(2)
830-4.10
NAS 1.55:2251
DEC 1 1982
ORIGINAL
COMPLETED
448

NASA Conference Publication 2251

Advanced Materials Technology

Proceedings of a seminar held at
NASA Langley Research Center
Hampton, Virginia
November 16-17, 1982

NASA

NASA Conference Publication 2251

Advanced Materials Technology

Compiled by
Charles P. Blankenship
and Louis A. Teichman
Langley Research Center
Hampton, Virginia

**Proceedings of a seminar sponsored by
NASA Langley Research Center, Hampton,
Virginia, and the American Institute of
Aeronautics and Astronautics, New York,
and held in Hampton, Virginia
November 16-17, 1982**

NASA
National Aeronautics
and Space Administration

**Scientific and Technical
Information Branch**

1982

I

Use of trade names or names of manufacturers in this report does not constitute an official endorsement of such products or manufacturers, either expressed or implied, by the National Aeronautics and Space Administration.

PREFACE

This publication is a compilation of papers presented at the NASA/AIAA Advanced Materials Technology Seminar held at NASA Langley Research Center on November 16-17, 1982. Collectively, these papers depict the broad scope of NASA's Materials Technology Program. Each paper provides a brief overview of a technical area in which NASA has a significant research focus. The technical areas include composites, polymer science, metallic materials (aluminum, titanium, and superalloys), materials processing technology, materials durability in the aerospace environment, ceramics, fatigue and fracture mechanics, tribology, and nondestructive evaluation (NDE). The technical program covers research being conducted at four NASA centers: Ames Research Center, Moffett Field, California; Langley Research Center, Hampton, Virginia [illegible] Research Center, Cleveland, Ohio; and Marshall Space Flight Center, Huntsville, Alabama.

Presentation of the NASA program in this format was selected to meet the following key seminar objectives:

1. Introduce the nonaerospace industry to the NASA Materials Technology Program.

2. Provide a convenient medium for technology exchange.

3. Provide industry with direct access to the NASA program, particularly for future follow-up activities in areas of high interest.

This Seminar was held as part of the continuing NASA/AIAA Industry Executive Seminar series. The NASA/AIAA program was designed to provide an early introduction and early exposure of the NASA research and development activities to the nonaerospace industry. Seminars of this type provide a convenient means to help transfer aerospace technology to the commercial mainstream in a systematic manner. The NASA/AIAA program is sponsored by the Division of Technology Utilization and Industry Affairs, NASA Headquarters, Washington, DC, and by the American Institute of Aeronautics and Astronautics, New York, New York.

Charles P. Blankenship
Seminar coordinator

BLANK PAGE

CONTENTS

PREFACE iii

1. OPPORTUNITIES FOR COMPOSITES IN COMMERCIAL TRANSPORT STRUCTURES 1
Herman L. Bohon

2. POLYMER RESEARCH AT NASA LANGLEY RESEARCH CENTER 29
Terry L. St. Clair and Norman J. Johnston

3. POLYMER MATERIALS RESEARCH AT NASA AMES RESEARCH CENTER 49
J. A. Parker, A. H. Heimbuch, and W. J. Gilwee

4. POLYMER MATRIX COMPOSITES RESEARCH AT NASA LEWIS RESEARCH CENTER 65
T. T. Serafini

5. FATIGUE AND FRACTURE RESEARCH IN COMPOSITE MATERIALS 91
T. Kevin O'Brien

6. PROCESSING COMPOSITE MATERIALS 115
R. M. Baucom

7. CONSERVATION OF STRATEGIC METALS 141
Joseph R. Stephens

8. SOLIDIFICATION PROCESS CONTROL FOR ADVANCED SUPERALLOYS 165
Hugh R. Gray and Robert L. Dreshfield

9. ADVANCED POWDER METALLURGY ALUMINUM ALLOYS AND COMPOSITES 183
W. B. Lisagor and B. A. Stein

10. ADVANCES IN METALS PROCESSING 201
Thomas T. Bales and Dick M. Royster

11. FATIGUE AND FRACTURE RESEARCH IN METALS 219
J. C. Newman, Jr. and J. R. Davidson

12. HIGH-TEMPERATURE FATIGUE IN METALS 233
Gary R. Halford

13. FIBROUS CERAMIC INSULATION 261
Howard E. Goldstein

14. RESEARCH ON ULTRA-HIGH-TEMPERATURE MATERIALS - MONOLITHIC CERAMICS, CERAMIC MATRIX COMPOSITES, AND CARBON/CARBON COMPOSITES 275
T. J. Miller and H. H. Grimes

15. RECENT ADVANCES IN CARBON-CARBON MATERIALS SYSTEMS 293
Donald R. Rummler

16. TURBINE ENGINE MATERIALS DURABILITY RESEARCH 313
S. R. Levine and C. A. Stearns

17. DURABILITY OF AIRCRAFT COMPOSITE MATERIALS 335
H. Benson Dexter

18. DURABILITY OF SPACECRAFT MATERIALS 357
Darrel R. Tenney

19. MATERIALS PROCESSING IN SPACE 381
W. A. Oran

20. TRIBOLOGY 391
Donald H. Buckley

21. FUNDAMENTALS OF ULTRASONIC NDE FOR MICROSTRUCTURE/MATERIAL PROPERTY INTERRELATIONS 411
A. Vary

22. ADVANCES IN NONDESTRUCTIVE EVALUATION TECHNOLOGY 421
Joseph S. Heyman

OPPORTUNITIES FOR COMPOSITES IN COMMERCIAL TRANSPORT STRUCTURES

Herman L. Bohon
NASA Langley Research Center
Hampton, Virginia

ACEE COMPOSITES PROGRAM-

INTRODUCTION

In recent years graphite/epoxy material has found widespread application in military aircraft and is now finding application in commercial transports. Because of special features of this material, such as high strength-to-density ratio, good formability and laminate tailoring, the next generation of military and commercial aircraft manufactured with composites could be significantly more efficient than current aircraft. Studies have shown that composites can reduce the structural weight of transport aircraft by as much as 25 percent over current aluminium structures with a corresponding reduction in fuel consumption of 12 to 15 percent. The NASA Aircraft Energy Efficiency (ACEE) composites program was established to foster the application of composite material in the next generation of aircraft. The primary objective of ACEE is to develop the essential technologies in cooperation with the commercial transport manufacturers to permit the efficient utilization of composites in airframe structure of future transport aircraft.

Specifically the ACEE composites program is to provide each of the commercial transport manufacturers both the technology and confidence required for a commitment to composite structures production. This means not only know-how for predictable designs and low-cost fabrication, but enough test and actual manufacturing experience to accurately predict durability for product warranty purposes and costs for product pricing, and to assure safety for certification by the FAA and maintainability for acceptance by the airlines.

OBJECTIVE

PROVIDE THE **TECHNOLOGY** AND **CONFIDENCE** SO THAT COMMERCIAL TRANSPORT MANUFACTURERS CAN COMMIT TO PRODUCTION OF COMPOSITES IN THEIR FUTURE AIRCRAFT:

SECONDARY STRUCTURE - 1980 TO 1985

PRIMARY STRUCTURE - 1985 - 1990

TECHNOLOGY	CONFIDENCE
° DESIGN CRITERIA, METHODS AND DATA	° DURABILITY/WARRANTY
° QUALIFIED DESIGN CONCEPTS	° QUANTITY COST VERIFICATION
° COST COMPETITIVE MANUFACTURING PROCESSES	° FAA CERTIFICATION
	° AIRLINE ACCEPTANCE

COMPONENT DEVELOPMENT TOWARD A PRODUCTION COMMITMENT

To support these objectives the manufacturers are developing composite versions of structural components on existing aircraft with NASA paying 90 percent of the cost. Development involves testing of various material options before selecting one and then extensive testing to develop an adequate data base of material strength and stiffness properties. Design options are narrowed through analysis and a varied spectrum of development tests on small and large subcomponents. In parallel with this, a suitable production process including economical ply preparation and cure at high temperature and pressure is evolved, tools are designed and fabricated, and full-scale components are then manufactured for ground qualification tests, flight tests, and airline service. The various tests include many that are required by the FAA for flight certification, which must precede airline service. Inspection and repair methods to insure adequate maintenance in service are also developed.

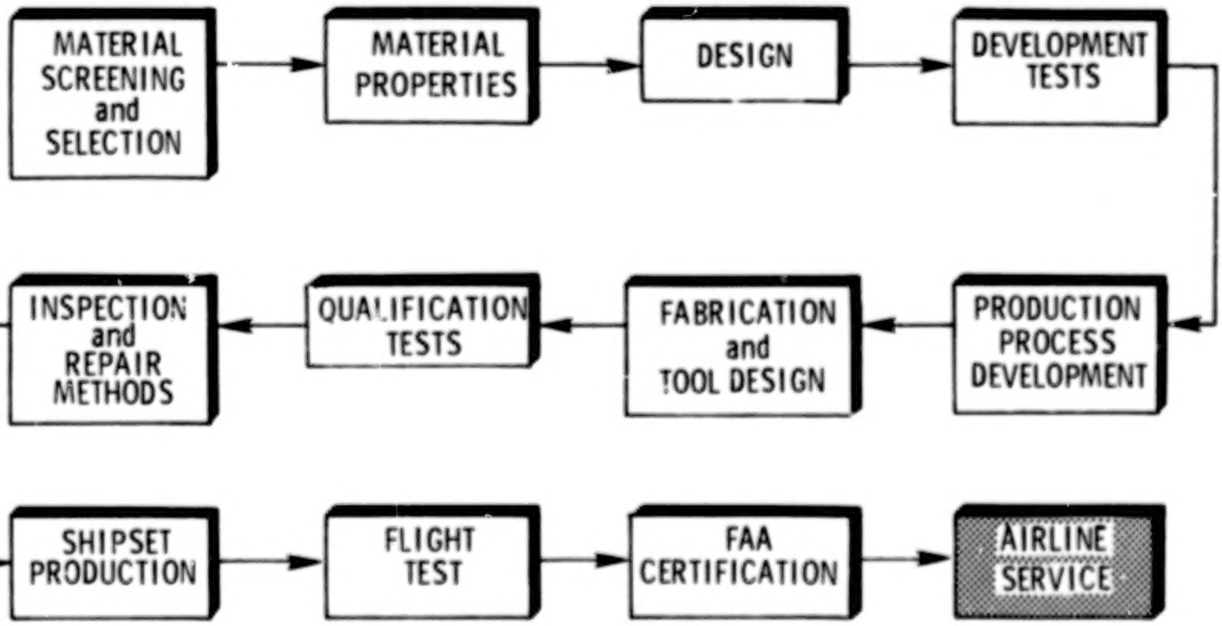
MATERIAL SCREENING and SELECTION
MATERIAL PROPERTIES
DESIGN
DEVELOPMENT TESTS
PRODUCTION PROCESS DEVELOPMENT
FABRICATION and TOOL DESIGN
QUALIFICATION TESTS
INSPECTION and REPAIR METHODS
SHIPSET PRODUCTION
FLIGHT TEST
FAA CERTIFICATION
AIRLINE SERVICE

ACEE COMPOSITE SECONDARY STRUCTURES

The commercial transport manufacturers were challenged to redesign selected secondary and medium primary components on existing aircraft with composite material. Secondary components include the Boeing 727 elevators, the Lockheed L-1011 ailerons and the Douglas DC-10 upper aft rudder. Such components are called "secondary" structures because they do not carry primary flight loads and are not critical to flight safety.

BOEING 727 COMPOSITE ELEVATOR

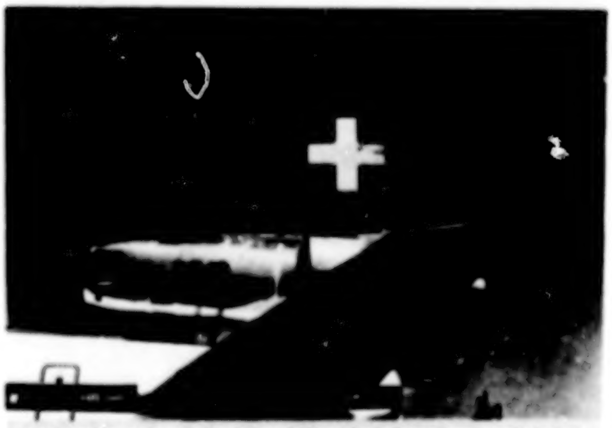

DOUGLAS DC-10 COMPOSITE RUDDER

LOCKHEED L-1011 COMPOSITE AILERON

DC-10 GRAPHITE/EPOXY UPPER AFT RUDDER

The DC-10 composite rudder program is now complete and one of the rudders is shown here. The rudder is 3 feet at the root chord by 13 feet in length and weighs only 67 pounds, corresponding to a 26-percent weight savings over the metal design. Douglas has fabricated 20 rudders under this program and to date 13 have been placed in flight service with several domestic and foreign commercial airlines.

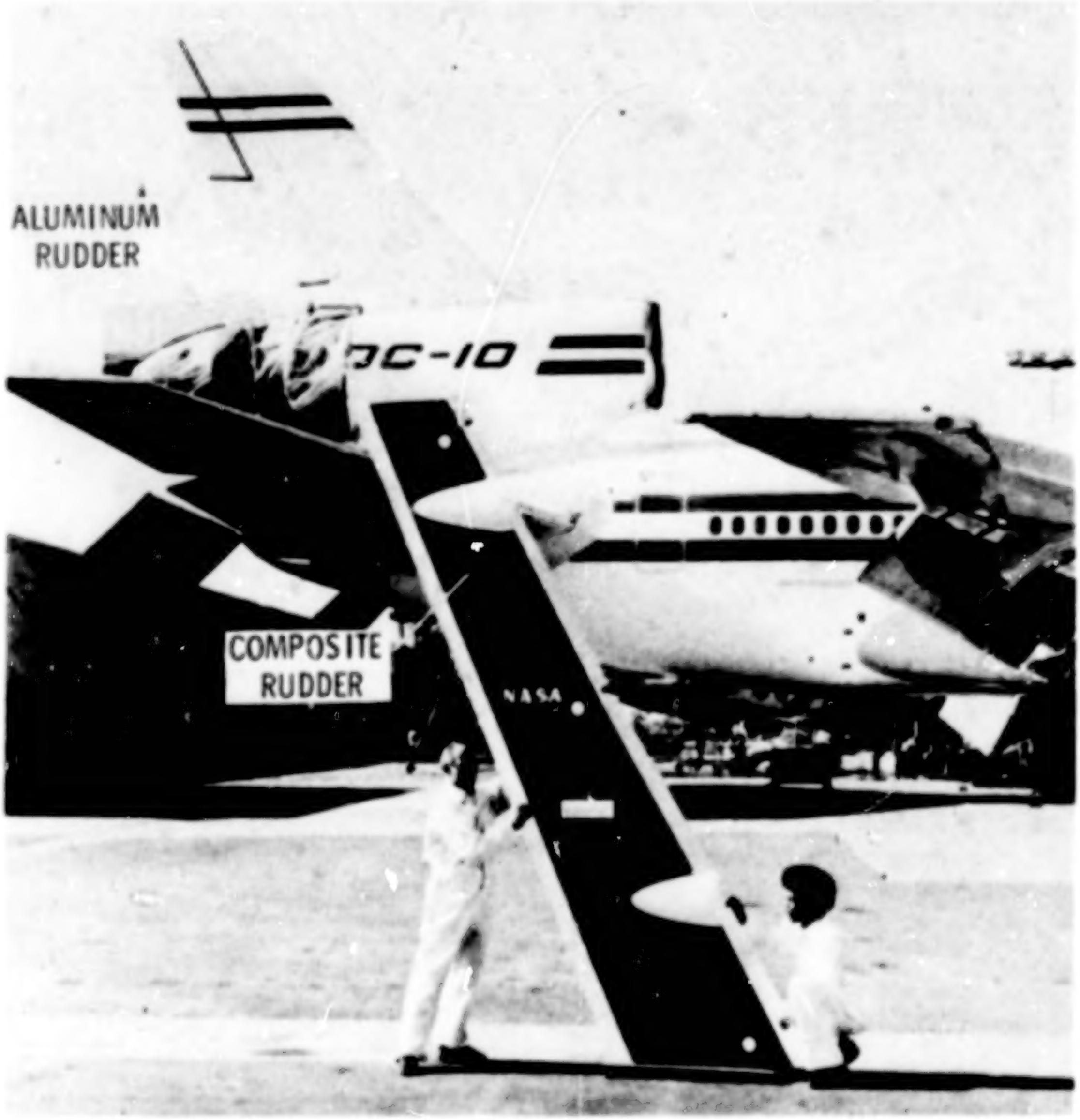

727 GRAPHITE/EPOXY ELEVATOR

In the Boeing 727 elevator program five shipsets of composite elevators have been fabricated and ground and flight tested. Four shipsets are shown here. This structure has been certificated by the FAA and all five shipsets have been placed into airline service with United Airlines. The elevators are 3-1/2 feet at the maximum chord by 17 feet in span and weigh 98 pounds. Weight reduction over the metal design is about 25 percent. The design and construction of these elevators provided the confidence and experience to place generically similar composite designs of secondary components on Boeing's new 767 and 757 aircraft.

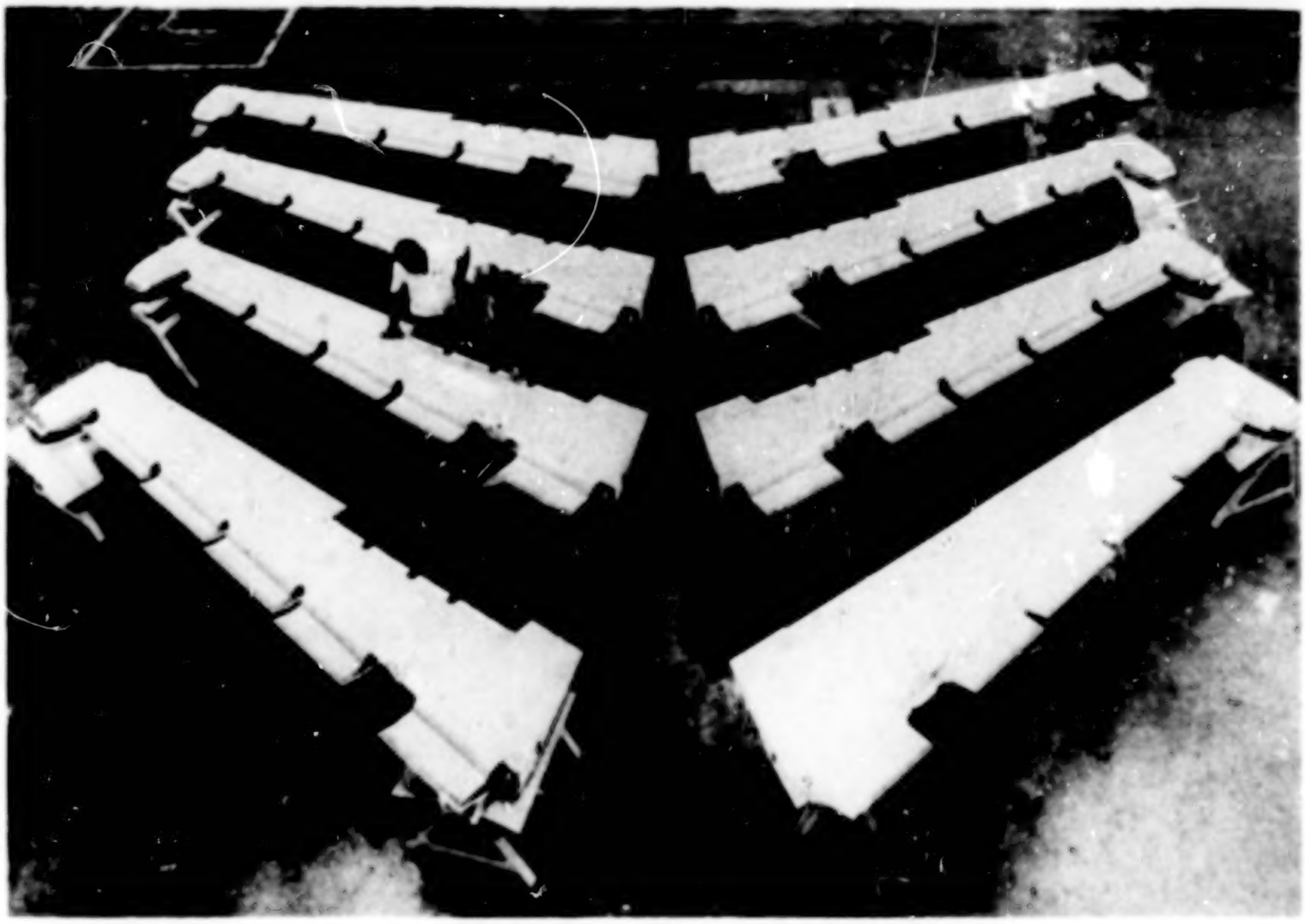

L-1011 GRAPHITE/EPOXY AILERON

The Lockheed L-1011 aileron program is also complete. Five shipsets of ailerons were successfully fabricated, ground and flight test qualified and certificated by FAA. One shipset is in service on the Lockheed Company airplane while the other four are in flight service on commercial aircraft, two with TWA and two with Delta. The ailerons are 4 feet by 8 feet and weigh 107 pounds, representing a 24-percent weight savings over the metal design.

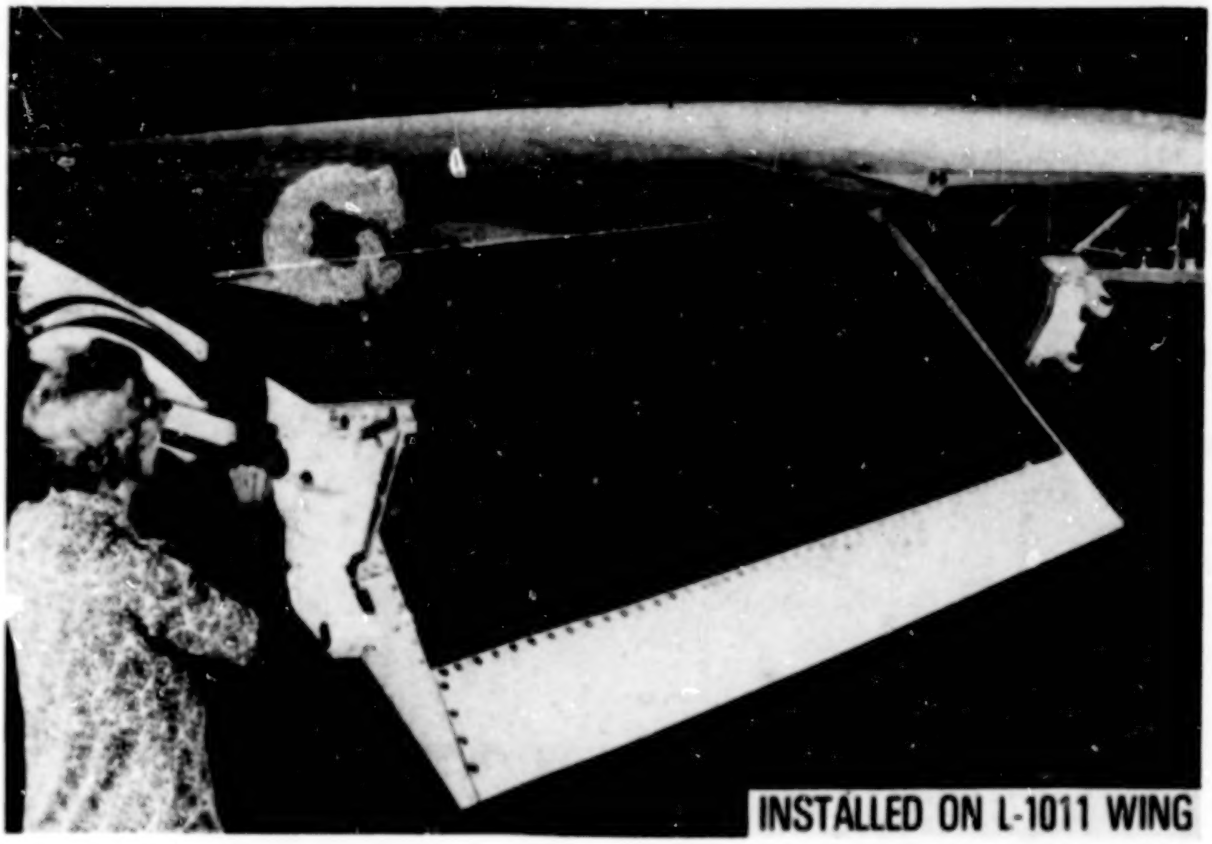
INSTALLED ON L-1011 WING

ACEE COMPOSITE MEDIUM PRIMARY STRUCTURES

The commercial aircraft manufacturers are also developing composite versions of empennage primary structures on their existing aircraft. The empennage components offer a significant increase in challenge for composites application compared to the secondary structures. In particular, physical size, design requirements, load interaction, manufacturing and tooling each present formidable technology development tasks beyond those required for secondary structure. Components selected for redesign are the horizontal stabilizers on the Boeing 737 and the vertical stabilizers of the Douglas DC-10 and the Lockheed L-1011. These programs are still in progress.

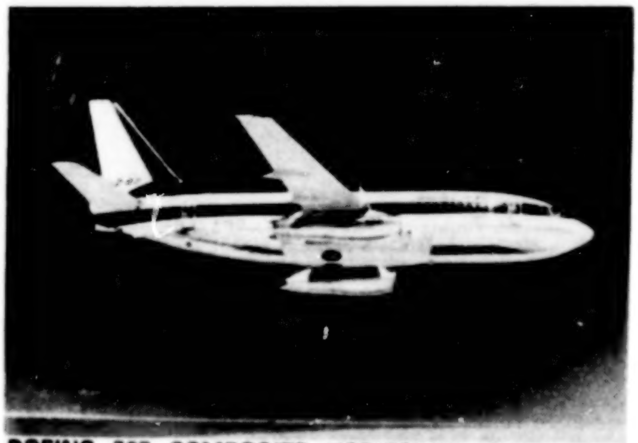

BOEING 737 COMPOSITE HORIZONTAL STABILIZER

DOUGLAS DC-10 COMPOSITE VERTICAL STABILIZER

LOCKHEED L-1011 COMPOSITE VERTICAL FIN

DC-10 GRAPHITE/EPOXY VERTICAL STABILIZER

All subcomponents (covers, spars, and ribs) of three full-scale composite vertical stabilizers for the DC-10 have been successfully fabricated and one stabilizer has been assembled for detailed ground qualification testing. The stabilizer is 7 feet at the root chord and 23 feet in span and weighs 779 pounds, representing a 23-percent weight savings over the metal design. The ground test program, which began in December 1981, was interrupted by premature failure initiating at the rear spar. Cause of failure has been identified and design modifications incorporated in the other two units. The second unit is being assembled to complete ground qualification testing, and the third unit will be flight tested to complete requirements for FAA certification. The third unit will then be placed in flight service with a commercial airline.

737 GRAPHITE/EPOXY HORIZONTAL STABILIZER

The 737 composite horizontal stabilizer is the smallest of the three empennage components and measures 4 feet at the root chord by 17 feet in span. The composite stabilizer weighs 204 pounds, which is a 22-percent weight reduction from the metal design. All ground and flight testing was completed successfully and FAA certification was granted in August 1982. This marks the first FAA certification of an empennage component for commercial transport aircraft. Boeing has fabricated and assembled five shipsets which are expected to be placed in flight service in the near future.

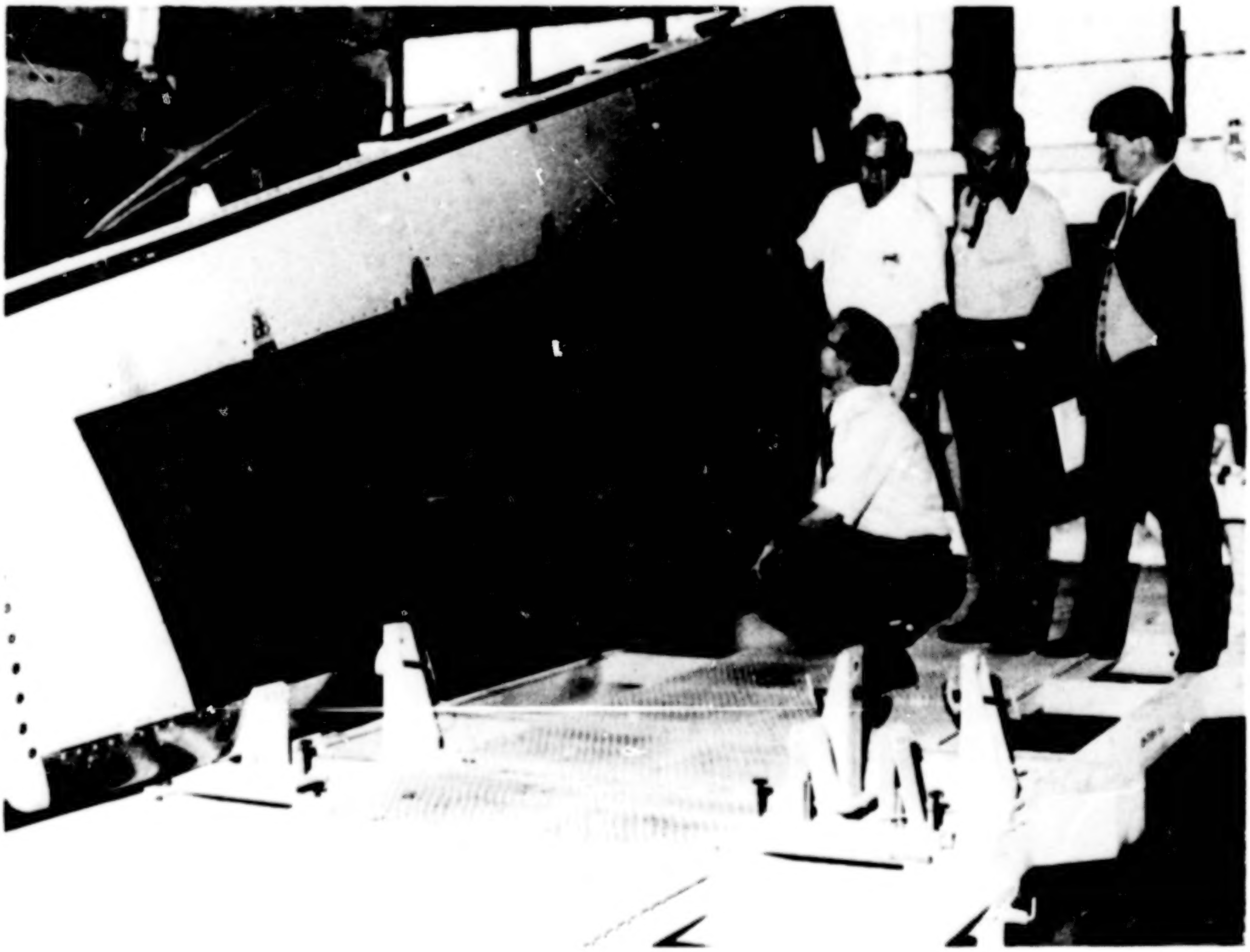

L-1011 GRAPHITE/EPOXY VERTICAL FIN

The L-1011 composite vertical fin is the largest in planform of the empennage components with a root chord of 9 feet and a span of 25 feet. The composite fin weighs 622 pounds, which is 28 percent lighter than the metal design. Two complete L-1011 composite fins have been assembled and one of these failed during ground qualification test just below design ultimate load, revealing a minor but significant design flaw. (Details of the failure will be discussed later.) The other fin was strengthened and successfully completed ground tests in June 1982 to qualify the modified design. Flight testing of the L-1011 composite fin is not planned.

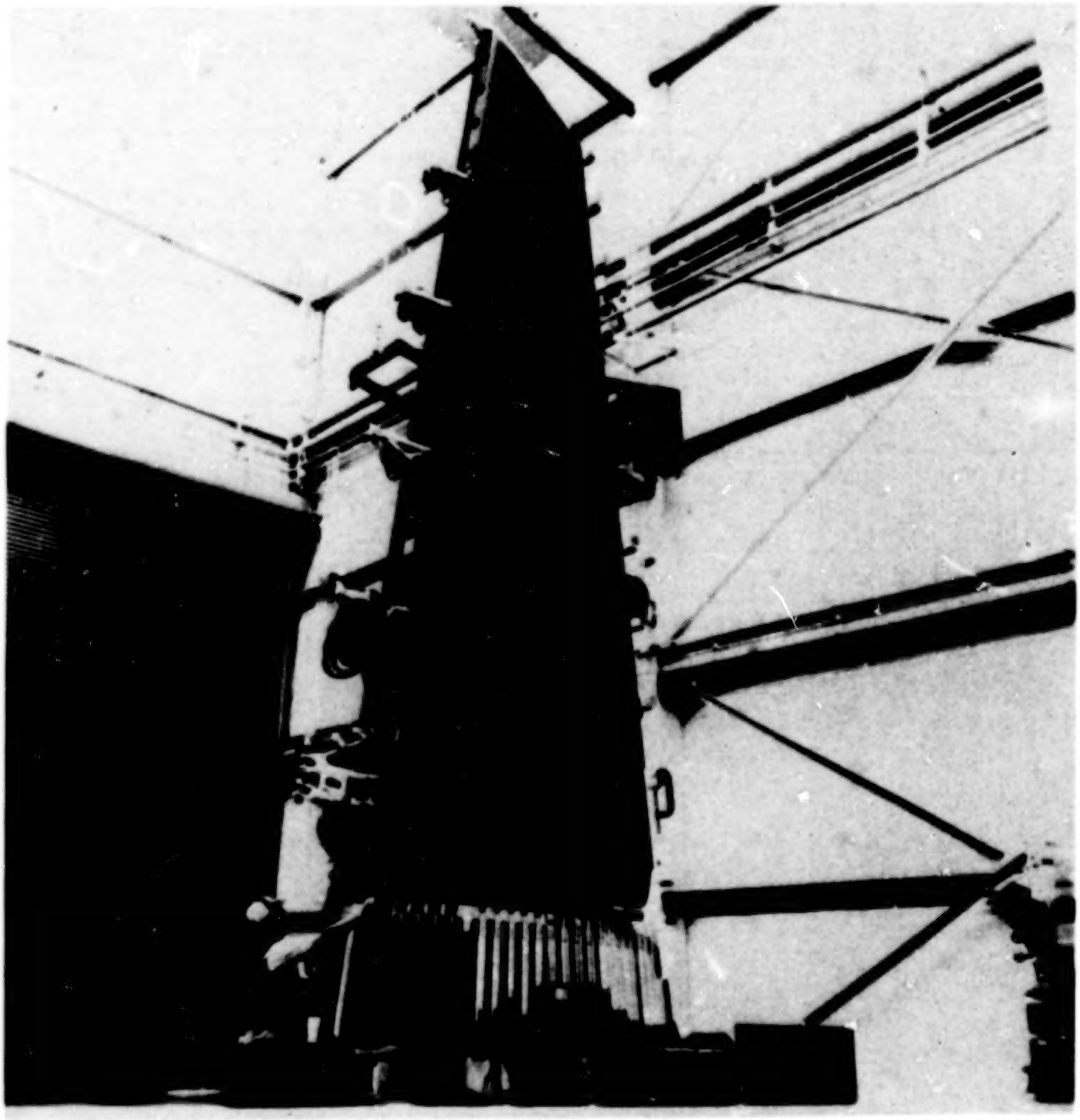

ACEE COMPOSITE COMPONENT STATUS

Key features of the three secondary and empennage primary components are summarized in this table. Each component was manufactured in a production environment as a direct replacement of existing metal components. Weight savings from 22 to 28 percent were obtained even though these composite designs were driven to some degree by the existing metal design requirements. All components placed in flight service are tracked by the airlines and the manufacturer and are inspected periodically to insure safety of flight.

COMPONENT	SIZE ROOT X SPAN FT.	METAL DESIGN WEIGHT (LBS.)	COMPOSITE DESIGN WEIGHT (LBS.)	WEIGHT REDUCTION	NUMBER OF PRODUCTION UNITS	FAA CERTIFICATION	REMARKS
SECONDARY STRUCTURES							
DC-10 RUDDER	3.2 x 13.2	91	67	26.4%	20	MAY 1976	13 UNITS IN FLIGHT SERVICE
727 ELEVATOR	3.4 x 17.4	130	98	24.6%	11	JAN. 1980	5 SHIPSETS (10 UNITS) IN FLIGHT SERVICE
L-1011 AILERON	4.2 x 7.7	140	107	23.6%	12	SEPT. 1981	4 SHIPSETS (8 UNITS) IN FLIGHT SERVICE
MEDIUM PRIMARY STRUCTURES							
DC-10 V. STABILIZER	6.8 x 22.8	1005	779	22.6%	5	SEPT 1984	FLIGHT C/O AUG 1984
737 H. STABILIZER	4.3 x 16.7	262	204	22.1%	11	AUG. 1982	FLIGHT C/O COMPLETE
L-1011 V. FIN	8.9 x 25	858	622	28.4%	2	No	NO FLIGHT TEST PLANS

CHARACTERISTICS OF GRAPHITE/EPOXY MATERIAL

The remainder of this paper will highlight lessons learned in the ACEE composites program first by looking at attributes of the graphite/epoxy composite system and then by examining areas requiring advanced technology development.

Throughout the program the manufacturers required all fabrication and assembly of full-scale parts to be carried out in their production shops in order to obtain reliable manufacturing cost data as well as to gain valuable experience with production personnel. Hands-on experience was essential, not only in laying up and curing the laminate material with consistency and repeatability, but in developing test procedures to properly validate structural performance. This figure lists several positive characteristics of the composite system in manufacturing and performance areas that became evident during the full scale production phase of the program. The next few figures are used to illustrate these characteristics.

MANUFACTURING

- TOLERANT RESIN CURE CYCLE
- UNIFORMITY OF HEAT DURING CURE OF PART IS ESSENTIAL
- PART SIZE LIMITED ONLY BY FACILITIES
- INNOVATIVE TOOLING PERMITS FABRICATION OF COMPLEX PARTS

PERFORMANCE

- FAILURE LOADS ARE PREDICTABLE
- FABRICATED PARTS ARE UNAFFECTED BY ENVIRONMENT

TYPICAL CURE CYCLES FOR GRAPHITE/EPOXY

The epoxy resin system used in the ACEE composites program is cured at 350°F and at high pressure (80 to 100 psi depending on the part). The structural performance of the part is found to be tolerant of the heat-up rate, a feature which offers considerable flexibility in utilization of facilities. A typical cure cycle matrix is shown in this figure. The three curves outline the fastest, average, and slowest heat rises used in an empennage program. The left and center curves show a heat rise to 250°F under vacuum, a dwell period, and pressure application. The right curve with a much slower heat rise has pressure applied at 225°F without a dwell period. The heat sink capacity of the tool generally determines the heat-up rate and care must be taken to assure uniformity of heat of the part during the cure cycle to avoid irregular resin flow.

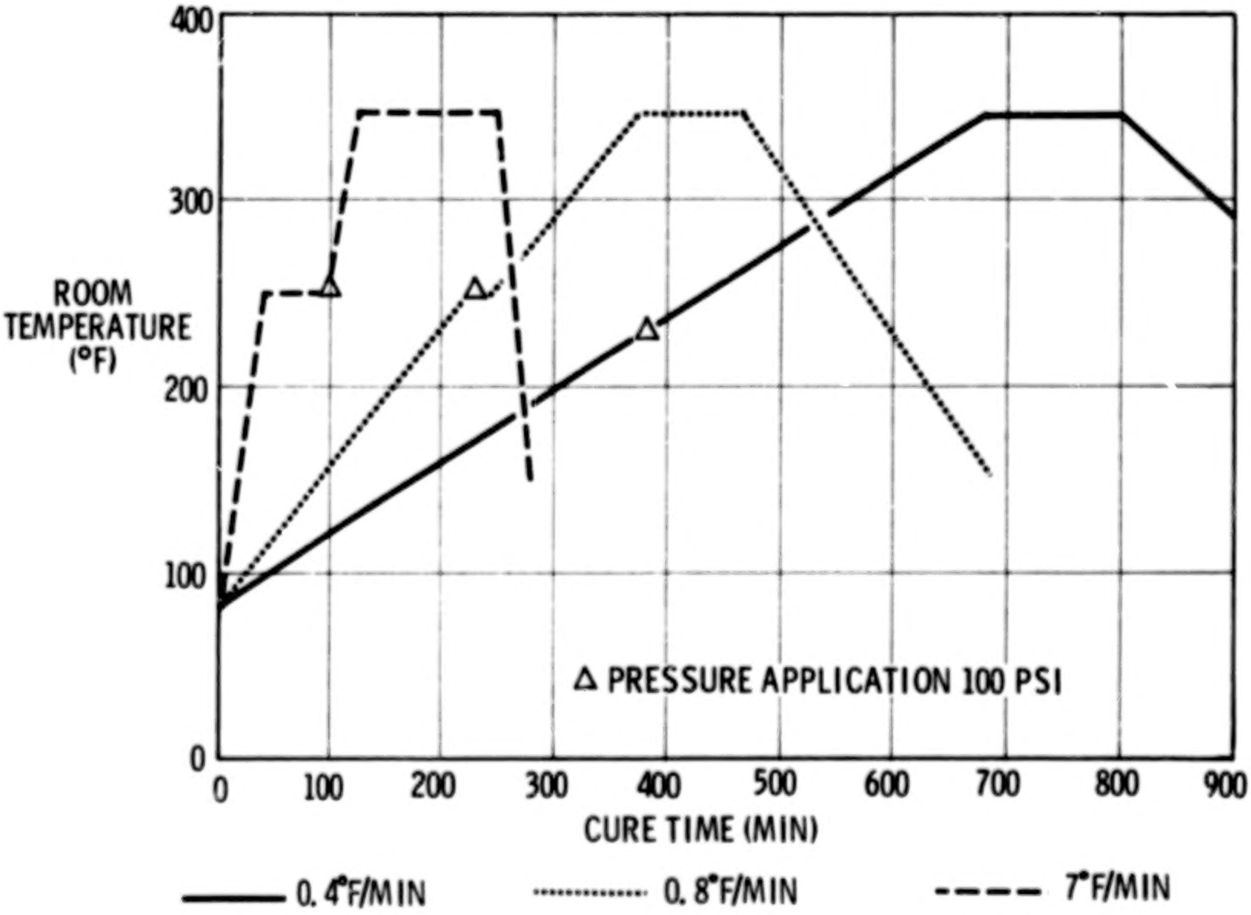

LARGE COMPLEX STRUCTURES MANUFACTURED

The largest single composite part in the empennage program is the cover panel of the L-1011 vertical fin. This structurally efficient hat-stiffened panel, which measures 8.9 feet at the root chord and 25 feet in span, was integrally cured in an autoclave and has no mechanical fasteners. The ease with which this part was cured suggests that the only limitation to part size may be the physical dimensions of the autoclave. The differential growth at cure temperature between the composite part and the hard tool (in this case steel) must, of course, be accounted for to assure dimensional control of critical elements and for tool release during cool-down following cure.

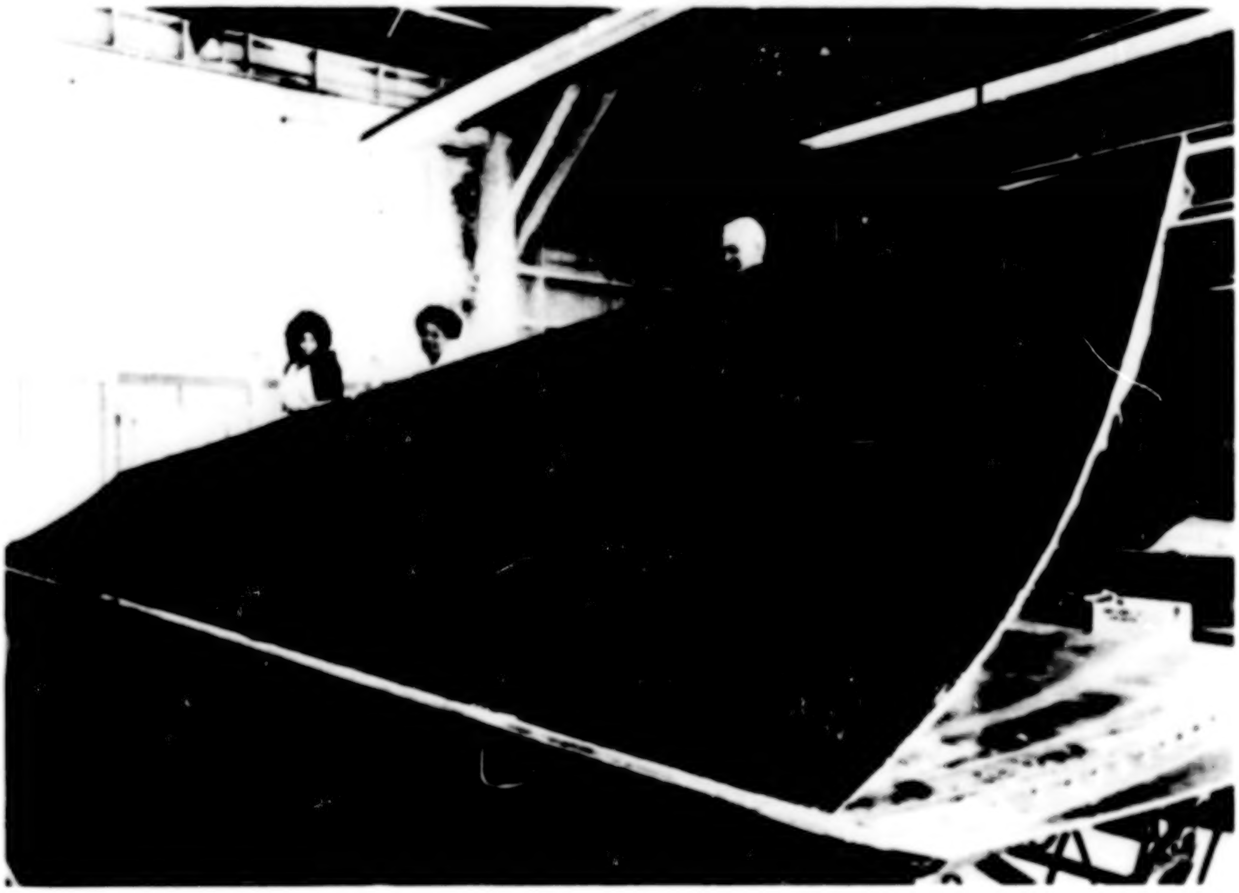

LIGHTWEIGHT STRUCTURAL COMPONENTS SIMPLIFY FINAL ASSEMBLY

One of the important features of the graphite/epoxy system is the unique opportunity to tailor stiffness properties and, with innovative tooling, to integrally mold efficient structural shapes that virtually eliminate mechanical fasteners. This figure illustrates one such example. The I-shaped spar configuration shown is 25 feet in length and is integrally (one step) cured, including the angle stiffeners on the shear web. Although some metallic parts are retained in final assembly, this single composite spar replaces 35 metal parts and 2,286 fasteners that were part of the all-metal design.

STRUCTURAL PERFORMANCE DEMONSTRATED

Following successful development of fabrication procedures for complex parts it is essential to validate the structural performance of cured parts. One program conducted by Lockheed to assess manufacturing tolerances on repeatability of performance is shown on the next three figures. Ten full-scale segments each of the L-1011 composite fin spar and cover were tested to destruction to obtain static strength characteristics. Each of the segments had measurable but acceptable manufacturing flaws such as thickness variations and small areas of porosity. The other twelve segments of each configuration are currently undergoing an accelerated 20 years of lifetime testing simulating flight cyclic loads, moisture, and temperature environments. Results from the static test program are shown in the next figure.

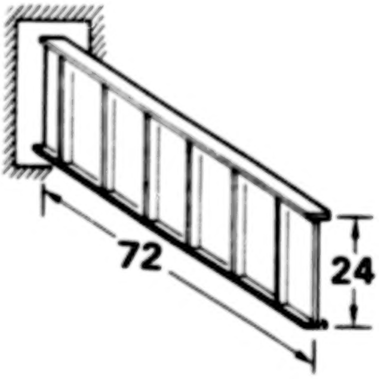

SPAR SEGMENT

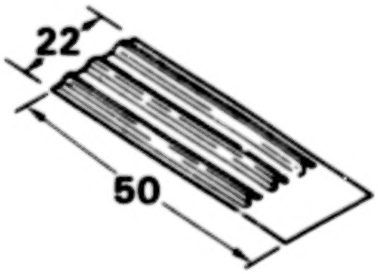

COVER SEGMENT

12	DURABILITY SPECIMENS	12
10	STATIC STRENGTH SPECIMENS	10
22		22

SPAR STATIC STRENGTH TESTS FOR MANUFACTURING VARIANCES

The results from the static strength tests of ten duplicate spar segments are shown in this figure. The spars were loaded in bending to produce a distribution of strain in the critical region equal to that of the full-size spar under flight loads. The load at failure is plotted as a percent of design ultimate load (DUL), which is 1.5 times the maximum aerodynamic load expected in flight. The test average is 135 percent DUL and about 15 percent higher than the predicted value based on conservative material properties from coupon tests. More importantly, all test values exceeded the predicted value, suggesting that the allowable manufacturing flaws have little effect on static strength.

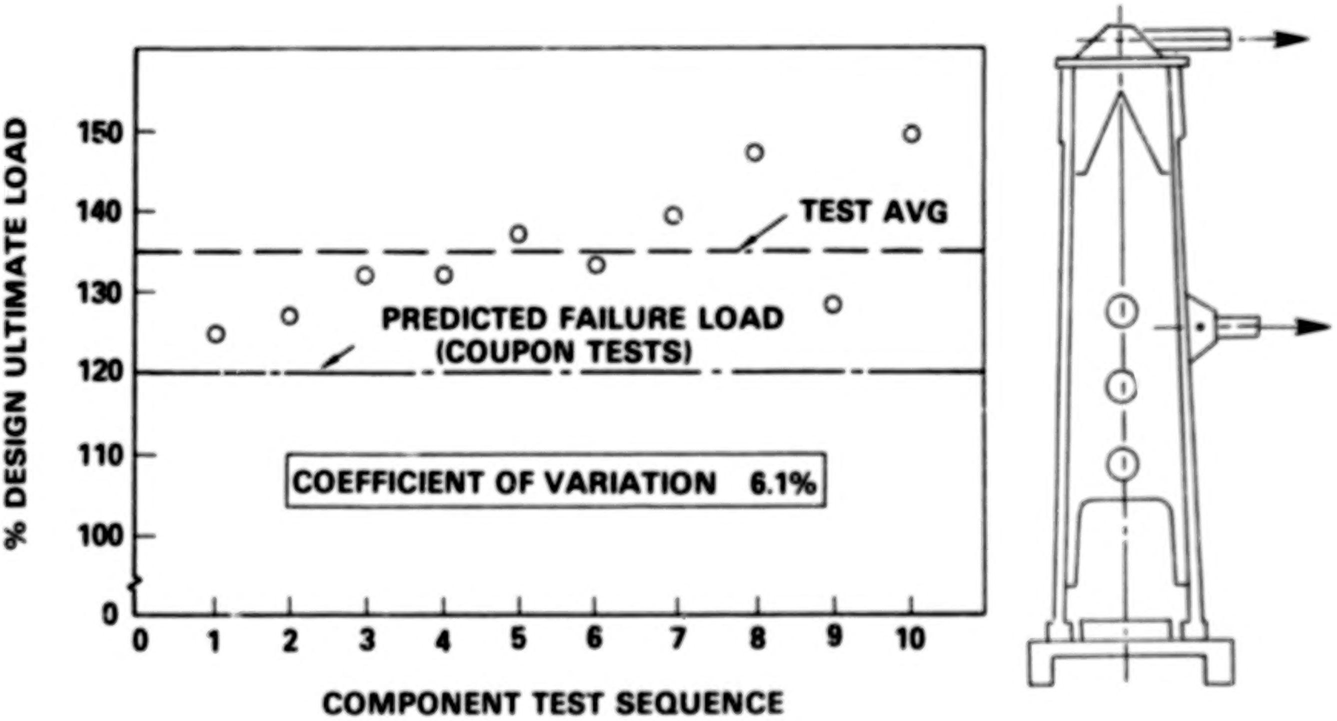

COMPARISON OF STATIC STRENGTH FOR STRUCTURAL MATERIALS

The coefficients of variation of the ten cover and spar segments were 3.3 and 6.1, respectively. These values, obtained from tests of complex structural components, are consistent with values obtained from composite coupons and other structural materials and attest to the predictability and repeatability of performance of composite parts manufactured in a production surrounding.

MATERIAL	COMPONENT	SPEC. NO.	LOADING	COEFFICIENT OF VARIATION PERCENT
Graphite-Epoxy	PRVT-Cover	10	Compression	**3.3**
Graphite-Epoxy	PRVT-Spar	10	Bending	**6.1**
Graphite-Epoxy	Spoiler	15	Bending	6.6
Graphite-Epoxy	Laminate Coupons	411	Tension	5.7
Graphite-Epoxy	Laminate Coupons	411	Ten-Modulus	4.0
Graphite-Epoxy	Laminate Coupons	290	Compression	9.0
Graphite-Epoxy	Laminate Coupons	290	Compr-Modulus	5.2
Wood	Mosquito Wings	5	Bending	10.3
Wood	Plywood Shear Wall	27	Shear	9.7
Concrete	Test Cylinders	216	Compression	10.6
Aluminum	7049-T73 Die Forging	384	Tension	3.2
Aluminum	A357-T6 Casting	804	Tension	5.5
Titanium	TI-SAL-2.5SN Sheet	565	Tension	3.9
Steel	Structural Steel	3982	Tension	7.1
Steel	17-7PH Sheet	88	Tension	5.1

INFLUENCE OF ENVIRONMENTAL PARAMETERS ON STRUCTURAL PERFORMANCE

Another important issue that required full-scale components to evaluate was the influence of flight environmental parameters (moisture and temperature) on the performance of the structure under flight loads. A key activity designed to assess the influence of variations of flight temperature and moisture on strain distribution in a three-dimensional structure was carried out by Douglas on a stub box component shown in this figure. This component is the lower 45 percent of the DC-10 composite vertical stabilizer. The entire stub box, including the metallic leading edge, was mounted in an environmental chamber and subjected to a series of tests to determine, among other things, if the range of temperature and moisture to be expected in routine flight would affect the distribution of strain. The article was tested to limit load in bending, torsion, and shear at ambient conditions (72°F and no moisture (dry)), and then in bending at 0°F. This was followed by moisture conditioning at 170°F and 95 percent humidity for 14 days to achieve about 1 percent by weight moisture in the laminated structure. The component was then cyclic loaded for one lifetime at 0°F/wet and again tested to limit load in bending at 0°F and 130°F. Following a second lifetime of cyclic loading and another limit load bending test at 0°F/wet the stub box was then loaded in bending to failure. Measured strains for the different test conditions are shown on the next figure.

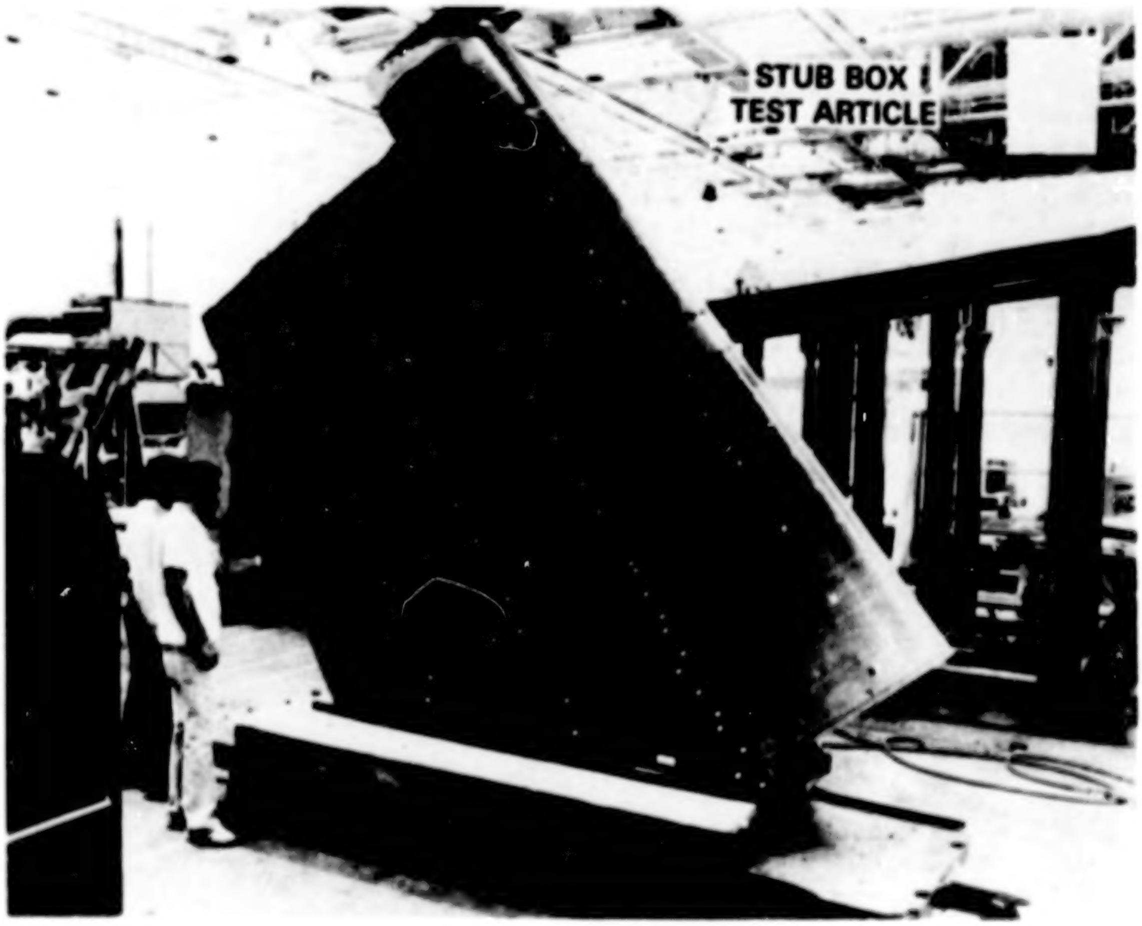

INFLUENCE OF MOISTURE AND TEMPERATURE ON STRAIN

The stub box strains shown are taken from the same strain gage at a cutout in the web of the rear spar. Data are plotted as a function of limit load for the four environmental conditions - ambient/dry, cold/dry, hot/wet, and cold/wet. The strain variation between the test conditions is small and suggests a negligible effect of moisture and temperature on strains in the three-dimensional structure.

REAR SPAR CUTOUT STRAINS

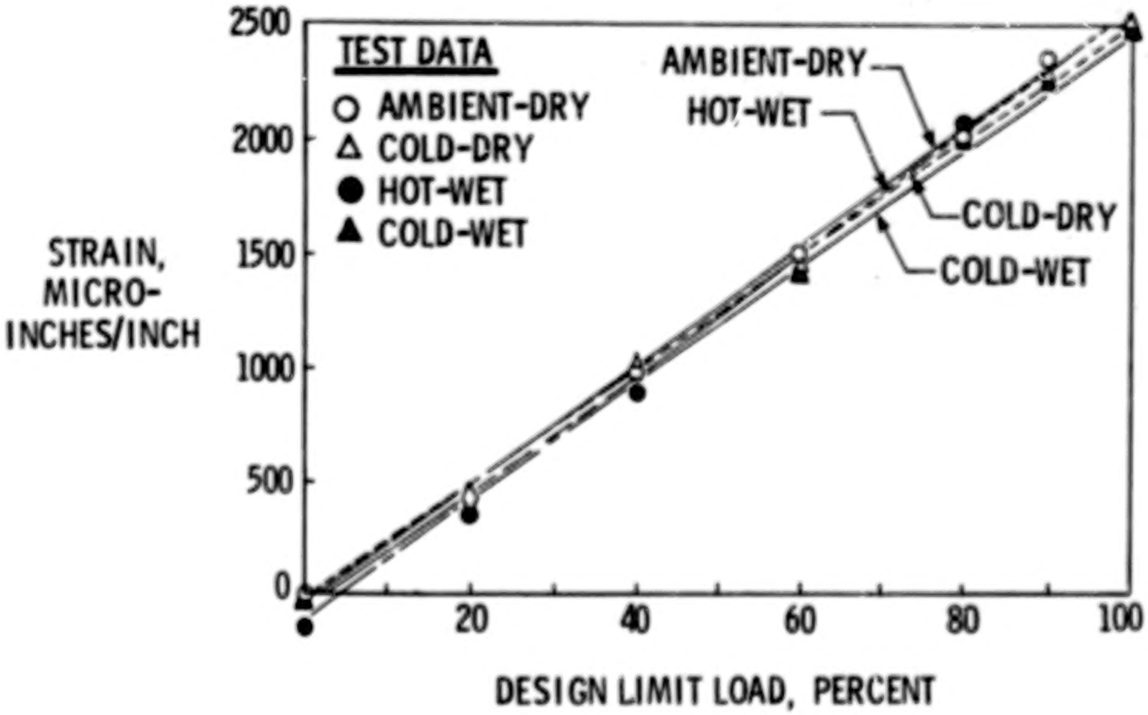

KEY AREAS FOR TECHNOLOGY ADVANCEMENT

With the ACEE composites program now near completion it is interesting to examine the state of technology, especially in light of requirements of the future. While the current material system is clearly adequate for application to lightly loaded (secondary and empennage) structure, there are identifiable areas where technology advancement could significantly enhance the utilization of composites in primary wing and fuselage components. Three areas for technology advancement of particular importance to primary structure application are listed on this figure. Of these, secondary loads are probably the least understood. It is agreed among designers that there is a general state of uncertainty with composites as to the source, magnitude, and effects of secondary loads. Yet secondary loads are virtually impossible to eliminate from a complex built-up structure. While these loads are properly ignored in metallic structures, the sensitivity of current composite materials to interlamina forces can lead to serious weaknesses being designed into a composite structure. Such loads may be produced by eccentricities, irregular shapes, stiffness changes, and discontinuities, and their effects are magnified by the nonyielding nature of composites, which precludes load redistribution due to plasticity effects. The influence of secondary loads was vividly illustrated during ground tests of the L-1011 vertical fin, an event discussed on the two subsequent figures.

- **IMPROVED UNDERSTANDING OF SOURCE, MAGNITUDE, AND EFFECTS OF SECONDARY LOADS**
- **ADVANCED MANUFACTURING PROCESSES**
- **TOUGHER RESIN TO IMPROVE DAMAGE TOLERANCE AND DURABILITY**

EFFECTS OF SECONDARY LOADS IN COMPOSITES

The L-1011 composite vertical fin failed during ground verification tests at 98 percent of design ultimate load (DUL) - 28 percent less than the predicted failure load. The failure caused separation of the cover and front spar, as shown in this figure, along the entire length of the component. After a careful investigation, the cause of failure was determined to be due to secondary loads caused by local buckling of the cover at the cover/spar interface. While local buckling beyond limit load was allowed in the design, the influence of these loads on the integrity of the structure was not expected. The interlamina tension forces caused delamination of the spar cap and ultimately separation along the line of the fasteners. Results from post-failure tests to assess the influence of such loads are shown on the next figure.

TYPICAL SPAR CAP DAMAGE IN PRIMARY FAILURE ZONE

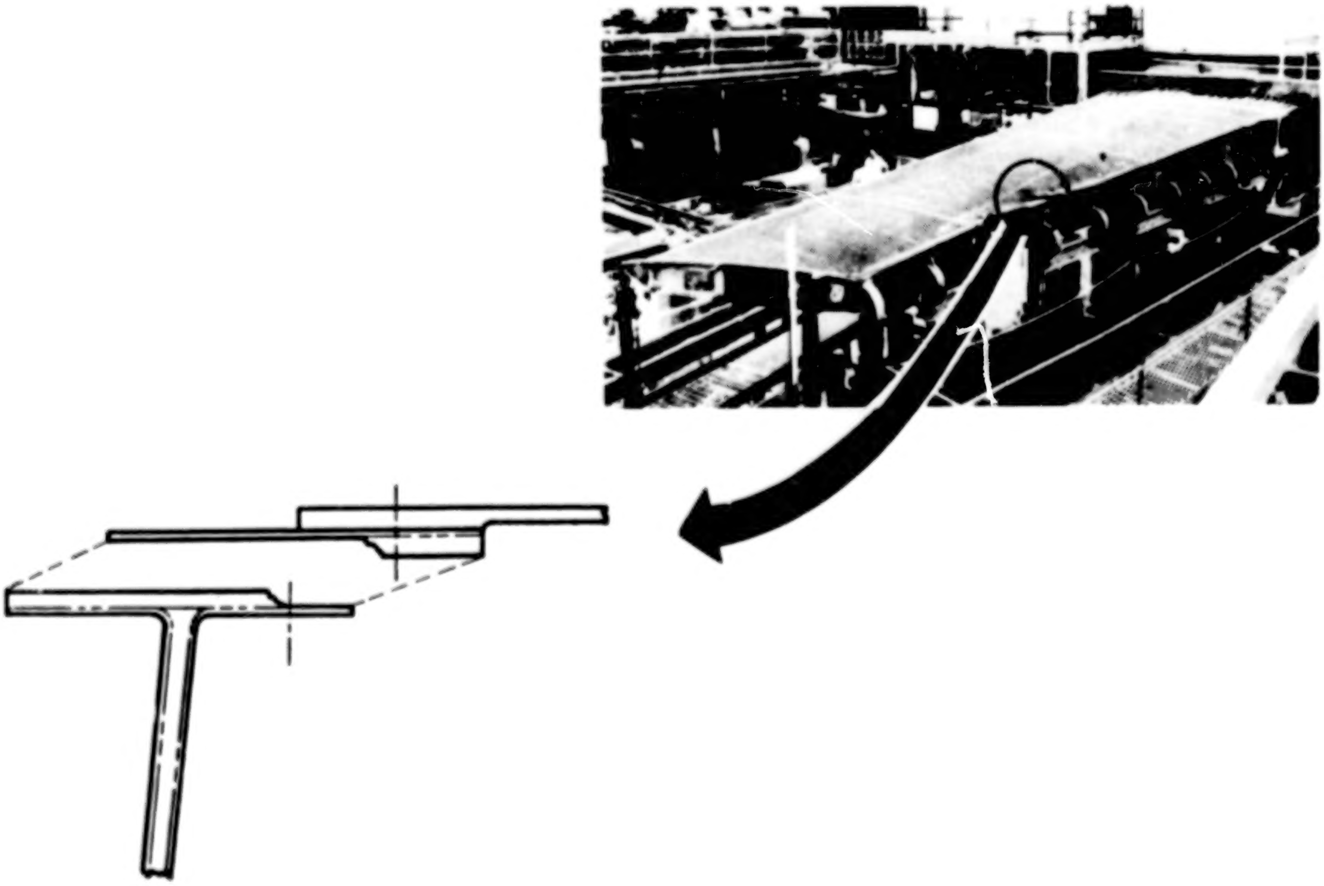

INFLUENCE OF LOAD CYCLING ON INTERLAMINA STRENGTH

Tests were conducted to determine the strength of the designs of the spar/cover intersection for secondary loads causing interlamina tension and transverse tension. The first test was on virgin material that had no prior loading and results were reasonable and indicated adequate margin. The estimated maximum interlamina tension load expected in flight was 68 pounds per fastener. The second test, on an undamage segment of the failed spar, showed large reductions in strength. This apparent influence of load cycling was verified by a third test on specimens subjected to load cycles similar to those of the ground test article prior to failure. This degradation in strength is the result of a design weakness in the spar cap, which can be avoided in future designs when criteria for secondary loads become a routine part of design practice.

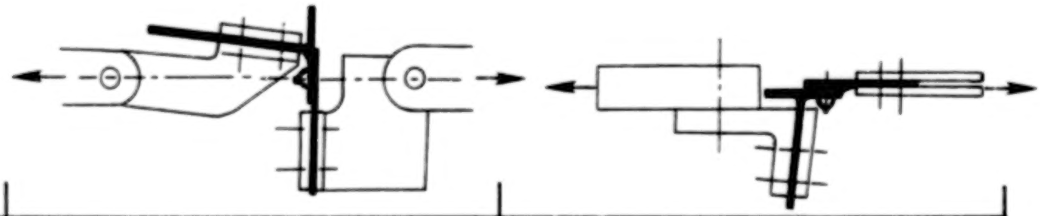

SPECIMEN CONDITIONING	INTERLAMINA TENSION (LB./FASTENER)	TRANSVERSE TENSION (LB./IN.)
NO PRIOR LOADING	88	445
SEGMENT OF SPAR OF FAILED GROUND TEST UNIT	34	256
PRIOR LOADING EQUAL TO GROUND TEST UNIT	56	225

INFLUENCE OF DAMAGE ON ALLOWABLE STRAIN

Another area in which technology advancement should pay off is the improvement of strain capability of the cured laminate. Limiting strain of current graphite/epoxy systems is determined primarily by sensitivity to impact damage. Typical results on this figure show the failure threshold of a compression-loaded graphite/epoxy plate as a function of impact energy. Designs of secondary and empennage structures have been governed primarily by stiffness requirements with design ultimate strains of about 0.003 μin./in.; and indeed, current resin systems can meet the strain requirements without a weight penalty. However, for large primary wing and fuselage structures, which are designed by strength requirements, higher strain capability is required if maximum utilization of composites is to be achieved. This is illustrated on the next figure.

EFFECT OF PROJECTILE IMPACT ON COMPRESSION STRENGTH

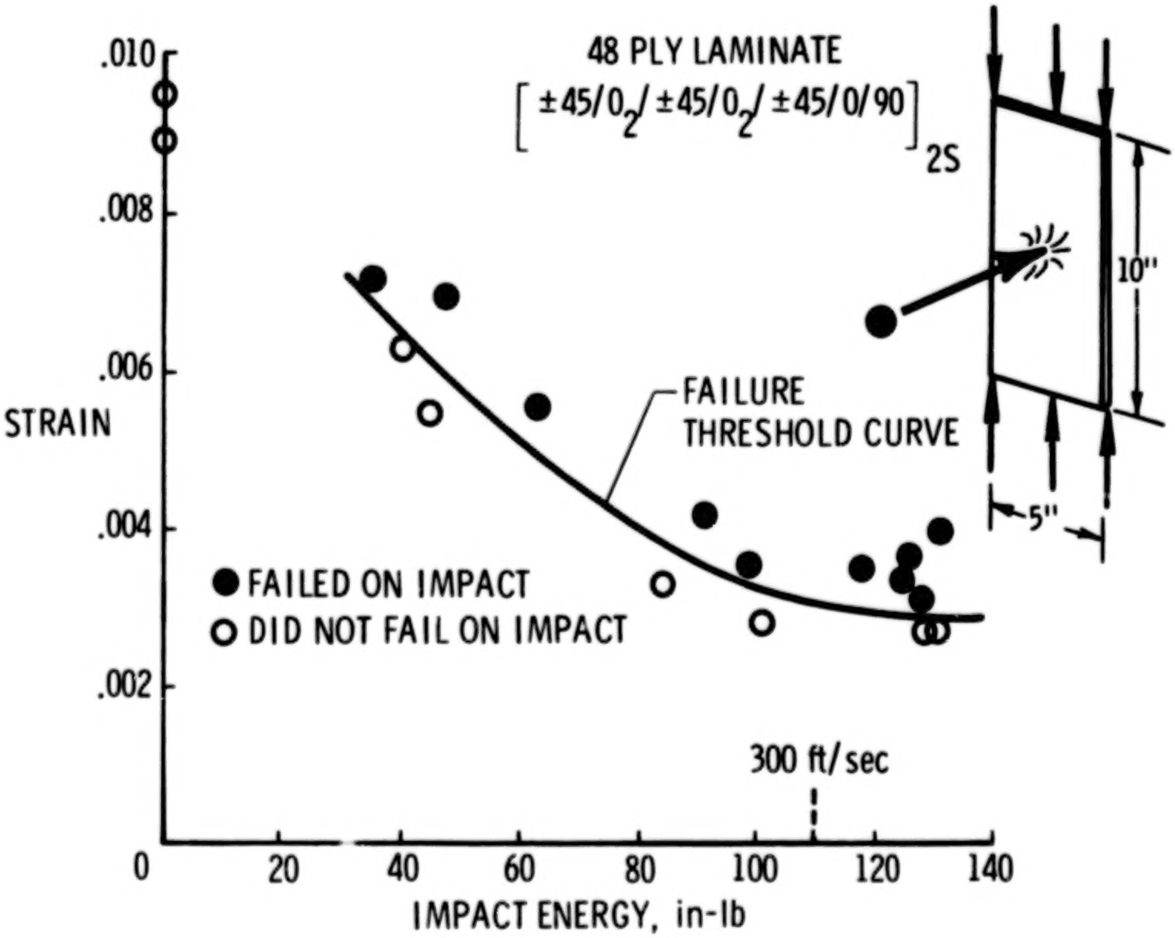

WEIGHT EFFECIENCY OF PRIMARY STRUCTURE DEPENDENT ON ALLOWABLE STRAIN

Wing structure of large transport aircraft carry considerably higher unit loads than other parts of the vehicle and element designs require thick laminates that are inherently stiff; consequently, strength rather than stiffness is the primary design driver. Recent wing surface design studies for commercial transports indicate that significant weight savings are permissible if design strains are not limited by impact requirements. This figure shows three structural configurations for wing surface panel designs; the curves on the figure show weight savings as a function of design strain for an optimized composite "blade" stiffened design over an aluminium design for the upper and lower surfaces. As can be seen a significant increase in weight savings for wing surface panels is possible if design strain can be increased from 0.004 to 0.006 μin./in. NASA is actively pursuing research in constituent relationships within the matrix and fiber/matrix interaction to achieve the higher strain capability.

WING SURFACE DESIGNS

CONCEPTS EVALUATED

BLADE STIFFENED

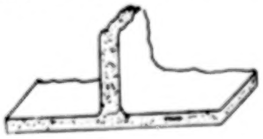

"I" STIFFENED

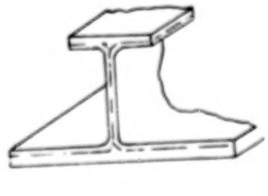

BONDED & BOLTED CORRUGATED SKIN

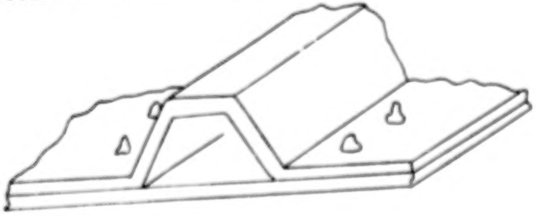

TYPICAL RESULTS

BLADE STIFFENED DESIGN

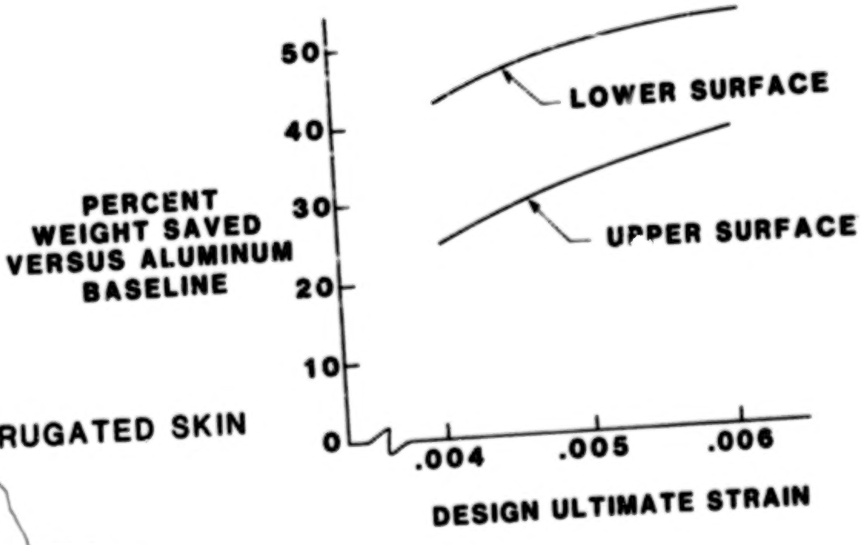

BEST DOCUMENT AVAILABLE

ACEE COMPOSITES PROGRAM CONCLUSIONS

The composite element of the NASA Aircraft Energy Efficiency (ACEE) program was initiated for the development of technology within the commercial airframe industry to foster the application of composites in future commercial aircraft. The program, which has been ongoing for nearly 6 years, has demonstrated the high potential for composites in commercial aircraft through the design and development of secondary and empennage primary components for existing aircraft. The composite material system used has been shown to be adaptable to variations in manufacturing processes, and it is readily formable into complex and highly efficient structural shapes with relatively good repeatability in performance. Large complex box structures have been fabricated, assembled, and ground tested and have provided a focus for technology advancements to further improve performance and assure flight safety.

The composites program has been very effective in developing confidence and experience within commercial airframe companies as engineering and manufacturing personnel have accepted and met challenges to develop and demonstrate weight and cost effective composite components. This level of confidence is strengthened by the generally widespread application of secondary composite components in flight service stemming from the ACEE composites program or prior NASA programs. This flight service experience is providing much needed airline participation and should pave the way for more committed involvement in composites in empennage primary and large primary structures in the next generation of aircraft.

- **LARGE STRUCTURAL COMPONENTS HAVE BEEN SUCCESSFULLY DESIGNED, FABRICATED, AND VERIFICATION TESTED**
- **WEIGHT SAVINGS UP TO 27 PERCENT DEMONSTRATED**
- **DESIGN AND MANUFACTURING CONFIDENCE IS HIGH**
- **TECHNOLOGY IS READY FOR SELECTIVE APPLICATION OF COMPOSITES IN NEW AIRCRAFT**
- **COMPONENTS PROGRAM PROVIDED FOCUS FOR ADVANCED RESEARCH**

BLANK PAGE

POLYMER RESEARCH
AT NASA LANGLEY RESEARCH CENTER

Terry L. St. Clair and Norman J. Johnston
NASA Langley Research Center
Hampton, Virginia

INTRODUCTION

The polymer program at NASA Langley Research Center has as a focus the synthesis and characterization of polymers for aerospace applications. Requirements for these materials vary according to the specific programs.

The synthesis effort involves preparation of polymers for both intermediate- and high-temperature applications. The systems under investigation are thermoplastics, thermosets, and hybrids of these two.

The characterization effort includes a wide variety of programs, such as methodology development, general testing, and specialized studies. This work deals with the elucidation of polymer behavior in composite, adhesive, and film applications for the various aerospace applications.

FOCUS

- o Polymer Synthesis
    - Thermoplastics
    - Pseudothermoplastics
    - Thermosets
- o Characterization
    - Methodology Development
    - General Testing
    - Specialized Studies

POTENTIAL APPLICATIONS

- o Matrix Resins
- o Adhesives
- o High Performance Films

TAILORING POLYMER STRUCTURES TO CONTROL PROPERTIES

The oxidative stability and color (transparency) of linear aromatic polymers can be tailored by altering chemical groups that bridge the aromatic rings. In the figure below, the $-\overset{O}{\overset{\|}{C}}-$ (carbonyl) bridging group is in the dianhydride-derived portion of the polymer and the -o- (oxygen) bridging group is in the diamine-derived portion of the commercial polyimide. When this polyimide was tested at 350°C the polymer film lost half of its initial weight in 80 hours. Other experimental polyimides were prepared and tested in the same manner, but the bridging groups were altered as shown in the figure. With the carbonyl bridge in both components (LARC Polyimide I), oxidative stability was improved by a factor of 2 without affecting the color transparency. Altering the structure by placing the oxygen bridge in both components (LARC Polyimide II) provided a polymer film with good transparency (colorless) and oxidative stability comparable to the commercial polyimide.

These results indicate the progress we are making in understanding how to control properties by tailoring the chemical structure of the polymer. For polymer coatings we can achieve good transparency without sacrificing oxidative stability, or the structure can be altered to achieve excellent gains in thermooxidative stability (ref. 1).

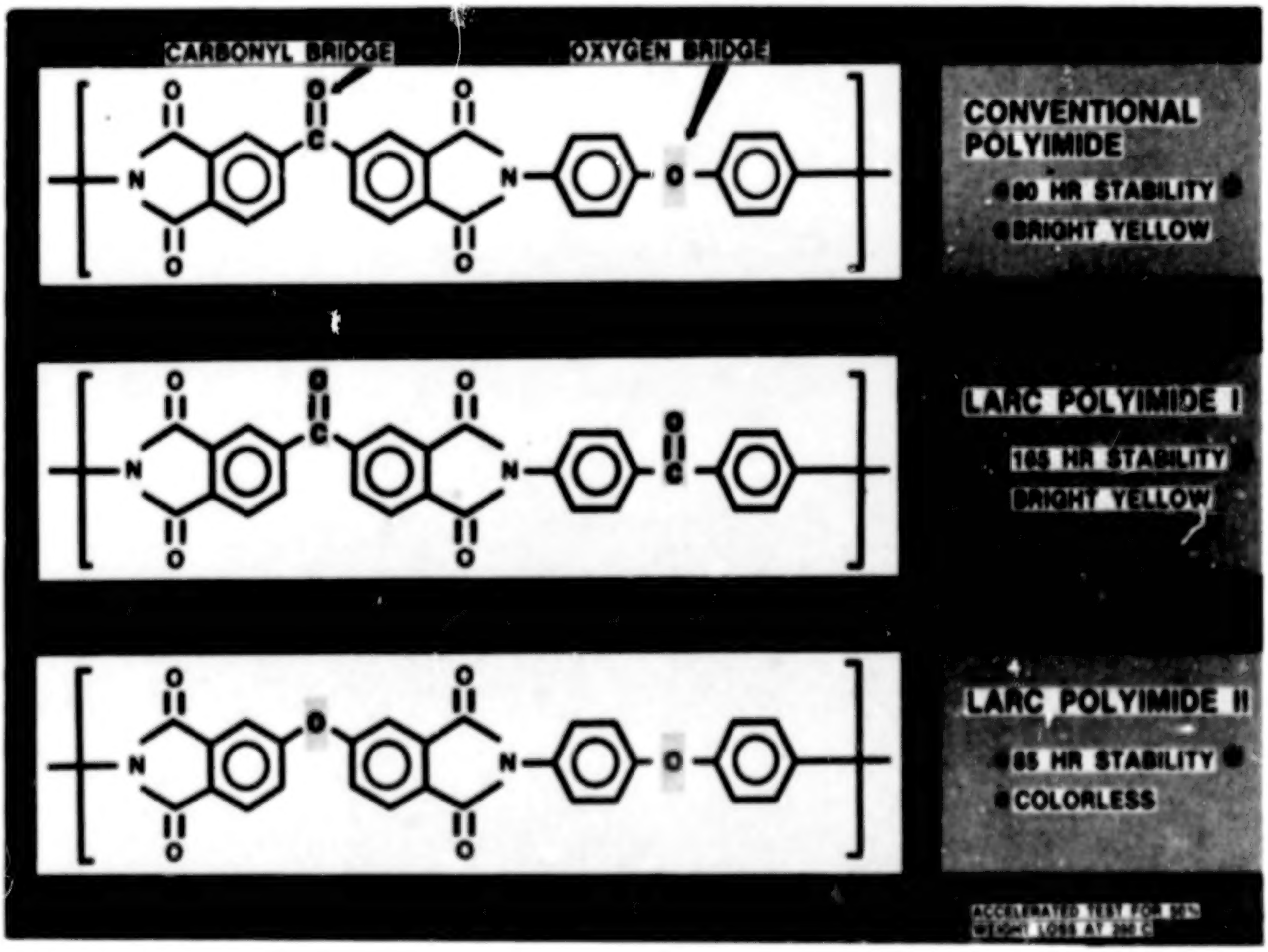
CARBONYL BRIDGE
OXYGEN BRIDGE
CONVENTIONAL POLYIMIDE
80 HR STABILITY
BRIGHT YELLOW
LARC POLYIMIDE I
165 HR STABILITY
BRIGHT YELLOW
LARC POLYIMIDE II
85 HR STABILITY
COLORLESS
ACCELERATED TEST FOR 50% WEIGHT LOSS AT 350°C

TOUGH SOLVENT RESISTANT POLYSULFONES

Polysulfones are engineering thermoplastics which are widely used in a variety of applications. They exhibit an excellent combination of processability, mechanical properties including impact strength, and cost. Their use, however, is generally restricted to environments where there is no exposure to polar organic solvents. Polysulfones are prone to solvent attack, especially in a stressed condition, undergoing solvent-induced crazing and cracking. As a result their use as structural adhesives and composite matrices on aerospace vehicles has been restricted.

Several synthetic routes are under investigation to transform polysulfones into solvent resistant materials while retaining their attractive properties. As shown in the figure, cured polymers from polysulfones endcapped with crosslinkable groups exhibit better solvent resistance and higher use temperatures than commercial polysulfone. As the solvent resistance of the polymer is improved, there is a corresponding loss of toughness. Acceptable trade-offs can be made by adjusting the molecular weight to maximize the attractive features without severely compromising other properties (e.g., toughness and thermoformability). This approach, along with other routes, offers the promise of providing polysulfones with improved solvent resistance, thereby making them more acceptable for use as structural adhesives and composite matrices on airplanes (ref. 2).

OBJECTIVE: DEVELOP SOLVENT RESISTANT, TOUGH, THERMOFORMABLE POLYSULFONES FOR MODERATE TEMPERATURE USE

CHEMISTRY

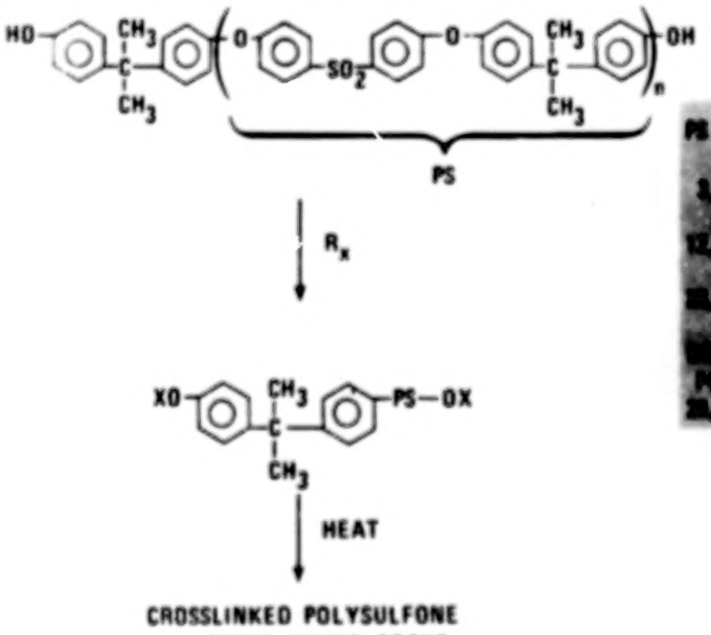

CROSSLINKED POLYSULFONE
X = CROSSLINKING GROUP

POLYMER PROPERTIES

PS mol. wt.	Tg°C	FILM	SOLVENT RESISTANCE
3,000	230	BRITTLE	INSOLUBLE
12,000	190	FLEXIBLE	SL. SWELLING
20,000	185	TOUGH	SWELLS
COMMERCIAL POLYSULFONE 20,000	190	TOUGH	DISSOLVES

APPLICATIONS

- STRUCTURAL ADHESIVES
- COMPOSITE MATRICES
- COATINGS
- MOLDINGS
- MEMBRANES

N-PROPARGYL-SUBSTITUTED AROMATIC POLYAMIDES

A study was conducted to crosslink methyl-substituted polyamides via pendent propargyl groups for the purpose of improving the applicability of this resin as a matrix for Kevlar fiber composites. Films of the polyamides containing 1-33% propargyl diamine were successfully crosslinked by heating in air at 280°-300°C. The thermal crosslinking of the latent propargyl groups was evidenced by a rise in the glass transition temperature of the films with increasing propargyl concentration, a loss in solubility, and the disappearance of propargyl-related peaks from the infrared film spectra. Thermal crosslinking was accomplished with a slight loss in thermooxidative stability.

From the results of this investigation, propargyl-containing polyamides have been determined to be feasible matrices for polyamide fiber (Kevlar) composites. These materials are processable at advantageously low temperatures and are thermally crosslinkable at temperatures below the relaxation temperature of the fiber. Compatibility of these resins with aromatic polyamide fibers gives them high potential for success as matrix resins for Kevlar composites (ref. 3).

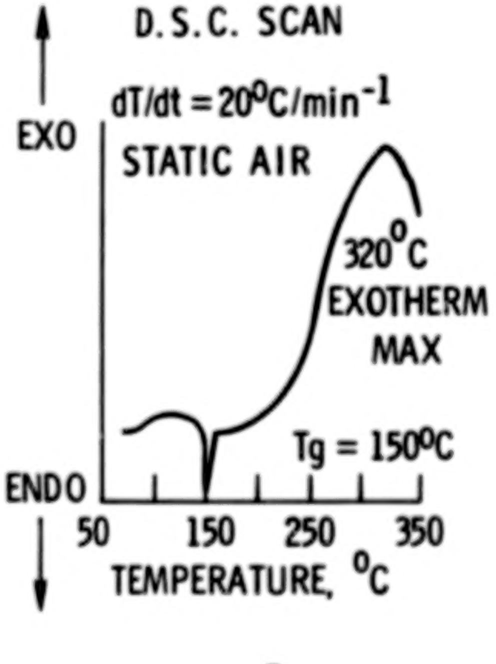
D.S.C. SCAN

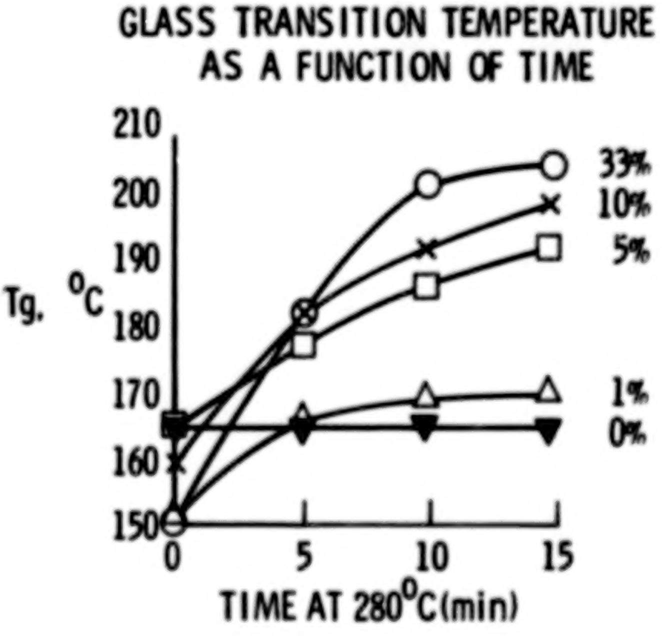
GLASS TRANSITION TEMPERATURE AS A FUNCTION OF TIME

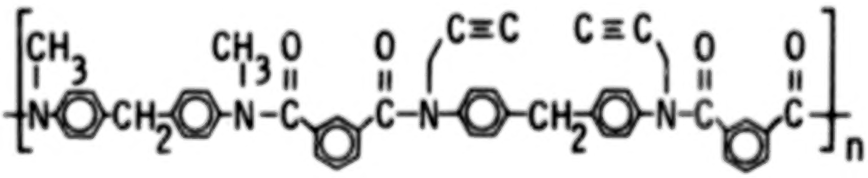

HOT MELT PROCESSABLE POLYIMIDE

Linear aromatic polyimides are a class of polymers which are generally not processable via conventional thermoplastic or hot-melt techniques. This class of polymer is, however, exceptionally thermally stable and has high glass transition temperatures. It is also resistant to attack by common organic solvents.

Linear aromatic polyphenylene oxides and sulfides, on the other hand, are more easily processed than the polyimides, generally exhibit lower glass transition temperatures, and still have relatively good thermal stability, although not equal to the polyimides. These systems also do not possess solvent resistance equal to the polyimides.

A novel linear aromatic polyphenylene ethersulfideimide has been synthesized which has some of the favorable characteristics of each parent system. The polymer has been molded, used as a resin, and cast into thin films. A limited characterization indicates this system can be processed via conventional thermoplastic techniques and may have a wide variety of applications (ref. 4).

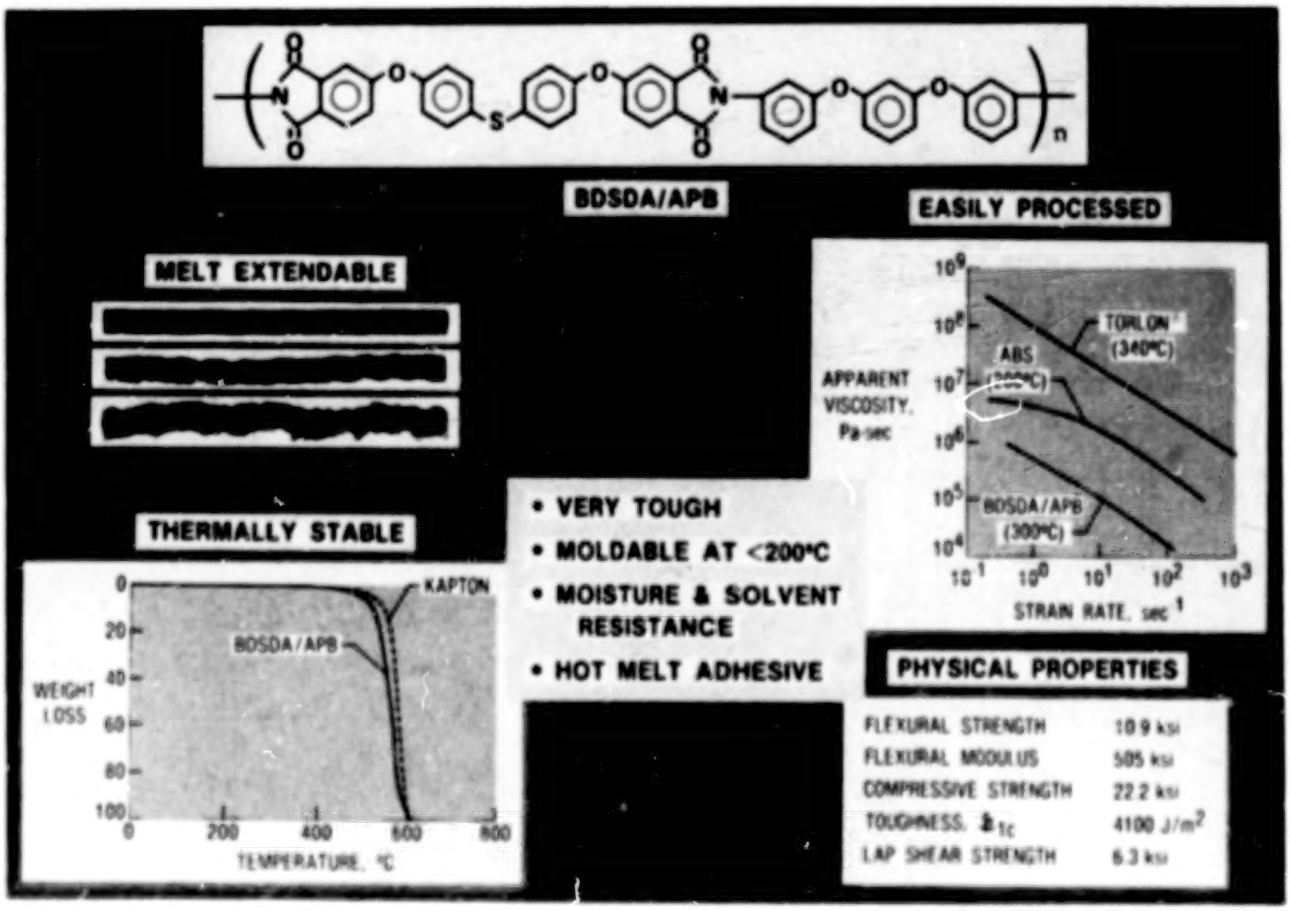

BDSDA/APB

EASILY PROCESSED

MELT EXTENDABLE

THERMALLY STABLE

- VERY TOUGH
- MOLDABLE AT <200°C
- MOISTURE & SOLVENT RESISTANCE
- HOT MELT ADHESIVE

PHYSICAL PROPERTIES

FLEXURAL STRENGTH	10.9 ksi
FLEXURAL MODULUS	505 ksi
COMPRESSIVE STRENGTH	22.2 ksi
TOUGHNESS, G_{Ic}	4100 J/m^2
LAP SHEAR STRENGTH	6.3 ksi

CROSSLINKING OF POLYPHENYLQUINOXALINES

In an attempt to overcome the shortcomings of thermoplastics without severely compromising their attractive features, work was initiated using polyphenylquinoxalines (PPQs) as a model system to demonstrate a general concept. Latent pendent groups (e.g. ethynyl and phenylethynyl) were incorporated on the linear molecules. These groups undergo a thermally induced reaction to provide controlled crosslinking. In this way, molecules are tied together (see figure) such that there is a significant improvement in their elevated temperature performance (e.g. creep resistance) and, more importantly, in their fluid and solvent resistance.

As indicated in the table, the T_g of a cured PPQ containing 5% of ethynyl (C≡CH) or phenylethynyl (C≡C-ϕ) groups was substantially higher than the parent PPQ void of latent crosslinking groups. At the 10% pendent group level, the cured PPQ containing the crosslinking groups became totally insoluble. Preliminary adhesive evaluation has also shown a marked increase in the 288°C lap shear strength. This concept is now being extended to polysulfones, which are lower temperature thermoplastics than PPQs, and it appears to be applicable to other thermoplastics such as polyesters, polyamides, and polyimides. This novel route offers the potential of modifying existing thermoplastics, particularly polysulfones, to improve their performance and make them acceptable for structural uses on future aircraft and spacecraft (ref. 5).

OBJECTIVE: DEVELOP SOLVENT RESISTANT HIGH TEMPERATURE STRUCTURAL RESINS

CHEMISTRY

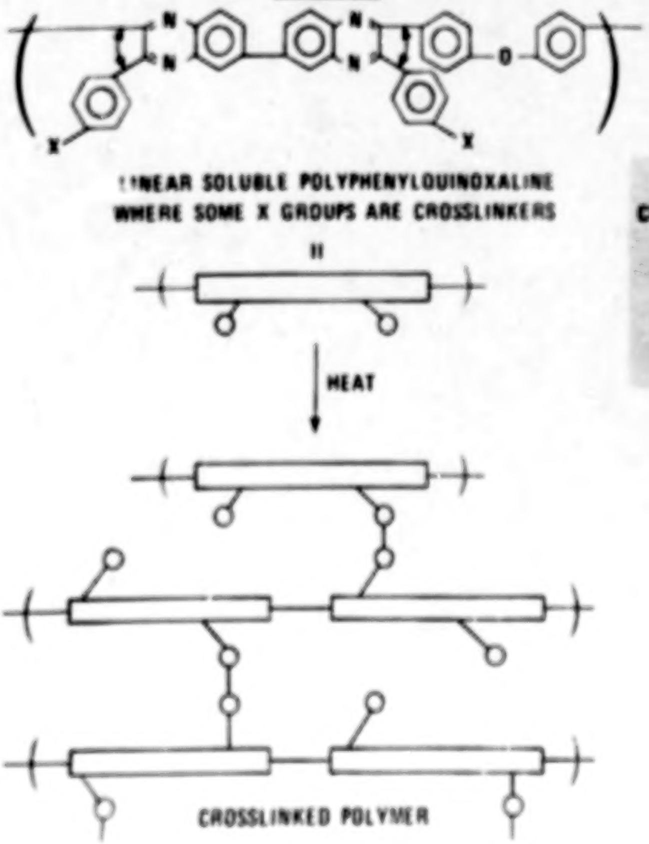

LINEAR SOLUBLE POLYPHENYLQUINOXALINE WHERE SOME X GROUPS ARE CROSSLINKERS

PROPERTIES

% OF CROSSLINKER	SOLVENT RESISTANCE	288°C LAP SHEAR STRENGTH, psi
0	DISSOLVES	1000
5	SWELLS	1000
10	INSOLUBLE	2200

APPLICATIONS

- HIGH TEMPERATURE ADHESIVES
- PROTECTIVE COATINGS
- HIGH TEMPERATURE COMPOSITE MATRICES
- ELECTRONIC COMPONENTS

BEST DOCUMENT AVAILABLE

ACETYLENE-TERMINATED PHENYLQUINOXALINES

A series of acetylene-terminated phenylquinoxaline (ATPQ) oligomers of various molecular weights were prepared and subsequently chain-extended by the thermally induced reaction of the ethynyl groups. The processability and thermal properties of these oligomers and their cured resins were compared with those of a relatively high molecular weight linear polyphenylquinoxaline (PPQ) with the same chemical backbone. The ATPQ oligomers exhibited significantly better processability than the linear PPQ but the PPQ displayed substantially better thermooxidative stability. Adhesive (Ti/Ti) and composite (graphite filament reinforcement) work was performed to evaluate the potential of these materials for structural applications. The PPQ exhibited better retention of adhesive and laminate properties than the ATPQ resins at 260°C after aging for 500 hr at 260°C in circulating air (ref. 6).

OBJECTIVE: IMPROVE THE PROCESSABILITY AND HIGH TEMPERATURE PERFORMANCE OF PPQ'S

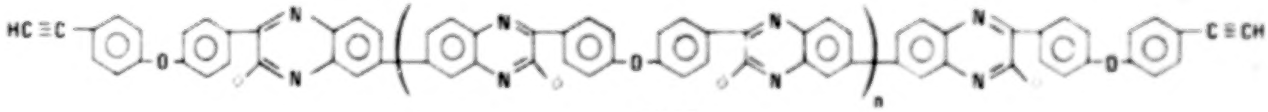

HEAT

CROSSLINKED POLYMER (ATPQ RESIN)

ADVANTAGES OVER EXISTING POLYMERS

- **BETTER PROCESSABILITY**
- **IMPROVED SOLVENT RESISTANCE**
- **HIGHER INITIAL ELEVATED TEMPERATURE STRENGTH**
- **AMENABLE TO TAILORING FOR SPECIFIC USE**

Ti/Ti ADHESIVE PROPERTIES

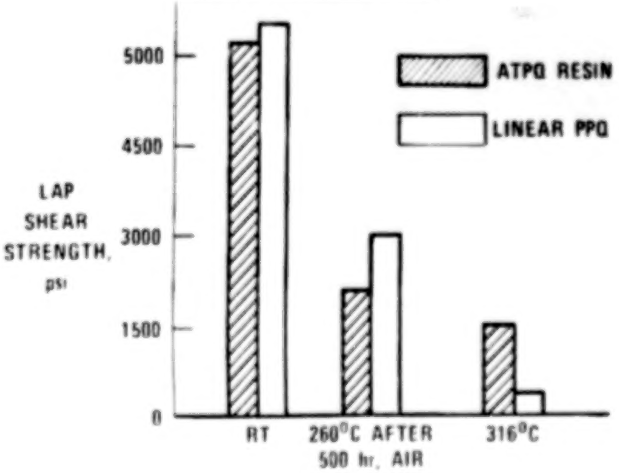

HT-S UNIDIRECTIONAL LAMINATE PROPERTIES

TEST CONDITION	FLEXURAL STRENGTH, Ksi	FLEXURAL MODULUS, Msi
RT	237	19.3
260°C	201	17.1
260°C AFTER 500 hrs, AIR	189	16.8

BEST DOCUMENT AVAILABLE

ADDITION POLYIMIDE ADHESIVES

Addition polyimide oligomers have been synthesized from 3,3',4,4'-benzophenone tetracarboxylic acid dianhydride and 3,3'-methylenedianiline using a variety of latent crosslinking groups as end caps. The nominal 1300-molecular-weight imide prepolymers were isolated and characterized for solubility in amide, chlorinated, and ether solvents; melt-flow and cure properties; glass transition temperature; and thermal stability on heating in an air atmosphere. The general structure of the prepolymer and the end caps is shown below. Adhesive strengths of the polyimides were obtained both at ambient and elevated temperatures before and after aging at 232°C. Properties of the novel addition polyimides were compared to a known nadic end-capped adhesive, LARC-13 (ref. 7).

END GROUP
R

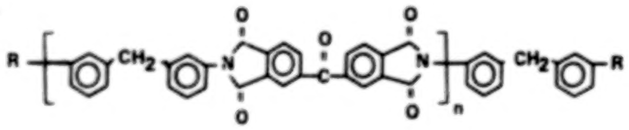

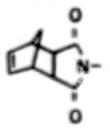
NADIC
(LARC-13)

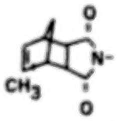
CH_3-NADIC

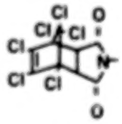
Cl_6-NADIC

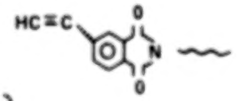
ACETYLENE

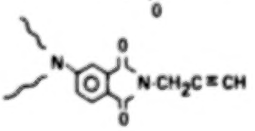
N-PROPARGYL

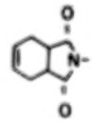
CYCLOHEXENE

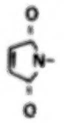
MALEIC

LAP SHEAR STRENGTHS (LSS) OF ADDITION POLYIMIDES AGED FOR 1000 HOURS AT 232°

OLIGOMER END GROUP	INITIAL LSS, psi		LSS AFTER 1000 hr AT 232°C, psi	
	RT	232°C	RT	232°C
NADIC (LARC-13)	3200	2600	2600	1960
ACETYLENE	2900	2500	2500	2800
N-PROPARGYL	3100	2800	800	1000

THERMOPLASTIC POLYIMIDESULFONE

Aromatic polysulfones, a class of high-temperature engineering thermoplastics, have a major deficiency in their tendency to swell and dissolve in many common solvents. This solvation can cause structural components which are fabricated from these polymers to be susceptible to damage by these solvents and thereby lose their structural integrity.

Aromatic polyimides, conversely, are a class of polymers which are known to be resistant to solvents, but they are generally not processable via thermoplastic means. These polyimides are known to be exceptionally thermally stable and like polysulfones and other thermoplastics their use temperature is governed by the softening temperature of each system.

A novel polymer system that possesses the processability of the polysulfones and the solvent resistance of the polyimides has been synthesized and characterized as a film, unfilled molding, filled molding, and adhesivse. The structure of this polyimidesulfone (PISO2) is shown below along with some adhesive and molding data (ref. 8).

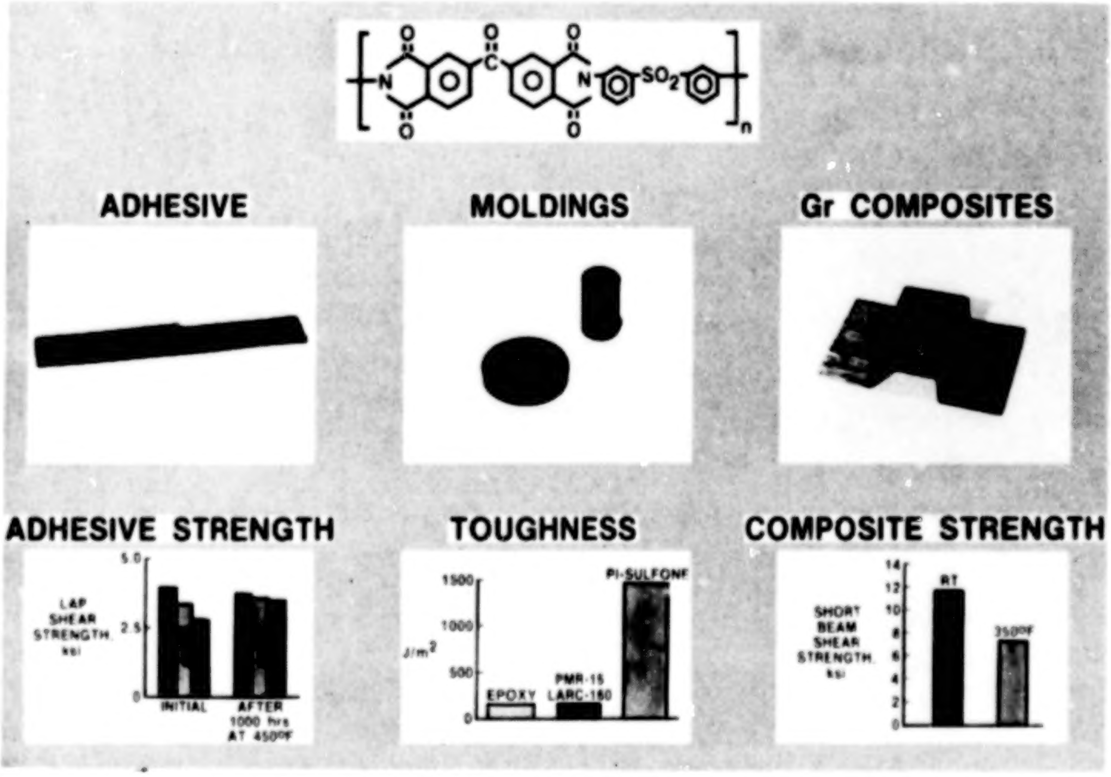

LARC-TPI

A linear thermoplastic polyimide, LARC-TPI, has been characterized and developed for a variety of high-temperature applications. In its fully imidized form this new material can be used as an adhesive for bonding metals such as titanium, aluminum, copper, brass, and stainless steel. LARC-TPI is being evaluated as a thermoplastic for bonding large pieces of polyimide film to produce flexible, 100% void-free laminates for flexible circuit applications. The further development of LARC-TPI as a potential molding powder, composite matrix resin, high-temperature film, and fiber will also be discussed (ref. 9).

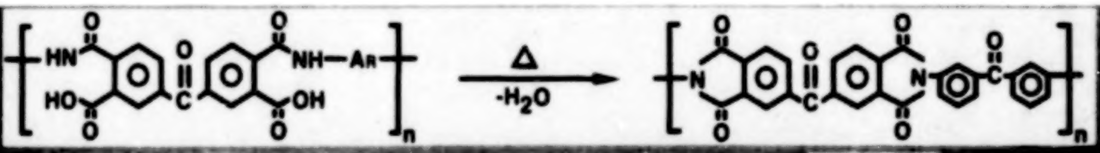

SOLAR SAIL ADHESIVE (POLYAMIC ACID)

LARC-TPI (THERMOPLASTIC POLYIMIDE)

LARC-TPI MOLDING

(1) STRUCTURAL ADHESIVE
(FOR METALS OR COMPOSITES)

(2) PI FILM LAMINATING ADHESIVE

(3) MOLDING POWDER

(4) COMPOSITE MATRIX RESIN

(5) HIGH-TEMP FILM

(6) HIGH-TEMP FIBER

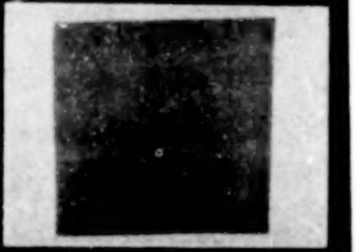

LARC-TPI FILM

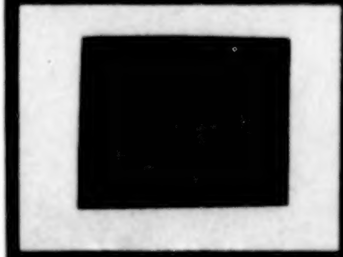

LARC-TPI/KAPTON® LAMINATE

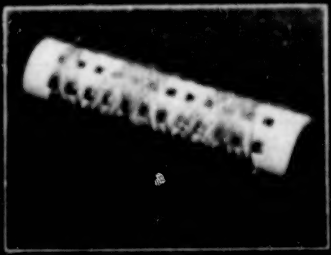

LARC-TPI FIBERS

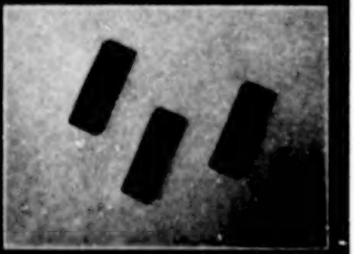

LARC-TPI/CELION® 6000 COMPOSITES

MEASUREMENT OF INTERLAMINAR FRACTURE TOUGHNESS BY COMPOSITE DOUBLE CANTILEVER BEAM TEST

The use of the double-cantilever-beam (DCB) test to measure the fracture toughness (G_{Ic}) of adhesives between metal adherends is well known. The application of the test to composite materials in which the crack is initiated in and propagated between two zero plies at the midplane is just now being pursued after the initial work of Bascom et al. (ref. 10). (See left-hand figure below.) Using a width-tapered DCB specimen, these investigators observed a noticeable improvement in fracture toughness of graphite cloth composites made with rubber-toughened epoxies or thermoplastics (P-1700 polysulfone) compared with state-of-the-art 250°F or 350°F cure epoxy systems. (See right-hand figure below.)

An extension of this work to laminates constructed from unidirectional tape (ref. 11 and right-hand figure) indicates that the G_{Ic} fracture toughness of the matrix varies widely and unpredictably depending upon the type of reinforcement. This work also shows that the G_{Ic} fracture toughness of neat resin cannot be used to predict the G_{Ic} value of composites made from that resin. However, the general trend seems to hold that neat resin G_{Ic} values are relative indicators of and can help rank fracture toughness in the corresponding composites.

NASA is pursuing an in-depth study of the composite DCB test in which the effects of matrix material, strain rate, specimen dimensions, stacking sequence, and environment are being investigated. A detailed analysis of the failure mechanics of various DCB specimens is also being done to help guide the development of an appropriate pure Mode I interlaminar fracture test method. Key investigators at the National Bureau of Standards, Hercules, Inc., and the University of Illinois, Urbana, are participating in this study.

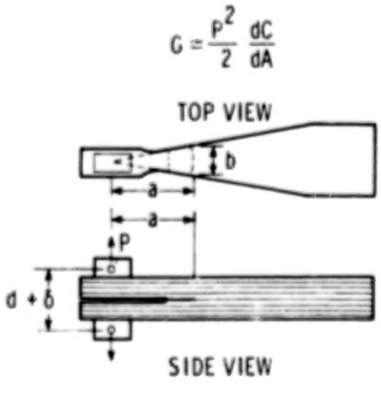

COMPACT TENSION AND WIDTH TAPERED DOUBLE CANTILEVER BEAM TESTS

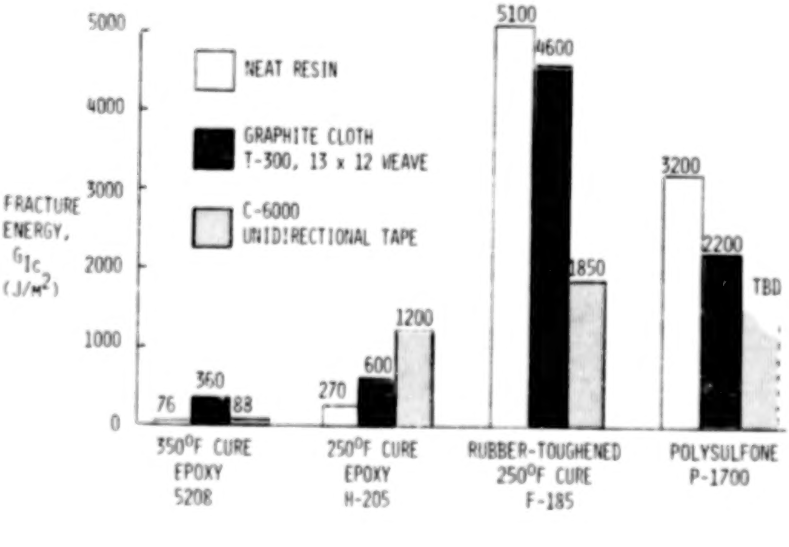

ELASTOMER-TOUGHENED POLYIMIDE ADHESIVES

Addition polyimides are presently being considered as candidate high-temperature adhesives for bonding composite materials and metals such as titanium on future aircraft and spacecraft. These thermoset polyimides undergo cure by an addition reaction involving unsaturated end groups that causes them to be highly crosslinked, insoluble, and extremely brittle.

The elastomer- (rubber) toughening process has been one of the most successful methods for modifying polymer toughness. Incorporation of small amounts of rubber into a polymer matrix has resulted in the significant enhancement of fracture resistance.

This chart illustrates the effects of various added elastomers on the T-peel strength and adhesive fracture energy of a high-temperature addition polyimide, LARC-13 (ref. 12).

- POLYIMIDE/RUBBER COMPATIBILITY ACHIEVED
- DATA SHOW IMPROVED TOUGHNESS
- TOUGHNESS ACHIEVED WITH SLIGHT SACRIFICE IN HIGH-TEMPERATURE ADHESIVE STRENGTH

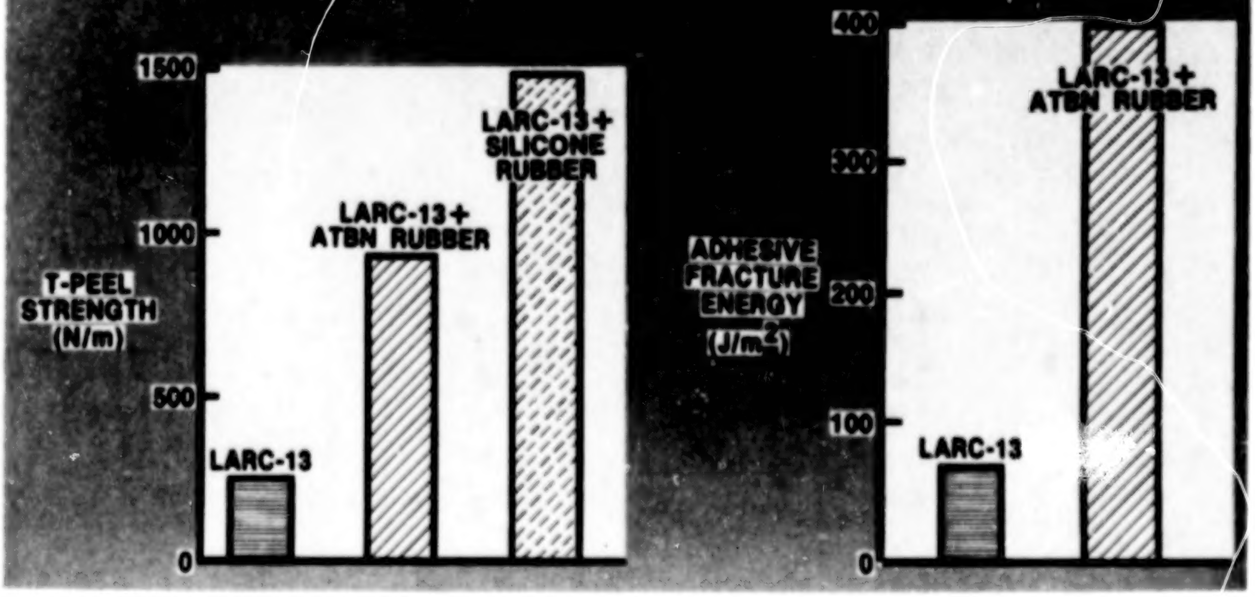

MECHANISM OF CURE IN NORBORNENE END-CAPPED IMIDE MODEL COMPOUNDS

Norbornene end-capped imide oligomers such as LARC-160, PMR-15 and LARC-13 display considerable promise for extensive use in various aerospace adhesive and composite applications (ref. 13). These materials were developed in a successful effort to retain the good thermal perfomance of linear condensation polyimides while improving overall processablity. However, very little is known about the mechanism by which these end-capped oligomers cure. This stdy (ref. 14) was designed to increase our fundamental understanding of the fate of the norbornene end-capper as the oligomer is heated.

Model compound I was heated to 285°C in air to yield a partially soluble product mixture that was separated by high-pressure liquid chromatography (HPLC) into three main fractions (A, B, and C). Spectroscopic techniques (NMR, FTIR, MS) were used to prove that the thermal reaction products were geometric isomers. Peak C, the only HPLC peak observed before heating, was starting material and proved to be the kinetically favored endo-endo isomer, II. Peaks B and A were shown to be the endo-exo (III) and exo-exo (IV) configurations, respectively. Further work proved that each isomer thermally isomerized to an equilibrium mixture of all three before further curing reactions took place that rendered the mixture insoluble.

Calorimetry and thermogravimetric analysis indicated that these materials behave differently in air than in nitrogen, suggesting different mechanisms of cure depending upon atmosphere. The data obtained is consistent with a reverse Diels-Alder mechanism leading to loss of cyclopentadiene in nitrogen and a more direct chain extension without weight loss in air.

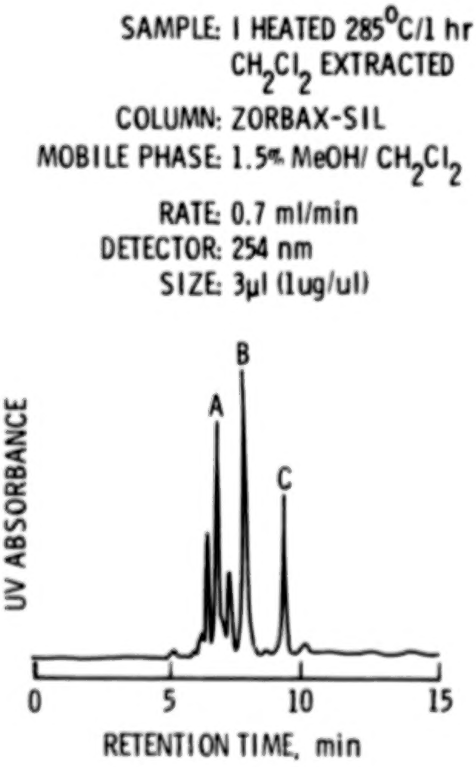

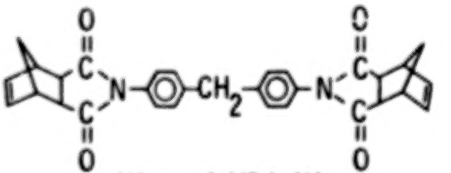

NA-p, p'-MDA-NA

I

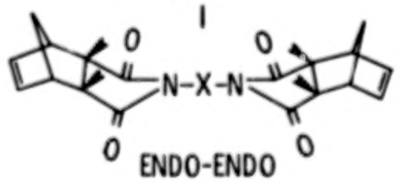

ENDO-ENDO

II

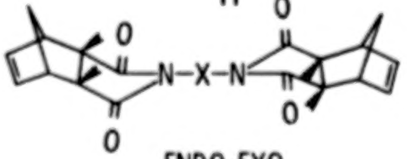

ENDO-EXO

III

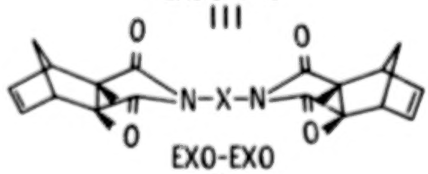

EXO-EXO

IV

EFFECT OF PENDENT ALKYL GROUPS ON POLYIMIDE PROPERTIES

An investigation was conducted to determine the effect on glass transition temperature (T_g), thermal stability and toughness of a polyimide when alkyl groups are attached pendent to the backbone. A series of polymers was prepared in dimethylacetamide (DMAc) using benzophenone tetracarboxylic dianhydride (BTDA) and five different p-alkyl-m,p'-diaminobenzophenones as monomers. The chemical structures are shown in the figure. The alkyl groups varied in length from C_1 (methyl) to C_9 (nonyl).

Poly(amic) acid solutions in DMA_c were vacuum cured to 280°C to afford flexible polyimide films whose T_g decreased with increasing alkyl group length, as determined from thermomechanical analysis. The largest effect, a 70°C decrease in T_g to 193°C, was observed for the polymer containing the nonyl pendent group compared to the T_g of the control polymer (R = H). During thermogravimetric analysis (air, 5°C/min. heating rate), the control exhibited a 10% weight loss at 525°C; the nonyl pendent polymer showed a 10% weight loss at 425°C. The thermooxidative stability of the other films fell between these extremes. Although no increase in the area under the stress-strain curve was observed during film tensile tests, an increase in elongation with a corresponding decrease in tensile strength was noted with increasing alkyl length.

The results of this study indicate that alkyl groups attached pendent to a polyimide backbone can be used to vary the T_g over a wide temperature range. This approach may offer a means of lowering the processing temperature of polyimides without a significant reduction in thermal stability (ref. 15).

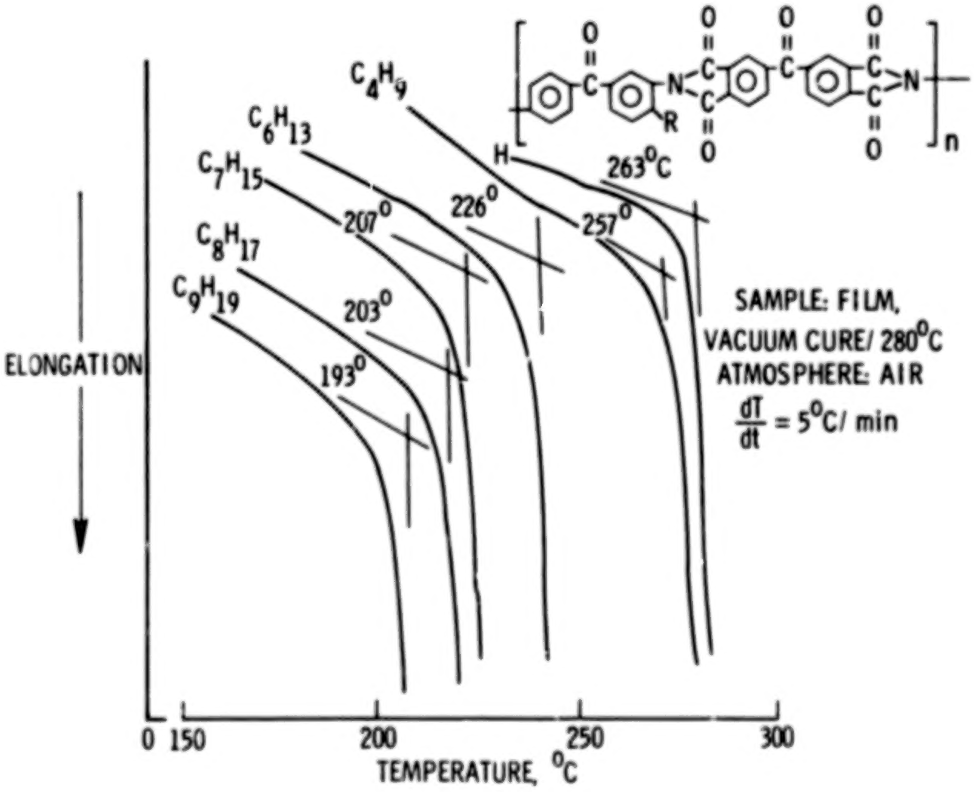

FILM LAMINATING

A need exists in the aerospace industry for reliable flexible electrical circuitry that can withstand extreme temperature variations and retain flexibility. Problems to date have been due partially to the presence of voids in film laminates caused by volatiles generated by the adhesive and/or the inherent rigidity of some adhesives. Because it is both flexible and imidized prior to bonding, LARC-TPI shows much potential as a high-temperature adhesive for laminating large areas of polyimide film.

A film-laminating process has been developed whereby films primed with a thin coat of LARC-TPI adhesive are bonded together using temperature and pressure. As an alternate process, LARC-TPI polyamic acid adhesive film may be imidized by heating prior to being sandwiched between polyimide film. When using either process to prouce flexible circuits, a conductive metal may be interposed between layers of the polyimide film. Metal-containing laminates have been made using aluminum, brass, copper and stainless steel sheets or foils (ref. 16).

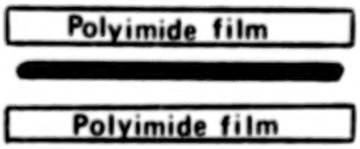
Polyimide film
Polyimide film

LARC-TPI
ADHESIVE
FILM

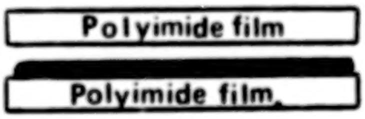
Polyimide film
Polyimide film

LARC-TPI
ADHESIVE

MULTI-PLY LAMINATES

METAL-CONTAINING
LAMINATES
(Al, Cu, Steel, Brass)

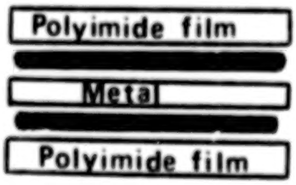
Polyimide film
Metal
Polyimide film

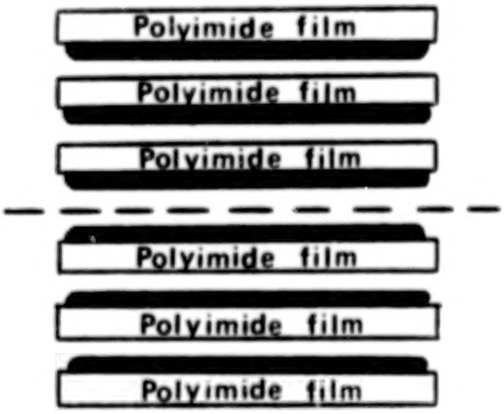
Polyimide film
Polyimide film
Polyimide film
Polyimide film
Polyimide film
Polyimide film

METAL IONS IMPROVE POLYIMIDE PROPERTIES

Polymer films are attractive for various aerospace applications such as antenna surfaces, adhesives, coatings, etc. However, covalently bonded polymers inherently lack the electrical conductivity desirable to resist spacecraft charging or to act as a Faraday Cage and even the most stable polymers developed to date have limited temperature capability.

Several options are available to increase electrical conductivity in a polymer film: (1) mix metallic flakes or powders into the formualtion; (2) laminate metallic/polymer films; and (3) add complex metallic ions to the backbone of the polymer structure. The latter is a very attractive option because the potential for conductivity increases with less increase in the characteristically low polymer film density than is experienced with the other options, but this application has had relatively little attention until recently.

Recent research activity has demonstrated the potential of certain selected metallic ion additions to a polyimide to increase electrical conductivity in a film and high-temperature performance in an adhesive. The addition of the aluminum-ion complex increased adhesive shear strength significantly at 275°C and 300°C. Even more dramatic was the increased electrical conductivity of polyimide films when palladium- and palladium/lithium-ion complexes were added. Electrical conductivity at room temperature was increased by 8 orders of magnitude.

This research is now directed towards elucidation of the mechanisms of electrical (and thermal) conductivity in these metallic ion containing polymers to provide a rational basis for the selection of the most effective ion additions for specific property improvements (ref. 17).

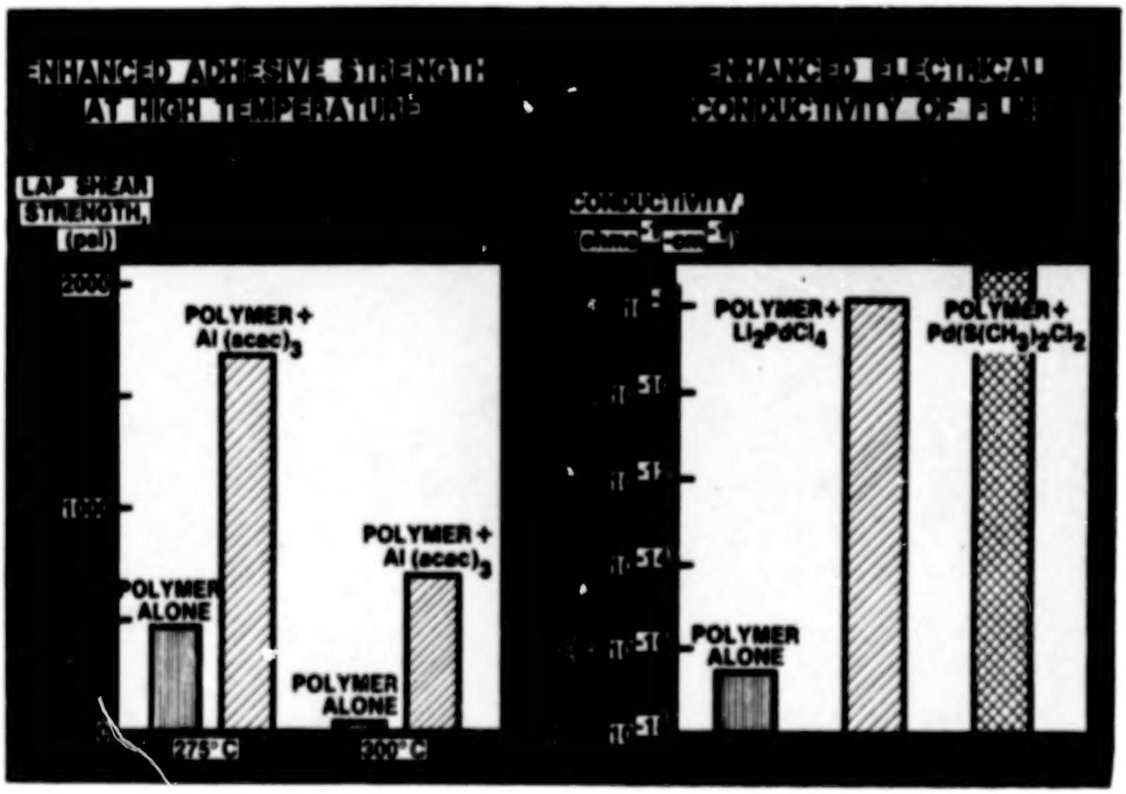

A STUDY OF THE MUTAGENICITY OF AROMATIC DIAMINES

Aromatic diamines are a class of chemicals that are vital for the preparation of high-performance polymers, including the polyurethanes, epoxies, polyamides, and polyimides. However, a number of them are toxic to humans. During the past decade Langley's polymer research has resulted in the synthesis of a broad collection of aromatic diamines with systematic variations in their chemical structures. Although the main reason for acquiring these chemicals was for polymer research, they were also used for a study to learn if any aspects of their chemical structures could be used to predict the mutagenic tendencies of diamines. Mutagenicity is a toxic feature of chemicals that is related to the carcinogenicity of the chemicals.

This comprehensive study has been performed by the Monsanto Research Corporation of Dayton, Ohio on Langley-supplied amines. The investigation disclosed that steric and chemical structural characteristics could be useful in predicting which of the diamines might be mutagenic. The chart below summarizes those results for the steric or spatial isomers (horizontal) of four chemical series (vertical) of aromatic diamines. For example, in general, the electronegative chemical groupings (C = 0 and especially SO_2) that join the two aniline functions cause the resulting diamines to be less mutagenic (a smaller number or absence of +'s). Conversely, the electropositive coupling groups (CH_2 and especially 0) cause the diamines to be more mutagenic. Also, the first three steric isomers on the left tend to be more mutagenic than the three on the right. Unfortunately, many of Langley's accomplishments in polyimide structure-property studies have been achieved using the meta, meta' diamine isomers (third from the left) which are quite mutagenic. But this study also showed that the meta, para' isomers (second from the right) are generally nonmutagenic, so they might be used for polyimides since they give polymers with properties not very different from those made with the meta, meta' diamines.

It is expected that this investigation will extend the usefulness of this novel group of diamine starting materials beyond the original polymer-oriented objectives by providing toxicologists with the means to predict the mutagenic tendencies inherent in aromatic diamines.

Z	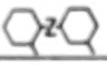	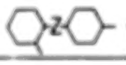	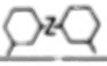	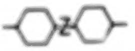	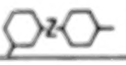	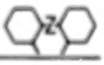
CH_2	+++++	++++	+++	++	-	-
C=0	+++ .	+++++	++++	-	-	-
SO_2	+	NT	+	-	-	-
0	NT	++++	+++++	++++	+++	NT

CODE: +++++ = VERY STRONG MUTAGEN; ++++ = STRONG; +++ = MODERATE;
++ = LOW; + = VERY LOW; - = NONMUTAGENIC, NT = NOT TESTED

SUMMARY

The polymer program at LaRC involves exploratory studies in polymer science. These include the synthesis of novel polymers and their characterization.

Polymer synthesis programs involve the development of novel thermoplastics, pseudothermoplastics, and thermosets. These systems are prepared to elucidate strucure-property relationships involving thermal capabilities, toughness, processability and environmental stability. Recent investigations have led to the development of more easily processable polyimides, solvent-resistant polysulfones and polyphenylquinoxalines, and tougher high- and intermediate-temperature polymers.

Characterization efforts have included high-pressure liquid chromatography methodology, the development of toughness tests for fiber-reinforced composites, a study of electrical properties of metal-ion-filled polyimides, and a study of the mutagenicity of aromatic diamines. Also the mechanism of cure/degradation of experimental polymers has been studied by rheology, mechanical behavior, separation techniques and spectroscopy. Some of these programs have involved the degradative crosslinking of alkyl-containing polyimides, the separation and identification of crosslinked phenylquinoxalines, the rheological behavior of hot-melt polyimides, and the elucidation of the cure of norbornene endcapped imides.

- o Synthesis Program for Polymers
- o Characterization of Monomers and Polymers
- o Development of Polymers for specific applications
    - Matrix Resins
    - Adhesives
    - Films

REFERENCES

1. St. Clair, T. L.; St. Clair, A. K.; and Smith, E. N.: Structure-Solubility Relationships in Polymers, Academic Press, Chapter 15, pp. 199-215, 1977.

2. Hergenrother, P. M.: Am. Chem. Soc. Div. Org. Coat. and Plastics, 46, 1982, p. 165.

3. Greenwood, T. D.; Armistead, D. M.; Wolfe, J. F.; St. Clair, A. K; St. Clair, T. L.; and Barrick, J. D.: Polymer, 23, Apr. 1982, pp. 621-625.

4. Burks, H. D.; and St. Clair, T. L.: NASA TM-84494, 1982.

5. Hergenrother, P. M.: Macromolecules, 14, 1981. pp. 891, 898.

6. Hergenrother, P. M.: Polymer Eng. and Sci., 21 (16), 1981, p. 1072.

7. St. Clair, A. K.; and St. Clair, T. L.: Polymer Eng. and Sci., 22 (1), 1982, pp. 9-14.

8. St. Clair, T. L.; and Yamaki, D. A.: A Thermoplastic Polyimidesulfone, to be presented at First Technical Conference on Polyimides, Society of Plastics Engineers, Inc. (Ellenville, NY), Nov. 10-12, 1982.

9. St. Clair, A. K.; and St. Clair, T. L.; SAMPE Quarterly, 13 (1), 1981, pp. 20-25.

10. Bascom, W. D.; Bitner, J. L.; Moulton, R. J.; and Siebert, A. R.: Composites, Jan. 1980, p. 9.

11. O'Brien, T. K.; Johnston, N. J.; Morris, D. H.; and Simonds, R. A.: SAMPE Journal, 18 (4), 1982.

12. St. Clair, A. K.; and St. Clair, T. L.: International J. of Adhesion and Adhesives, 1 (5), 1981, pp. 249-255.

13. Dexter, H. B.; and Davis, J. G. (Eds.): Graphite/Polyimide Composites, NASA CP-2079, 1979.

14. Young, P. R.: NASA TM-83192, 1981.

15. Jensen, B. J.; and Young, P. R.: Polyimide Characterization Studies: Effect of Pendent Alkyl Groups, to be presented at First Technical Conference on Polyimides, Society of Plastics Engineers, Inc. (Ellenville, NY), Nov. 10-12, 1982.

16. St. Clair, A. K.; and St. Clair, T. L.: U.S. Patent Application, serial no. 189,234, Sept. 22, 1980.

17. Taylor, L. T.; St. Clair, A. K.; Carver, V. C.; and Furtsch, T. A.: U.S. Patent 4,311,615, Jan. 19, 1982.

POLYMER MATERIALS RESEARCH AT NASA AMES RESEARCH CENTER

J. A. Parker, A. H. Heimbuch, and W. J. Gilwee
NASA Ames Research Center
Moffett Field, California

POLYMER MATERIALS RESEARCH AT NASA AMES RESEARCH CENTER

Research at NASA Ames to discover new polymers and the principles governing their physical and chemical behavior in severe environments has been organized to provide advanced materials for specific space applications such as reentry thermal protection heat shields (ref. 1), thermal coatings (ref. 2), and solar sails (ref. 3), as well as advanced components for service conditions encountered by aeronautical systems (ref. 4). This paper deals primarily with polymer activities that have led to new aeronautical materials that are providing significant improvements in both efficiency and safety for civilian transport aircraft and military combat aircraft. High strength to weight structures such as carbon fiber composites with long-term durability are requirements common to both classes of aircraft.

Aircraft safety improvements in fire resistance and crashworthiness of primary and secondary structures are long-term objectives for transport aircraft. Void filler ballistic foams (ref. 5), intumescent coatings (ref. 6), and radiation-resistant transparent plastics (ref. 7) are NASA Ames contributions to vulnerability reduction in combat military aircraft. As applied polymer research, the NASA Ames program is driven by aeronautical design requirements to improve both low- and high-velocity impact tolerance, fire resistance, thermal stability, and long-term durability of polymers and components derived therefrom.

Aerospace polymeric materials have several important constraints not usually encountered in usual commercial polymer applications. Most often, materials selection criteria are dominated by component weight minimization needs to achieve energy efficiency and operational capabilities. Neoprene fire-blocking layers (ref. 8) are perfectly adequate for ground-based applications, for example, but for cost-effective use in transport aircraft, a fire-blocking material with one-fourth the aerial density is required (ref. 9). This requirement has been met, surprisingly, with high-temperature-resistant, non-conductive fiber arrays and fabrics based on preoxidized PAN or PBI, so-called space age fibers (ref. 10). Weight constraints such as the specific stiffness requirements are typified by the extensive use of facesheet bonded honeycomb structures utilizing graphite and other organic fibers such as Kevlar, and high-performance polymeric film formers such as polyethetherketone and matrix resins and adhesives based on polyimide technology.

The research at Ames has been concerned with the synthesis, characterization, and evaluation of new carbon fibers (ref. 11), new transparent self-supporting films derived from fluorenone monomers, and matrix resins derived from bismaleimide derivatives (ref. 12), new phenolics and stilbazole derivatives (ref. 13), and recently phthalocyanine (ref. 14) and phosphonitriles. These unusual polymers possess outstanding environmental properties that are not readily accessible with state-of-the-art polymers.

These polymers, although expensive by ordinary standards, have been designed to accommodate the kinds of environmental effects encountered in aerospace polymer applications. Here the environmental parameters often exceed the flux density and energy usually encountered in earthbound applications, such as temperature, photon energy and flux, creep-fatigue stress, impact energy, vacuum outgassing and chemical environments. Combined environmental effects are the rule. Hot wet strength is needed for supersonic applications of structural graphite composites. Impact- and fire-resistance properties are sought in the case of transport aircraft structure. High-energy particle and temperature resistance is generally required for new space structures. High-temperature- and impact-resistant turbine fan blades for jet engines would be economically useful.

There are few if any off-the-shelf standard tests that adequately simulate these aerospace environments needed to assess the time-dependent behavior of aerospace polymers. This is especially true in the case of thermal environments and impact effects. Analytical modeling, the development of special simulation facilities and often full-scale testing play a large role in most aerospace polymer research programs, and these test programs are generally long term and expensive.

Economically practical fabrication methods for large complex shapes such as composite structures for aircraft and spacecraft components impose inherent constraints on processing options. Spray molding of foams, tape, fabric, and fiber-wound lay-ups for composites; reaction injection molding (RIM); casting; and coatings are representative of some of these options. Particular classes of polymers are especially suitable. Reactive prepolymers which finally take the form of crosslinked binders and film formers satisfy these needs. The polymers discussed in this paper are concerned with these classes of materials.

AEROSPACE MATRIX RESINS FOR COMPOSITES

It is well known that aromatic polycyclic ring structures generally exhibit high-temperature and high-energy-radiation resistance due to high interchain bond strengths possible with such structures. Typically, polybenzimidazoles, "pyrones", polyphenylenes, and some polyimides exhibit these properties. All of these polymers have been examined in the NASA polymer program. Additional high-temperature stability, fire resistance, and thermochemical char formation for ablation efficiency may be obtained by elimination of processing solvents and introduction of crosslinked structures. Crosslink ability from a melt phase is constant with the processing requirements discussed previously, as well as with ultimate polymer properties.

A large part of the research at Ames is concerned with optimizing polymer properties for composite matrix resin binders by systematically manipulating the molecular structure of what may be conveniently described as crosslinked polycyclic aromatic structures in the form of liquid oligomers or fluid prepolymers. Inclusion of phosphorous and nitrogen heteroatoms in the basic ring systems is more the rule than not. As matrix resins these polymers must accommodate a substantial weight fraction of fiber for reinforcement such as glass, carbon, Kevlar, and hybrid blends. Often density reduction devices are included such as foaming gases, syntactic fillers and honeycomb structures. Formulation of aerospace components often include all of these elements. Combinations of widely diverse polymeric materials are necessary to obtain the combination of properties needed for cost-effective aeronautical applications.

It was clear from the outset of polymer research at Ames, that the development of weight-efficient ablative heat shields required that the chemist get control over the thermochemical rates of vapor and char formation to optimize heat shield design for different kinds of reentry environments. A significant observation was made at Ames in 1966 (ref. 15) which clearly demonstrated that in the one-dimensional heat transfer case, the pyrolysis vapor production rate was proportional to the applied cold-wall heating rate and inversely related to the number of multibonded aromatic rings in the neat resin. The generality of this result is shown in figure 1. Here the anaerobic thermochemical char yield (inversely related to the vapor production rate) is plotted as a function of the estimated concentration of multiply bonded aromatic rings. Linear polyphenylene is found to give the theoretical amount of residual carbon at 800°C in an inert atmosphere of 94 percent, epoxides are between 20-35, and phenolics and imides occupy an intermediate position of 60-65 percent.

Although this is a convenient relationship, a rather complete understanding of the bulk anerobic thermochemical reactions is required to estimate the effective number of stable aromatic rings. Thermochemical decomposition temperature and glass or heat distortion temperatures follow similar trends but much less regularly than these char yield values. It follows intuitively from these relationships that if one is seeking the most thermally stable polymers, those polymers with more stable bonded aromatic ring systems such as those polycyclic aromatic structures which are bonded by relatively stable bridging linkages such as imides, imidazoles, sulfones, aromatic ethers, carbonyls, silicones, and even metal ligands should be examined. These thermochemical principles were first applied in the formulation of the fabrication of the Apollo reentry charring ablative heat shield which was based on an epoxy novolac-phenolic resin system, the starting point for polymer research at the Ames Research Center.

This reentry heat shield polymer technology was first exploited in technology transfer to explain and predict the fire resistance of polymeric materials (ref. 16). As shown in figure 2, it is possible to correlate many of the important flammability properties with this easily measured anaerobic char yield, measured thermogravimetrically at 800°C. It can be seen that those properties usually associated with flammability, such as flame spread, ignition and toxic gas emission, decrease linearly with increasing char yield where those thermal properties associated with fire containment, that is the ablation efficiency, reach a maximum value in the fire environment between 45-50 percent.

These results have been used to select polymers for the design and fabrication of a number of new fireworthy interior panel structures for transport aircraft of the generic type shown in figure 3, where the relatively flammable epoxy glass facesheets have been replaced with comparably processable aromatic bismaleimide or phenolic resins. This at present is the best available compromise of the desired fire containment and fire involvement characteristics. The phenolic system is in the form of a crushed-core configuration, as adopted for use in the new Boeing 757 and 756 interior panels (ref. 17). Although considerable improvement in the fire resistance of this class of panels has been demonstrated in both laboratory and full-scale simulations, further improvements in decorative films and bonding adhesives are possible. These represent other new project developments, and they will be discussed subsequently.

It is obvious from the results shown in figure 2 that flammability and fire containment can not be optimized in a given polymer. It is also common knowledge that highly crosslinked aromatic polymers are generally very brittle, with low strain to failure and high impact sensitivity. Current research at Ames on fire-resistant polymers is aimed at solving both of these problems. It has recently been found (ref. 18) that the virtually totally fire resistant matrix resins with anerobic char yields greater than seventy-five percent are readily available from the condensation of alkyl-substituted pyridines such as collidone and lutidine with aromatic dialdehydes, as shown in figure 4. Carbon fiber composites formulated from this resin have been exposed to relatively severe fire environments (5 to 8 W/cm^2) for periods of 5 minutes. They do not burn and they retain most of their mechanical integrity after such exposure. They exhibit no tendency to delaminate under severe high-speed impact. These are somewhat remarkable results. As shown in the figure, these new polystyrylpyridine polymers (PSP) have a "buried" thermochemically reactive functionality in the form of a conjugated stilbazole double bond. At modest temperatures, the stilbazole remains uncrosslinked providing some linear chain runs and points of flexibility. The stilbazole double bond appears to react thermally at temperatures in excess of 400°C in the thermal environment to crosslink, giving an extremely fire resistant structure and retaining its mechanical integrity (ref. 19). The stilbene-like double bond has a high bond strength and meets the thermochemical requirements for a multiple bonding segment.

This matrix resin was first applied in the NASA Ames polymer program as a means of overcoming the phenomenon of accidental carbon fiber release to eliminate electrical hazards from carbon composites exposed to a crash fire environment (ref. 19). As shown in figure 5, the rate of carbon fiber release varies linearly with the increased anaerobic char yield. As expected, minimum fiber release was obtained under simulated fire impact conditions with carbon composites formulated from the PSP resin system. The long-term high-temperature stability of PSP-based carbon composites is apparent in comparing the effect of temperature on the dynamic modulus as measured by dynamic mechanical analysis (DMA). The results obtained for carbon composite formulated from PSP compared with conventional epoxides are compared in figure 6. Rapid loss of the epoxy-based composite occurs around 250°C whereas no change in the mechanical properties of the PSP composite is observed to occur up to 400°C. As should be expected, the application of these new PSP polymers requires special attention to the fiber sizing employed. Unsized fibers or those coated with polyimides in preliminary tests provide basic mechanical properties at least equivalent to standard aerospace epoxy composites.

Recent preliminary studies by the aircraft companies on vendor-prepared aircraft interior honeycomb sandwich panels have shown that these PSP composites withstand at least five minute exposure to simulated post-crash fire environments with virtually no loss in mechanical strength.

For the first time, a new matrix resin system has been developed for carbon fiber composites which clearly demonstrates the concept of using a stable, thermochemically reactive functionality which in the case of PSP has provided maximum fire resistance and adequate strength over a wide range of temperature conditions. Compound panels are being prepared wherein one sheet is derived from the highly ablatively efficient bismaleimide for fire containment, with PSP face sheets for complete interior resistance to fire involvement. Such systems are expected to provide optimum future designs for transport aircraft interiors and other aerospace vehicles.

Higher cure and post-cure temperatures are required for the basic PSP polymer shown in figure 4 than for those usually considered conventional for large aircraft parts. This concern has been overcome by altering the condensation cure to basic prepolymer reaction by means of vinyl end group termination through reaction with vinyl methyl pyridine, as shown in figure 7. The easily polymerized vinyl groups permit curing of these matrix resins under conventional epoxy curing conditions. In addition to providing low-temperature gelation of the matrix resin and cure, replacement of the condensation cure (elimination of water) with terminal vinyl groups gives low-void composites with acceptable mechanical properties with carbon fibers. It is interesting to note that these vinyl-modified PSP's still exhibit the same high char yields, that is, around seventy-five percent, due to high-temperature conversion of the stilbazole double bonds, and give the expected fire-resistant properties. It is clear that easy control of molecular weight of the divinyl PSP derivatives is possible by changing the concentration of the vinyl methyl pyridine to provide a series of stilbazole derivatives which can be used as reactive oligomers and reactive diluents for other matrix resins. Modification of bismaleimides and other unsaturated matrix resins of particular interest are currently under investigation. Sensitivity of high-modulus carbon fiber composites to the effects of both low- and high-speed impact and the potential limitations these responses place on the use of such composites as primary aircraft structures are well known. The use of polyphase rubber dispersions in matrix resins has been examined in some detail (ref. 20). There are other important factors such as fiber resin interface adhesion and the nature of the fiber lay-up, orientation, and fabric weaves which also contribute to fracture toughness in such systems. Although high-strength properties of composites are largely influenced by matrix resin properties, composite tolerance to both low- and high-speed impact is controlled by the microstructural features of such compositions.

The effect of rubber modification of conventional aerospace-grade carbon fiber epoxy on the short beam shear strength as a function of low-speed impact is shown in figure 8. It can be seen that it requires as much as twenty-five percent addition of carboxy-terminated butadiene acrylonitrile elastomers to minimize the rate of change in short beam shear strength with impact energy. These modifications, although reducing the effect of low-speed impact, degrade the strength properties of the high-stiffness composites. The initial flexural strength is reduced by as much as ten to fifteen percent, the hot wet strength is reduced by as much as sixty percent, and the flexural modulus is reduced by as much as forty percent. This general degradation of mechanical properties through conventional rubber modification to improve impact tolerance may be sufficient to make this modification inappropriate. These results have been interpreted to mean that the controlling factor in rubber toughening, in addition to the well-known particle size and distribution of the rubber phase, is the phase distribution of rubber in resin and resin in rubber, the former plasticizing the resin phase and the latter reducing the dampening effectiveness of the dispersed elastic particle.

To examine this question, a trifunctional epoxy novolac, TEN, provided by the Dow Chemical Company, which is a much more aromatic matrix resin than the conventional TGMDA (shown in figure 9), was modified by addition of CTBN. The data is shown in Table 1. It is clear that the improvement in impact tolerance is maximized at a ten percent addition of CTBN elastomer with a three-fold increase in the shear strength after 10 in/lb impact with about a twenty percent improvement in the flexural strength over the control. Although the initial properties of the TEN/DDS control are somewhat lower than those obtained for the TGMDA/DDS control, in addition to higher impact tolerance possible with the ten percent modification of TEN/DDS, all of its mechanical properties are superior to both initial and any modification possible with the less aromatic TGMDA. Further improvements in impact tolerance, if required, may be possible by further tailoring the solubility parameters of the resin-elastomer system. Rubber modifications to provide large differences in solubility parameters of the resin-rubber system were examined by replacing the hydrocarbon by a fluorocarbon elastomer from preliminary results of rubber-toughening a standard EPON 828/DDS epoxy resin (ref. 21) in a glass laminate as shown in Table 2. As in the former case the improvement in retention of shear strength after impact goes through a maximum of eight percent addition of the fluoroelastomers of fluoropropylene oxide with a significant improvement of the impact tolerance and improvement of the mechanical properties as indicated. Since these fluoroelastomers have thermal stabilities in excess of 400°C as well as excellent fire resistance, they show considerable promise as fracture-toughening agents for high-temperature matrix resins such as the bismaleimides and PSP polymers described above.

It may be concluded from the brief overview of polymer research being conducted at the Ames Research Center with aerospace matrix resins for composites that liquid oligomers formulated from stilbazole derivatives alone or in combination with other unsaturated imide monomers such as bismaleimides may be modified with selected elastomers to provide high-stiffness-molecule composites with an optimum combination of high-temperature, impact, and fire resistance required for many aerospace applications. It is believed that although these resin systems may be somewhat specialized for general commercial use, the principles that have been employed in their development have a broad range of applicability to the polymer industry at large.

Total polymer design as illustrated in the case of the stilbazole polymers probably offers the best route to effect the best combination of properties required for advanced aerospace applications. We have, however, investigated some simple modifications of conventional matrix resins which have improved both the thermal- and fire-resistant properties. Soluble phthalocyanine tetramines of copper, cobalt, nickel as shown in figure 9, are easily prepared (ref. 22). We have used these tetramines to prepare a variety of high-temperature imides with use temperatures in air in excess of 600°C. In addition, we have found that with borontrifluoride catalysis these organometallic tetramines react easily with conventional epoxides as shown in figure 10. The resulting polymers are useful as matrix binders for carbon-fiber composites with substantially improved fire resistance. Limiting oxygen index values in excess of 50 with anaerobic char yields corresponding to values greater than 70-75 percent have been obtained for carbon-fiber composites with acceptable mechanical and processing properties. Although the thermochemistry of these modifications is not well understood, the results may be very useful in conventional epoxy technology.

REFERENCES

1. J. A. Parker and G. F. D'Alelio, "Ablative Plastics", Marcel Dekker, Inc., New York, NY (1971).

2. C. B. Neel, R. N. Griffin, Jr., and J. P. Millard, Solar Plastics, 6, 235 (1969). "Studies Related to Satellite Thermal Control: Measurements of Earth-Reflected Sunlight and Thermal-Control Coatings".

3. T. Wydeven, C. C. Johnson, M. A. Golub, M. S. Hsu and N. R. Lerner, ACS Symposium Series, 108, 299 (1979).

4. M. A. Golub and J. A. Parker, Eds., "Polymeric Materials for Unusual Service Conditions", Appl. Polym. Symp., No.22, (1973).

5. R. W. Rosser, R. H. Fish and J. A. Parker, U. S. Patent 3,916,060, October 28, 1975.

6. J. A. Parker, G. M. Fohlen, P. M. Sawko and R. N. Griffin, Jr., SAMPE Journal, August/September 1968, "The Use of Acid Salts of p-Nitroaniline as a Component of Intumescent Coatings".

7. J. A. Parker, G. M. Fohlen and P. M. Sawko, Technical Report AFML-TR-73-126, February 1973.

8. J. A. Parker and D. A. Kourtides, "Optimization of Fire Blocking Layers for Aircraft Seating", presented at the 7th International Conference on Fire Safety, Menlo Park, CA, January 1982 .

9. D. A. Kourtides and J. A. Parker, J. of Fire and Flammability, 15, 56 (1982).

10. D. E. Cagliostro, Textile Research Journal, 50, 632 (1980).

11. D. E. Cagliostro, Surface Analysis of Carbon Fibers Modified from PAN Fibers at Low Accepted Carbonization Temperatures. Accepted for publication in Textile Research Journal.

12. I. K. Varma, G. M. Fohlen, and J. A. Parker, ACS Symposium Series, 195, 253, 1982.

13. A. H. Heimbuch and J. A. Parker, "Polystyrylpyridine: Chemistry and Technology", presented at Gordon Research Conference on Polymers (Santa Barbara, CA), Jan. 15, 1982.

14. B. N. Achar, G. M. Fohlen, and J. A. Parker, J. Polymer Sci., Polymer Chemistry Edition, 20, 269, 1789, 1982.

15. J. A. Parker and E. L. Winkler, NASA TR R-276, 1967.

16. J. A. Parker, D. A. Kourtides, R. H. Fish, and W. J. Gilwee, Proceedings of the AGARD Propulsion and Energetics Panel (Rome, Italy), April 1975.

17. J. A. Parker and D. A. Kourtides, Fireworthiness of Transport Aircraft Interior Systems, Aircraft Fire Safety, AGARD Lecture Series No. 123, 1982.

18. Ming-ta Hsu, Mark L. Rosenberg, John A. Parker, and Alvin H. Heimbuch, J. Appl. Polymer Sci., 26, 1975, 1981.

19. W. J. Gilwee and R. H. Fish, NASA TM-81179, 1980.

20. W. J. Gilwee and A. Jayarajan, Proceedings of National Symposium of Polymers, ACS (Washington, D.C.), June 9-11, 1980.

21. R. W. Rosser, M. Taylor, and T. Chen, Modification of Epoxy-Reinforced Glass Cloth Composites with a Perfluorinated Alkyl Ether Elastomer. Accepted for publication in J. Polymer Eng. & Sci.

22. B. N. Achar, G. M. Fohlen, and J. A. Parker, Phthalocyanine Polymers IV: Novel Type of Thermally Stable Polyimides Derived from Methyl Phthalocyanine Tetramine and Benzophenone Tetracarboxylic Dianhydride. Accepted for publication in J. Polymer Sci., Polymer Chemistry Edition.

TABLE I.- MECHANICAL PROPERTIES

Sample	Density	Shear Strength		Flexural Strength		Flex. Mod. 10^6		Moisture abs
		Initial	10 in/lb impact	Dry	200°F Wet	Dry	200°F Wet	
DEN*/DDS	1.4886	6673	2866	83,265	78,146	9.4	8.8	2
DEN/DDS + CTBN								
2%	1.5418	5737	2303	80,643	71,862	9.5	9.8	1.3
5%	1.509	7137	3058	98,278	66,018	9.5	8.5	1.28
6%	1.555	8206	2587	113,825	85,362	9.5	7.4	0.71
10%	1.5373	9362	6302	105,838	89,430	7.6	8.2	0.30
15%	1.518	7919	4252	99,327	78,858	7.8	7.9	0.40
20%	1.4678	5404	3633	74,250	52,989	7.6	7.2	0.88

* Trifunctional Epoxy Novolac
Composite fiber vol. 61.8±2.8

TABLE 2.- FLUOROETHER ELASTOMER MODIFIED EPOXY GLASS CLOTH COMPOSITES

	Tg (°C)	Flexural Toughness (ft. lbs/in^3	Flexural Strength (psix10^4)	Flexural Modulus (psix10^6)	Retention of Shear Strength After 15 in. lbs impact (%)
EPON 828/DDS (DGEBA)	203	40.5	6.56	3.10	70.3
EPON 828/DDS 8% fluoroether	225	60.4	9.52	4.29	86.2
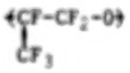 $\leftarrow\underset{CF_3}{CF}-CF_2-O\rightarrow$					

BEST DOCUMENT AVAILABLE

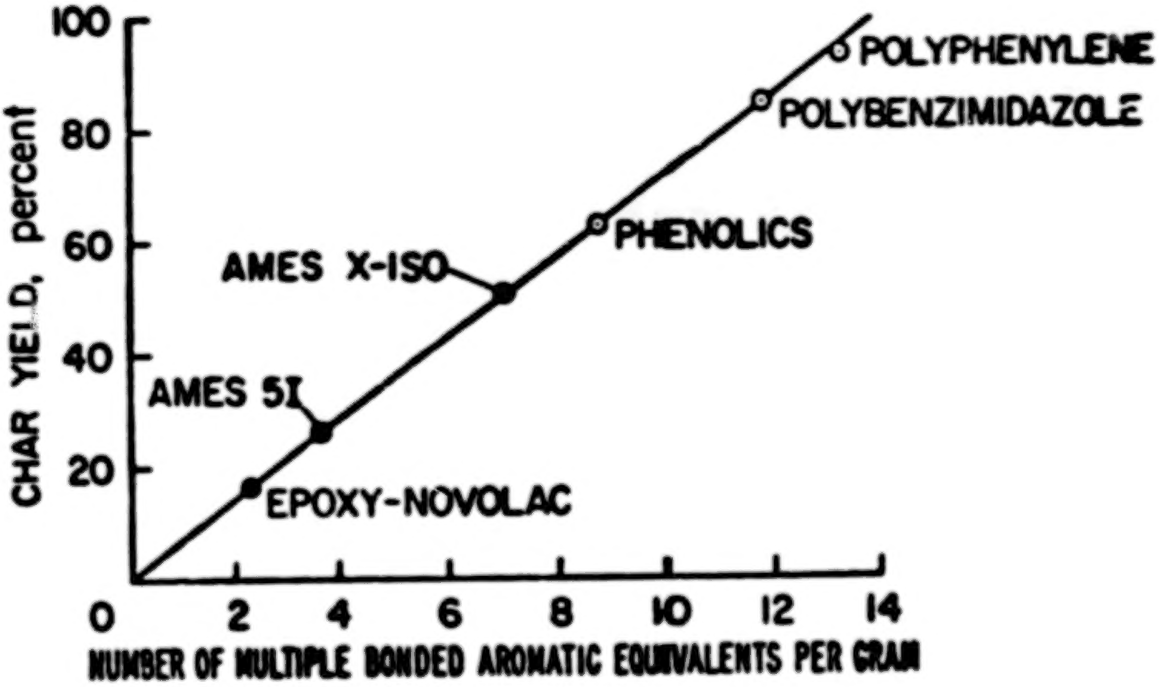

Figure 1.- Correlation of primary thermochemical char yield with molecular structure.

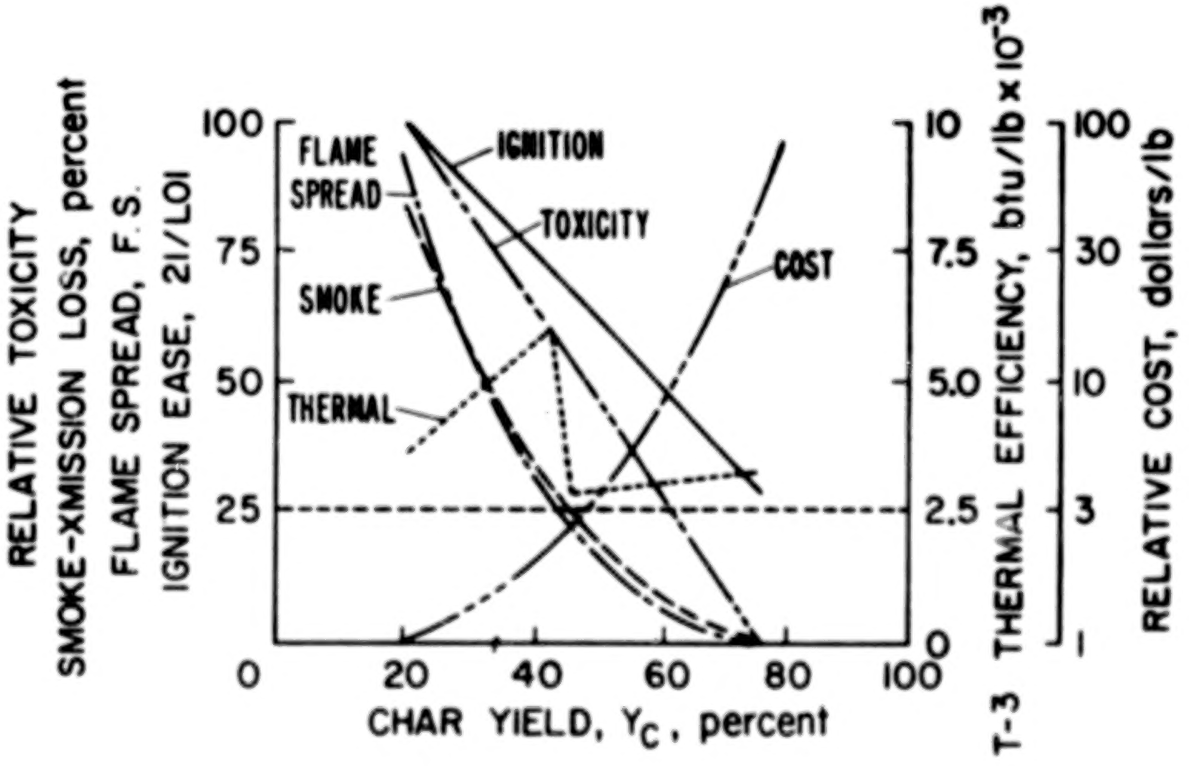

Figure 2.- Summary of properties of char-forming foamed polymers.

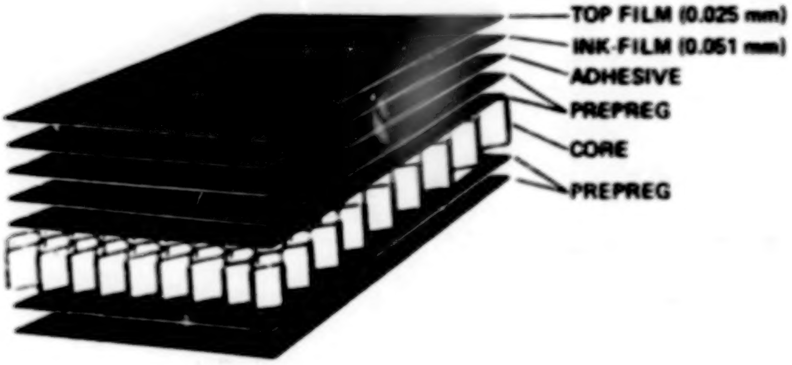
TOP FILM (0.025 mm)
INK-FILM (0.051 mm)
ADHESIVE
PREPREG
CORE
PREPREG

- CANDIDATE RESIN SYSTEMS FOR PREPREG
  - BASELINE EPOXY
  - BISMALEIMIDE
  - PHENOLIC
  - POLYIMIDE
- TESTING MATRIX
  - FLAMMABILITY, SMOKE, AND TOXICITY
  - MECHANICALS AND AESTHETICS

Figure 3.- Sandwich panel configuration.

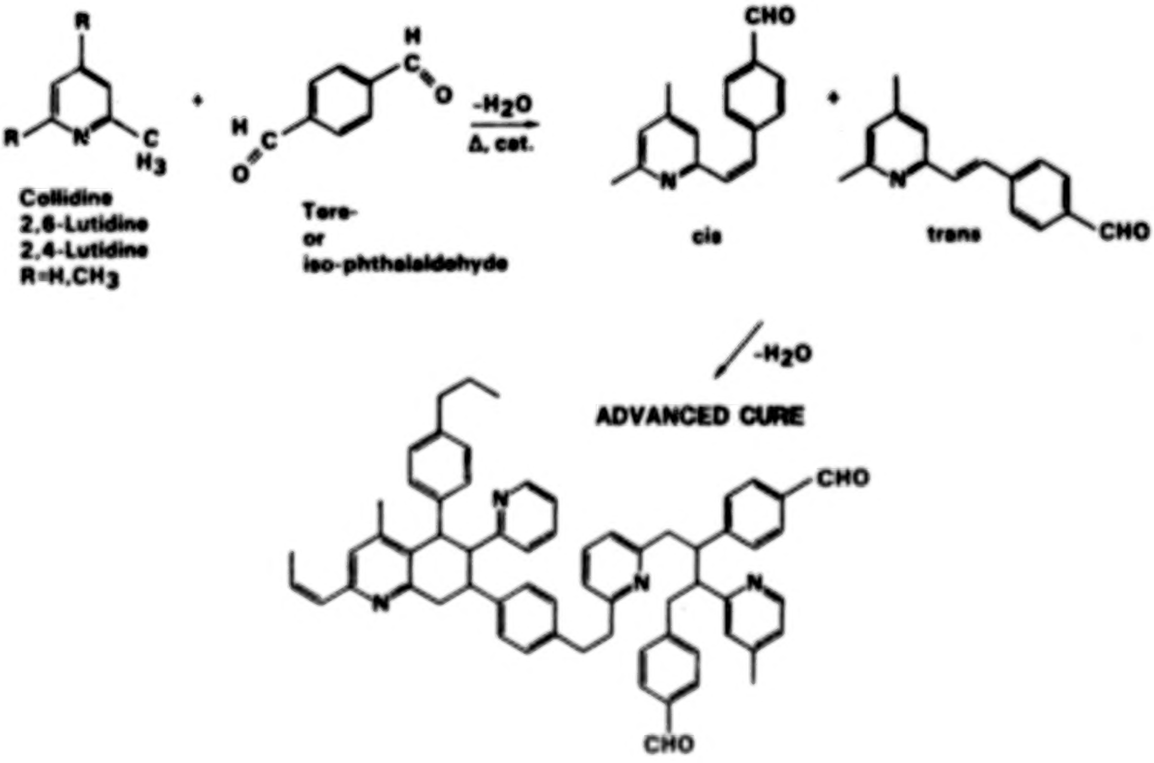
R
R
N
C
H3
H
C
O
H
C
O
-H2O
Δ, cat.
CHO
N
N
CHO
Collidine
2,6-Lutidine
2,4-Lutidine
R=H,CH3
Tere-
or
iso-phthalaldehyde
cis
trans
-H2O
ADVANCED CURE
N
N
N
N
N
CHO
CHO

Figure 4.- Reaction scheme for linear or crosslinked polystyrylpyridine (PSP).

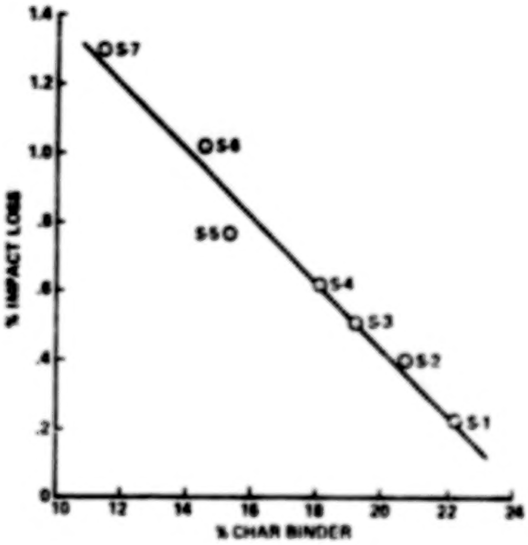

Figure 5.- Char versus impact loss after burn - satin weave.

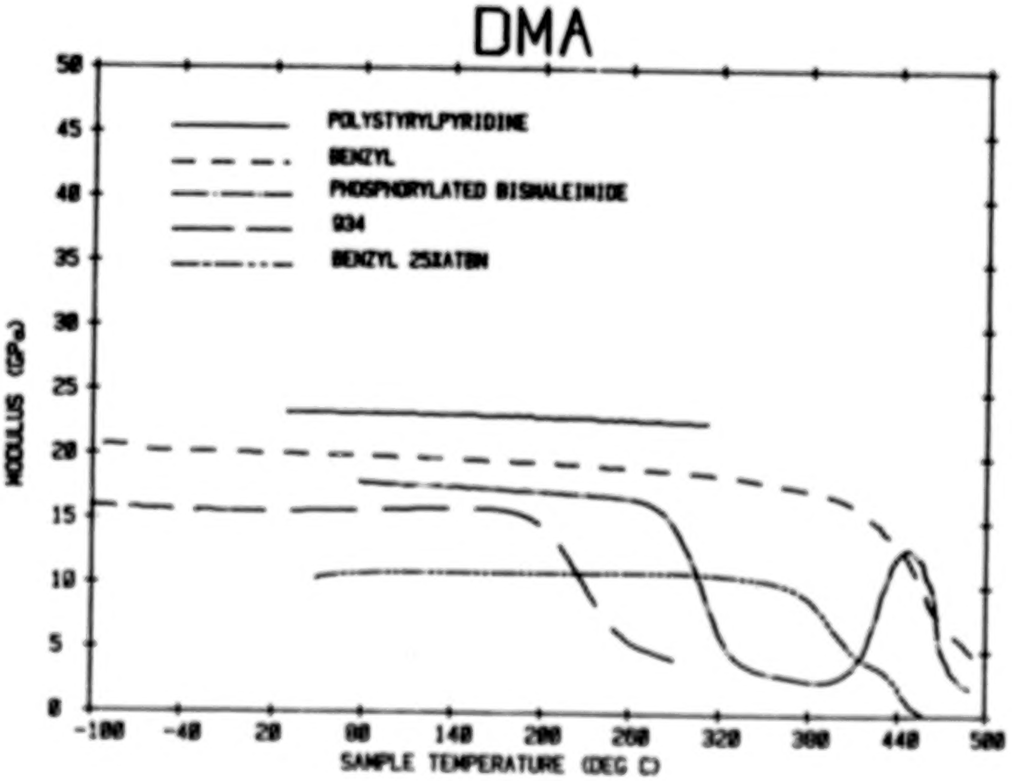

Figure 6.- Effect of temperature on dynamic modulus of carbon composites.

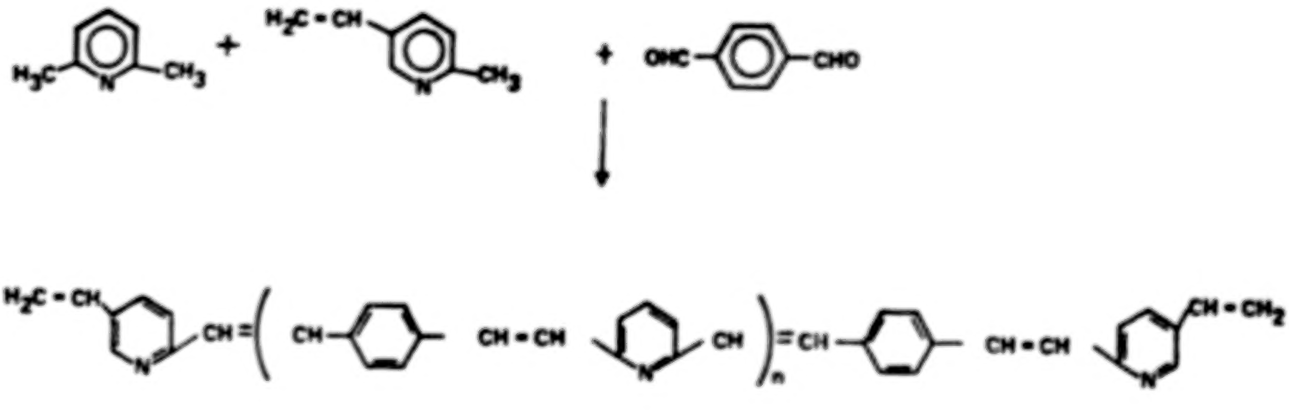
H₃C
N
CH₃
+
H₂C = CH
N
CH₃
+
OHC
CHO
H₂C = CH
CH =
CH
CH = CH
N
CH
n
= CH
CH = CH
N
CH = CH₂

Figure 7.- Synthesis of PSP (vinyl-terminated polystyrylpyridine).

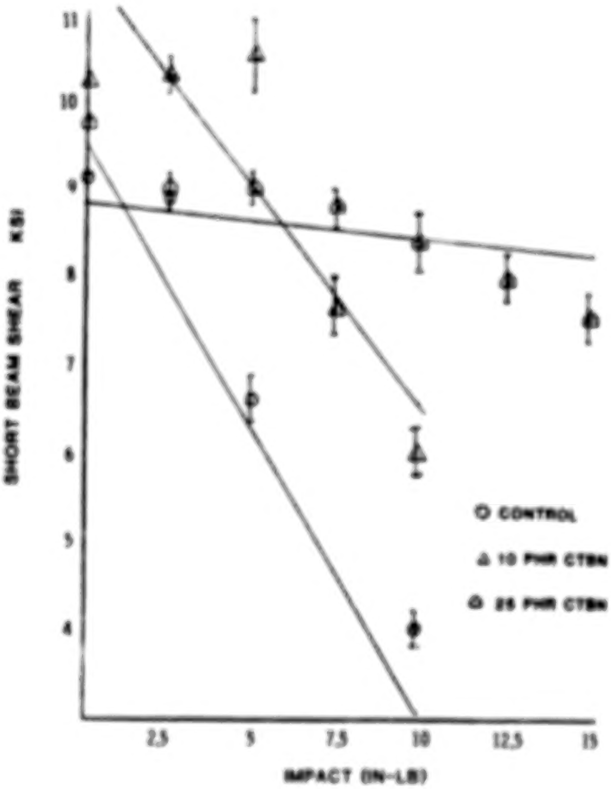

Figure 8.- Shear strength after impact.

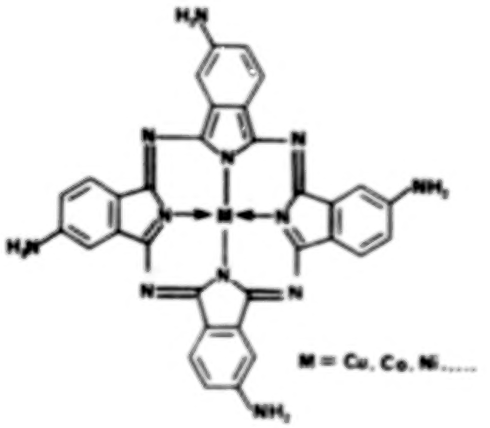

Figure 9.- Tetraminophthalocyanine monomer.

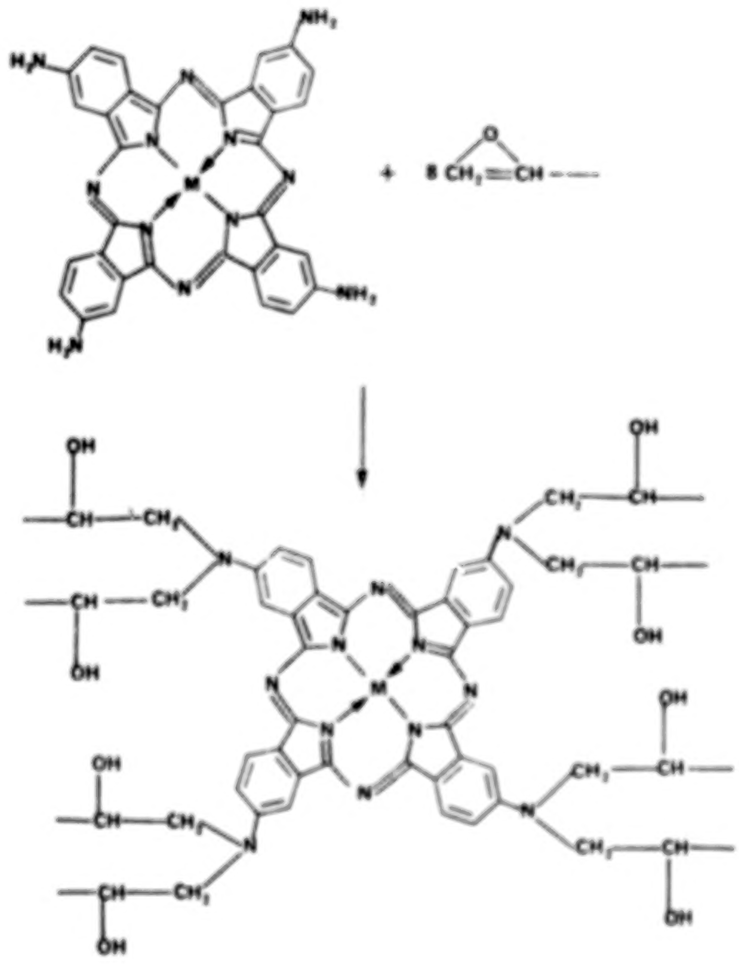

Figure 10.- Polymer structure of the reaction of tetraminophthalocyanine with conventional epoxides.

BLANK PAGE

POLYMER MATRIX COMPOSITES RESEARCH AT NASA LEWIS RESEARCH CENTER

T. T. Serafini
NASA Lewis Research Center
Cleveland, Ohio

CURRENT PROGRAM THRUSTS

The objective of the polymer matrix composites research at the NASA Lewis Research Center is to develop technology for new generations of polymer matrix composites intended for application in advanced aeropropulsion systems. Other applications for the newly developed technology are in airframe and space structures. Research is performed in the following areas: 1) monomer/polymer synthesis, 2) polymer/composites characterization, 3) cure/degradation mechanisms, 4) polymer/composites processing, 5) environmental effects, and 6) thermo-mechanical properties. Emphasis is given not only to developing improved materials, but also to achieving a fundamental understanding of materials' behavior at the molecular level.

The current thrusts of the Lewis polymer matrix composites program are listed in figure 1. In keeping with the Lewis role as the lead center for propulsion research, the major emphasis of the Lewis program is in the area of engine applications. Research is also being conducted to develop matrix resins with improved toughness to support the inter-center program, with the lead center responsibility at the Langley Research Center, to develop improved composites for airframe applications. Highlights of recent progress in each of the program thrusts are discussed with the exception of the thrust to develop a 700° F matrix resin. Emphasis is given to reviewing key advances in improving the processability of PMR polyimides and the application of PMR-15 composites in engine static structures.

ENGINE APPLICATIONS

- DEVELOP MATRIX RESINS FOR USE AT 700° F
- DEVELOP PMR POLYIMIDES WITH IMPROVED PROCESSABILITY
- DEVELOP COMPOSITES MECHANICS METHODOLOGY TO PREDICT LIFE/DURABILITY OF COMPOSITES IN ENGINE ENVIRONMENTS
- ESTABLISH FABRICATION TECHNOLOGY FOR ENGINE STATIC STRUCTURES

AIRFRAME APPLICATIONS

- DEVELOP TOUGHER MATRIX RESINS

Figure 1

LEWIS PMR POLYMIDE TECHNOLOGY

Studies conducted at the Lewis Research Center led to the development of the concept and class of polyimides known as PMR (for in situ polymerization of monomer reactants) polyimides (refs. 1 and 2). The PMR concept has been adopted by other investigators, and PMR polyimide materials are being offered commercially by the leading suppliers of composite materials. Figure 2 outlines some salient features of the PMR polyimide approach for the fabrication of composites. The reinforcing fibers are hot-melt or solution impregnated with a mixture of monomers dissolved in a low-boiling-point alkyl alcohol. Following fiber impregnation, in situ polymerization of the monomers is caused by heating at temperatures in the range of 250° to 450° F. The final polymerization, an addition reaction, occurs at temperatures in the range of 525° to 660° F without the evolution of undesirable reaction by-products, making it possible to fabricate void-free composite structures. The highly processable polyimides are now making it possible to realize much of the potential of high-temperature polymer matrix composites.

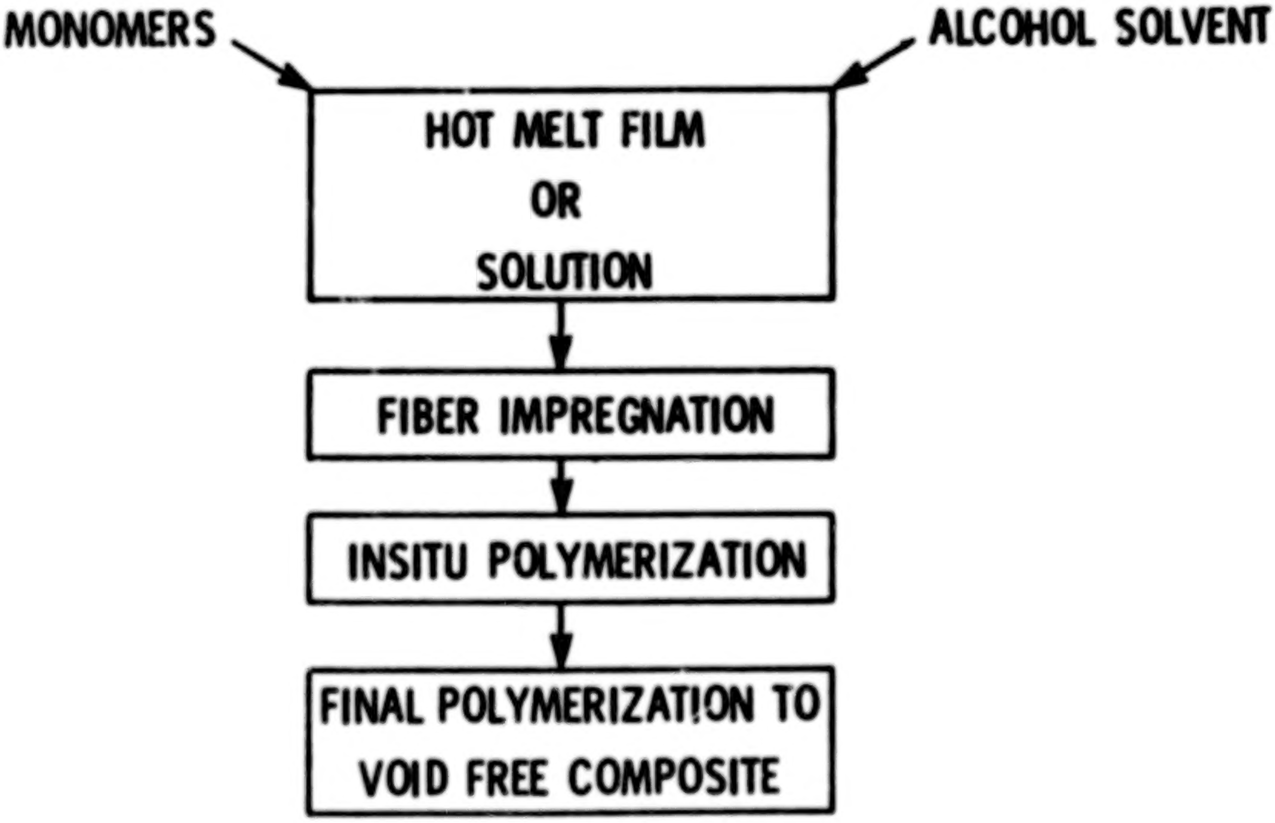
MONOMERS
ALCOHOL SOLVENT
HOT MELT FILM OR SOLUTION
FIBER IMPREGNATION
INSITU POLYMERIZATION
FINAL POLYMERIZATION TO VOID FREE COMPOSITE

Figure 2

MONOMERS USED FOR PMR-15 POLYIMIDE

The excellent elevated temperature properties and processability of PMR polyimide composites based on the PMR matrix known as PMR-15 have led to their acceptance as viable engineering materials for high-performance structural applications. The structures of the monomers used in PMR-15 are shown in figure 3. The number of moles of each monomer reactant is governed by the following ratio: 2:n:(n + 1), where 2, n, and (n + 1) are the number of moles of NE, BTDE, and MDA, respectively. In PMR-15 the value of n is 2.087, corresponding to a formulated molecular weight of 1500. This PMR composition was found to provide the best overall balance of processing characteristics and thermo-oxidative stability at 600° F (ref. 3). Solutions having solids contents in the range of 50 to 85 percent are prepared by simply dissolving the monomer reactants in an alcohol such as methanol. Higher solids content solutions are used for psuedo-hot-melt fiber impregnation techniques.

STRUCTURE	NAME	ABBREVIATION
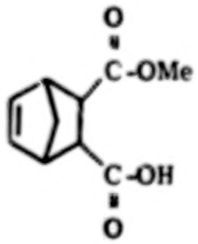	MONOMETHYL ESTER OF 5-NORBORNENE-2,3-DICARBOXYLIC ACID	NE
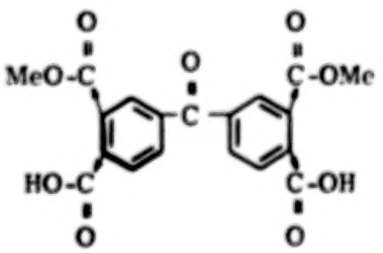	DIMETHYL ESTER OF 3,3',4,4'-BENZOPHENONETETRACARBOXYLIC ACID	BTDE
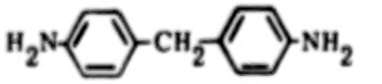	4,4'-METHYLENEDIANILINE	MDA

Figure 3

VERSATILITY OF PMR APPROACH

The early studies (ref. 1 and 3) conducted at Lewis clearly demonstrated the versatility of the PMR approach. By varying either the chemical composition of the monomers or the monomer stoichiometry, or both, PMR matrices having a broad range of processing characteristics and properties can be readily synthesized. A PMR composition, designated as PMR-II, has been identified which exhibited improved thermo-oxidative stability compared to PMR-15 (ref. 4). PMR-II has not been accepted as a matrix material because of the lack of a commercial source for one of the monomer reactants used in formulating the resin. A modified PMR-15, called LARC-160, has been developed by substituting an aromatic polyamine for MDA (ref. 5). Other studies (ref. 6) demonstrated the feasibility of using the PMR approach "to tailor make" matrix resins with specific properties. For example, as shown in figure 4, the resin flow characteristics (based on weight of resin flash formed during molding) of PMR polyimides can be varied, or "tailored", over a broad range by simply varying the formulated molecular weight. The higher flow formulations did exhibit decreased thermo-oxidative stability at 550° F.

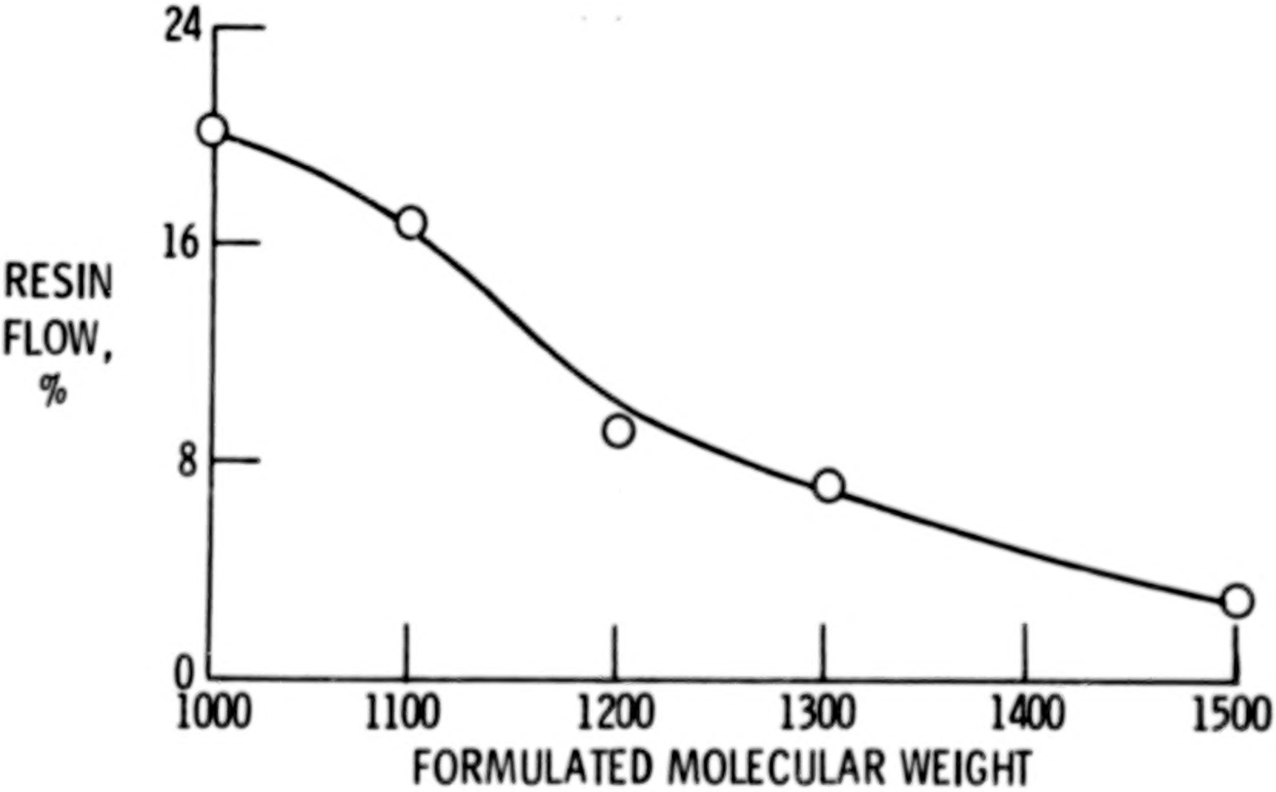

Figure 4

PMR-15 POLYIMIDE MODIFICATIONS FOR IMPROVED PREPREG TACK

Current-technology PMR-15 polyimide prepreg solutions are generally prepared by dissolving the monomer mixture in methanol. Although the volatility of methanol is highly desirable for obtaining void-free composites, it does limit the tack and drape retention characteristics of unprotected prepreg exposed to the ambient. PMR-15 monomer reactants and a mixed solvent have been identified which provide prepreg materials with improved tack and drape retention characteristics without changing the basic cure chemistry or processability (ref. 7). The modifications consist of substituting higher alkyl esters for the methyl esters in NE and BTDE and using a solvent mixture (3:1 methanol/1-propanol) in lieu of pure methanol. As can be seen in figure 5 (left), the ester and solvent modifications extend the tack retention of PMR-15 prepreg to beyond 12 days under ambient conditions. Figure 5 (right) shown that the 600° F interlaminar shear strength (ILSS) properties of Celion 6000 graphite fiber composites made with the modified PMR-15 system are identical to the 600° F (ILSS) properties of composites made with the control, or unmodified, system. The improved tack PMR-15 system should facilitate the fabrication of large complex structures which require long layup times and provide cost savings because of reduced material scrap.

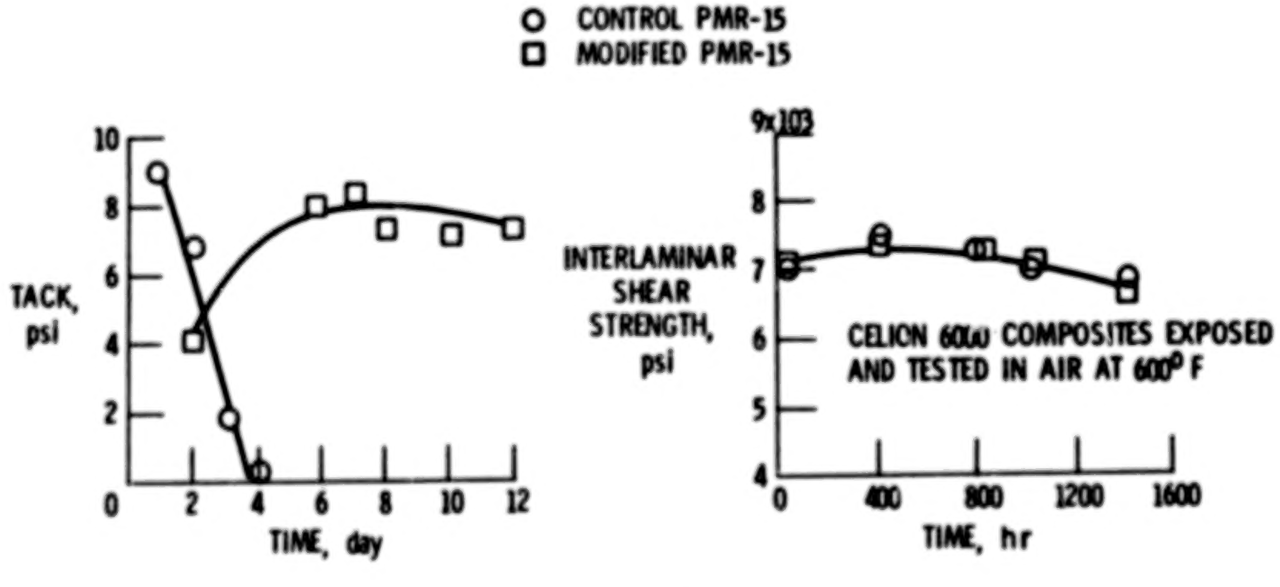

Figure 5

LOWER-CURING-TEMPERATURE PMR POLYIMIDES

The recommended temperature for final cure of PMR-15 is 600° F. This temperature exceeds the temperature capabilities of many industrial autoclave facilities which were originally acquired for curing of epoxy matrix composites. Recent studies (ref. 8) have shown that a significant reduction in cure temperature of PMR-15 can be achieved by replacing 50 mole percent of the NE with p-aminostyrene. Cure studies of the modified system, designated PMR-NV, showed that final cure temperature of PMR-15 could be reduced to 500° F (figure 6, upper left) without sacrificing its 600° F thermo-oxidative stability (figure 6, upper right). As can be seen in figure 6 (bottom), the 600° F interlaminar shear strength (ILSS) properties of Celion 6000 composites made with the PMR-NV matrix are equivalent to the ILSS properties of Celion 6000/PMR-15 composites. The lower cure temperature of the PMR-NV system should be more compatible with existing autoclave facilities and should lead to wider usage of PMR materials.

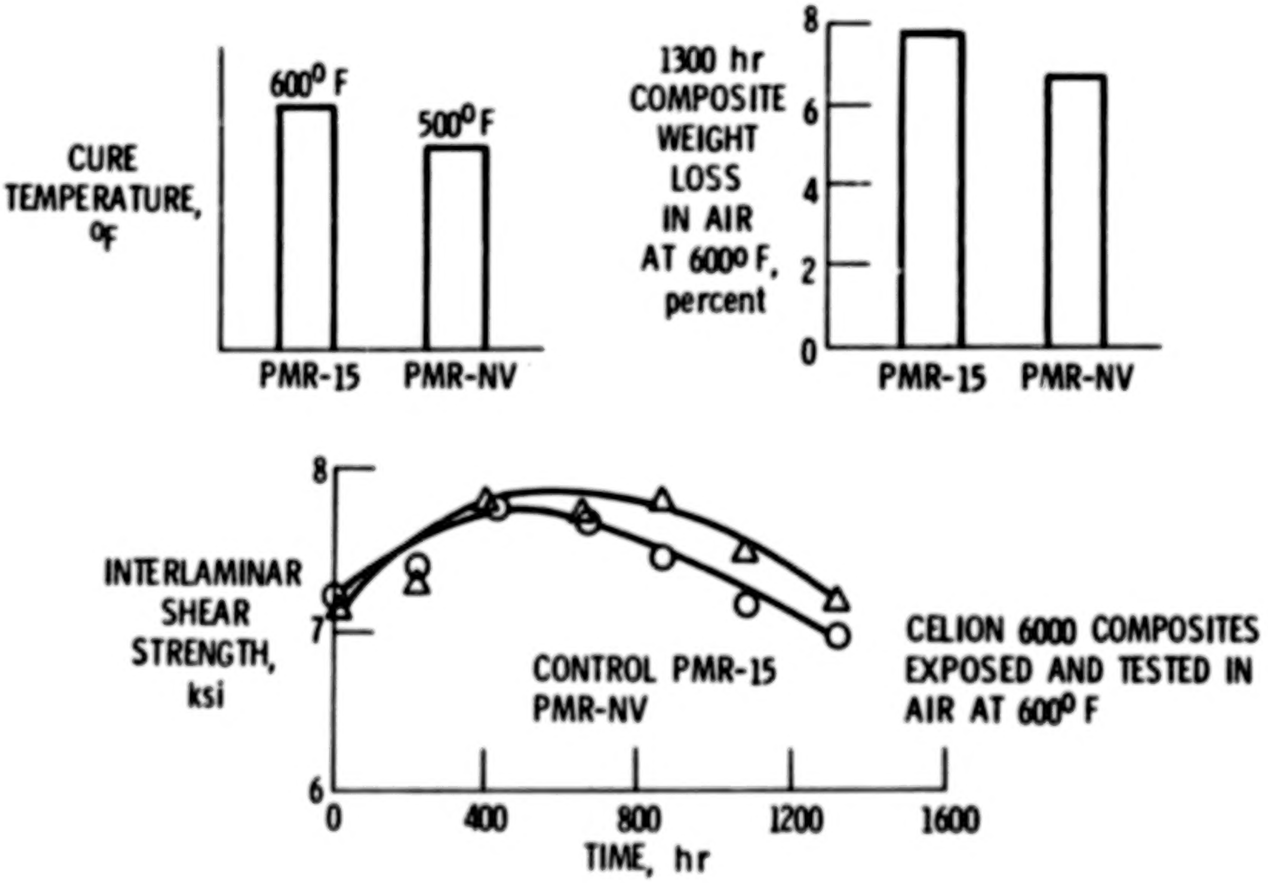

Figure 6

IMPROVED CELION 6000/PMR-15 COMPOSITES

Our continuing research with PMR polyimides has identified a fourth monomer reactant which improved the thermo-oxidative stability and resin flow during composite fabrication (ref. 9). Figure 7 (left) shows the 1500-hour composite weight loss in air at 600° F of Celion 6000 composites made with PMR-15 containing 0 to 20 mole percent N-phenylnadimide (PN). It can be seen that PN levels of 4 and 9 mole percent resulted in improved 600° F thermo-oxidative stability. Figure 7 (right) shows the variation of resin flow during composite processing as a function of PN content. It can be seen that increased resin flow results from the addition of PN. Although the PN-modified PMR-15 composites exhibited lower initial properties at 600° F than unmodified PMR-15 composites, the addition of PN appears to be a promising approach to improve the thermo-oxidative stability of PMR-15.

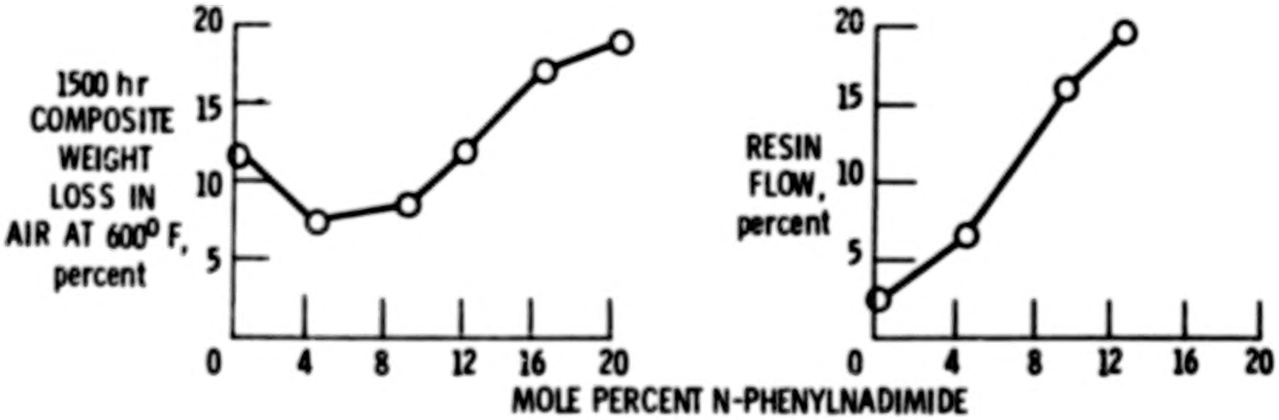

Figure 7

IMPROVED SHEAR STRAIN OF IMIDE-MODIFIED EPOXY

The approach of introducing imide groups into the molecular structure of epoxy resins by reacting epoxy oligomers with novel bis(imide-amine) curing agents was developed by Lewis investigators as a means of improving the thermal characteristics of epoxies (ref. 10). Studies are presently under way at United Technologies Research Center, under contract to NASA, to establish the potential of imide-modified epoxies for improving composite toughness. Figure 8 (left) compares the 10-degree off-axis tensile strengths (ref. 11) of Celion 6000 composite made with a conventional epoxy (A) and an imide-modified epoxy (B). Figure 8 (right) compares calculated resin shear strain for the two composite systems. The resin shear strains were calculated from data generated using 10-degree off-axis tensile tests. It can be seen that the imide-modified resin exhibited more than a two-fold increase in calculated shear strain compared to the conventional epoxy. Studies are currently in progress to establish the correlation between composite toughness and resin shear strain calculated from 10-degree off-axis tensile tests.

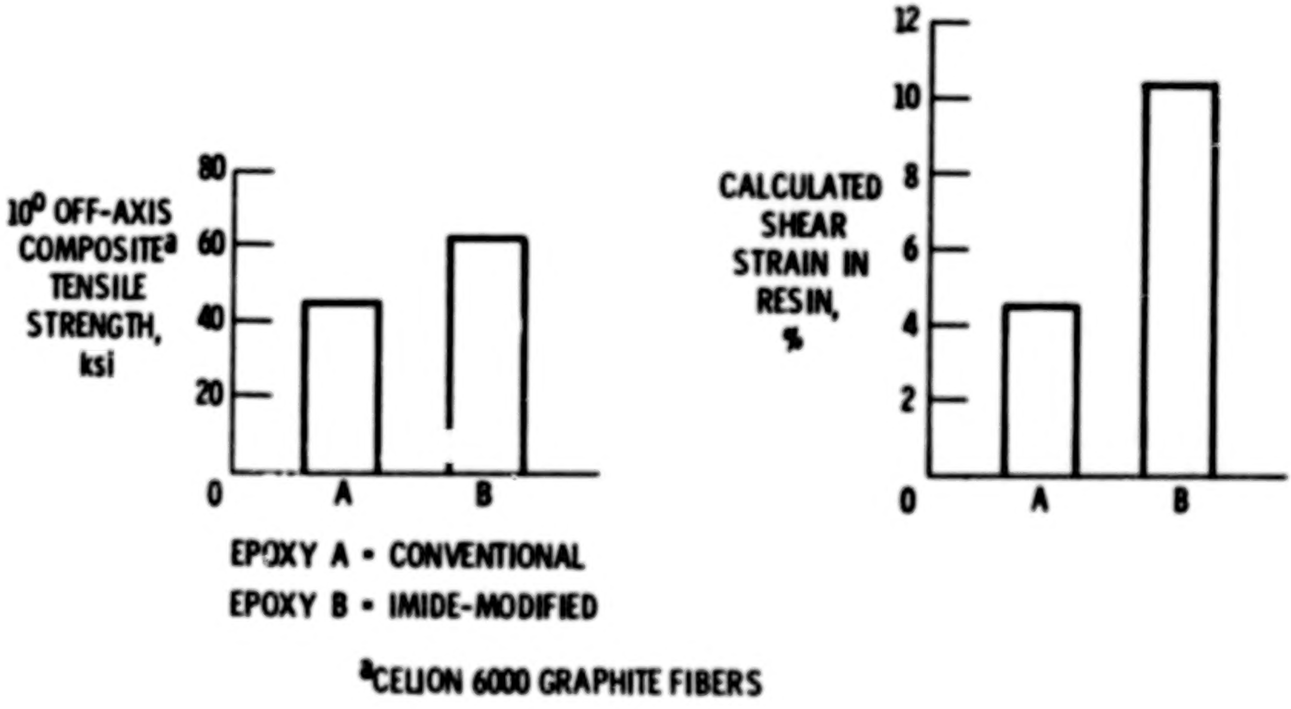

Figure 8

COMPOSITE DURABILITY

Research is being conducted at the Lewis Research Center to develop methodology to predict the life and/or durability of composite structural components in engine service environments. Service environments of major concern are various combinations of temperature, moisture, and mechanical loads. A "generalized" predictive model for predicting the life/durability of graphite fiber/resin matrix composites has been developed (ref. 12). Figure 9 compares experimental data (individual data points) and data predicted by the "generalized" model (parallel lines) for AS graphite/epoxy composites subjected to compression-compression fatigue at room temperature under dry or wet conditions. The important point to note is that the measured data at fracture is above the predicted lines. This indicates the conservative nature of the "generalized" predictive model and should provide credence for its use in preliminary designs.

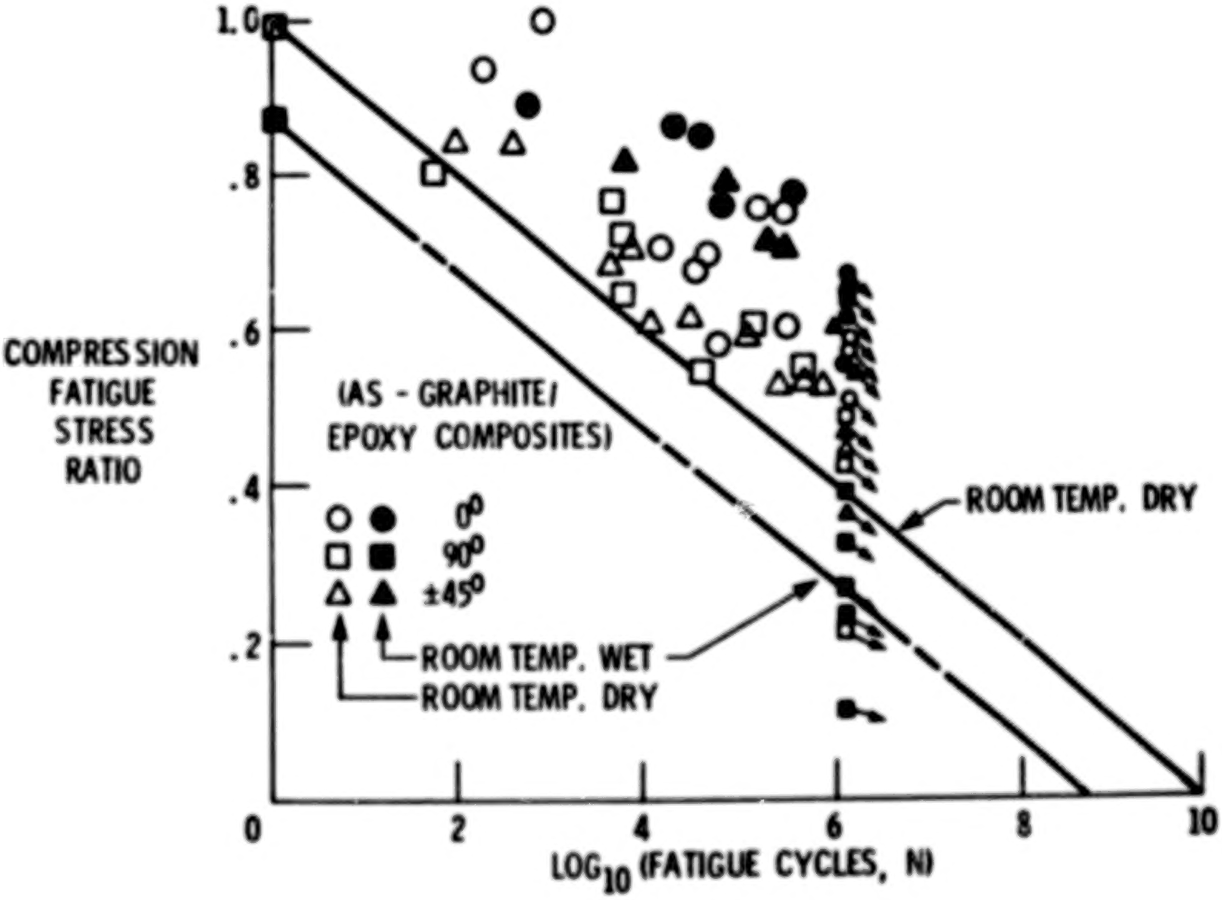

Figure 9

APPLICATIONS OF PMR-15 POLYIMIDE COMPOSITES

One of the most rewarding aspects of the PMR polyimide development has been the successful demonstration of PMR-15 polyimide composite materials as viable engineering materials. Prepregs, molding compounds and even adhesives based on PMR-15 have been commercially available from the major suppliers of composite materials since the mid-seventies. Because of their commerical availability, processability, and excellent retention of properties at elevated temperatures, PMR-15 composites have been used to fabricate a variety of structural components. These components range from small compression-molded bearings to large autoclave-molded aircraft engine cowls and ducts. Processing technology and baseline materials data are being developed for the application of PMR-15 composites in aircraft engines, space structures, and weapon systems. Some representative applications of PMR-15 composites are listed in figure 10. None of the components listed in the figure, with the exception of the ion engine beam shield, are applications in the sense that the components are currently being produced. However, several of the components listed in figure 10 are scheduled for production introduction in the near future. A brief discussion of each of the components listed in figure 10 follows.

COMPONENT	AGENCY	COMPANY
ULTRA-HIGH TIP SPEED FAN BLADES	NASA-LeRC	PWA/TRW
QCSEE INNER COWL	NASA-LeRC	GE
F404 OUTER DUCT	NAVY/NASA-LeRC	GE
F101 DFE INNER DUCT	AIR FORCE	GE
T700 SWIRL FRAME	ARMY	GE
JT8D REVERSER STANG FAIRING	NASA-LeRC	McDONNELL-DOUGLAS
EXTERNAL NOZZLE FLAPS		
PW1120	----	PWA[a]
PW1130	AIR FORCE	PWA
SHUTTLE ORBITER AFT BODY FLAP	NASA-LaRC	BOEING
ION THRUSTER BEAM SHIELD	NASA-LeRC	HUGHES

[a] COMPANY FUNDED

Figure 10

ULTRA-HIGH-TIP-SPEED FAN BLADES

The blade illustrated in figure 11 was the first structural component fabricated with a PMR-15 composite material. The reinforcement is HTS graphite fiber. The blade design was conceived by Pratt & Whitney Aircraft (PWA) for an ultra-high-speed fan stage (ref. 13). Blade tooling and fabrication were performed by TRW Equipment (ref. 14). The blade span is 11 in. and the chord is 8 in. The blade thickness ranges from about 0.5 in. just above the midpoint of the wedge-shaped root to 0.022 in. at the leading edge. At its thickest section the composite structure consists of 77 plies of material arranged in varying fiber orientation. The "line of demarkation" visible at approximately one-third the blade span from the blade tip resulted from a required change in fiber orientation from 40 degrees in the lower region to 75 degrees in the upper region to meet the torsional stiffness requirements. Ultrasonic and radiographic examination of the compression-molded blades indicated that they were defect free. Although some minor internal defects were induced in the blades during low-cycle and high-cycle fatigue testing, the successful fabrication of these highly complex blades established the credibility of PMR-15 as a processable matrix resin.

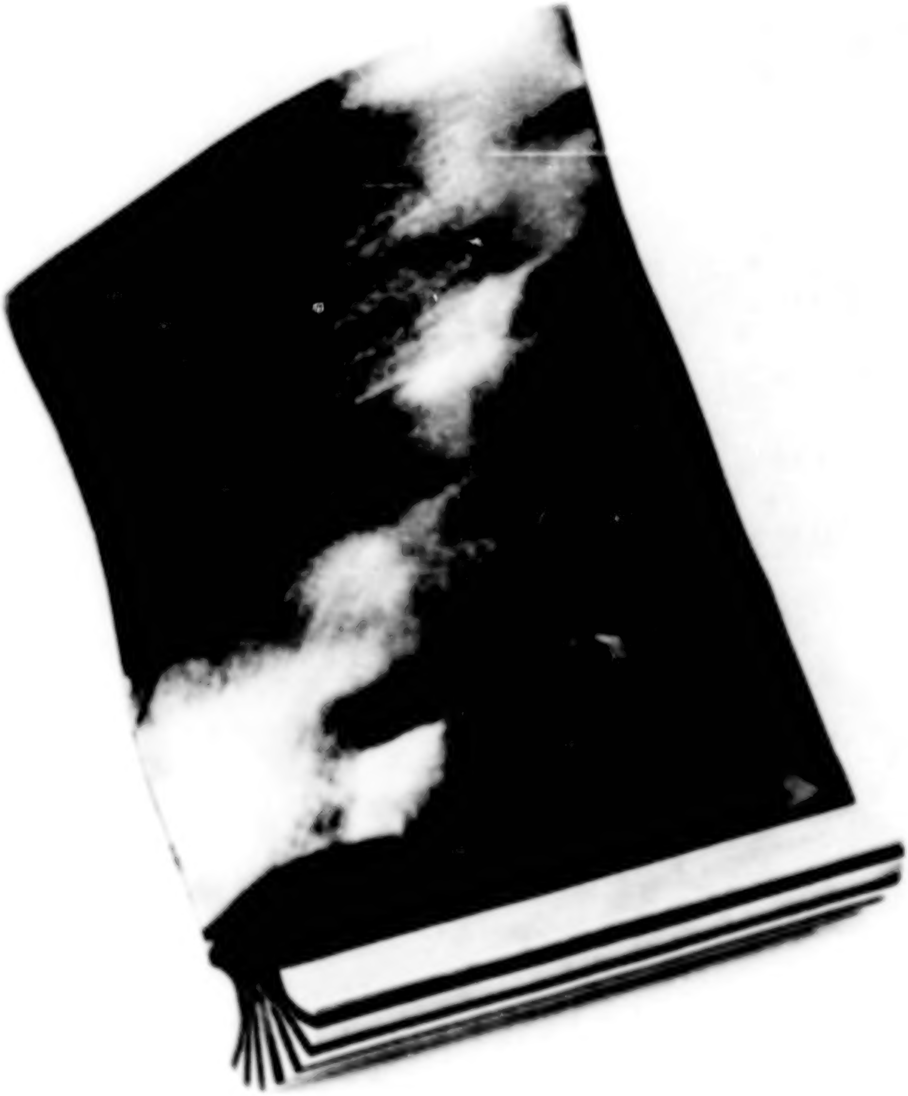

Figure 11

APPLICATION OF COMPOSITES ON QUIET CLEAN SHORT-HAUL EXPERIMENTAL ENGINE (QCSEE)

The Quiet, Clean, Short-Haul Experimental Engine (QCSEE) program was initiated to develop a propulsion technology base for future powered-lift short-haul aircraft. One of the major areas of new technology investigated under the QCSEE program was the application of advanced composite materials to major engine hardware. Figure 12 shows a cutaway drawing of the under-the-wing (UTW) QCSEE engine. Composite materials were used for fan blades, the fan frame, and nacelle components. The blades, frame and all nacelle components with the exception of the inner cowl were fabricated from Kevlar or graphite fibers in an epoxy matrix resin. The inner cowl was made of graphite fibers in PMR-15 polyimide.

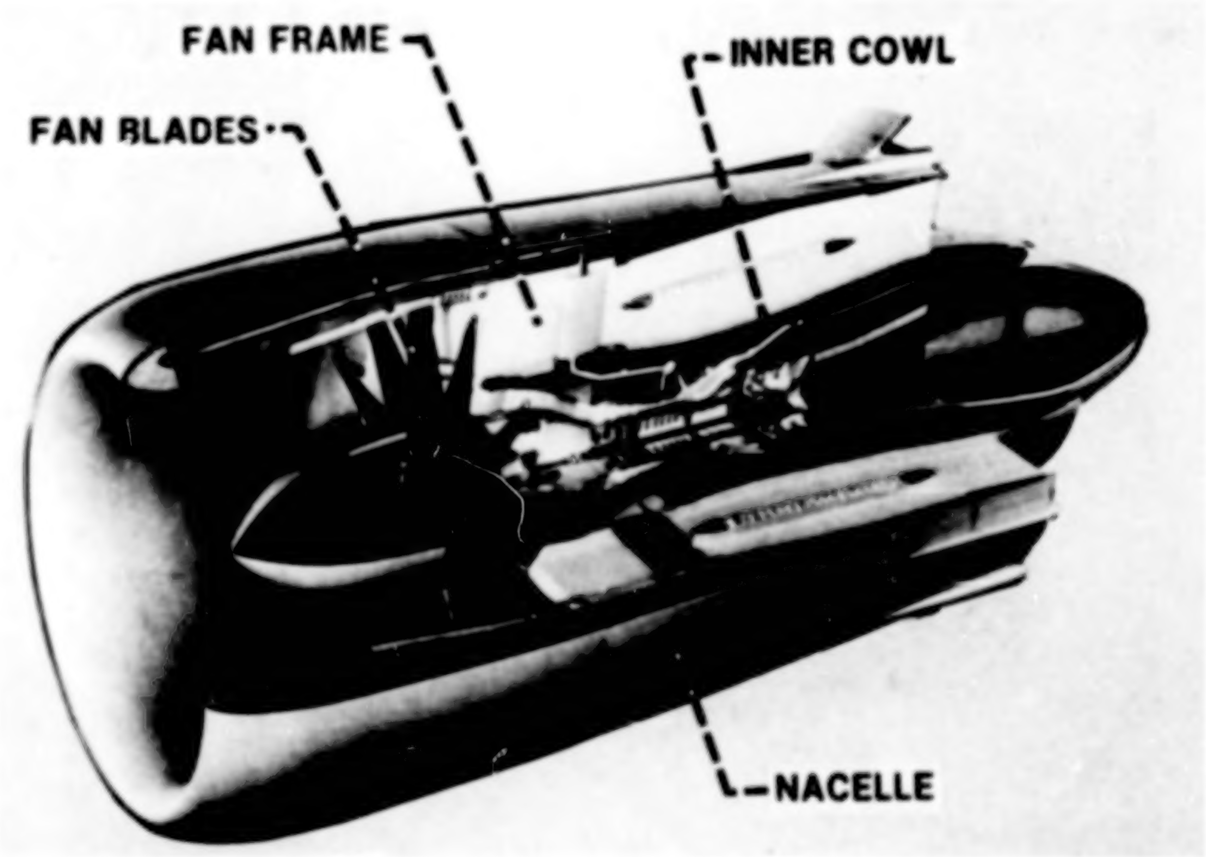

Figure 12

GRAPHITE FIBER/PMR-15 QCSEE INNER COWL

Figure 13 shows the composite inner cowl installed on the UTW QCSEE engine developed by General Electric (GE) under contract with the Lewis Research Center (ref. 15). The cowl defines the inner boundary of the fan air flowpath from the fan frame to the engine core nozzle. The cowl was autoclave-fabricated by GE from PMR-15 and T300 graphite fabric. The cowl has a maximum diameter of about 36 in. and is primarily of honeycomb sandwich construction. HRH327 fiberglass polyimide honeycomb was used as the core material. Complete details about the cowl fabrication process are given in reference 16. The cowl was installed on the QCSEE engine and did not exhibit any degradation after more than 300 hours of ground engine testing. The maximum temperature experienced by the cowl during testing was 500° F (ref. 17). The successful autoclave fabrication and ground engine test results of the QCSEE inner cowl established the feasibility of using PMR-15 composite materials for large engine static structures.

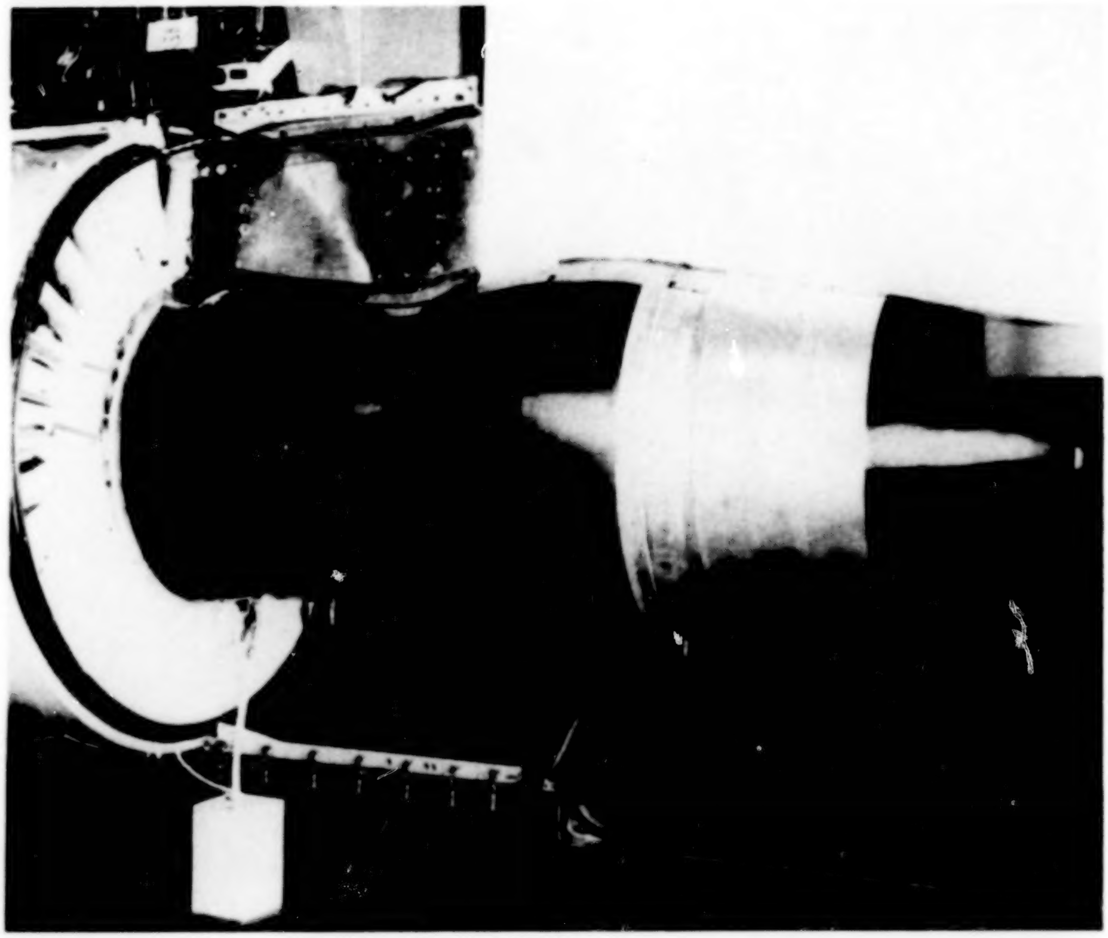

Figure 13

GENERAL ELECTRIC F404-GE-400 TURBOFAN

Under a jointly sponsored U. S. Navy/NASA Lewis program (NAS3-21854), GE is developing a T300 graphite fabric/PMR-15 composite outer duct to replace the titanium duct presently used on the F404 engine, shown in figure 14, for the Navy's F18 strike fighter. The titanium duct (the waffle-like structure) is a sophisticated part made by forming and machining titanium plates followed by chem-milling to reduce weight. A preliminary cost-benefit study indicated that significant cost and weight savings (ref. 18) could be achieved by replacing the titanium duct with a composite duct.

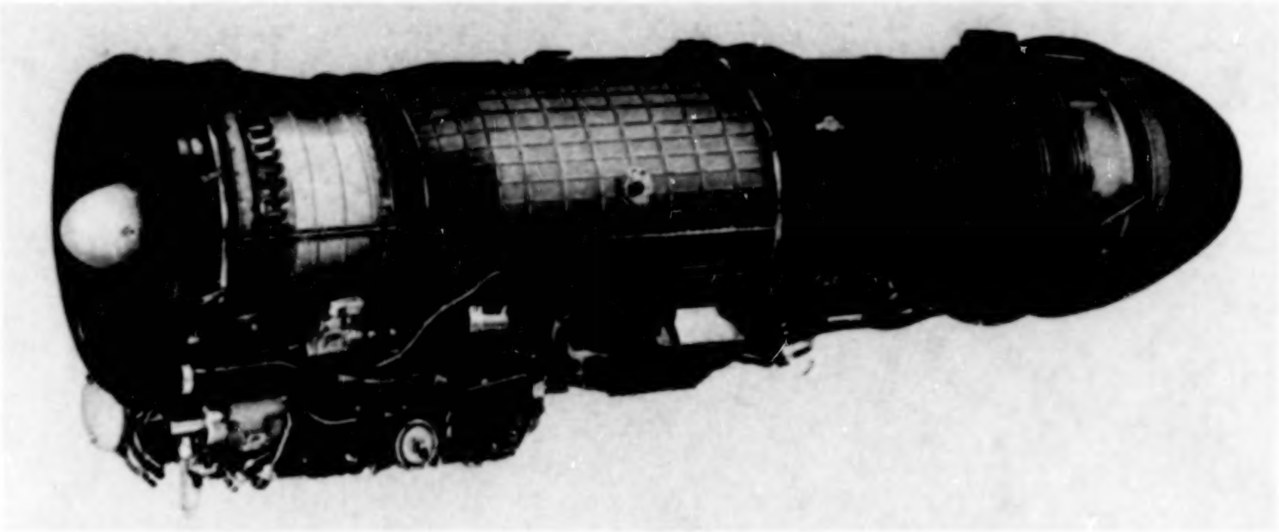

Figure 14

GRAPHITE FIBER/PMR-15 POLYIMIDE OUTER DUCT FOR GE F404 ENGINE

Figure 15 is a photograph of the full-scale composite duct (38 in. diameter x 65 in. length x 0.080 in. wall thickness) that was autoclave-fabricated from T300 graphite fabric and PMR-15 polyimide. The duct was proof pressure checked successfully, prior to ground engine testing, to 108 psi (150 percent of operating pressure). The F404 composite outer duct differs from the QCSEE inner cowl in several important respects. The F404 duct is a monolithic composite structure and needs to withstand fairly high loads, and perhaps most importantly, the F404 duct is to be a production component and not a "one-of-a-kind" demonstration component.

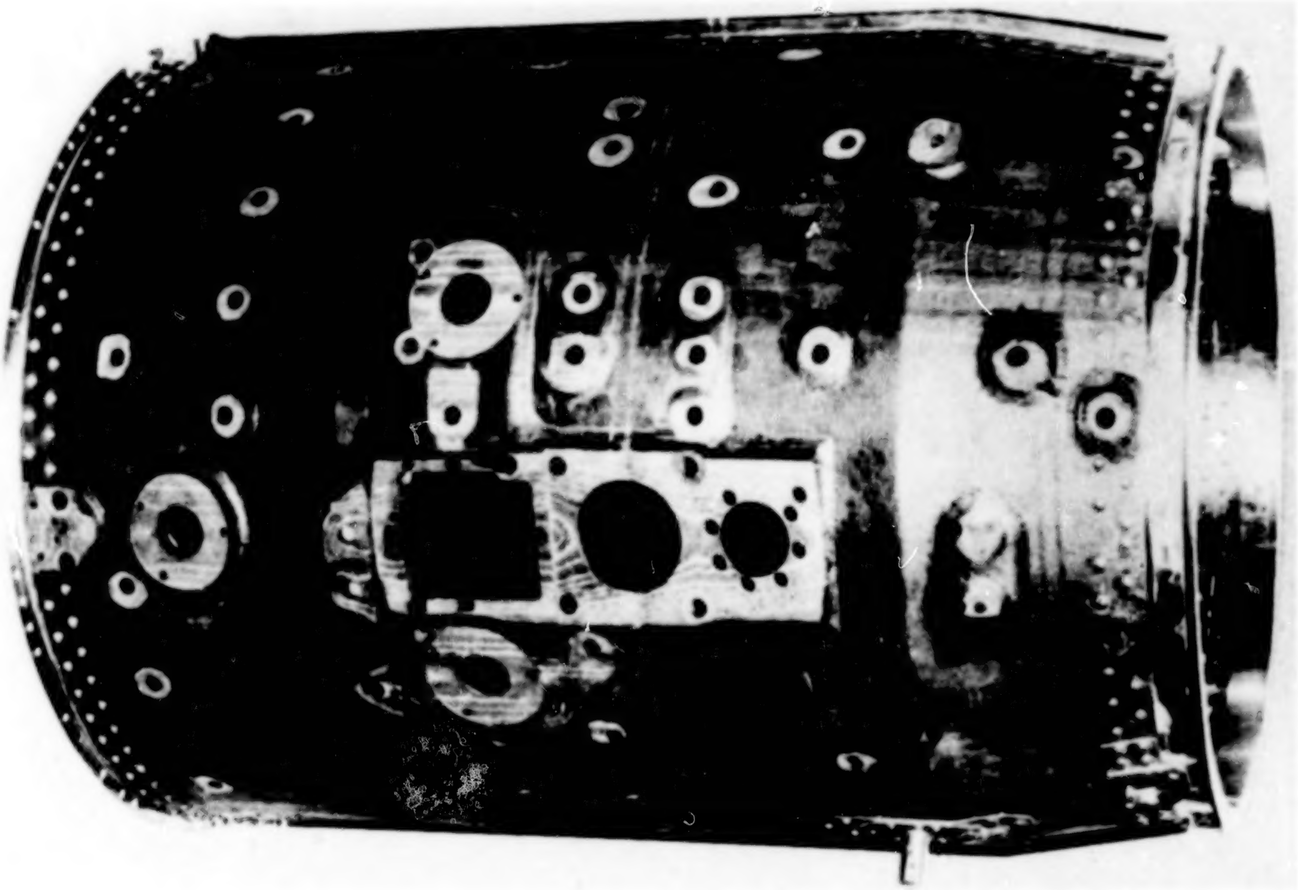

Figure 15

GRAPHITE FIBER/PMR-15 POLYIMIDE OUTER DUCT ON GE F404 ENGINE

Figure 16 shows the composite duct installed on an F404 test engine. The composite duct has successfully withstood over 1000 accelerated mission test cycles during a total engine exposure time of 700 hours. The graphite/PMR-15 polyimide composite duct is scheduled for production introduction in 1985.

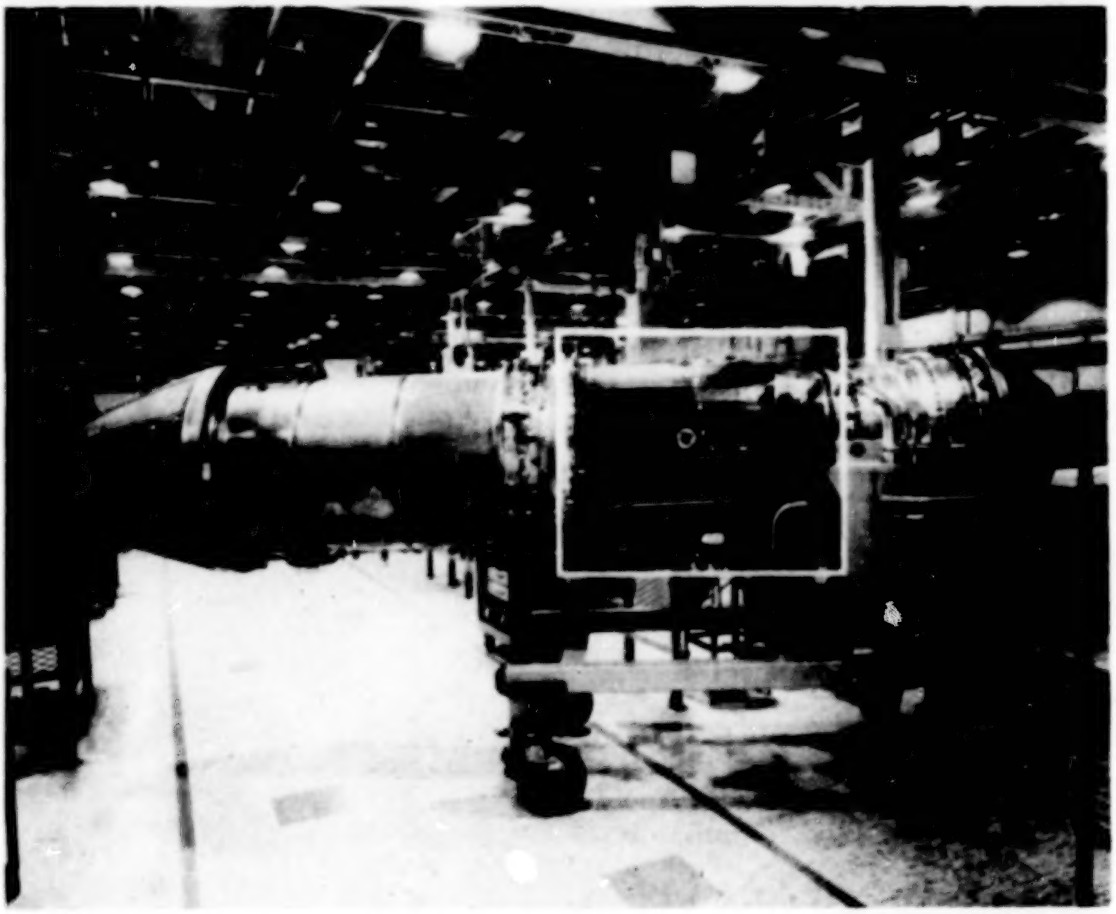

Figure 16

SCHEMATIC OF GE T700 PMR-15 COMPOSITE SWIRL FRAME

The current bill-of-materials inlet particle separator swirl frame on GE's T700 engine is an all-metal part that involves machining, shape-forming, welding, and brazing operations. Design studies conducted under U. S. Army contract number DDAK51-79-C-0018 indicated that the fabrication of a metal/composite swirl frame could result in cost and weight savings of about 30 percent. Figure 17 shows a schematic diagram of a section of the metal/composite swirl frame that was fabricated from 410 stainless steel and various kinds of PMR-15 composite materials. The outer casing uses stainless steel in the flow path area to meet anti-icing temperature requirements and T300 and glass fabric/PMR-15 hybrid composite to meet structural requirements. The T300/glass hybrid composite was selected on the basis of both cost and structural considerations. An aluminum-coated glass fabric PMR-15 composite material is utilized in the inner-hub flowpath to meet heat transfer requirements for anti-icing. The glass fabric/PMR-15 composite utilized for the front edge and front inner surface was selected because of cost as well as temperature considerations. A full-scale (O.D. ~ 20 in.) metal/composite swirl frame has been subjected to sand erosion and ice ball impact tests. The metal/composite swirl frame provided improved particle separation and successfully met the impact test requirements. Fabrication feasibility has been demonstrated, and if the metal/composite swirl frame successfully meets all of the performance requirements, the metal/composite T700 swirl frame will be introduced into production in 1985.

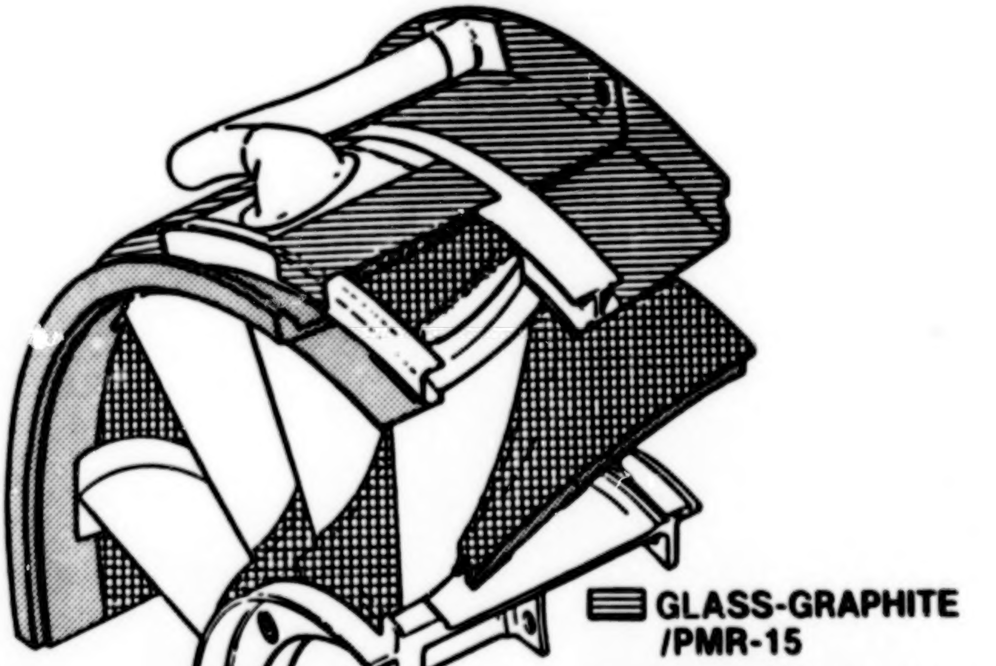

Figure 17

APPLICATIONS OF GRAPHITE FIBER/PMR-15 POLYIMIDE COMPOSITES ON PW1120 ENGINE

Figure 18 is a schematic showing "committed" and "possible" applications of graphite/PMR-15 composite materials on the PW1120 turbojet currently being developed by Pratt & Whitney Aircraft/Government Products Division (PWA/GPD). A committed application is an application for which a metal back-up component is not being developed. The committed applications for graphite/PMR-15 composites on the PW1120 at this time are the external nozzle flaps and the airframe interface ring. PWA/GPD is in the process of completing its assessment of the various "possible" applications and anticipates that many of these will also become "committed", if engine test schedules can be met. The PW1120 engine is currently scheduled for production deliveries in 1986. Graphite/PMR-15 external nozzle flaps have been committed for production by PWA/GPD for its PW1130 turbofan engine. Production deliveries of the PW1130 are scheduled for 1984. Prepregs made from T300 or Celion 3000 uniweave fabrics and PMR-15 are being evaluated for fabrication of the nozzle flaps used on both the PW1120 and PW1130 engines.

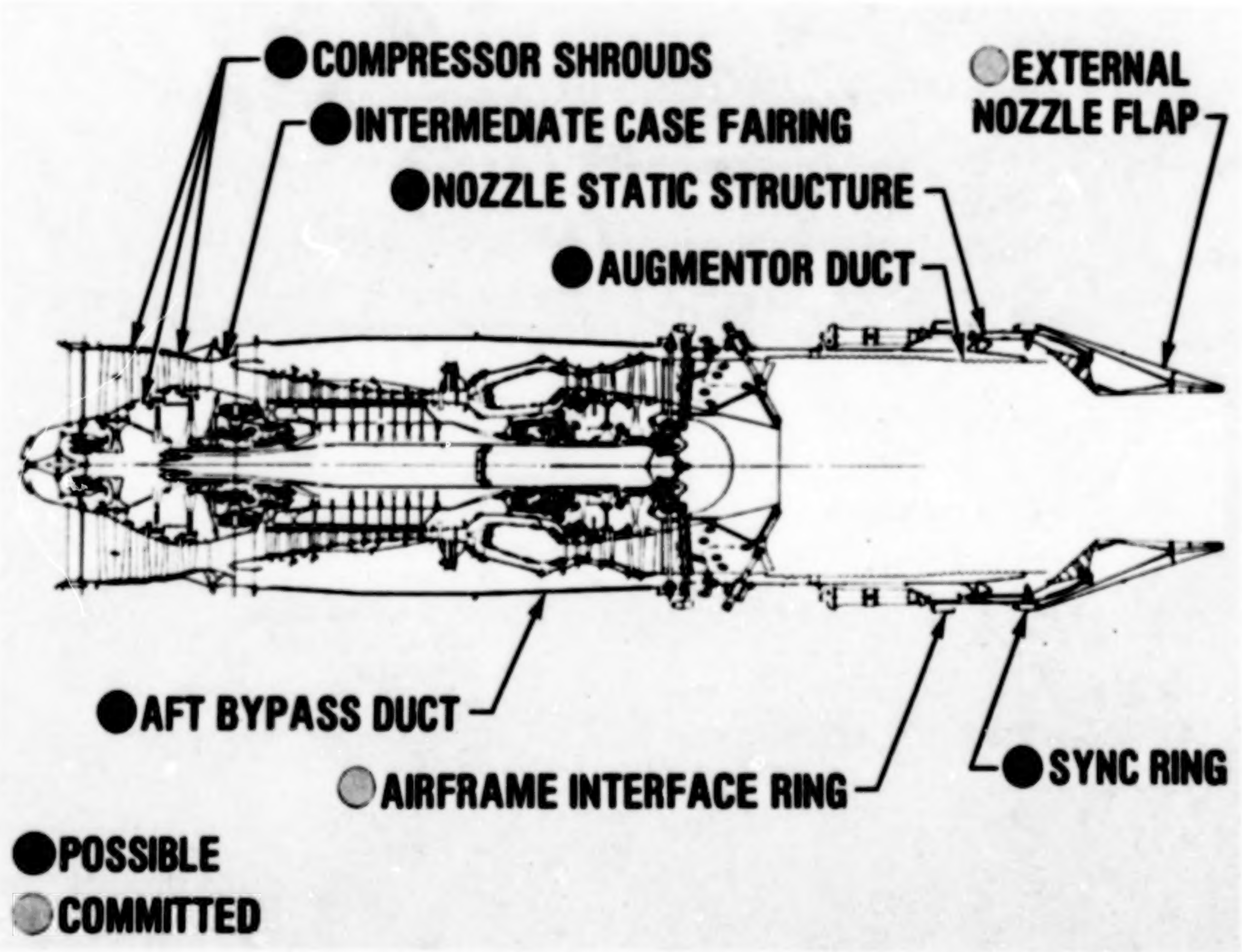
● COMPRESSOR SHROUDS
● INTERMEDIATE CASE FAIRING
● NOZZLE STATIC STRUCTURE
● AUGMENTOR DUCT
○ EXTERNAL NOZZLE FLAP
● AFT BYPASS DUCT
○ AIRFRAME INTERFACE RING
● SYNC RING
● POSSIBLE
○ COMMITTED

Figure 18

DC-9 DRAG REDUCTION

Figure 19 shows a photograph of a DC-9. The inserts schematically depict the design of the presently used metal reverser stang fairing and a composite redesigned fairing developed by Douglas Aircraft Company under the NASA Lewis Engine Component Improvement Program (ref. 19). Studies had shown that a redesigned fairing provided an opportunity to reduce baseline drag and would result in reduced fuel consumption. The fairing serves as the aft enclosure for the thrust reverser actuator system on the nacelle of the JT8D and is subjected to an exhaust temperature of 500° F during thrust reversal. A Kevlar fabric/PMR-15 composites fairing has been autoclave fabricated and flight tested. Compared to the metal component, the composite fairing resulted in a one percent airplane drag reduction (1/2 percent had been anticipated) and a 40-percent reduction in component weight.

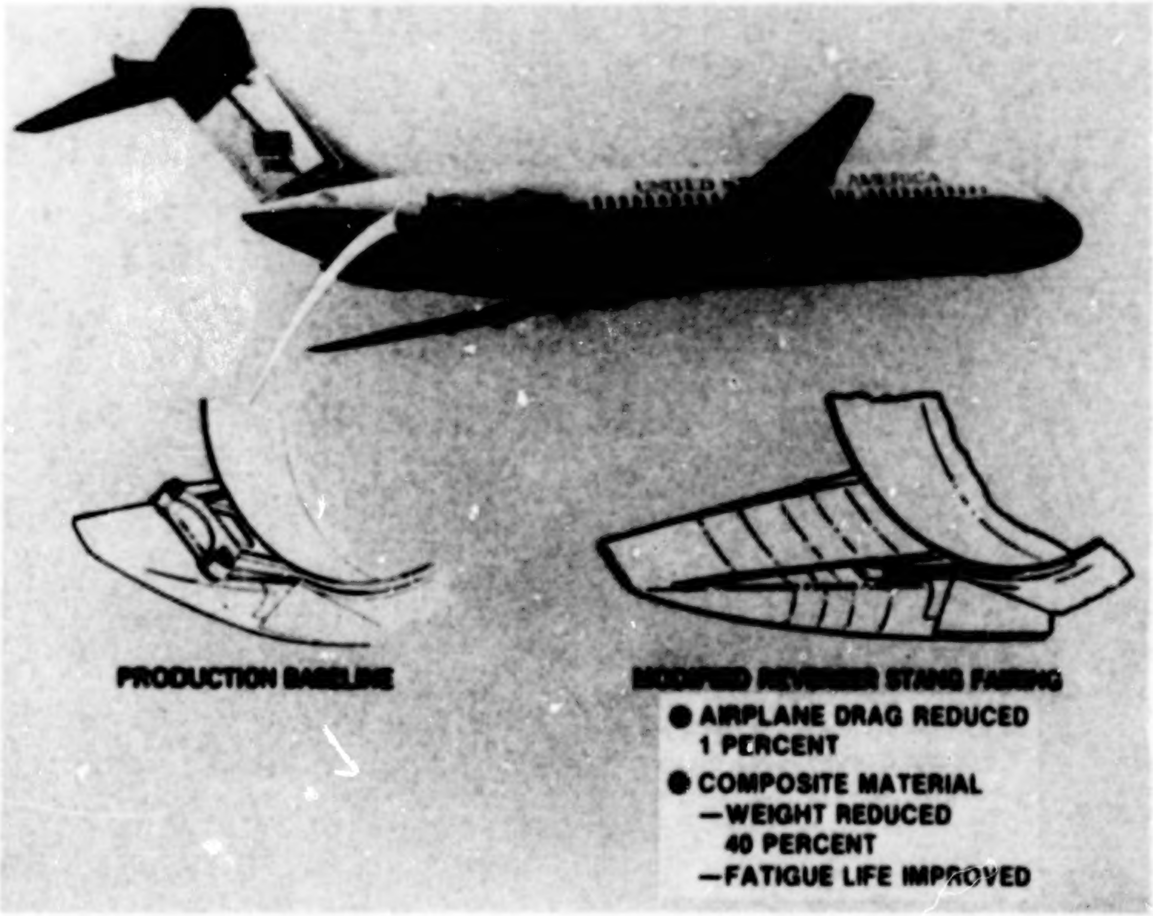
UNITED
AMERICA
PRODUCTION BASELINE
MODIFIED REVERSER STANG FAIRING
● AIRPLANE DRAG REDUCED
1 PERCENT
● COMPOSITE MATERIAL
—WEIGHT REDUCED
40 PERCENT
—FATIGUE LIFE IMPROVED

Figure 19

KEVLAR FABRIC/PMR-15 REVERSER STANG FAIRING

Figure 20 shows a photograph of the Kevlar fabric/PMR-15 reverser stang fairing. The weight of the composite fairing was found to be 40 percent less than the calculated weight of a fairing of the same shape made from aluminum.

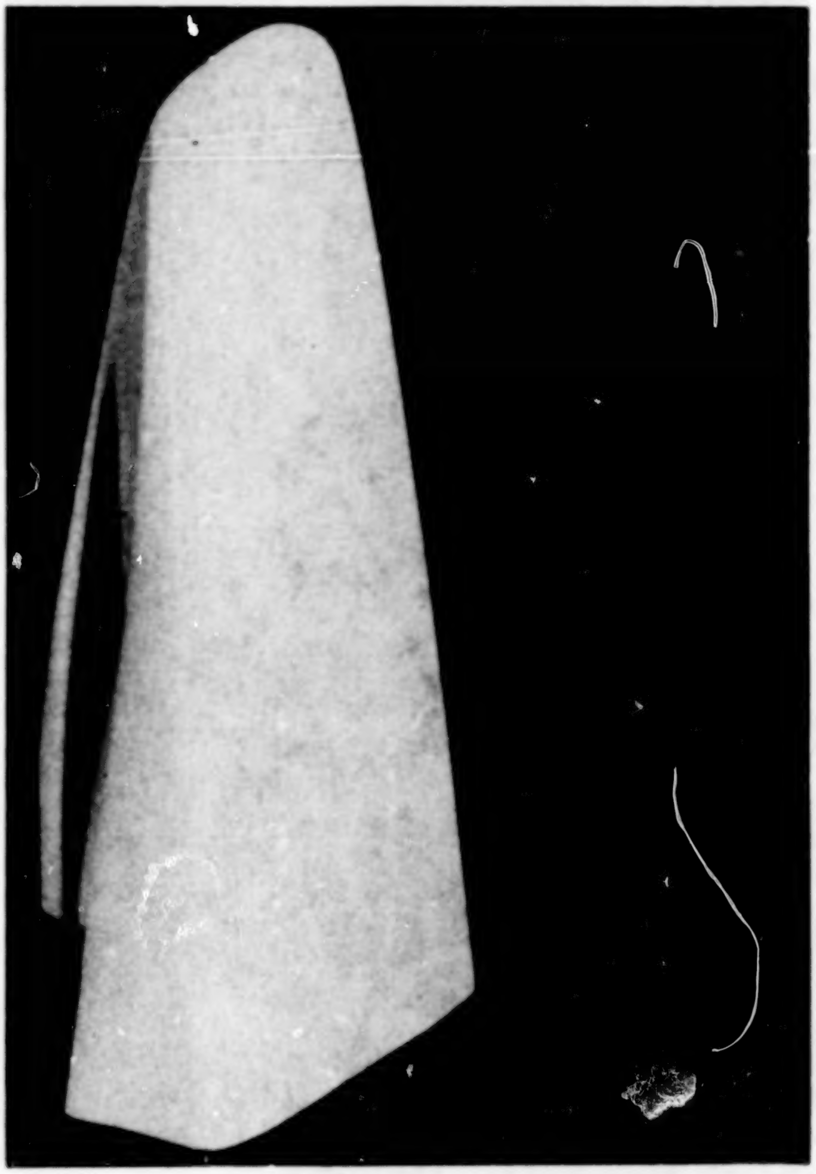

Figure 20

GLASS FABRIC/PMR-15 BEAM SHIELD INSTALLED ON MERCURY ION THRUSTER

Figure 21 shows a mercury ion thruster for an auxiliary propusion system being built by Hughes Space and Communications Group under contract to NASA Lewis. The ion propulsion system is scheduled for launch and testing on a future Shuttle flight. The thruster is equipped with a glass fabric/PMR-15 composite beam shield to protect the solar cell arrays and sensitive instrumentaion on the spacecraft from ion-beam damage. The composite shield (approximate dimensions: 10 in. diameter by 8 in. length by 0.040 in. thickness) was selected over tantalum and titanium because of weight and structural considerations. The feasibility of using a glass fabric/PMR-15 composites shield was initially demonstrated by in-house fabrication and testing of full-scale beam shields.

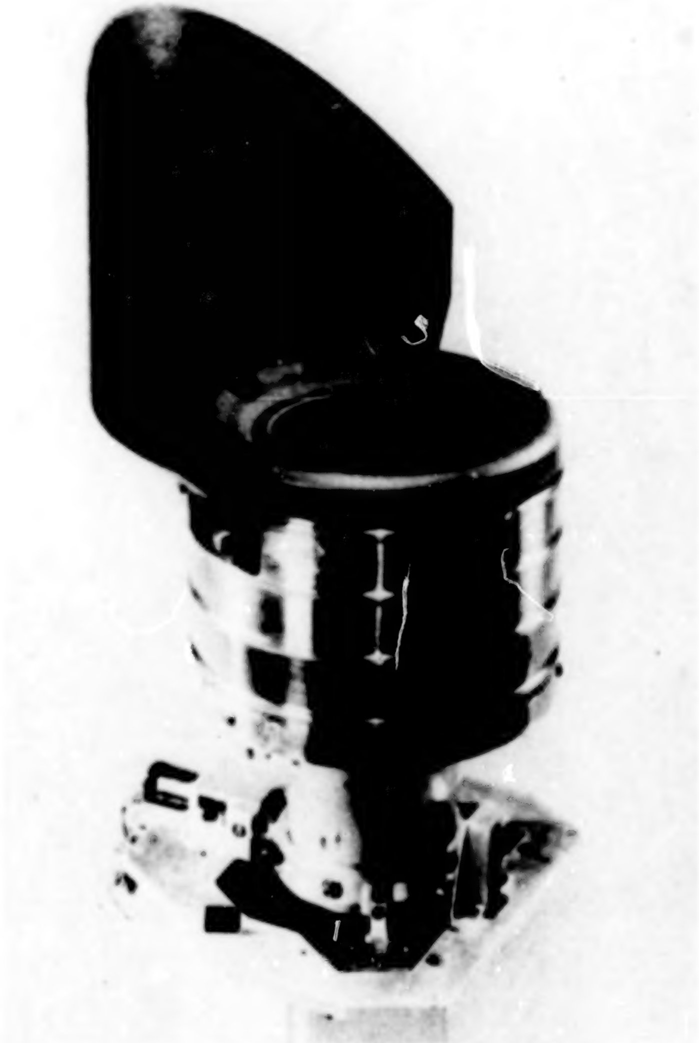

Figure 21

CONCLUDING REMARKS

The in situ polymerization of monomer reactants (PMR) approach has been demonstrated to be a powerful approach for solving many of the processing difficulties associated with the use of high-temperature resistant polymers as matrix resins in high-performance composites. PMR-15, the PMR polyimide discovered in the early seventies, provides the best overall balance of processing characteristics and elevated temperature properties. The excellent properties and commercial availability of composite materials based on PMR-15 have led to their acceptance as viable engineering materials. PMR-15 composites are currently being used to produce a variety of high-quality structural components. Increased use of these materials is anticipated in the future.

PMR-15 POLYIMIDE COMPOSITES:

- PROVIDE EXCELLENT PROCESSABILITY
- PROVIDE EXCELLENT HIGH TEMPERATURE PROPERTIES
- BEING ACCEPTED AS VIABLE ENGINEERING MATERIALS
- BEING USED TO FABRICATE HIGH QUALITY STRUCTURAL COMPONENTS

Figure 22

REFERENCES

1. Serafini, T. T.; Delvigs, P.; and Lightsey, G. R.: Thermally Stable Polyimides from Solutions of Monomeric Reactants, J. Appl. Polym. Sci., Vol. 16, 1972. pp. 905-915.

2. Serafini, T. T.; Delvigs, P.; and Lightsey, G. R.: Preparation of Polyimides from Mixtures of Monomeric Diamines and Esters of Polycarboxylic Acids, U.S. Patent 3,745,149, July 10, 1973.

3. Delvigs, P.; Serafini, T. T.; and Lightsey, G. R.: Addition-Type Polyimides from Solutions of Monomeric Reactants, NASA TN D-6877, 1972. (Also Proc. of 17th SAMPE National Symposium and Exhibition, April 1972.)

4. Serafini, T. T.; Vannucci, R. D.; and Alston, W. B.: Second Generation PMR Polyimides, NASA TM X-71894, 1976.

5. St. Clair, T. L. and Jewell, R. A.: Solventless LARC-160 Polyimide Matrix Resin. Proc. of 23rd SAMPE National Symposium and Exhibition, May 1978.

6. Serafini, T. T. and Vannucci, R. D.: Tailor Making High Performance Graphite Fiber Reinforced PMR Polyimides, NASA TM X-71616, 1975. (Also Proc. of 30th SPI RP/Composites Institute Conference, February 1975.)

7. Vannucci, R. D.: PMR Polyimides Modifications for Improved Prepreg Tack, NASA TM-82951, 1982.

8. Delvigs, P.: Lower-Curing-Temperature PMR Polyimides, NASA TM-82958, 1982.

9. Pater, R. H.: Novel Improved PMR Polyimides, NASA TM-82733, 1981. (Also Proc. of 13th SAMPE National Technical Conference, October 1981.)

10. Serafini, T. T.; Delvigs, P.; and Vannucci, R. D.: Curing Agent for Polyepoxides and Epoxy Resins and Composites Cured Therewith, U.S. Patent 4,244,857, January 13, 1981.

11. Chamis, C. C. and Sinclair, J. H.: Ten-Deg Off-Axis Test for Shear Properties in Fiber Composites, Experimental Mechanics, Vol. 17, No. 9, 1977, pp. 339-346.

12. Chamis, C. C. and Sinclair, J. H.: Durability/Life of Fiber Composites in Hygrothermomechanical Environments, Composite Materials: Testing and Design, Sixth Conference, ASTM STP 787, I. M. Daniel, Ed., ASTM 1982, pp. 498-512.

13. Halle, J. E.; Burger, E. D.; and Dundas, R. E.: Ultra-High Speed Fan Stage with Composite Rotor, NASA CR-135122, 1977.

14. Cavano, P. J.: Resin/Graphite Fiber Composites, NASA CR-134727, 1974.

15. Adamson, A. P.: Proc. of Conference on Quiet Powered-Lift Propulsion, NASA CP-2077, 1978, pp. 17-29.

16. Ruggles, C. L.: QCSEE Under-the-Wing Graphite/PMR Cowl Development, NASA CR-135279, 1978.

17. Stotler, C. L.: Proc. of Conference on Quiet Powered-Lift Propulsion, NASA CP-2077, pp. 83-109.

18. Stotler, C. L.: Development Program for a Graphite/PMR-15 Polyimide Duct for the F404 Engine, Proc. of 25th SAMPE National Symposium and Exhibition, May 1980, pp. 176-187.

19. Kawai, R. T. and Hrach, F. J.: Development of a Kevlar/PMR-15 Reduced Drag DC-9 Nacelle Fairing, AIAA-80-1194, AIAA/SAE/ASME 16th Joint Propulsion Conference, June 1980.

BLANK PAGE

FATIGUE AND FRACTURE RESEARCH IN
COMPOSITE MATERIALS

T. Kevin O'Brien
NASA Langley Research Center
Hampton, Virginia

INTRODUCTION

NASA Langley has a major research program to understand and characterize the fatigue, fracture, and impact behavior of composite materials (fig. 1). Bolted and bonded joints are included. The scope of this work is generic so that the solutions developed will be useful for a wide variety of structural applications. The analytical tools developed are used to demonstrate the damage tolerance, impact resistance, and useful fatigue life of structural composite components. Furthermore, much recent emphasis is on developing and analyzing standard tests for screening improvements in materials and constituents.

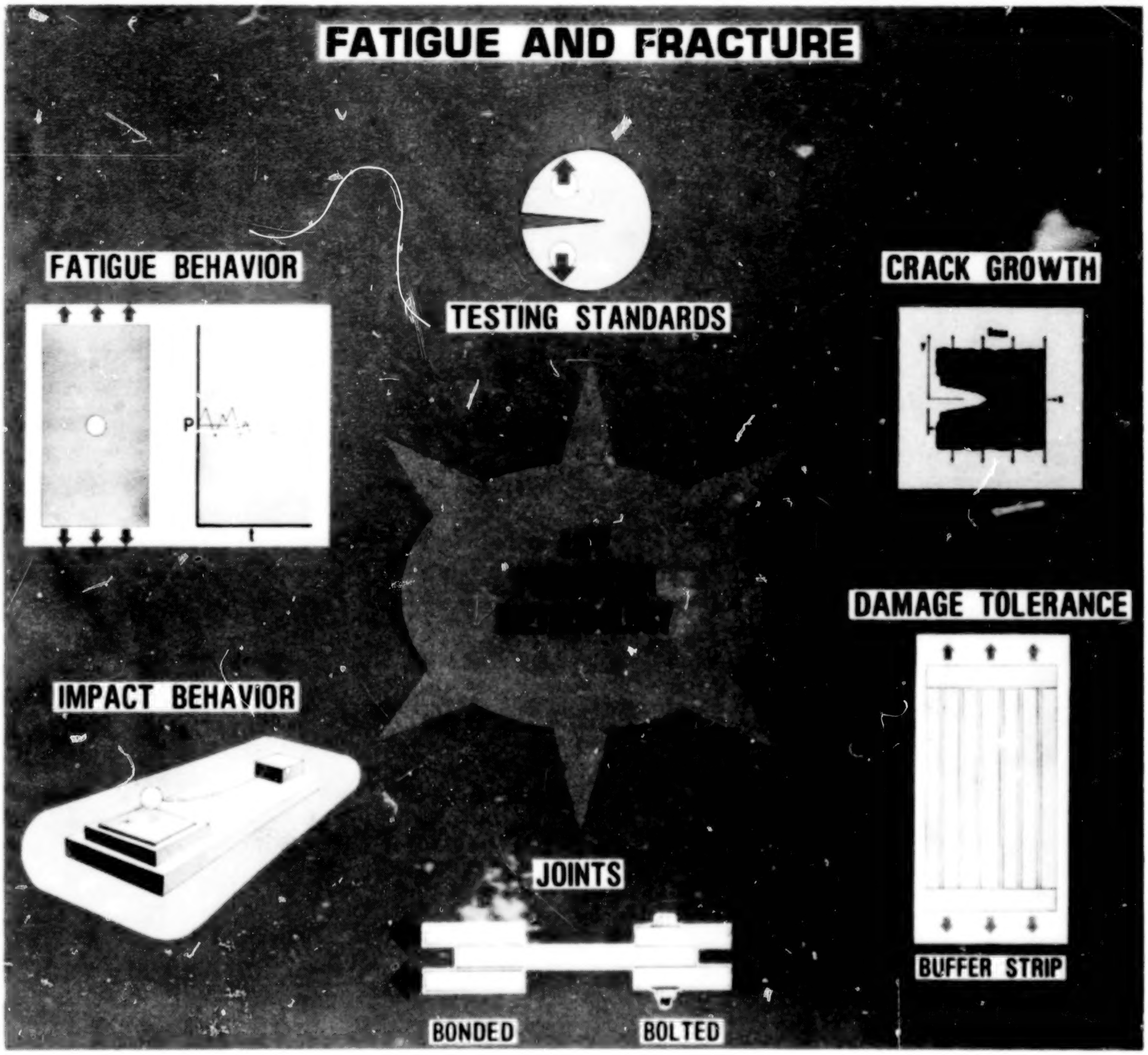
FATIGUE AND FRACTURE
FATIGUE BEHAVIOR
P
t
TESTING STANDARDS
CRACK GROWTH
DAMAGE TOLERANCE
BUFFER STRIP
IMPACT BEHAVIOR
JOINTS
BONDED
BOLTED

Figure 1

A UNIFYING STRAIN CRITERION TO PREDICT FRACTURE TOUGHNESS OF COMPOSITE LAMINATES

In references 1 and 2 a method was developed to predict composite fracture toughness from fiber and matrix properties. A laminate was assumed to fail when the strains at the crack tips in the principal load-carrying plies reach a critical level, regardless of layup. (See fig. 2.) The singular term in a series representation of the orthotropic strain field was chosen to represent the fiber strains. The fibers in the principal load-carrying plies were oriented at an angle θ to the applied load. The singular coefficient Q_c is given by $Q_c = K_Q\xi/E_y$, where K_Q is the usual stress intensity factor, E_y is the laminate modulus in the loading direction, and ξ is a function that depends only on the laminate elastic constants and the angle of the principal load-carrying plies. A critical level of strains at failure implies a constant value of Q_c, independent of ply orientations. Furthermore, Q_c is proportional to the ultimate tensile failing strain of the fibers, independent of the matrix material. (See fig. 2.) Therefore, the fracture toughness of all fibrous composite laminates can be computed from the ultimate tensile failing strain of the fibers and the elastic constants.

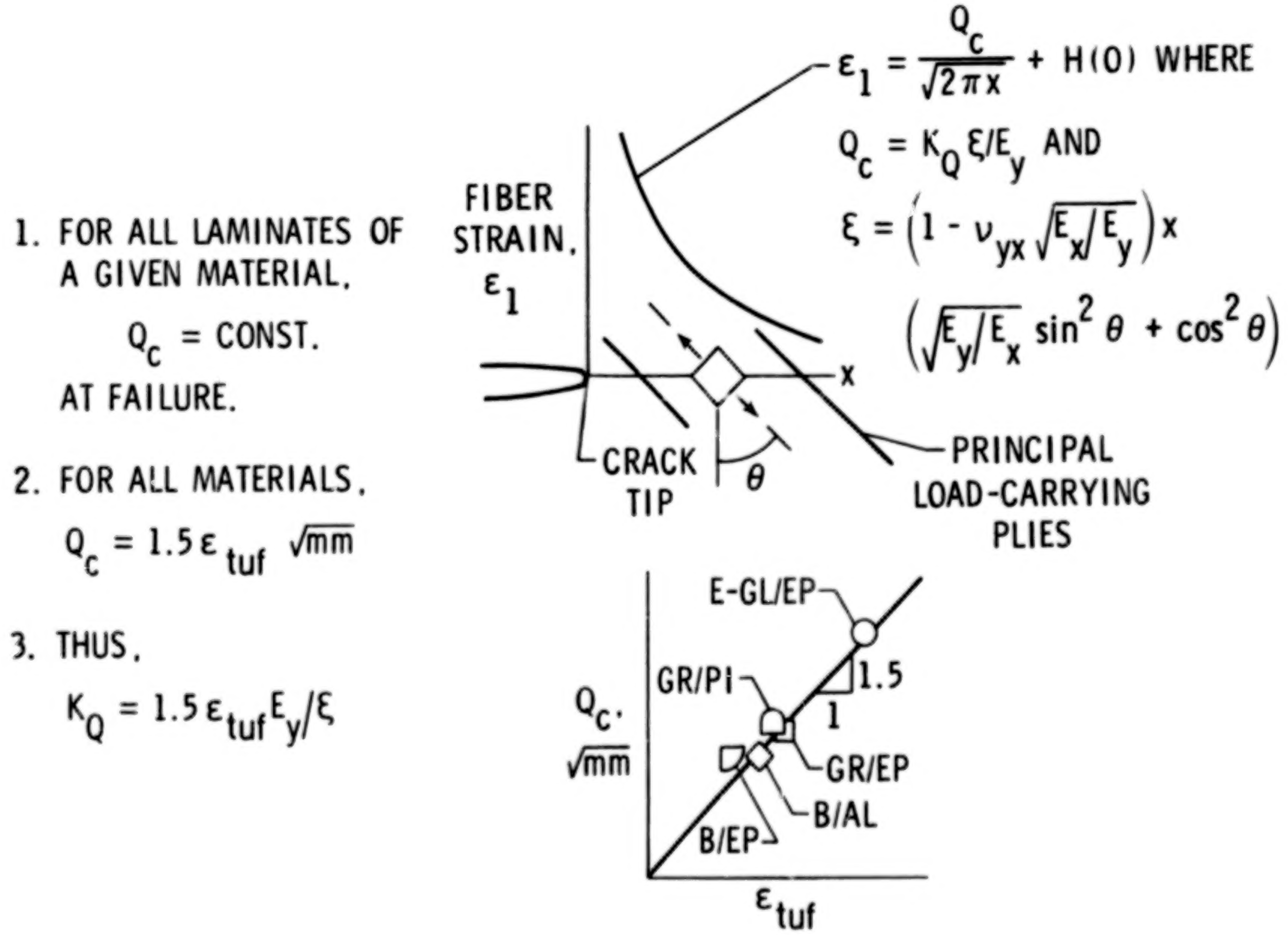

1. FOR ALL LAMINATES OF A GIVEN MATERIAL,
Q_c = CONST.
AT FAILURE.
2. FOR ALL MATERIALS,
$Q_c = 1.5\,\varepsilon_{tuf}\ \sqrt{mm}$
3. THUS,
$K_Q = 1.5\,\varepsilon_{tuf}E_y/\xi$
$\varepsilon_1 = \frac{Q_c}{\sqrt{2\pi x}} + H(0)$ WHERE
$Q_c = K_Q\,\xi/E_y$ AND
$\xi = \left(1 - \nu_{yx}\sqrt{E_x/E_y}\right)x$
$\left(\sqrt{E_y/E_x}\,\sin^2\theta + \cos^2\theta\right)$
FIBER STRAIN, ε_1
x
CRACK TIP
θ
PRINCIPAL LOAD-CARRYING PLIES
E-GL/EP
GR/PI
1.5
1
GR/EP
B/AL
B/EP
Q_c, $\sqrt{mm}$
ε_{tuf}

Figure 2

MEASURED AND PREDICTED VALUES OF FRACTURE TOUGHNESS

Figure 3 shows predicted and measured values of composite fracture toughness for a number of different layups and materials. The value of K_Q increases in proportion to fiber strength. Hence, the laminates with boron fibers have the highest K_Q and those with E-glass the lowest. The predictions, which are usually within 10 percent of the measurements, are quite good. The discrepancies between predicted and measured values of K_Q may be due largely to matrix and fiber failures at the crack tips that occur before overall failure. These crack tip failures, which alter the local fiber stresses, are not presently accounted for in the analysis. Micromechanical analyses are being developed that do account for these failures. In addition, experiments are being conducted to measure the type and extent of crack tip failures for various layups.

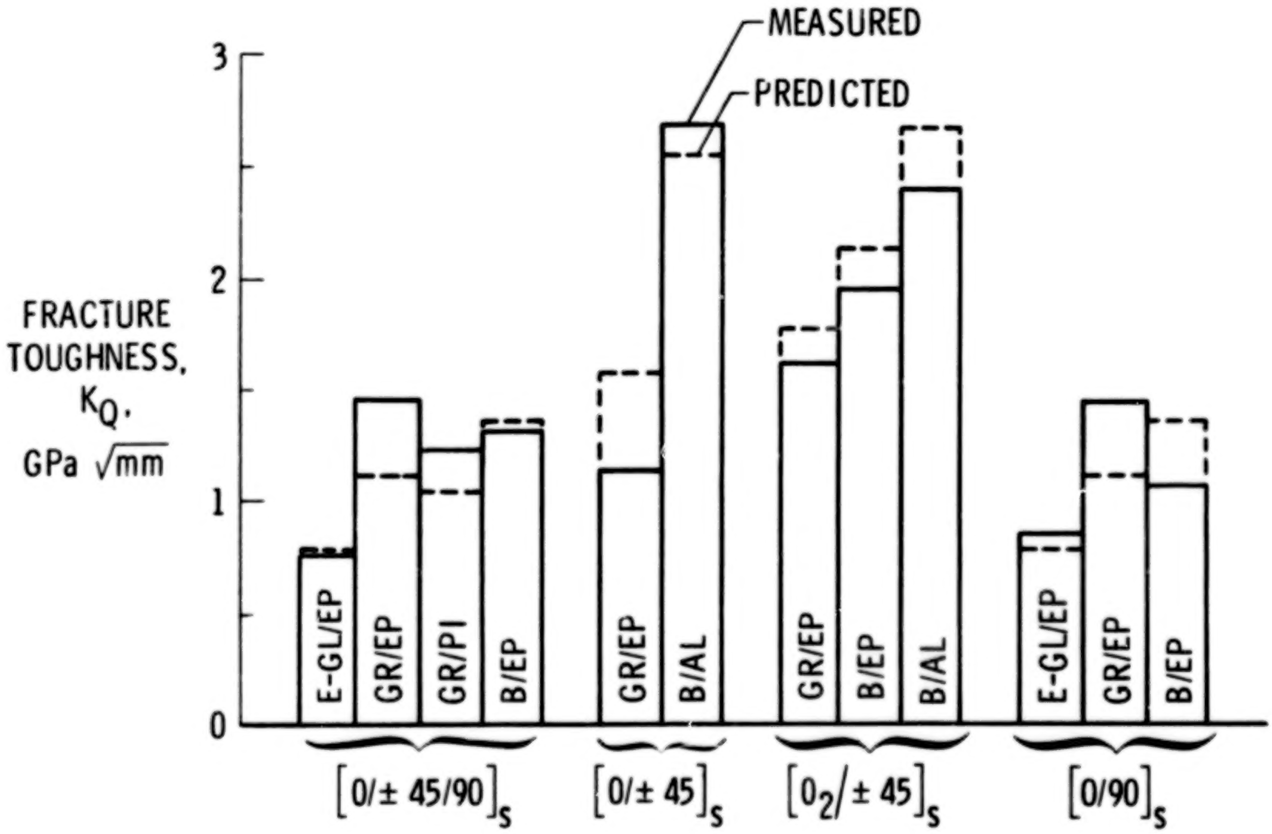

Figure 3

BEST DOCUMENT AVAILABLE

IMPROVING DAMAGE TOLERANCE OF COMPOSITE LAMINATES

WITH BUFFER STRIPS - TEST RESULTS

Buffer strips can greatly increase the tensile strength of damaged graphite/epoxy laminates while increasing weight only a little. In addition, recent work has shown that S-glass buffer strips can be woven into the 0° graphite plies with little additional expense (ref. 3). Figure 4 shows the remote strain for three quasi-isotropic panels containing center slits and S-glass buffer strips. Fracture initiates in panels with (filled symbols) and without (dashed curve) buffer strips at the same remote strain. However, the buffer strips arrest the fractures because they have a higher modulus of resilience than the graphite. The eventual failing strains of the panels are more than two times the strain at which the fracture initiated from the longest slit. Thus, in a damage tolerance situation, the strengths of these panels can be twice that of plain laminates.

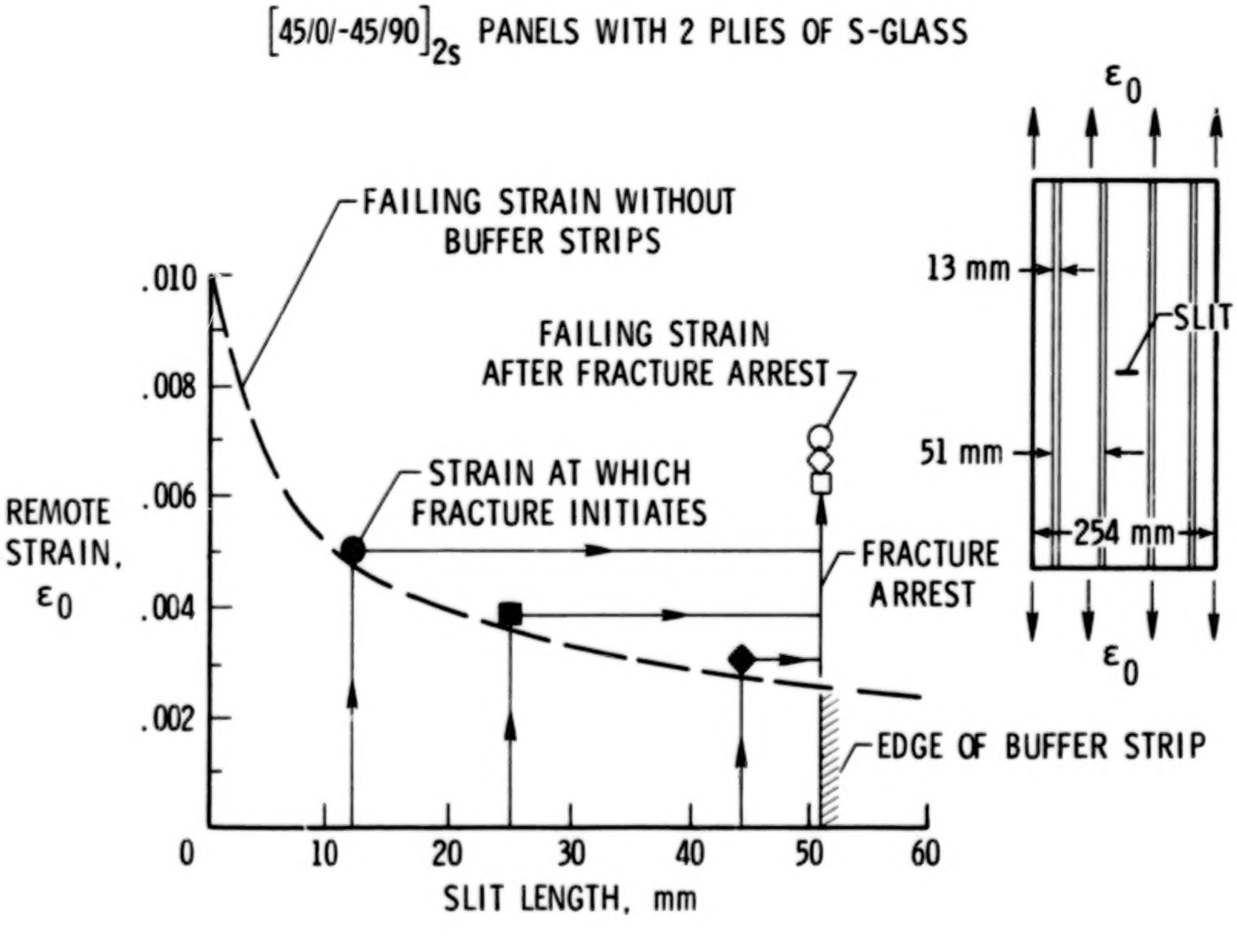

Figure 4

IMPROVING DAMAGE TOLERANCE OF COMPOSITE LAMINATES WITH BUFFER STRIPS - ANALYSIS

In addition to the buffer strip panels in figure 4, panels were also made with other buffer materials, various numbers of buffer plies and spacings, and various layups (ref. 3). Figure 5 shows the ratios of cracked to uncracked strength for these tests plotted against the buffer strip spacing (which is the arrested crack length) multiplied by the ratios of number of 0° plies and modulus of resilience for graphite to buffer material. Each symbol represents an average of three tests. Round symbols represent S-glass buffer strips; square symbols represent Kevlar buffer strips. Filled and open symbols differentiate between the two layups (shown in the key) used for the main panel material. A shear-lag analysis indicates that for large values of the abscissa, the strength ratio should vary inversely with the square root of the abscissa. S-glass has the highest modulus of resilience, and hence gives the highest strengths. For small values of the abscissa, the strengths are limited to the ultimate net section strength, which is 75 percent of the uncracked strength. (The buffer strip spacing, W_a, is 25 percent of the panel width.) The test data agree very well with this relationship. Additional tests are currently being conducted for a [illegible] buffer strip parameters and for woven buffer material. Tests are [illegible] conducted to determine the influence of environment and fatigue loading [illegible]gths. Furthermore, analyses are being developed to better predict the [illegible]hs in terms of the buffer strip parameters.

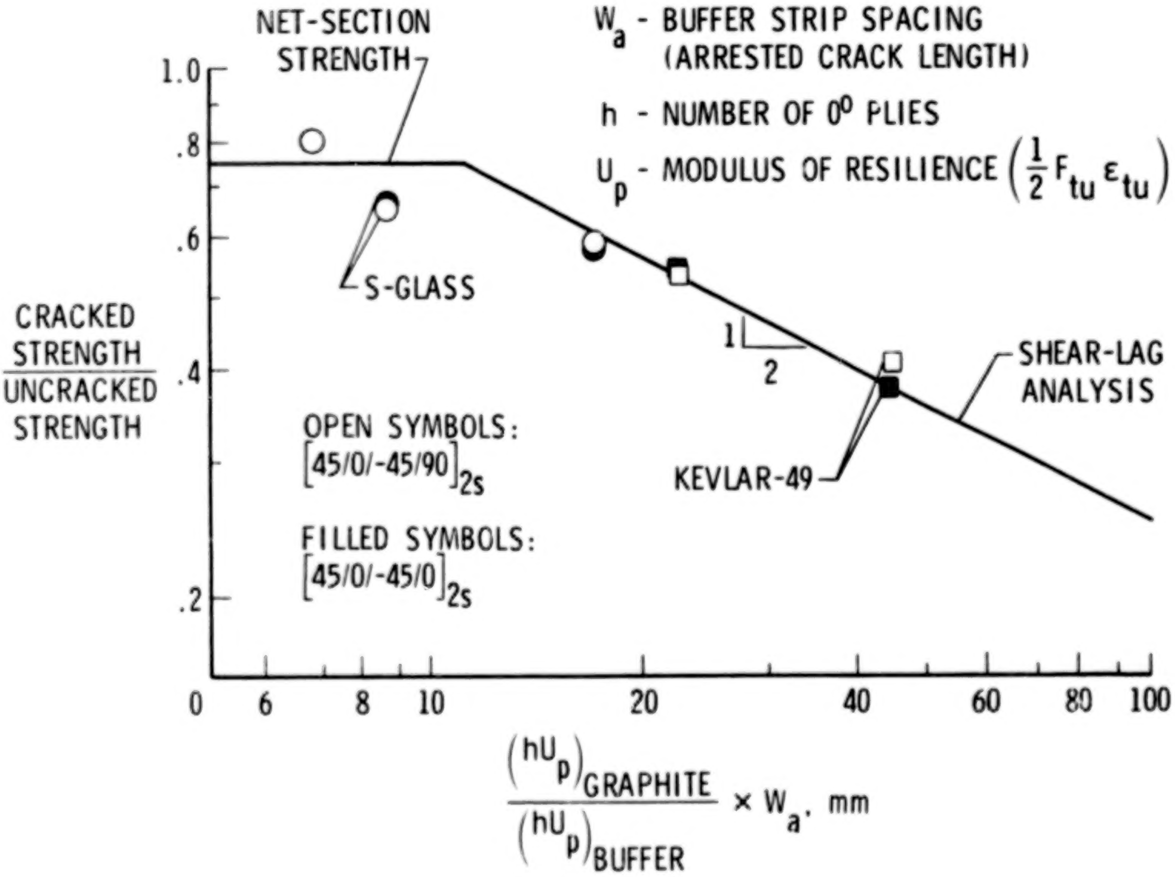

Figure 5

HOLE ELONGATION UNDER CYCLIC LOADING IN BOLTED COMPOSITE JOINTS

Bolt holes in composite joints can elongate under cyclic loading and thereby reduce joint stiffness. Single-fastener joints were tested in reference 4 using different combinations of tension-tension fatigue loading and bolt clampup torques. Figure 6 shows measured hole elongations from three tests that produced about the same fatigue life. This figure shows the influence of clampup on hole elongation. For the case of pin bearing with no clampup constraint, the figure shows that the bolt hole did not elongate before it failed in fatigue. But with "finger-tight" clampup and a higher cyclic stress, the hole elongated extensively before it failed. Much less elongation is shown for the third case, which has a typical 2.82 N·m clampup for the 6.35-mm-diameter bolt. Other tests were conducted to measure hole elongation and strength under static loading. Future research will focus on analyzing damage mechanisms for bearing-loaded holes.

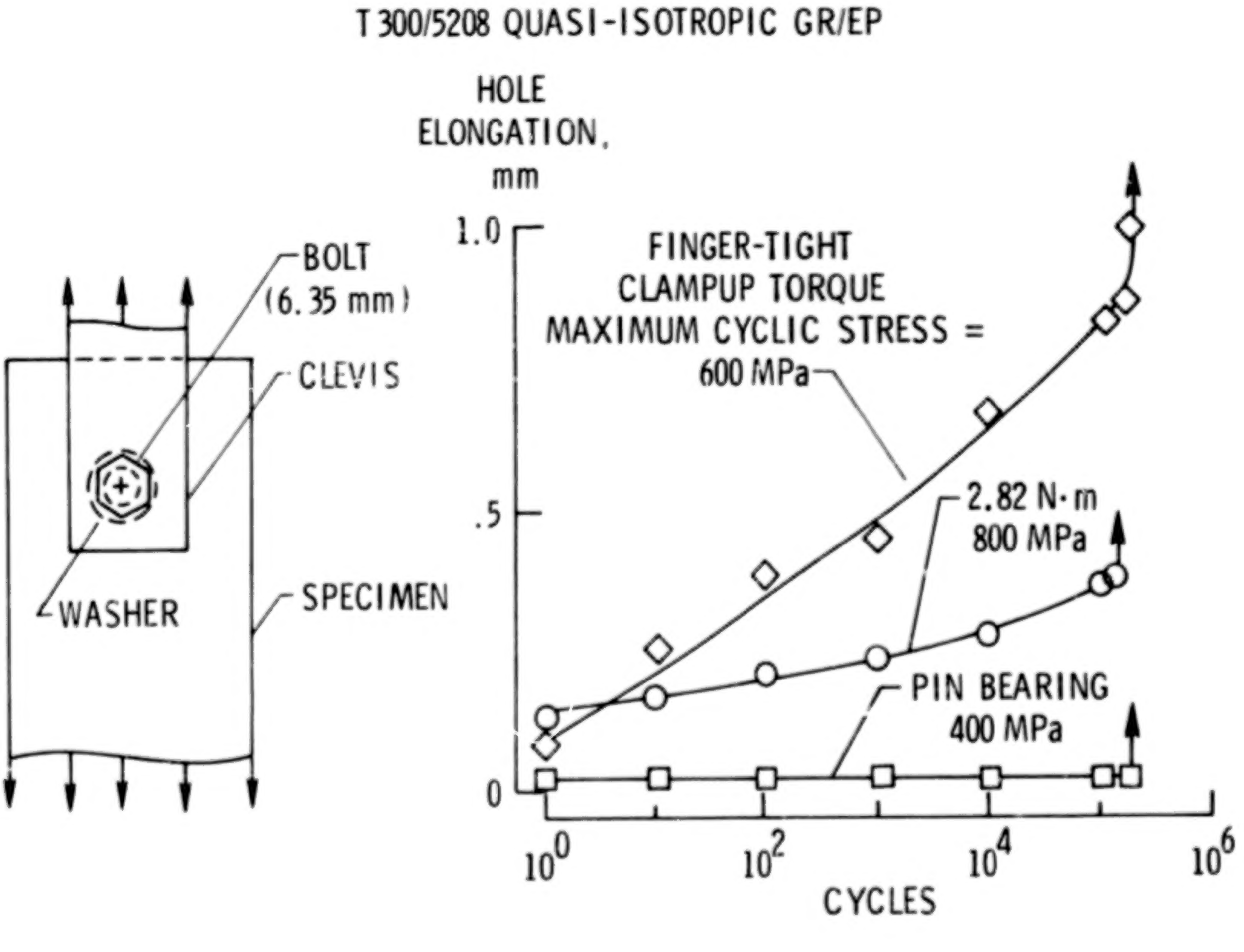

Figure 6

BOLT CLAMPUP RELAXATION

Recent studies have shown that bolt clampup improves the strength of composite joints. This improvement, however, may decrease somewhat if the bolt clampup force relaxes during long-term exposure. A viscoelastic relaxation analysis has been developed (ref. 5) for steady-state exposure conditions. A simple double-lap bolted joint was analyzed using a finite-element procedure. Typical results are shown as symbols in the accompanying figure 7. For the room-temperature-dry (RTD) reference case, relaxations of 8, 13, 20, and 30 percent were calculated for 1 day, 1 week, 1 year, and 20 years, respectively. As expected, moisture increased the clampup relaxation compared to the RTD case. Reference 5 also includes results for elevated-temperature exposures. In addition to the finite-element analyses, a simple empirical equation was developed to calculate clampup relaxation. First, this equation was fitted (dashed curve) to the RTD finite-element results to establish two constants (F_1 and n). Then the equation was generalized to account for moisture by substituting viscoelastic shift factors a_{TH} from the literature. The solid curves show that this equation agrees quite closely with the finite-element results. Recently, this equation was extended to account for transient environments (ref. 6).

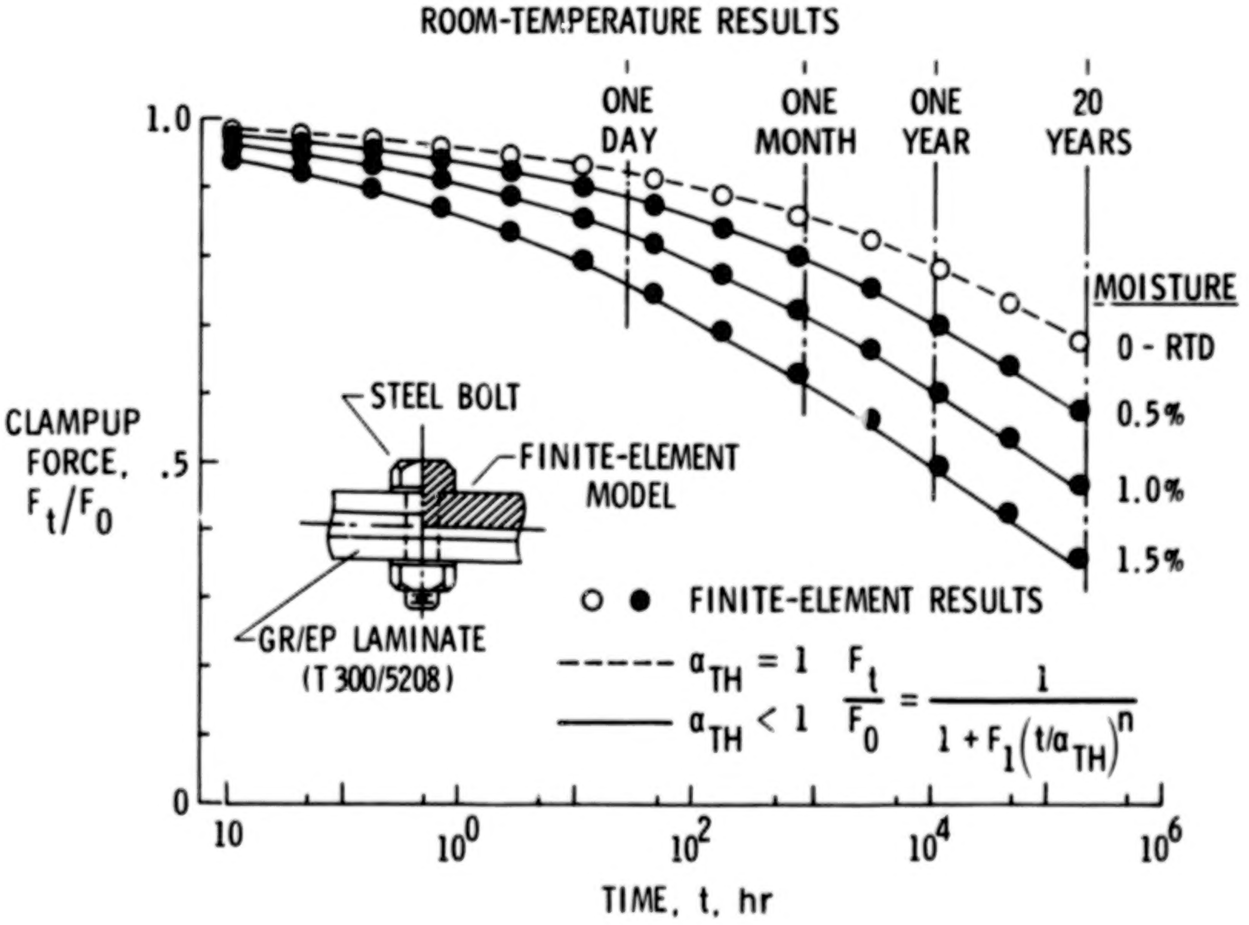

Figure 7

3-D STRESSES AT LAMINATE BOLT HOLES

High interlaminar stresses develop near holes in composite laminates. These interlaminar stresses were analyzed in reference 7 for a $[0/90]_s$ graphite/epoxy laminate with a circular hole and remote uniaxial loading. These stresses were calculated using a 3-D finite-element model with a very high mesh refinement near the ply interface. Typical stress results are presented in figure 8, and for convenience they are normalized by the remote stress S_g. The two curves in this figure represent the interlaminar normal and shear stresses, σ_z and $\sigma_{z\theta}$, respectively, along the hole boundary. These stresses provide a basis for locating delaminations at laminate holes. The 3-D finite-element procedures are currently being extended to calculate interlaminar stresses due to thermal and hygroscopic effects.

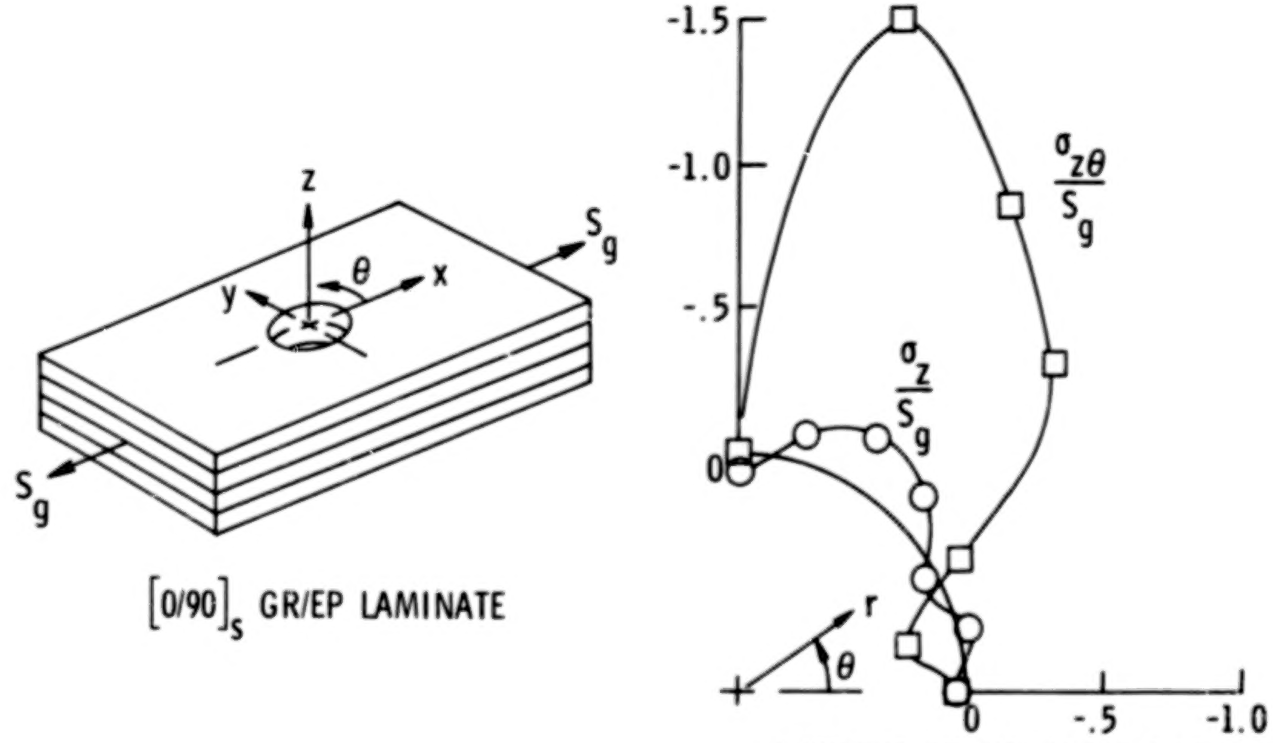

$[0/90]_s$ GR/EP LAMINATE

STRESSES AT 0/90 INTERFACE

Figure 8

DAMAGE THRESHOLD UNDER LOW-VELOCITY IMPACT OF COMPOSITES

Low-velocity impact can easily damage composite laminates by delaminating bonded layers or breaking fibers. Impact damage was studied to analyze the impact mechanics, determine failure criteria, and develop a simple impact test method. The test device consists of a hardened 1-inch-diameter steel ball at the end of a cantilevered rod (fig. 9). The ball strikes a 4-inch-square composite plate that is bonded to an aluminum support plate. The support plate has a circular aperture ranging in diameter from 1/2 to 3-1/2 inches. The ball and laminate are wired so that while they are in contact a circuit is completed and contact time is recorded on an oscilloscope. The expected impact duration, maximum impact force, and maximum shear and flexural stresses are calculated from an analysis based on the static first-mode deformations. The predicted durations and the test results agree within ±3 percent. The criteria for failure were found to be matrix ultimate shear stress and fiber ultimate stress. The right-hand figure shows that the analysis correctly predicts the damage threshold within about ±10 percent.

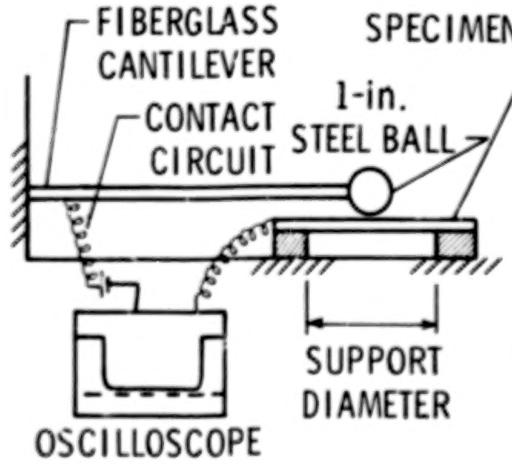

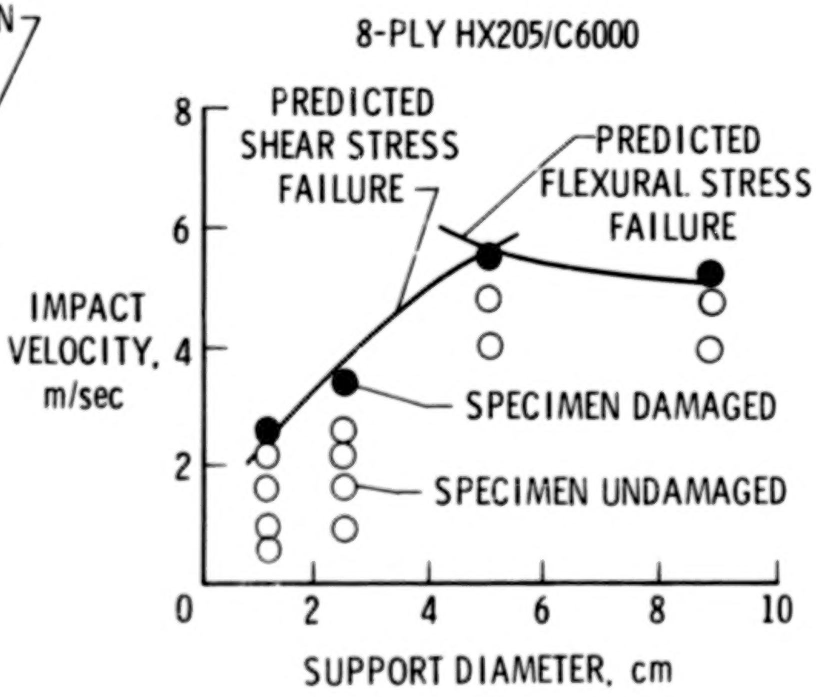

- MEASUREMENTS
  - VELOCITY OF IMPACT
  - DURATION OF IMPACT
- MODEL
  - DYNAMIC ANALYSIS OF DURATION, FORCE, ETC.
  - ONLY FIRST-MODE DEFORMATIONS CONSIDERED

- MODEL FAILURE PREDICTION AGREES WITH EXPERIMENT TO WITHIN ±10%

Figure 9

COMPOSITE IMPACT SCREENING BY STATIC INDENTATION TESTS

Graphite/epoxy laminates can lose up to 50 percent of their original strength from low-velocity impact damage. For laminates up to at least 16 plies, a static indentation test on a specimen bonded between two aperture plates yields failures almost identical to the failures from an impact (ref. 8). A static test, however, allows sufficient time for analysis of the failure sequence (fig. 10). The load deflection curve for an undamaged plate with a small span is shown in the left figure; the flexural stiffness from the shear strength of the matrix transfers most of the load to the supports. Damage progression occurs as matrix shear failure causes delaminations to grow, until only a membrane of delaminated fibers supports the load. Then membrane failure controls penetration load. For this configuration, matrix shear strength dominates the low-level impact damage, and the extent of delamination is limited by the fiber toughness. The figure on the right indicates that for larger aperture plates, failure is dominated by the failure energy of the overall membrane. Matrix failure, in this case, releases little energy; failure here is governed predominantly by fiber strength.

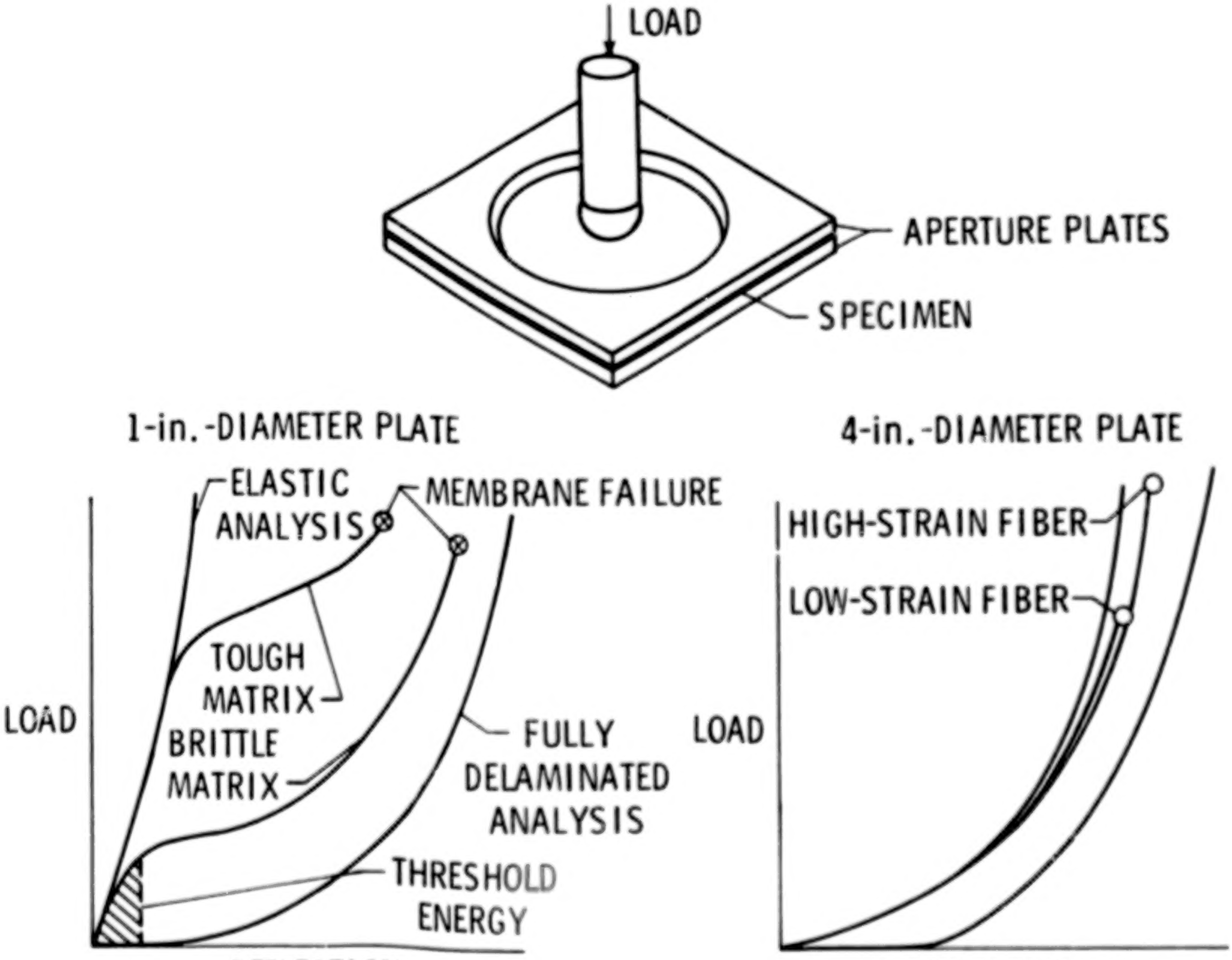
LOAD
APERTURE PLATES
SPECIMEN
1-in.-DIAMETER PLATE
ELASTIC ANALYSIS
MEMBRANE FAILURE
TOUGH MATRIX
LOAD
BRITTLE MATRIX
FULLY DELAMINATED ANALYSIS
THRESHOLD ENERGY
DEFLECTION
4-in.-DIAMETER PLATE
HIGH-STRAIN FIBER
LOW-STRAIN FIBER
LOAD
DEFLECTION

Figure 10

STRAIN ENERGY RELEASE RATE FOR DELAMINATION GROWTH DETERMINED

A simple expression was derived for the strain energy release rate, G, for edge delamination growth in an unnotched laminate (ref. 9). This simple expression shown in figure 11 has several advantages. First, G is independent of delamination size. It depends only on the applied strain, ε, the specimen thickness, t, the stiffness of the undamaged laminate, E_{LAM}, and the stiffness of the laminate when it was completely delaminated, E^*. Second, E_{LAM} and E^* can be calculated from simple laminated-plate theory. Third, because E^* depends on the location of the delaminated interface(s), E^*, and hence G, are sensitive to the location of damage in the laminate thickness. The simple equation was used to develop criteria to predict the onset and growth of delaminations in realistic, unnotched laminates.

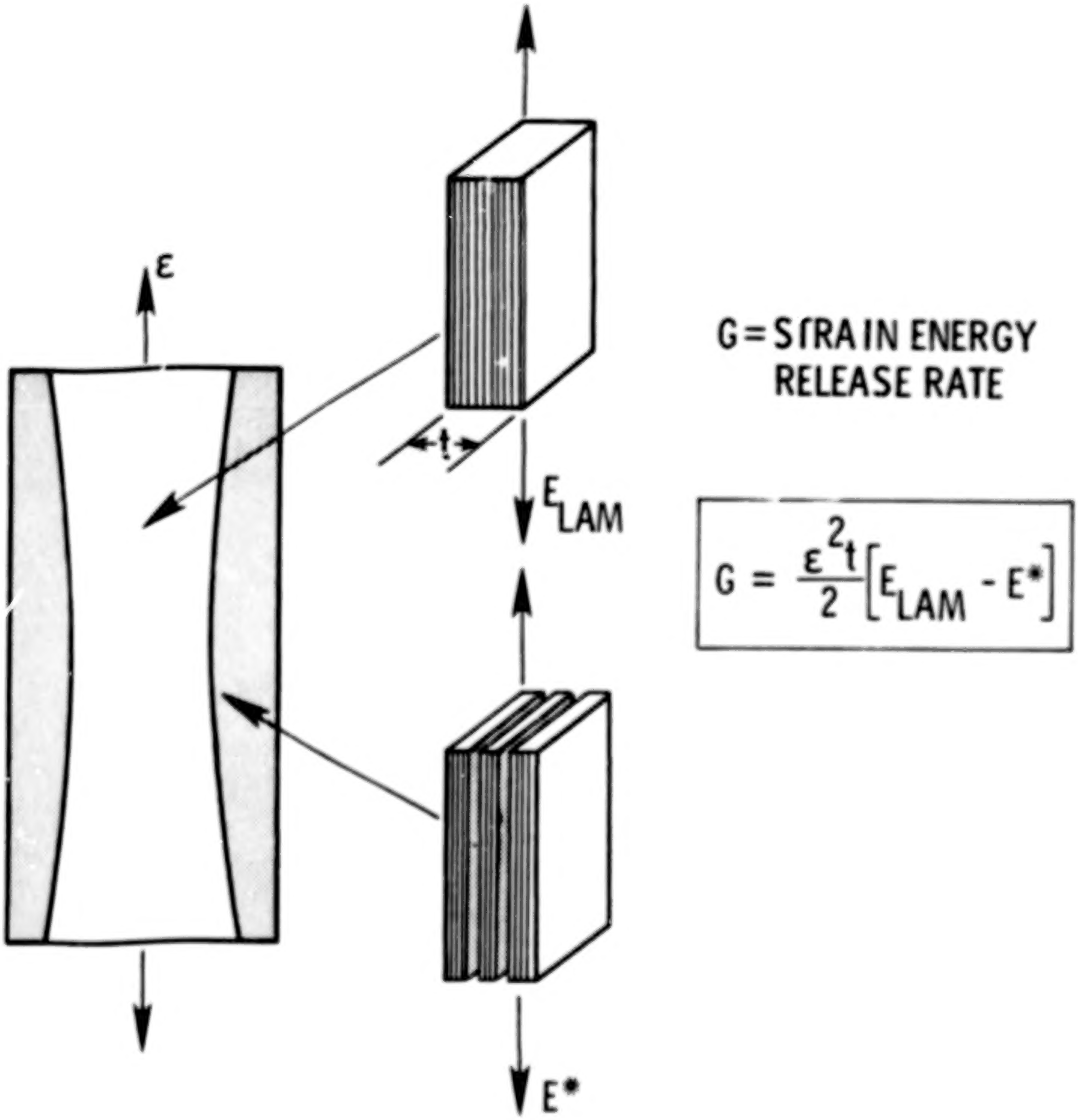

$$G = \frac{\varepsilon^2 t}{2}\left[E_{LAM} - E^*\right]$$

Figure 11

DELAMINATION ONSET PREDICTED

To predict the onset of delaminations in realistic unnotched laminates (ref. 9), quasi-static tension tests were conducted on the $[\pm 30/\pm 30/90/\overline{90}]_s$ laminates. The applied strain recorded at the onset of delamination, ε_c, was used to calculate a critical strain energy release rate, G_c. Then, G_c was used to predict the onset of delamination in more complex laminates. Figure 12 shows data and predictions for three $[+45_n/-45_n/0_n/90_n]_s$ laminates all having the same layup but with different ply thicknesses. For example, n = 1 is an 8-ply laminate, n = 2 is a 16-ply laminate, and n = 3 is a 24-ply laminate. The predictions agreed well with experimental data, indicating that G_c was a material property. Furthermore, the trend of lower ε_c for thicker laminates was correctly predicted. This trend could not be predicted by a critical interlaminar stress criterion.

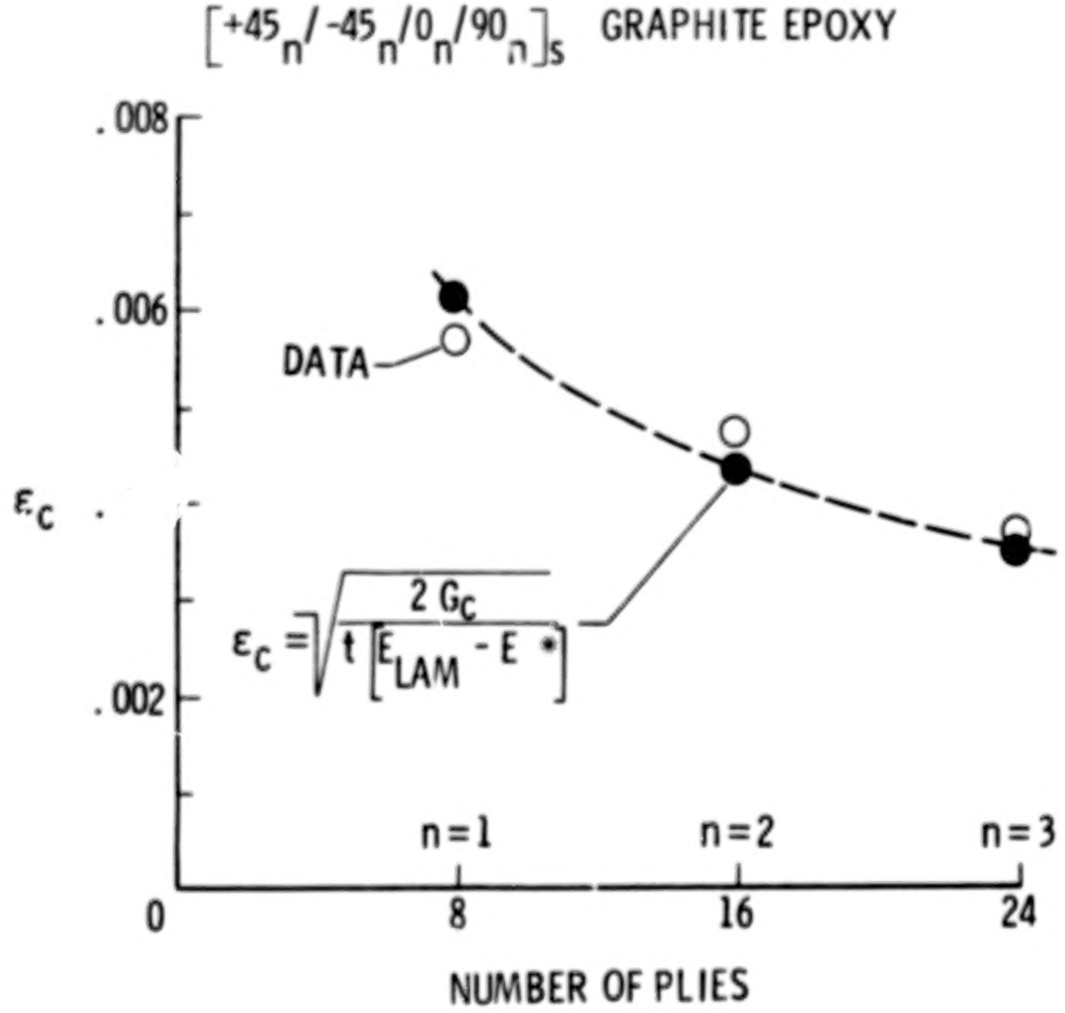

$$\varepsilon_c = \sqrt{\frac{2\,G_c}{t\left[E_{LAM} - E^*\right]}}$$

Figure 12

EDGE DELAMINATION TENSION TEST MEASURES

INTERLAMINAR FRACTURE TOUGHNESS

A simple test has been developed for measuring the interlaminar fracture toughness of composites made with toughened matrix resins (ref. 10). The test involves measuring the stiffness, E_{LAM}, and nominal strain at onset of delamination, ε_c, during a tension test of an 11-ply $[\pm 30/\pm 30/90/\overline{90}]_s$ laminate (fig. 13). These quantities, along with the measured thickness t, are substituted into a closed-form equation for the strain energy release rate, G, for edge delamination growth in an unnotched laminate (ref. 9). The E^* term in the equation is the stiffness of the $[\pm 30/\pm 30/90/\overline{90}]_s$ laminate if the 30/90 interfaces were completely delaminated. It can be calculated from the simple rule of mixtures equation shown in figure 13 by substituting the laminate stiffness measured during tension tests of $[\pm 30]_s$ and $[90]_n$ laminates. The critical value of G_c at delamination onset is a measure of the interlaminar fracture toughness of the composite. This edge delamination test is being used by Boeing, Douglas, and Lockheed under the NASA ACEE (Aircraft Energy Efficiency) Key Technologies contracts to screen toughened resin composites for improved delamination resistance (ref. 11).

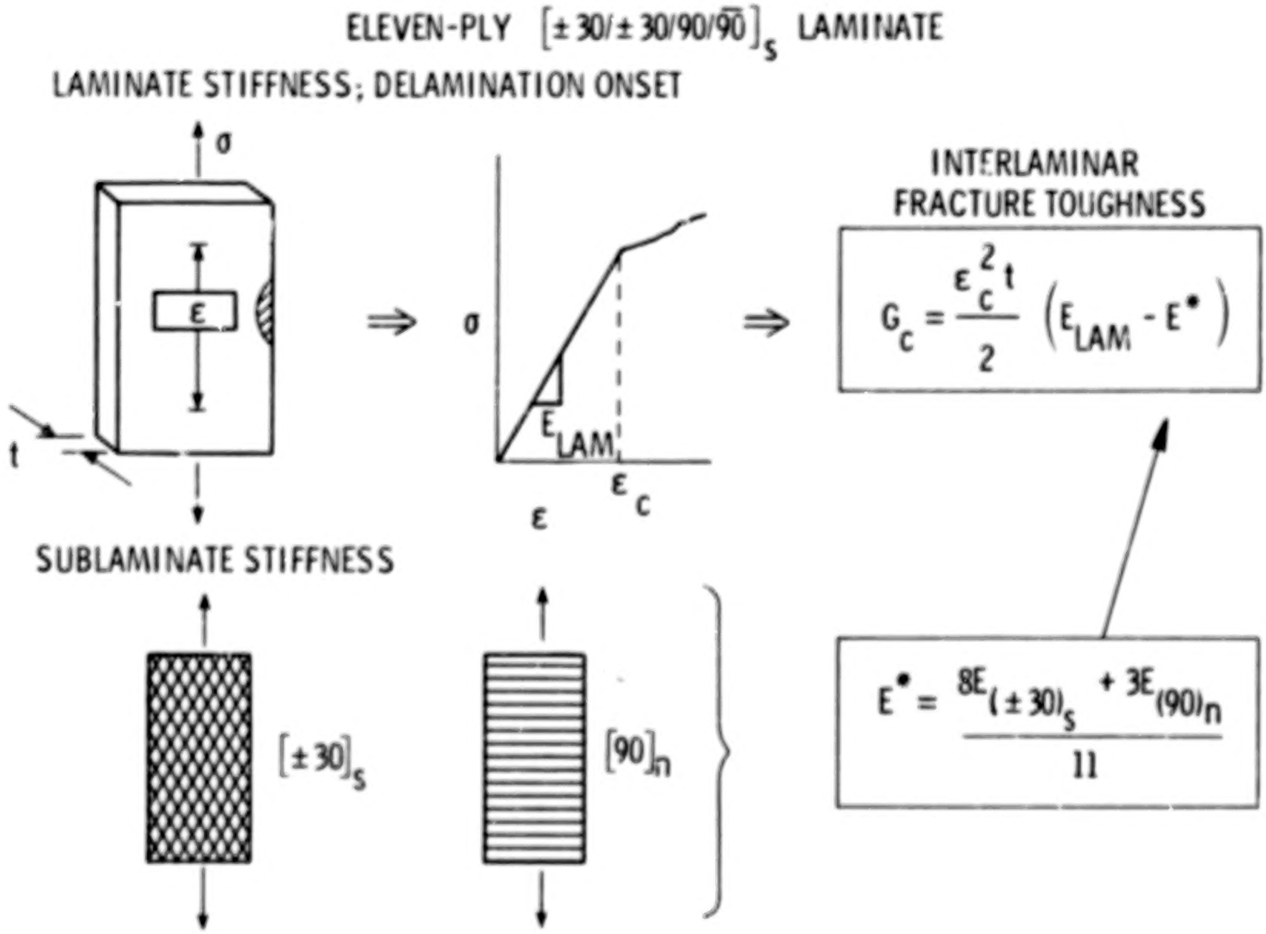
ELEVEN-PLY $[\pm 30/\pm 30/90/\overline{90}]_s$ LAMINATE
LAMINATE STIFFNESS; DELAMINATION ONSET
σ
ε
t
σ
E_{LAM}
ε_c
ε
INTERLAMINAR FRACTURE TOUGHNESS
$G_c = \frac{\varepsilon_c^2 t}{2}\left(E_{LAM} - E^*\right)$
SUBLAMINATE STIFFNESS
$[\pm 30]_s$
$[90]_n$
$E^* = \frac{8E_{(\pm 30)_s} + 3E_{(90)_n}}{11}$

Figure 13

MIXED-MODE STRAIN ENERGY RELEASE RATES DETERMINED

A quasi-three-dimensional finite-element analysis (ref. 12) was performed to determine the relative crack opening (mode I) and shear (mode II) contributions of the $[\pm 30/\pm 30/90/\overline{90}]_s$ edge delamination specimen (ref. 10). Delaminations were modeled in the 30/90 interfaces where they were observed to occur in experiments. Figure 14 indicates that the total G represented by G_I plus G_{II} reaches a value prescribed by the closed-form equation derived from laminated-plate theory and the rule of mixtures. Furthermore, like the total G, the G_I and G_{II} components are also independent of delamination size. In addition, the percentage, G_I/G_{II}, is fixed for a particular layup and does not change significantly for different resin composites as long as the laminates have the same kinds of fibers.

FINITE ELEMENT ANALYSIS OF MIXED MODE PERCENTAGES

$[\pm 30/\pm 30/90/\overline{90}]_s$ LAMINATE

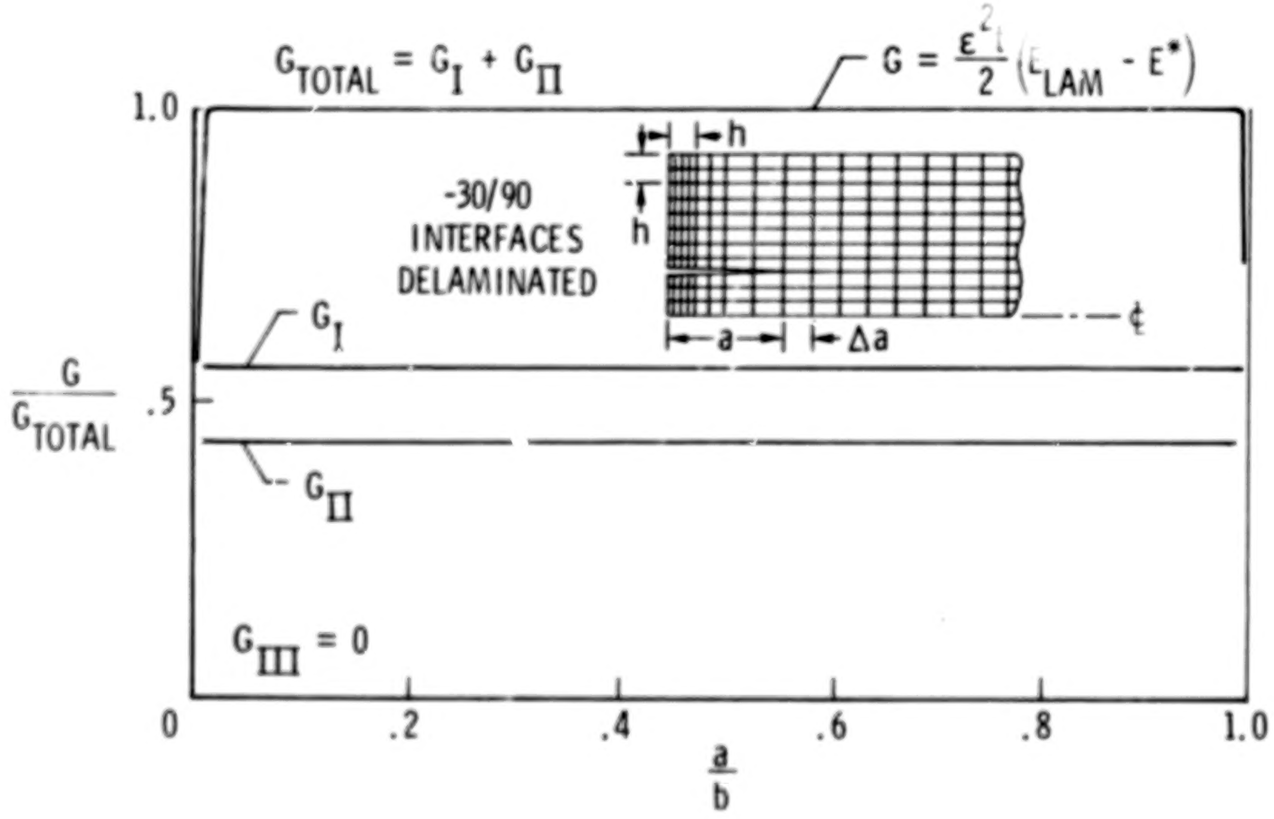

Figure 14

BEST [illegible]

INTERLAMINAR FRACTURE TOUGHNESS OF GRAPHITE COMPOSITES MEASURED

Two test methods are being developed to measure the interlaminar fracture toughness of graphite-reinforced composites (ref. 10). The first is a pure crack opening (mode I) double-cantilever-beam test. The second is the NASA-developed crack opening and shear, mixed-mode (modes I and II), edge delamination tension test (refs. 10 and 11). Figure 15 shows results of these measurements for a relatively brittle 350°F-cure epoxy (5208), a tougher 250°F-cure epoxy (H-205), and a still tougher rubber-toughened 250°F-cure epoxy (F-185). Results indicate that for the brittle epoxy, even in the mixed-mode test, only the crack opening fracture mode contributes to delamination. However, for the tougher 250°F-cure epoxy and its rubber-toughened version, both the crack opening and shear fracture modes contribute to delamination. Hence, although both tests indicate relative improvements among materials, one test alone is not sufficient to quantify interlaminar fracture toughness.

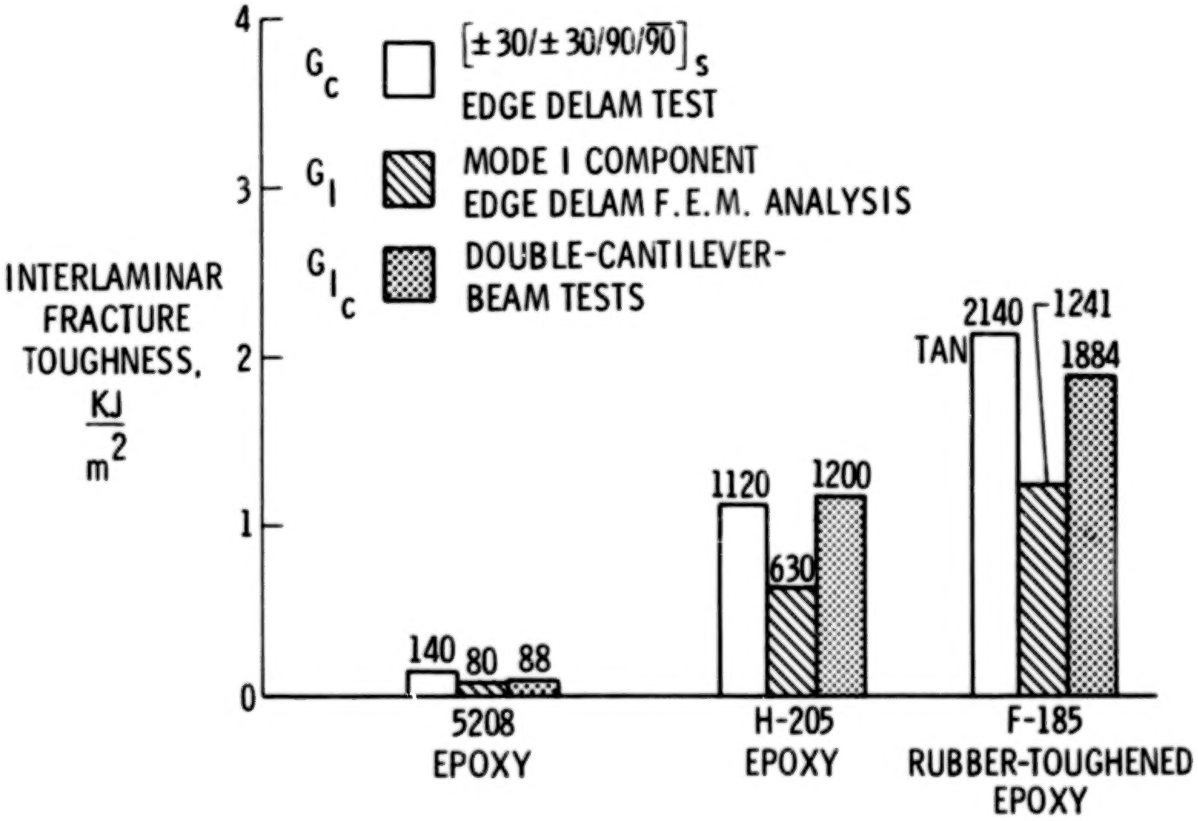

Figure 15

INVESTIGATION OF INSTABILITY-RELATED DELAMINATION GROWTH

Under compression load fatigue, delaminations in composites sometimes induce localized buckling, causing high interlaminar stresses at the ends of the delamination. Rapid delamination growth and loss of structural stability often ensue. Because delamination growth can lead to structural instability, the growth process must be understood. To improve our understanding, through-width delaminations (fig. 16) were studied experimentally and analytically (ref. 13). The figure shows a comparison of measured growth rates and calculated strain energy release rates, which are a measure of the intensity of stresses at the crack tip. In the figure, G_I and G_{II} are the energy release rates related to peel and shear stresses, respectively. Note that both G_I and the growth rate first increase then decrease rapidly with crack extension; G_{II} increases monotonically and does not reflect the change in growth rate. Apparently, the rate of delamination growth is governed by the intensity of the peel stress field. Hence, prediction of crack growth depends on an accurate assessment of the peel stress field around the crack tip. Further work will concentrate on quantifying the relationship between calculated peel stress or related parameters (e.g., G_I) and delamination growth rates.

COMPARISON OF STRAIN-ENERGY-RELEASE RATES AND DELAMINATION GROWTH RATES

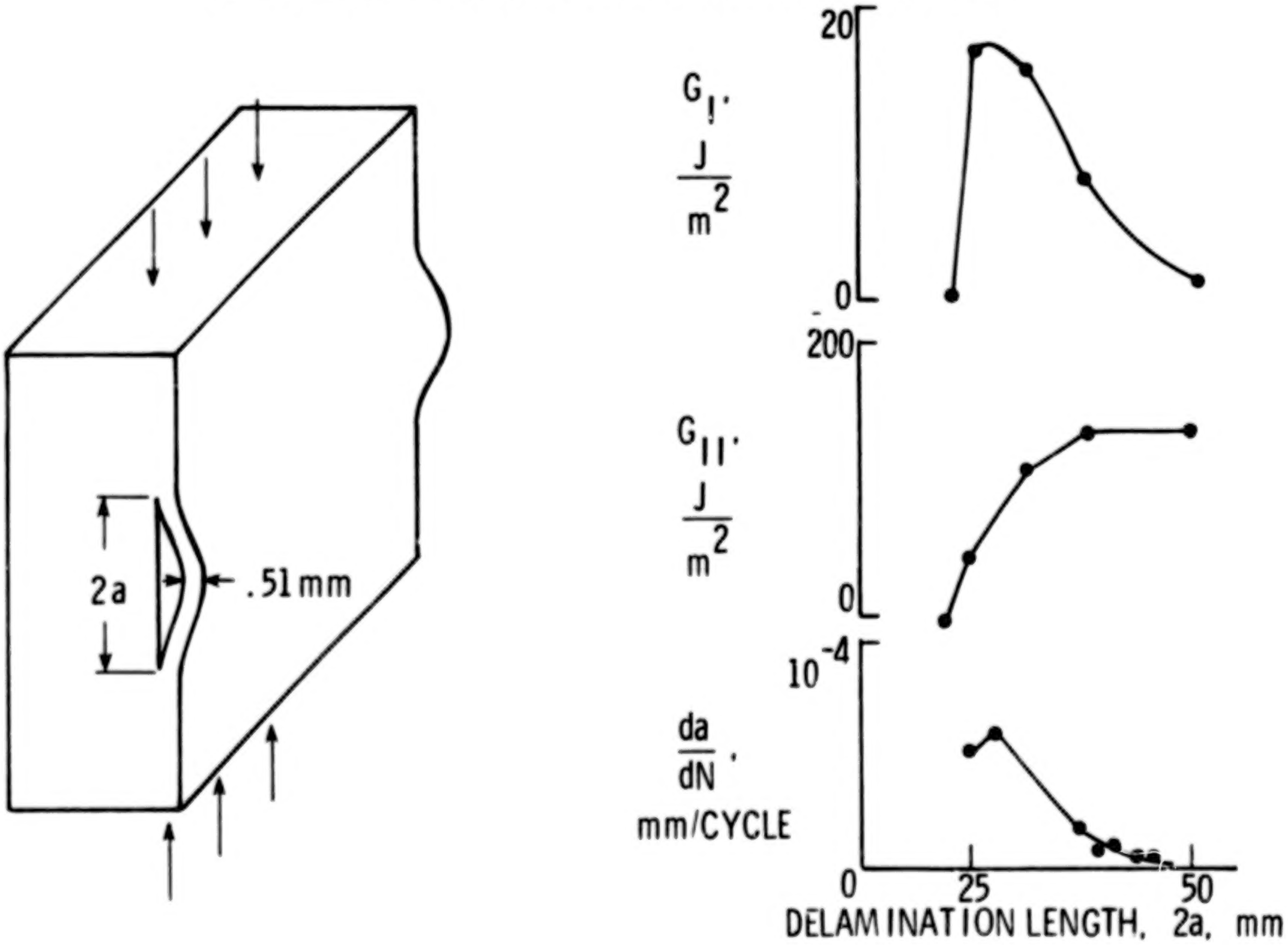

Figure 16

TEST METHODS FOR COMPRESSION FATIGUE OF COMPOSITES

Test methods developed for the fatigue evaluation of airframe metals, primarily aluminum alloys, may not be appropriate for composites. The results of two investigations (ref. 15) aimed at development of test methods for composites loaded primarily in cyclic compression are shown in figure 18. The left side of the figure shows the results of simple cyclic load tests that were conducted to select a method for preventing column buckling in fatigue tests of thin coupons containing an open hole. The test results show that the best configuration is one that does not limit the localized buckling that develops near the hole due to fatigue-induced delaminations. Limiting the localized buckling causes the test to yield an unrealistically long life estimate. The right side of the figure shows the results of simulated flight loading tests that were conducted to determine what parts of the flight load spectrum could be deleted from the simulation to shorten test time without affecting the test result. The results show that deletion of 90 percent of the low loads did not change the test life very much, but that deletion of just a few of the rare, high loads led to very long test lives. Therefore, to be on the safe side in tests on composite structure, the high loads must not be deleted from the test spectrum as would normally be done in tests on aluminum structure.

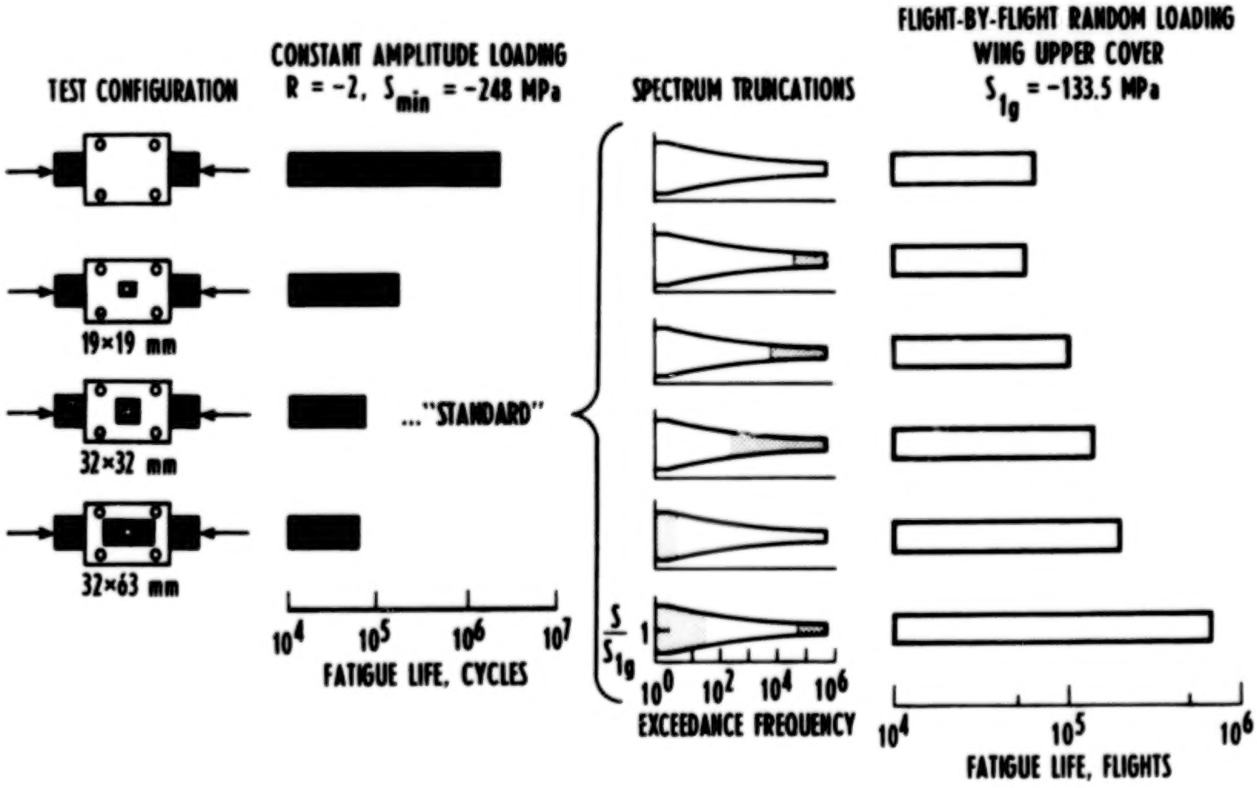

Figure 18

TEST METHODS FOR COMPRESSION FATIGUE OF COMPOSITES

Test methods developed for the fatigue evaluation of airframe metals, primarily aluminum alloys, may not be appropriate for composites. The results of two investigations (ref. 15) aimed at development of test methods for composites loaded primarily in cyclic compression are shown in figure 18. The left side of the figure shows the results of simple cyclic load tests that were conducted to select a method for preventing column buckling in fatigue tests of thin coupons containing an open hole. The test results show that the best configuration is one that does not limit the localized buckling that develops near the hole due to fatigue-induced delaminations. Limiting the localized buckling causes the test to yield an unrealistically long life estimate. The right side of the figure shows the results of simulated flight loading tests that were conducted to determine what parts of the flight load spectrum could be deleted from the simulation to shorten test time without affecting the test result. The results show that deletion of 90 percent of the low loads did not change the test life very much, but that deletion of just a few of the rare, high loads led to very long test lives. Therefore, to be on the safe side in tests on composite structure, the high loads must not be deleted from the test spectrum as would normally be done in tests on aluminum structure.

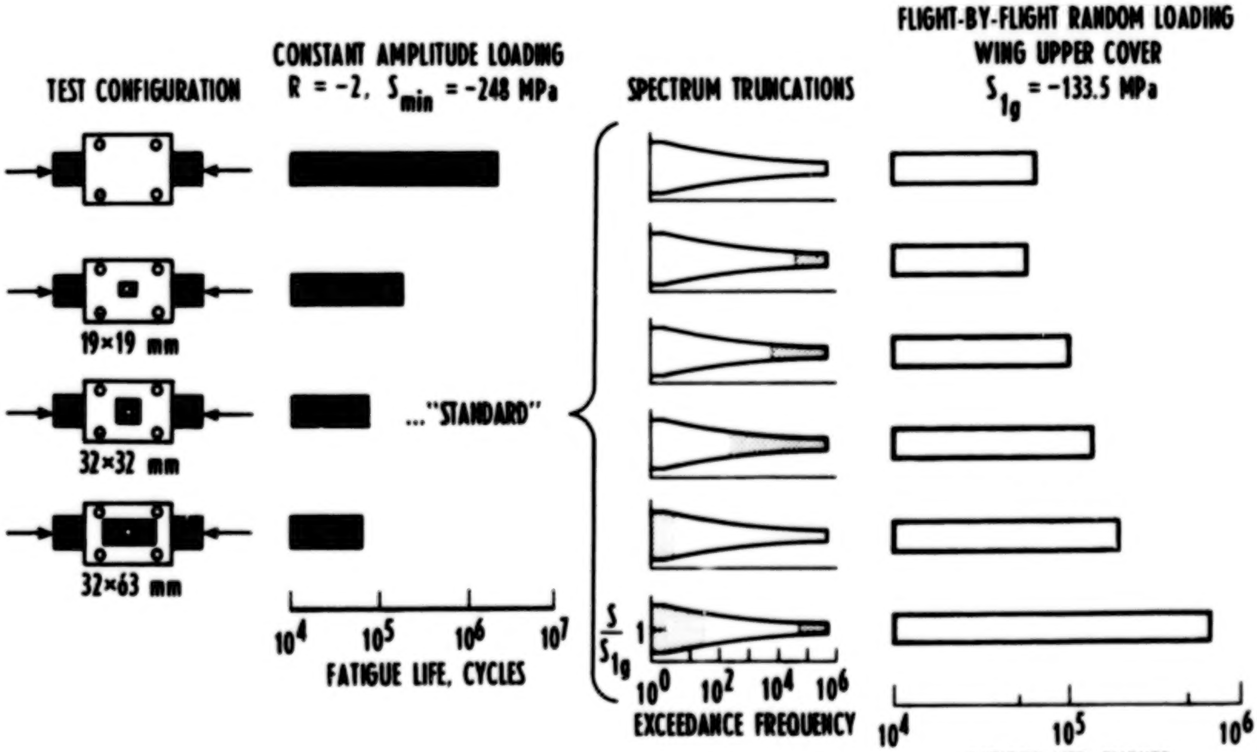

Figure 18

BEST DOCUMENT AVAILABLE

FATIGUE DAMAGE IN BORON/ALUMINUM LAMINATES

Because an aluminum matrix has a modulus 20 times higher than a polymer matrix, matrix cracking in aluminum matrix composites strongly influences laminate stiffness. After long periods of fatigue loading, matrix cracks form in boron/aluminum composites and stiffness may drop significantly (ref. 16). A simple analysis has been developed to predict these laminate stiffness reductions due to fatigue (ref. 17). The analysis is based upon the elastic modulus of the fiber and matrix, fiber volume fraction, fiber orientation, and cyclic-hardened yield stress of the matrix material. It readily predicts the laminate secant modulus of the composite at the stabilized damage state (after approximately 500,000 cycles) for a given cyclic stress range or cyclic strain range. Figure 19 illustrates the agreement between prediction and experiment. The material is $[0_2/\pm45]_s$ boron/aluminum, with a fiber volume fraction of 0.45. The solid line represents the predicted laminate stiffness loss. Since the relation between cyclic stress range and cyclic strain range does not depend upon stress ratio, either can be used to predict secant modulus degradation. The secant modulus is shown to decrease with increasing stress or strain range. This particular laminate's secant modulus dropped over 40 percent without impending failure. The data were generated under either strain-controlled or load-controlled conditions.

$[0_2/\pm45]_s$ AND $[\pm45/0_2]_s$

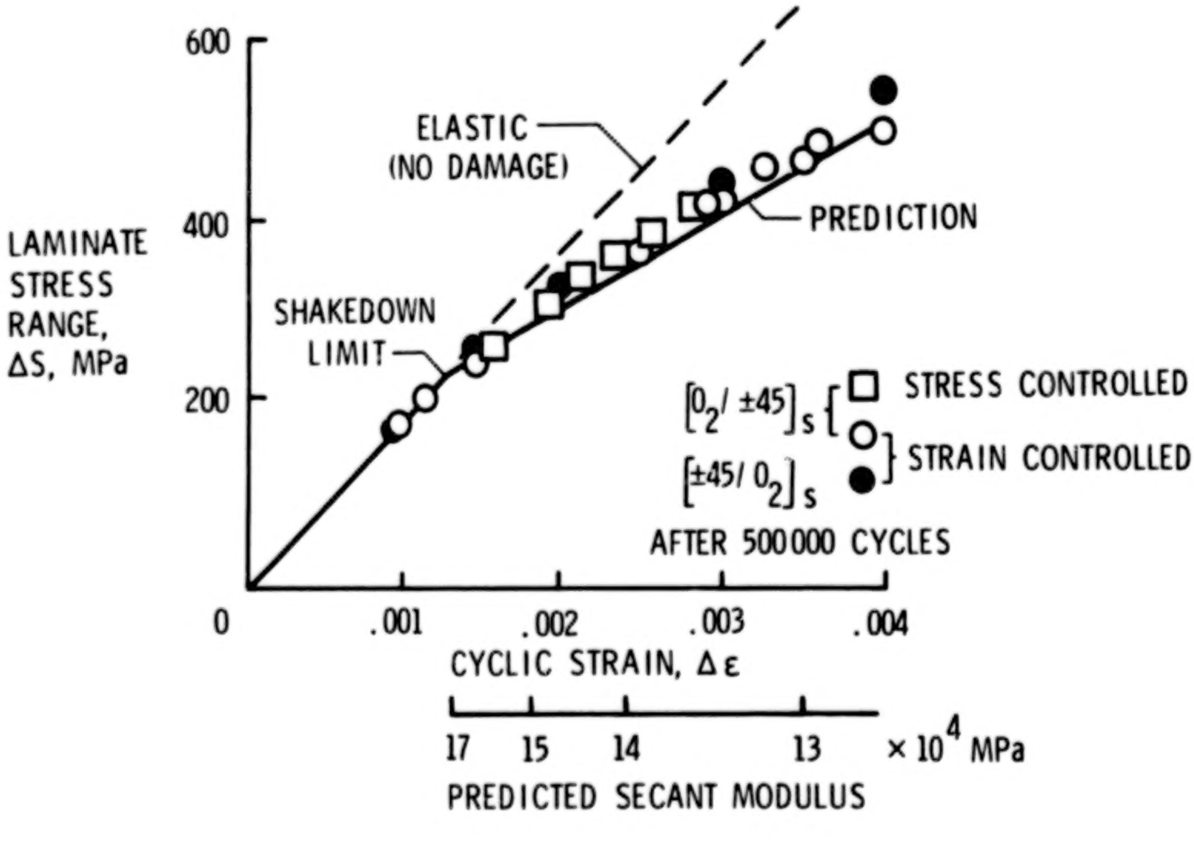

Figure 19

BEST DOCU... T AVAILABLE

DEBONDING OF ADHESIVELY BONDED COMPOSITES UNDER FATIGUE LOADING

An experimental and analytical investigation based on fracture mechanics methodology was undertaken to study fatigue failure (such as the gradual growth of debonded area when loads are repeated) of adhesively bonded composite joints. A cracked lap-shear specimen was used to test the adhesives. This specimen simulates a realistic adhesive joint where a combination of shear and peel stresses are present. Different configurations of cracked lap-shear specimens are being investigated. The different configurations have different percentages of the strain energy release rate, G, associated with debond opening tension, G_I, and debond shearing, G_{II} (ref. 18). Specimens were made from T300/5208 graphite/epoxy and Kevlar/epoxy (ref. 19). The EC-3445 and FM-300 adhesives tested were cured at 121°C and 177°C, respectively. Specimens are being studied for the combination of both composites and adhesives. For example, figure 20 shows the correlation between the experimentally measured debond growth rate, da/dN, and the value of strain energy release rate, G_I, for the two adhesive systems measured using graphite/epoxy specimens. The FM-300 has a slower growth rate than EC-3445 for an equivalent G_I. The purpose of the program is to develop a model to relate strain energy release rate to debond behavior for any structural geometry. This would then in turn be used to design safe, efficient, bonded composite structures.

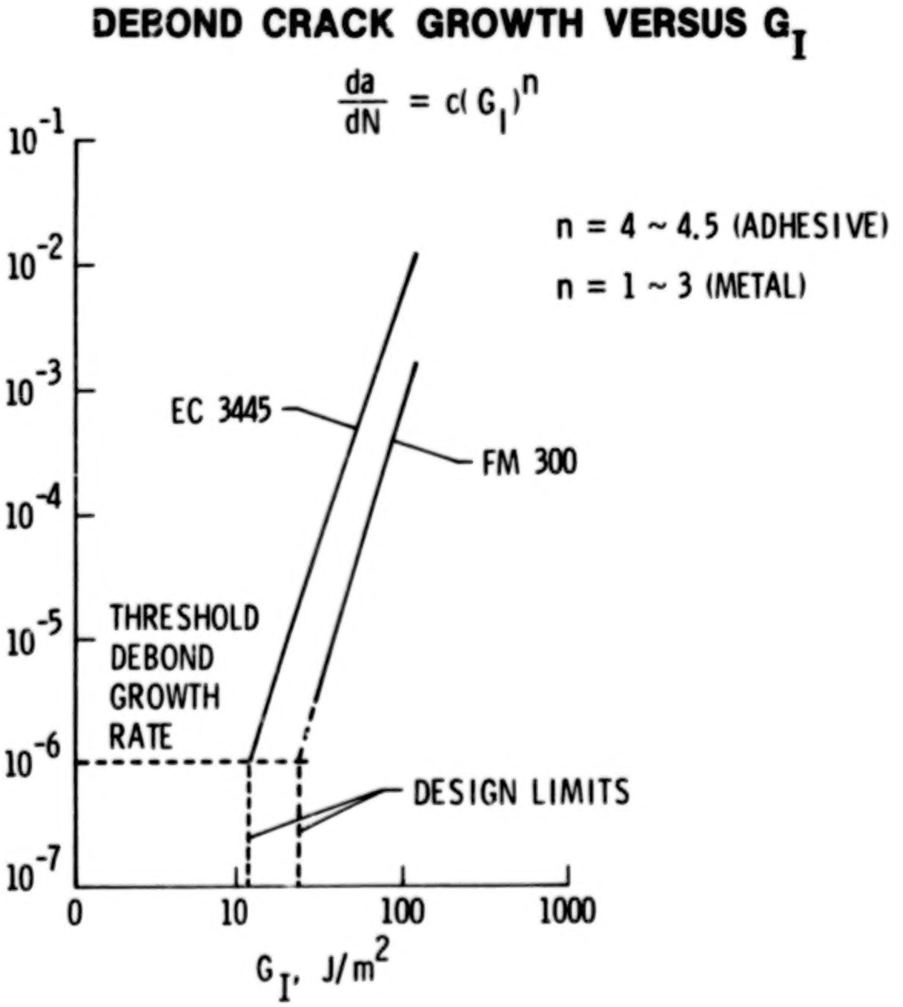

Figure 20

FUTURE WORK

As a result of these recent activities, work is planned in the following areas.

- Develop analyses for buffer strips with a wide range of parameters.

- Analyze damage mechanisms for bearing loaded holes.

- Extend finite-element analysis of bolt clampup to account for transient environments.

- Extend 3-D finite-element analyses of interlaminar stresses to account for thermal and hygroscopic effects.

- Determine static and fatigue delamination failure criteria for a variety of mixed-mode loadings.

- Predict delamination growth due to local instabilities.

- Predict fatigue endurance limits for arbitrary composite laminates.

- Predict fatigue endurance limits for adhesively bonded joints.

- Evaluate second-generation composites for improved delamination and impact resistance.

REFERENCES

1. Poe, C. C., Jr.; and Sova, J. A.: Fracture Toughness of Boron/Aluminum Laminates With Various Proportions of 0° and ±45° Plies. NASA TP-1707, 1980.

2. Poe, C. C., Jr.: A Single Fracture Toughness Parameter for Fibrous Composite Laminates. NASA TM-81911, 1981.

3. Poe, C. C., Jr.; and Kennedy, J. M.: An Assessment of Buffer Strips for Improving Damage Tolerance of Composite Laminates. Journal of Composite Materials Supplement, vol. 14, no. 1, 1980, pp. 57-70.

4. Crews, J. H., Jr.: Bolt-Bearing Fatigue of a Graphite/Epoxy Laminate. Joining of Composite Materials, K. T. Kedward, ed., ASTM STP 749, American Society for Testing and Materials, 1981, pp. 131-144.

5. Shivakumar, K. N.; and Crews, J. H., Jr.: Bolt Clampup Relaxation in a Graphite/Epoxy Laminate. NASA TM-83268, 1982. (Also to appear in Long-Term Behavior of Composites, T. K. O'Brien, ed., American Society for Testing and Materials Special Technical Publication.)

6. Shivakumar, K. N.; and Crews, J. H., Jr.: An Equation for Bolt Clampup Relaxation in Transient Environments. NASA TM-84480, 1982. (Also accepted for publication in Composites Technology Review.)

7. Raju, I. S.; and Crews, J. H., Jr.: Three-Dimensional Analysis of $[0/90]_s$ and $[90/0]_s$ Laminates with a Central Circular Hole. NASA TM-83300, 1982. (Also accepted for publication in Composites Technology Review.)

8. Bostaph, G. M.; and Elber, W.: Static Indentation Tests on Composite Plates for Impact Susceptibility Evaluation. Paper presented at the U.S. Army Symposium on Solid Mechanics: Critical Mechanics Problems in Systems Design (Cape Cod, MA), Sept. 21-23, 1982.

9. O'Brien, T. K.: Characterization of Delamination Onset and Growth in a Composite Laminate. Damage in Composite Materials, K. L. Reifsnider, ed., ASTM STP 775, American Society for Testing and Materials, 1982, pp. 140-167. (Also NASA TM-81940, 1981.)

10. O'Brien, T. K.; Johnston, N. J.; Morris, D. H.; and Simonds, R. A.: A Simple Test for the Interlaminar Fracture Toughness of Composites. SAMPE Journal, vol. 18, no. 4, 1982, pp. 8-15.

11. Standard Tests for Toughened Resin Composites. NASA RP-1092, 1982.

12. Raju, I. S.; and Crews, J. H., Jr.: Interlaminar Stress Singularities at a Straight Free Edge in Composite Laminates. Journal of Computers and Structures, vol. 14, no. 1-2, 1981, pp. 21-28.

13. Whitcomb, J. D.: Finite Element Analysis of Instability-Related Delamination Growth. Journal of Composite Materials, vol. 15, 1981, pp. 403-426.

14. O'Brien, T. Kevin: Tension Fatigue Behavior of Quasi-Isotropic, Graphite/Epoxy Laminates. Fatigue and Creep of Composite Materials, H. Lilholt and R. Talreja, eds., Risø National Laboratory, Roskilde, Denmark, 1982, pp. 259-264.

15. Phillips, E. P.: Effects of Truncation of a Predominantly Compression Load Spectrum on the Life of a Notched Graphite/Epoxy Laminate. Fatigue of Fibrous Composite Materials, ASTM STP 723, American Society for Testing and Materials, 1981, pp. 197-212. (Also NASA TM-80114, 1979.)

16. Johnson, W. S.: Mechanisms of Fatigue Damage in Boron/Aluminum Composites. Damage in Composite Materials, K. L. Reifsnider, ed., ASTM STP 775, American Society for Testing and Materials, 1982, pp. 83-102. (Also NASA TM-81926, 1980.)

17. Johnson, W. S.: Modeling Stiffness Loss in Boron/Aluminum Below the Fatigue Limit. NASA TM-83294, 1982. (Also to appear in Long-Term Behavior of Composites, T. K. O'Brien, ed., American Society for Testing and Materials Special Technical Publication.)

18. Dattaguru, B.; Everett, R. A., Jr.; Whitcomb, J. D.; and Johnson, W. S.: Geometrically Nonlinear Analysis of Adhesively Bonded Joints. Paper presented at 23rd AIAA/ASME/ASCE/AHS Structures, Structural Dynamics, and Materials Conference (New Orleans, LA), May 10-12, 1982. (Also accepted for publication in Journal of Engineering Materials and Technology.)

19. Mall, S.; Johnson, W. S.; and Everett, R. A., Jr.: Cyclic Debonding of Bonded Composites. Paper presented at International Symposium on Adhesive Joints: Their Formation, Characteristics, and Testing (Kansas City, MO), September 13-16, 1982.

PROCESSING COMPOSITE MATERIALS

R. M. Baucom
NASA Langley Research Center
Hampton, Virginia

INTRODUCTION

Langley Research Center has an active role in the development of composite materials for aerospace applications. This activity was initiated over ten years ago and has included a variety of study efforts that have led to several production commitments to use composite materials in structural components. The overall composites program at Langley includes basic polymer studies, composites processing research, materials evaluation, analysis, and applications. In order to support the composite research activities, the current annual consumption of graphite, Kevlar and fiberglass reinforced polymer materials is approximately 1000, 400, and 800 pounds, respectively. An additional 50 pounds of fiber reinforced metal matrix composite materials are also consumed. Annually, approximately 300 structural laminates ranging in size up to 20 square feet and in thickness up to 1.2 inches are fabricated from these materials. Structural articles weighing up to several hundred pounds are also frequently fabricated. In addition to conventional vacuum molding capability, 12 heated platen presses, 4 research autoclaves, 2 thermoforming machines and a pultruder are available for composites fabrication. This paper will review composite processing methods and illustrate selected examples of components produced by Langley as well as components produced by our aerospace contractors.

COMPOSITE PROCESSING AND APPLICATIONS

Fiber reinforced polymer composite materials can be processed into structural articles by a vareity of different methods. The application of pressure or force to composite materials to shape and cure is accomplished by means of the application of vacuum, autoclave pressurization, trapped rubber expansion or hydraulic presses. Vacuum molding is a widely used method for the fabrication of large production, non-aerospace articles from general use composite materials such as fiberglass reinforced polyester and epoxy. Advanced composite materials such as Kevlar and graphite reinforced epoxies and polyimides are generally processed by autoclave molding, by trapped rubber expansion, or by hydraulic presses. To complete the processing cycle the articles fabricated by these methods are normally subjected to nondestructive inspection to verify the structural integrity of the finished part.

This presentation will feature the fabrication of several composite structural articles including DC-10 upper aft rudders, L-1011 vertical fins and composite biomedical appliances. Also, a discussion on innovative composite processing methods will be included.

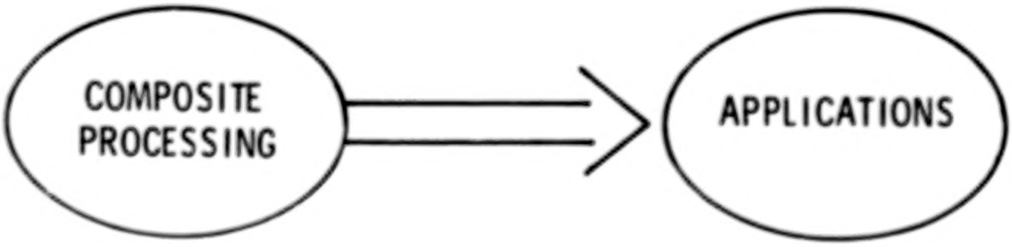

COMPOSITE PROCESSING

APPLICATIONS

CONVENTIONAL

- VACUUM MOLDING
- AUTOCLAVE
- TRAPPED RUBBER
- PRESS MOLDING
- INSPECTION

ADVANCED

- INTEGRATED LAMINATING CENTER
- HOT MELT FUSION

- DC-10 UPPER AFT RUDDER
- L-1011 VERTICAL FIN
- BIOMEDICAL APPLIANCES

COMPOSITE MOLDING METHODS

The three most widely used methods for applying pressure to mold composites are thermal expansion of trapped rubber, autoclave pressurization, and hydraulic presses. The selection of the appropriate molding method depends primarily on the structural article size and maximum cure temperature and pressure. The trapped rubber or thermal expansion molding technique has the capability of developing very high pressures during composite cure and care must be exercised in the design of the tooling in order to maintain the selected pressures. This method is utilized in composite processing where uniform pressure application in complex shapes is difficult with other methods. Composite article size is limited only by oven size and tool mass with the thermal expansion molding technique. Autoclave processing of composite materials is widely used due to the precise control of pressure and temperature offered by the method.

Structural article size and maximum pressure are limited by the design of the autoclave pressure vessel. Hydraulic presses equipped with heated platens are generally utilized for applications which require high pressures and fast cycle times during composite molding. Hydraulic presses are widely used to fabricate small, intricate parts in matched metal tooling.

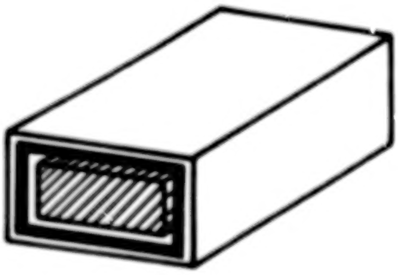
THERMAL EXPANSION

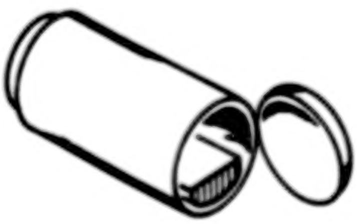
AUTOCLAVE

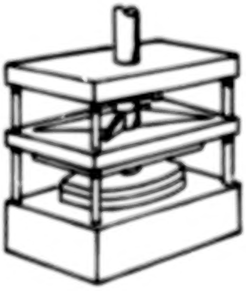
HYDRAULIC PRESS

COMPOSITE MOLDING BY THERMAL EXPANSION

Most rubber compounds possess the physical characteristic of expanding upon the application of heat. This characteristic can be used to apply uniform pressure to composite materials to form and cure a structural article. Typically, a block or plug of rubber is cast into the desired shape with appropriate allowances for expansion prior to contacting the mold cavity during heat up. The composite material is applied over the rubber plug and the assembly is placed in the mold cavity which serves as the pressure containment chamber during cure. As the temperature is increased the composite material is forced against the mold. Since the rubber expands uniformly, the composite material is subjected to near-hydrostatic pressure as the temperature approaches the cure temperature. After an appropriate dwell time at the cure temperature the assembly is cooled and the part is removed. The cast rubber mold is then removed from the part and the assembly is prepared for the next fabrication cycle. The cast rubber block can be used for several cycles without degrading the material or losing its pressurization capability which, in turn, reduces the tooling costs.

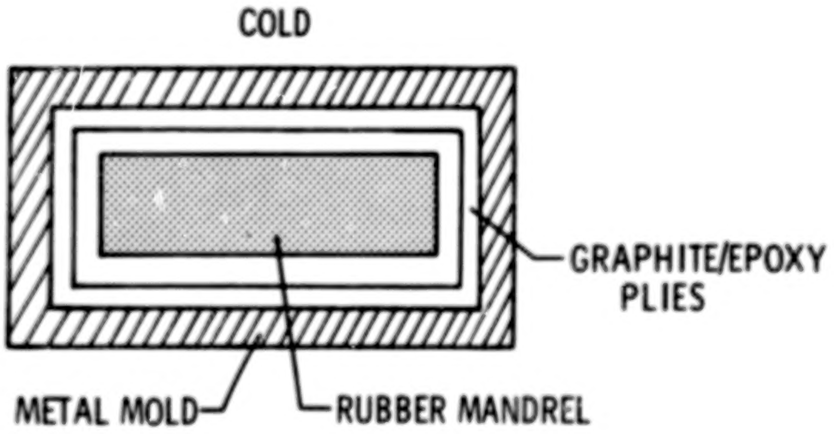

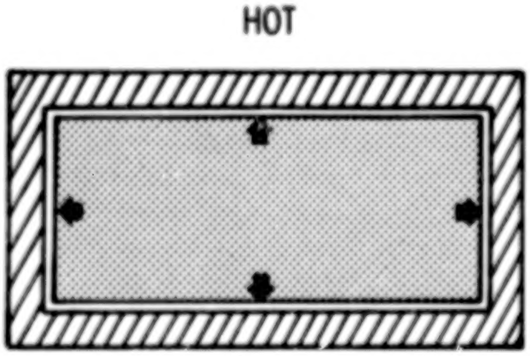

AUTOCLAVE MOLDING OF COMPOSITES

Autoclaves are utilized for processing a wide variety of composite materials into flat laminates and structural shapes. A typical autoclave process begins with assembling the part from the appropriate composite prepreg material. This assembly, commonly referred to as the layup, is placed on a metal caul plate that has been coated with spray release agent or a nonporous release film. The composite material is then covered with a porous release film and the required number of plies of breather material. A vacuum bag is then installed over the assembly and sealed around its periphery with gasket sealant material. A vacuum line is attached to the caul plate, vacuum is applied to the part, and the entire assembly is inserted into the autoclave. During heat-up to the composite cure temperature the viscosity of the resin in the prepreg material is lowered and the excess resin is drawn into the breather plies through the porous release fabric. Volatile products generated during cure are also removed in the same manner. After the temperature and autoclave pressure are held for the appropriate time to cure the prepreg, the vacuum bag assembly is removed from the autoclave, the vacuum bag is stripped away, and the fully cured part is removed. The materials utilized in this fabrication process are selected to withstand the temperature and pressure required for the particular composite material being processed. Autoclave molding is the most widely used process in the aerospace industry for manufacture of large graphite/epoxy and graphite/polyimide structural articles.

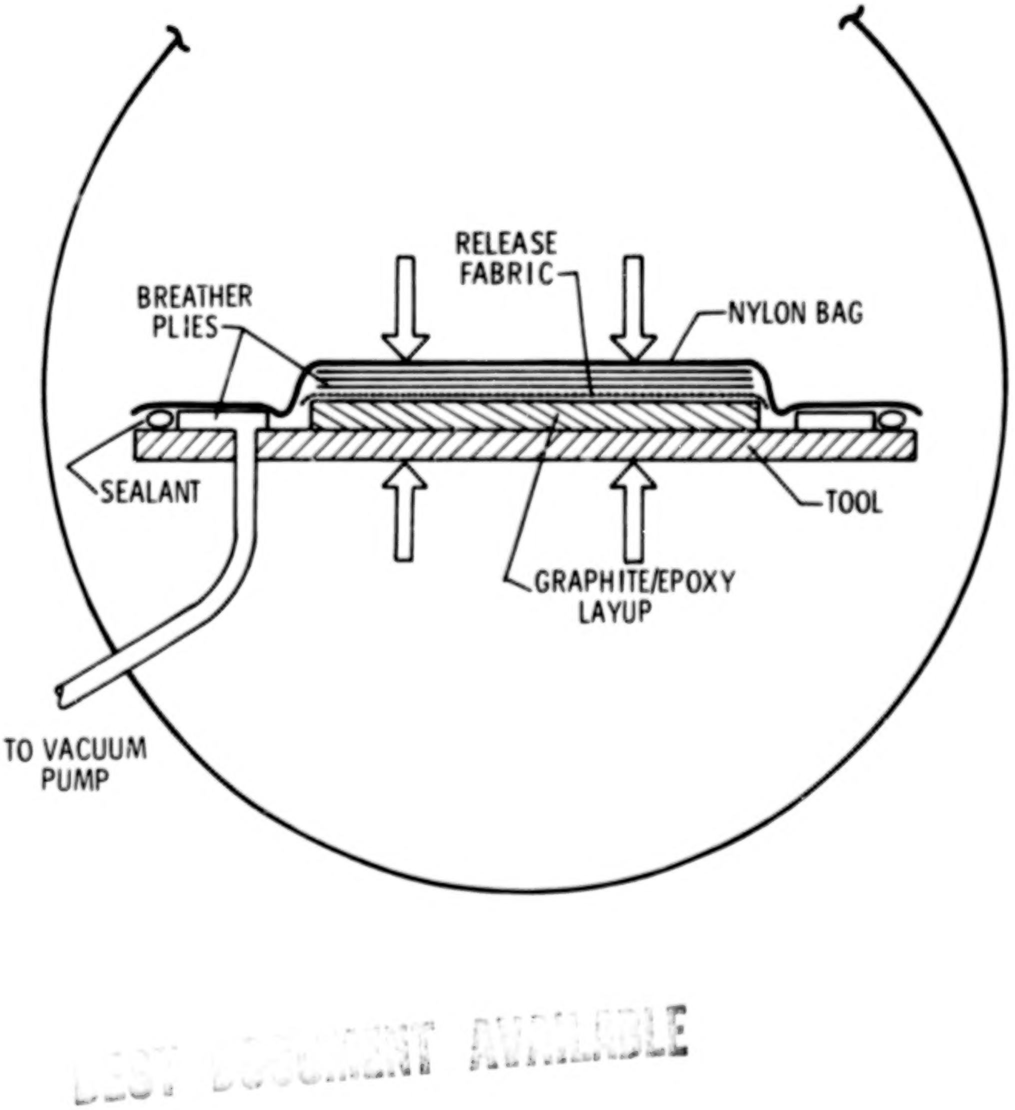

TYPICAL COMPOSITE CURE CYCLE

Polymer matrices for fiber reinforced composite materials generate reaction by-products during cure. In addition, the viscosity of the polymer matrix varies substantially during cure. In order to accommodate these physical phenomena during composite processing, the application of heat, vacuum, and pressure must be precisely controlled to avoid incomplete cures, voids, delaminations, and excess resin and fiber movement. A typical cure cycle for fabricating graphite/epoxy is shown in the figure. Vacuum is applied to the composite material and it is heated to an intermediate temperature of approximately 250-275°F. This condition is held for a period of time to allow excess solvent, water and reaction by-products to be removed. Prior to matrix gellation, the vacuum is removed and positive pressure is applied. The composite material is heated to the cure temperature, typically 350°F, and allowed to soak for 1 to 2 hours to effect a complete matrix cure. The part is then cooled to room temperature, the pressure is vented, and the part is removed. With minor variations to accommodate different composite material combinations, this profile is representative of most engineering composite material cure cycles.

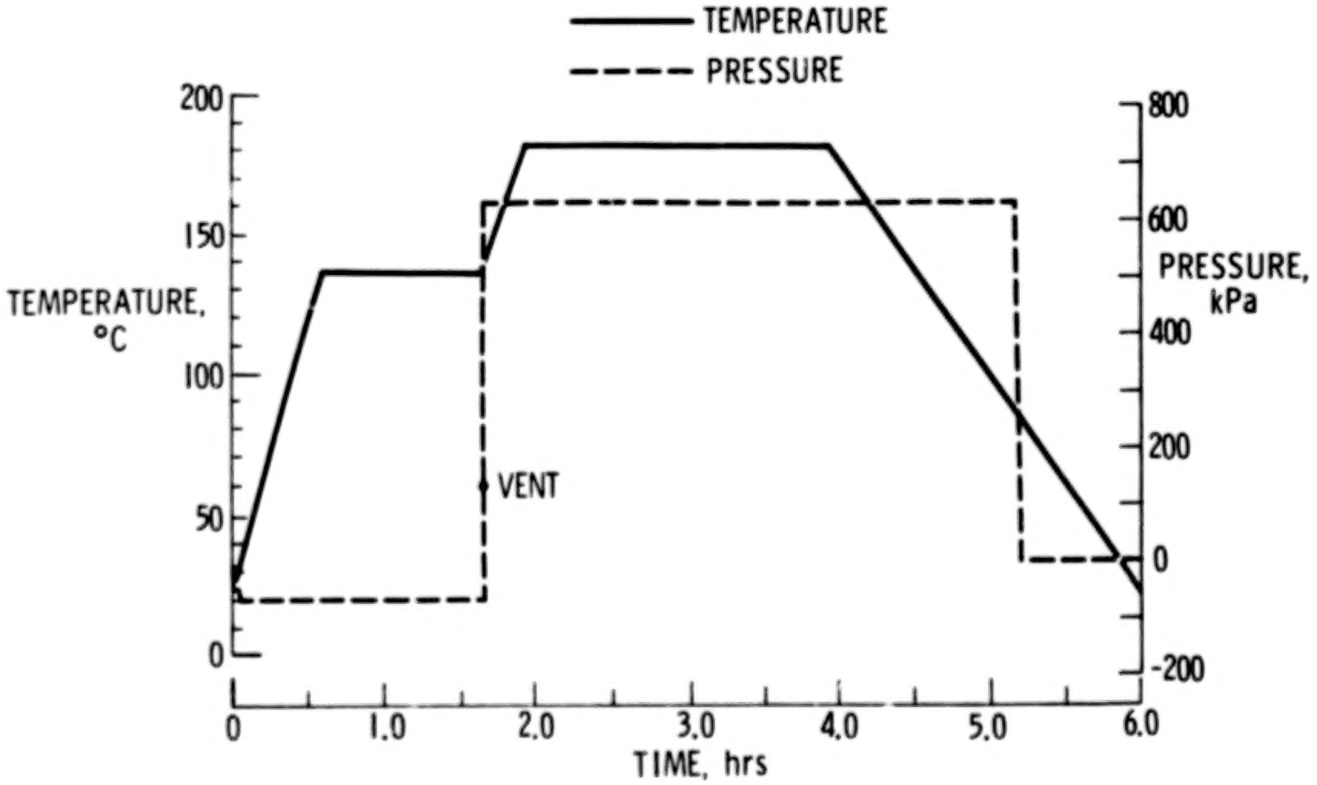

ULTRASONIC INSPECTION OF COMPOSITES

After composite articles are fabricated it is necessary to establish the structural integrity of the finished part. An initial visual examination is performed to identify areas of gross disbonding, delamination, fiber misalignment, laminate cracking, warped areas, etc. This inspection is normally followed by nondestructive ultrasonic evaluation of the article to ensure that the article is free of internal defects. This method requires that the article be acoustically coupled to the ultrasound transducer. The most convenient way to establish positive acoustic coupling is to immerse the article in a water tank equipped with a traveling bridge for attachment of the transducer. As the transducer travels along the bridge, sound is directed through the water and into the article. When a discontinuity is detected in the composite, the decibel level of the sound transmitted back to the transducer is reduced. This data can be displayed on an oscilloscope in the form of signal amplitude changes or on a printer which highlights the defect area. Voids, delaminations, cracks and porosity absorb the sound transmitted by the transducer and can be readily identified by this inspection process. Transducer frequency, focal distances, and focal diameters are selected to accommodate article thickness, shape, and fiber and resin type.

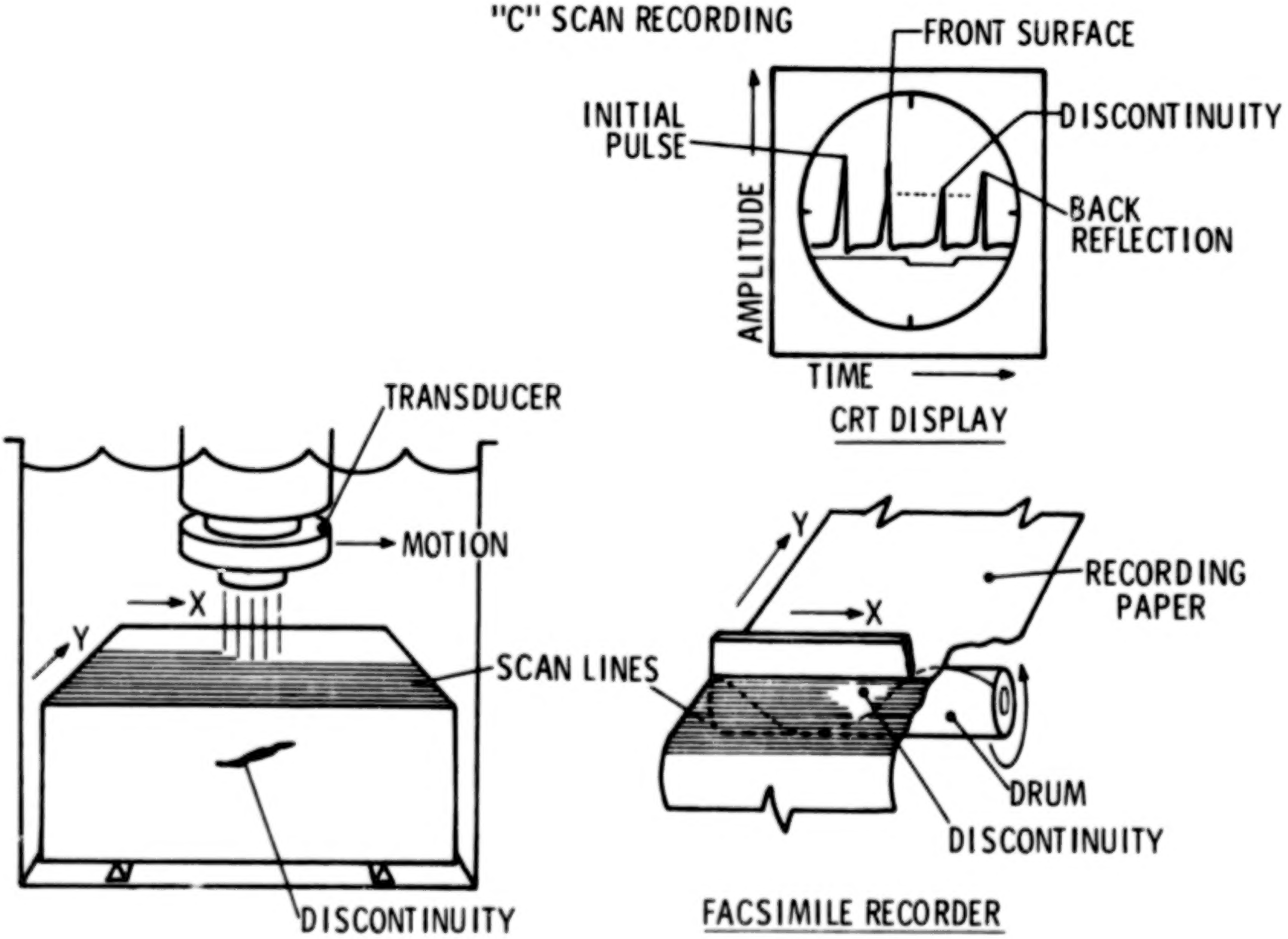
"C" SCAN RECORDING

FRONT SURFACE
INITIAL PULSE
DISCONTINUITY
BACK REFLECTION
AMPLITUDE
TIME
TRANSDUCER
MOTION
X
Y
SCAN LINES
DISCONTINUITY
RECORDING PAPER
X
Y
DRUM
DISCONTINUITY

CRT DISPLAY

FACSIMILE RECORDER

INSPECTION TECHNIQUES

The capability of ultrasonic inspection to verify the structural integrity composites has been demonstrated by machining, polishing, and visually inspecting the suspected defect areas. The ultrasonic C-scan image, shown in the upper left of the figure, indicates a structurally sound laminate. The small black dots on the C-scan represent the metal support pins used to elevate the laminate off the base of the water immersion tank to avoid undesirable artifacts in the C-scans. The photomicrograph of the laminate shown in the upper right of the figure verified the assessment. The ultrasonic C-scan in the lower left portion of the figure shows evidence of internal voids which absorbed the sound beam during inspection. This laminate was also sectioned, polished and visually inspected to verify the ultrasonic display of voids. Large discontinuities between laminate plies are evident in the defective areas indicated by ultrasonic inspection. The criteria for accept/reject of a composite article vary widely as a function of the data base generated for the particular composite system and the mission for the composite article. In particular, the criticality of void size, type, and location plays a major role in establishing the acceptable limits for anomalies discovered by ultrasonic inspection.

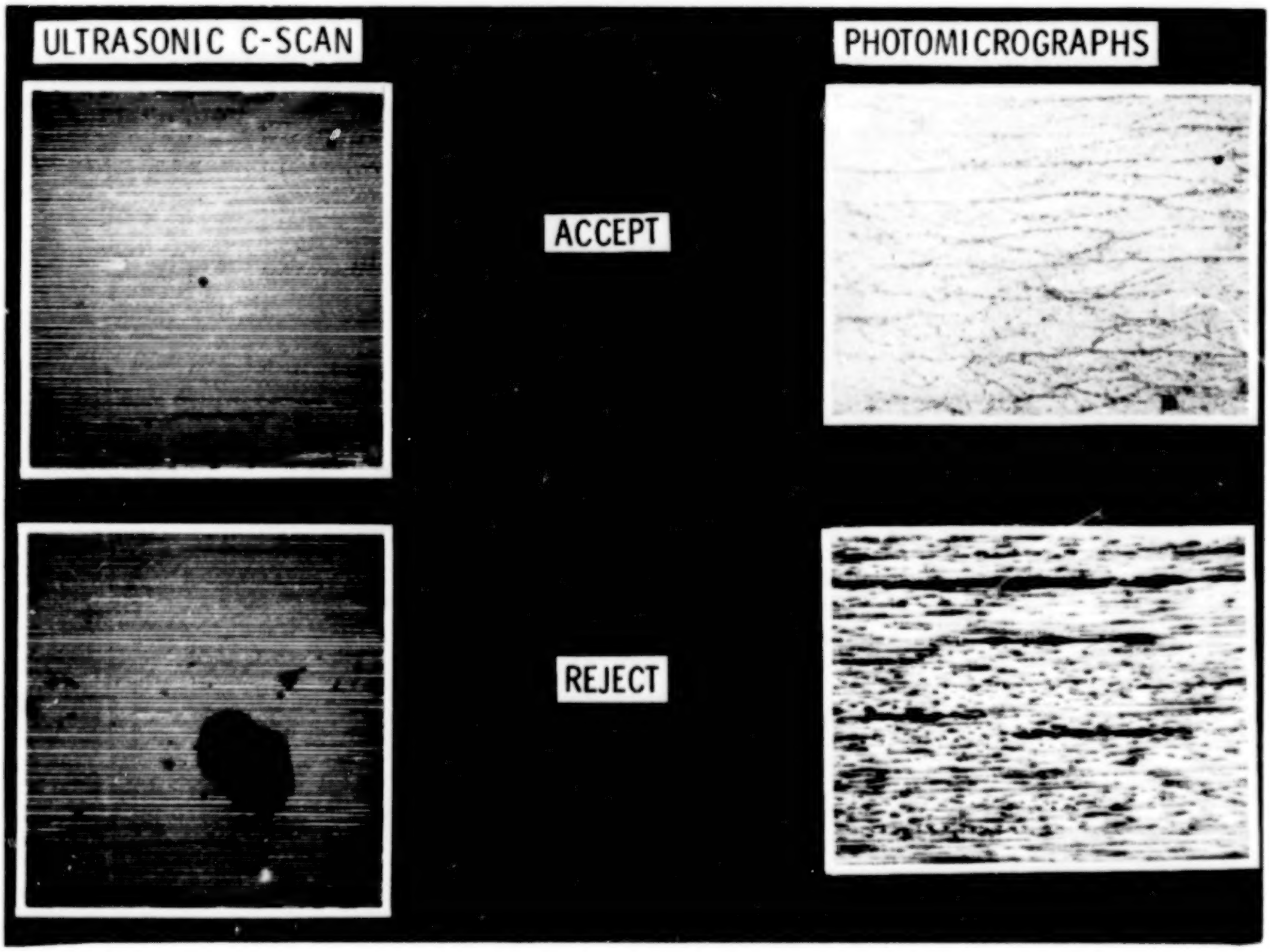

DC-10 UPPER AFT RUDDERS

One of the composite structural components developed under the NASA ACEE (Aircraft Energy Efficiency) program is the upper aft rudder for the DC-10 aircraft. The component is approximately 13 feet in length. The aluminum production design weighs 93 pounds whereas the composite rudder weighs only 61 pounds. The structural box was fabricated from graphite/epoxy material. The leading and trailing edges were fabricated from glass/epoxy material.

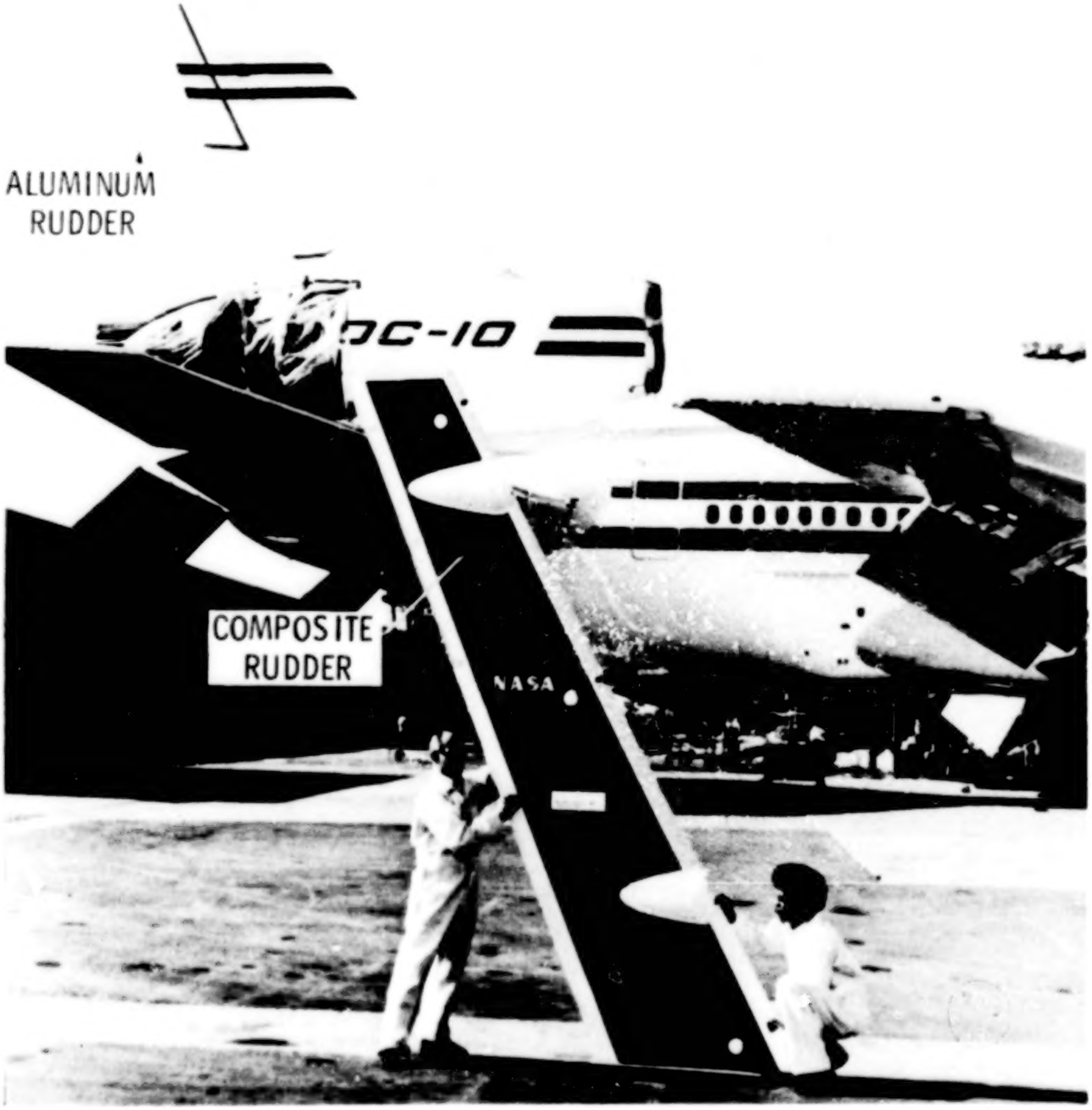

COMPOSITE DC-10 UPPER AFT RUDDER ADVANTAGES

The graphite/epoxy upper aft rudder for the DC-10 was fabricated using the trapped rubber thermal expansion technique. Principal advantages of using this fabrication procedure were: (1) the component was molded to net size and machining operations were minimized, (2) the complete assembly was cured in one cycle thereby saving costs and limiting exposure time of the composite to 350°F temperatures, and (3) the requirement for secondary bonding of subassemblies was eliminated. Composite rudders fabricated in this manner weigh approximately 30 percent less than the production aluminum rudders.

GRAPHITE/EPOXY COCURED COMPONENT

- MOLDED NET TO SIZE
- CURED IN ONE CYCLE
- NO SECONDARY BONDING
- SIGNIFICANT WEIGHT REDUCTION OVER METAL CONFUGURATION

DC-10 UPPER AFT RUDDER MANUFACTURING SEQUENCE

Fabrication of the DC-10 graphite/epoxy upper aft rudder began with layup and predensification of the skins, front and rear spars and ribs from unidirectional tape and broadgoods. These parts were then loaded into the rubber molding tool along with the internal metal and rubber mandrels. Steel side plates were bolted into place and the assembly was placed in the oven. The assembly was heated to 350°F and held for 2 hours and 15 minutes to fully cure the graphite/epoxy. The finished rudder was removed from the tool.

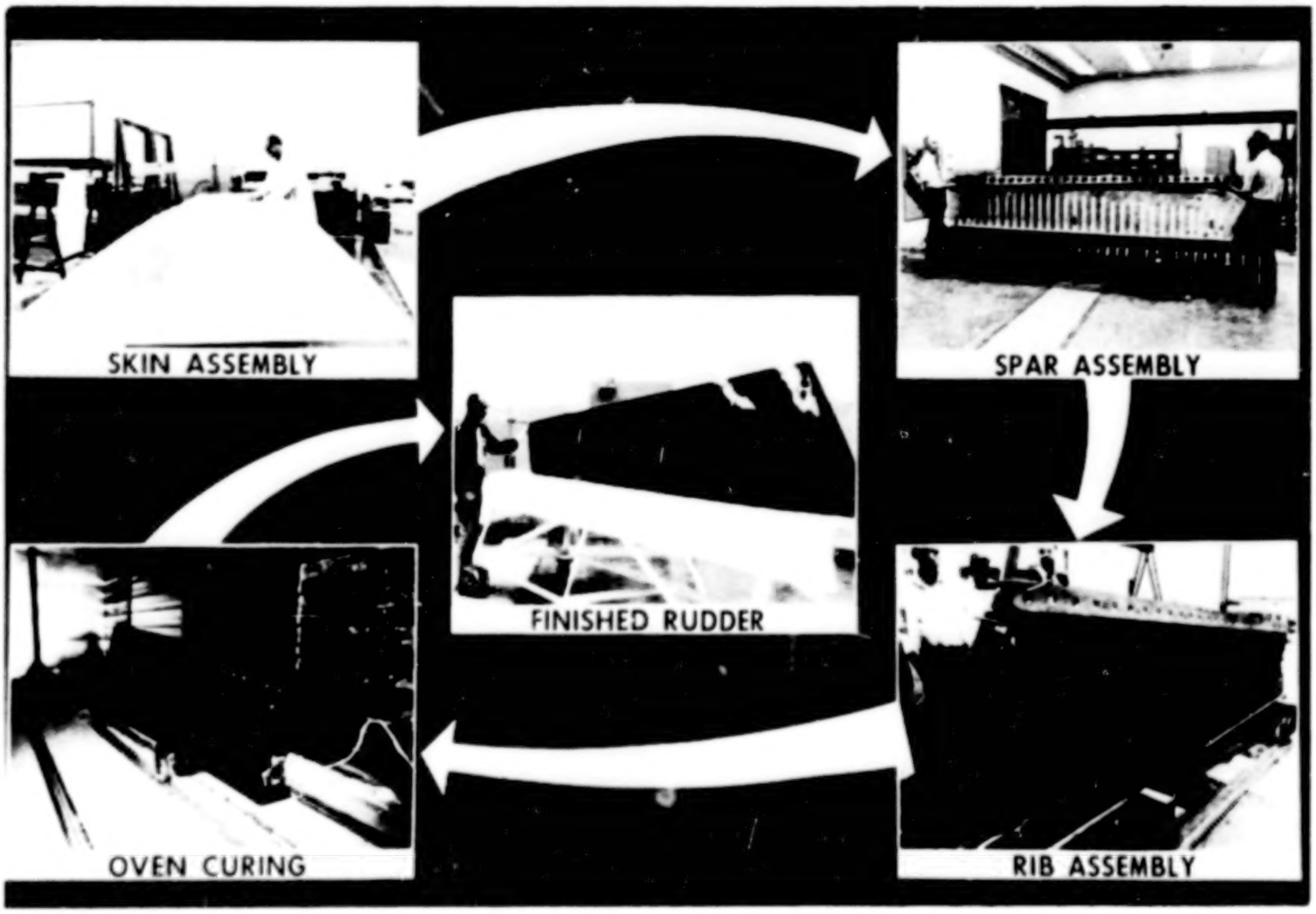
SKIN ASSEMBLY
SPAR ASSEMBLY
FINISHED RUDDER
OVEN CURING
RIB ASSEMBLY

THERMAL EXPANSION MOLDING TECHNIQUE

Thermal expansion molding technique (trapped rubber processing) is predicated on the fact that silicone rubber, when confined within a vessel and subjected to heat, thermally expands and generates internal pressure. As in the case of the upper aft rudder of the DC-10, graphite/epoxy details are laid up, densified on wooden form blocks, trimmed and prepared for freezer storage. The formed details are then loaded into the rudder tool, the rubber mandrel is properly positioned, and the tool vessel is closed. The loaded tool is then placed in an oven and cured for 2 hours at 350°F after initial heat-up. Advantages of the process include elimination of the autoclave and vacuum bagging operations.

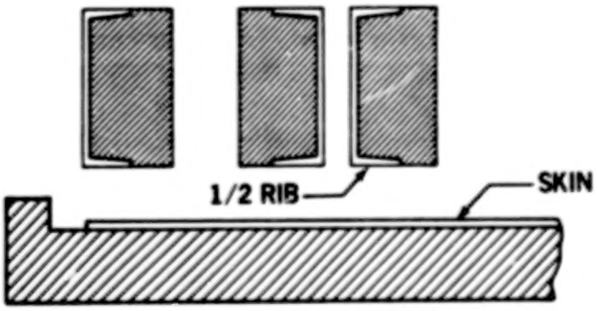

- **LAYUP INDIVIDUAL PIECES ON ANCILLARY TOOLS**
- **DENSIFY**
- **TRIM TO SIZE**
- **STORE IN FREEZER**

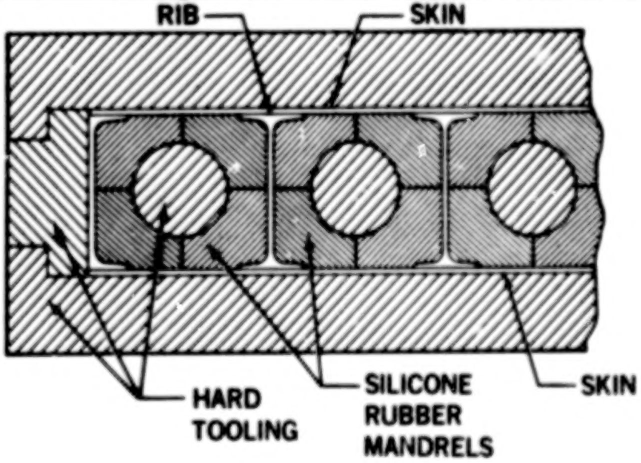

- **ASSEMBLE PIECES IN CURE TOOL**
- **APPLY HEAT**
- **PRESSURE SUPPLIED BY EXPANSION OF SILICONE RUBBER WITHIN TOOL CAVITY**
- **NO BAGGING, BLEED-OFF, OR ADHESIVE REQUIRED**

L-1011 ADVANCED COMPOSITE VERTICAL FIN

Two structural components on the L-1011 airplane were selected for fabrication from graphite/epoxy composite as part of the NASA ACEE program. One component, the vertical fin, is a primary load-carrying structural element. The objectives of the Advanced Composite Vertical Fin (ACVF) research were to develop low-cost manufacturing processes for large composite structural aircraft articles and to verify the structural integrity and durability of the article.

L-1011
Lockheed
Lockheed TriStar

L-1011 ACVF STRUCTURAL CONFIGURATION

The ACVF is 25 feet long, 9 feet wide at the root, and weighs 622 pounds. It is comprised of 10 ribs, front and rear spars, and hat-stiffened cover skins. Unidirectional and woven graphite/epoxy prepreg is utilized in the construction of the ACVF subassemblies.

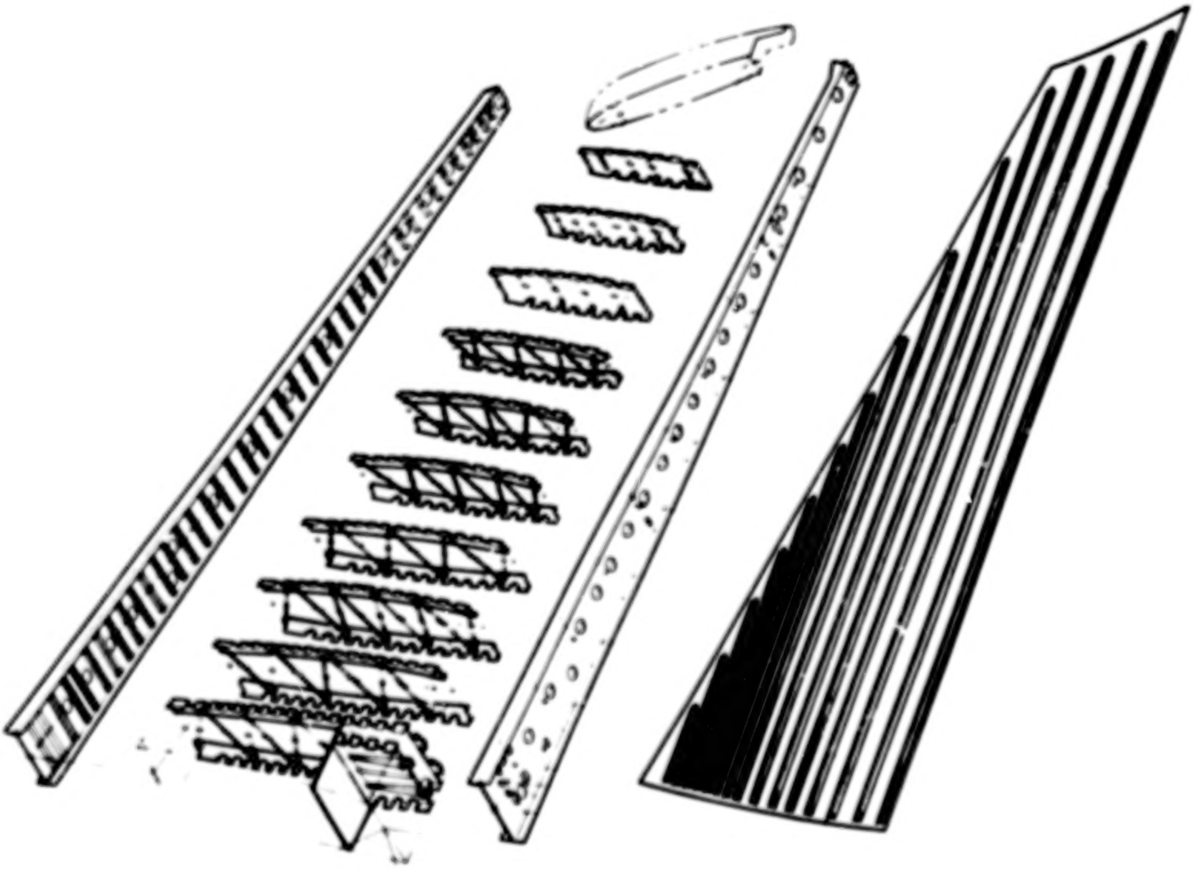

ACVF SKIN LAY-UP SCHEMATIC

The skin of the L-1011 composite fin (ACVF) is comprised of a ply buildup which is 34 plies at the root end (to match the existing L-1011 metallic mating structure) and tapers progressively to 16, 14, and 10 ply areas as shown. The buildup consists of five plies over the complete fin area, oriented ±45°, 0°, ∓45°. This is followed by 10 partial plies, principally 0° orientation, building up toward the root end, and a core of four ±45° plies at the midpoint in the symmetrical layup. Additional partial plies are included at the tip and along the front and rear spar attach areas to provide a reinforced bearing pad for fastening.

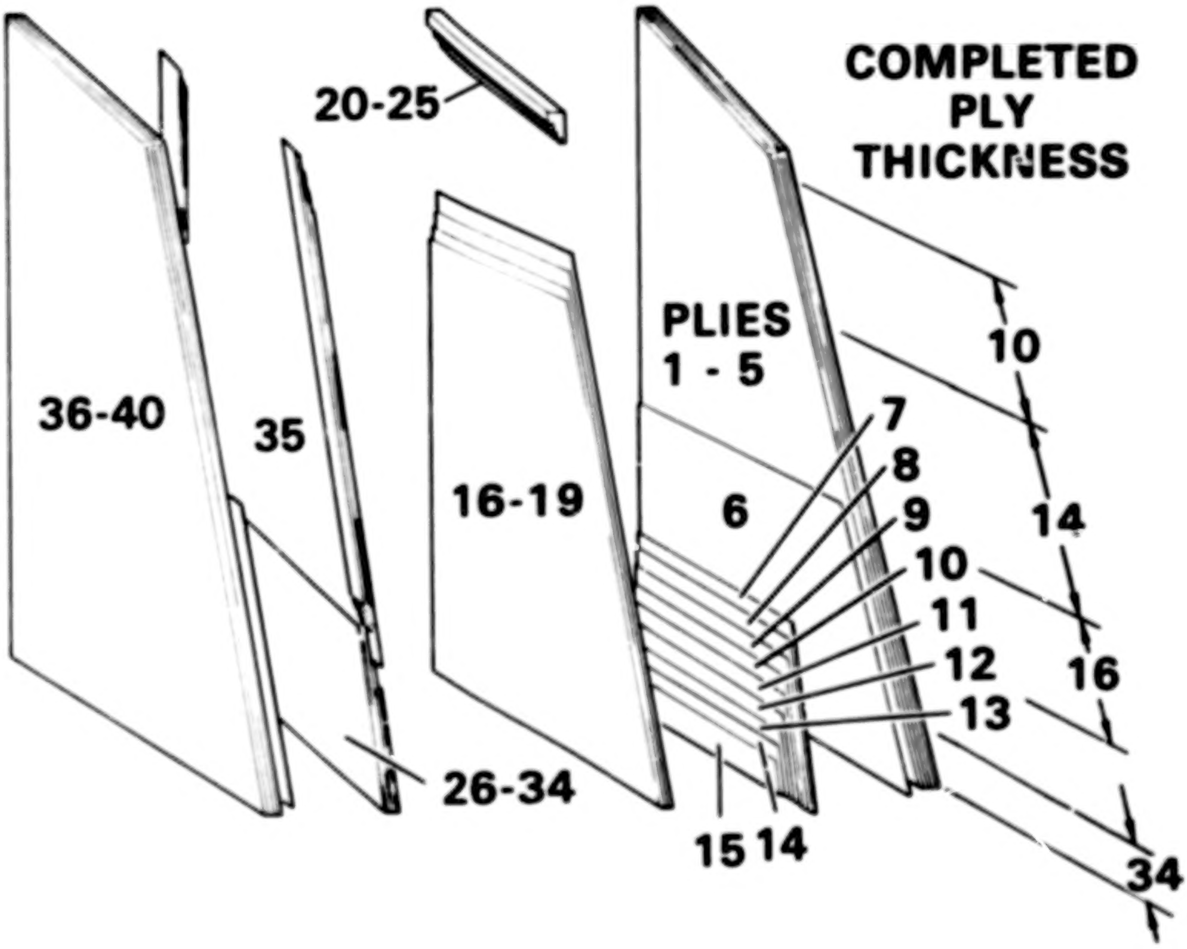

20-25
COMPLETED
PLY
THICKNESS
PLIES
1 - 5
10
36-40
35
16-19
7
8
6
9
14
10
11
12
16
13
26-34
15
14
34

ACVF HAT/SKIN VACUUM BAG ASSEMBLY

The various types of materials which are used in the cure of a typical hat-stiffened bay of the ACVF cover assembly are shown in the figure. A barrier film is used next to the tool surface and also under the hat cauls to prevent resin adhesion to the tooling components. A nylon peel ply is placed immediately adjacent to the graphite layup, both on the tool side of the skin and over the hats and between hat flanges. Bleeder material is located between hat flanges and around the periphery of the part. Breather plies cover the completed stack to assure a continuous vacuum path to the vacuum ports located around the tool base. A vacuum bag covers the complete assembly and is sealed at the edges of the tool. The inflatable bladder penetrates the vacuum bag to admit autoclave pressure to the bladder interior.

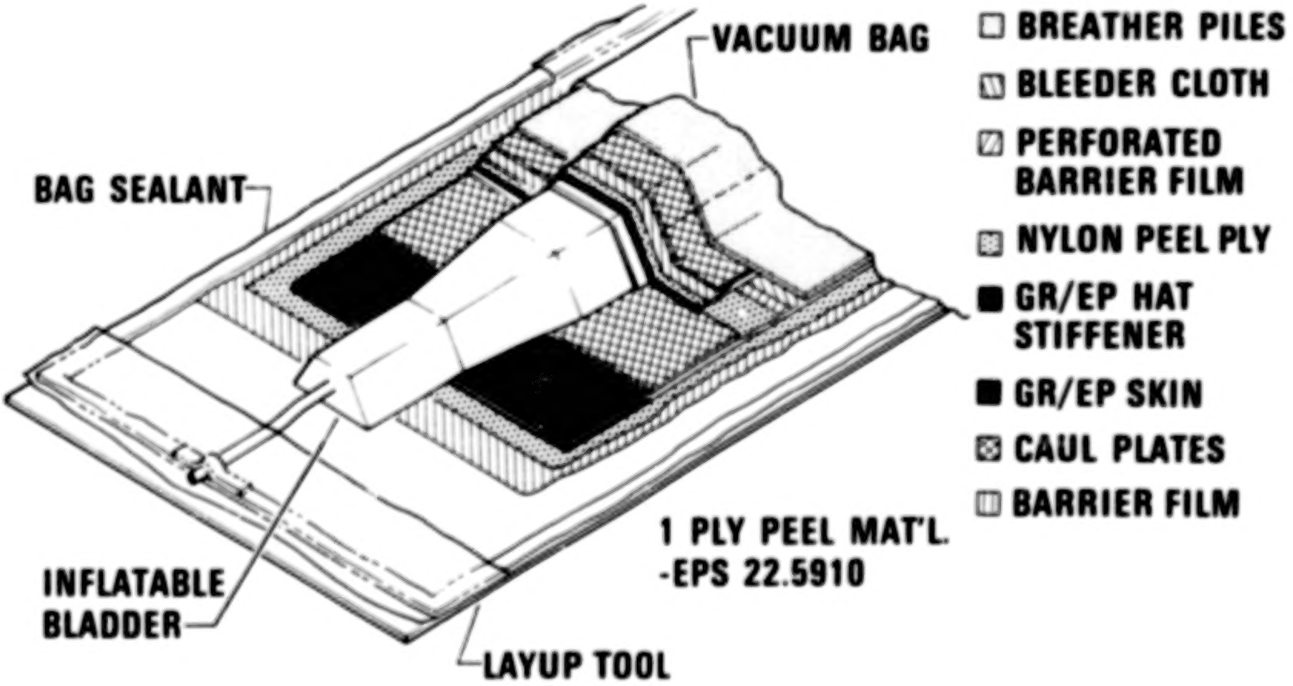
VACUUM BAG
BAG SEALANT
INFLATABLE BLADDER
LAYUP TOOL
1 PLY PEEL MAT'L.
-EPS 22.5910
☐ BREATHER PILES
▧ BLEEDER CLOTH
▨ PERFORATED BARRIER FILM
▦ NYLON PEEL PLY
■ GR/EP HAT STIFFENER
■ GR/EP SKIN
▩ CAUL PLATES
▥ BARRIER FILM

ACVF COVER FABRICATION

After the ACVF components are laid up, densified, and cured they are removed from the autoclave. The vacuum bag assembly for the fin cover shown in the figure has been removed and the inflatable rubber mandrels utilized for presurization of the hat stiffened elements during cure are being removed.

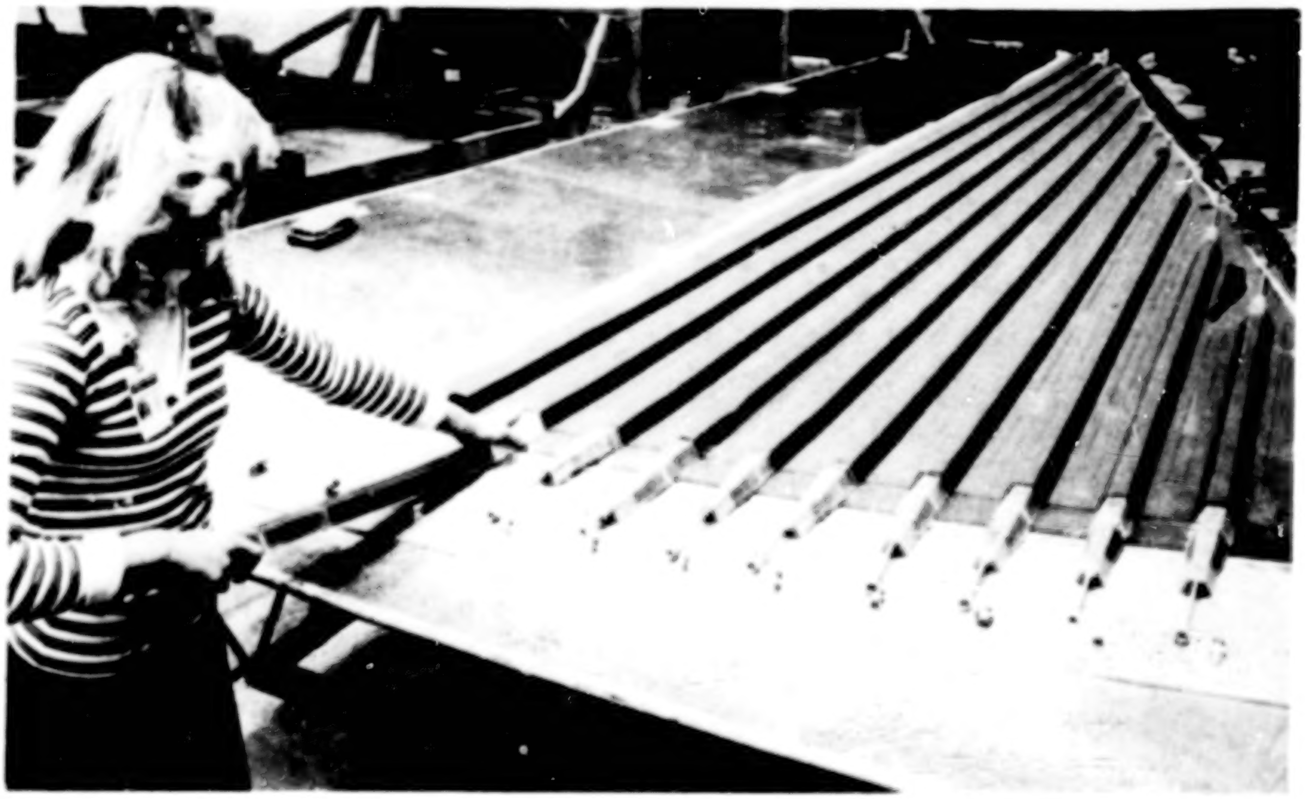

COMPLETE GRAPHITE/EPOXY ACVF COVER

The graphite/epoxy ACVF cover skin with integral cocured hat stiffener elements is shown being removed from the autoclave cure tool. After removal from the tool, the covers are subjected to a complete ultrasonic scan inspection to ensure that the part is free of voids, delaminations, or other anomalies that may affect structural integrity. The skins are then machined for mechanical attachment to the rib and spar assemblies.

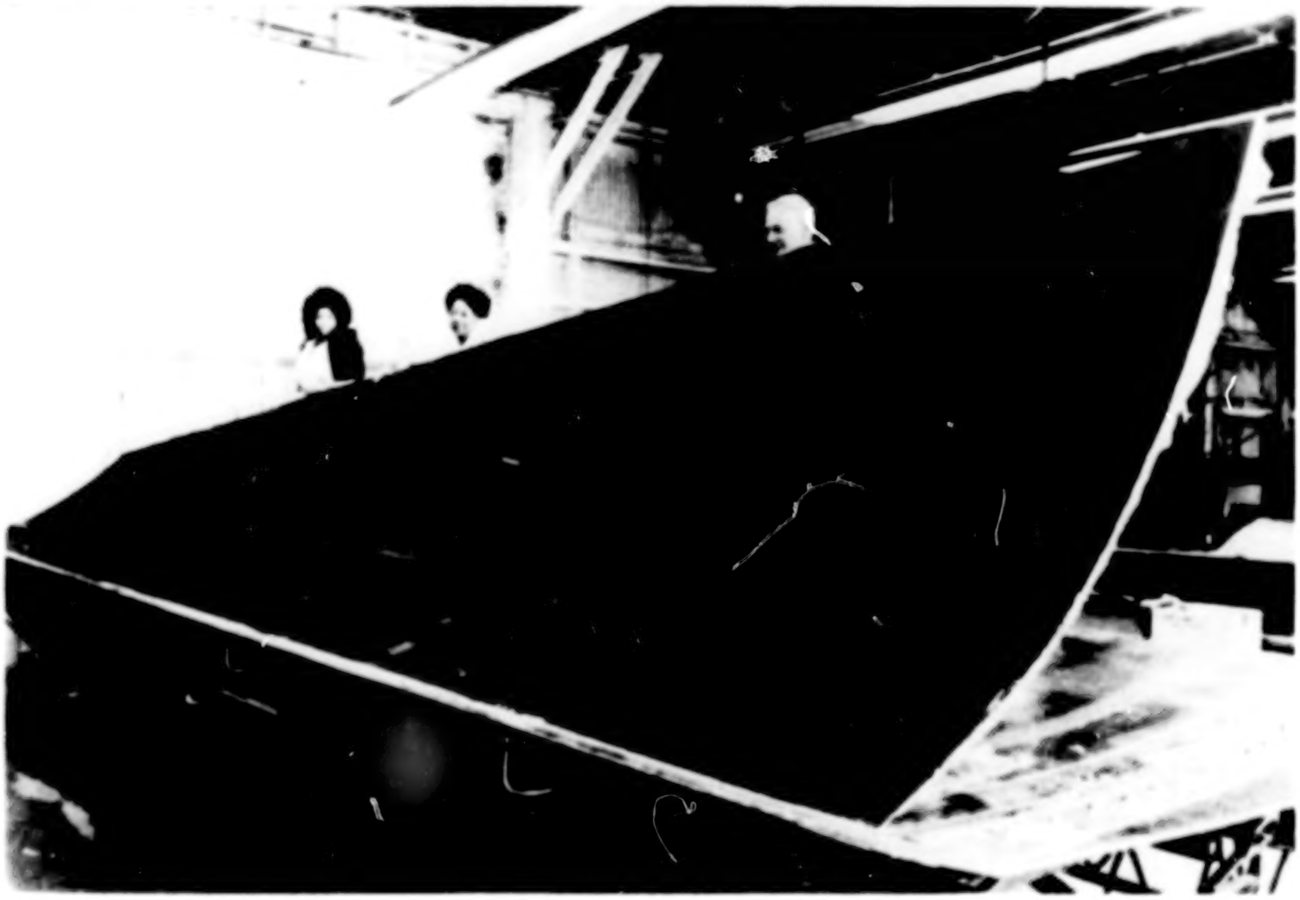

AUTOMATED INTEGRATED MANUFACTURING SYSTEM

During the 1970's, as composites became more generally accepted, the need for mechanized equipment to fabricate severely contoured, integrally stiffened, complex structures for aircraft was identified. This led to the development and implementation of a number of automated composites processing centers in the aircraft industry. The Automated Integrated Manufacturing System (AIMS) shown in the figure was developed by the Grumman Aerospace Corporation under Air Force sponsorship. This system has the capability to automatically dispense and laser trim composite tape and broadgoods. The prepreg details can then be automatically transferred to a contour ply handler or translaminar stitching machine for final layup and assembly into structural articles.

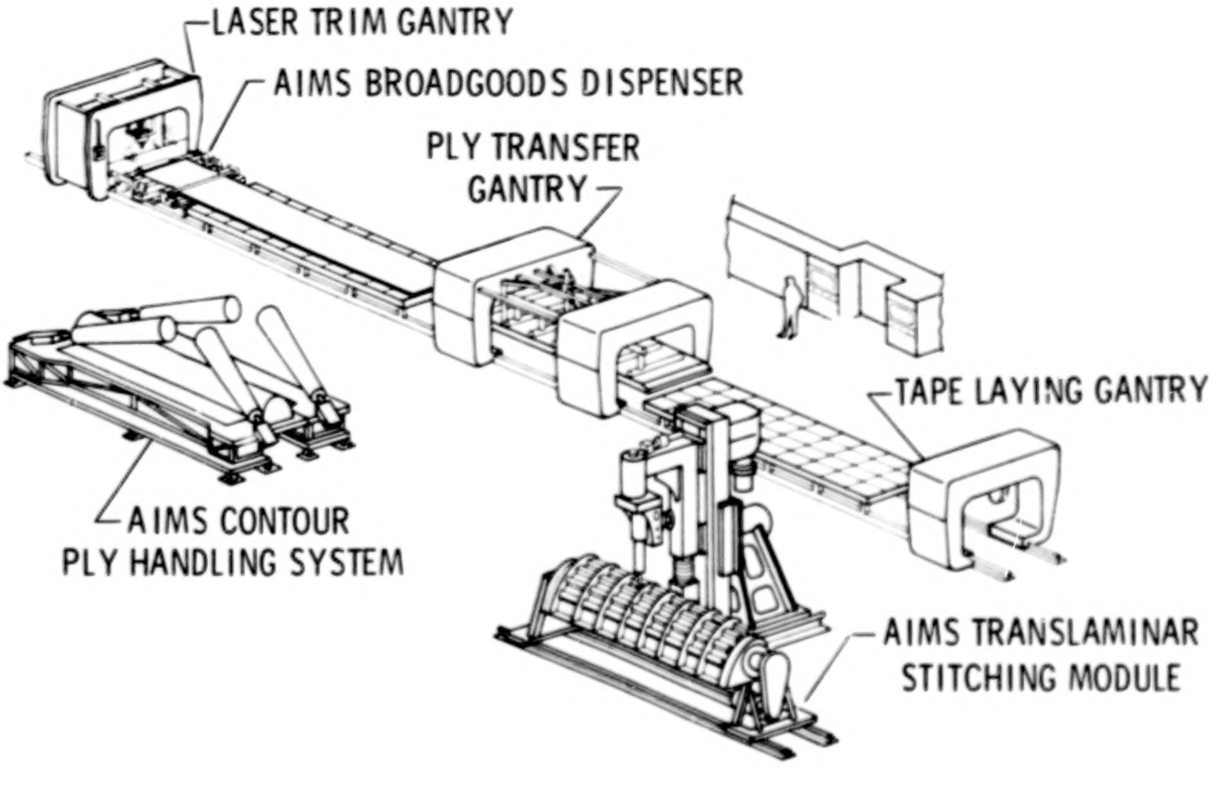
LASER TRIM GANTRY
AIMS BROADGOODS DISPENSER
PLY TRANSFER GANTRY
TAPE LAYING GANTRY
AIMS CONTOUR PLY HANDLING SYSTEM
AIMS TRANSLAMINAR STITCHING MODULE

INTEGRATED LAMINATING CENTER

The heart of the Grumman AIMS is the Integrated Laminating Center which is comprised of three traveling gantrys and two separate layup racks. The composite tape or broadgoods are dispersed onto the appropriate rack and trimmed by the laser trim gantry. The composite details can then be removed by the ply transfer gantry and placed on the appropriate layup tool.

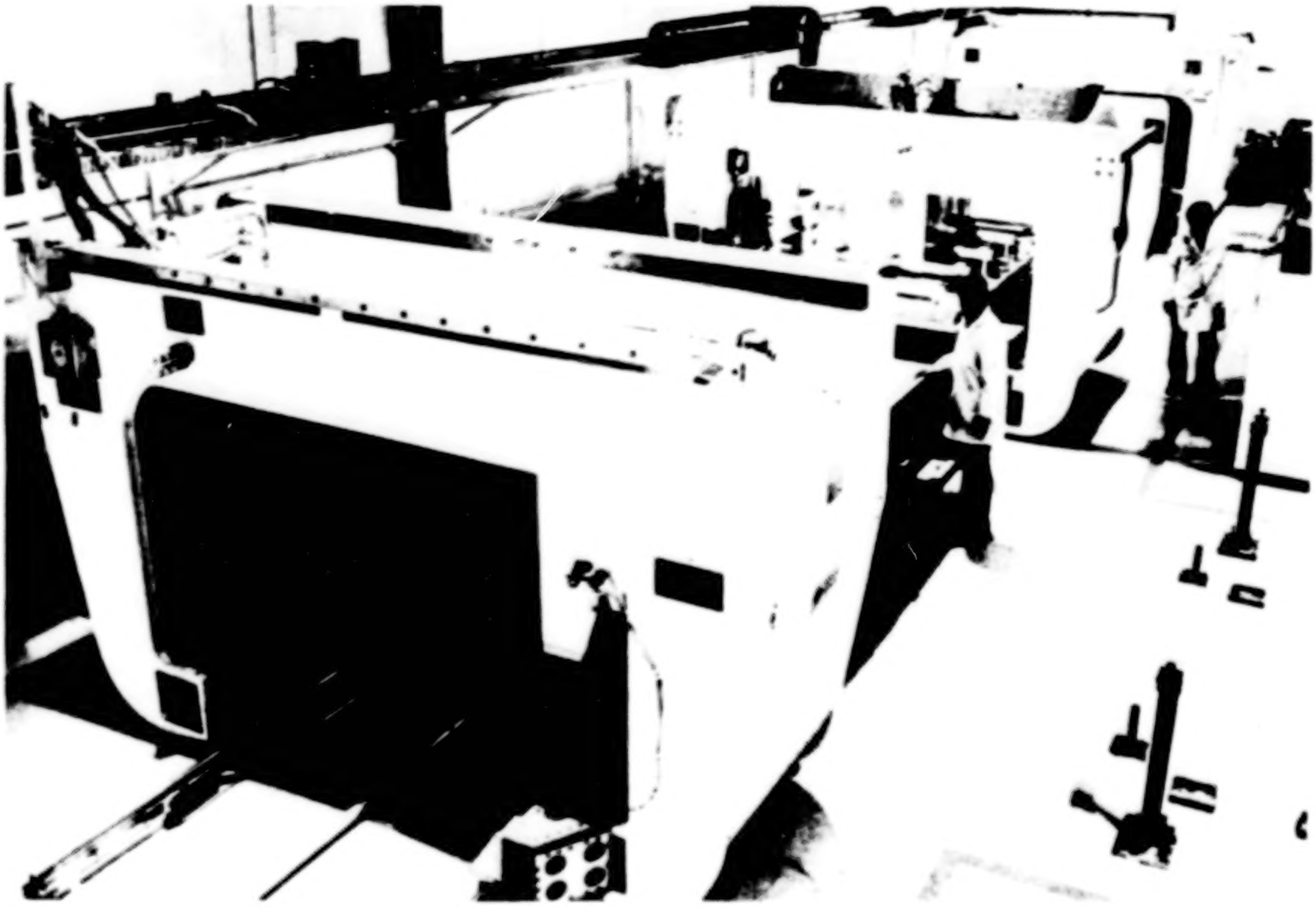

HOT MELT FUSION COMPOSITES

The state of the art for fabrication of fiber reinforced thermoplastic composite materials requires the impregnation of the reinforcement fiber with thermoplastic polymers that have been placed in solution with appropriate solvent systems. The matrix polymer materials that lend themselves to being placed in solution for impregnation naturally have limited resistance to exposure to various solvents after fabrication of a structural article. One obvious solution to this problem is to utilize a solvent-resistant polymer matrix material for impregnation of the composite. Since these matrix materials cannot be readily placed in solution, the reinforcing fibers must be impregnated by some form of hot-melt fusion of the matrix polymer. Performing this function by coating the fibers with films has met with limited success due to the inability to penetrate fiber bundles with the high-viscosity, solvent-resistant matrix materials. The technique of blending reinforcing fibers with nearly equal dimater thermoplastic matrix fibers is under investigation in the Materials Division at Langley Research Center. Preliminary results with laboratory-scale graphite/PBT thermoplastic composites fabricated in this manner indicate that very good wetting of the reinforcing fiber with the matrix fiber takes place during application of heat and pressure to form the composite. Work is under way to scale this technique up to fabricate broadgoods with graphite/thermoplastic PBT tows and subsequently manufacture structural articles from the graphite/PBT cloth.

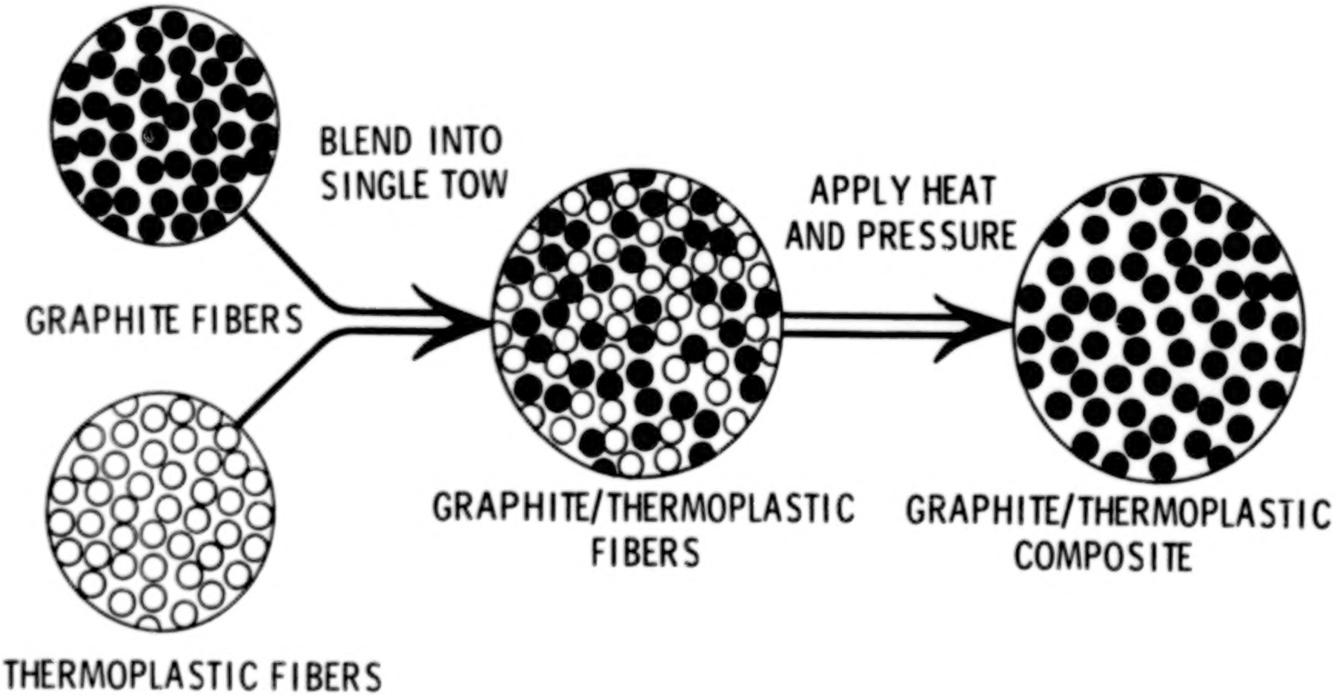

KEVLAR/EPOXY FACEGUARD

One physical impairment that frequently occurs as a result of cerebral palsy is the onset of seizures ranging from very mild to violent. Uncontrolled falls frequently result from these seizures which, without proper protection, can cause serious injury to the upper body and facial area of a person. One of the standard protection devices for uncontrolled falls is a helmet very similar to a football linemans' helmet. Due to the very heavy weight of this type of helmet, patients often refuse to wear them, which in turn eliminates the protection afforded by the helmet. A prototype Kevlar/epoxy protective face protection mask was fabricated at Langley for the boy shown in the figure. The mold for the mask was made from plaster and four plies of epoxy-impregnated Kevlar cloth were applied to the mold. After curing the mask it was removed from the plastic mold and the mouth and eye openings were cut. The resultant weight of this composite mask was 4 ounces compared to approximately 2 pounds for the football lineman's helmet. The patient in the figure has freely worn the Kevlar/epoxy mask for more than a year and has sustained no injuries in this time period. Prior uncontrolled falls without protection had resulted in several serious injuries to this patient including multiple jaw and nose breaks and loss of several permanent teeth.

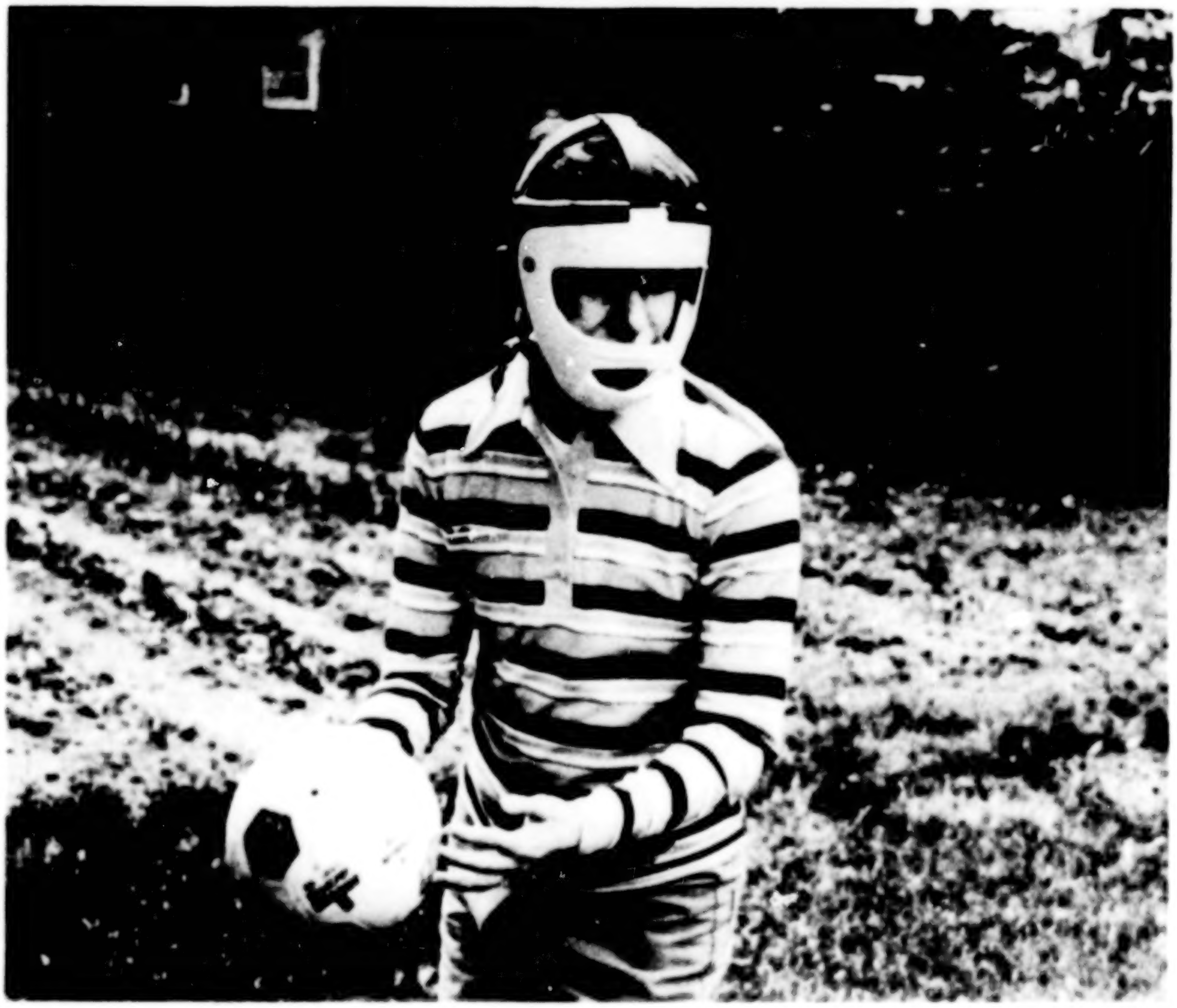

COMPOSITE WHEELCHAIR PROJECT

NASA Langley Research Center and the University of Virginia Rehabilitation Engineering Center are working together to design, fabricate, and evaluate a durable, lightweight composite wheelchair for general use. The graphite/epoxy wheelchair shown in the figure was the forerunner for the current NASA/UVA effort. All of the major structural components for the wheelchair in the figure were fabricated from graphite/epoxy to develop confidence in the fabricability of wheelchair elements from composites. This wheelchair was designed to transport invalid passengers aboard aircraft. The current general-use wheelchair under development will employ a variety of composite materials in its construction. The side, seat, and foot rest elements will be fabricated from a composite system composed of graphite/epoxy and Kevlar/epoxy hybrid skins bonded to each side of a special high strength inert polyimide foam core. This structurally efficient composite system has been subjected to a variety of bending and flexural tests to identify the optimum combination of elements. The target weight for the composite wheelchair is 25 pounds, whereas conventional general-purpose metal wheelchairs weigh over 50 pounds. Three prototype composite wheelchairs are scheduled to be completed by March 1983 for structural and clinical evaluation.

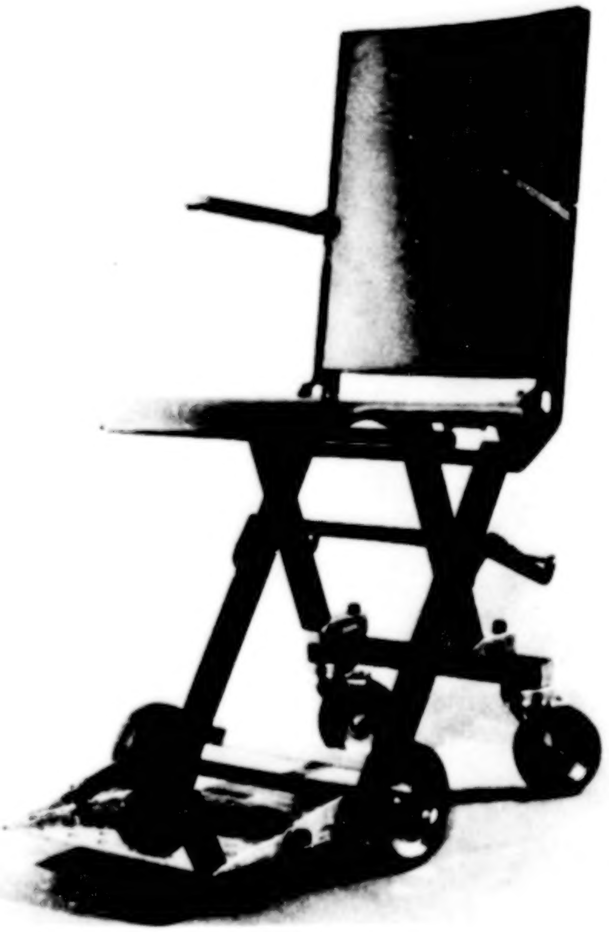

SUMMARY

Composite materials processing at Langley Research Center encompasses a wide variety of concepts and applications ranging from the construction of exotic models for research to the computer-assisted identification of critical molecular changes in polymer systems during cure. Along with the research support functions performed by highly specialized technicians, research is continuing in composite materials processing to identify and provide the concepts necessary to fabricate low-cost, reliable, and efficient structures. Facilities are continually being updated to provide support for this research. New composite systems formulated in-house are assessed on a continuing basis to establish their utility for a variety of commercial and aerospace applications.

CURRENT TECHNOLOGY

- ESTABLISHED FABRICATION PROCEDURES
- FLIGHT QUALITY COMPONENTS PRODUCED

FUTURE EMPHASIS

- AUTOMATION OF COMPOSITE PROCESSING
- PROCESSING TECHNIQUES FOR ADVANCED RESINS

SPINOFF

- BIOMEDICAL
- SPORTS
- TRANSPORTATION

BLANK PAGE

CONSERVATION OF STRATEGIC METALS

Joseph R. Stephens
NASA Lewis Research Center
Cleveland, Ohio

INTRODUCTION

NASA Lewis Research Center has undertaken a long-range program in support of the aerospace industry aimed at reducing the use of strategic materials in gas turbine engines (refs. 1 and 2). The program, which is called COSAM (Conservation of Strategic Aerospace Materials), has three general objectives:

(1) Contribute basic scientific understanding to the turbine engine "technology bank" so that our national security is not jeopardized if our strategic material supply lines are disrupted

(2) Help reduce the dependence of United States military and civilian gas turbine engines on worldwide supply/price fluctuations in regard to strategic materials

(3) Through research, contribute to the United States position of preeminence in the world gas turbine engine markets by minimizing the acquisition costs and optimizing the performance of gas turbine engines

NASA plans to accomplish these objectives of the COSAM Program by three major research thrusts: strategic element substitution; advanced processing concepts; and alternate material identification. Results from research and any required supporting technology will give industry the materials technology options it needs to make tradeoffs in material properties for critical components against the cost and availability impacts related to their strategic metal content. This paper presents an overview of the COSAM Program and briefly highlights the early progress that has been made.

VULNERABILITY OF U.S. AEROSPACE TO SUPPLY INSTABILITIES

The COSAM Program uses the following as a working definition of strategic metals: "those predominantly or wholly imported elements contained in the metallic alloys used in aerospace components which are essential to the strategic economic health of the U.S. aerospace industry." As a result of meetings with the ASME Gas Turbine Panel in 1979 and a survey of aerospace companies in 1980, the COSAM Program was focused primarily on the needs of the aircraft engine industry. Based on these findings and other discussions with several aircraft engine manufacturers, four elements emerged that were of particular concern. The alloys used to build the critical high-temperature components for aircraft propulsion systems require the use of the four metals - cobalt, tantalum, columbium, and chromium. Today we are almost totally dependent on foreign sources for these metals (fig. 1). In several of the countries listed in figure 1, political disturbances have led to supply interruptions. Therefore, the U.S. aircraft engine industry is very vulnerable to supply instabilities of the essential metals needed for engine manufacturing.

METAL	% IMPORTED	MAJOR FOREIGN SOURCES
COBALT	97	ZAIRE, ZAMBIA
COLUMBIUM	100	BRAZIL, CANADA
TANTALUM	97	THAILAND, MALAYSIA
CHROMIUM	91	SOUTH AFRICA, ZIMBABWE

Figure 1

STRATEGIC MATERIAL RESOURCES IN AFRICA

Currently, the African Third World nations of Zaire, Zambia, Zimbabwe, and South Africa play a major role in supplying strategic materials to the United States (fig. 2). Foreign cartels, political unrest, and production limitations have led to severe market availability/cost fluctuations. In fact, such problems could lead to a total interruption of flow of such strategic metals in times of world crisis. There are regions of instability (ref. 3) in Africa where some political groups might be able to wage "a long-term resource war against the U.S." (ref. 4).

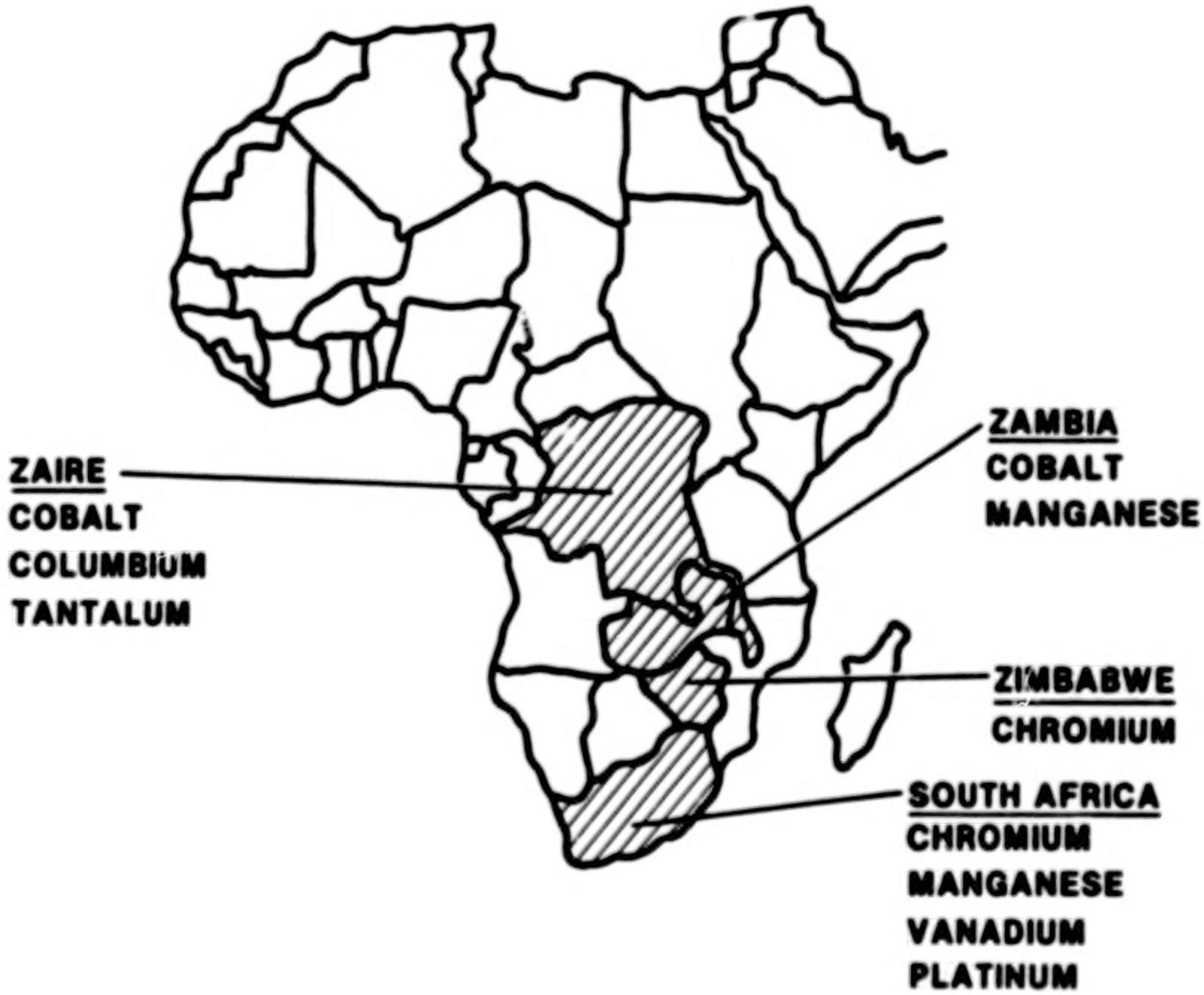
ZAIRE
COBALT
COLUMBIUM
TANTALUM
ZAMBIA
COBALT
MANGANESE
ZIMBABWE
CHROMIUM
SOUTH AFRICA
CHROMIUM
MANGANESE
VANADIUM
PLATINUM

Figure 2

DEPENDENCE OF GAS TURBINE ENGINES ON STRATEGIC METALS

The strategic metals cobalt, tantalum, columbium, and chromium are contained in superalloys, steels, and stainless steels that are used in engine manufacturing. The locations of these metals in aircraft engine compressors, turbines, and combustors are shown in figure 3. The need for these metals has increased as the demands have grown for higher durability plus higher performance fuel efficient aircraft turbine engines. Based on the essential nature of these metals and in order for the U.S. aircraft industry to maintain its competitive position, supplies must be readily available at a reasonably stable cost.

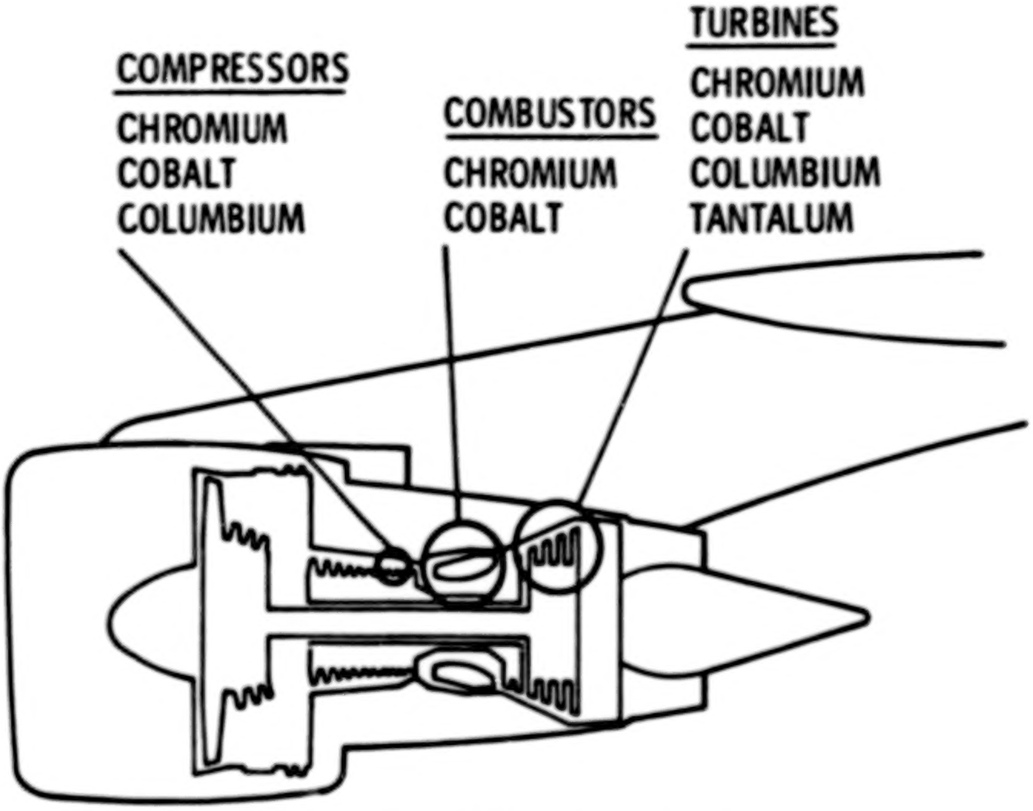
COMPRESSORS
CHROMIUM
COBALT
COLUMBIUM
COMBUSTORS
CHROMIUM
COBALT
TURBINES
CHROMIUM
COBALT
COLUMBIUM
TANTALUM

NEEDED FOR PERFORMANCE AND LONG LIFE

COBALT - HIGH TEMPERATURE STRENGTHENER
COLUMBIUM - INTERMEDIATE TEMPERATURE STRENGTHENER
TANTALUM - OXIDATION RESISTANCE
CHROMIUM - CORROSION RESISTANCE

Figure 3

VOLATILE AND UNPREDICTABLE PRICES OF STRATEGIC MATERIALS

Because of supply disruption or increased demand, it is not uncommon for price changes of several hundred percent to occur (fig. 4 and ref. 5). These rapid price increases illustrate the vulnerability of the U.S. aircraft engine industry to cost fluctuations. The essential nature of chromium, cobalt, columbium, and tantalum and their vulnerability to supply instabilities and cost fluctuations combine to cause these metals to be classified as strategic aerospace metals. The possibility of a total supply disruption during a time of worldwide crisis is, of course, readily recognizable.

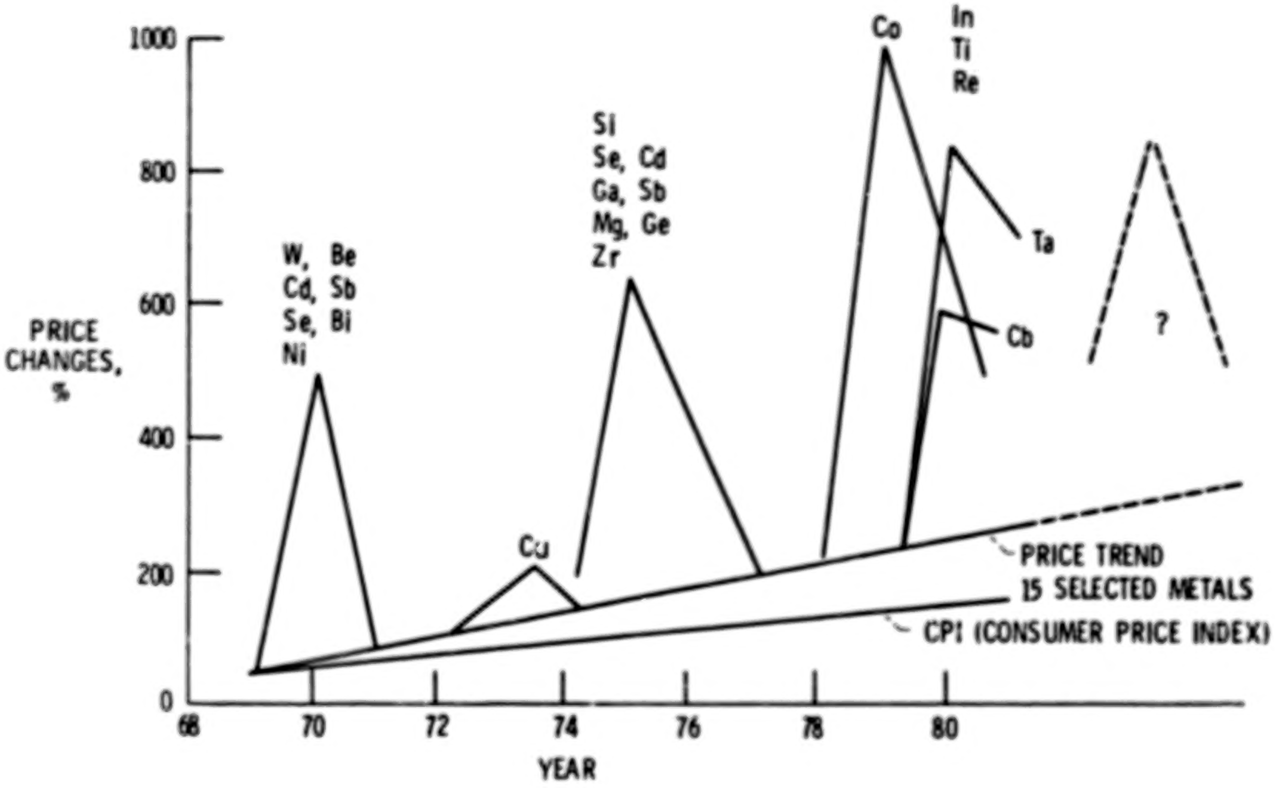

Figure 4

BEST [illegible]LE

MAJOR THRUSTS OF COSAM PROGRAM

The three objectives of the COSAM Program given in the INTRODUCTION are being accomplished by a systematic basic research and technology effort aimed at reducing the need for strategic metals in advanced aerospace components. The COSAM Program is aimed at providing industry with options so that they can make their own property versus availability/cost tradeoffs when selecting aerospace alloys. The three-pronged approach to COSAM is shown in figure 5. It consists of research on strategic element substitution, advanced processing concepts, and development of alternate materials. Conservation, as well as reduced dependence on strategic metals, will be achieved in the area of strategic element substitution by examining systematically the effects of replacing cobalt, columbium, and tantalum with less strategic elements in current, high use engine alloys. Conservation through advanced processing concepts research will be approached by investigating the interface stability in a simulated dual alloy or tailored structure (use strategic metal containing alloys only where needed) component. In the longer term, developing (higher risk) alternate materials that are readily available in the U.S. to replace the most strategic metals could lead to a dramatic reduction in our dependence on foreign sources. These last two technology areas will also help conserve the strategic metals cobalt, tantalum, columbium, and chromium.

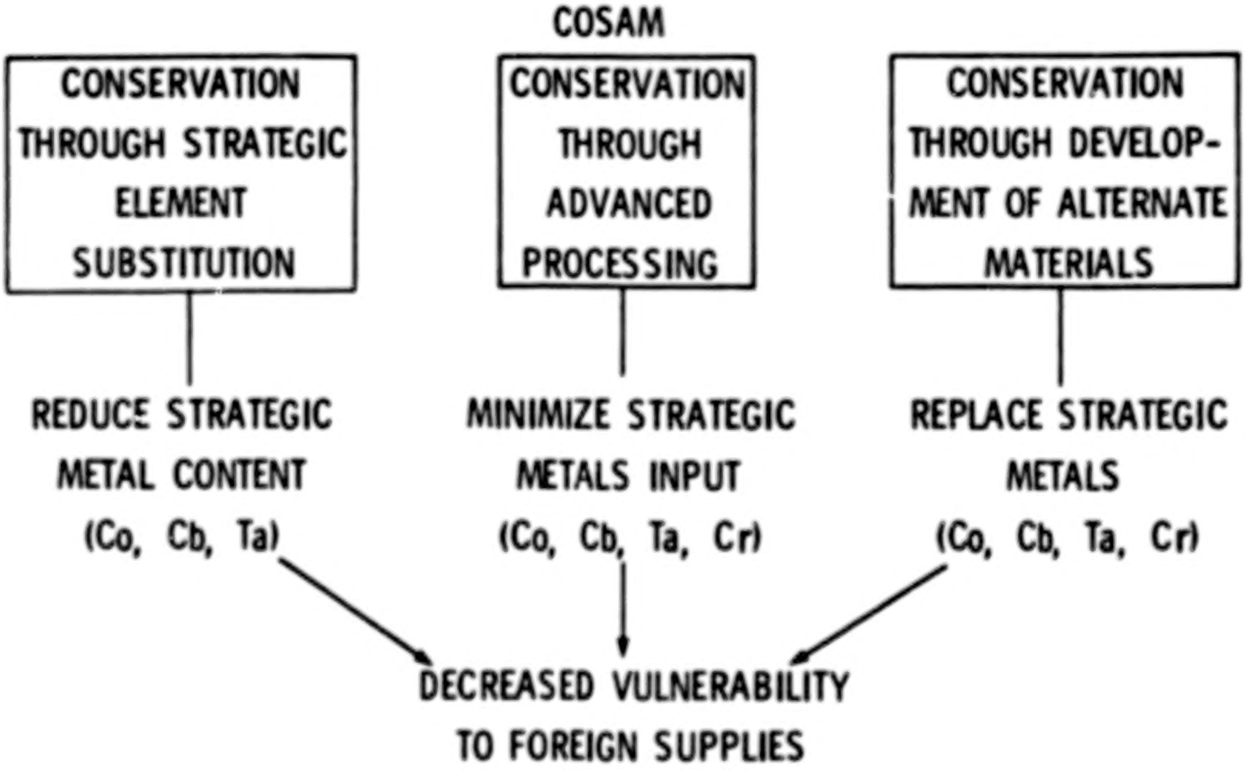
COSAM
CONSERVATION THROUGH STRATEGIC ELEMENT SUBSTITUTION
CONSERVATION THROUGH ADVANCED PROCESSING
CONSERVATION THROUGH DEVELOPMENT OF ALTERNATE MATERIALS
REDUCE STRATEGIC METAL CONTENT (Co, Cb, Ta)
MINIMIZE STRATEGIC METALS INPUT (Co, Cb, Ta, Cr)
REPLACE STRATEGIC METALS (Co, Cb, Ta, Cr)
DECREASED VULNERABILITY TO FOREIGN SUPPLIES

Figure 5

COOPERATIVE NASA-INDUSTRY-UNIVERSITY PROGRAMS

Various research efforts are being conducted under the overall programmatic management of the NASA Lewis Research Center. Some of this work is being conducted in-house at Lewis. There are also cooperative programs under way involving Lewis with both industry and universities to optimize the expertise at each organization and to seek synergistic results from the combined efforts. This research cooperation is presented graphically in figure 6. Typical roles for each organization are shown. These roles, of course, vary from program to program. For example, one project can involve an industry contract or a university grant for the bulk of the effort with a range of supporting contributions from the other partners. Another project may be conducted mainly in-house at Lewis with a range of support from industry or a university. The subsequent figures outline some of the current projects and present limited highlights of results obtained to date.

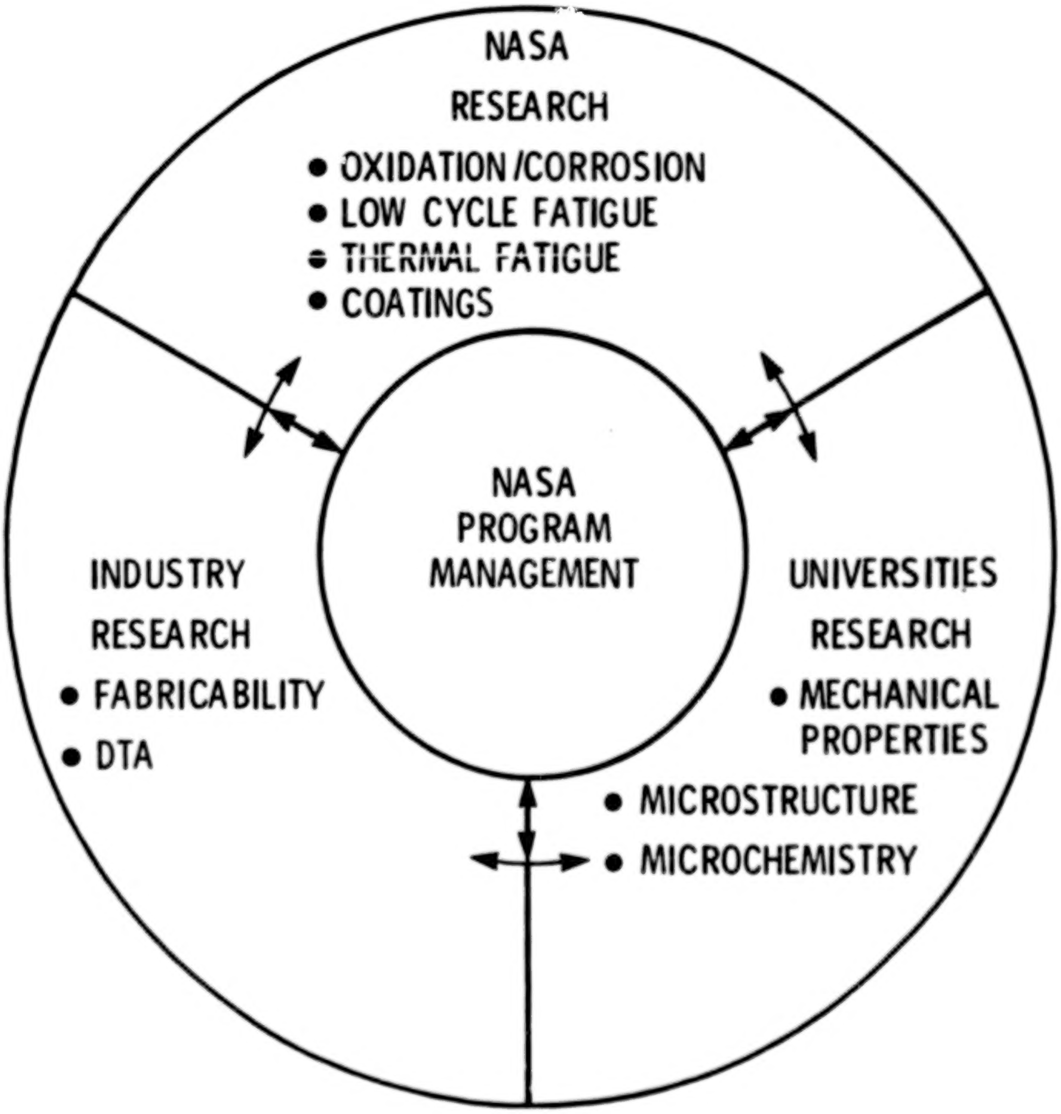
NASA
RESEARCH
• OXIDATION/CORROSION
• LOW CYCLE FATIGUE
• THERMAL FATIGUE
• COATINGS
NASA
PROGRAM
MANAGEMENT
INDUSTRY
RESEARCH
• FABRICABILITY
• DTA
UNIVERSITIES
RESEARCH
• MECHANICAL PROPERTIES
• MICROSTRUCTURE
• MICROCHEMISTRY

Figure 6

RECENT TRENDS IN UNITED STATES AND AEROSPACE COBALT USAGE

As a result of the high cost of cobalt in 1978 and 1979, the United States has experienced a decline in cobalt usage (ref. 6). Figure 7 shows that 20 million pounds of cobalt were consumed in 1978 but that by 1981 usage was down to an estimated 13.6 million pounds, a reduction of about 33 percent in only 3 years. During this same period, the use of cobalt to produce superalloys, primarily nickel-base alloys for aircraft engines, increased from 4 million pounds in 1978 to a peak of 7.2 million pounds in 1980 before it declined to an estimated 5.4 million pounds in 1981.

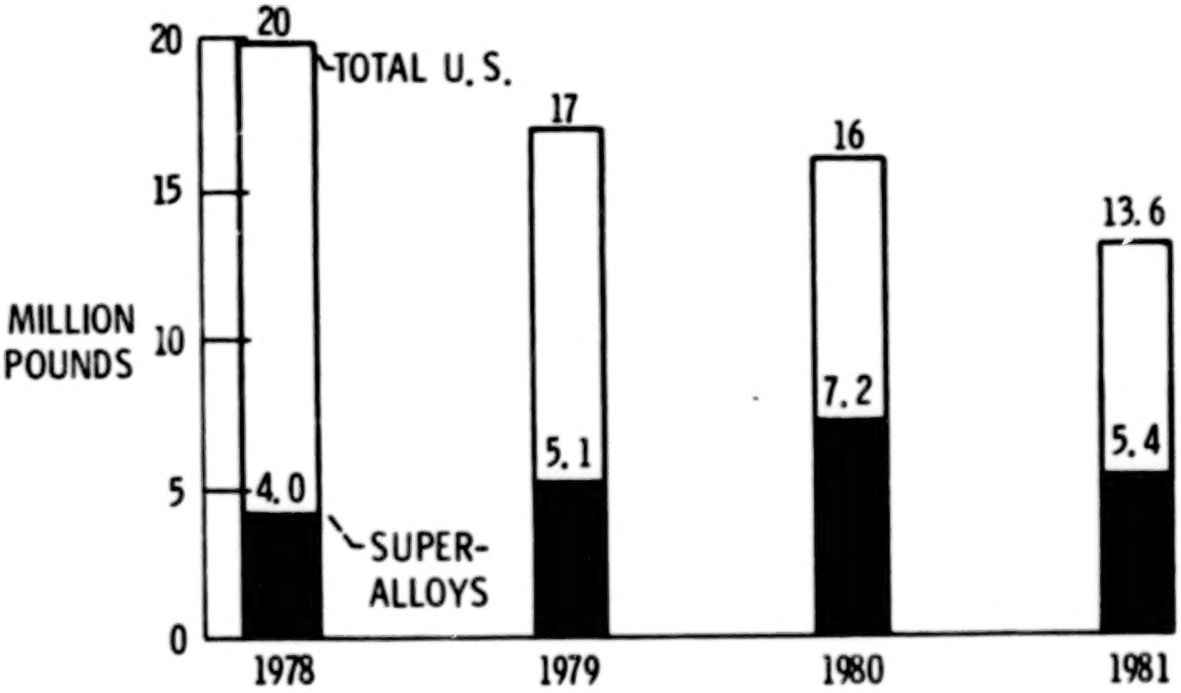

Figure 7

DISTRIBUTION OF 1981 UNITED STATES COBALT CONSUMPTION

The importance of cobalt to superalloy production is illustrated in figure 8. Of the 13.6 million pounds of cobalt consumed by the United States in 1981, 40 percent of it went for superalloy production. Because of the importance of cobalt to the aircraft engine industry and its high cost and lack of availability in 1979 and 1980, several programs were initiated to identify substitutes for it in a variety of nickel-base superalloys. Such programs could have long-term national benefits, and, in addition, the methodology developed in these programs could serve as a model for future efforts involving other strategic elements.

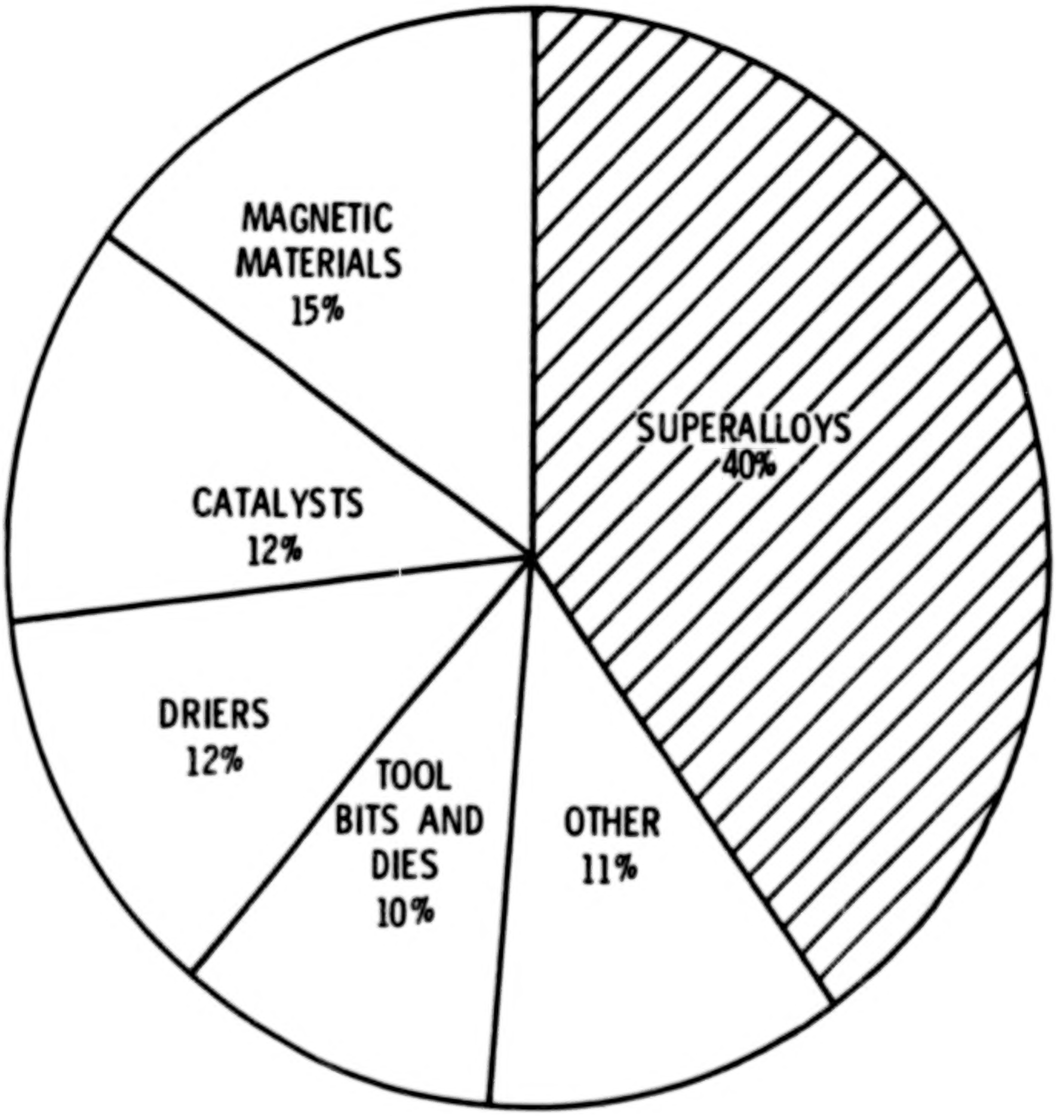

Figure 8

SUPERALLOYS SELECTED FOR COBALT SUBSTITUTION

Four nickel-base superalloys were selected for the COSAM investigation on cobalt. The four alloys are listed in figure 9 with their typical applications in the aircraft engine industry, the forms in which they are used and remarks as to why they were selected for the COSAM activity. Applications include turbine disks as well as low- and high-pressure turbine blades. A variety of product forms are represented by the applications of the four alloys as noted in the figure. The selection of the four alloys was based primarily on the considerations given in this figure. Waspaloy was selected because it represented the highest tonnage of cobalt in commercial aircraft engines. Udimet-700 was selected because it has a composition similar to many of the cobalt-containing nickel-base superalloys, and it is used in the as-cast, as-wrought ingot, as-wrought powder, and as-HIP powder metallurgy fabricated conditions. Thus, the composition versus processing study opportunities were great. The potential for determining the impact of cobalt on both conventionally cast and D.S. polycrystalline and single crystal turbine blades was the reason for selecting MAR-M247. René 150 was chosen because it is an advanced directionally solidified alloy.

ALLOY	TYPICAL ENGINE APPLICATION	FORM	REMARKS
WASPALOY	TURBINE DISK	FORGED	HIGHEST USE WROUGHT ALLOY IN CURRENT ENGINES
UDIMET-700	TURBINE DISK	FORGED	SIMILAR ALLOYS USED IN VARIOUS FORMS AND APPLICATIONS
(LC) ASTROLOY	TURBINE DISK	AS-HIP-POWDER	
(RENÉ 77)	TURBINE BLADES	CAST	
MAR-M247	TURBINE BLADES & WHEELS	CAST	CONVENTIONALLY-CAST, D.S. AND SINGLE CRYSTAL
RENÉ 150	TURBINE BLADES	DS-CAST	HIGHLY COMPLEX DIRECTIONALLY-CAST ALLOY

Figure 9

PARTICIPANTS' ROLES IN COOPERATIVE PROGRAM ON WASPALOY AND UDIMET-700

The cooperative nature of the research being conducted on Waspaloy and Udimet-700 is illustrated in figure 10. The role of industry, as represented by Special Metals Corporation, is to characterize and optimize fabrication and heat-treating procedures for the reduced cobalt Waspaloy and Udimet-700 alloys. The roles of Columbia University and Purdue University are also shown in the figure. Columbia University is conducting mechanical property characterization, structural stability, microstructural feature evaluation, and theoretical formulations to identify future alloy modifications, if required, for the second portion of the project. Purdue University is responsible primarily for microstructural and microchemistry characterization of the reduced cobalt content alloys. NASA Lewis is involved in special mechanical and physical metallurgy characterization of the alloys. The result of this cooperative effort is expected to be a clearer understanding of the role of cobalt in nickel-base superalloys.

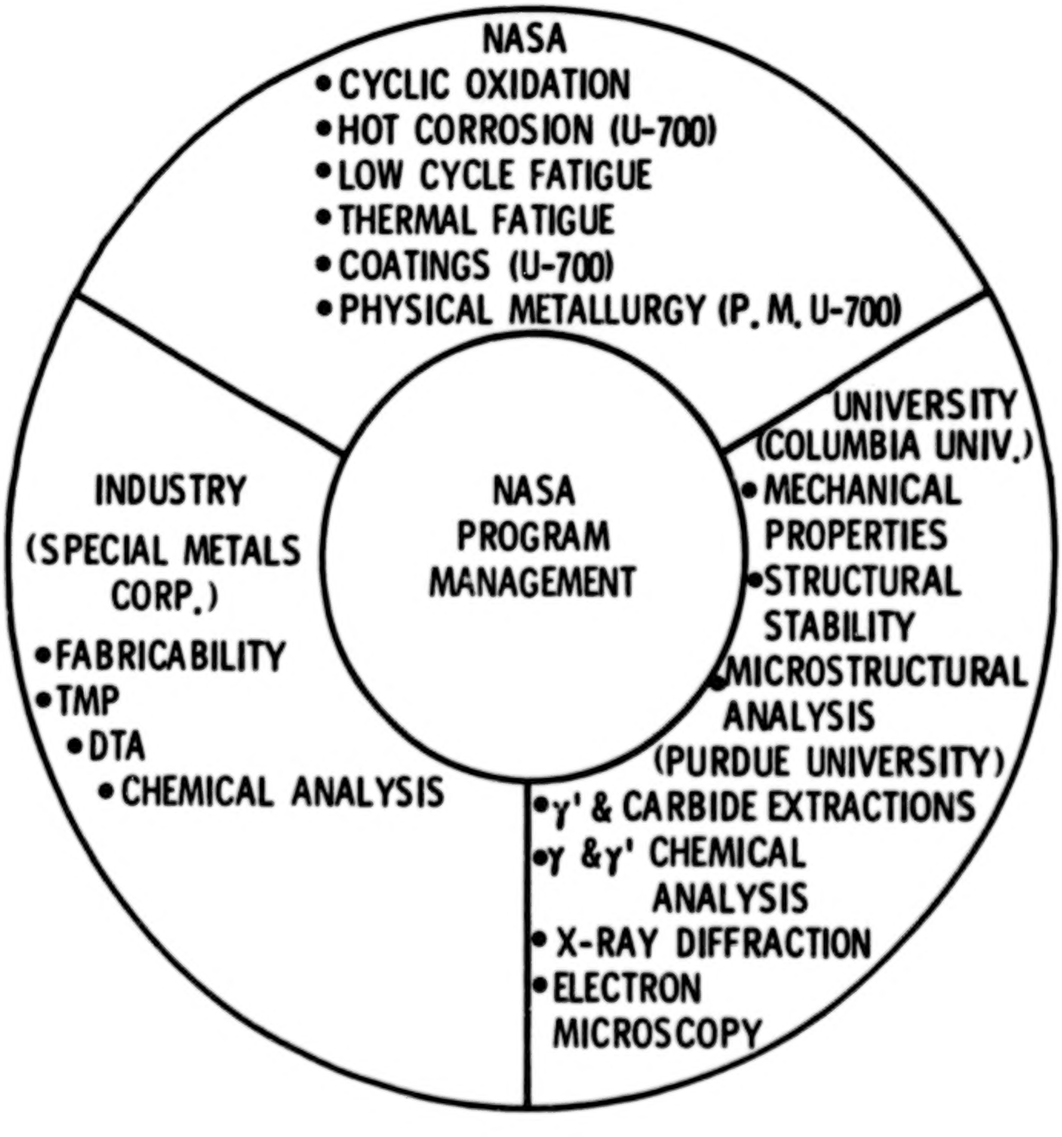
NASA
• CYCLIC OXIDATION
• HOT CORROSION (U-700)
• LOW CYCLE FATIGUE
• THERMAL FATIGUE
• COATINGS (U-700)
• PHYSICAL METALLURGY (P. M. U-700)
NASA PROGRAM MANAGEMENT
INDUSTRY
(SPECIAL METALS CORP.)
• FABRICABILITY
• TMP
• DTA
• CHEMICAL ANALYSIS
UNIVERSITY
(COLUMBIA UNIV.)
• MECHANICAL PROPERTIES
• STRUCTURAL STABILITY
• MICROSTRUCTURAL ANALYSIS
(PURDUE UNIVERSITY)
• γ' & CARBIDE EXTRACTIONS
• γ & γ' CHEMICAL ANALYSIS
• X-RAY DIFFRACTION
• ELECTRON MICROSCOPY

Figure 10

EFFECT OF COBALT CONTENT IN WASPALOY ON RUPTURE LIFE AND TENSILE STRENGTH

Some preliminary results on the effects of reducing cobalt in Waspaloy (13-percent cobalt alloy) were reported by Maurer et al. (ref. 7) of Special Metals Corporation. Highlights of that study are shown in figure 11. Tensile strength decreases only slightly as the amount of cobalt in the alloy decreases. However, rupture life decreased substantially with decreasing amounts of cobalt in Waspaloy.

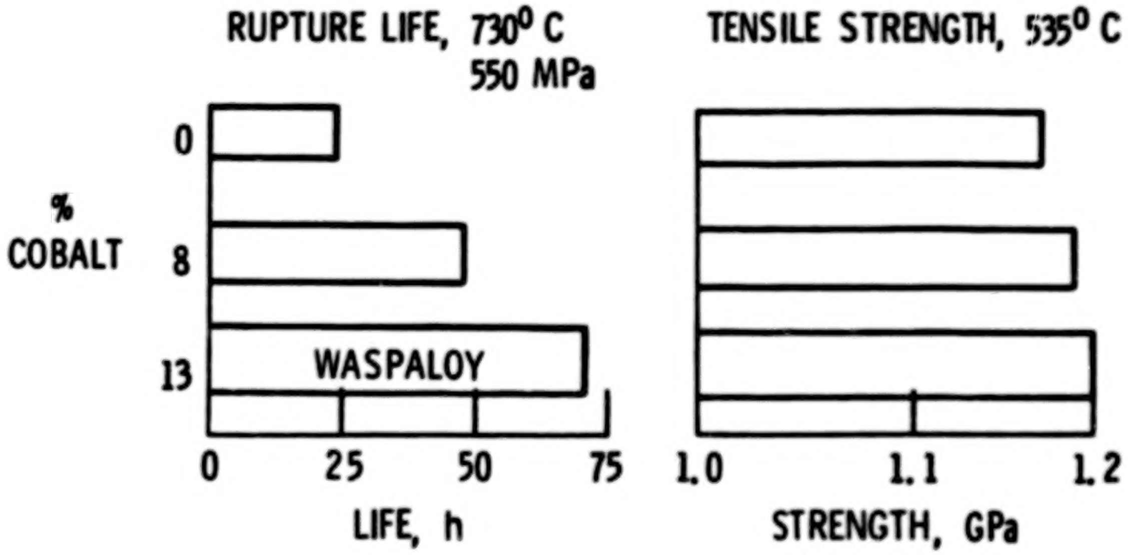

Figure 11

EFFECT OF COBALT ON CYCLIC OXIDATION RESISTANCE OF UDIMET-700

Research at NASA Lewis has focused on the cyclic oxidation resistance of the low/no cobalt Udimet-700 alloys. Initial results of this study are shown in figure 12. At 1100° C, removing cobalt from Udimet-700 improved the cyclic oxidation resistance based on specific weight change data; however, confirmatory metallographic analyses of the depths of attack have yet to be conducted. Tests at 1000° and 1150° C revealed a similar behavior. Hot corrosion resistance of the low/no cobalt Udimet-700 alloys is also under investigation at NASA Lewis. Initial qualitative results from tests using NaCl-doped flames in a Mach 0.3 burner rig indicate that corrosion resistance also increases with decreasing cobalt content.

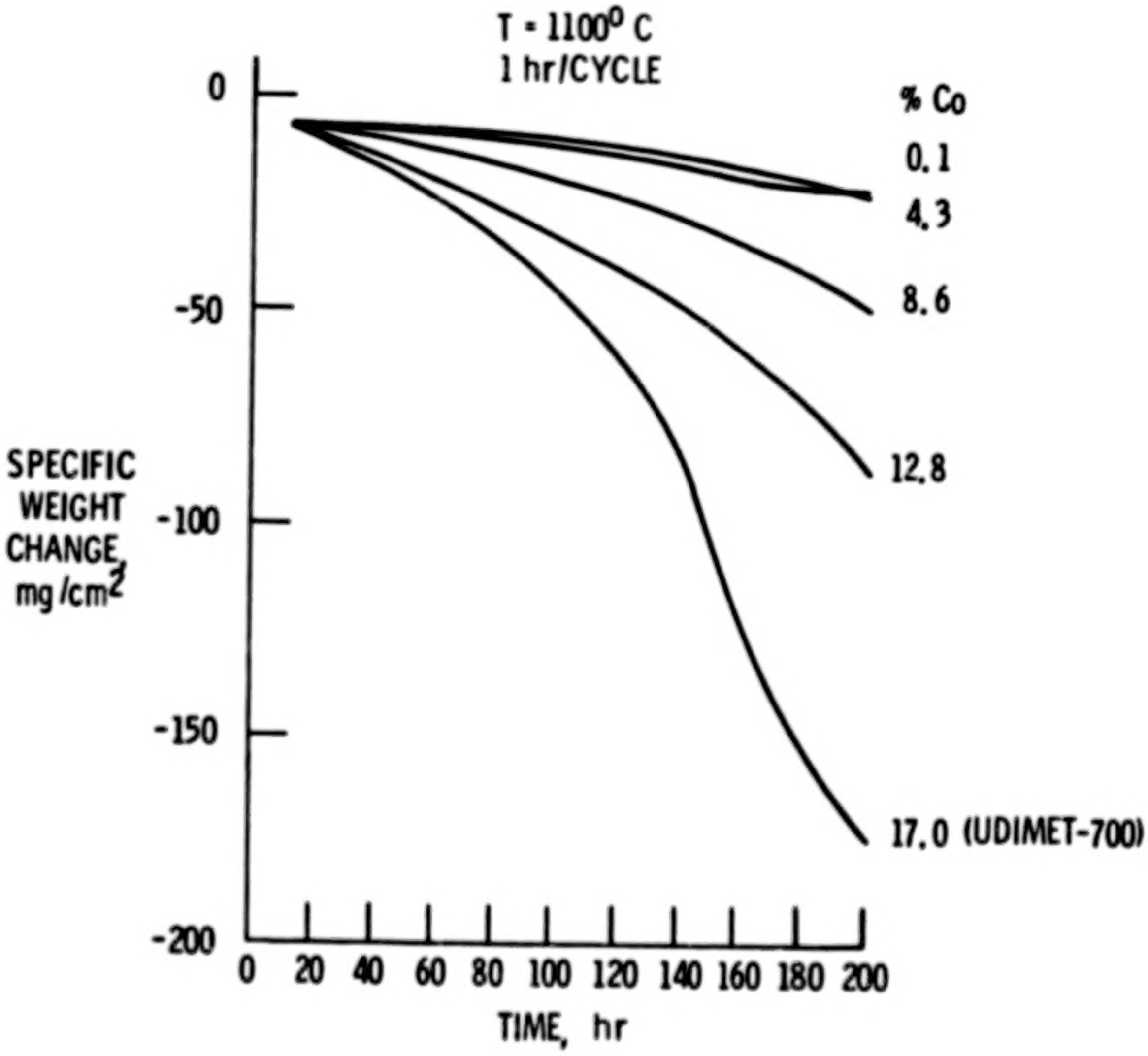

Figure 12

PARTICIPANT ROLES IN COOPERATIVE PROGRAM ON COLUMBIUM IN INCONEL 718

Columbium is considered to be a strategic aerospace metal because the United States imports 100 percent of it and because this metal is becoming increasingly important as an alloying element in nickel-base superalloys. The response of the aerospace industry to the cobalt shortage in 1978-79 was, in some instances, to switch to columbium-containing alloys as substitutes for cobalt-bearing alloys - for example, Inconel 718 (5-percent Cb - 0-percent Co) for Waspaloy (0-percent Cb - 13-percent Co). In 1980, 29 percent of the United States consumption of columbium went into the production of superalloys - the largest single use of columbium in the United States. Within the aerospace industry, Inconel 718 is probably the largest consumer of columbium. Inconel 718 is used as a turbine disk material. Disks are large, heavy components that contain the bulk of the columbium used. The increased demand for columbium in the aerospace industry has focused attention on identifying potential substitutes for it in nickel-base superalloys. A program has recently been initiated to identify potential substitutes for columbium in Inconel 718. This program is being conducted primarily under a grant with Case Western Reserve University. Special Metals Corporation has prepared the modified composition alloys and NASA Lewis is involved in evaluating alloy properties. The program organization is illustrated in figure 13.

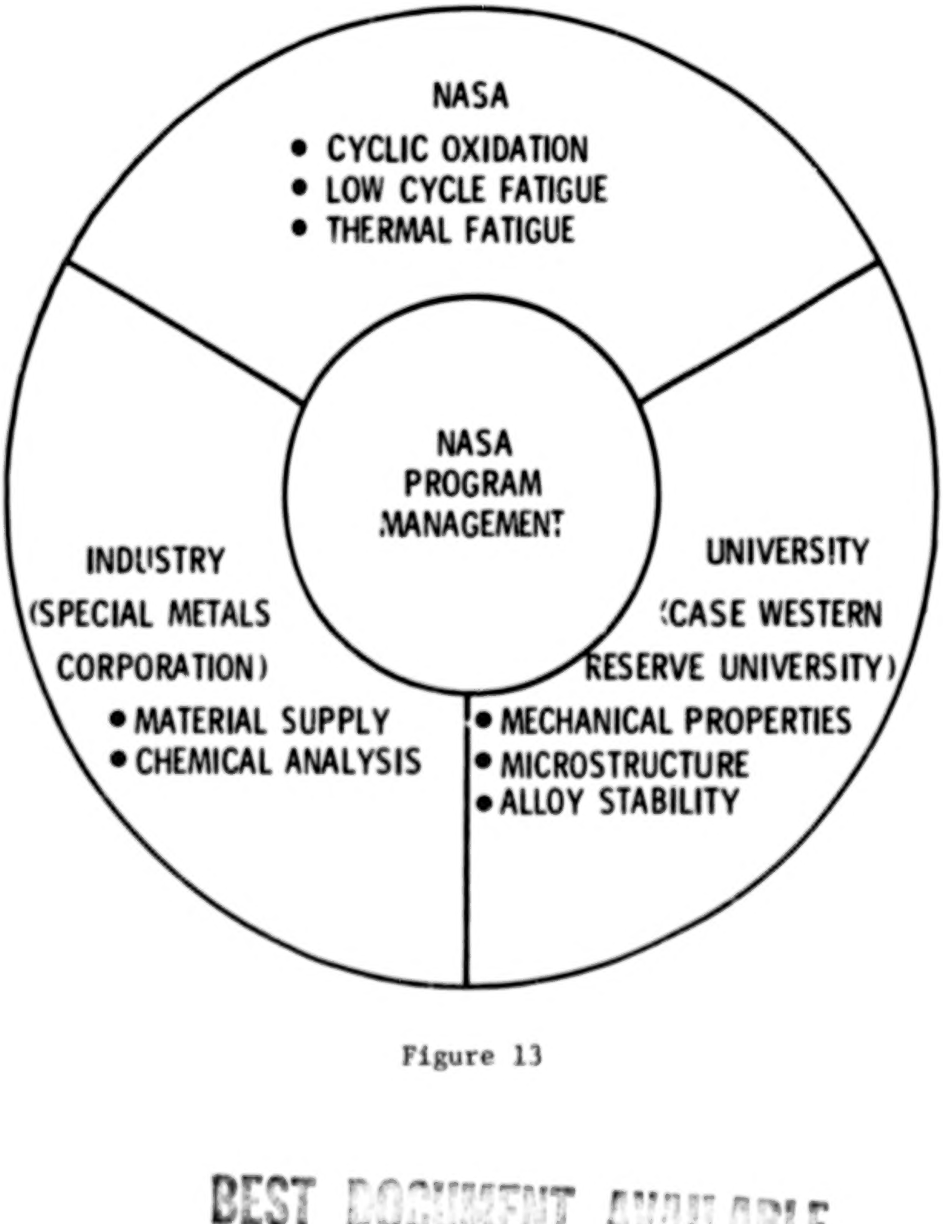
NASA
• CYCLIC OXIDATION
• LOW CYCLE FATIGUE
• THERMAL FATIGUE
NASA PROGRAM MANAGEMENT
INDUSTRY
(SPECIAL METALS CORPORATION)
• MATERIAL SUPPLY
• CHEMICAL ANALYSIS
UNIVERSITY
(CASE WESTERN RESERVE UNIVERSITY)
• MECHANICAL PROPERTIES
• MICROSTRUCTURE
• ALLOY STABILITY

Figure 13

PARTICIPANT ROLES IN COOPERATIVE PROGRAM ON TANTALUM IN SUPERALLOYS

Tantalum is being used in advanced nickel-base superalloys primarily to improve oxidation resistance and to increase strength. Because of the increased use of tantalum in the aerospace industry and because the United States imports over 97 percent of it, this element is strategic and is of concern for the long term. Its major usage is for capacitors, another high national priority application, while the total use of tantalum in superalloys constitutes only about 6 percent of total United States consumption. However, tantalum is critical to advanced nickel-base superalloys. A joint Michigan Technological University/ General Electric/NASA Lewis program is just beginning to determine the role of tantalum in nickel-base superalloys. The program organization is shown in figure 14. Primary initial emphasis is on exploring the effects of reducing tantalum in conventionally cast, D.S. polycrystalline and single-crystal MAR-M247, an alloy that contains 4 percent tantalum. In addition, some limited studies will be conducted on B-1900+Hf, an alloy which contains 4.3 percent tantalum. Material for this part of the program is being supplied by TRW. Case Western Reserve University is exploring the effects of substituting tungsten for tantalum in single-crystal MAR-M247 alloys.

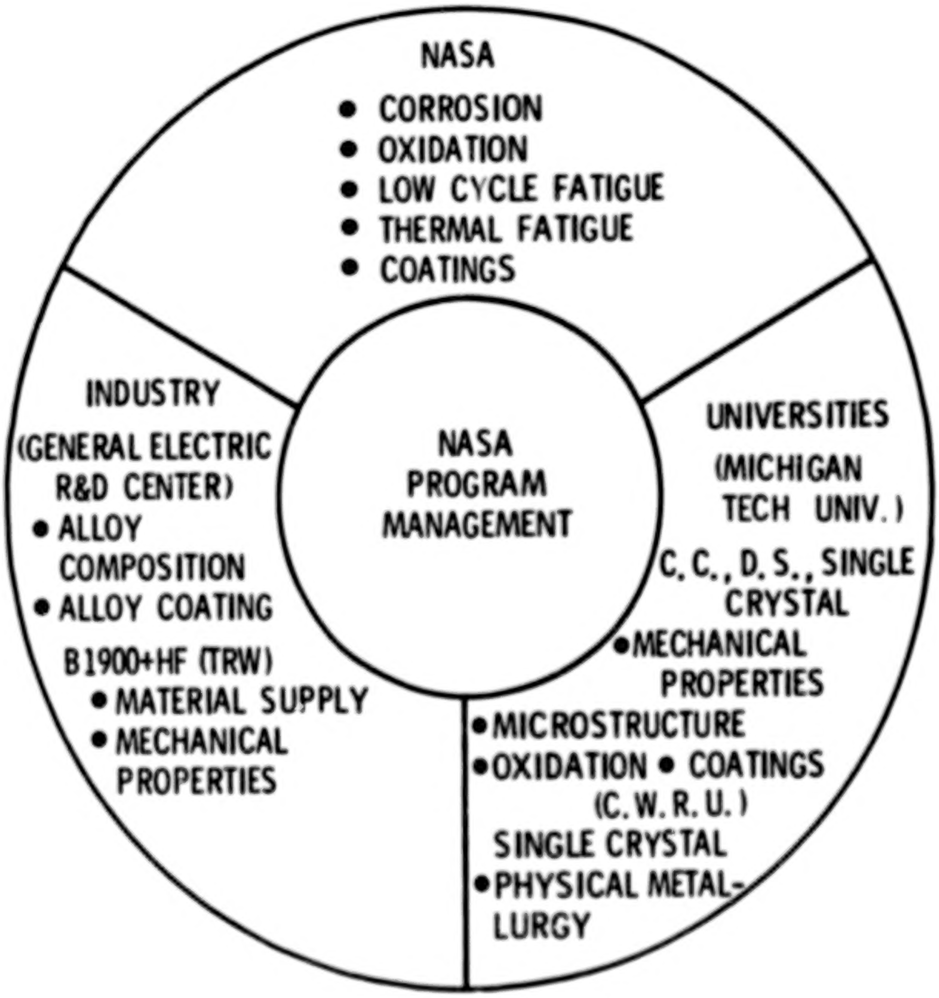
NASA
• CORROSION
• OXIDATION
• LOW CYCLE FATIGUE
• THERMAL FATIGUE
• COATINGS
INDUSTRY
(GENERAL ELECTRIC R&D CENTER)
• ALLOY COMPOSITION
• ALLOY COATING
B1900+HF (TRW)
• MATERIAL SUPPLY
• MECHANICAL PROPERTIES
NASA PROGRAM MANAGEMENT
UNIVERSITIES
(MICHIGAN TECH UNIV.)
C.C., D.S., SINGLE CRYSTAL
• MECHANICAL PROPERTIES
• MICROSTRUCTURE
• OXIDATION • COATINGS
(C.W.R.U.)
SINGLE CRYSTAL
• PHYSICAL METALLURGY

Figure 14

DUAL ALLOY INTERFACE STABILITY

The second major COSAM Program thrust is that of advanced processing. Turbine disks constitute a major portion of the weight of superalloys (and thus strategic materials) used in gas turbine engines. These components typically operate at higher temperatures in the rim and at lower temperatures in the hub area. In addition, creep is the primary deformation mechanism in the rim while fatigue resistance is required in the hub. Monolithic disks currently used are fabricated and heat treated to compromise the creep resistance that can be achieved with a large grain size material and fatigue resistance of a fine grain size material. An alternate approach would be to fabricate dual property disks (different heat treatments at the bore and rim) or dual alloy disks to optimize the required properties at the rim and hub. The concept of joining two P.M. nickel-base superalloys to achieve this goal was investigated by Kortovich (ref. 8) in a NASA Lewis sponsored program. The COSAM Program will carry this technique further by studying the feasibility of HIP joining a nickel-base alloy rim material and an iron-base alloy (low strategic metal content) hub material. The dual alloy joining concept is shown schematically in figure 15 along with the planned extension of this process to conserve strategic materials. Emphasis will be placed on HIP joint integrity, microstructural stability, and mechanical properties as compared to the base alloys. This program will be conducted on laboratory size test specimens and will not involve prototype or component fabrication.

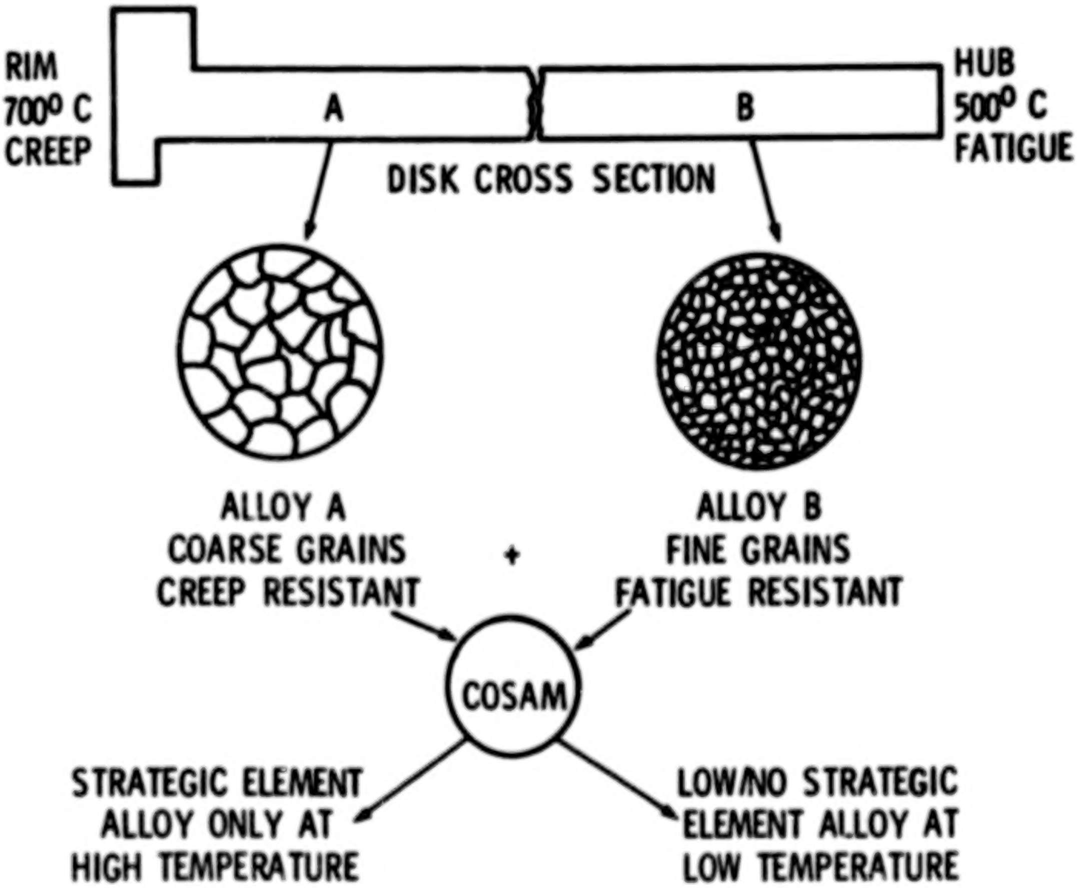
RIM
700° C
CREEP
A
B
HUB
500° C
FATIGUE
DISK CROSS SECTION
ALLOY A
COARSE GRAINS
CREEP RESISTANT
+
ALLOY B
FINE GRAINS
FATIGUE RESISTANT
COSAM
STRATEGIC ELEMENT
ALLOY ONLY AT
HIGH TEMPERATURE
LOW/NO STRATEGIC
ELEMENT ALLOY AT
LOW TEMPERATURE

Figure 15

PARTICIPANTS' ROLES IN COOPERATIVE INTERMETALLIC COMPOUND PROGRAM

The third major COSAM Program thrust, alternate materials, has the potential of eliminating most or all of the cobalt, tantalum, and columbium containing alloys and also of replacing some of the strategic element chromium that is now used in gas turbine engines. One aspect of this thrust of the COSAM Program is focusing on the equiatomic iron and nickel aluminides (i.e., FeAl and NiAl) as potential alternatives to nickel-base superalloys. This program emphasizes a basic research approach toward understanding the deformation mechanisms that control high-temperature creep as well as those that control the lack of room temperature ductility. By necessity, the program is a long-term, high-risk effort, but it offers the potential of a substantial payoff if materials evolve which permit conserving all four currently identified strategic metals -- cobalt, tantalum, columbium, and chromium. These binary aluminides have several advantages:

(1) They exist over a wide range of compositions and have a large solubility for substitutional third element additions.

(2) They have a cubic crystal structure.

(3) They have very high melting points (except for FeAl which has a somewhat lower melting point).

(4) They contain inexpensive, readily available elements.

(5) They possess potential for self protection in oxidizing environments.

Their chief disadvantage is that they lack room temperature ductility. Figure 16 illustrates the organizational structure of the current intermetallic compound program.

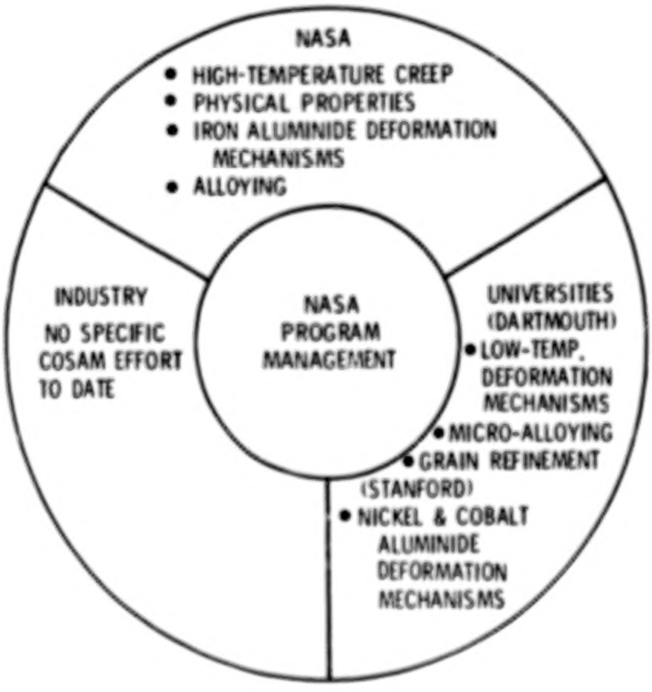
NASA
• HIGH-TEMPERATURE CREEP
• PHYSICAL PROPERTIES
• IRON ALUMINIDE DEFORMATION MECHANISMS
• ALLOYING
INDUSTRY
NO SPECIFIC COSAM EFFORT TO DATE
NASA PROGRAM MANAGEMENT
UNIVERSITIES
(DARTMOUTH)
• LOW-TEMP. DEFORMATION MECHANISMS
• MICRO-ALLOYING
• GRAIN REFINEMENT
(STANFORD)
• NICKEL & COBALT ALUMINIDE DEFORMATION MECHANISMS

Figure 16

BEST DOCUMENT A[illegible]BLE

CREEP BEHAVIOR OF ALUMINIDES AT 1125° C

The in-house program is focused on understanding the slow plastic deformation behavior of extruded powder metallurgy polycrystalline aluminides in terms of existing deformation models and structural parameters. Some initial results of compressive creep testing of the three aluminides are shown in figure 17 along with data for two commercial superalloys for comparative purposes. In addition to creep testing, thermal expansion and lattice parameter measurements are also being evaluated. A transmission electron microscopy evaluation of dislocation interactions in deformed specimens is being conducted in-house on the iron aluminides. In support of these high-temperature deformation studies, Stanford University has a grant to explore similar dislocation interactions in the nickel aluminide.

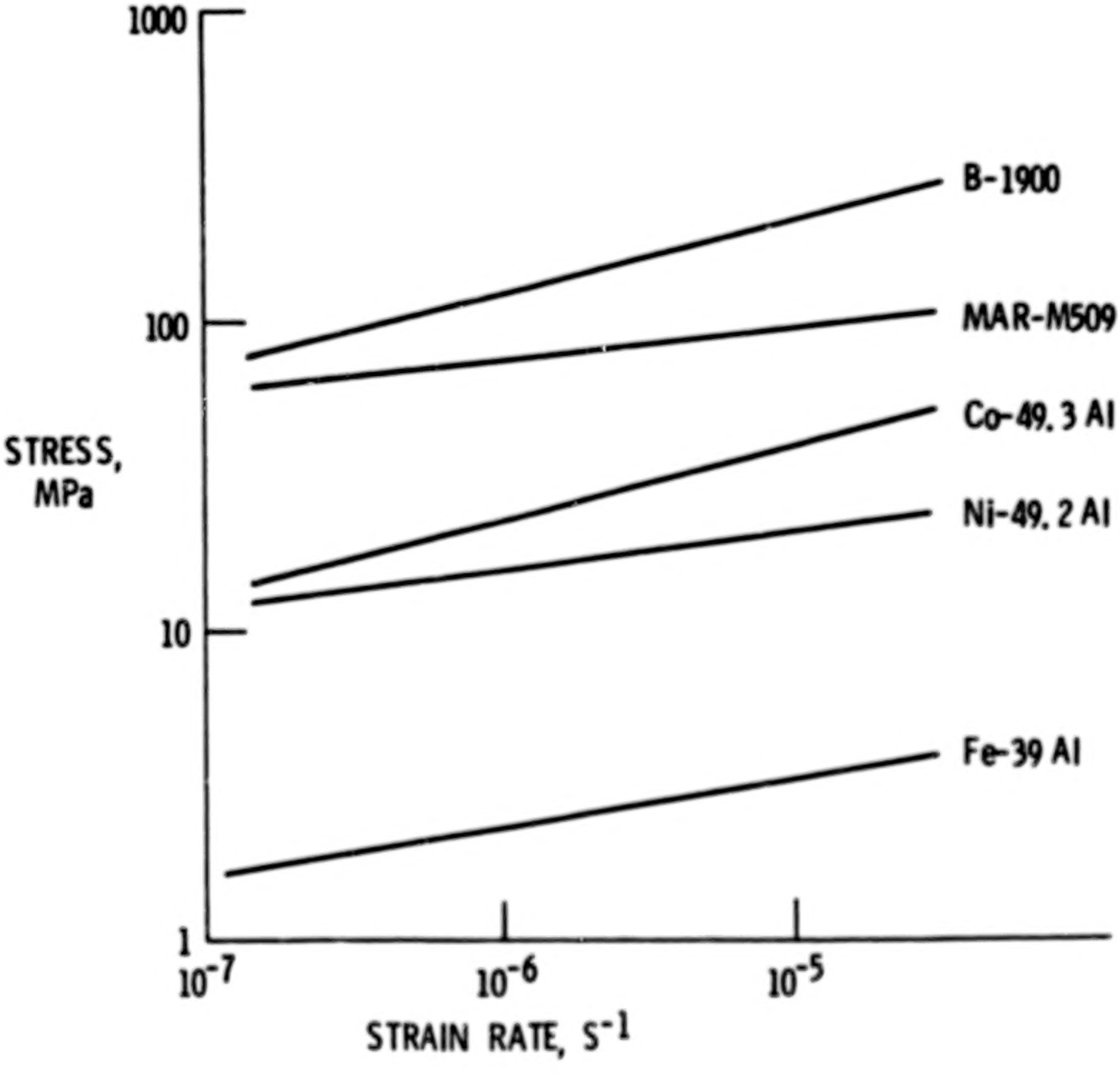

Figure 17

GRAIN SIZE EFFECTS ON DUCTILITY OF NICKEL ALUMINIDE AT 295° C

A COSAM investigation is being conducted at Dartmouth College on the low-temperature deformation mechanisms of nickel aluminide. Emphasis centers on grain size effects and microalloying to improve low-temperature ductility. The effect of decreasing grain size on tensile elongation at 295° C is shown in figure 18. Results indicate that below a grain size of about 10 micrometer diameter tensile ductility at 295° C can be achieved in nickel aluminide. Various microalloyed materials have been prepared and they are being tested.

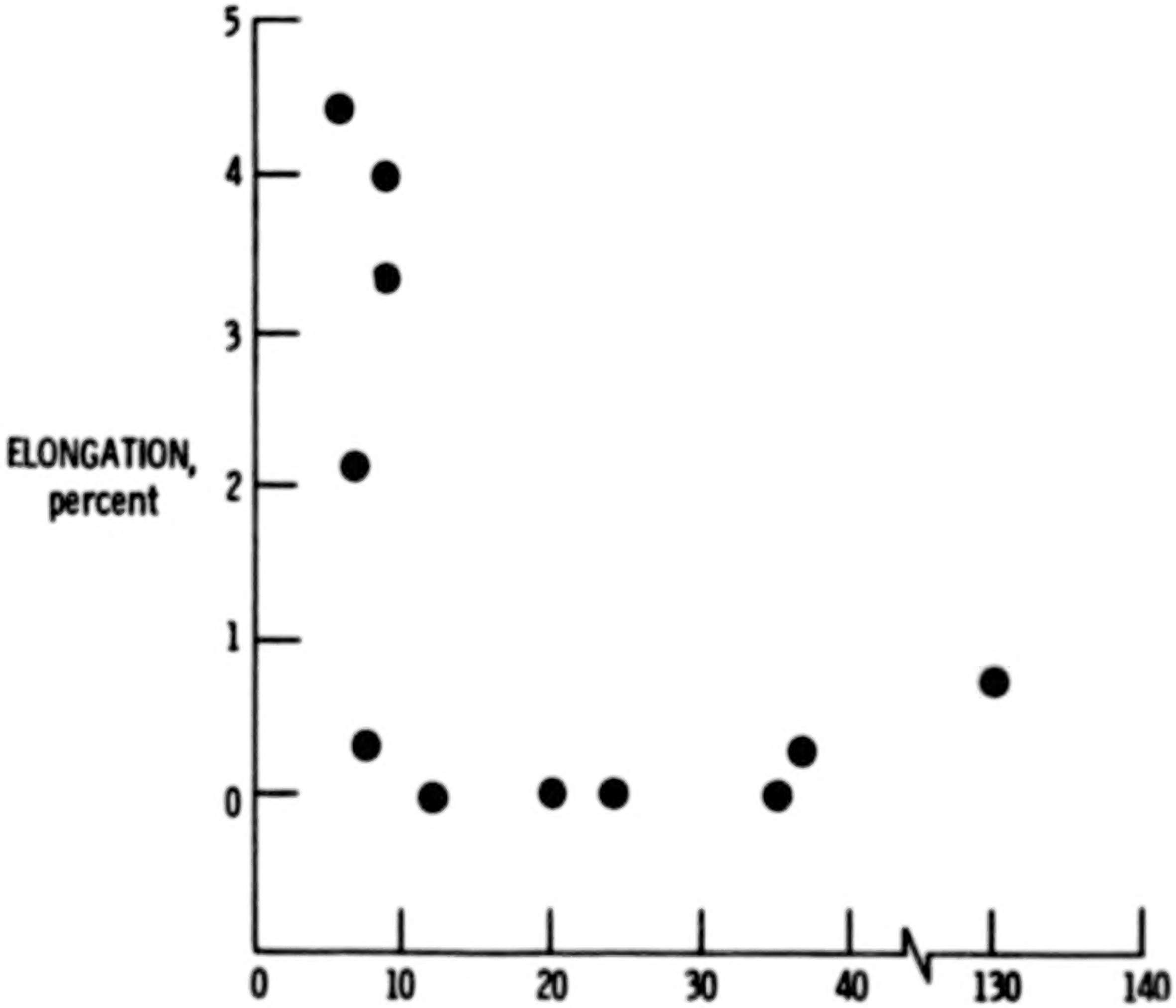

Figure 18

PARTICIPANTS' ROLES IN COOPERATIVE IRON-BASE PROGRAM

With the successful development of high-strength nickel-base superalloys (and to some extent cobalt-base superalloys) over the last 30 years, there has been little recent interest in developing iron-base alloys for the higher temperature gas turbine engine components. However, with the threat of strategic material supply disruptions or interruptions, iron-base alloys with low strategic metal contents are attractive as alternative materials for United States industrial consideration. A program has been initiated within the alternate materials thrust to investigate iron-base superalloys with aligned carbides for further strengthening as potential alternatives to current high strategic element content nickel- and cobalt-base superalloys. This is a joint program involving the University of Connecticut, United Technologies Research Center (UTRC), and NASA Lewis. Roles of the participants are illustrated in figure 19.

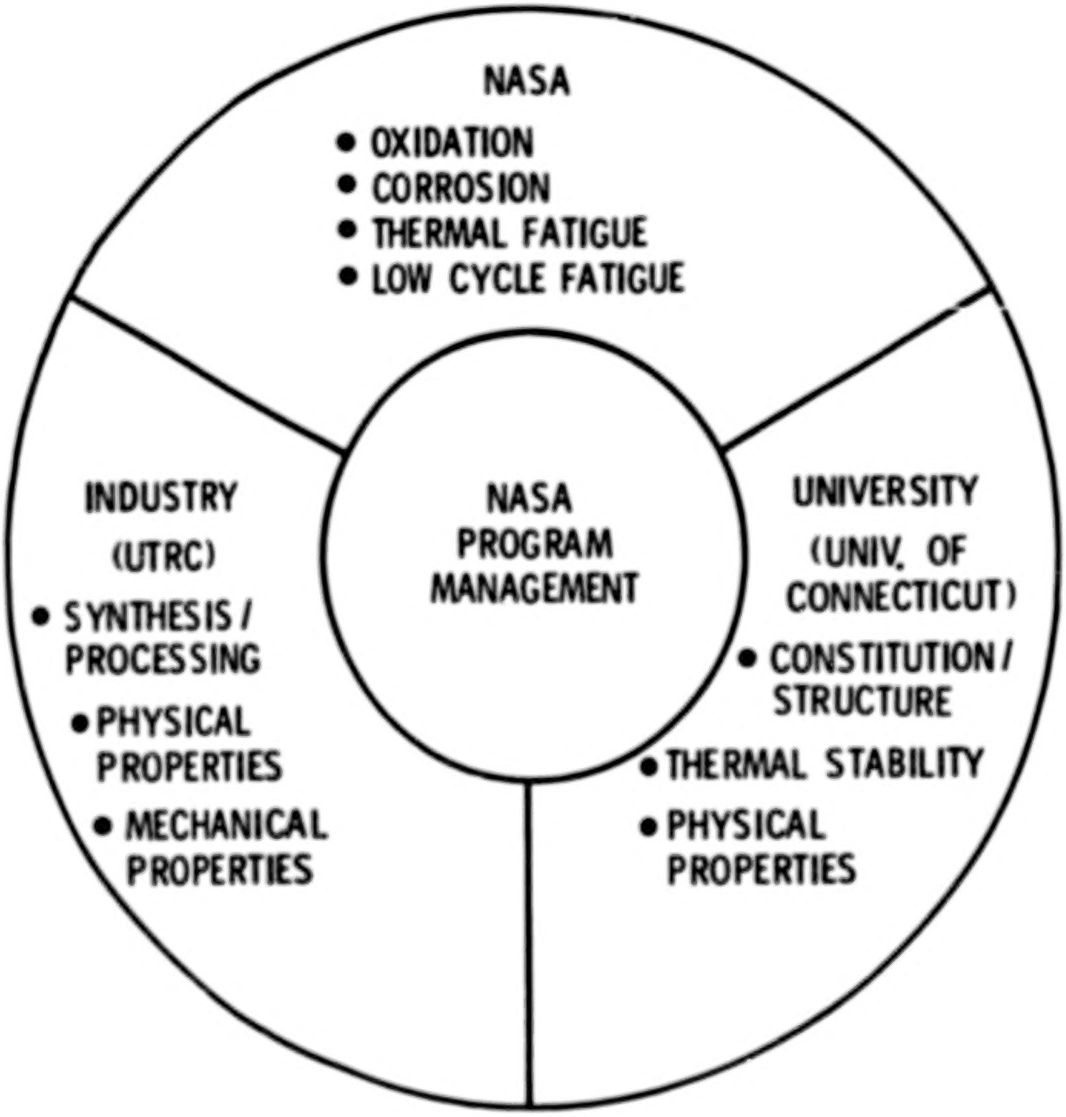
NASA
• OXIDATION
• CORROSION
• THERMAL FATIGUE
• LOW CYCLE FATIGUE
NASA PROGRAM MANAGEMENT
INDUSTRY
(UTRC)
• SYNTHESIS / PROCESSING
• PHYSICAL PROPERTIES
• MECHANICAL PROPERTIES
UNIVERSITY
(UNIV. OF CONNECTICUT)
• CONSTITUTION / STRUCTURE
• THERMAL STABILITY
• PHYSICAL PROPERTIES

Figure 19

STRESS-RUPTURE POTENTIAL OF Fe - 20-Cr - 10-Mn - 3.2-C ALLOY

The rupture lives (determined by United Technologies Research Center) of iron-chromium-manganese-aluminum-carbon-type alloys are compared in figure 20 with the rupture lives of other iron-, nickel-, and cobalt-base alloys. Results indicate that the experimental iron-base alloy offers a strength advantage over the commercial cobalt-base alloy MAR-M509.

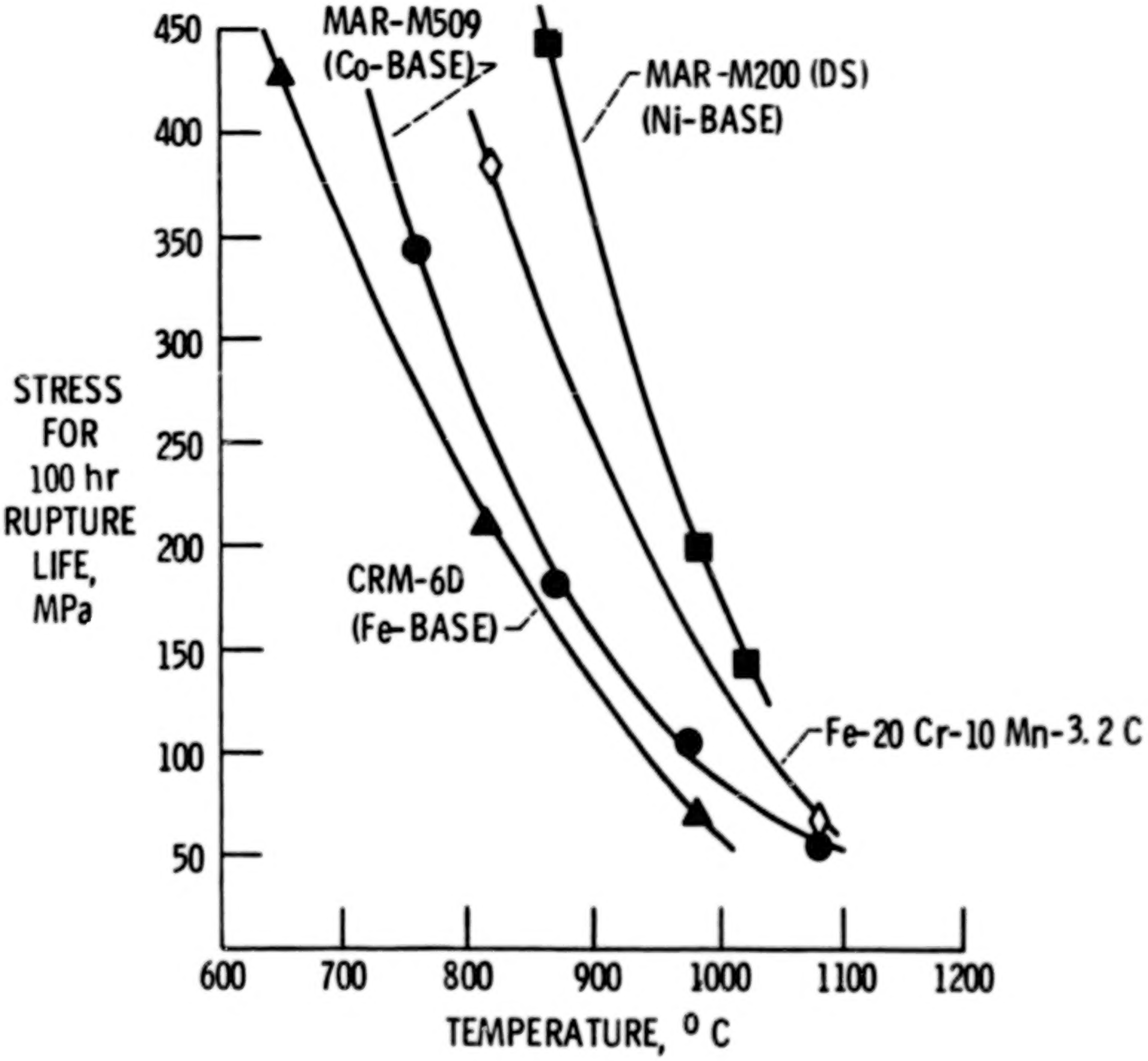

Figure 20

CONCLUDING REMARKS

NASA Lewis Research Center has undertaken a long-range program called COSAM (Conservation of Strategic Aerospace Materials):

(1) Program is in support of the aerospace industry and is aimed at reducing the use of strategic materials in gas turbine engines.

(2) Three-pronged approach to COSAM consists of research on strategic element substitutions, advanced processing concepts, and alternate materials.

(3) Program emphasizes cooperative research efforts with industry, universities, and Lewis Research Center.

(4) Program will help provide a technology base to serve as a guide for future gas turbine engine material development.

REFERENCES

1. Stephens, J. R.: NASA's Activities in the Conservation of Strategic Aerospace Materials. NASA TM-81617, 1980.
2. Stephens, J. R.: A Status Review of NASA's COSAM (Conservation of Strategic Aerospace Materials) Program. NASA TM-82852, 1982.
3. Egypt's Technology Shift - Soviets Focus on Control of Oil Flow from Region. Aviat. Week Space Technol., vol. 115, no. 24., Dec. 14, 1981, pp. 48-54.
4. Sheets, K. R.: American's Gap in Strategic Minerals. U.S. News and World Report, vol. 92, no. 5, Feb 8, 1982, p. 59.
5. Monthly Digest of Significant Developments in Strategic Metals Intelligence. B. O. Szuprowicz, Publisher, Oct. 1981, p. 3.
6. Bureau of Mines: Mineral Industry Surveys, Cobalt in 1978, 1979, 1980, and 1981. Department of Interior.
7. Maurer, G. E.; Jackman, L. A.; and Domingue, J. A.: Role of Cobalt in Waspaloy. Superalloys 1980, J. K. Tien, ed., American Society for Metals, 1980, pp. 43-52.
8. Kortovich, C. S.; and Marder, J. M.: Development of Materials and Process Technology for Dual Alloy Disks. (TRW-ER-8001-F, TRW, Inc.; NASA Contract NAS3-21351.) NASA CR-165224, 1981.

BLANK PAGE

SOLIDIFICATION PROCESS CONTROL FOR ADVANCED SUPERALLOYS

Hugh R. Gray and Robert L. Dreshfield
NASA Lewis Research Center
Cleveland, Ohio

SOLIDIFICATION PROCESS CONTROL FOR ADVANCED SUPERALLOYS

Advances in performance and reduction in fuel consumption in aircraft gas turbines have, in the past, been the result of advances in both design techniques and high temperature alloy technology. The alloys used in the hotter sections are nickel-base superalloys which have undergone remarkable growth in use temperatures (~ 1500 to ~ 1800°F) during the three decades of jet turbine transport. In this presentation we will show the importance of understanding and controlling the basic solidification process. Resultant tailoring of the superalloy macro- and microstructure offers significant potential for continued advances in superalloy use temperatures in turbine engines.

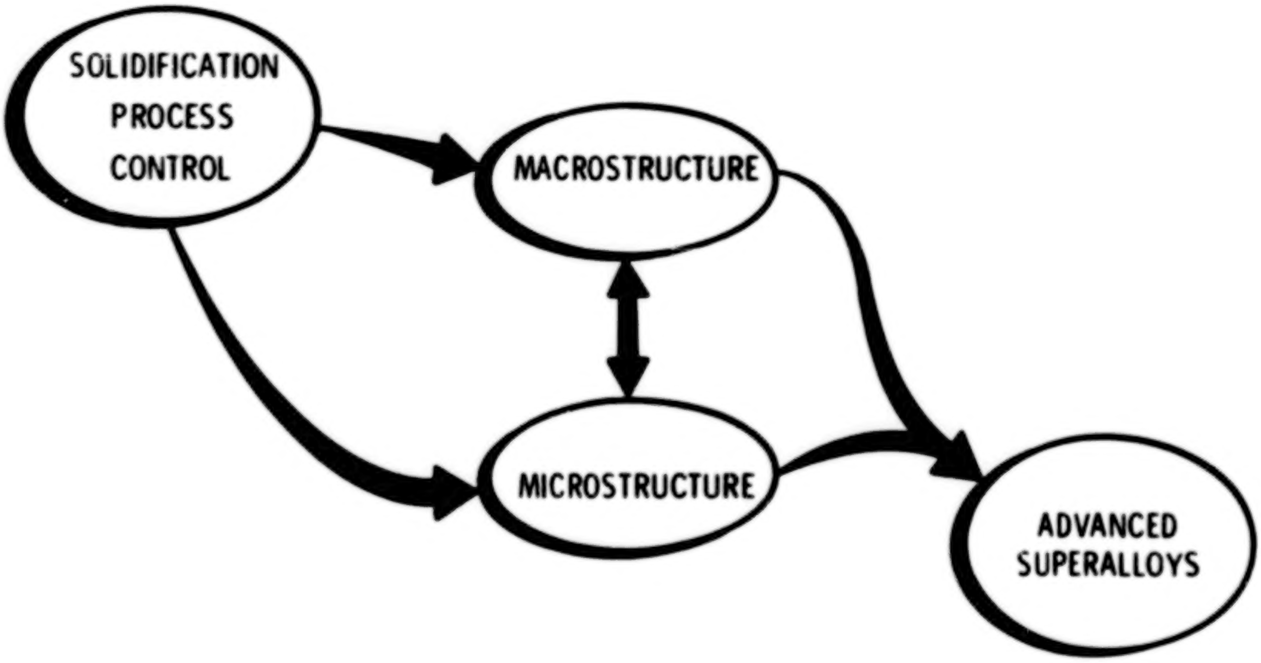
SOLIDIFICATION PROCESS CONTROL
MACROSTRUCTURE
MICROSTRUCTURE
ADVANCED SUPERALLOYS

SOLIDIFICATION PROCESS CONTROL FOR ADVANCED SUPERALLOYS

An important parameter in cast metals relates to the segregation spacing of chemical alloying elements. Segregation may lead to inferior mechanical properties and as the spacing becomes large, long times at high temperatures are required to homogenize the castings. If the segregation spacing is reduced then shorter, lower temperature, more economical processes become possible and properties are improved. The segregation distance is a strong function of the solidification rate (ref. 1). The segregation spacing varies from several millimeters (mm) in ingot castings with cooling rates of a few degrees per minute to 10^{-1} micrometers (μm) for surface melted material solidified at about 10^7 degrees per second. The slope of the linear relation between segregation spacing and cooling rate varies somewhat for various alloy systems and even varies slightly for different alloy compositions within the nickel-base superalloy family. Advanced superalloys are being investigated throughout the aerospace industry covering a broad range of solidification rates.

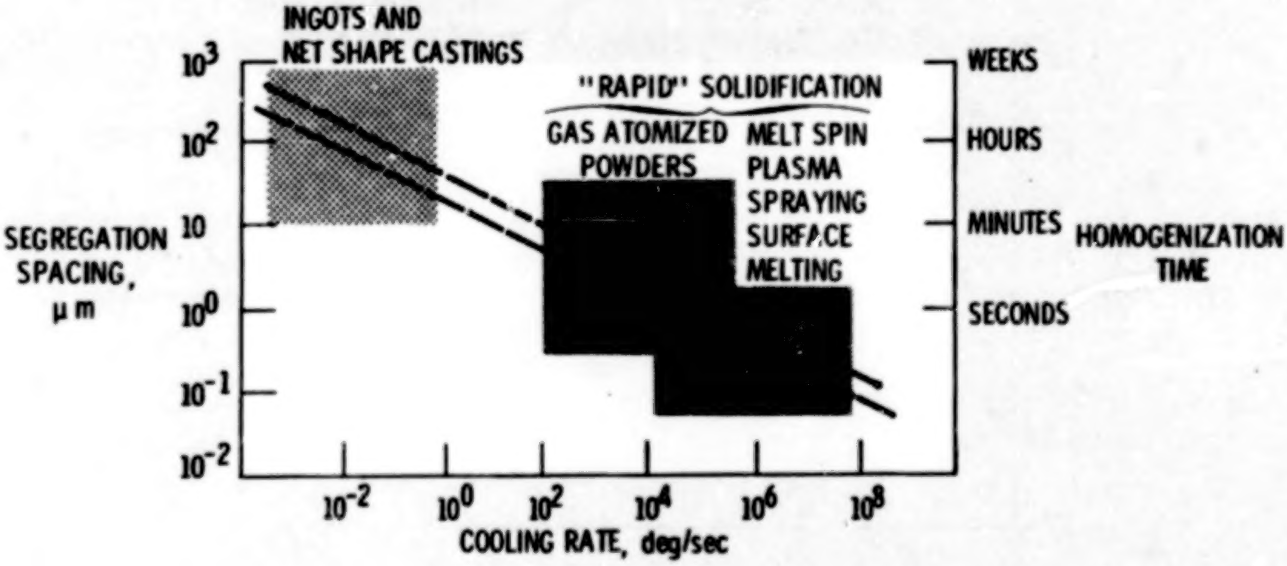

(ADAPTED FROM MEHRABIAN)

NEW ALLOYING CONCEPTS

In order to fully exploit the advantages offered by controlling the solidification process and rate, one must apply appropriate alloying concepts. In some cases solidification control permits the use of new alloying concepts. In this presentation we shall briefly describe programs at the Lewis Research Center in single crystal turbine blades, powder metallurgy turbine components and the recently initiated program concerned with rapidly solidified flakes and ribbons. These programs span the solidification rate spectrum and range from net shape MACROCASTINGS to extremely small MICROCASTINGS which then must be consolidated into usable structural components.

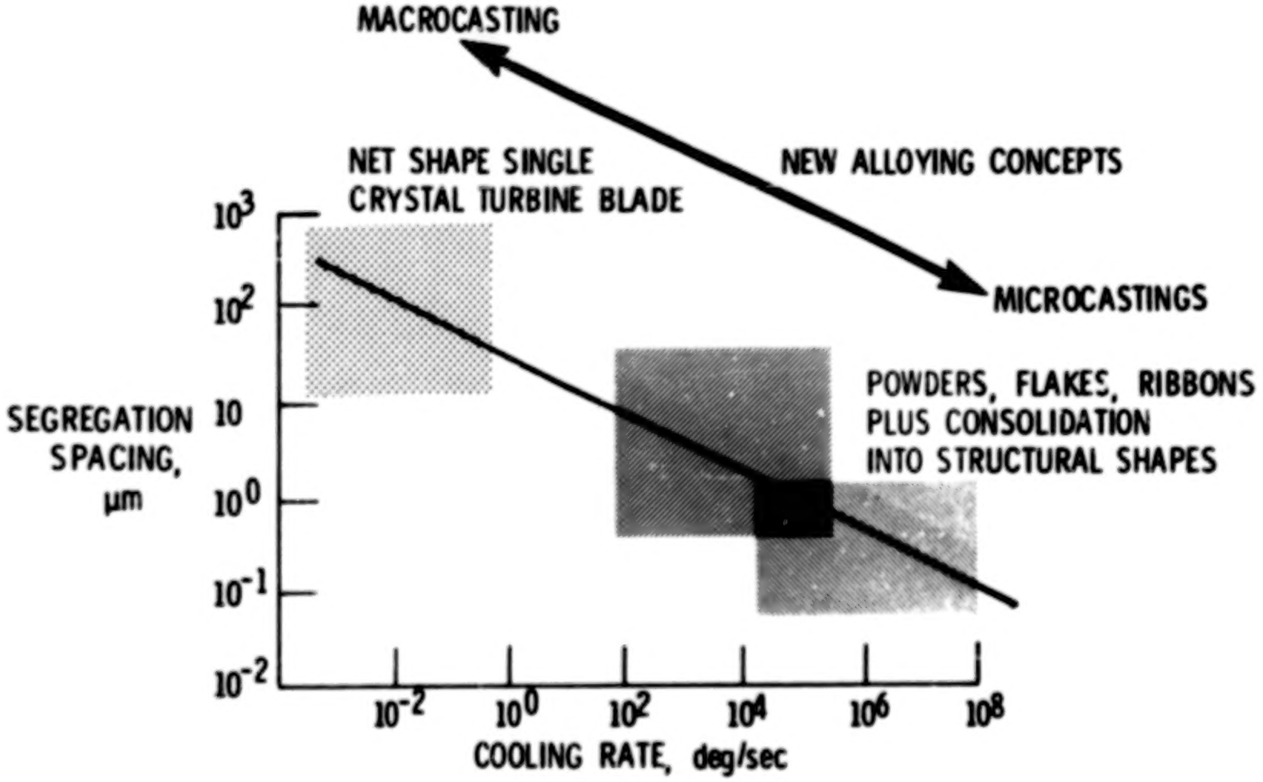

SINGLE CRYSTAL TURBINE BLADES

Single crystal turbine blades are cast by causing solidification to occur in a unidirectional manner and by using a geometrical restriction to allow only one grain to grow from the starter to the blade. The unidirectional solidification is accomplished by casting on a water cooled chill plate which causes the heat flow to be directional into the plate. This process typically results in rather low solidification rates in the order of 10^{-1} degrees per second. Both solid and air-cooled turbine blades in a large range of sizes are currently being evaluated for or are in use in turbine engines (refs. 2 and 3).

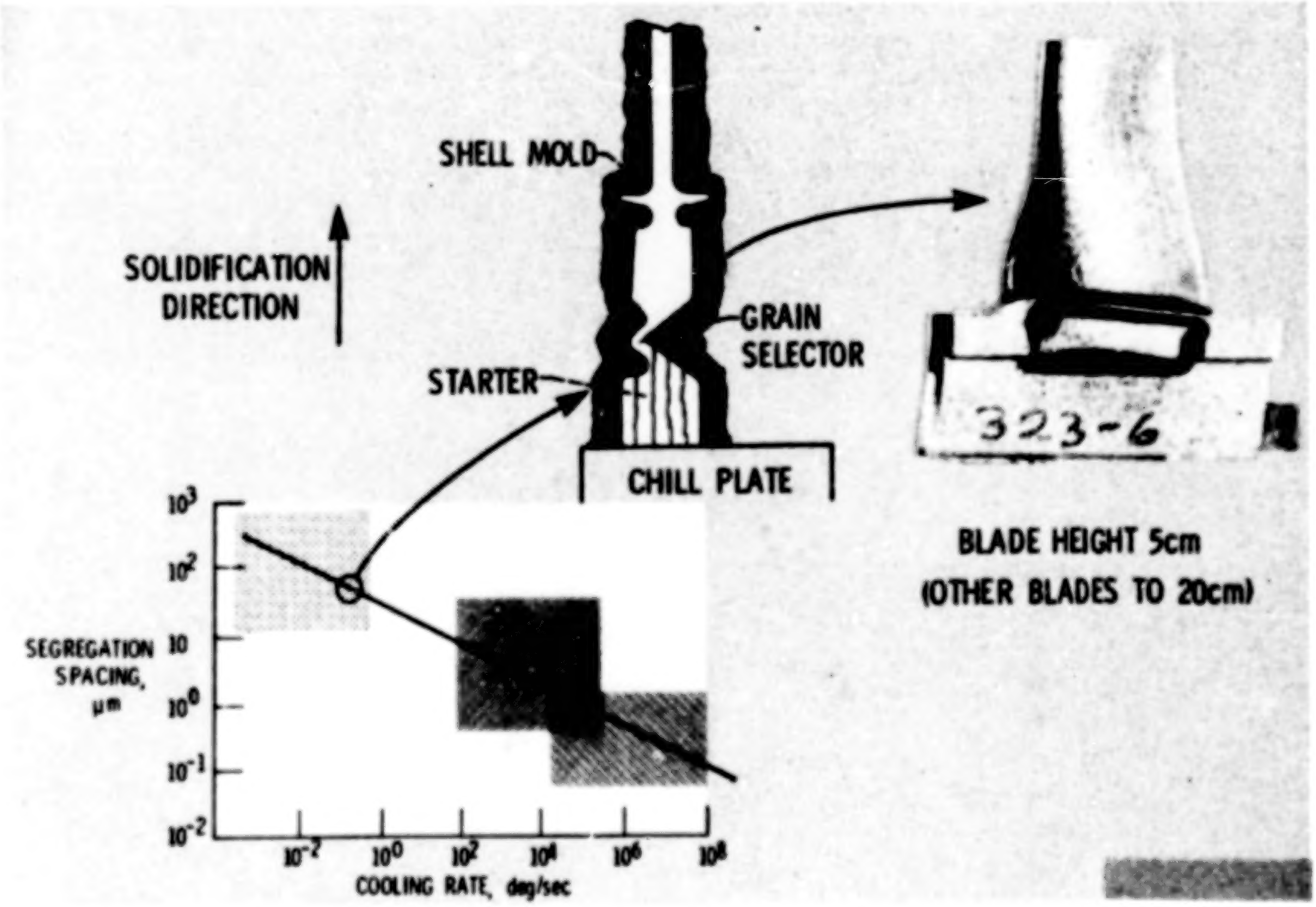
SHELL MOLD
SOLIDIFICATION DIRECTION
GRAIN SELECTOR
STARTER
CHILL PLATE
323-6
BLADE HEIGHT 5cm
(OTHER BLADES TO 20cm)
SEGREGATION SPACING, μm
10³
10²
10
10⁰
10⁻¹
10⁻²
10⁻²
10⁰
10²
10⁴
10⁶
10⁸
COOLING RATE, deg/sec

SINGLE CRYSTAL SUPERALLOYS
MICROSTRUCTURAL HOMOGENEITY THROUGH COMPOSITIONAL ADJUSTMENT AND HEAT TREATMENT

The casting process used to produce single crystal superalloys results in segregation spacings of about 50 μm. In order to produce optimum mechanical properties this chemical segregation is reduced through the use of high temperature heat treatment. It can be seen that 2 hours at 2400°F results in good homogeneity for the alloy shown while after 2 hours at 2300°F considerable casting segregation remains (ref. 4). In order to allow the single crystal superalloys to be annealed at these high temperatures without melting, it is necessary to alter their chemical compositions to raise the melting points. A typical nickel-base superalloy may contain 15 Cr, 10 Co, 5(Mo+W), 7 (Al+Ti), and 0.02-2(B, C, Hf, Zr)(all in weight percent). However, for single crystals, alloying elements such as B, C, Hf, Zr which are melting point depressants are removed, thus permitting heat treating at higher temperatures without melting. It should also be noted that, since the traditional role of these alloying elements is to strengthen the grain boundaries of polycrystalline nickel-base superalloys, they are indeed unnecessary for single crystal alloys.

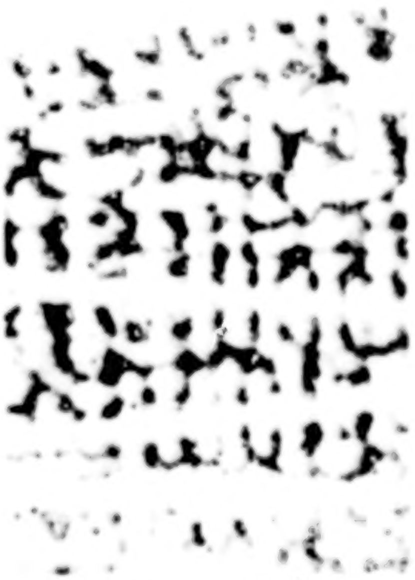

AS-CAST

SEGREGATION SPACING

2300° F FOR 2 HOURS

2400° F FOR 2 HOURS

SINGLE CRYSTAL SUPERALLOYS
INCREASED STRENGTH BY CONTROL OF FINE MICROSTRUCTURE

High temperature strength improvements have been achieved in single crystals by careful control of the fine microstructure. Specifically, achievement of the very homogeneous composition described in the previous figure now permits precise control of the size and amount of the gamma prime (γ') phase which is the strengthening phase in nickel-base superalloys. Up to 60 volume percent can be precipitated in a fine, controlled network thus providing optimum strengthening. Recent research has shown that the high temperature load carrying capacity of the single crystal superalloys can be further increased by causing the fine γ' phase to form small platelets or "rafts" (ref. 5). Work is currently in progress at the Lewis Research Center on these super single crystals in order to more fully understand the basic phenomena which cause the rafted microstructure.

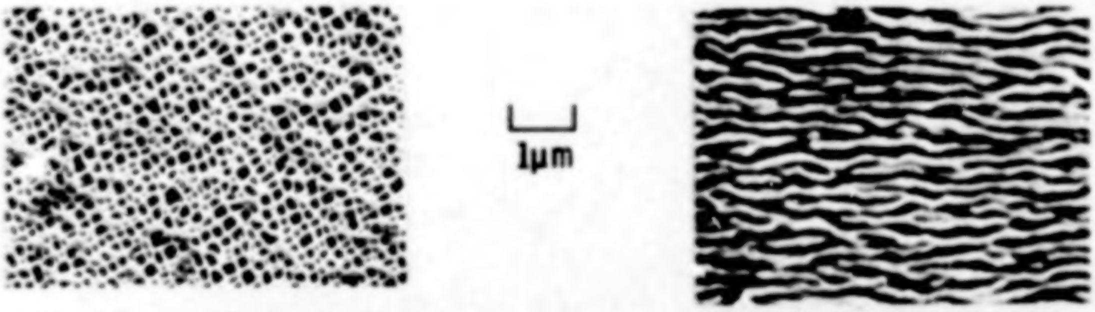

60% FINE γ' STRENGTHENING PHASE

SPECIALLY PROCESSED RAFTED γ'

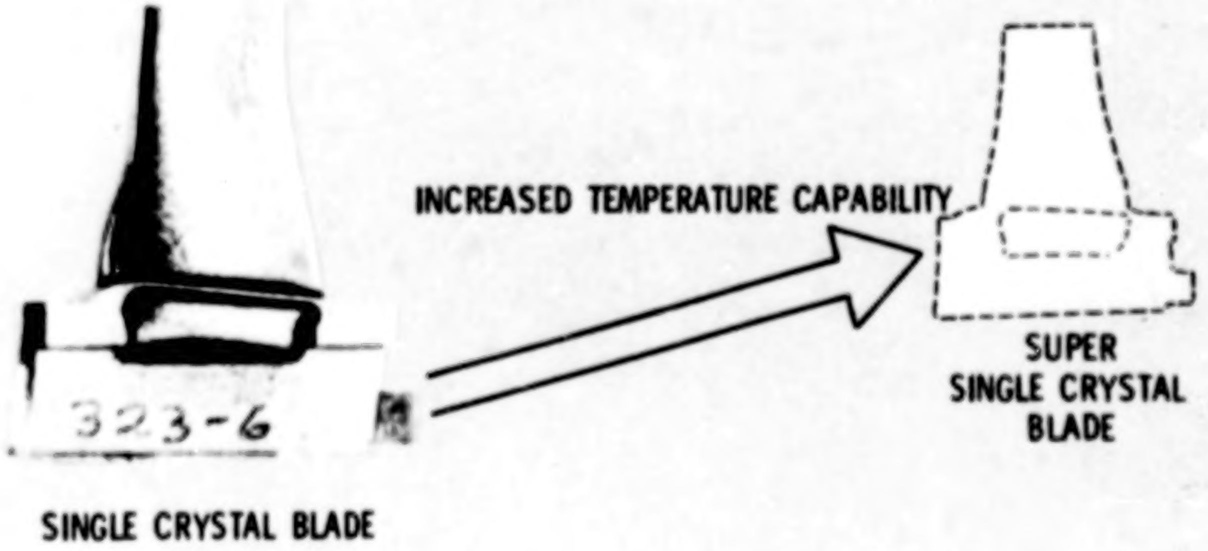

IMPROVED PROPERTIES THROUGH MACRO/MICROSTRUCTURAL CONTROL

The objective of controlling the structure shown in the previous figure has been to increase the capability of the alloys to perform at higher temperatures. In the top figure it can be seen that at a stress of about 25 ksi, the temperature for 1000 hours life is raised from about 1670°F for an equiaxed alloy to about 1800°F for a rafted or super single crystal. Directional solidification and single crystal processing each allowed a 45°F increase in temperature capability. The lower figures show that both the high cycle and low cycle fatigue behavior also benefit from single crystal processing (ref. 3). It is important to recognize that these three mechanical properties and several other mechanical, chemical and physical properties need to be mutually optimized to permit a turbine blade to operate successfully at higher temperatures.

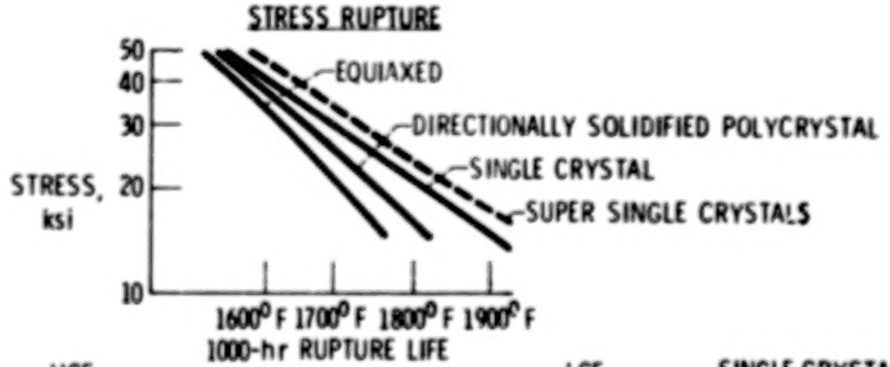

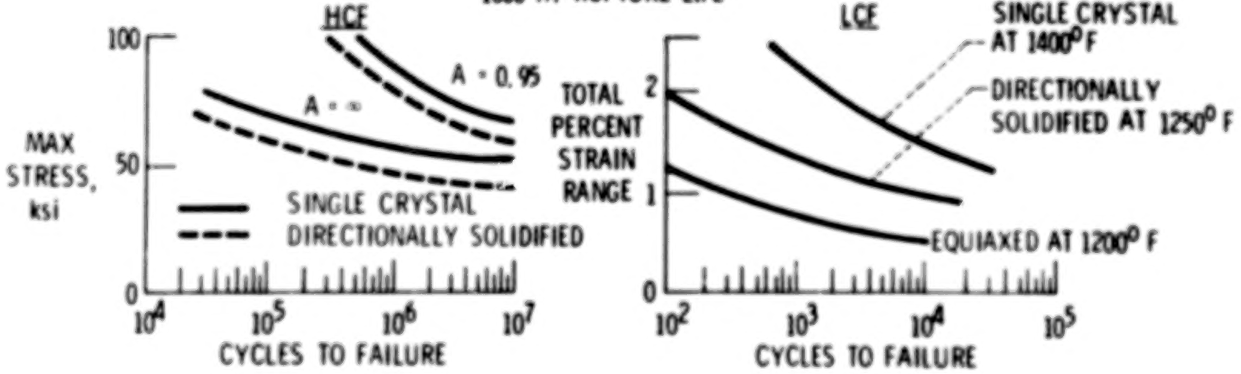

ATOMIZED POWDER TURBINE COMPONENTS

Gas atomized metal powder demonstrates another regime of solidification process control. Superalloys produced by gas atomization processes have been estimated to have solidification rates of about 10^3 degrees per second. The resultant segregation spacing is about 2 μm. As a result it is possible to process alloys having larger amounts of strengthening elements with reduced segregation than through ingot metallurgy and forging. These powders must then be consolidated to a structural shape, such as a turbine disk, as will be discussed subsequently.

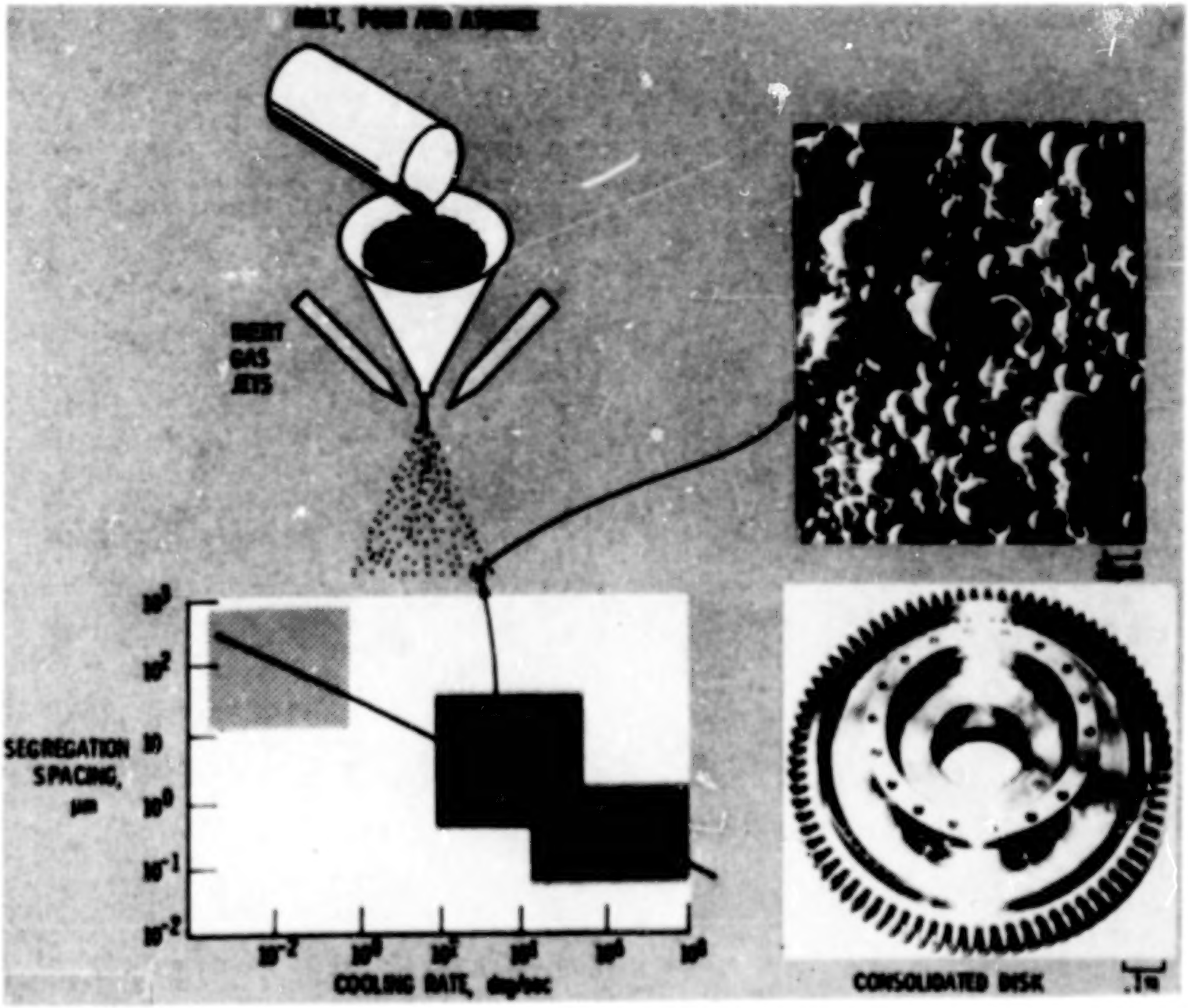
MELT, POUR AND ATOMIZE
INERT GAS JETS
SEGREGATION SPACING, μm
10^3
10^2
10
10^0
10^{-1}
10^{-2}
10^{-2}
10^0
10^2
10^4
10^6
10^8
COOLING RATE, deg/sec
CONSOLIDATED DISK
1 in

ATOMIZED SUPERALLOY POWDER

The atomized powder particles are essentially microcastings. The figure shows the cast structure of the powder spheres and illustrates the fine scale of the segregation spacing. The cooling rate and resultant segregation spacing are a function of the particular method of atomization and the particle size. The smaller particles solidified at faster cooling rates. Within reasonable constraints, one can tailor the cooling rate of the material. As was the case with single crystal alloys, it was found beneficial to alter the chemical composition of powder alloys to more fully take advantage of the process. Specifically, the amount of alloying elements such as C and/or Hf is usually reduced in powder superalloys.

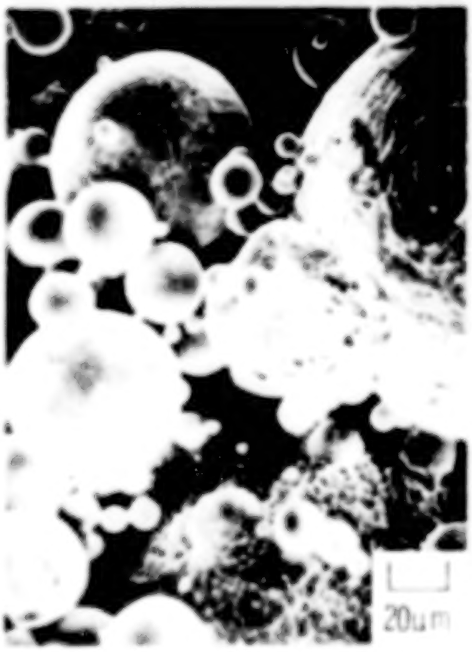

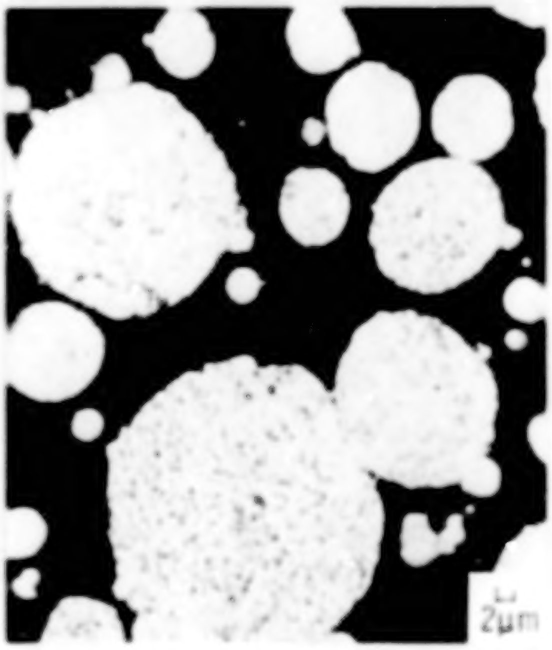

SEGREGATION SPACING

RAPIDLY SOLIDIFIED SUPERALLOYS FOR ADVANCED TURBINE COMPONENTS

The melt spinning process is capable of solidification rates of about 1,000,000 degrees per second. The superalloy charge is melted in a crucible in a vacuum chamber and then ejected through a hole(s) or slit in the bottom of the crucible by pressurization. The molten metal stream impinges on the surface of a wheel rotating at several thousand revolutions per minute. Wetting conditions and heat extraction rates can be carefully controlled by proper selection of wheel material, surface conditions and temperature. Thus, a variety of microcasting morphologies ranging from fine powder to flake and continuous lengths of ribbon can be produced. A systematic study of the interrelationships between processing variables and the resultant structure of the microcastings is currently under way in a NASA Lewis research program.

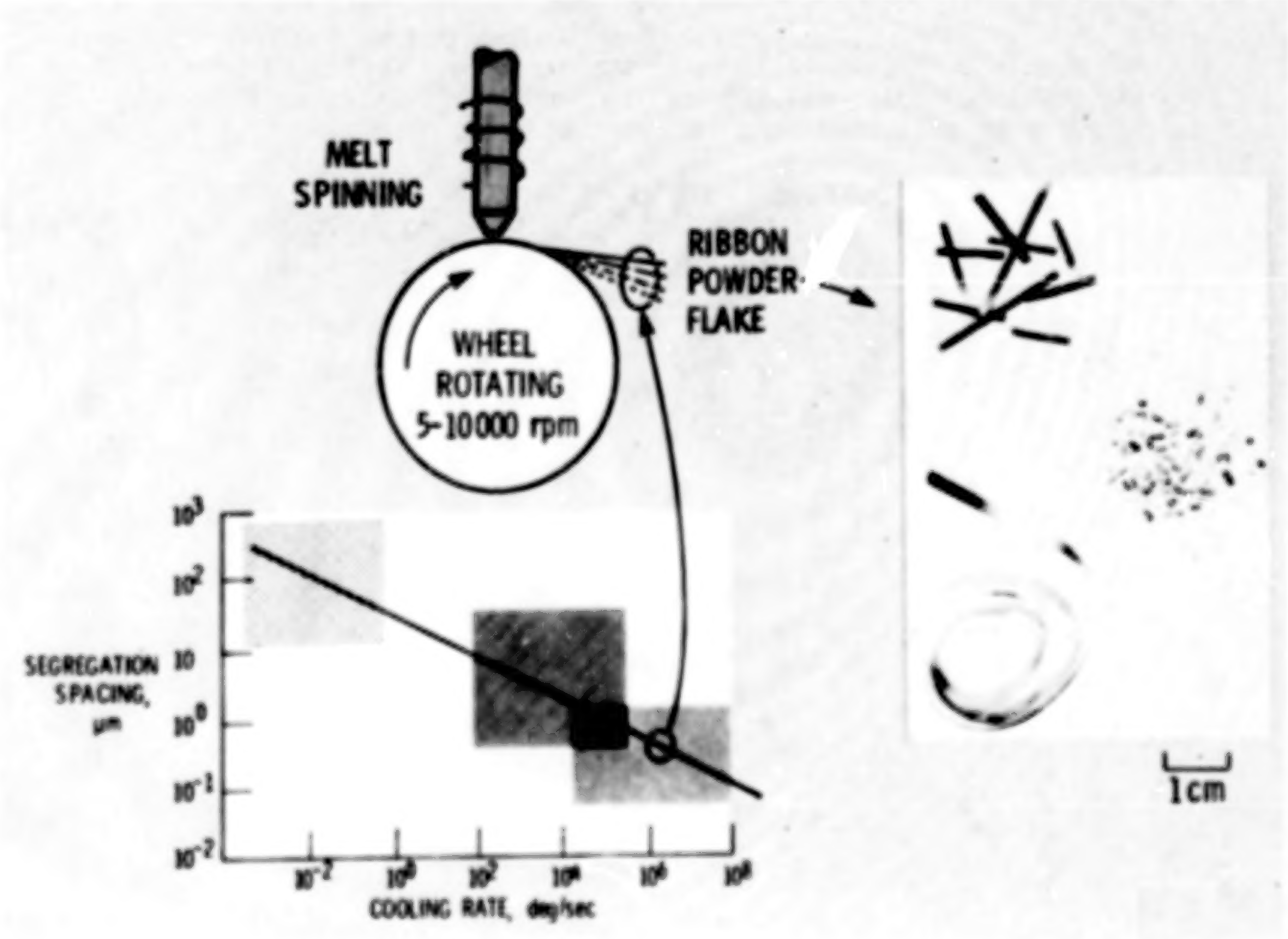
MELT SPINNING
RIBBON
POWDER
FLAKE
WHEEL ROTATING 5-10000 rpm
SEGREGATION SPACING, µm
10^3
10^2
10
10^0
10^{-1}
10^{-2}
10^{-2}
10^0
10^2
10^4
10^6
10^8
COOLING RATE, deg/sec
1cm

RAPID SOLIDIFICATION PRODUCES ULTRAFINE, UNIQUE MICROSTRUCTURES

A typical nickel-base superalloy, 713 LC, was recently solidified at a wheel surface speed of about 3000 feet per minute in order to produce a relatively thick foil of 15 μm. The cross section of this foil when viewed at high magnification provides a pictorial history of the rapid solidification process. The bottom of the foil which was in contact with the quenching wheel solidified at the fastest rate thus producing fine grains near the bottom surface. These grains gradually transitioned into fine columnar grains in the lower half of the foil and then dendritic grains in the slower cooling upper portion of the foil. However, even the dendritic structure is extremely fine (0.5 μm) because the solidification rate is indeed significantly more rapid than processes described earlier in this paper. Ultrafine precipitate particles are contained in the dislocation tangles as shown in the transmission electron micrograph taken at 70,000x. Thinner foils representative of only the lower columnar grain portion of this foil have been produced simply by quenching onto a wheel rotating at a faster speed. Entirely new classes of alloys with extended solid solubilities and metastable phase strengthening concepts are being evaluated in our current program.

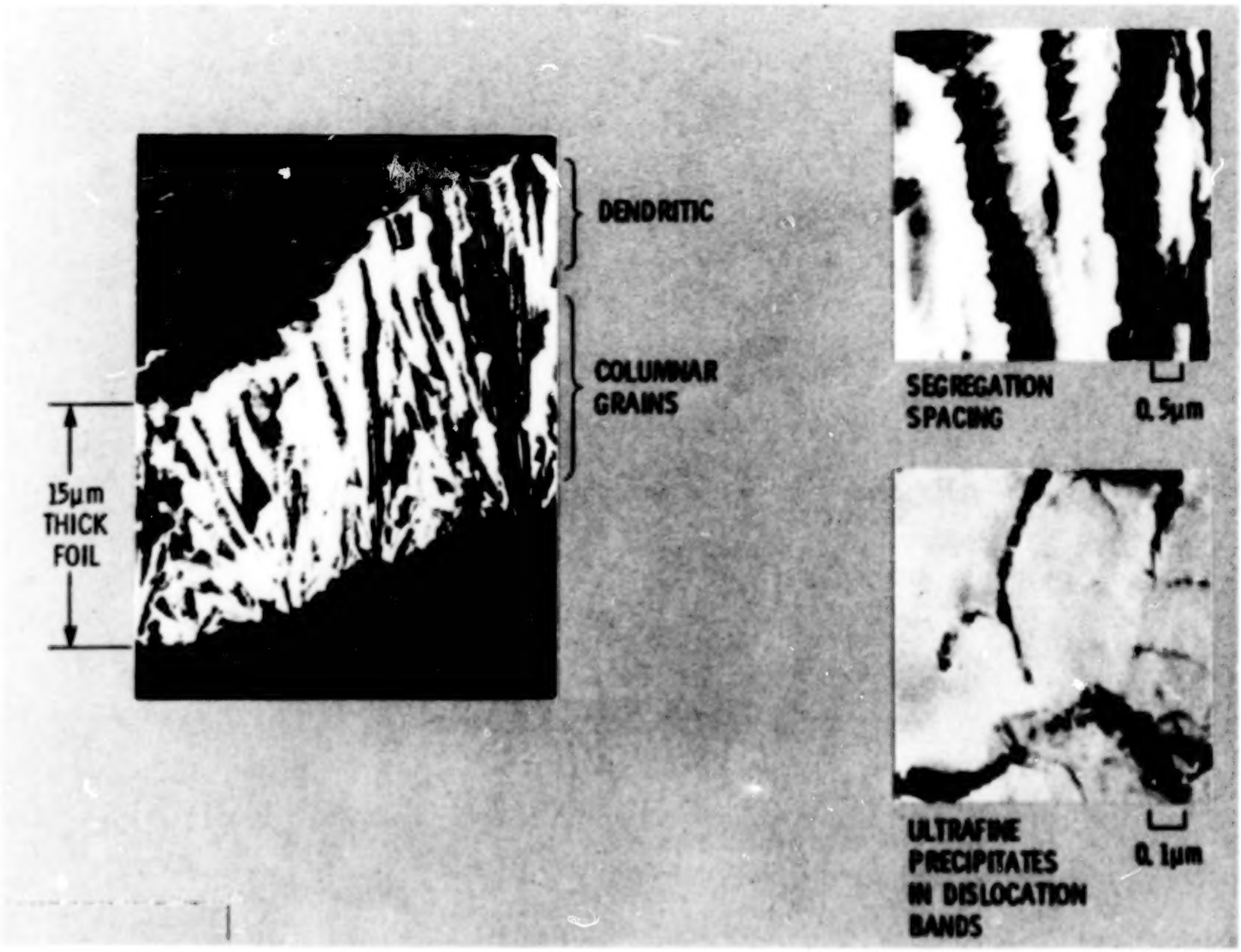

RAPIDLY SOLIDIFIED SUPERALLOY TURBINE COMPONENTS

As discussed previously, all of these rapid solidification processes are designed to produce microcastings of various controlled sizes and morphologies -- powder, flake, or ribbon. It is essential that these microcastings be consolidated for their eventual use as structural materials. Control of the macro/micro-structure of these materials during and after consolidation is critically related to their intended application. Consolidation processes may include extrusion, hot isostatic pressing (HIP) and/or isothermal forging. Each of these processes will produce a microstructure consisting of fine, equiaxed grains which is ideal for high-strength and high-fatigue-resistant turbine applications up to about 1400°F, such as disks, shafts and seal rings. However, if the desired application is intended for higher use temperatures, such as blades, vanes, or combustors, the consolidated microcastings must be subjected to an additional process called directional recrystallization. This process converts the fine grains to large, elongated grains necessary for strength at 2000+°F.

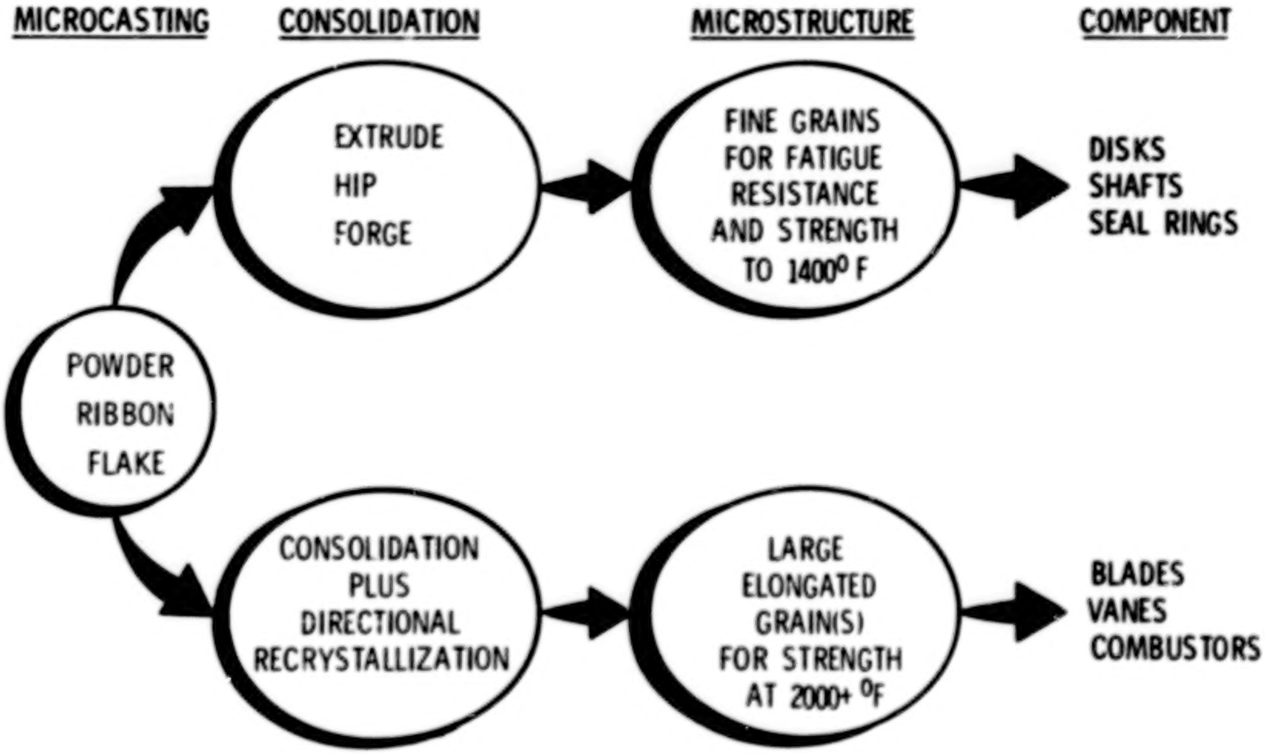
MICROCASTING
CONSOLIDATION
MICROSTRUCTURE
COMPONENT
EXTRUDE
HIP
FORGE
FINE GRAINS FOR FATIGUE RESISTANCE AND STRENGTH TO 1400° F
DISKS
SHAFTS
SEAL RINGS
POWDER
RIBBON
FLAKE
CONSOLIDATION PLUS DIRECTIONAL RECRYSTALLIZATION
LARGE ELONGATED GRAIN(S) FOR STRENGTH AT 2000+ °F
BLADES
VANES
COMBUSTORS

POWDER SUPERALLOYS CONSERVE MATERIALS AND DOLLARS

The conventional process of producing turbine disks from cast ingot materials involves a substantial number of forging steps, heat treating steps, and a lot of machining (ref. 6). The ratio of the initial materials input weight to final component weight may range from 10:1 to 20:1 depending on the actual configuration of the turbine disk. Obviously large amounts of expensive and strategic metals as well as huge amounts of energy are consumed in such conventional processing. Powder metallurgy processing permits significant savings in quantities of starting materials, energy consumption, and amount of machining time and chips. Powders have been consolidated by extrusion or HIP followed by isothermal forging to near net shape. Alternatively powders have been consolidated by HIP directly to net sonic shape. Several recent NASA MATE (Materials for Advanced Turbine Engines) programs have demonstrated input material weight savings of ~ 1/2 and cost savings of ~ 1/3 relative to conventional processing (refs. 7 to 9).

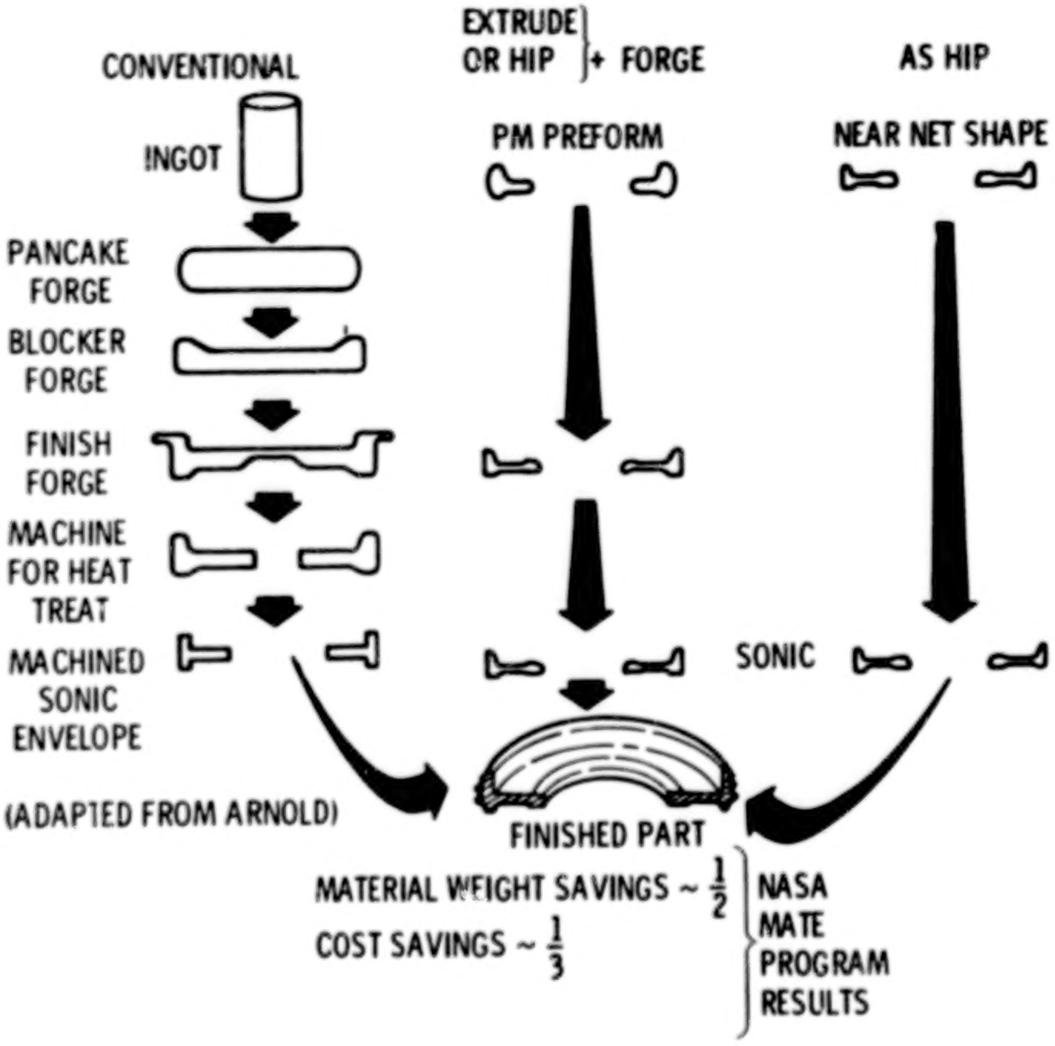
CONVENTIONAL
EXTRUDE OR HIP + FORGE
AS HIP
INGOT
PM PREFORM
NEAR NET SHAPE
PANCAKE FORGE
BLOCKER FORGE
FINISH FORGE
MACHINE FOR HEAT TREAT
MACHINED SONIC ENVELOPE
SONIC
FINISHED PART
MATERIAL WEIGHT SAVINGS ~ 1/2
COST SAVINGS ~ 1/3
NASA MATE PROGRAM RESULTS

(ADAPTED FROM ARNOLD)

POWDER SUPERALLOYS KEY TO ADVANCED DISKS

In addition to material and cost savings, powder metallurgy processing offers a unique opportunity to solve current problems and provide for future advancements in disk operating conditions. Turbine disks operate over a wide range of temperatures, up to ~ 800°F near the bore and up to ~ 1400°F at the rim. Yield strength, stress rupture strength, and resistance to fatigue crack initiation and propagation are the critical mechanical property requirements for disks. Significant improvements have been achieved in increasing strength and resistance to fatigue crack initiation via powder metallurgy because the microcastings contain a greater amount of and a more uniform distribution of strengthening phases in their microstructure. However, the crack propagation characteristics of these high-strength alloys are relatively poor. A current Lewis Research Center research program (refs. 10 to 12) is focused on a basic understanding of the relations between alloy processing - microstructure - crack propagation behavior of these materials in order to increase the cyclic life of turbine disk alloys.

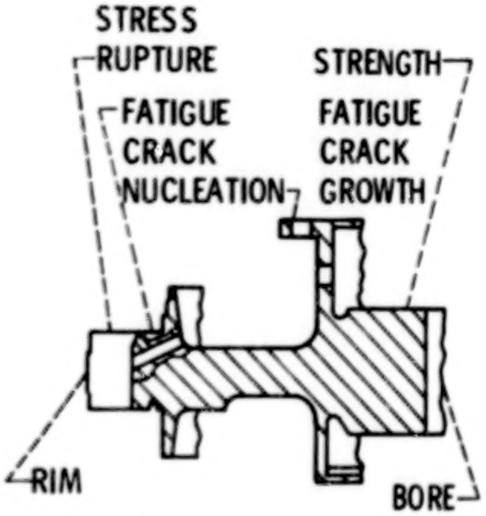

PROPERTY REQUIREMENTS FOR TURBINE DISKS

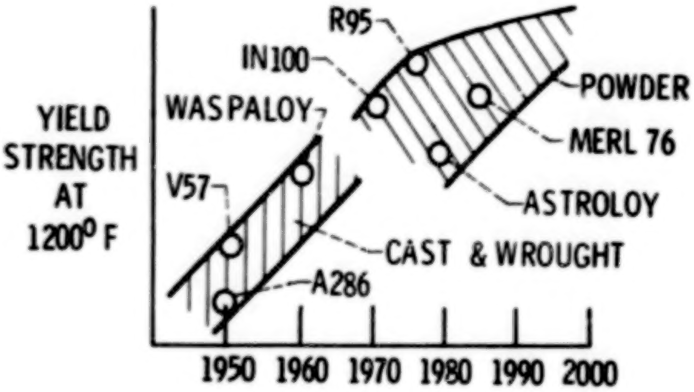

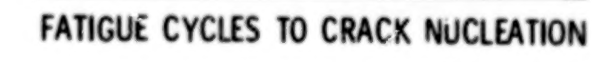

RAPIDLY SOLIDIFIED SUPERALLOYS HAVE POTENTIAL FOR HIGH-TEMPERATURE APPLICATIONS

As mentioned previously, rapidly solidified microcastings must not only be consolidated, but must also have their initial fine-grain structure converted to large elongated grains for strength at high temperatures. Powders or flakes can be consolidated by the previously described process of extrusion into bar or rod and then sliced into sheet or laminates (Strangman, T. E., AiResearch Co., private communication), or split blade halves. Alternatively, melt spun foil may be used directly. Complex air cooling passages may be photochemically etched into the laminates prior to subsequent bonding into a blade assembly. The critical step in converting the fine grain into large, elongated grain(s) is called directional recrystallization. The laminates or the bonded assembly are passed through a steep temperature gradient at a slow, controlled rate. This causes the grains to grow in size and parallel to the direction of the thermal gradient. It is even possible to control the process so that only one grain survives, thus resulting in a single crystal produced in the solid state rather than by solidification as described previously.

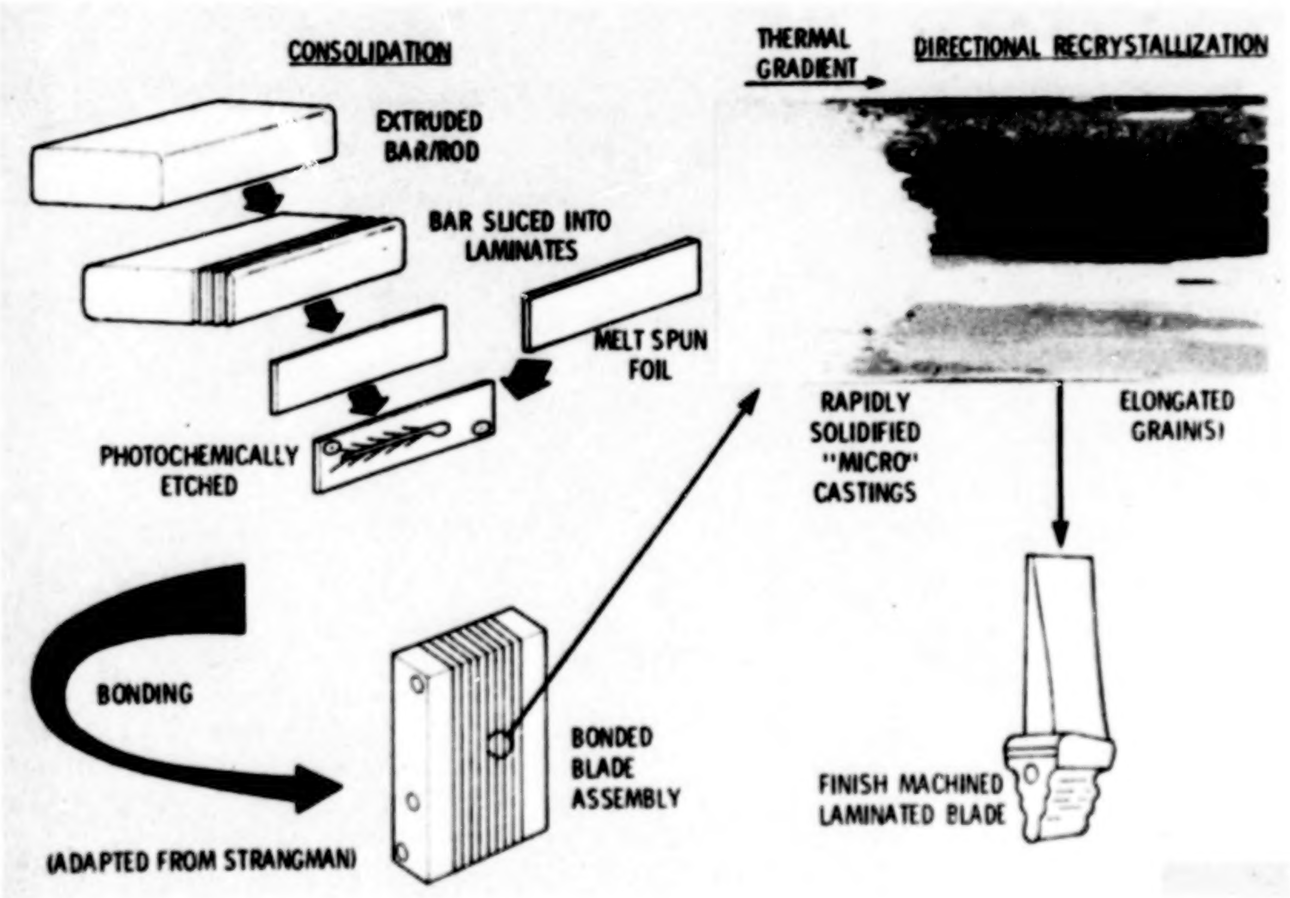
CONSOLIDATION
EXTRUDED BAR/ROD
BAR SLICED INTO LAMINATES
MELT SPUN FOIL
PHOTOCHEMICALLY ETCHED
BONDING
BONDED BLADE ASSEMBLY
THERMAL GRADIENT
DIRECTIONAL RECRYSTALLIZATION
RAPIDLY SOLIDIFIED "MICRO" CASTINGS
ELONGATED GRAIN(S)
FINISH MACHINED LAMINATED BLADE

(ADAPTED FROM STRANGMAN)

SOLIDIFICATION PROCESS CONTROL FOR ADVANCED SUPERALLOYS

We have described research programs conducted at or sponsored by the Lewis Research Center which rely on solidification process control to achieve improvements in nickel-base superalloy turbine components. These programs include single-crystal turbine blades, powder metallurgy components, and melt-spun flake or ribbon technology. These programs span the solidification rate spectrum and result in net-shape macrocastings or extremely small microcastings which then must be consolidated into usable structural components. Continued advances in turbine engine performance and reductions in fuel consumption can be realized by understanding and control of superalloy solidification processing. Concurrent tailoring of superalloy macro- and microstructure offers significant potential for further increases in superalloy use temperatures.

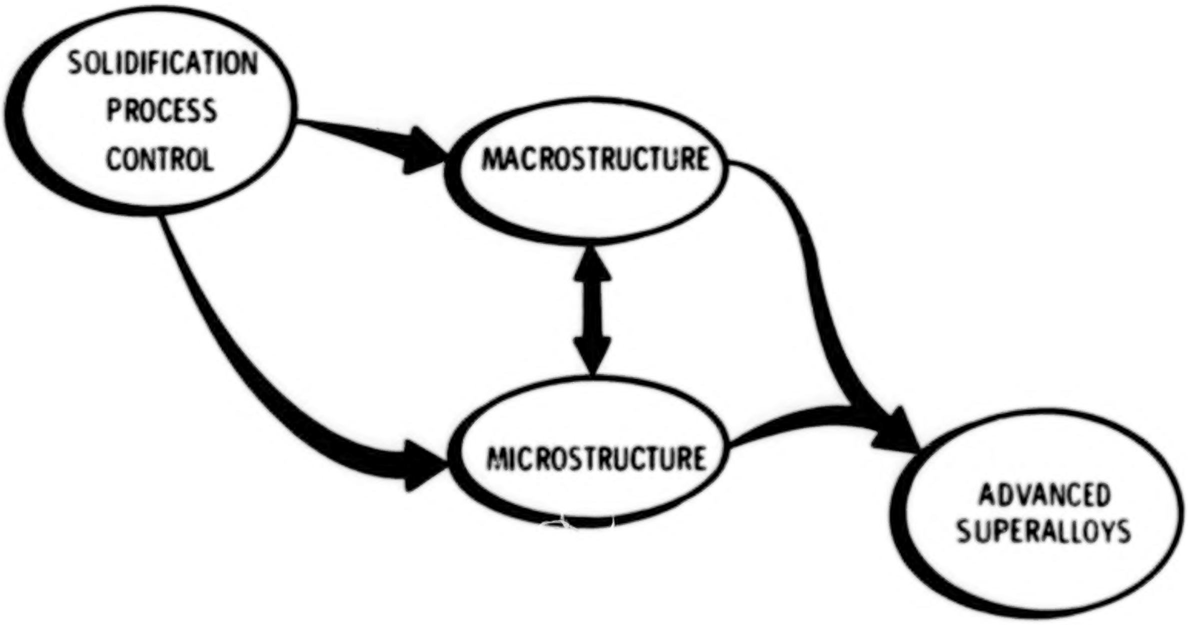

REFERENCES

1. Mehrabian, Robert: Relationship of Heat Flow to Structure in Rapid Solidification Processing. Rapid Solidification Processing - Principles and Technologies. Claitor's Publishing Div., 1978, pp. 9-27.

2. Gell, M.; Duhl, D. N.; and Giamei, A. F.: The Development of Single Crystal Superalloy Turbine Blades. Superalloys 1980. American Society for Metals, 1980, pp. 205-214.

3. Strangman, T. E.: Low-Cost, Single Crystal Turbine Blades. NASA Contract NAS 3-20073, Garrett Turbine Engine Co., 1982, also Superalloys 1980, pp. 215-224.

4. Strangman, T. E.; Hoppin, G. S. III; Phipps, C. M.; Harris, K.; and Schwer, R. E.: Development of Exothermically Cast Single-Crystal MAR-M247 and Derivative Alloys. Superalloys 1980, pp. 215-224.

5. Pearson, D. D.; Lemkey, F. D.; and Kear, B. H.: Stress Coarsening of γ' and Its Influence on Creep Properties of a Single Crystal Superalloy. Superalloys 1980, pp. 513-520.

6. Arnold, David B.: Rene' 95 Powder Metallurgy Opportunities for Gas Turbine Applications. Agard Conf. Proc. No. 200, Advanced Fabrication Techniques in Powder Metallurgy and Their Economic Applications. 1976, pp. P.6-1 to P.6-6.

7. Eng, R. D.; and Evans, D. J.: High Strength HIP Consolidated MERL 76 Disks, Superalloys 1980, pp. 491-500. (also NASA CR-165549, 1982).

8. Eng, R. D.; and Evans, D. J.: Manufacture of Low Carbon Astroloy Turbine Disk Shapes by Hot Isostatic Pressing, NASA CR-135409, 1978.

9. Pfouts, W. R.; et al: Powder Metallurgy Rene' 95 - Rotating Turbine Engine Ports. NASA CR-159802, 1979.

10. Dreshfield, R. L.; and Miner, R. V. Jr.,: Application of Superalloy Powder Metallurgy for Aircraft Engines, Metal Powder Reports, 35, No. 11, pp. 516-520, 1980.

11. Miner, R. V.; Gayda, J.; and Maier, R. D.: Fatigue and Creep-Fatigue Deformation Behavior of Nickel-Base Superalloys at 650°C, Metallurgical Transactions, 13A, no. 10, 1982.

12. Cowles, B. A.; Warren, J. R.; and Haake, F. K.: Evaluation of the Cyclic Behavior of Aircraft Turbine Disk Alloys. NASA CR-165123, 1980.

ADVANCED POWDER METALLURGY ALUMINUM ALLOYS AND COMPOSITES

W. B. Lisagor and B. A. Stein
NASA Langley Research Center
Hampton, Virginia

INTRODUCTION

Improvements in design properties of structural aluminum alloys over the past three decades had become a slow, evolutionary process as alloy chemistries were developed and refined. By about 1970, the limited equilibrium solubility of alloying additions to 7000- and 2000-series aluminum alloys synthesized by conventional ingot metallurgy (IM) processing portended increasing difficulty in achieving higher levels of balanced properties. However, the emerging technology of rapidly solidified or mechanically alloyed powder metallurgy (PM) aluminum alloys promises to change that situation dramatically.

By employing cooling rates of 10^2 to 10^6°C per second in the production of particulate powders or flakes, alloying element concentrations can be substantially increased through supersaturated solid solutions and grain sizes in consolidated product forms reduced by an order of magnitude from those in conventional ingot metallurgy products. Another method used to achieve small grain size and controlled dispersoid amount and distribution is the mechanical alloying process. Via both processes, the resulting uniform distribution of alloying elements and dispersoids has provided (in laboratory to pilot plant quantity materials) superior property combinations of tensile and creep strength, ductility, fracture toughness, fatigue strength, and corrosion resistance compared to commercial ingot alloys.

The conclusions of a National Materials Advisory Board (NMAB) Survey (reference 1) of advanced powder metallurgy aluminum research were as follows:

o Rapidly solidified PM alloys offer high potential of superior properties compared to ingot metallurgy alloys.

o Broad usage of rapidly solidified PM alloys is foreseen for aerospace applications.

o Current knowledge of phase relationships, microstructure, and structure/property interaction is inadequate.

That survey recommended vigorous support of rapidly solidified PM aluminum at all levels of research, development, testing, and manufacturing, with special emphasis on continuing long-range basic research and development programs.

This paper outlines the differences between powder and ingot metallurgy processing of aluminum alloys, indicates the potential payoff in the use of advanced PM aluminum alloys in future transport aircraft, and reviews briefly the national program (in response to the NMAB challenge) to bring this technology to commercial fruition and the NASA Langley Research Center role in this program. We also present some initial results of research in 2000-series PM alloys and composites to highlight the property improvements possible.

CONVENTIONAL INGOT METALLURGY

The mature technology in structural aluminum alloys for aerospace, ground, and water transportation and for a wide range of consumer products is a result of two generations of developments and refinements of ingot metallurgy (IM) processes. The aluminum metal is recovered from its ore, usually bauxite, by an electrolytic process. As figure 1 shows, the alloy constituents are melted and a direct casting process using water-cooled molds produces ingots of various sizes. Cooling rates as high as 10°C per second may be achieved by this method but IM cooling rates for aluminum alloys are generally lower and can be as low as 10^{-2}°C per second for large ingots. Thus, equilibrium restrictions of solid solubility limit ingot chemistries, and grain sizes in ingots are relatively coarse. The cast ingot is warm- and/or cold-worked by forging, extrusion, or rolling to produce the mill product form. The latter is heat treated (or thermomechanically processed), which consists of solution treatment plus precipitation hardening (plus cold work) for structural alloys, then formed or machined to final product dimensions.

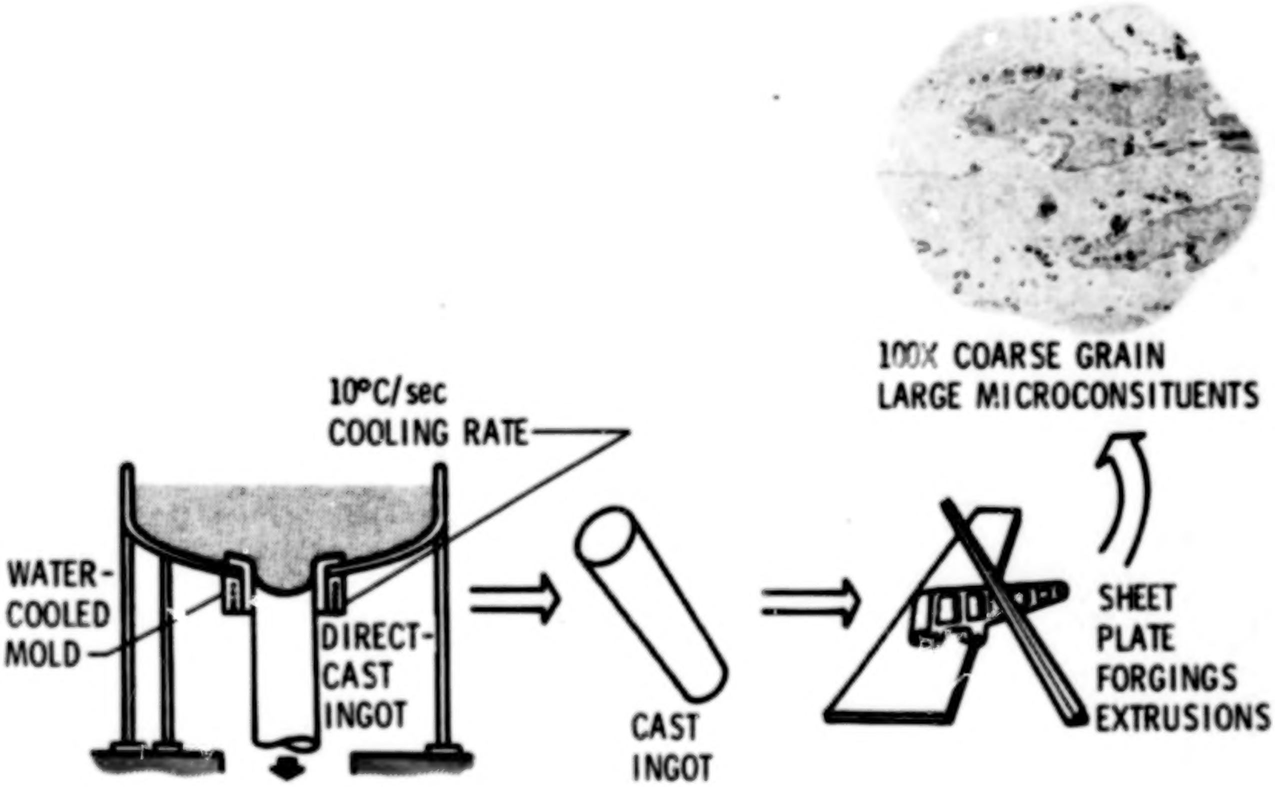
100X COARSE GRAIN
LARGE MICROCONSITUENTS
10°C/sec
COOLING RATE
WATER-
COOLED
MOLD
DIRECT-
CAST
INGOT
CAST
INGOT
SHEET
PLATE
FORGINGS
EXTRUSIONS

Figure 1

RAPIDLY SOLIDIFIED OR MECHANICALLY ATTRITED POWDER METALLURGY

Two generic processes are currently being commercialized to produce aluminum alloy powders for subsequent consolidation into billets which are then converted into product forms and structural components using conventional aluminum processing and fabrication technology. The powder process under most extensive study is that of rapid solidification from the melt. As illustrated in figure 2, one process to produce such powders is to impinge a jet of molten alloyed aluminum from a vacuum melting furnace onto a rapidly spinning disk in an inert gas quench chamber; the "atomized powders" which result are roughly spherical and micron-sized. Alternative versions of this process can produce other micromorphologies such as very thin flakes or ribbons. The cooling rates achieved typically range from 10^2 to 10^6°C per second. The powders produced can retain relatively high percentages of alloying elements (miscible in the melt) in metastable, supersaturated solid solutions. Supersaturation opens up a wide range of possibilities for new aluminum alloy chemistries which could not be produced by conventional ingot melting techniques (with their slow cooling rates), because equilibrium solid solubility of many elements in aluminum is at low concentrations.

The other generic powder production process - mechanical alloying - is also illustrated in figure 2. Elemental and/or partially prealloyed powders of the alloy chemistry desired are subjected to high energy mixing processes which result in a powder in which each particle contains all desired alloying constituents in a uniform chemical/dispersoid distribution. Figure 2 shows this result achieved in a high energy ball mill with steel balls driven by a rotating impeller in a water-cooled tank. The steel balls pressure weld the aluminum, iron, and other elemental powders into micron-sized prealloyed powders.

The fine powders resulting from both generic processes should have these desirable qualities: (1) relatively uniform matrix chemistry with controlled levels of alloying elements, (2) fine, uniformly spaced, thermally stable dispersoids (i.e.-oxides and/or intermetallics).

In either case, the powders are classified and packaged, usually in metallic cans, prior to cold compaction. Cold compacts are vacuum degassed followed by hot compaction in a conventional set of dies or by hot isostatic pressing to produce a billet (compacted ingot) of fine grain size compared to a cast ingot.

The subsequent rolling, extrusion, forging, and heat treating/thermomechanical processing procedures for the powder metallurgy billets are similar to those used for the cast ingot products, using equipment currently available in aluminum material producer, aerospace, and consumer product industries. Parameters of the particular cold/hot working or heat treatment process will probably be somewhat different for powder product forms (to achieve optimum balanced properties) than they were for cast ingots of similar chemistry. Considerable research is under way to investigate such parameters. Conventional aluminum alloy component mechanical joining processes (e.g.-riveting, bolting) should be applicable to the advanced PM alloys. Development of welding procedures to retain the desired properties may be very difficult; however, PM alloys will likely be used in applications where welding is not a primary joining method.

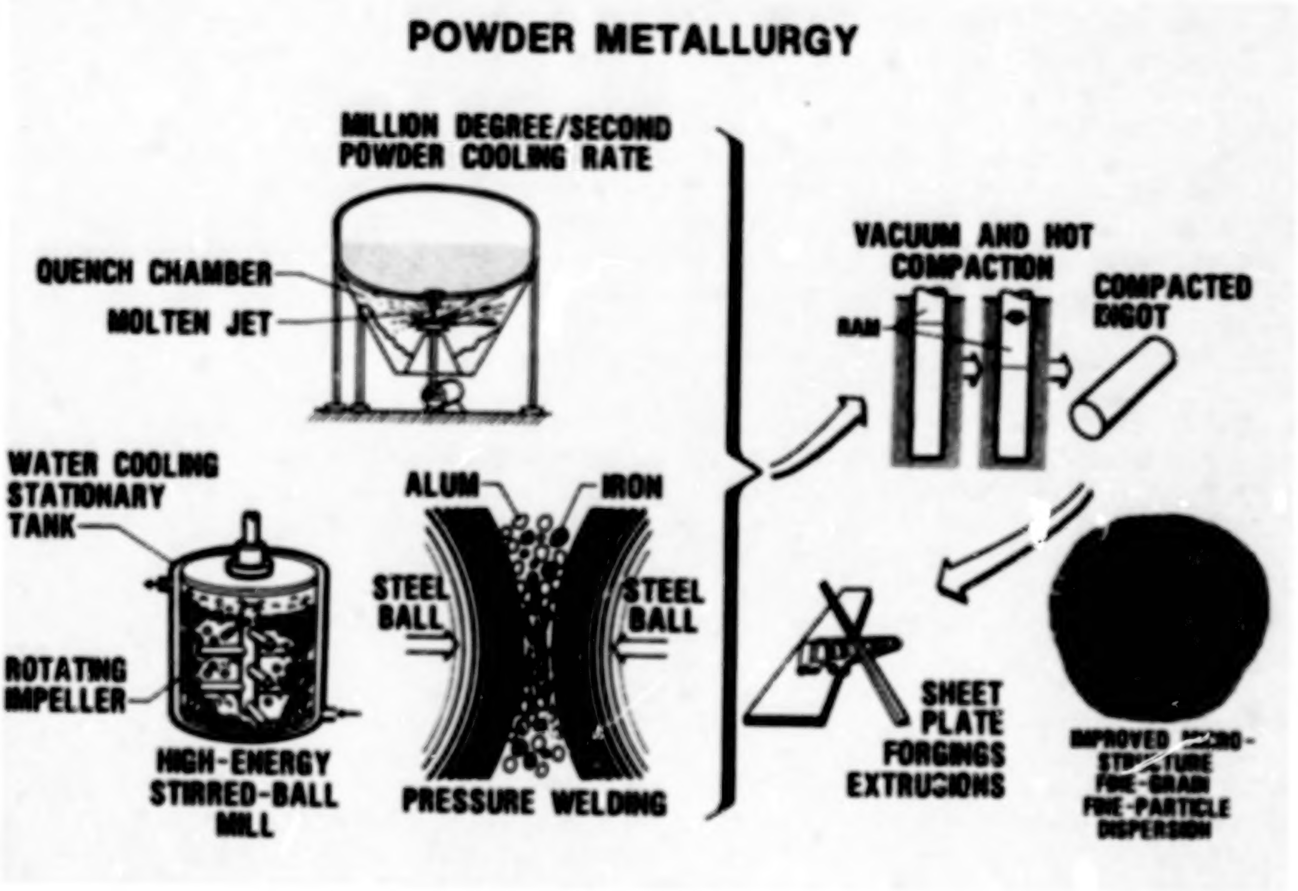
POWDER METALLURGY
MILLION DEGREE/SECOND POWDER COOLING RATE
QUENCH CHAMBER
MOLTEN JET
WATER COOLING STATIONARY TANK
ROTATING IMPELLER
HIGH-ENERGY STIRRED-BALL MILL
ALUM
IRON
STEEL BALL
STEEL BALL
PRESSURE WELDING
VACUUM AND HOT COMPACTION
RAM
COMPACTED INGOT
SHEET
PLATE
FORGINGS
EXTRUSIONS
IMPROVED MICRO-STRUCTURE
FINE-GRAIN
FINE-PARTICLE DISPERSION

Figure 2

STATUS OF NATIONAL ADVANCED ALUMINUM ALLOY PROGRAM

The national technology development program in advanced aluminum alloys is a more or less coordinated effort of materials producers and aerospace manufacturers, with Federal Government support in most areas. That support is provided mainly by the Department of Defense, with significant contributions from the U.S. Air Force, Army, Navy, and Defense Advanced Research Projects Agency, particularly in the materials development and applications areas. NASA support is generally aimed at the materials research area.

The strong direction to date in materials research (figure 3) has been aimed at minor chemistry and heat treatment modification of the conventional ingot metallurgy 7000-series (Al-Zn-Mg-Cu-X) and 2000-series (Al-Cu-Mg-X-X) alloys to take advantage of the small grain size/uniform dispersoid capabilities of the powder process without making major diversions from known aluminum alloy technology. Only limited alloy formulation of entirely new chemistries in powder metallurgy aluminum alloy has been pursued to date. Most notable of these is the development of Al-Fe-Ce alloys and other chemistries which produce thermally stable dispersoids for applications at temperatures above 400°F. Another research area receiving increased recent emphasis is aluminum-lithium alloys synthesized by both ingot and powder metallurgy techniques. Al-Li-X-X alloys promise important increases in elastic modulus-to-density ratios compared to conventional alloys at moderate temperatures, an important factor in stiffness critical applications.

Materials development has been under way for several years with some government support, but largely financed by the major aluminum suppliers - ALCOA, Kaiser, and Reynolds - for the rapidly solidified powder alloys and by INCO/Novamet for the mechanically alloyed materials. There have been commitments to commercial development with ALCOA rapidly solidified powder alloy X7091 and the INCO IN9021 mechanically alloyed material. Further alloy chemistry/processing development studies are under way at several companies and pilot process scaleup has been initiated.

Applications of advanced aluminum alloys have been studied for several years by major aerospace manufacturers (e.g.-Lockheed, Boeing, McDonnell Douglas, Northrop, General Dynamics/Convair), under both company and government funding. Evaluations to date have covered a broad range of material property tests of laboratory specimens from laboratory or pilot-plant quantities of material. The materials data have been used in preliminary design studies to forecast the most promising applications. Specific aerospace structural applications with high potential payoffs have been identified and the "spinoff" to nonaerospace applications has been addressed. The most promising potential nonaerospace applications for advanced aluminum alloys appears to be in ground transportation.

STATUS OF NATIONAL ADVANCED ALUMINUM ALLOY PROGRAM

- MATERIAL RESEARCH
    - GOVERNMENT/PRODUCER/USER COMBINED R&D EFFORTS
    - FOCUS ON MODIFICATION OF I/M CHEMISTRIES IN 2000- AND 7000-SERIES ALLOYS
    - NEW ALLOY FORMULATIONS FOR HIGH-TEMPERATURE APPLICATIONS
    - Al-Li ALLOYS
- MATERIAL DEVELOPMENT
    - MAJOR MATERIAL SUPPLIERS INVOLVED
    - COMMITTED TO COMMERCIAL DEVELOPMENT
    - PILOT PROCESS SCALEUP INITIATED
- APPLICATIONS
    - BROAD PROPERTY EVALUATION BY MAJOR AEROSPACE MANUFACTURERS AND GOVERNMENT UNDER WAY
    - ALL EVALUATIONS TO DATE BASED ON LABORATORY QUANTITIES
    - POTENTIAL NONAEROSPACE USAGE IN ADVANCED GROUND TRANSPORTATION SYSTEMS

Figure 3

ADVANCED ALUMINUM ALLOY TECHNOLOGY: RESEARCH AND DEVELOPMENT COSTS

The cost of bringing each new advanced aluminum alloy from the initial synthesis through the research and development (R&D) stage to the application stage - is shown in figure 4. It takes about 3 years of materials research with cumulative costs accruing relatively slowly to reach the point where a decision to scale up to product form characterizaton and structural element testing can be made. That stage and the following pre-application stages, design property generation and proof-of-concept testing of complex structures, consume rapidly increasing funding to about the 5th year. When a positive application decision is reached, R&D support is usually required to enhance the material for the specific application and to solve material/processing problems in the early production runs. The total cost of this R&D effort in today's dollars is $6- to $10-million for each alloy brought to full commerical production.

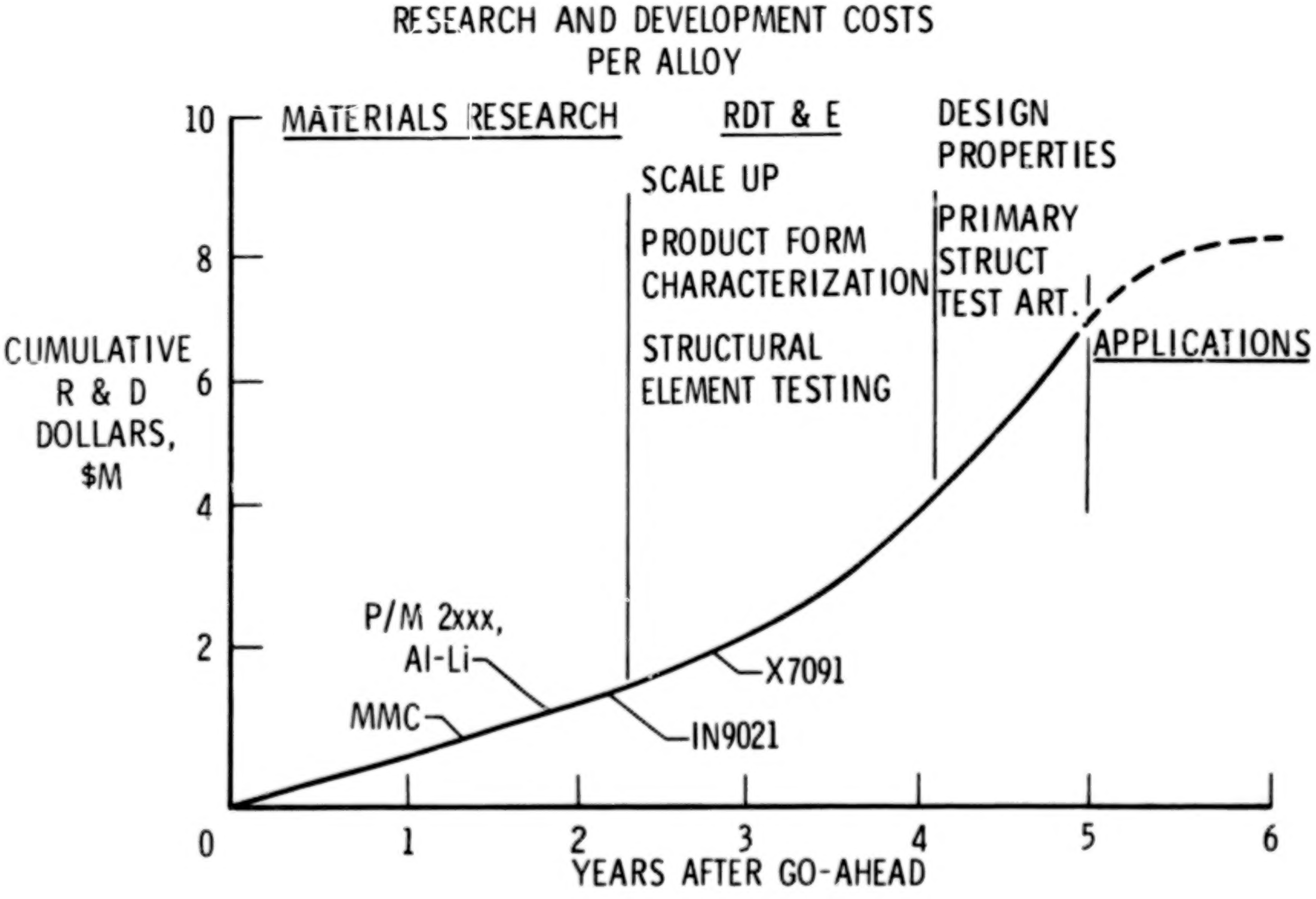

Figure 4

RELATIVE COST DIFFERENTIAL FOR CONVENTIONAL AND ADVANCED ALUMINUM ALLOYS: LONG-HAUL TRANSPORT APPLICATIONS

As in any other application, the aerospace industry must convince itself that increased costs inherent in a new technology will be more than offset by the advantages resulting from that technology, in a specific product or component. This subject was addressed in a NASA supported study for three types of commercial vehicles - a long-range transport aircraft, a short/medium-range transport aircraft, and a short-haul commuter aircraft (reference 2). Examples of the results are shown in figures 5 through 7.

The relative cost differentials between conventional commercial ingot Al alloys and advanced aluminum alloys is shown in figure 5. Cost per pound of material or structure is shown in 3 sets of bars, with the costs plotted on a logarithmic scale. The raw material (in sheet, plate, extrusion or forging product form) costs of conventional alloys ranges from about $2.25 to $4.50 per pound; the advanced alloys are twice to four times as expensive. However, a comparison on that basis only can be highly misleading. The center bars in the figure indicate the actual costs per pound of a structural component produced with conventional alloys ranges from about $92 to $114 per pound; the related components in advanced alloys will cost about 20 percent more. The two bars on the right, which reflect the total aircraft production cost per pound of structural weight, show a further reduction in the cost differential between conventional and advanced aluminum to about 16%. When the weight savings is taken into account, the projected cost per aircraft using advanced aluminum is actually slightly lower than its conventional aluminum counterpart, as indicated in figure 6.

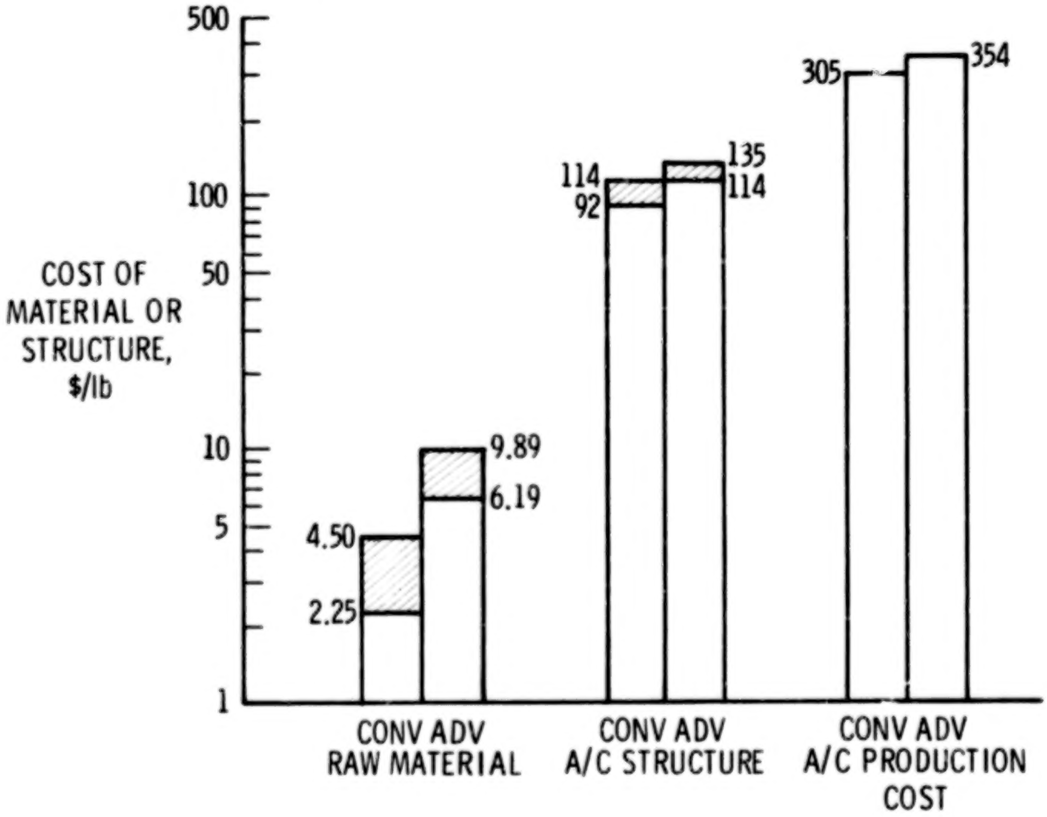

Figure 5

BEST DOCUMENT AVAILABLE

ADVANCED LONG-RANGE TRANSPORT FOR THE 1990s: NET VALUE OF ADVANCED ALUMINUM TECHNOLOGY

The most attractive generic aircraft application of advanced aluminum alloy technology found in the study reported in reference 2 is the long range transport. A sketch of such a vehicle, an extension of Lockheed L-1011 technology, is in figure 6. This concept was analyzed for a primary structure of either conventional aluminum or advanced aluminum alloy. The shaded areas indicate major structural and aerodynamic improvements from the current aircraft. The 1990s aircraft also has composite secondary structure components and improved flight station electronics, controls, etc.

The table in the lower part of figure 6 shows that (in spite of the increased costs per pound of advanced material and structure shown in figure 5), the increased structural efficiency (i.e. - decreased structural weight fraction) of the advanced aluminum aircraft shows a cost benefit in all significant cost factors. Most importantly, the operational cost per year benefit for a fleet of 300 aircraft is highly significant even at fuel costs at $1.00 per gallon and rises sharply as fuel price increases. The specific property improvements required in the advanced Al alloys to achieve these benefits are addressed in the next figure.

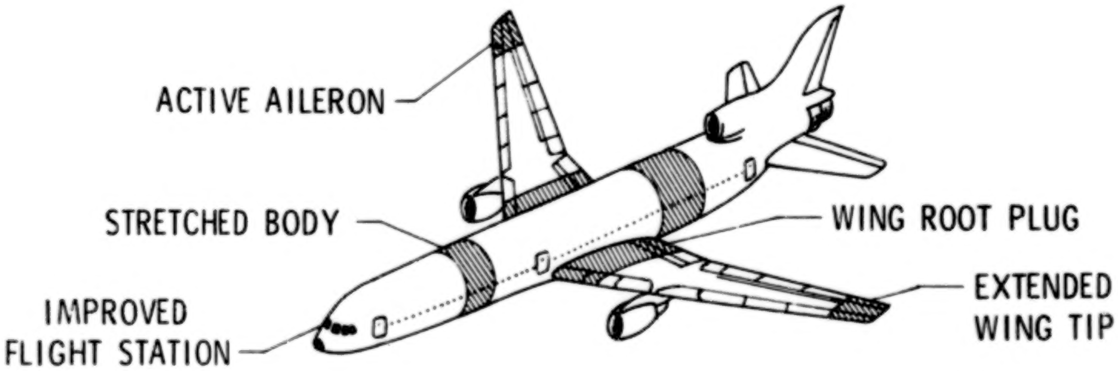

ATX-3501 LONG RANGE TRANSPORT AIRCRAFT	TOTAL OPERATIONAL COST* FUEL PRICE, $			FLYAWAY COST, $		RDT&E COST, $
	$264/m^3$ (1.00/gal)	$528/m^3$ (2.00/gal)	$792/m^3$ (3.00/gal)	PER AIRCRAFT	300 AIRCRAFT	300 AIRCRAFT
REFERENCE AIRCRAFT (CONVENTIONAL ALUMINUM)	10585M	12779M	14948M	68.49M	20547M	2823M
ADVANCED ALUMINUM AIRCRAFT	10265M	12275M	14271M	66.79M	20037M	2753M
NET COST BENEFIT	320M	504M	677M	1.70M	510M	70M

*ANNUAL COST FOR 300 AIRCRAFT BASED ON AVERAGE STAGE LENGTH OF 4630 km (2500 n. mi.)

Figure 6

PRELIMINARY MATERIAL PROPERTY GOALS

It is important to realize that in any complex structure, materials are utilized in a variety of product forms and specific components put a premium on different properties and combinations of properties. Thus, several different alloys (or the same alloy with different thermomechanical treatment to enhance given properties) are utilized in conventional aluminum alloy aircraft structures. Accordingly, several types of advanced alloys are envisioned for future applications. Increases in a given property, such as strength or stiffness, will usually not be enough to satisfy the goals. A balance of properties is required, with an increase over the current alloy in several parameters and at least comparable values in other properties.

A preliminary set of material property goals to achieve the benefits shown in the the preceding figure is shown in figure 7. The table shows that the aircraft structural applications can be divided into five classifications, from strength to low-density/high-stiffness (left-hand column). The product forms and typical conventional alloys used in current long-range transport structures are indicated in the center columns. One to three product forms are utilized in each classification. The right column shows the target goals as percentage increases in various properties for each classification. An advanced alloy must meet or exceed these targets to provide the required structural benefits. However, substantial exceedence of one property without maintaining the required balance of properties usually will not achieve the desired result.

CLASSIFICATION ALLOY REQUIREMENT	ALLOY CODE	BASELINE ALLOY - PRODUCT FORM				TARGET GOALS PERCENT IMPROVEMENT
		SHEET	PLATE	EXTRUSION	FORGING	
STRENGTH	A	7075-T6clad	–	7075-T6	–	20-25% STRENGTH 20% FATIGUE COMPARABLE TOUGHNESS
STRENGTH AND CORROSION RESISTANCE	B	–	7075-T76	7075-T76	7075-T73	20-30% STRENGTH 20% FATIGUE COMPARABLE TOUGHNESS & CORROSION RESISTANCE
STRENGTH, STIFFNESS AND CORROSION RESISTANCE	C	–	7075-T76	7075-T76	–	10-20% STRENGTH 10% FATIGUE 8% STIFFNESS COMPARABLE TOUGHNESS & CORROSION RESISTANCE
DURABILITY AND DAMAGE TOLERANCE	D	2024-T3clad	2024-T3	–	–	20% FATIGUE 25% TOUGHNESS CORROSION RESISTANCE COMPARABLE TO 7075-T76
LOW DENSITY/ HIGH STIFFNESS	E	2024-T3clad	–	–	–	10% FATIGUE 10% DENSITY COMPARABLE STRENGTH

Figure 7

LaRC ADVANCED ALUMINUM ALLOY
PROGRAM PHILOSOPHY

Considering the national Advanced Al Alloy Program (figure 3) and the conclusions and recommendations of the NMAB Study (see Introduction), the decision was made to focus the LaRC program on research aimed at a quantitative understanding of structure property relationships in advanced aluminum alloys. The elements of this program philosophy are shown in figure 8. The five elements at the left (composition.....thermomechanical processing....product form processing) are all factors which will affect the microstructural qualities listed in the center (grain and subgrain structure...microconstituent particles) and, in turn, must be adjusted to achieve desired microstructures or microstructural distributions. The latter are directly related to the three elements listed at the right, the physical and mechanical properties (including those which are time dependent). Learning and quantifying these structure-property relationships will enable prediction of new chemistry/processing directions for further PM aluminum improvements, understanding of difficulties encountered in the application of these advanced alloys, and thus (as the information is digested in the materials and fabrication communities) the t[illegible]g of aluminum properties for aerospace structures.

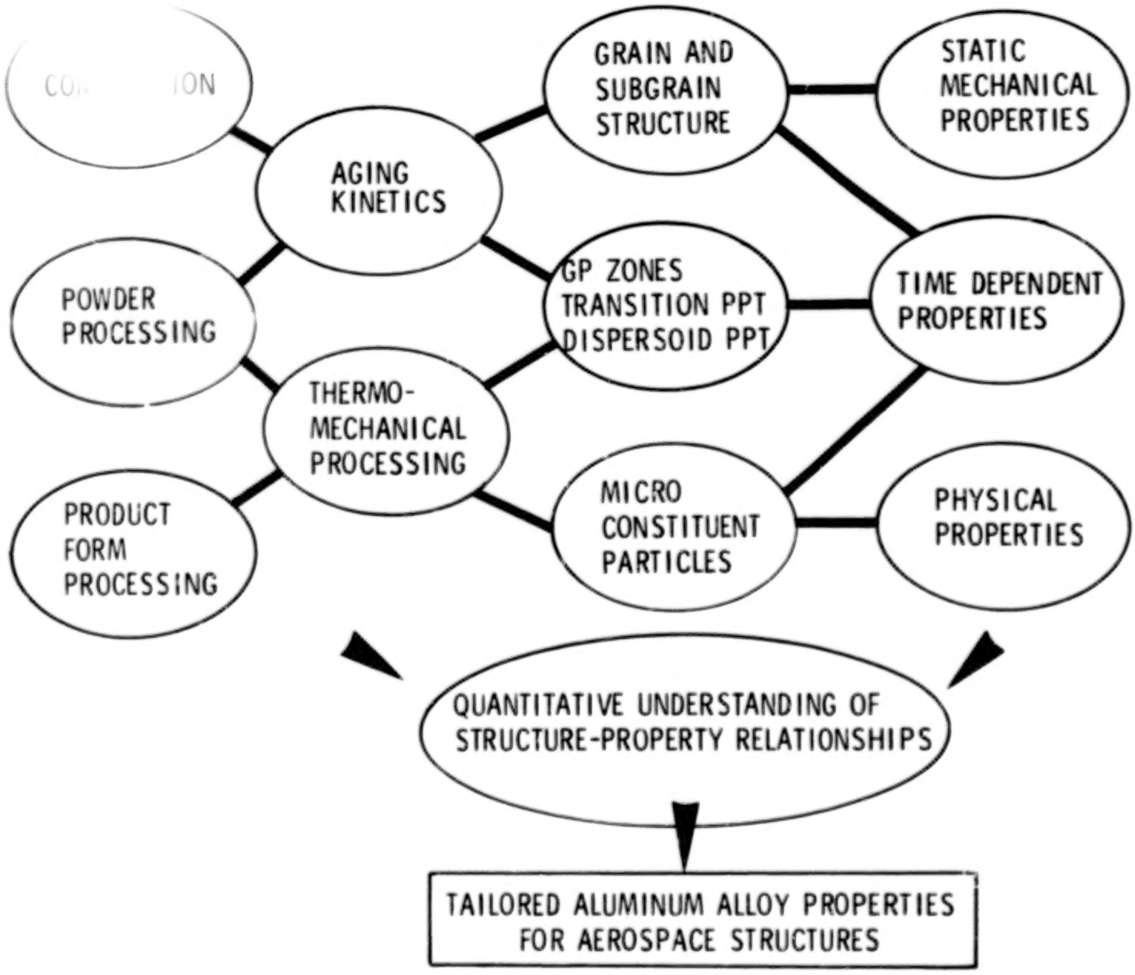
CO[illegible]ION
AGING KINETICS
POWDER PROCESSING
THERMO- MECHANICAL PROCESSING
PRODUCT FORM PROCESSING
GRAIN AND SUBGRAIN STRUCTURE
GP ZONES TRANSITION PPT DISPERSOID PPT
MICRO CONSTITUENT PARTICLES
STATIC MECHANICAL PROPERTIES
TIME DEPENDENT PROPERTIES
PHYSICAL PROPERTIES
QUANTITATIVE UNDERSTANDING OF STRUCTURE-PROPERTY RELATIONSHIPS
TAILORED ALUMINUM ALLOY PROPERTIES FOR AEROSPACE STRUCTURES

Figure 8

LaRC ADVANCED ALUMINUM ALLOY PROGRAM APPROACH

Implementing the philosophy shown in figure 8, and narrowing the range of possible aluminum alloy types to be studied, LaRC decided to concentrate on the alloy chemistry developed for high-toughness, intermediate-temperature (to about 350°F in long cumulative service) applications. That family is the 2000-series alloys, the Al-Cu-Mg-X-X chemistries. As indicated in Figure 9, the focus will be on understanding of: (1) the possibilities in powder chemistry/processing optimization, (2) the structure-property relationships, (3) aging kinetics and thermomechanical processing variables; and (4) component processing methodology opportunities. The program will be a combined effort of in-house, contract, and university grant activity. Selected results of initial powder metallurgy alloy studies are shown on the following figures.

- CONCENTRATE ON Al-Cu-Mg-X-X CHEMISTRY
- FOCUS ON UNDERSTANDING
    - POWDER CHEMISTRY/PROCESSING OPTIMIZATION
    - STRUCTURE-PROPERTY RELATIONSHIPS
    - AGING KINETICS AND THERMOMECHANICAL PROCESSING
    - COMPONENT PROCESSING METHODOLOGY
- COMBINED IN-HOUSE, GRANT, AND CONTRACT ACTIVITY

Figure 9

COMPARISON OF NOTCHED TENSILE STRENGTH/YIELD STRENGTH RATIOS

Implementation of the LaRC advanced aluminum alloy research program has concentrated to date on the systems study of transport aircraft (results of which are described previously herein) and on studies to evaluate the potential of 2000 series PM aluminum alloys with chemistry modifications from the corresponding IM alloys (ref. 3). Laboratory quantities of several 2000-series powder alloys have been evaluated, including 2124, 2219, and the 2124 alloy with silicon carbide whisker reinforcement.

The objective of this part of the LaRC effort is to determine powder metallurgy chemistries/heat treatments on 2000-series alloys which can meet the target material property goals for advanced transport aircraft shown in figure 7. The chemistry modifications have been limited initially to adjustments in the amount of dispersoid forming elements present in the PM product. The purpose of these adjustments was to promote formation of more thermally stable dispersoids and to take advantage of the naturally occurring oxide dispersoids present in the P/M product. The desired result is an increase in yield strength at ambient and elevated temperatures while maintaining high toughness.

Figure 10 shows recent results indicating that combined goals of tensile yield-strength and toughness (as measured by notched tensile strength) can be met with extrusions of powder metallurgy aluminum alloys. The dashed line for the ingot metallurgy 2124-T8510 alloys shows that data for specimens of this material do not meet the goal, falling below or to the left of the target goal outlines. The powder metallurgy, modified chemistry form of the 2124 alloy with the similar heat treatment can reach the notch strength ratio target goal at a yield strength of about 62 ksi. Similarly, certain PM chemistry modfications of the 2618 alloy can meet the goals at yield strengths from about 62 to 65 ksi, whereas the 2618 PM alloy with the identical chemistry of the IM alloy does not meet the goals. The P/M HID 543 alloy can also meet the goals at yield strengths of about 63 ksi.

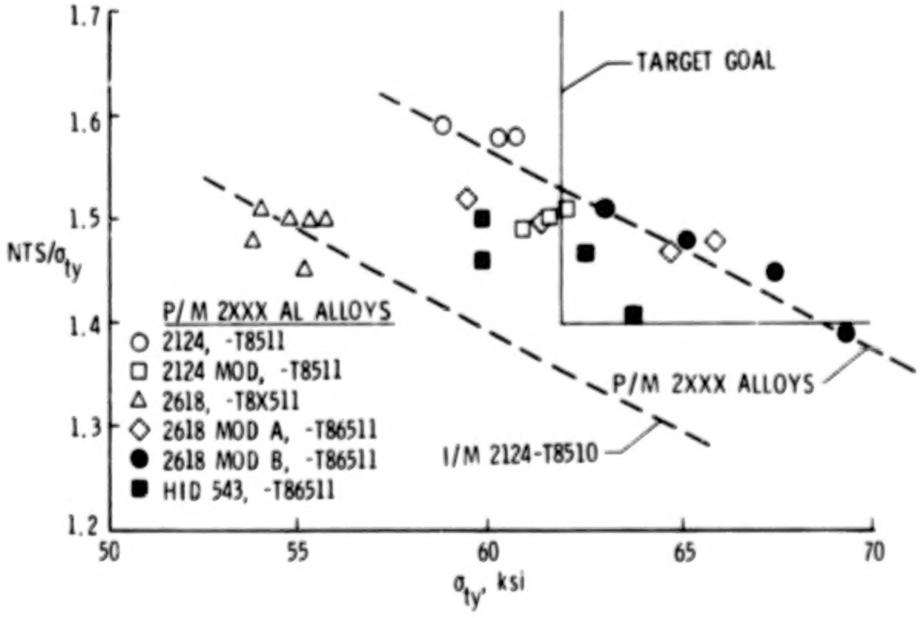

Figure 10

COMPARISON OF TENSILE PROPERTIES FOR PM 2219 Al

Improving the properties of an aluminum alloy via powder metallurgy is achieved through a combination of parameters. Minor chemistry modifications are made in the alloy to take advantage of the inherent capability of the powder process to retain higher percentages of strengthening elements in solid solution and to distribute dispersoids more finely and uniformly than is possible with ingot alloys. Solution treatment and aging or thermomechanical treatment conditions usually require modifications for the powder metallurgy alloy to achieve the best balance of properties in the advanced material.

A case in point is shown in figure 11. The ultimate tensile strength (σ_{tu}), tensile yield strength (σ_{ty}), elongation (e), and reduction in area (RA) are shown for extruded bars of conventional 2219 alloy (Al-6.3 Cu-0.3 Mn-0.2 Zr) ingot material and for the PM alloy modification of it (Al-5.5 Cu-.35 Mg-.3 Mn) after several temperature/time conditions of solution treatment (ST) and aging. It is generally desirable to process P/M alloy product at the lowest temperatures practicable in order to retain the uniformity of chemistry and dispersoids inherent in the powders. Attempts to solution treat at temperatures below that of conventional processing were made to limit tendency for recrystallization and grain growth. Figure 11 shows that P/M alloy properties can be altered significantly by solution treat temperature, but that highest strengths were attained at a solution treat temperature near that of the conventional I/M alloy. However, strength improvements were obtained for all P/M conditions.

TENSILE PROPERTIES FOR P/M 2219 Al MOD - T8511 TEMPER

MODIFIED SOLUTION TREATMENT SCHEDULE

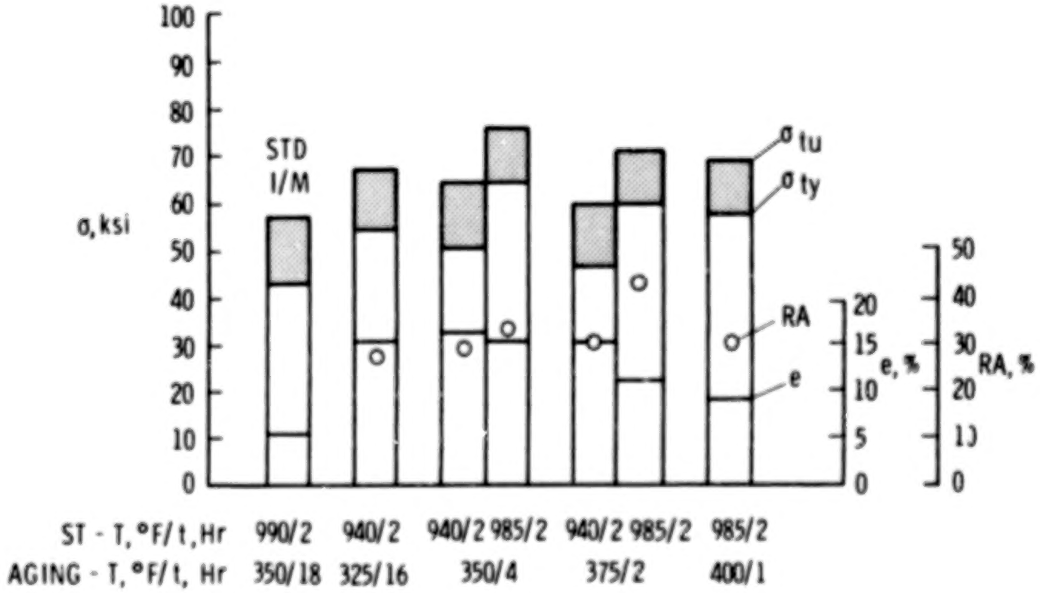

Figure 11

SPECIFIC ELASTIC MODULUS OF 2124 AND 2219 Al MMC/SiC EXTRUSIONS

Another advantage of the powder metallurgy process is its capability to consolidate alloys with uniform dispersions of high-strength, high-stiffness microconstituents which can further enhance important design properties of advanced aluminum alloys.

Two 2000-series alloys were fabricated with different amounts of silicon carbide whiskers (nominal 0.5 μm diameter with typical length/diameter ratio of 60) to produce whisker-reinforced metal matrix composites, and heat treated to the T4 condition. As shown in figure 12, small extrusions exhibit very attractive specific elastic moduli compared to the conventional 2000-series ingot metallurgy alloy, IM 2024-T4 (dashed curve). The four solid curves show that the specific elastic modulus for two powder aluminum alloys, 2124-T4 and 2219-T4, each reinforced with 15 and 25 percent silicon carbide whiskers (SiC_w) is 30 to 75% higher than the IM 2024 over a temperature range from 75 to 350°F. Many aerospace structural components are stiffness limited. Such improvements in specific stiffness can be highly significant, if other properties can be maintained at adequate levels for each specific design.

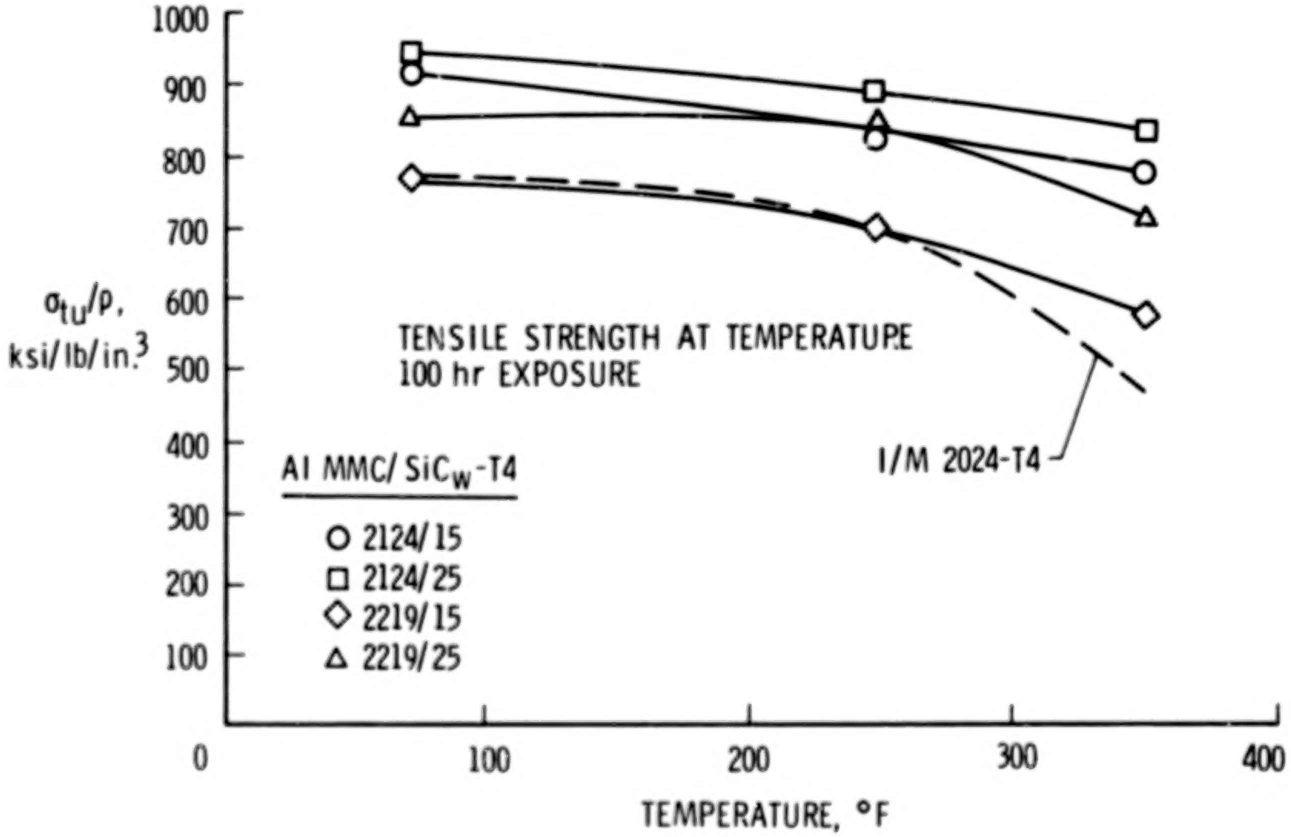

Figure 12

SPECIFIC TENSILE STRENGTH OF 2124 and 2219 Al MMC/SiC EXTRUSIONS

Figure 13 shows the specific tensile strength data which corresponds to the specific elastic modulus data shown for the SiC whisker reinforced aluminum alloys in figure 12. Specific strengths ranged from equivalent to unreinforced IM 2024-T4 for the 2219-T4 with 15 percent whiskers to a 21 percent increase over I/M 2024-T4 for PM 2124-T4 with 25% SiC_w at room temperature. At 350°F (after 100 hrs exposure at 350°F) specific strength increases over IM 2024-T4 ranged from 25% for PM 2219-T4 with 15%SiC_w to 73 percent for PM 2124-T4 with 25% SiC_w in the laboratory extruded bar specimens. However, current materials have typical elongations to failure of less than 3%, a property which must be improved if conventional philosophy is to be utilized in designing with these metal matrix composites. Further research is needed to enhance ductility in these materials, to develop these properties in other product forms such as sheet and plate, and to scale up to large billets, but the promise of these powder metallurgy aluminum matrix composites, especially for elevated temperature aerospace structural applications, appears bright.

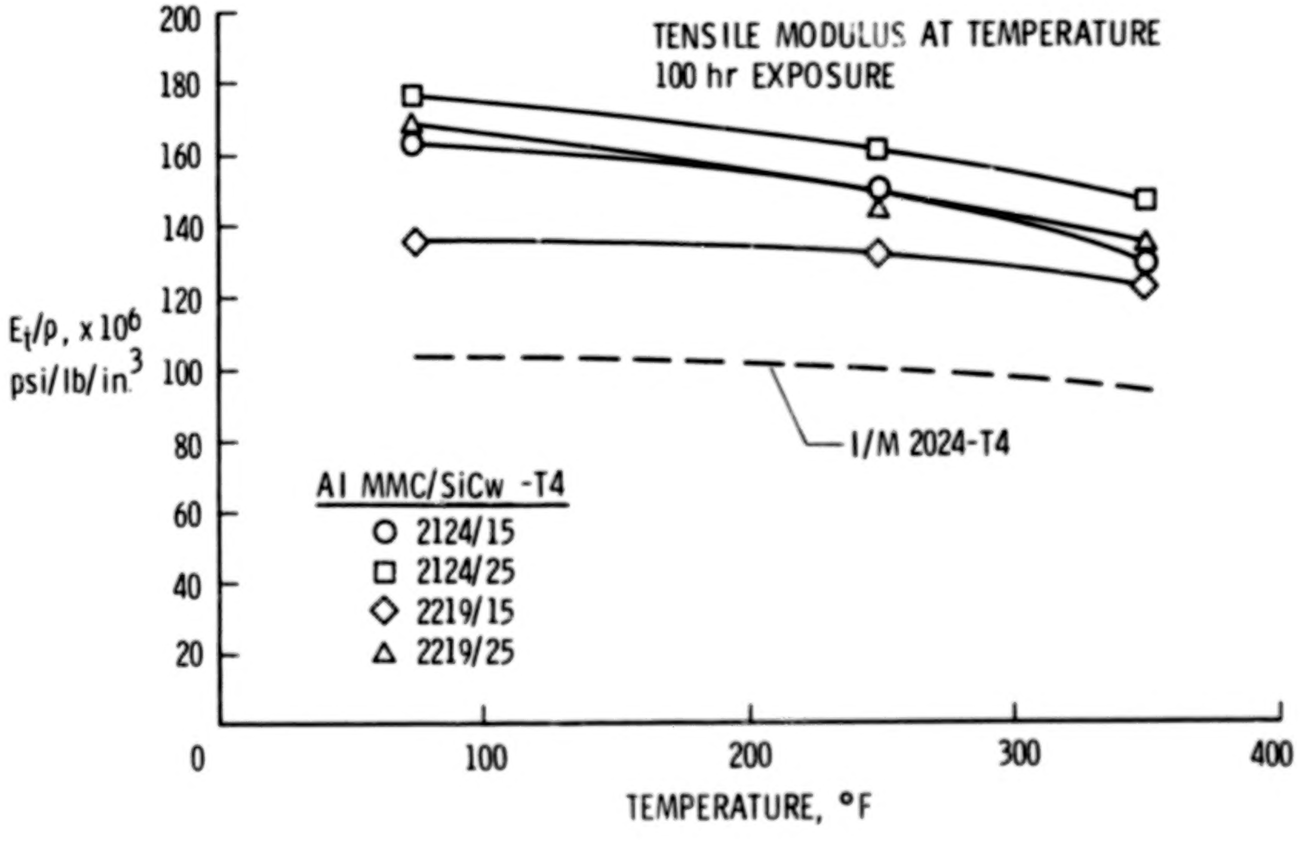

Figure 13

CONCLUSIONS

Based on this survey of advanced aluminum technology status and plans, the following can be concluded:

- Powder metallurgy aluminum alloys can be synthesized with the required balance of properties that offer high potential for efficient aerospace structures for the 1990s and beyond
- Future applications in nonaerospace industries are expected as the technology matures.
- A comprehensive national long range program of research, development, and applications is underway
- The NASA-LaRC contribution to that program concentrates on P/M 2000-series alloys and on those alloys as composite matrices reinforced with silicon carbide. The focus is on the understanding of chemistry/metallurgical/structure/thermomechanical processing/mechanical property relationships

REFERENCES

1. NMAB Committee on Powder Aluminum Alloys: "Rapidly Solidified (RS) Aluminum Alloys - Status and Prospects". National Materials Advisory Board Report No. 368, 1981.

2. Sakata, I. F.: "Systems Study of Transport Aircraft Incorporating Advanced Aluminum Alloys - Final Report". NASA CR-165820, January 1982.

3. Wald, G. G.: Supersonic Cruise Vehicle Technology Assessment Study of an Over/Under Engine Concept - Advanced Aluminum Alloy Evaluation. NASA CR-165675, May 1981.

ADVANCES IN METALS PROCESSING

Thomas T. Bales and Dick M. Royster
NASA Langley Research Center
Hampton, Virginia

INTRODUCTION

Research on metals processing is being conducted at the Langley Research Center to develop improved forming and joining methods with the potential of reducing the weight and cost of future aerospace structures. The approach followed is to assess the state of the art for fabricating a given structural system, define candidate methods for improving processing, evaluate the merits of each, fabricate and test subelement components, and then scale up the process to demonstrate validity.

This paper reports on the development and the state of the art of weldbrazing, superplastic forming (SPF), superplastic forming and codiffusion bonding (SPF/DB) and superplastic forming and weldbrazing (SPF/WB) for titanium and the SPF of aluminum. While the technology was developed for aerospace applications, potential uses are anticipated in the nonaerospace industries.

WELDBRAZING OF TITANIUM

Weldbrazing is a process developed at the Langley Research Center that combines the use of resistance spotwelding and brazing to produce structural joints having mechanical properties superior to similar joints produced by either of the processes alone (ref. 1). The steps employed in the process for fabricating a titanium structural component are shown in figure 1. The two mating parts are formed, chemically cleaned, and spotwelded together. Spotwelding parameters were selected so that a uniform faying surface gap was established between mating parts due to weld nugget expansion. A 3003 aluminum braze alloy (foil strips) was then placed adjacent to faying surfaces. The assembly was placed in a vacuum furnace and heated to the brazing temperature. Due to the spotwelds fixing and maintaining alignments of the components, no tooling was required for brazing. Upon melting the braze was drawn into the faying surface gap by capillary action to establish a hermetically sealed joint. The braze foil, which was originally placed adjacent to the flange of the hat component, completely penetrated the joint to form a filet between the face sheet and hat stringer, as shown in the photomicrograph below. Structural joints produced by this process have been shown to have superior tension, compression, and fatigue properties, as well as improved corrosion resistance compared to joints produced by riveting, spotwelding, or brazing alone. Additional studies by the Northrop Corporation have shown that weldbrazing can offer a 30-percent reduction in labor costs compared to riveting (ref. 2). Although the process was developed for joining titanium, the technology should also be applicable for use with other metals that can be joined by welding and brazing. A similar process for joining aluminum also exists, called weldbonding, where spotwelding and adhesive bonding are combined to produce joints having similar advantages.

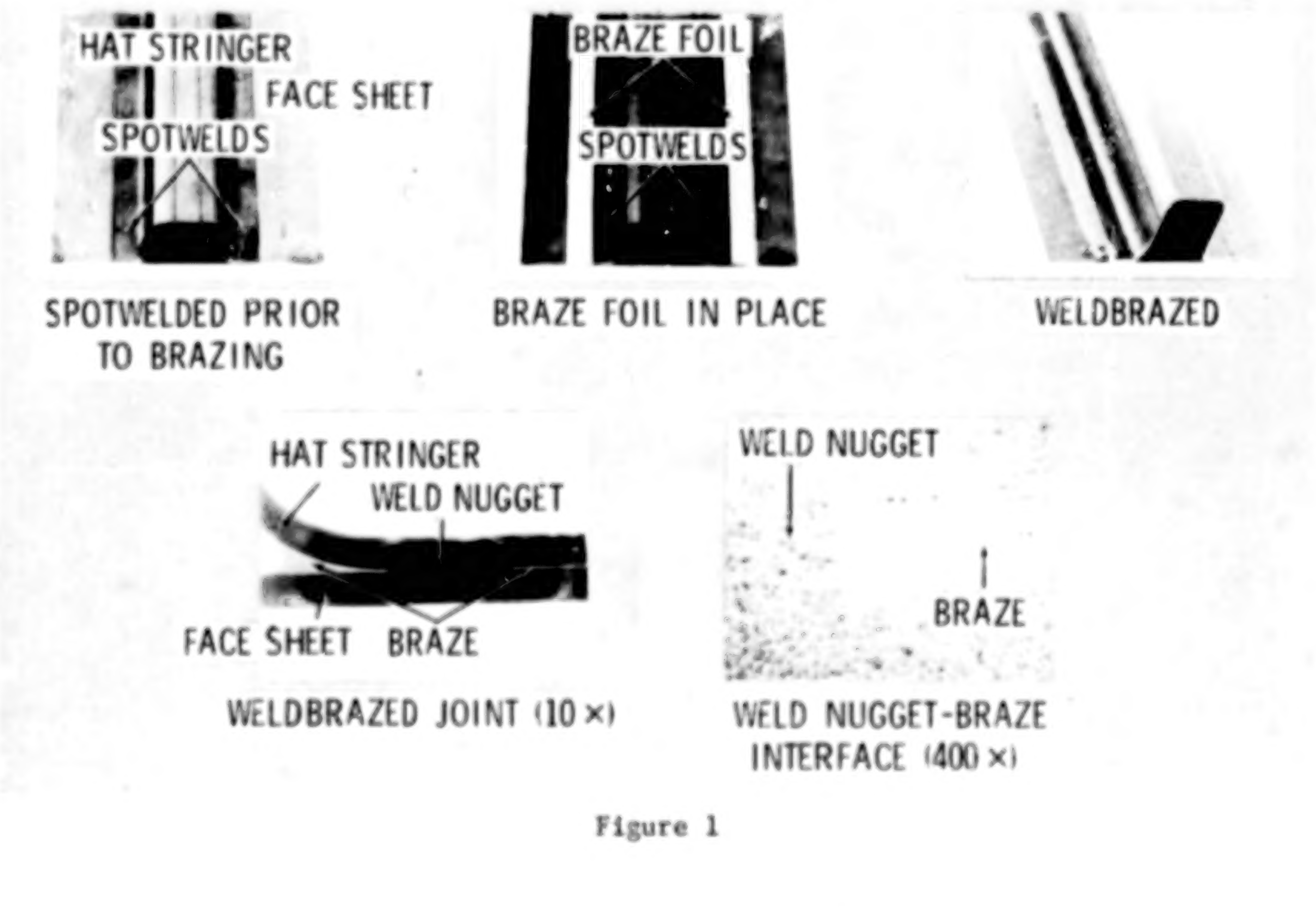

SPOTWELDED PRIOR TO BRAZING

BRAZE FOIL IN PLACE

WELDBRAZED

WELDBRAZED JOINT (10 ×)

WELD NUGGET-BRAZE INTERFACE (400 ×)

Figure 1

SUPERPLASTIC FORMING OF TITANIUM

Superplastic forming of titanium is an emerging technology which has the potential to revolutionize the fabrication of many titanium components. An example of the superplastic behavior exhibited by titanium is depicted in figure 2, which shows a specimen as machined and following superplastic stretching. The as-machined specimen was heated to 1700°F in vacuum, loaded in tension to a stress of 2 ksi, and stretched to a total elongation of over 1000 percent. As shown, the specimen elongated uniformly without experiencing localized necking. Since the flow stress required for stretching is low, the use of gas pressure to blow form or superplastically form the material was developed. Early studies shows that titanium parts could be superplastically formed to exacting tolerances to eliminate the springback and minimum bend radii problems encountered in conventional forming. Also, the high degree of formability permitted the fabrication of configurations not possible with conventional methods. These features have led to the fabrication of new design concepts having improved structural efficiency. Further work demonstrated that superplastically forming multiple parts in a large tool and a single operation resulted in cost savings of 50-70 percent compared to forming by conventional means.

Titanium can also be easily diffusion bonded at the superplastic forming temperature of 1700°F, and as a result methods have been developed to exploit the combined use of superplastic forming and diffusion bonding (SPF/DB). Early studies predicted cost savings of 30-50 percent and weight savings of 20-30 percent for SPF/DB titanium structure compared to similar components fabricated conventionally. As a result, NASA Langley initiated studies to evaluate the potential of SPF/DB titanium structures for application on future high performance aircraft.

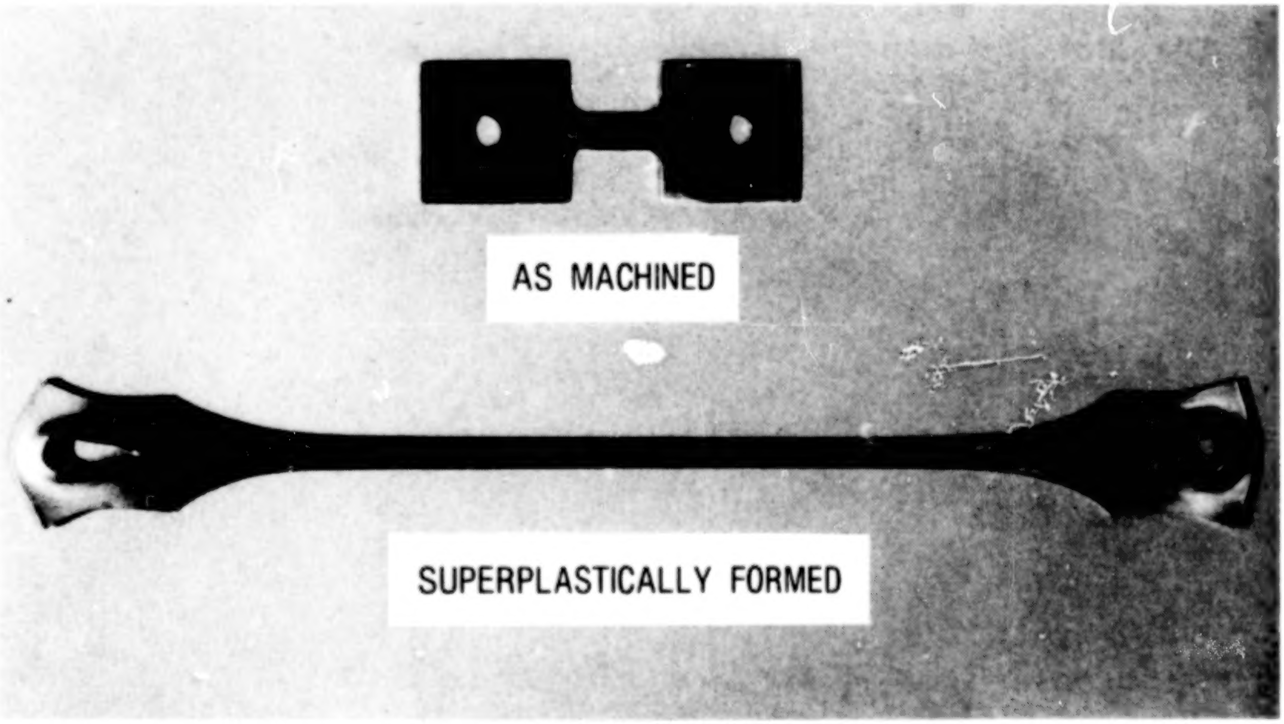

Figure 2

SPF/DB OF TITANIUM TRUSS CORE SANDWICH STRUCTURE

The method for superplastically forming and codiffusion bonding titanium sandwich structure, using the selective application of stop-off material, (ref. 3), is schematically represented in figure 3. In the first step, both sides of the center sheet are selectively coated with a ceramic stop-off material. The three sheets are then stacked and placed in the tool. The assembly is then positioned between resistance-heated ceramic platens that are mounted in a press or loading device. Load is applied and a gas-tight seal is established between the tool and the three titanium sheets due to the pinching action of the projections machined on the upper tool. The cavity of the tool is then purged with argon gas and the assembly heated to 1700°F. Argon gas is then injected into the tool at a pressure of 300 psi to compress the three sheets against the flat side of the tool. Pressure is maintained for three hours to diffusion bond the titanium sheets together in the regions where stop-off was not applied. Gas pressure in the tool cavity is then released and inert gas is injected through the preplaced tubes into the stop-off material between the sheets. Once separation of the sheets occurs, the gas pressure is increased at a programmed rate to a pressure of 100 psi to superplastically form the outer sheets to the contour of the mold cavity. As the face sheets are separated by the gas pressure, the center core sheet is superplastically stretched to form the truss core configuration. Gas pressure is equalized within the sandwich during forming by means of premachined holes. Following SPF/DB the panel is chemically milled to remove surface contamination and to obtain the desired skin thicknesses. This process has been patented and has been used to fabricate a wide variety of large components.

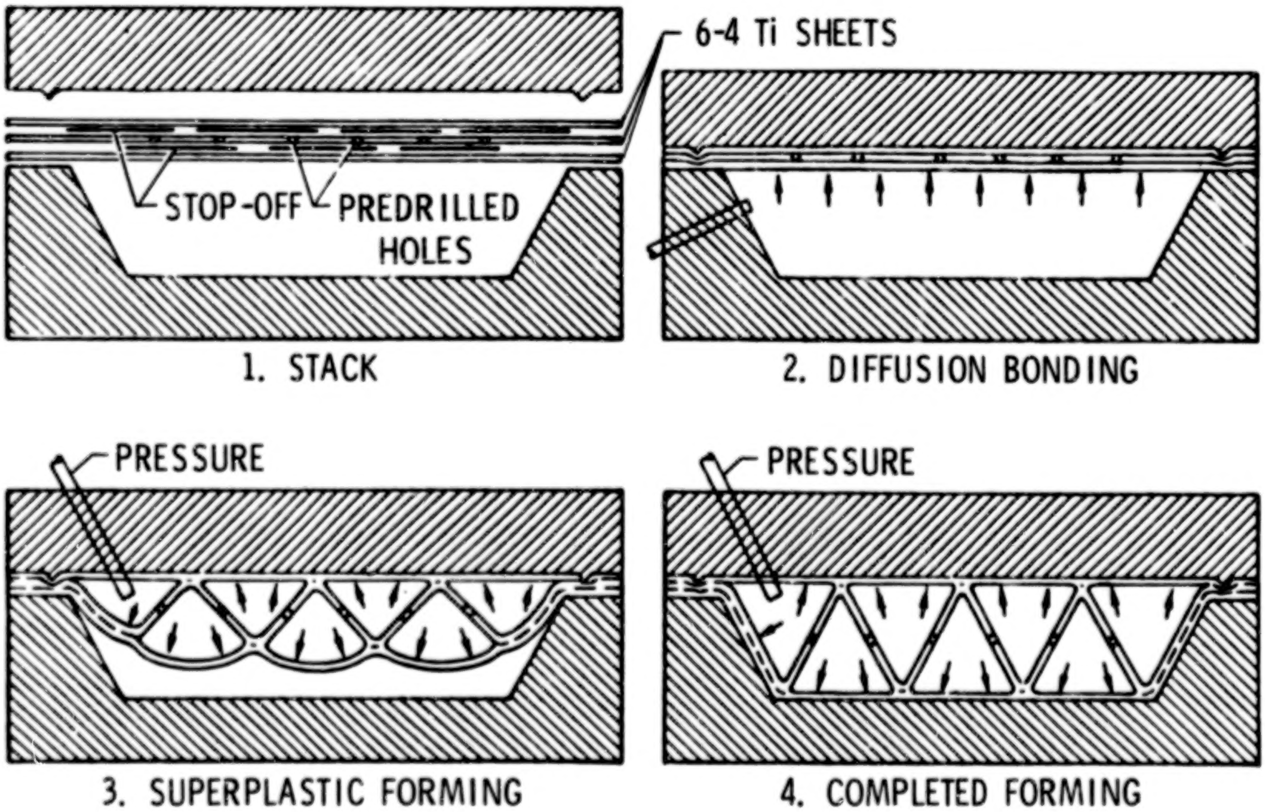

Figure 3

SCR YF-12 PANEL PROGRAM

In support of NASA's Supersonic Cruise Research (SCR) Program, LaRC initiated a study to develop and evaluate innovative processes suitable for use in fabricating flight-quality hardware for use on future supersonic aircraft. The study, designated as the YF-12 structural panel program, was a joint NASA Langley and Dryden Research Center activity.

To focus this research, an upper wing panel on the NASA YF-12C airplane was selected as a suitable structural component to validate processing methods for incorporating advanced materials into flight-quality hardware. The panel location on the YF-12 is shown in figure 4. This 16- × 28-inch panel was considered to be part of the primary structure and design critical in shear. The original wing panel was an integrally stiffened structure machined from a single plate. Panels were fabricated and evaluated through both ground tests and flight tests on the YF-12 at airspeeds up to Mach 3. Seven different panel concepts were evaluated in the program (ref. 4). Details on the fabrication of weldbrazed and SPF/DB panel concepts are discussed in following figures.

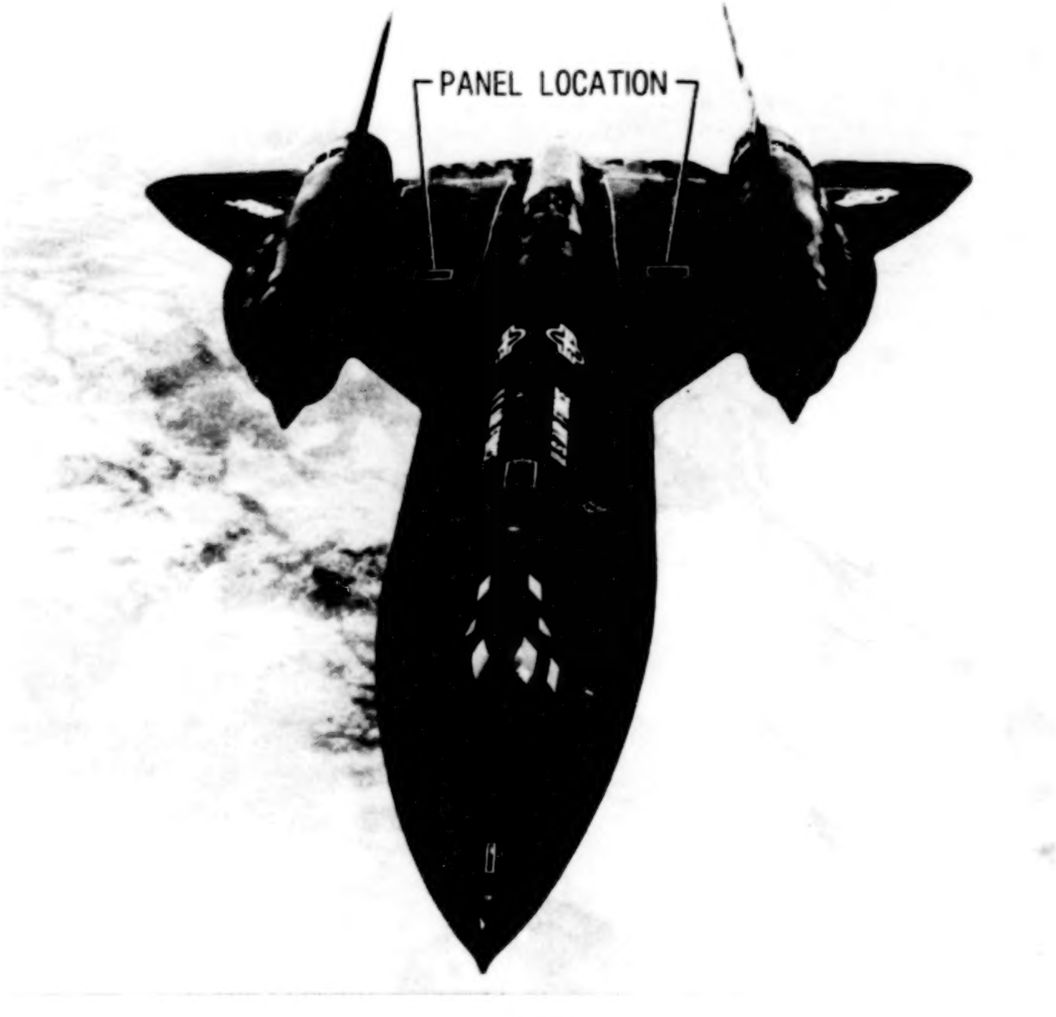

Figure 4

WELDBRAZED TITANIUM SKIN-STRINGER YF-12 PANEL

The first panel concept for the YF-12 panel program was a Ti-6AL-4V titanium alloy skin-stringer structure. The panel was fabricated by Lockheed-Advanced Development Projects using the NASA LaRC weldbrazing process. The general configuration and construction details of the weldbrazed YF-12 panel assembly are shown in figure 5. The panel measures 16 inches × 28 inches and consists of an annealed Ti-6AL-4V titanium alloy skin, chemically milled in the center to a thickness of 0.70 inch, and thirteen Ti-6AL-4V "Z" stiffeners formed from 0.050-inch sheet. The stiffeners were spot-welded to the skin using a welding schedule that produced a 0.003- to 0.004-inch gap at the faying surface. Narrow strips of 0.016-inch-thick 3003 aluminum alloy alloy sheet, scarfed to a knife-edge along one side, were wedged in the faying surface gap at the foot of each stiffener to hold them in place during brazing. Brazing was accomplished in a vacuum furnace at 1290°F for 10 minutes at a vacuum of 10^{-5} torr. A total of ten panels were fabricated. Test results obtained showed that all panels exceeded design requirements. One panel was installed on the NASA YF-12 airplane and flown for a total of approximately 100 hours with 30 hours at airspeeds in excess of Mach 2.6. Based on these results, weldbrazing is considered to be a simple and viable process for fabricating flight-quality titanium structure.

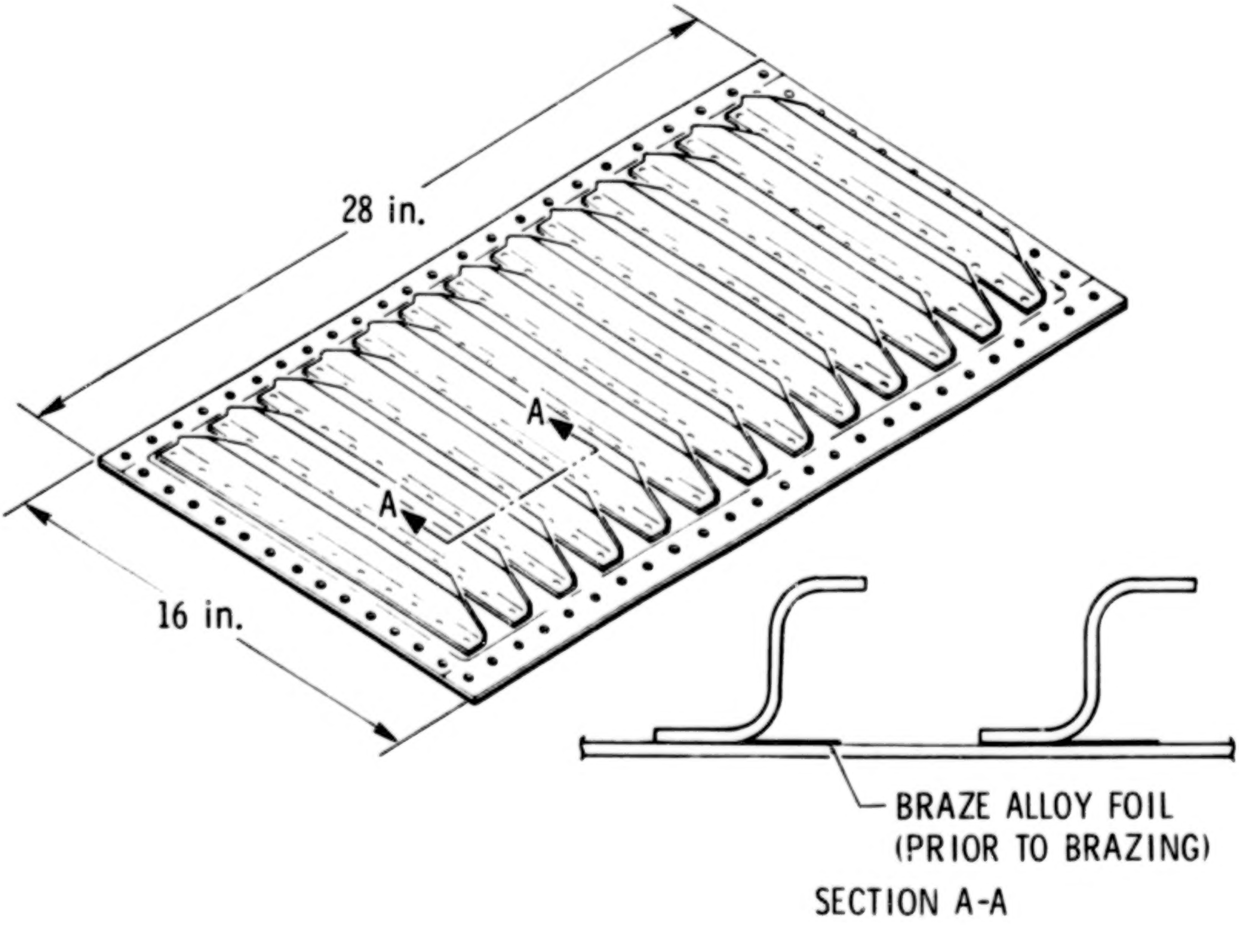

Figure 5

SPF/DB TITANIUM SINE WAVE TRUSS CORE SANDWICH YF-12 PANEL

To assess the potential of SPF/DB for fabricating efficient titanium structure a YF-12 wing panel was designed and fabricated using the selective stop-off process. The panel concept developed is shown in figure 6 and consists of a sine wave truss core sandwich structure. The design thickness of the inner and outer face sheets was 0.029 inch and the core web thickness was 0.013 inch. The panel was fabricated from three flat sheets using the process described in figure 3. The next figure shows the center core sheet of the panel prior to SPF/DB and fabrication details are presented in the accompaning text.

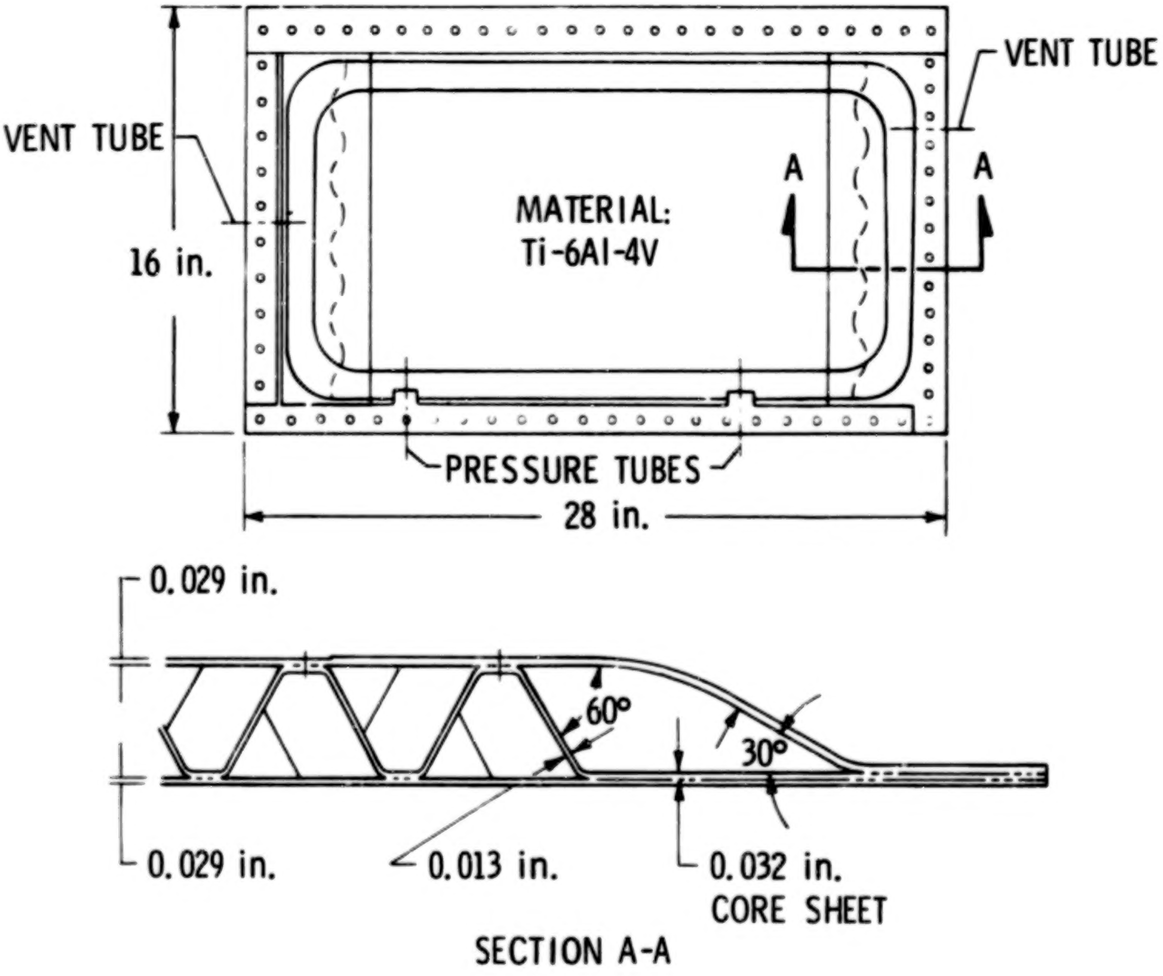
VENT TUBE
VENT TUBE
A
A
MATERIAL:
Ti-6Al-4V
16 in.
PRESSURE TUBES
28 in.
0.029 in.
60°
30°
0.029 in.
0.013 in.
0.032 in.
CORE SHEET
SECTION A-A

Figure 6

CORE SHEET FOR SPF/DB YF-12 PANEL

The center core sheet used in fabricating the SPF/DB titanium sine-wave truss core sandwich panel for the YF-12 program is shown on figure 7. The core sheet was slotted to accommodate stainless steel pressure and vent tubes and ceramic stop-off material was selectively applied to both sides using a silk screening process. The core sheet was then sandwiched between the two face sheets and tack welded together with the vent and pressure tubes in place. This assembly was then placed in a steel tool between ceramic platens and the panel was SPF/DB in accordance with the Rockwell process previously described. A total of seven panels were successfully fabricated. Six panels were tested to demonstrate structural adequacy prior to installing one panel on the YF-12 for flight service evaluation. All panels met the requirements of the program and demonstrated that SPF/DB is a viable process for fabricating titanium structure for high-performance aircraft.

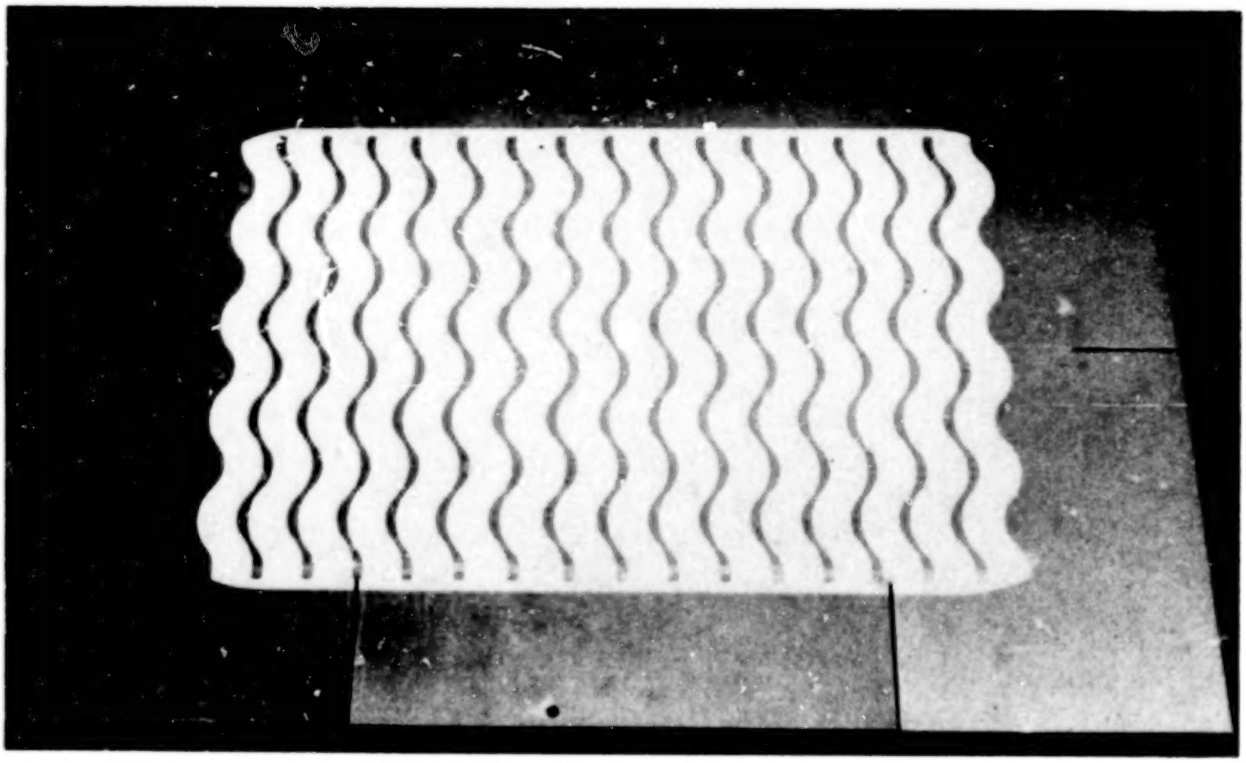

Figure 7

FOUR-SHEET SPF/DB TITANIUM PANELS

A process which combines the use of resistance spotwelding and SPF/DB to fabricate titanium sandwich panels has also been developed (ref. 5). The steps involved in this process are shown in figure 8. The two titanium sheets which make up the core are first spotwelded together in a selected geometric pattern as shown in the upper part of the figure. Gaps are periodically left between the overlapping welds to provide for equalization of pressure during forming. The welded core sheets are positioned between the face sheets in an appropriate tool, and the assembly is heated to 1700°F using ceramic heated platens. Gas pressure is introduced between the core sheets and the core sheets separate in a pillow fashion as shown in the center of the figure. Forming continues using an argon gas pressure of 30 to 100 psi until the individual sections of the core sheets contact the face sheets and each other. Argon gas pressure is then increased to 300 psi and maintained for 3 hours to diffusion bond all mating surfaces. The part is then cooled and removed from the tool. Limited chemical milling is required to remove surface contamination. The process has been used to fabricate a wide variety of parts containing different core geometries.

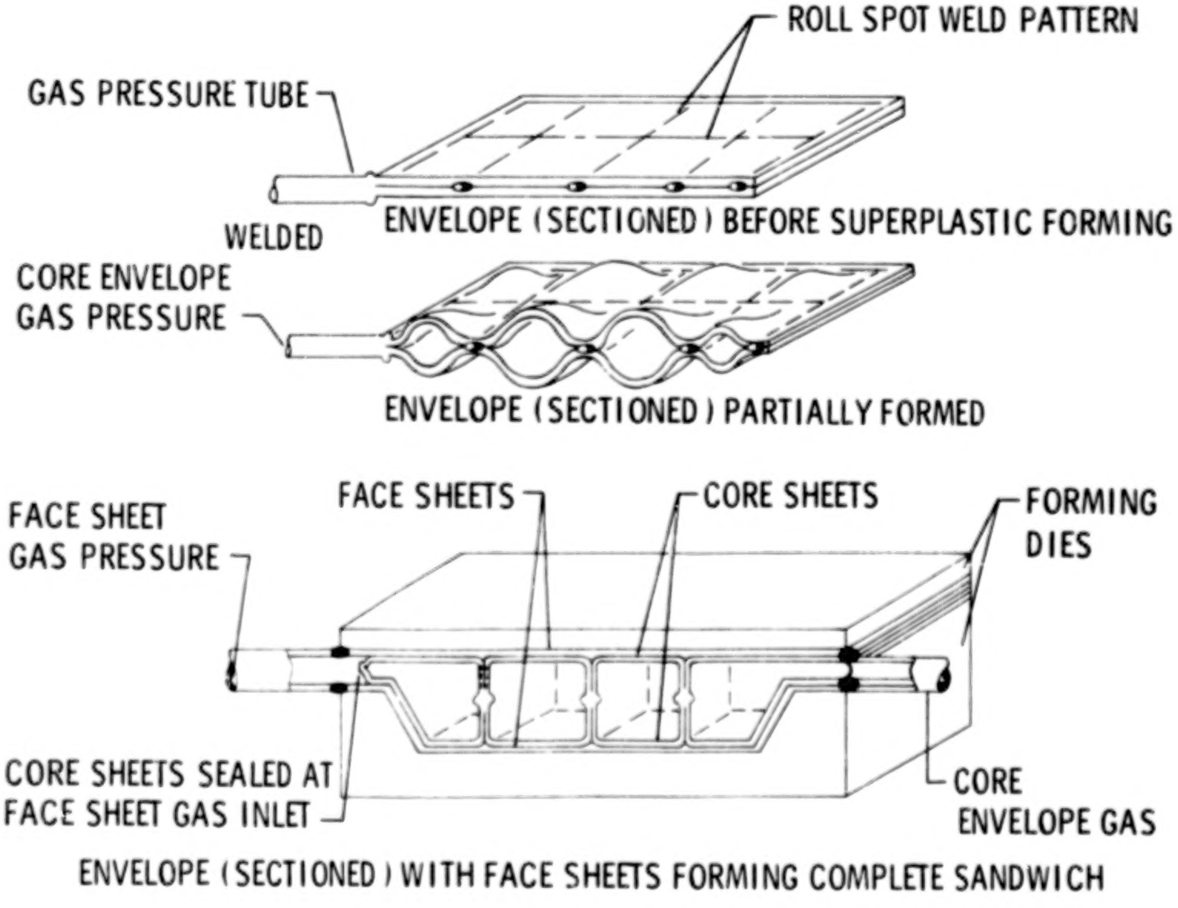
ROLL SPOT WELD PATTERN
GAS PRESSURE TUBE
ENVELOPE (SECTIONED) BEFORE SUPERPLASTIC FORMING
WELDED
CORE ENVELOPE
GAS PRESSURE
ENVELOPE (SECTIONED) PARTIALLY FORMED
FACE SHEET
GAS PRESSURE
FACE SHEETS
CORE SHEETS
FORMING
DIES
CORE SHEETS SEALED AT
FACE SHEET GAS INLET
CORE
ENVELOPE GAS
ENVELOPE (SECTIONED) WITH FACE SHEETS FORMING COMPLETE SANDWICH

Figure 8

SPF/DB FOUR-SHEET TITANIUM WING PANEL

To further evaluate the potential of the SPF/DB four-sheet process, a processing study was conducted for a large structural component. A 3- × 5-foot panel was selected and designed to meet the loading requirements of a supersonic transport wing. Also, selected studies were made to determine the effects of the SPF/DB process on the mechanical properties of Ti-6Al-4V. Two full-size panels were fabricated on the rectangular cell core expanded sandwich design. Figure 9 shows one of the completed panels. Spectrum fatigue and compression testing of the panels were conducted at the design conditions. Both panels met the design requirements. Mechanical properties of the SPF/DB titanium were comparable to conventionally processed material.

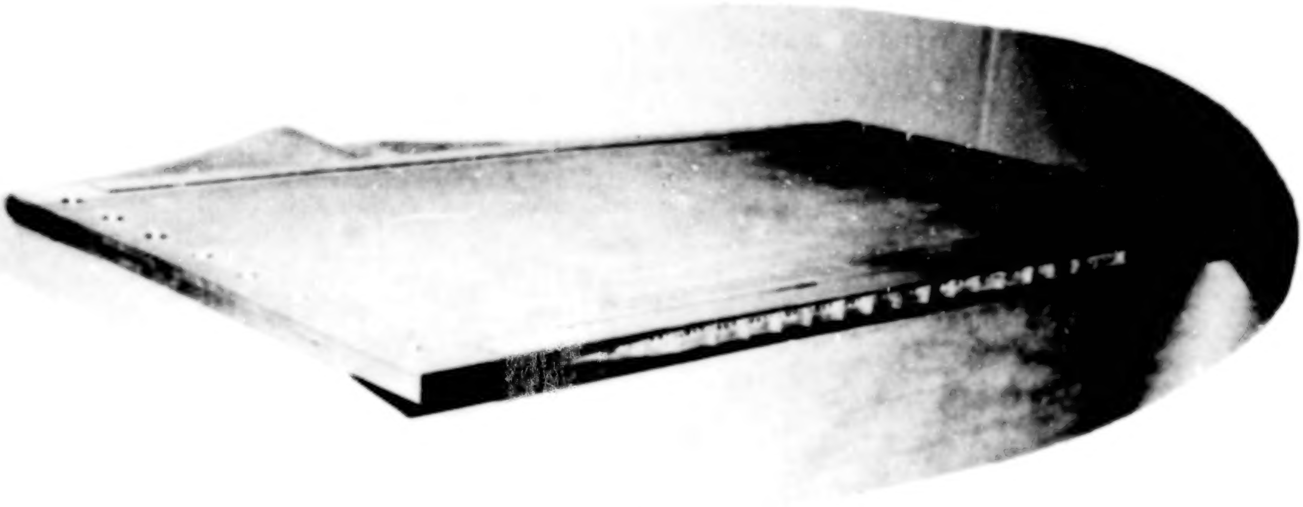

Figure 9

SUPERPLASTIC FORMING AND WELDBRAZING

While SPF/DB components are reported to have significant potential for reducing the weight and cost of titanium structure, processing times of 6 to 10 hours are commonly required. In an attempt to simplify processing, NASA LaRC initiated a study to separate the forming and joining processes. The process selected for study was the combined use of superplastic forming and weldbrazing (SPF/WB). The specimen selected for evaluation was a small 10-inch-long compression panel.

The steps involved in the process are shown in figure 10. A pan-like component is first superplastically formed to fabricate the stringer. To form the part, a single sheet of titanium is placed in the tool and blown or superplastically formed over a male tool. Forming requires processing at 1700°F for a period of 30 minutes. The formed stringer is then spotwelded to a flat face sheet. Strips of 3003 aluminum braze alloy are then positioned adjacent to the joint and the assembly is placed in a vacuum furnace for brazing. Brazing requires no tooling and is accomplished at a temperature of 1250°F for a period of 5 minutes. Total elevated-temperature processing time required for a SPF/WB component is approximately 35 minutes. Following weldbrazing the final specimen shown on the lower portion of the figure is machined. Advantages of SPF/WB compared to SPF/DB for the fabrication of selected components are reduced elevated-temperature processing and improved inspectability (ref. 6).

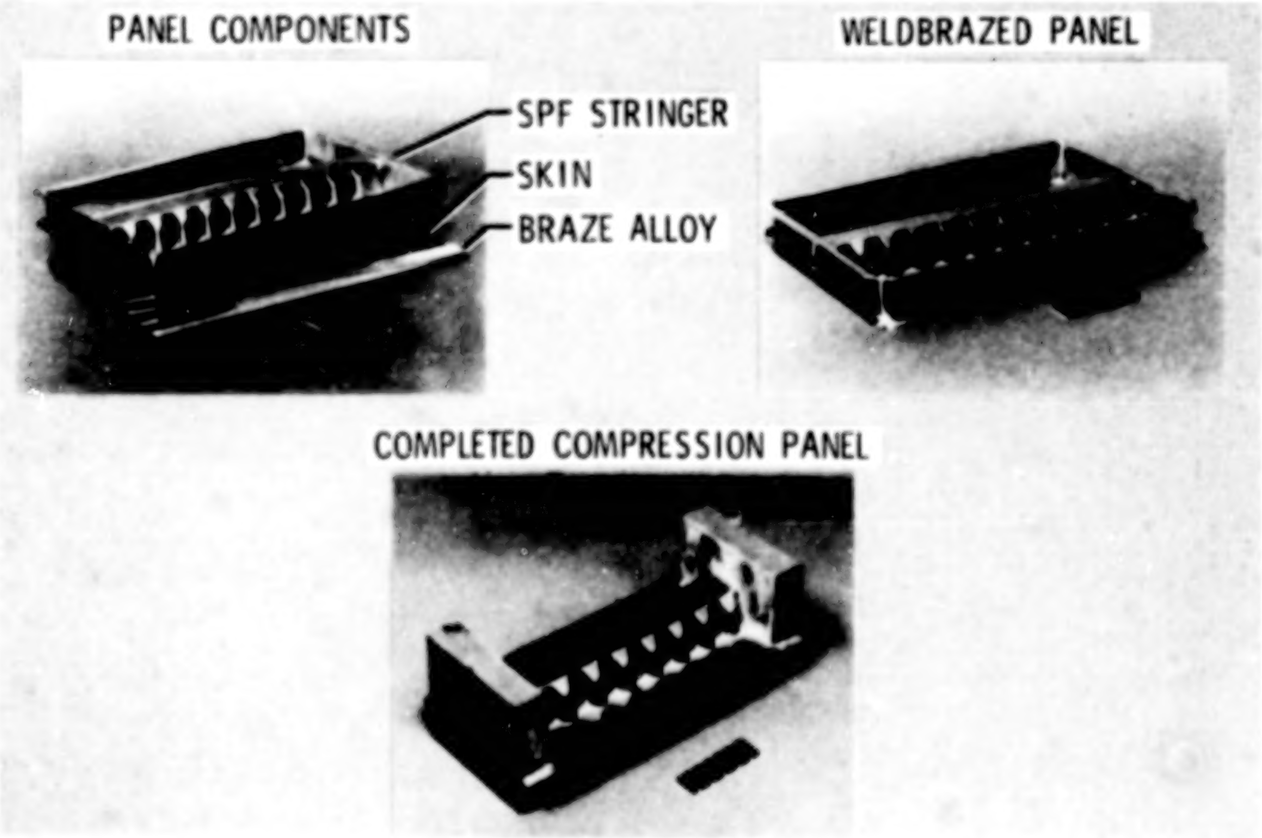

Figure 10

SPF TOOLING AND STRINGER CONFIGURATIONS

The simple steel female tool and the various male inserts used to superplastically form the titanium stringers for the superplastic forming and weldbrazing (SPF/WB) study are shown in figure 11. The stringer configurations selected for evaluation were based on their potential to offer increased structural efficiency in compression compared to conventional hat stiffeners. The configurations selected also exploited the increased formability of superplastic forming. Other than the conventionally shaped stringer, the configurations would be difficult if not impossible to form using conventional titanium fabrication methods. As shown in the figure, the stringer configurations that were evaluated consisted of a conventional hat, a stepped hat, a ribbed-web hat and a beaded-web hat. As previously stated, the stringers were superplastically formed at 1700°F using a single sheet of titanium which was blown down into the cavity using argon gas at a pressure of 30 to 125 psi. Each of the stringers formed in this manner were of equal weight. Following forming the pan-shaped stringer components were chemically cleaned for subsequent weldbrazing.

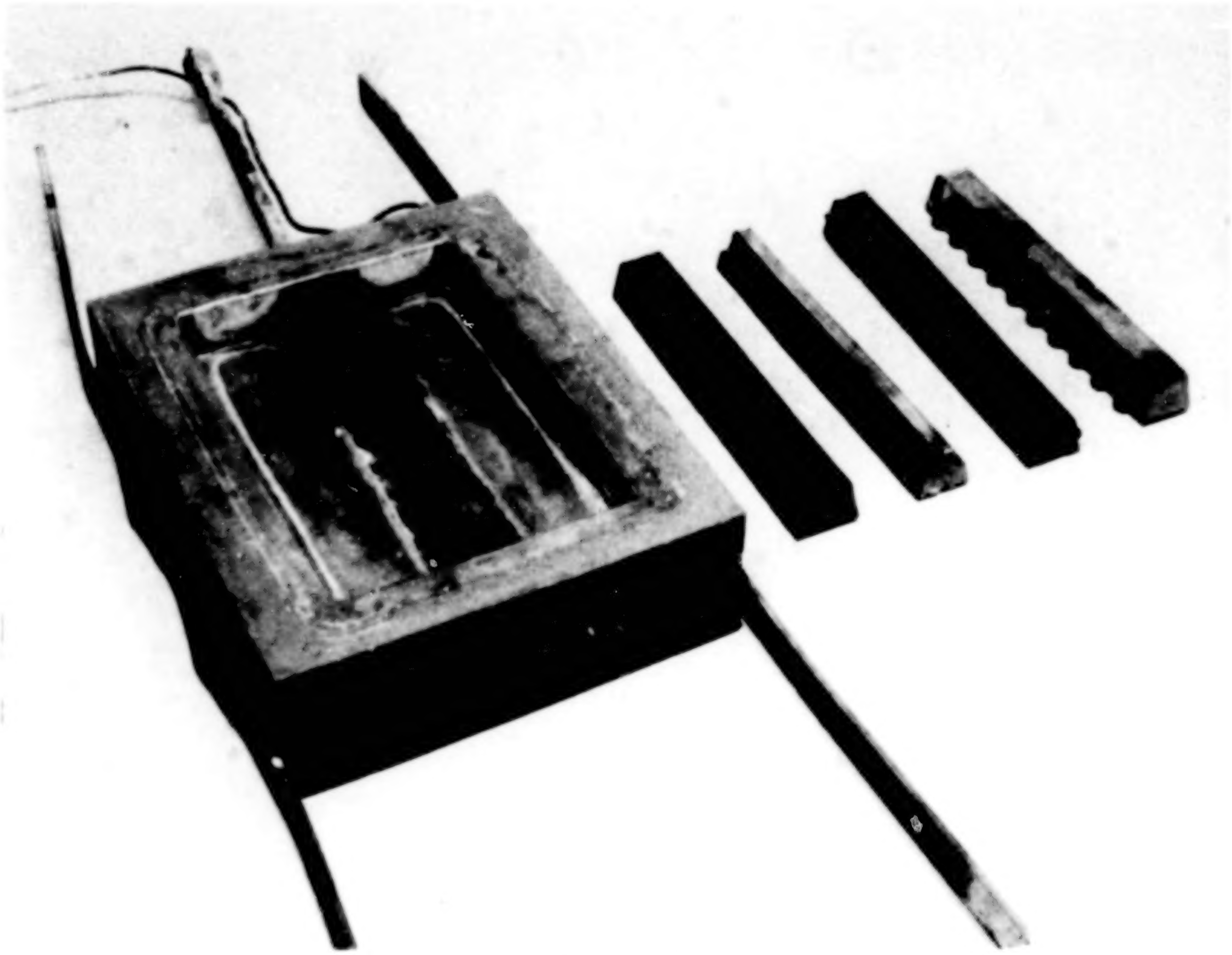

Figure 11

RELATIVE BUCKLING STRENGTHS OF SPF/WB TITANIUM PANELS

Three compression specimens of each of the four stringer configurations described on the previous figure were fabricated and tested. The relative local buckling loads of these specimens are shown in figure 12. Each bar represents the average value of three tests. Since each of the specimens were of equal weight, regardless of configuration, the data are also an indication of relative structural efficiency. As shown on the figure, the buckling strengths of the beaded web hat, the ribbed hat, and the stepped hat specimens were all greater than the buckling strenghts of the specimen fabricated with a conventional hat stringer. The buckling loads or strengths of specimens with beaded-web, ribbed-web, and stepped-web shaped stringers were 20 percent, 50 percent, and 60 percent higher, respectively, than the specimens with conventional hat stringer configuration. As demonstrated by these data, superplastic forming affords appreciable opportunities for improvements in structural efficiency and corresponding weight reductions of titanium structures designed to carry compression loads.

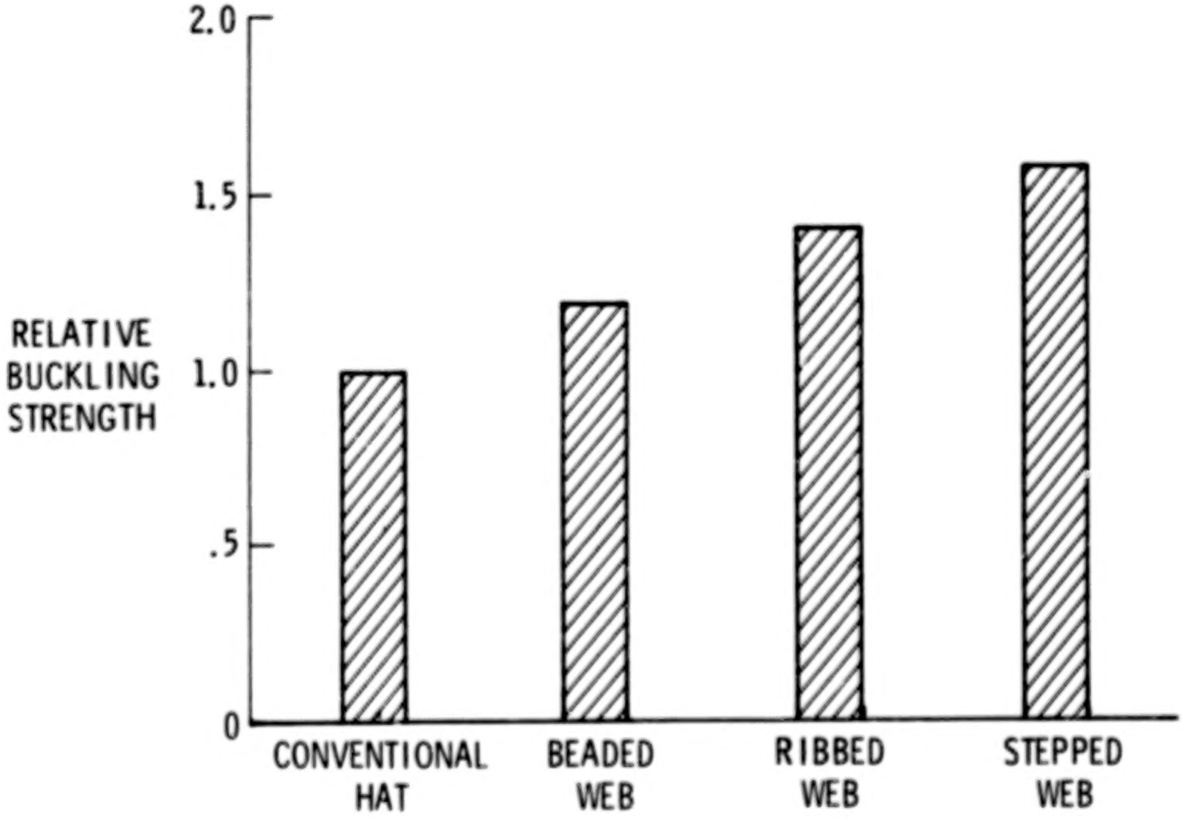

Figure 12

SPF/WB MULTIPLE STRINGER TITANIUM COMPRESSION PANELS

To further assess the potential of SPF/WB for fabricating titanium compression panels, LaRC is scaling up the SPF/WB process to fabricate and test multiple stringer panels. A tool having multiple inserts has been fabricated to superplastically form a multiple stringer or corrugated sheet from a single piece of titanium using the same parameters and processes established for the small single stringer specimens described in figures 10, 11 and 12. A photograph of a 22-inch × 30-inch SPF/WB panel fabricated having nine conventional hat stringers is shown in figure 13. This panel will be tested to serve as a baseline for comparison with multiple-stringer panels having a stepped-hat or beaded-web configurations. Panels will also be fabricated with stringers running in the longer direction to evaluate the column buckling behavior of SPF/WB titanium compression panels having different stringer configurations. Based on the results obtained to date, SPF/WB is considered to be a promising process for fabricating titanium compression panels and offers significant improvements in structural efficiency.

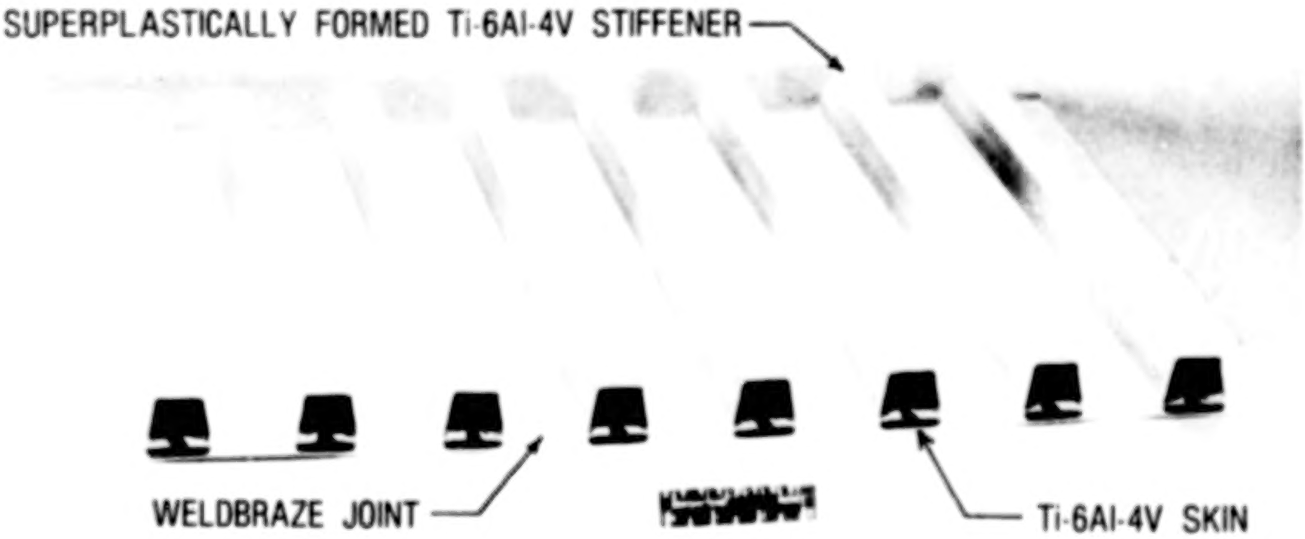

Figure 13

SUPERPLASTIC FORMING OF ALUMINUM ALLOYS

The advent of the superplastic forming of titanium created an interest in the aerospace community regarding the superplastic behavior of other metals and the benefits that may be derived. A natural focus of this interest was on high-strength aluminum structural alloys such as 7075, 2024 and 6061. However, early studies showed that the large elongated grains inherent in conventionally processed aluminum sheet severly limited their degree of superplasticity. Subsequent studies sponsored by the Army and conducted at Rockwell International Science Center showed that refinement of the grain size of 7475 aluminum sheet by thermomechanical treatment resulted in material having a high degree of superplasticity. The major aluminum companies have also recently developed fine-grained 7475 aluminum alloy sheet for superplastic forming. An example of the superplastic behavior of 7475 aluminum is shown in figure 14. The as-machined specimen was heated to 960°F and pulled at a strain rate of 1×10^{-4} in./in.-sec. Total elongation to failure was approximately 800 percent. The flow stress or stress to superplastically stretch the specimen was 4 ksi, which indicates that there is a similar potential for blow-forming or gas-pressure-forming aluminum as has been demonstrated for titanium. Consequently, superplastic forming of aluminum has been projected to have the potential of reducing the weight of future aerospace structures by 20 percent and the cost by approximately 30 to 50 percent. As a result NASA LaRC has initiated a study to evaluate the potential of SPF aluminum for aerospace structural applications. The program will follow a similar course as the programs for titanium. Processing parameters and methods will be evaluated to provide for improved structural efficiency of future aluminum structures.

Several low-strength aluminum alloys (Al-Zn,Al-Ca-Zn,Al-Cu-Zn) have also been developed which exhibit a high degree of superplastic behavior. A United Kingdom firm, Superform Metals, Ltd., is currently in production on a large number of superplastically formed aluminum components. Applications appear aimed at the nonaerospace industry for fabricating automotive body components, typewriter covers, and various types of deep containers. The improved formability offered by superplastic forming makes it possible to fabricate components which cannot be formed by conventional means and to reduce the cost of others made by conventional forming methods.

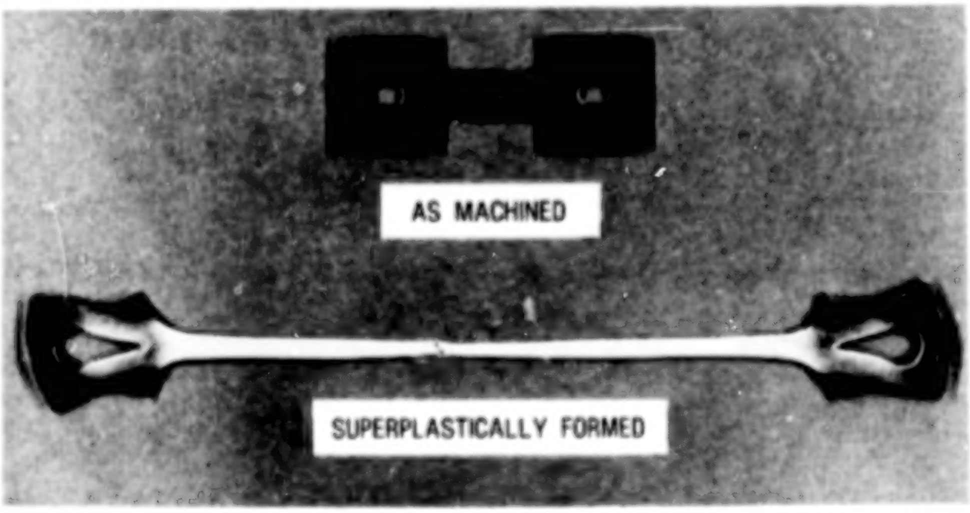

Figure 14

SUMMARY

Significant advances have been made in the processing of titanium in recent years (fig. 15). Research studies have demonstrated that weldbrazing, SPF, SPF/DB, and SPF/WB are viable processes for fabricating titanium structures that exhibit improved efficiency. The large reduction in manufacturing costs afforded by these processes will substantially reduce the finished-part cost of titanium components. This cost driver combined with the high mechanical properties at temperatures up to 600°F and the excellent corrosion resistance of titanium should promote wider spread applications in industries involved with chemical processing, food handling and processing, manufacturing products exposed to a marine environment, and, possibly, components for high-performance internal-combustion engines. Due to the relative simplicity of SPF alone, compared to the other combined processes discussed, it is considered to have the greatest impact in the near term.

The development of the superplastic forming of high-strength aluminum alloys may substantially expand the use of aluminum for structural and nonstructural applications. If the projected cost savings for the technology are realized, aluminum components will be increasingly cost competitive with other metal and nonmetal products.

TITANIUM - WB, SPF, SPF/DB, SPF/WB

- ADVANCED Ti-PROCESSING TECHNOLOGY

  GREATER STRUCTURAL EFFICIENCY POSSIBLE THROUGH FORMING OF UNIQUE COMPONENTS
- TECHNOLOGY BASE REASONABLY MATURE
- COST SAVINGS POTENTIAL COULD INCREASE NONAEROSPACE APPLICATIONS

ALUMINUM - SPF

- POTENTAIL FOR WEIGHT AND COST SAVINGS
- FORMABILITY OFFERED BY SPF MAY EXPAND APPLICATIONS
- TECHNOLOGY BASE EMBRYONIC FOR HIGH-STRENGTH STRUCTURAL ALLOYS
- U.K. WORLD LEADER IN PRODUCTION OF COMPONENTS USING LOW-STRENGTH ALLOYS

Figure 15

REFERENCES

1. Bales, Thomas T., Royster, Dick M., and Arnold, Winfrey E., Jr.: Development of the Weldbraze Joining Process. NASA TN D-7281, June 1973.

2. Hocker R. G.: Weldbraze Airframe Components. AFML-TR-77-171, Nov. 1977.

3. Isreali, L., Arvin, H. G., and Ascani, L. A.: Evaluation of Superplastic Forming and Co-Diffusion Bonding for Ti-6AL-4V Titanium Alloy Expanded Sandwich Structure for Supersonic Cruise Research (SCR) Applications. NASA CP-2160, 1980.

4. Bales, Thomas T., Hoffman, Edward L., Payne, Lee, and Reardon, Lawrence, F.: Fabrication Development and Evaluation of Advanced Titanium and Composite Structural Panels. NASA TP-1616, March 1980.

5. Fischler, J. E.: SPF/DB Development Program for AST Low-Cost Light-Weight Structures. NASA CP-2160, 1980.

6. Royster, Dick M., Bales, Thomas T., and Wiant H. Ross: Superplastic Forming/Weldbrazing of Titanium Skin-Stiffened Compression Panels. Proceedings of the 27th National SAMPE Symposium, May 1982.

FATIGUE AND FRACTURE RESEARCH IN METALS

J. C. Newman, Jr. and J. R. Davidson
NASA Langley Research Center
Hampton, Virginia

INTRODUCTION

Fatigue and fracture of structural materials have always been a concern for design engineers. Notable structural failures have occurred throughout all historical periods. Categories of prominent fatigue and fracture failures have shifted from bridges (1700 to about 1850) to railroads (1850 to early 1900's) to storage tanks (1890's to 1930's) to ships (1940's to 1960) and to aircraft (1940's to present).

Since the 1940's extensive investigations have been undertaken to both explain and solve the fatigue and fracture problems. These studies have revealed that flaws, low metal toughness, and stress concentrations not anticipated in design are responsible for most failures. Conventional design criteria were based on tensile strength, yield stress, and buckling stress. Although these criteria were adequate in many engineering situations they were insufficient under conditions where cracks or crack-like defects were present in the structure.

Fatigue and fracture research at NASA Langley Research Center on monolithic and laminated metals has been concentrated in three areas: (1) stress analyses of two- and three-dimensional cracked bodies, (2) fatigue crack growth, and (3) fracture toughness. Analytical methods have been developed to predict fatigue crack growth and fracture strengths of cracked specimens. Such specimens represent typical aircraft structural details (such as cracks from holes). These specimens were subjected to simple constant-amplitude loading and to more complex flight load histories. Test data from both in-house tests and from the literature are used to substantiate the analytical methods. These analyses have extended the theory of fracture mechanics to deal with fatigue crack growth and fracture of complex crack configurations that are typical of aircraft materials and structural details. Several of these analyses are now used in ASTM standards and ASME codes and by several aircraft companies for damage tolerance studies. This paper will provide a summary of this research area and highlight recent advances in understanding the fatigue and fracture behavior of metals.

MATERIALS TEST AND ANALYSIS METHODOLOGY

Structural components are subjected to cyclic load time histories and operate in various environments. They may develop cracks from material defects, stress concentrations, or inadvertent damage. Such cracks grow at rates that depend upon applied load levels and environmental conditions. Catastrophic failure occurs when the crack reaches a critical length.

Several American Society for Testing and Materials (ASTM) Committees (E9, E24, and G1) are developing or have developed testing standards and test specimens for characterizing fatigue crack growth [1], stress-corrosion cracking, and fracture toughness [2] of engineering materials. The NASA Langley Research Center has contributed to the analyses of several of these standard test specimens. A few of these, shown in figure 1, will be discussed here.

The stress intensity factor (K) (a crack tip characterizing parameter) has been calculated at Langley for several standard laboratory specimens: the compact specimen, the round compact specimen, and the bolt-loaded double-cantilever-beam (DCB) specimen. Compact and round compact specimens, used for fatigue crack growth and fracture toughness tests, were analyzed by Newman [3] using a boundary-collocation analysis. (The round compact specimen has been shown to be about 40 percent cheaper to machine than the rectangular specimen.) The DCB specimen, used in stress-corrosion cracking tests, was analyzed by Fichter [4] using asymptotic and collocation methods.

These analyses provided more accurate K-solutions over a wider range of crack lengths than previous solutions. For example, the failure loads on 2219-T851 aluminum alloy compact specimens are plotted as a function of crack-length-to-width (a/W) ratio in figure 1. The solid and dashed curves show the predicted results using the new and old analyses, respectively. The new analysis [3] was much more accurate than the old analysis at low and high values of a/W. The new K-solutions for the compact specimens are in current ASTM standards [2].

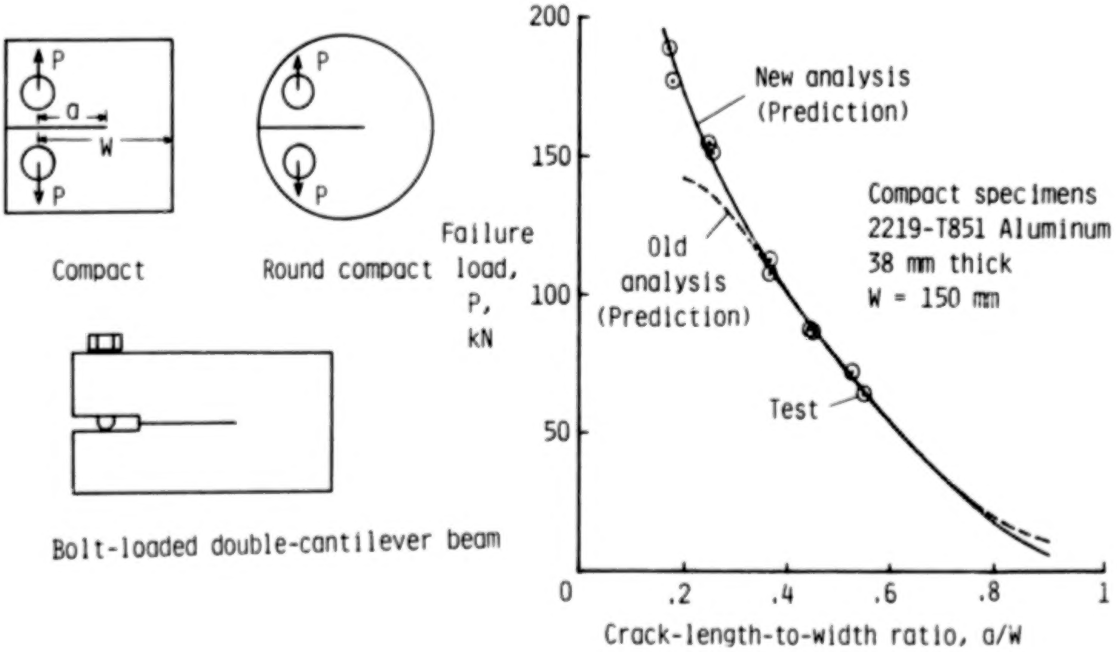

Figure 1.- Laboratory test specimens and experimental verification of analysis.

THE SURACE CRACK

In 1969 the catastrophic failure of the wing on an F-111 aircraft was caused by a surface crack. A photograph of the cracked area is shown in figure 2. This failure, more than any other, initiated present U.S. Air Force airworthiness regulations [5]. These regulations are based on considerations of "damage tolerance." The underlying philosophy for damage tolerance is to acknowledge that accidental or normal service-induced damage is inevitable, and that periodic inspections are needed to detect such damage. Airworthiness is then assured by demonstrating that damage that escapes one inspection will not grow to critical size before the next inspection. Two evaluations must be made: first, the rate of crack growth under expected service loading; and second, the residual static strength with the crack present. Such evaluations employ fracture mechanics analyses, in particular the stress intensity factors for various crack configurations.

Many stress intensity factor (K) solutions have been proposed for the surface crack. However, for large crack-depth-to-plate-thickness ratios (like that in the F-111 failure), the solutions differed considerably (up to 80 percent). To provide an accurate solution, three-dimensional finite-element analyses of semi-elliptical surface cracks subjected to tension and bending loads have been conducted by Raju and Newman [6]. The K-equations for surface cracks in plates under tension and bending loads, as well as in pressurized cylinders, have also been developed [7,8]. The K-equation for the surface crack has been experimentally verified by Newman and Raju [7]. The ratio of predicted to experimental failure loads for brittle epoxy specimens containing various size surface cracks is plotted as a function of crack-depth-to-plate-thickness (a/t) ratio in figure 2. The equation was able to predict failure loads within about ±10 percent of experimental failure loads.

These new K-solutions have been used in an ASTM standard practice on surface crack testing [9], and in the newly revised ASME pressure vessel and piping codes.

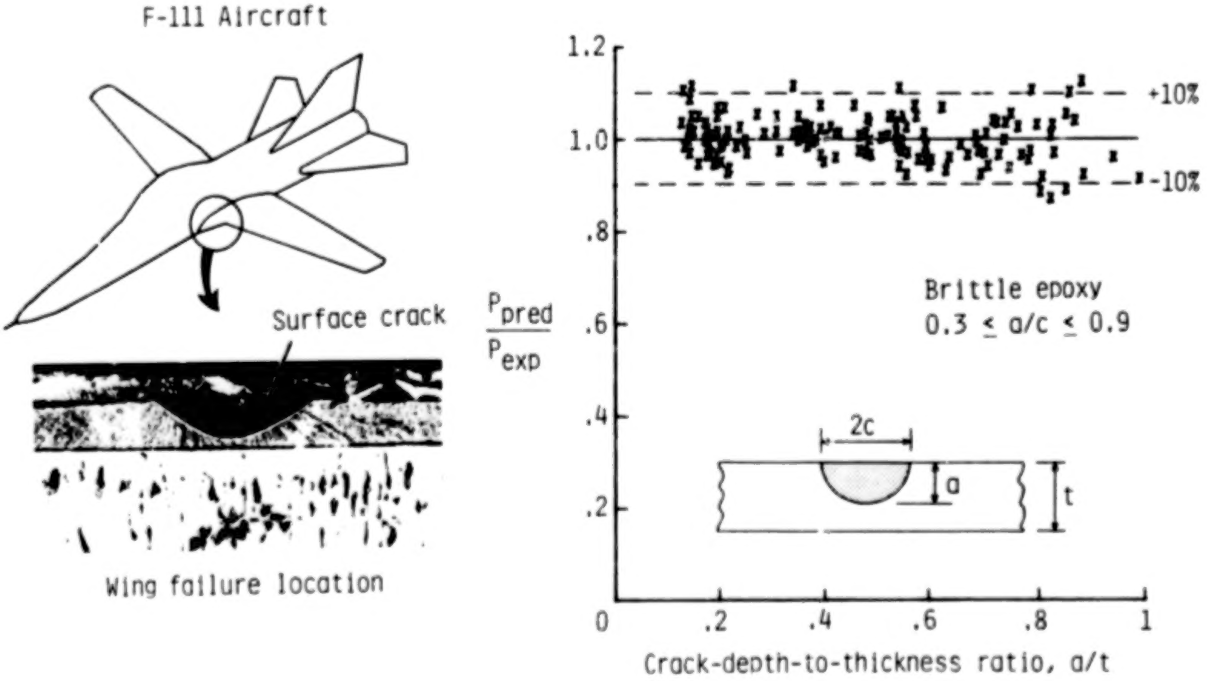

Figure 2.- Aircraft failure due to surface crack and experimental verification of analysis.

MOST COMMON CRACK IN AEROSPACE STRUCTURES

Corner cracks and through cracks at holes are among the most common flaws in aircraft structures. The photograph in figure 3 shows a corner crack at a hole in a plank on a fractured wing structure. Accurate stress analyses of such configurations are needed to reliably predict crack growth rates and fracture strengths, and to establish inspection intervals so that failures like this one can be avoided.

A three-dimensional finite-element analysis was again conducted at Langley by Raju and Newman [10] to determine stress intensity factors for quarter-elliptical corner cracks at the edge of a hole under various loading. These stress intensity factor solutions are used to predict the number of load cycles required to grow a crack from a small defect at the edge of a hole to failure. Figure 3 shows a comparison between experimental and predicted crack length versus number of cycles for a corner crack growing from a circular hole in a 7075-T651 aluminum alloy specimen subjected to constant-amplitude tensile loading. The predicted crack propagation life was in good agreement with the experimental value.

Equations for stress intensity factors for other three-dimensional crack configurations (such as an embedded elliptical crack, a quarter-elliptical corner crack, a semi-elliptical surface crack, and semi-elliptical surface cracks at a hole in finite-thickness plates) have also been developed by Newman and Raju [11]. Several aircraft companies have incorporated these equations into computer programs for the design of damage-tolerant structures.

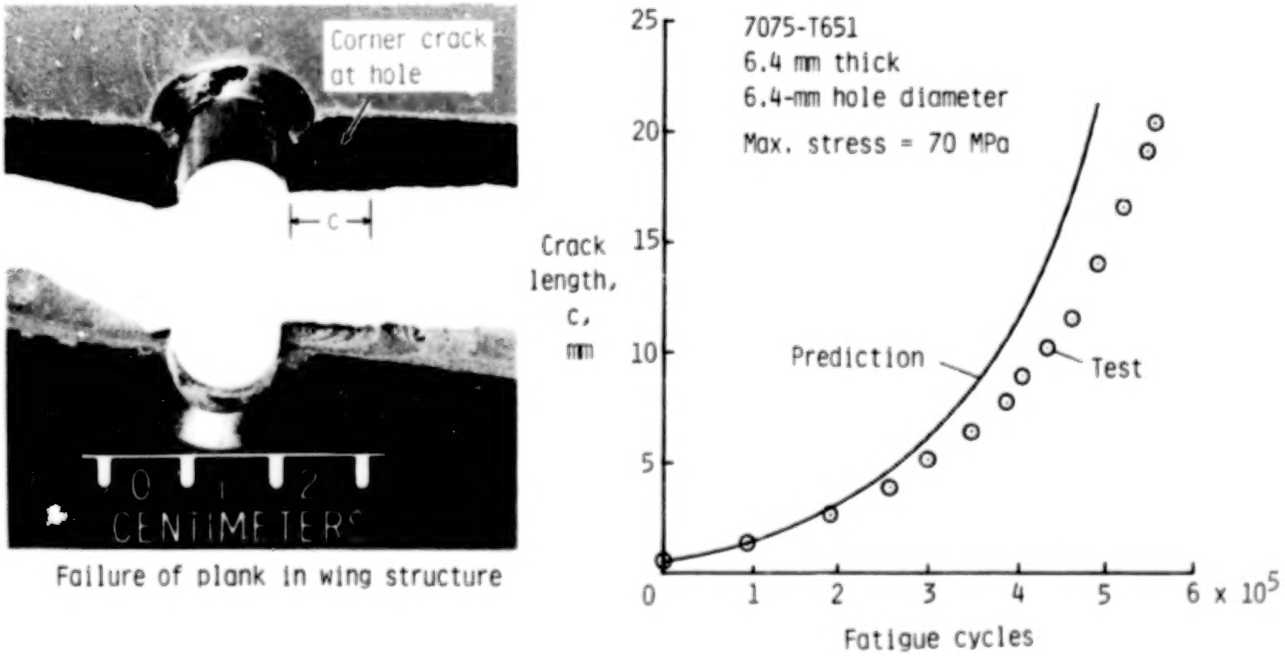

Failure of plank in wing structure

Figure 3.- Wing failure due to corner crack at hole and experimental verification of analysis.

THE CRACK CLOSURE PHENOMENON

Elber [12] was the first to identify and quantify the phenomenon of crack closure during cyclic loading. He showed that the crack surfaces near the crack tip close before a specimen is completely unloaded. Such behavior was not expected in an elastic specimen until an infinitesimal compressive load was applied.

The reason for crack closure is depicted in figure 4. The presence of a plastic zone ahead of a crack tip (shown with double crosshatch) is accepted as a feature of crack tip behavior. But the feature that had been commonly ignored was the plastically deformed material left in the wake of a crack. As the load on a specimen is reduced, this deformed material comes together. It then transfers compressive forces across the crack surfaces before the load is reduced to zero. Many investigators have conducted detailed experiments to verify crack closure. The intuitive consequence of this behavior is that those portions of a load cycle during which the crack tip is closed will not contribute to crack growth.

The closure behavior has been analyzed by Newman using an elastic-plastic finite-element analysis [13]. This analysis showed that cracks open and close at predictable stress levels. Figure 4 shows a comparison between experimental and predicted crack-opening stresses normalized by the maximum applied stress (S_o/S_{max}) plotted against stress ratio (ratio of minimum to maximum applied stress). The predicted values agreed well with the experimental values. The finite-element analysis was, however, very complicated and required a large computer. More recently, Newman [14] developed a simple strip-yield model of closure that needs only a small computer but can accommodate many hundreds of thousands of variable load cycles. The use of this model to predict crack growth under aircraft spectrum loading will be discussed later.

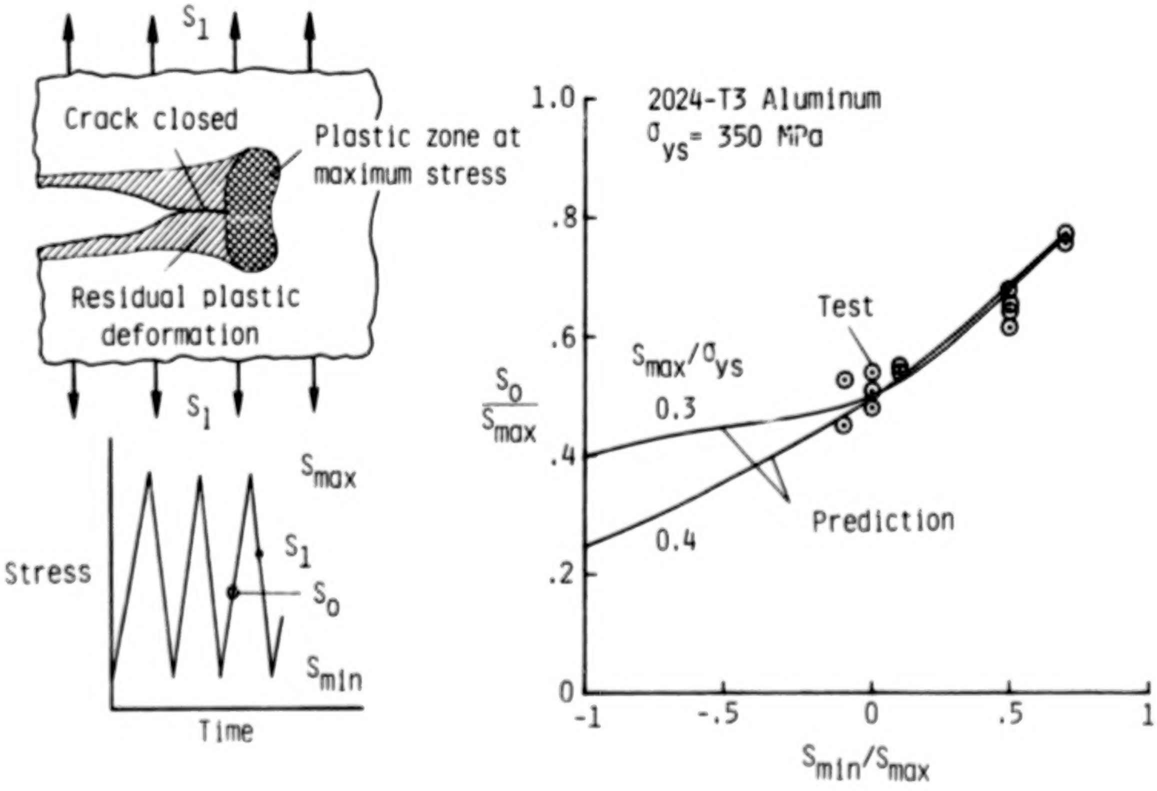

Figure 4.- Fatigue crack closure concept: test and analysis.

FATIGUE CRACK GROWTH IN METALS

Most studies on fatigue crack growth have been conducted on "large" cracks with lengths in excess of 2 mm. However, in many engineering structures crack growth from "small" preexisting flaws is a major portion of the component's fatigue life. But the growth of small cracks (10^{-2} to 1 mm) in plates and at notches differs from that of large cracks. Such behavior is illustrated in figure 5, in which the crack growth rate is plotted against the stress intensity factor range, ΔK, for a constant ratio of minimum to maximum load, R. The solid curve shows a typical result usually obtained from tests with large cracks. At low growth rates the threshold stress intensity factor range, ΔK_{th}, is usually obtained from load reduction tests. Some typical results for small cracks are shown by the dashed curves. These results show that small cracks grow faster than large cracks at the same ΔK level and that they also grow at ΔK levels below threshold.

To explain these differences, the crack closure model mentioned previously was used to study crack growth and closure behavior of small cracks in plates and at notches [15]. At equivalent ΔK levels the model predicts that small cracks should grow faster than large cracks because the applied stress level needed to open a small crack is less than that needed to open a large crack. Results from the model also imply that many of the ΔK_{th} values that have been obtained in tests with large cracks and with load reduction schemes do not apply to the growth of small cracks; that is, the load reduction scheme is causing the threshold. Consequently, the large crack data at low applied stress levels may possibly follow the dash-dot curve.

These results indicate the importance of considering crack closure when using large-crack data to predict the growth of small cracks from preexisting defects.

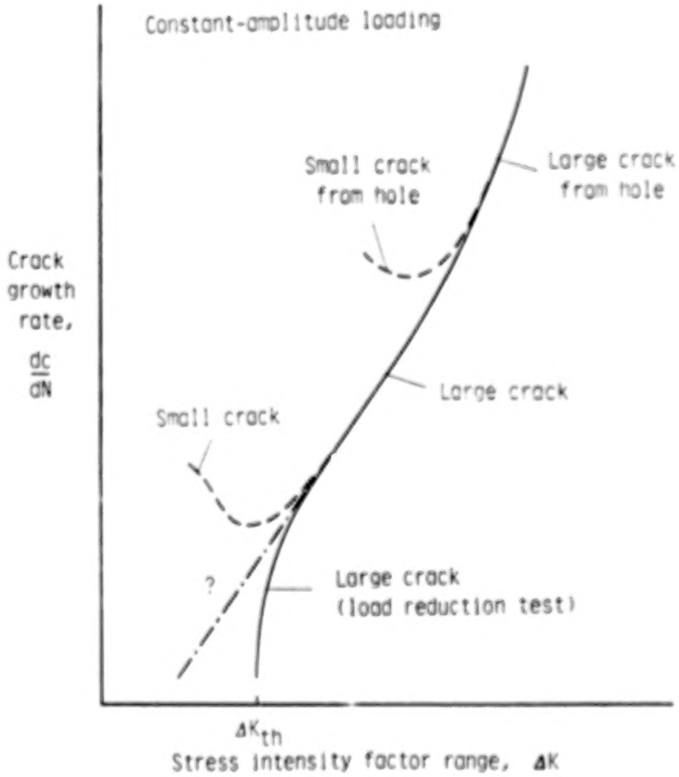

Figure 5.- Typical fatigue crack growth rate data for small and large cracks.

PREDICTION OF CRACK GROWTH UNDER AIRCRAFT SPECTRUM LOADING

Predictions of crack growth rates are used in aircraft design to determine inspection intervals and damage tolerance. Under aircraft spectrum load conditions, load interaction effects sometimes retard and sometimes accelerate crack growth.

Various models have been developed to account for load interaction. Two of the most widely accepted concepts are being studied at Langley. One, the CGR-LaRC computer program developed by Johnson [16], uses the multiparameter yield zone (MPYZ) model. Like the well-known Willenborg model [17], the MPYZ model is based on residual stresses in the crack tip region. The MPYZ model uses crack growth rate data from constant-amplitude loading tests. Four parameters must also be obtained from variable-amplitude load tests.

The other concept is the FAST computer program, which is based on the crack closure model developed by Newman [14]. The closure model requires only crack growth rate data under constant-amplitude loading to predict crack growth under variable-amplitude loading.

ASTM Subcommittee E24.06 on Applications recently completed a round robin study of crack growth predictions under aircraft spectrum loads. The accuracy of the predictions made from the CGR-LaRC and FAST programs on 2219-T851 aluminum alloy specimens for the round robin is shown in figure 6. Both methods gave good results on 13 different aircraft spectrum load tests. The mean value and standard deviation of the ratio of predicted cycles (N_{PRED}) to test cycles (N_{TEST}) for each method are shown in the figure.

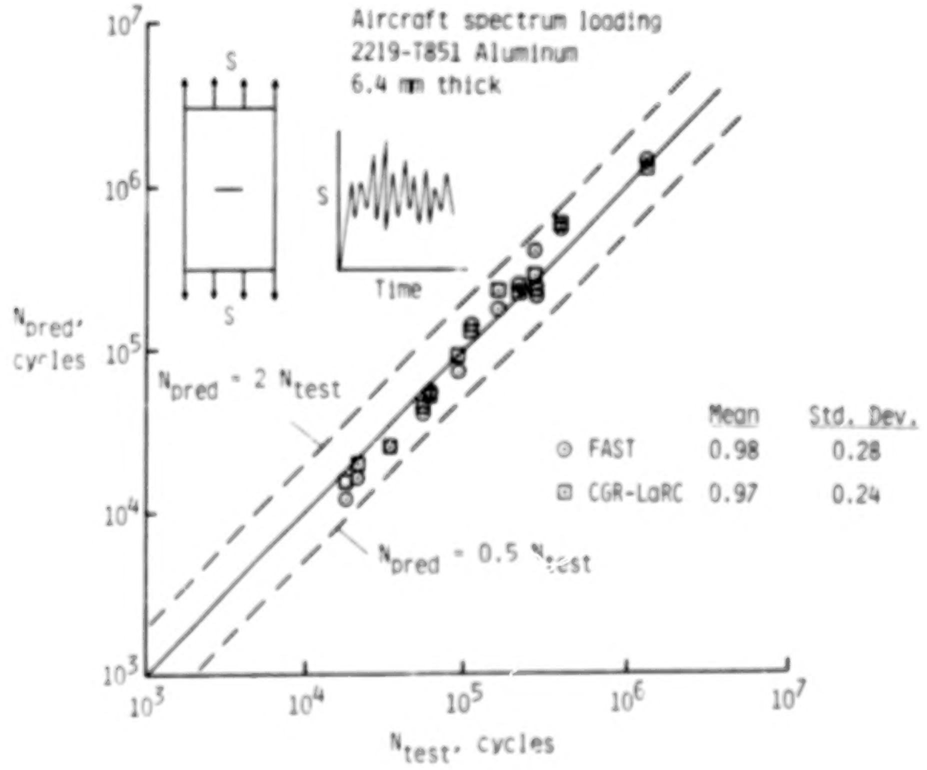

Figure 6.- Comparison of predicted and experimental cycles to failure using two crack growth models.

ELASTIC-PLASTIC FRACTURE OF METALS

Under an increasing load, a crack growing in metal leaves plastically stretched material behind. The stretching is very dramatic in ductile materials, as is shown in the photograph of a copper specimen failing (fig. 7). An arrow points out the plastic wake of material formed during the final load cycle of a fatigue test. (The photograph shows the lower half of the crack surface; the upper half was outside the field of view.) Although the plastic wakes are much smaller in aerospace structural materials, their formation still controls stable crack growth and instability. If the plastic wakes were not there, any crack extension (Δa) would precipitate unstable growth and catastrophic failure.

Elastic-plastic finite-element analyses of the crack growth process conducted by Newman [18] have confirmed the importance of the plastic-wake concept. The analysis was used with a critical crack tip opening displacement (CTOD) criterion to study crack initiation, stable crack growth, and instability under monotonic loading to failure for several materials (7075-T651 and 2024-T351 aluminum alloys and 304 stainless steel). Comparisons between calculated and experimentally measured CTOD values (δ_c) at initiation agreed well for compact specimens made of the two aluminum alloys. These critical CTOD values, determined from compact specimens, were used to predict failure loads on laboratory specimens (center-crack tension) and on a structurally configured specimen (typical of aircraft structural details) made of the three materials. Figure 7 shows a comparison between experimental (symbols) and predicted (solid curves) failure loads on center-crack tension specimens made of the three materials. Predicted failure loads were within ±10 percent of the experimental failure loads for these specimens and were generally within ±15 percent of the experimental failure loads on the structurally configured specimens for all three materials.

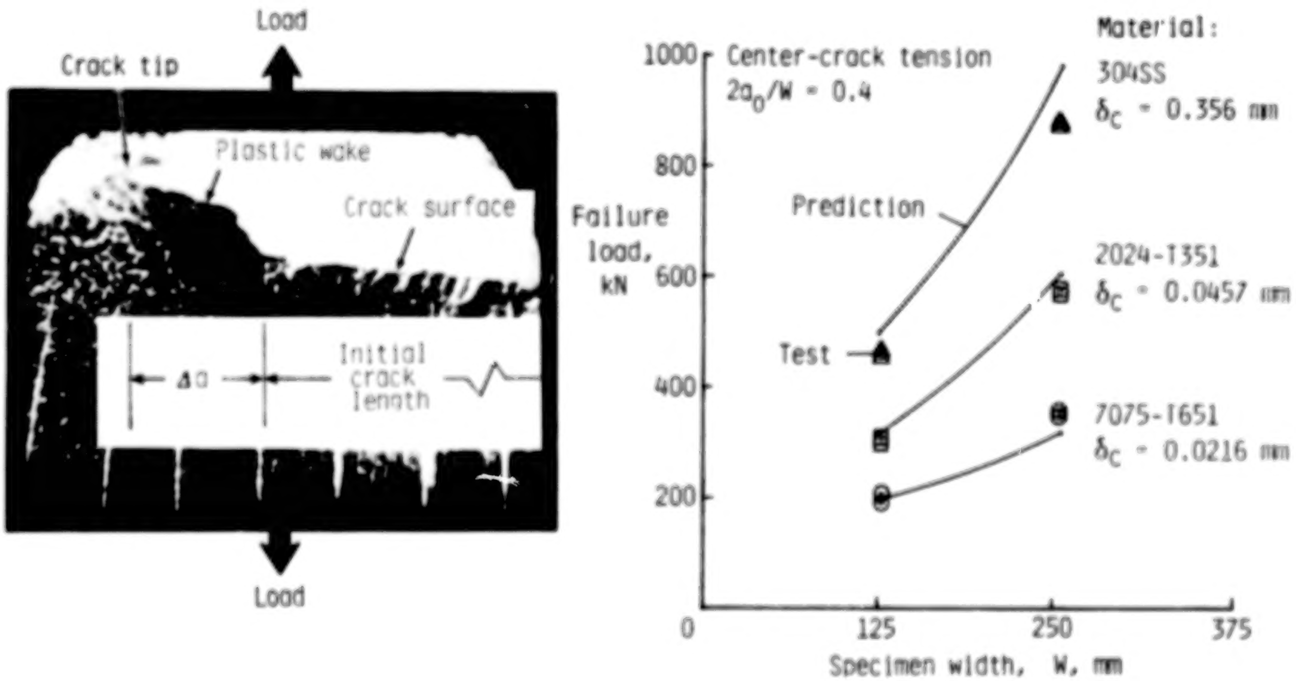

Figure 7.- Plastic-wake concept: test and finite-element predictions.

STATE OF THE ART IN FRACTURE ANALYSES FROM ASTM ROUND ROBIN

The results of an experimental and predictive round robin conducted by Langley and ASTM Task Group E24.06.02 on Application of Fracture Analysis Methods are shown in figure 8. The objective of the round robin was to verify whether the fracture analysis methods currently used can or cannot predict, from the fracture results of a "standard" compact specimen, failure loads of complex structural components containing cracks.

Results of fracture tests conducted on various-sized compact specimens of 7075-T651 aluminum alloy, 2024-T351 aluminum alloy, and 304 stainless steel were supplied as baseline data to 17 participants. These participants (from industry, university, and government) used several different fracture analysis methods to predict failure loads on a structurally configured specimen that typified aircraft structural details. The specimen contained three circular holes with a crack emanating from one of the holes (see insert in figure). The specimen was loaded in tension. The failure loads on the structurally configured specimens were unknown to the participants.

The accuracy of the prediction methods was judged by the variation in the ratio of predicted to experimental failure loads, as shown in figure 8 for the 2024-T351 aluminum alloy specimens. The various methods used and the range and mean of the predictions are indicated on the figure. A few methods were able to predict failure loads within about ±10 percent of the experimental loads. Several methods were totally inadequate. On the basis of the predictions made on all three materials, some crack growth resistance methods (with proper limit load calculations), the two-parameter fracture criteria, and the finite-element analyses appear to be the best methods for predicting failure loads on cracked components.

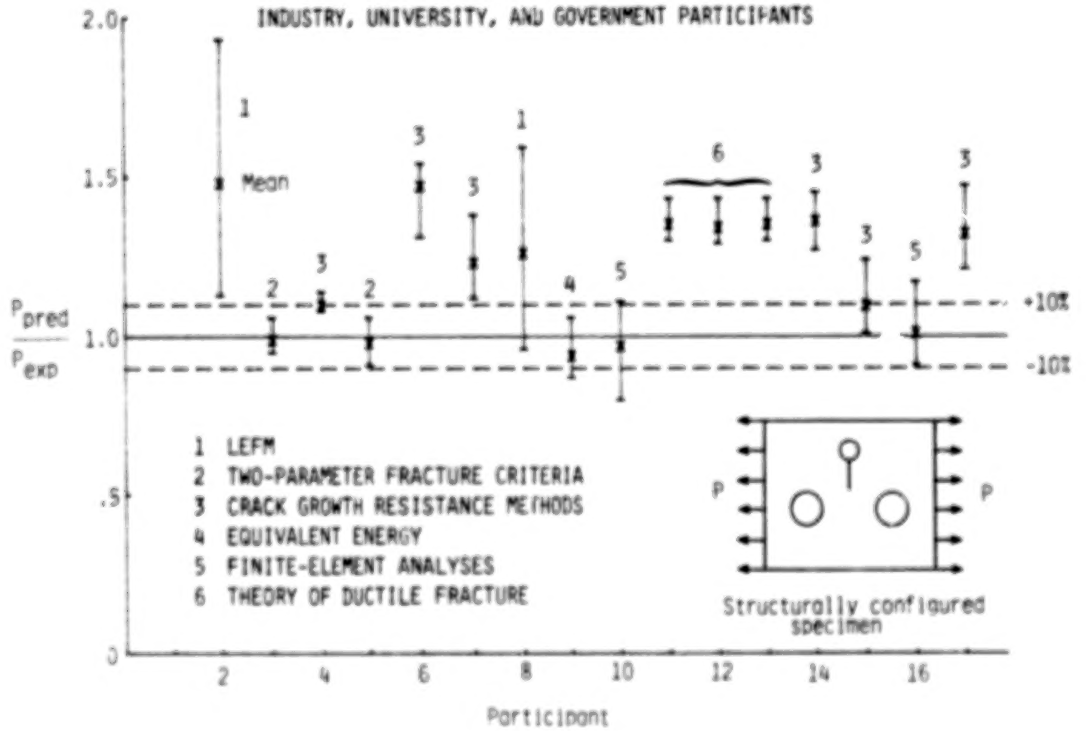

Figure 8.- Summary of predicted to experimental failure loads on 2024-T351 aluminum alloy cracked structural components.

FATIGUE LIVES AND FRACTURE TOUGHNESS OF LAMINATED METALS

Titanium's high strength-to-weight ratio and high temperature stability are desirable structural properties. However, under cyclic loads the crack growth rates are high compared to aluminum alloys at comparable applied-stress-to-density ratios, and its toughness-to-density ratio is low (between brittle D6AC steel and ductile 2024 aluminum). The high crack growth rates and low toughness lead to short damage-tolerant life. To improve the damage-tolerant capability of titanium structures the concept of adhesively bonded titanium sheets was assessed by Johnson [19].

In this investigation six thin sheets of Ti-6Al-4V titanium were bonded together with AF-147 adhesive. They formed a laminated plate 9 mm thick from which specimens were cut. Specimens similar in planform and about the same thickness as the laminate were cut from a monolithic plate. Electric-discharge-machined (EDM) surface flaws were cut into each type of specimen, as shown in figure 9. All specimens were subjected to the same fighter load spectrum. The ratio of maximum spectrum load to specimen density was the same for each specimen. The figure shows that the laminated specimen survived 15 times longer than the monolithic one did. This increased life happened in part because when one ply failed, the others supported the load. Because the adhesive was relatively weak, flaws were inhibited from crossing from one lamina to another.

Toughness tests were also conducted on compact specimens made of both the six-ply titanium laminate and the monolithic plate. Figure 9 shows that the laminated plate has a fracture toughness K_c about 40 percent higher than that of the monolithic plate. The higher toughness implies that a crack in a laminated structure can grow to about twice the length of a crack in a similar monolithic structure before failure. These results show that the adhesive lamination process is a viable way to improve the fatigue life and toughness of titanium for structural applications.

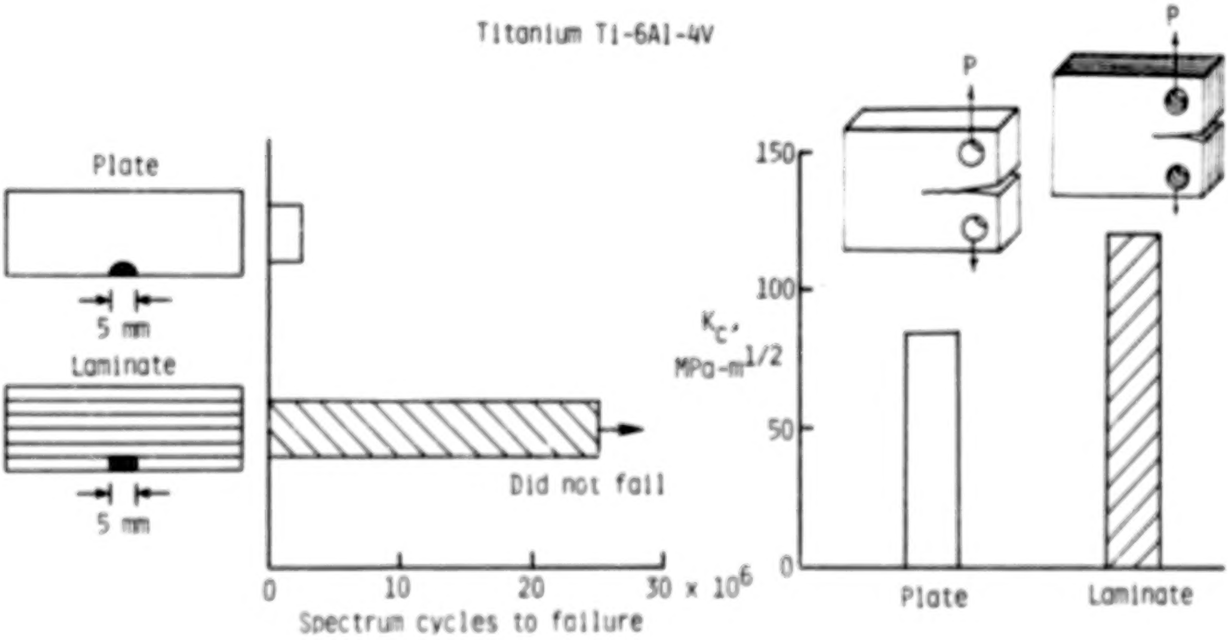

Figure 9.- Fatigue lives and fracture toughness of monolithic and laminated metal.

CURRENT RESEARCH FOR FATIGUE AND FRACTURE OF METALS

- Three-dimensional elastic stress analyses of other crack configurations
- Three-dimensional elastic-plastic analyses of fatigue crack growth and fracture
- Development of a simple fracture model based on the plastic-wake concept
- Scanning electron microscope studies of crack growth under variable-amplitude loading
- Experimental studies on crack closure in thick plates
- Elastic-plastic fracture of surface-cracked plates
- Study effects of holes and bolt loading on the damage tolerance of laminated metal
- Fatigue crack growth measurements in various thickness materials
- Develop and experimentally verify new threshold testing procedures

REFERENCES

1. ASTM E647, Standard Test Method for Constant-Load-Amplitude Fatigue Crack Growth Rates Above 10^{-8} m/cycle, 1981.

2. ASTM E399, Standard Test Method for Plane-Strain Fracture Toughness of Metallic Materials, 1981.

3. Newman, J. C., Jr.: Stress-Intensity Factors and Crack-Opening Displacements for Round Compact Specimens. International Journal of Fracture, vol. 17, no. 6, 1981, pp. 567-578.

4. Fichter, W. B.: Stress-Intensity Factors for the Double-Cantilever-Beam Specimen. Accepted for publication in International Journal of Fracture.

5. Airplane Damage Tolerance Requirements. MIL-A-83444, U.S. Air Force, 1974.

6. Raju, I. S.; and Newman, J. C., Jr.: Stress-Intensity Factors for a Wide Range of Semi-Elliptical Surface Cracks in Finite-Thickness Plates. Engineering Fracture Mechanics, vol. 11, no. 4, 1979, pp. 817-829.

7. Newman, J. C., Jr.; and Raju, I. S.: Analyses of Surface Cracks in Finite Plates Under Tension or Bending Loads. NASA TP-1578, 1979.

8. Newman, J. C., Jr.; and Raju, I. S.: Stress-Intensity Factors for Internal Surface Cracks in Cylindrical Pressure Vessels. Journal of Pressure Vessel Technology, vol. 102, 1980, pp. 342-346.

9. ASTM E740, Standard Practice for Fracture Testing with Surface-Crack Tension Specimens, 1981.

10. Raju, I. S.; and Newman, J. C., Jr.: Stress-Intensity Factors for Two Symmetric Corner Cracks. Fracture Mechanics, C. W. Smith, ed., ASTM STP 677, 1979, pp. 411-430.

11. Newman, J. C., Jr.; and Raju, I. S.: Stress-Intensity Factor Equations for Cracks in Three-Dimensional Finite Bodies. NASA TM-83200, 1981.

12. Elber, W.: Fatigue Crack Closure Under Cyclic Tension. Engineering Fracture Mechanics, vol. 2, no. 1, 1970, pp. 37-45.

13. Newman, J. C., Jr.: A Finite-Element Analysis of Fatigue-Crack Closure. Mechanics of Crack Growth, ASTM STP 590, 1976, pp. 281-301.

14. Newman, J. C., Jr.: A Crack-Closure Model for Predicting Fatigue-Crack Growth Under Aircraft Spectrum Loading. Methods and Models for Predicting Fatigue Crack Growth Under Random Loading, J. B. Chang and C. M. Hudson, eds., ASTM STP 748, 1981, pp. 53-84.

15. Newman, J. C., Jr.: A Nonlinear Fracture Mechanics Approach to the Growth of Small Cracks. Paper presented at the AGARD Specialists Meeting on Behavior of Short Cracks in Airframe Components (Toronto, Canada), Sept. 20-21, 1982.

16. Johnson, W. S.: Multi-Parameter Yield Zone Model for Predicting Spectrum Crack Growth. Methods and Models for Predicting Fatigue Crack Growth Under Random Loading, J. B. Chang and C. M. Hudson, eds., ASTM STP 748, 1981, pp. 85-102.

17. Willenborg, J. D.; Engle, R. M., Jr.; and Wood, H. A.: A Crack Growth Retardation Model Using Effective Stress Concept. AFFDL-TM-71-1-FBR, Jan. 1971.

18. Newman, J. C., Jr.: Finite-Element Analysis of Initiation, Stable Crack Growth, and Instability Using a Crack-Tip-Opening Displacement Criterion. Paper presented at the 15th National Symposium on Fracture Mechanics (College Park, Maryland), July 6-8, 1982.

19. Johnson, W. S.: Improved Damage Tolerance of Titanium by Adhesive Lamination. NASA TM-84525, 1982.

HIGH-TEMPERATURE FATIGUE IN METALS

Gary R. Halford
NASA Lewis Research Center
Cleveland, Ohio

INTRODUCTION

The presentation focuses primarily on the progress we at NASA Lewis Research Center have made in the understanding of the phenomenological processes of high-temperature fatigue of metals for the purpose of calculating lives of turbine engine hot section components. Improved understanding has resulted in the development of accurate and physically correct life prediction methods such as Strain-Range Partitioning (SRP) for calculating creep-fatigue interactions and the Double Linear Damage Rule (DLDR) for predicting potentially severe interactions between high- and low-cycle fatigue. Examples of other life prediction methods are also discussed.

FATIGUE LIFE PREDICTION APPROACH

The major technology areas needed to perform fatigue life predictions of turbine engine hot section component parts are shown in figure 1. The NASA Lewis Research Center has substantial efforts in each of these areas.

We begin with a determination of the operating environment and a calculation of the thermal and mechanical loading of combustor liners, inlet guide vanes, turbine blades, and disks. We then determine the cyclic stress-strain and creep behavior of the engine materials so that the finite element structural analyses can be made. The results of the analyses are the local stress strain temperature versus time response of the material at the most critical locations in the component part. Finally, from a knowledge of the fatigue, creep, and fracture resistance of the materials, we can make a prediction of the lifetime of the component part.

The presentation will focus primarily on the progress we at NASA Lewis have made in the areas of material characterization and failure analysis for the purpose of calculating turbine engine hot section component fatigue and thermal fatigue lives. We have recognized for many years that our fatigue research has applicability beyond the aeronautical and space arenas, and have maintained an interface with other industries in order that they may benefit in some measure. This conference is another example of our desire to share the fruits of our research.

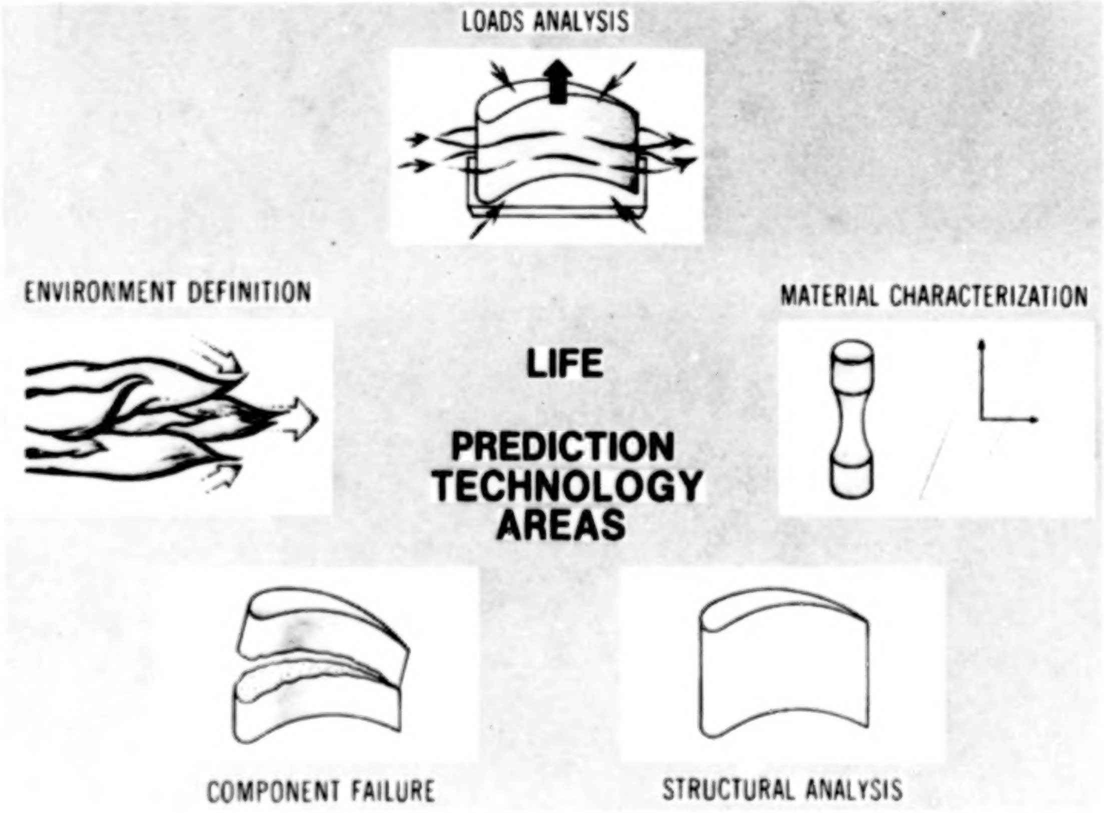

Figure 1

LIFE PREDICTION PROBLEMS IN ENGINE HOT SECTIONS

The specific problem areas within the hot section are shown in figure 2. Typical modes of failure are listed for each of the components that suffer degradation during engine operation.

Combustor liners -- Thermal fatigue and creep buckling

Seals -- Wear

Disks -- Low-cycle fatigue

Vanes and Blades -- Thermal low-cycle fatigue and chemical attack

With the exception of the centrifugal loads on the blades and disks, the primary source of cyclic fatigue loading is due to the severe thermal cycling associated with each startup and shutdown of the engine, although high-frequency excitation problems are sometimes encountered.

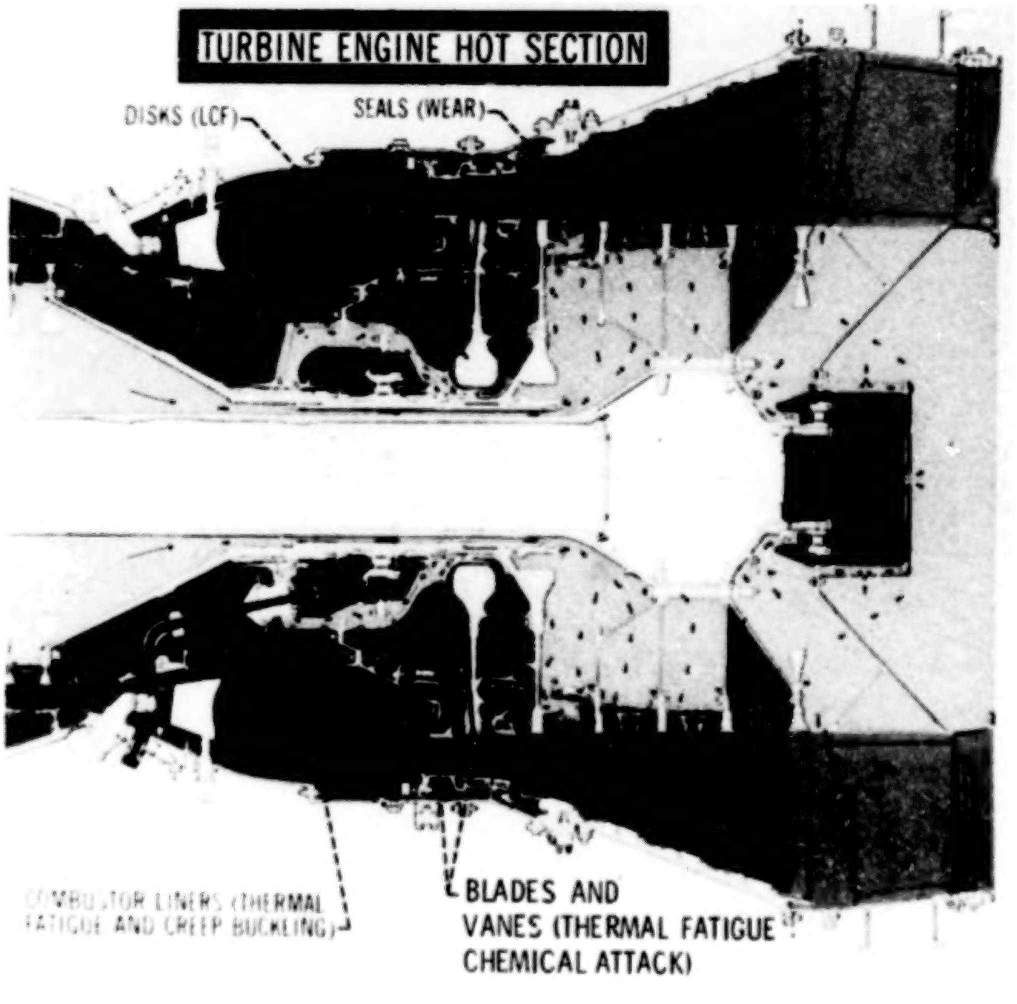
TURBINE ENGINE HOT SECTION
DISKS (LCF)
SEALS (WEAR)
COMBUSTOR LINERS (THERMAL FATIGUE AND CREEP BUCKLING)
BLADES AND VANES (THERMAL FATIGUE CHEMICAL ATTACK)

Figure 2

LOW-CYCLE THERMAL FATIGUE

Low-cycle fatigue and thermal fatigue occur in component parts where the strain in a small localized region is larger than in the surrounding region because of notches that concentrate the strain, or because of constrained thermal expansion as in the case of thermal fatigue. The key feature is that the local strain is prevented from exceeding certain bounds because the bulk of the component part remains elastic. Hence, the local material is caused to cycle between approximately constant strain limits. When the local strains are large, inelastic strains occur and the cyclic stress-strain behavior becomes nonlinear with a hysteresis loop forming, as shown schematically in figure 3. Note the terms used to describe the characteristics of the hysteresis loop. The stress range, $\Delta\sigma$, and the elastic strain range, $\Delta\varepsilon_e$, are related by the modulus of elasticity, E. The total strainrange, $\Delta\varepsilon$, is the sum of the elastic strainrange, $\Delta\varepsilon_e$, and the inelastic strainrange, $\Delta\varepsilon_{in}$.

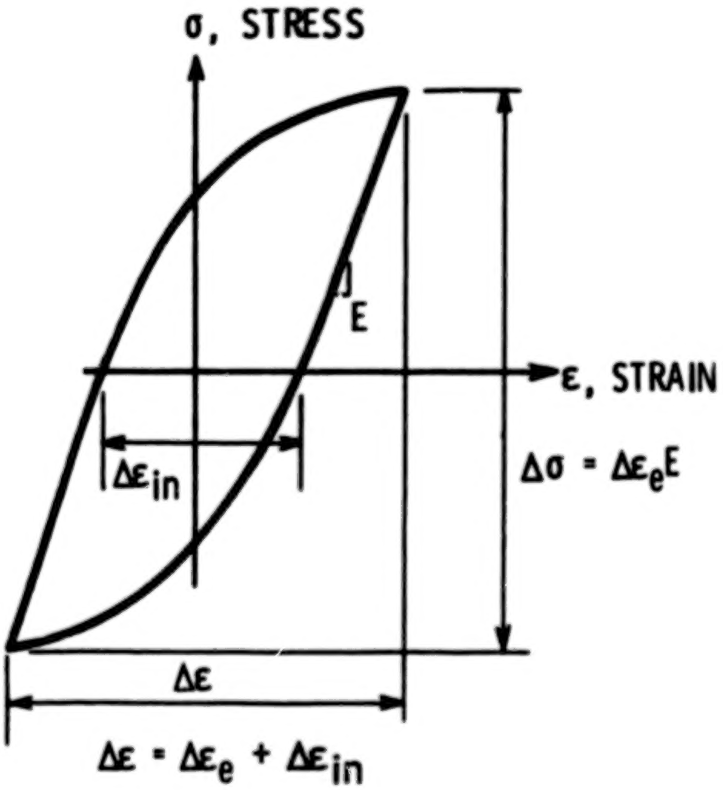
σ, STRESS
E
ε, STRAIN
$\Delta\varepsilon_{in}$
$\Delta\sigma = \Delta\varepsilon_e E$
$\Delta\varepsilon$
$\Delta\varepsilon = \Delta\varepsilon_e + \Delta\varepsilon_{in}$

Figure 3

HOW DO WE ATTACK THIS PROBLEM?

To study the problem of large cyclic strains, it was necessary to evolve an entirely new testing philosophy and to develop new testing equipment. To measure the cyclic stress-strain and low-cycle fatigue behavior of materials at large strains, axially loaded, strain-controlled testing was required. Consequently, cyclic strain extensometers were developed for measuring and controlling the inelastic strains encountered during testing. Closed loop, servocontrolled testing machines were designed, built, and perfected. A closeup view of a resistance heated, axially loaded, elevated temperature specimen is shown in figure 4. An extensometer measures the change in diameter of the round bar specimen. The sensing element is a linear variable differential transformer. Strains as small as 20 microinches per inch can be detected with this device.

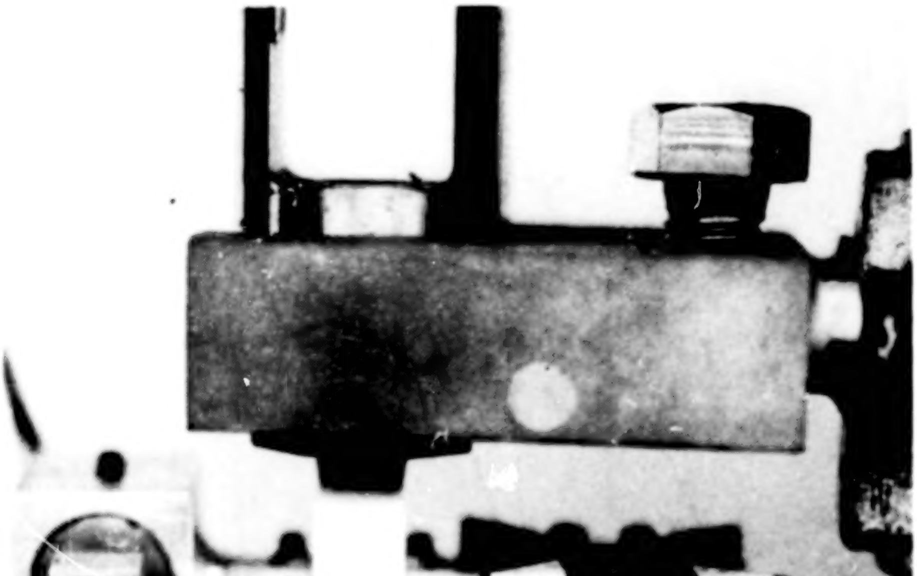

Figure 4

LOW-CYCLE FATIGUE RESISTANCE OF ALLOYS

Figure 5 serves to illustrate that the cyclic strainrange is used to correlate the low-cycle fatigue resistance of alloys. Results of low-cycle fatigue tests are displayed on logarithmic coordinates of strainrange versus cycles to failure. Note that the total strainrange curve is asymptotic to the inelastic strainrange curve at very low cyclic lives and is asymptotic to the elastic strainrange curve at long cyclic lives. As indicated earlier, the total strainrange is simply the sum of the elastic and inelastic strainranges. For most materials, the elastic and inelastic strainrange curves are straight lines on the logarithmic coordinates. This representation of fatigue behavior is usually valid up to 10^6 cycles to failure.

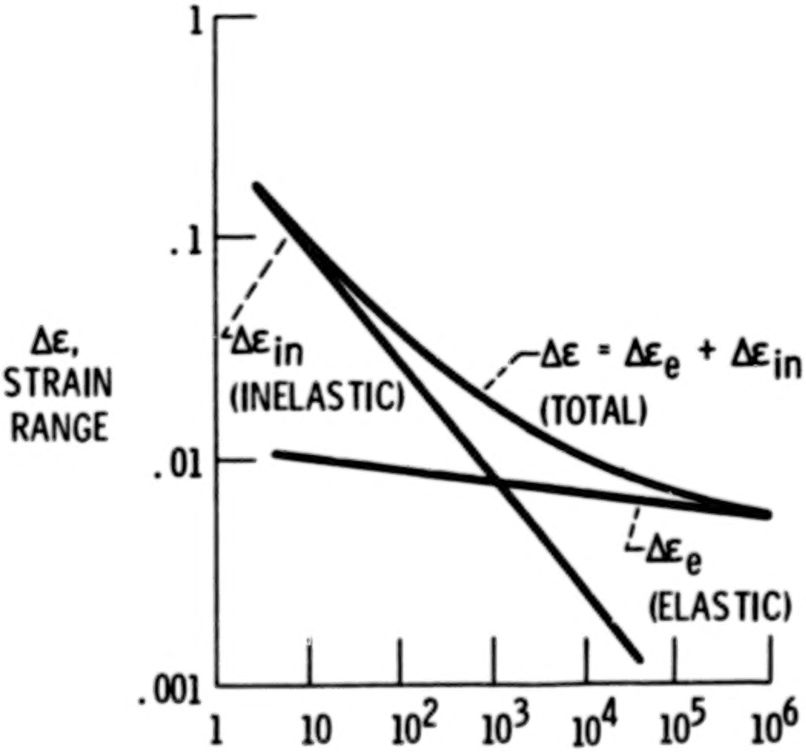

Figure 5

MANSON-COFFIN LAW FOR LOW-CYCLE FATIGUE

With that introduction, I would like to now present a brief historical overview of the contributions made by NASA Lewis engineers in the development of material life prediction methods for low-cycle and thermal fatigue. Our first contribution came in the early 1950's when S. S. Manson (now a professor at Case Western Reserve University) first proposed the power law relationship between the inelastic strainrange and cycles to failure (ref. 1). This law has come to be known as the Manson-Coffin Law for low-cycle fatigue. It expresses the observation that for almost all materials, at room temperature, the slope of the logarithmic straight line is constant (see fig. 6). Furthermore, the coefficient "C" is related to the ductility measured in a tensile test. The greater the ductility, the greater is "C". The Manson-Coffin Law served to provide a better understanding of what causes the fatigue process (reversed crystallographic slip with properly oriented crystals of the metal). However, to apply the law to the prediction of low-cycle fatigue life required that the inleastic strainrange in a component part be known accurately. At the time, the technology was lacking for calculating inelastic strains in a component part. Hence, a more practical approach was needed.

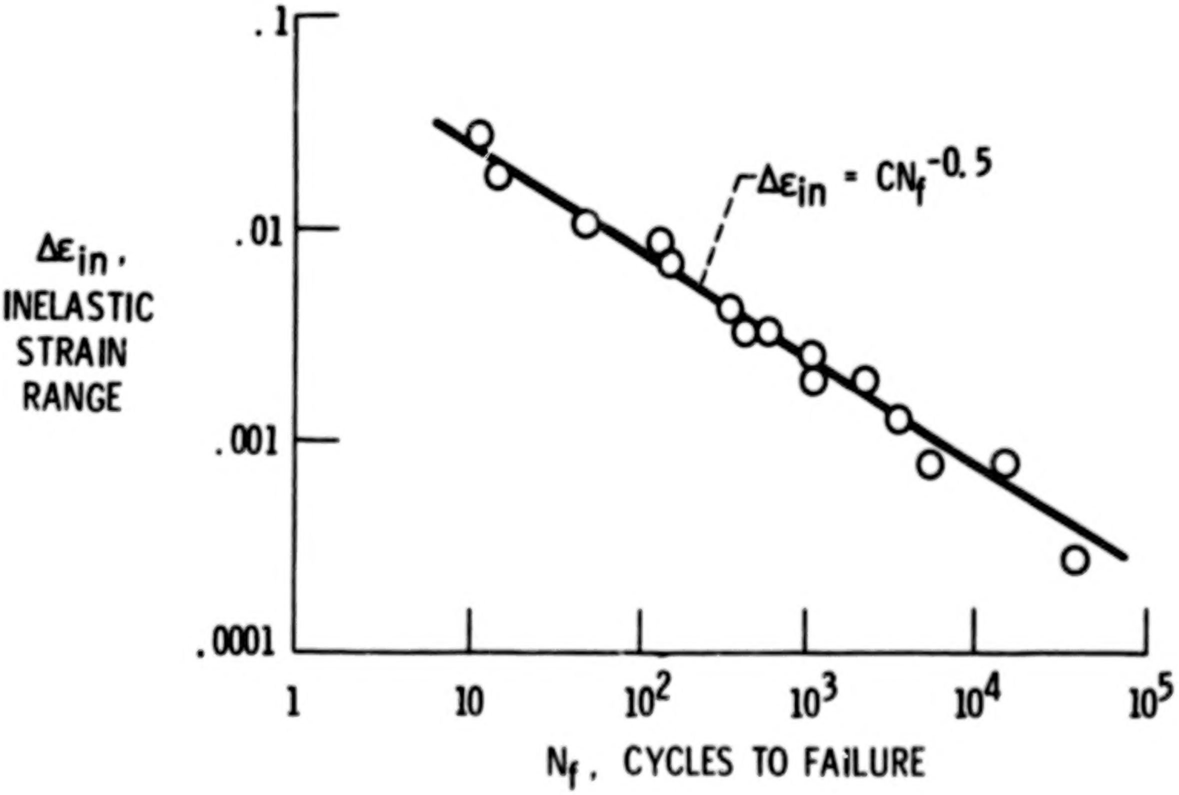

Figure 6

UNIVERSAL SLOPE METHOD FOR ESTIMATING FATIGUE LIFE

Although the inelastic strainrange could not always be calculated accurately, the total strain could be by using the concept of strain invariance along with an elastic stress analysis. Thus, by expressing the low-cycle fatigue resistance of a material in terms of total strainrange versus cycles to failure, practical predictions of life could be made. In 1964, Manson and Hirschberg (ref. 2) recognized the importance of this viewpoint and developed a procedure for representing the low-cycle fatigue curves in terms of the total strainrange. Then, they proposed a procedure for estimating the total strainrange versus cycles to failure curve from only a knowledge of a material's tensile test properties. Their method was called the Method of Universal Slopes since it assumed a constant slope of -0.12 for the elastic line and a constant slope of -0.60 for the inelastic line (see fig. 7). Furthermore, the intercept of the elastic line was related directly to the σ_u (ultimate tensile strength) and the E (modulus of elasticity) of the material. The intercept of the inelastic line was related to D (the ductility in a tensile test). The approach was an immediate success and is used widely during preliminary design.

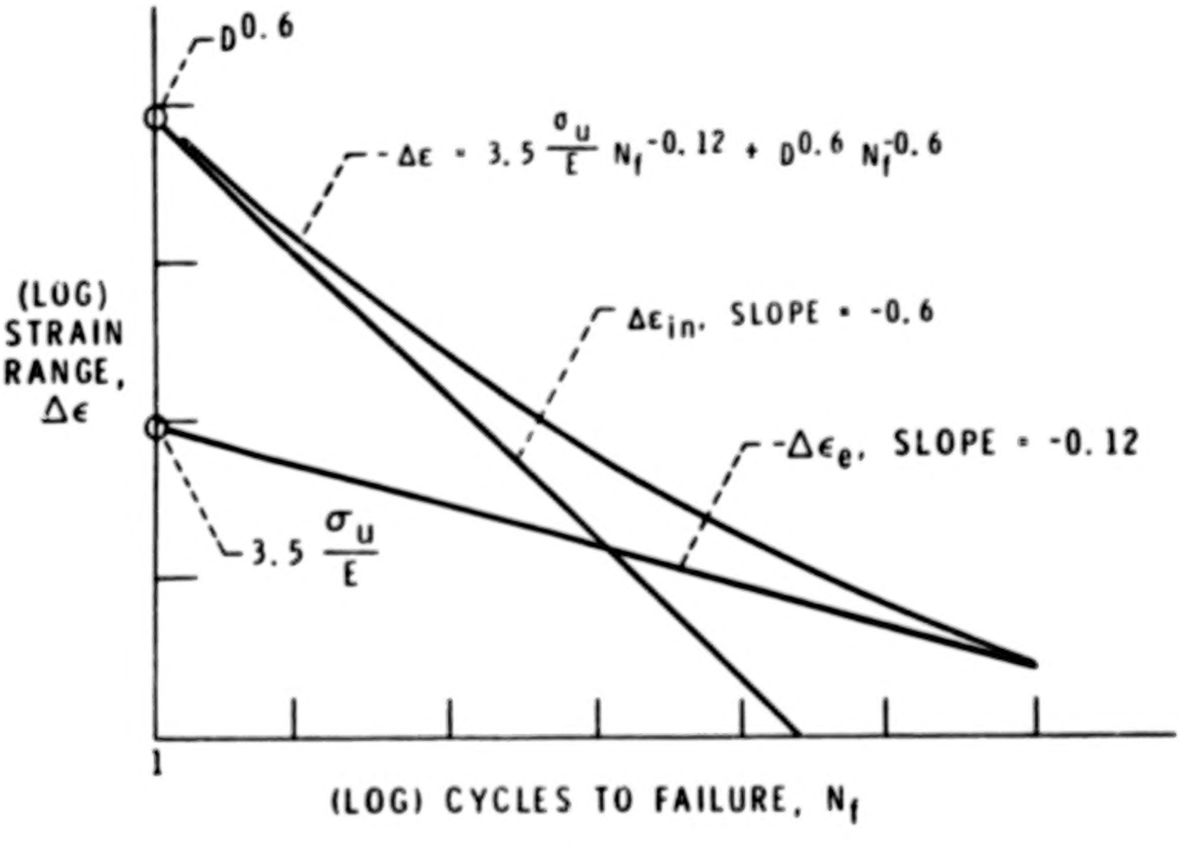

Figure 7

PREDICTIVE CAPABILITY OF METHOD OF UNIVERSAL SLOPES

As seen in figure 8, the Method of Universal Slopes (ref. 2) follows the trend of low-cycle fatigue data reasonably well over a range of six orders of magnitude in cyclic life. For any given material, the predicted cycles to failure may be wrong by as much as a factor of ten in the extreme. However, this uncertainty is usually acceptable considering the fact that fatigue tests are not required -- only materials tensile properties are needed to estimate the fatigue behavior. Since the Method of Universal Slopes was developed on the basis of low-temperature data, its applicability to high-temperature, low-cycle fatigue was in question.

First attempts to apply this method at high temperatures, using high-temperature tensile properties, resulted in overpredictions of life. The cyclic lives were lower than expected because at the high testing temperature, detrimental attack of the material grain boundaries occurred from oxidation and cyclic creep strain. Short-time tensile properties were unaffected by these factors and hence were no longer directly appropriate for use in estimating cyclic lifetimes.

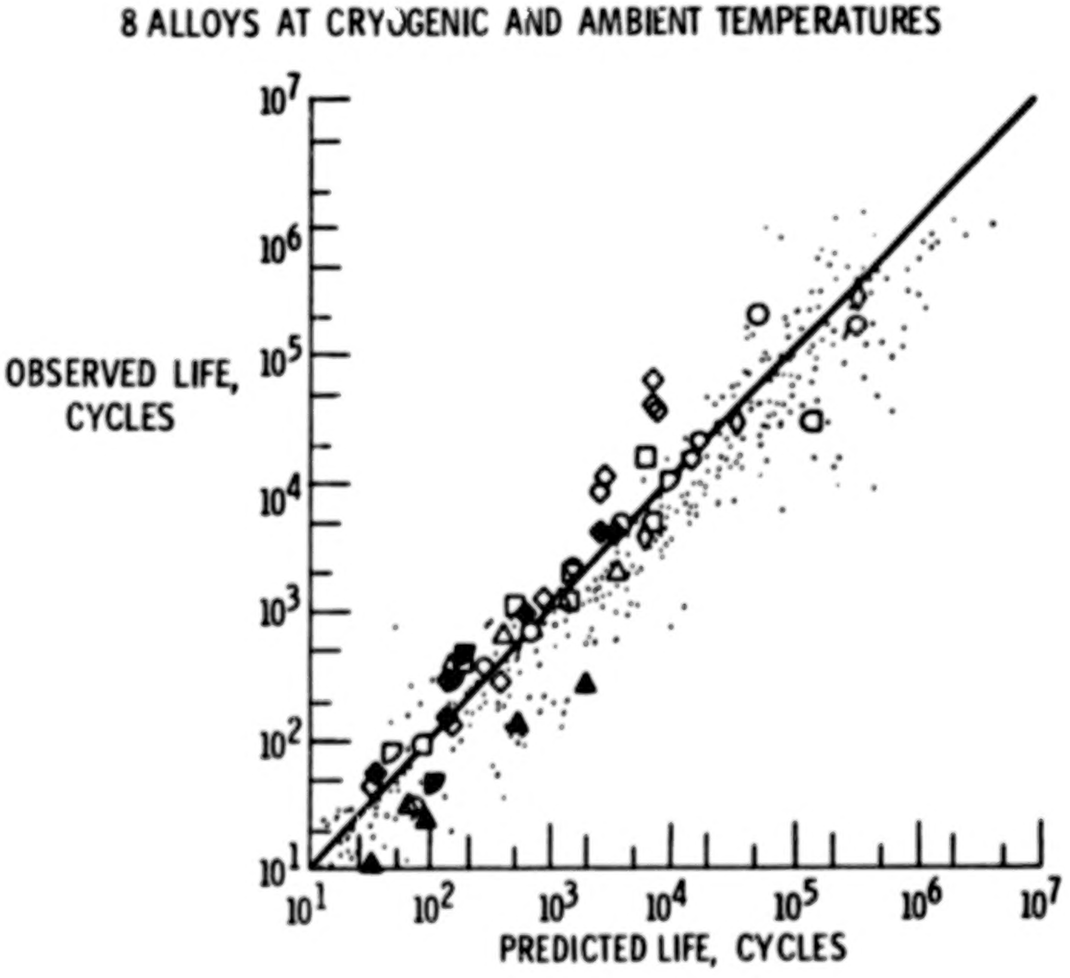

Figure 8

10% RULE FOR PREDICTING HIGH-TEMPERATURE LOW-CYCLE FATIGUE

As a first approximation to the effects of grain boundary attack on the fatigue process, it was recognized that the micro-crack initiation process was being bypassed, leaving only the crack propagation portion of the total life. Since the propagation life could be as low as about 10% of the total life in low-cycle fatigue, it was reasoned that an estimate of the minimum high-temperature low-cycle fatigue behavior of a material could be taken as equal to 10% of the life calculated by the Method of Universal Slopes (fig. 9). This rule referred to as the "10% Rule" was proposed in 1967 by Manson and Halford (ref. 3) and applied to all of the high-temperature low-cycle fatigue data available at the time.

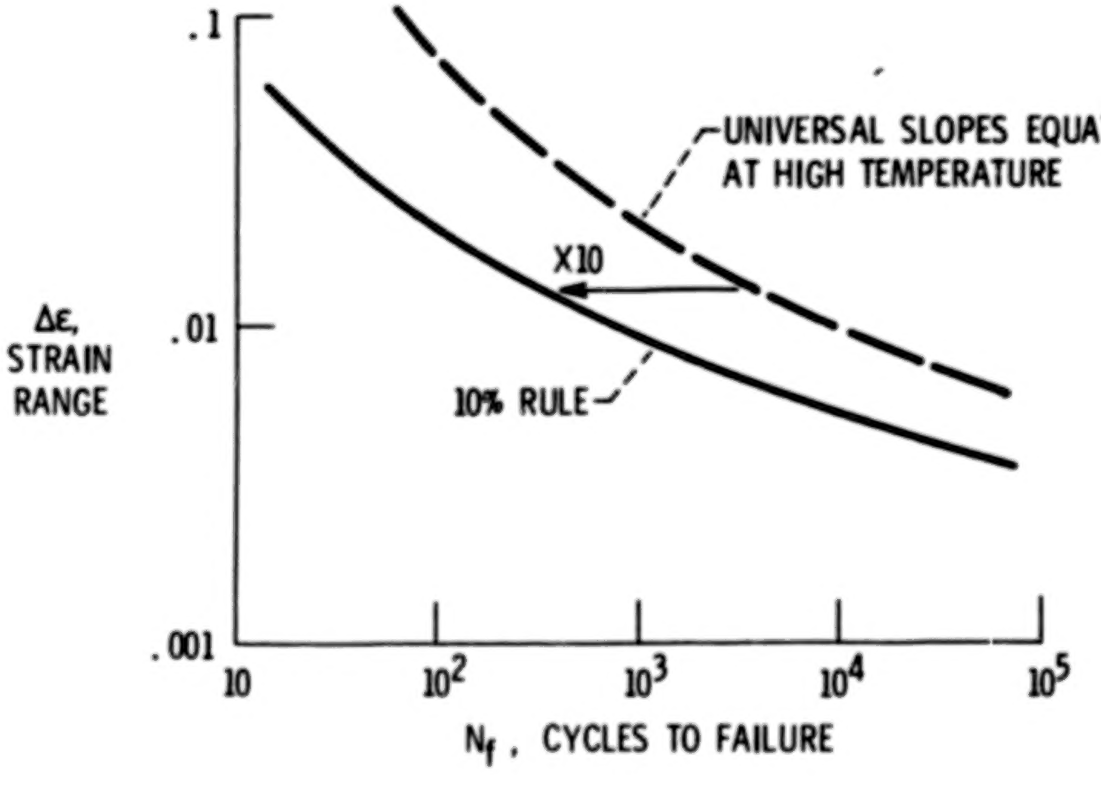

Figure 9

PREDICTIVE CAPABILITY OF 10% RULE

As seen in figure 10, we were able to verify that the method did indeed predict the trends in the available data over the range of 10 to 10^5 cycles to failure. The accuracy of the predictions was on the same order as the accuracy of the Method of Universal Slopes for lower temperature fatigue. Because of the method's simplicity, it has been used on many occasions when no high-temperature low-cycle fatigue data were available, but high-temperature tensile properties were. However, it did not account for details of a high-temperature cycle which have since been found to be important. Some of these details are: Frequency, Hold Times, Temperature, and Cycle Wave Shape.

Thus, we were motivated to seek a high-temperature life prediction method that could account for these important cycle details. The Time and Cycle Fraction Method that Professor Taira of Japan had been working on (ref. 4) possessed some of the desirable features we were looking for.

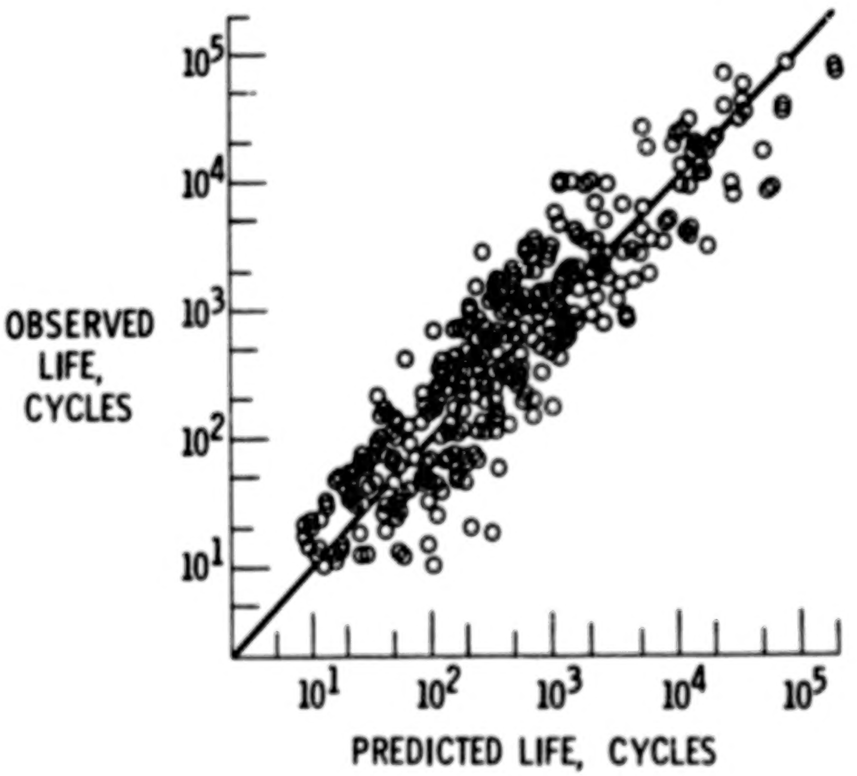

Figure 10

TIME AND CYCLE FRACTION METHOD

We made modifications (ref. 5) to Taira's method to make it more appropriate to low-cycle fatigue life prediction. Creep damage and fatigue damage are calculated independently, then the damages are summed linearly. Failure is predicted to occur when damage reaches 100%. Creep damage is expressed as a life fraction, that is, the ratio of the time spent at a stress divided by the time to rupture at that stress. Similarly, the fatigue damage is expressed as a life fraction determined from the number of cycles applied at a given total strain range divided by the number of cycles to failure at that strain range in a high-frequency fatigue test. The final expression for predicting the lifetime of any creep-fatigue cycle is indicated at the bottom of figure 11.

Although the method does have the capability to handle frequency, hold time, and temperature effects on the expected cyclic lifetime, the method does suffer limitations. Notable among these are that, (a) Creep damage is highly sensitive to stress, thus highly accurate stress calculations are needed. This is difficult to accomplish under high-temperature high-strain loading conditions, (b) Compressive creep damage is difficult to define since compressive creep rupture does not occur, yet compressive cyclic creep damage does, and (c) The method does not build in any synergistic effect of creep on fatigue or fatigue on creep.

Because of these limitations, we sought a more unifying framework for predicting cyclic lifetime under creep-fatigue conditions.

FAILURE MODE	STRESS-TIME-DEPENDENT	STRAIN-CYCLE-DEPENDENT
FAILURE CRITERION	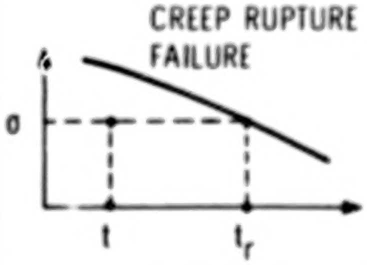	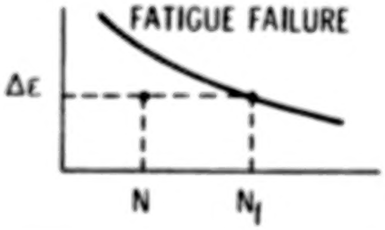
MEASURE OF DAMAGE	LIFE FRACTION t/t_r	LIFE FRACTION N/N_f
ACCUMULATION OF DAMAGE	LINEAR SUMMATION TO 1 $\sum \frac{t}{t_r} = 1$ (AT FAILURE)	LINEAR SUMMATION TO 1 $\sum \frac{N}{N_f} = 1$ (AT FAILURE)
COMBINATION	$\sum \frac{t}{t_r} + \sum \frac{N}{N_f} = 1$ (AT FAILURE)	

Figure 11

FOUR BASIC CYCLES OF SRP

In 1971, Manson, Halford, and Hirschberg (ref. 6) proposed an entirely new life prediction method that had the potential to overcome previously encountered limitations. It is a strain-based approach and recognizes the desirability of dividing (or partitioning) the inelastic strain into its creep and plastic strain components. The creep strain is thermally activated, diffusion controlled, and is the time-dependent portion. The plastic strain is time independent and is a result of crystallographic slip within metallic grains. The two basic types of inelastic strain can then be combined in the two directions of uniaxial loading -- tension and compression. This combination leads to four distinct types of cycles which are shown in figure 12. We call these the four basic cycles of Strainrange Partitioning (SRP). In a short-hand notation, these are PP (plastic strain in tension and compression), CP (creep in tension, plasticity in compression), PC (plasticity in tension and creep in compression), and finally, CC (creep in both tension and compression). Strain cycling tests can be conducted in the laboratory that feature these four types of cycles. A series of such tests conducted to failure gives the results shown schematically in the next figure.

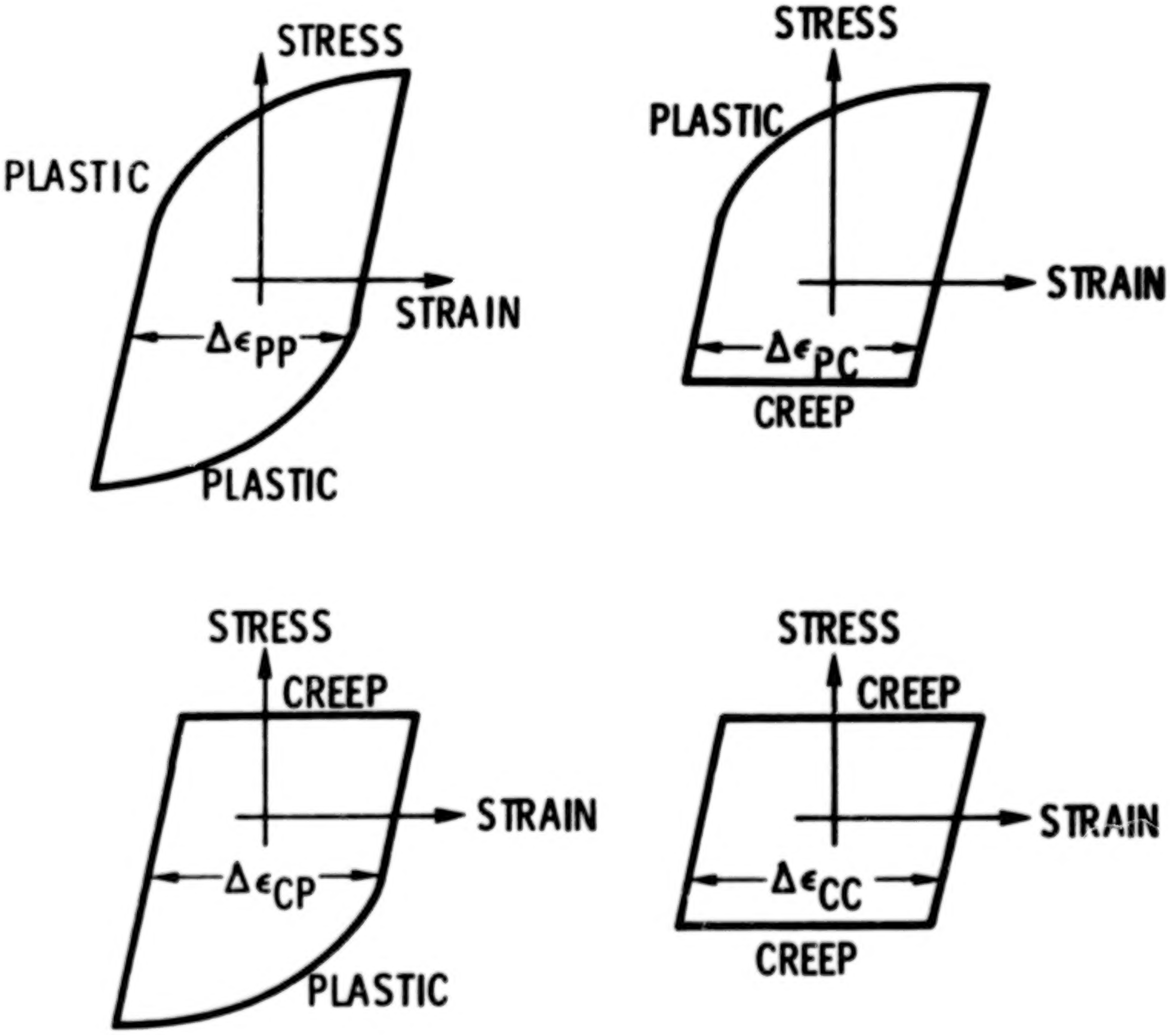
STRESS
PLASTIC
STRAIN
$\Delta\epsilon_{PP}$
PLASTIC
STRESS
PLASTIC
STRAIN
$\Delta\epsilon_{PC}$
CREEP
STRESS
CREEP
STRAIN
$\Delta\epsilon_{CP}$
PLASTIC
STRESS
CREEP
STRAIN
$\Delta\epsilon_{CC}$
CREEP

Figure 12

TYPICAL SRP LIFE RELATIONS

Each cycle type produces a unique curve of inelastic strainrange versus cycles to failure on logarithmic coordinates. These curves are called the SRP life relations. As shown in figure 13, the PP curve is usually the highest and the CP curve is usually the lowest with the PC and the CC curves being intermediate. It should be noted that these relations represent extremes in cyclic lives, and that any closed cycle is a combination of components of these types of cycles and thus will have a cyclic life that lies somewhere between these extremes.

Using the Strainrange Partitioning Method, it is possible to characterize the creep-fatigue properties of high-temperature alloys. Because the approach is generic, it is applicable to any material that undergoes high-temperature cyclic inelastic deformation, and it is applicable to any conceivable inelastic strain cycle.

A likely reason for the generality of the approach is that it is based upon a micromechanistic deformation model that is physically sound. The next figure illustrates this schematically and with photomicrographs of an alloy that has been cyclically deformed according to each of the four basic SRP cycles.

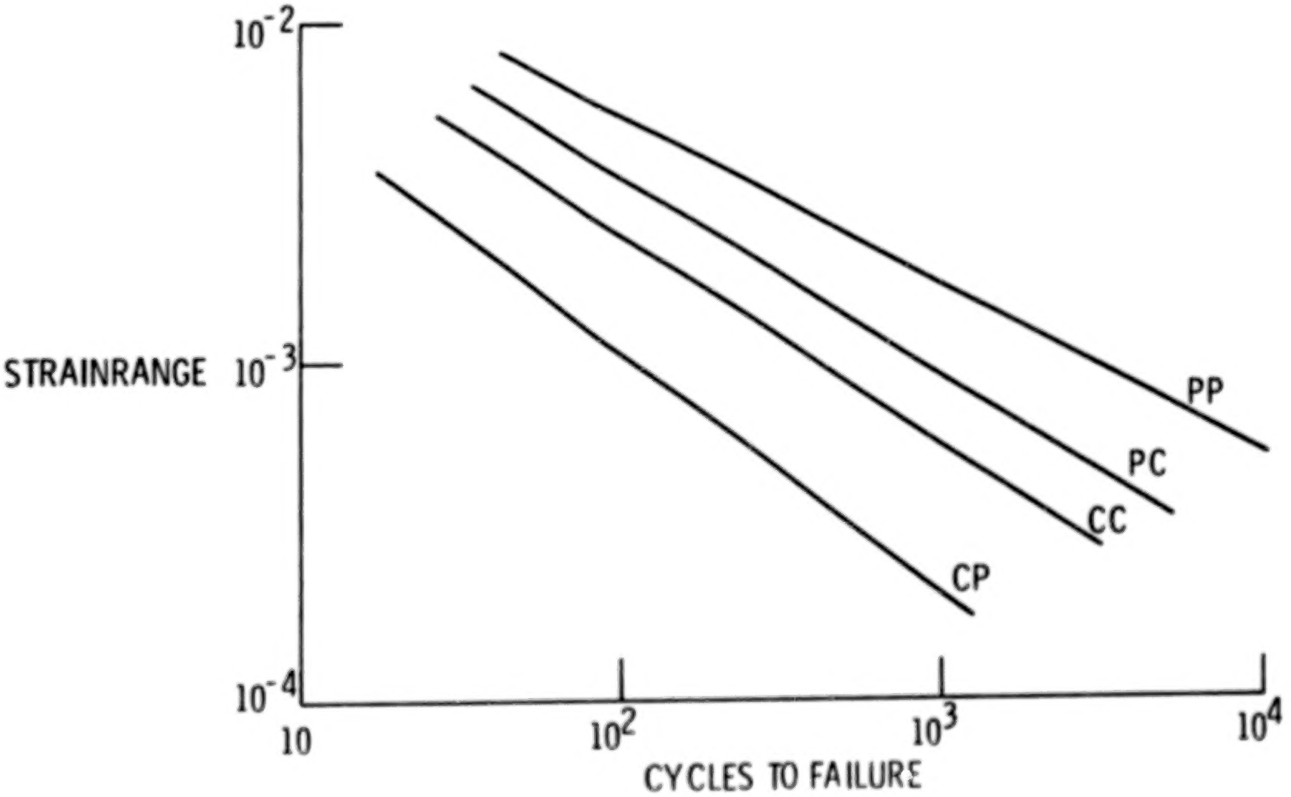

Figure 13

MECHANISMS OF SRP

A set of four simple cyclic deformation models is shown schematically in figure 14 for one complete cycle of PP, PC, CP, and CC type SRP's. Plastic strain is shown by a slip along a crystallographic slip plane while creep is shown as sliding along with a grain boundary. When these two types of strain are applied in the two directions of loading, the result is four completely different looking deformation models. The general agreement between the simple deformation model and the microstructures that develop has given credence to the validity of the SRP method of describing high-temperature creep-fatigue behavior of materials. The method has been shown to correlate the creep-fatigue behavior of a wide variety of alloys.

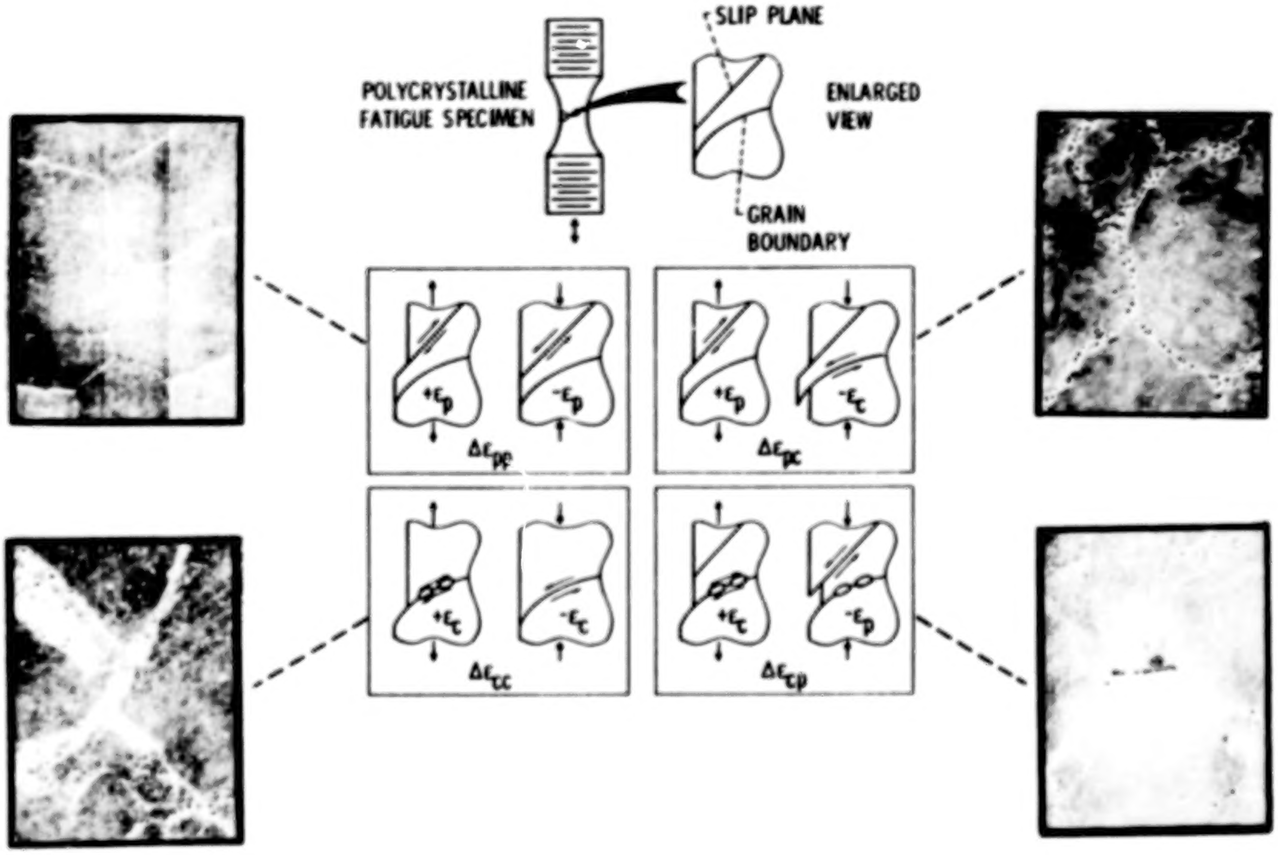
SLIP PLANE
POLYCRYSTALLINE FATIGUE SPECIMEN
ENLARGED VIEW
GRAIN BOUNDARY
$+\epsilon_p$
$-\epsilon_p$
$\Delta\epsilon_{pp}$
$+\epsilon_p$
$-\epsilon_c$
$\Delta\epsilon_{pc}$
$+\epsilon_c$
$-\epsilon_c$
$\Delta\epsilon_{cc}$
$+\epsilon_c$
$-\epsilon_p$
$\Delta\epsilon_{cp}$

Figure 14

AVAILABLE

CHARACTERIZING MATERIALS BY STRAINRANGE PARTITIONING

For a number of different materials, including nickel-, cobalt-, iron-, tantalum- and even copper-base alloys, the method of SRP has been able to correlate the cyclic life behavior of laboratory specimens to within factors of two (fig. 15). We consider this to be excellent correlation, since repeat data may vary by as much as a factor of two. For these data, there were variations in details of the cycles that the method of SRP was able to take into account. In particular, these included variations in cyclic frequency, hold times, a variety of temperatures, and of course, the cycle wave shape.

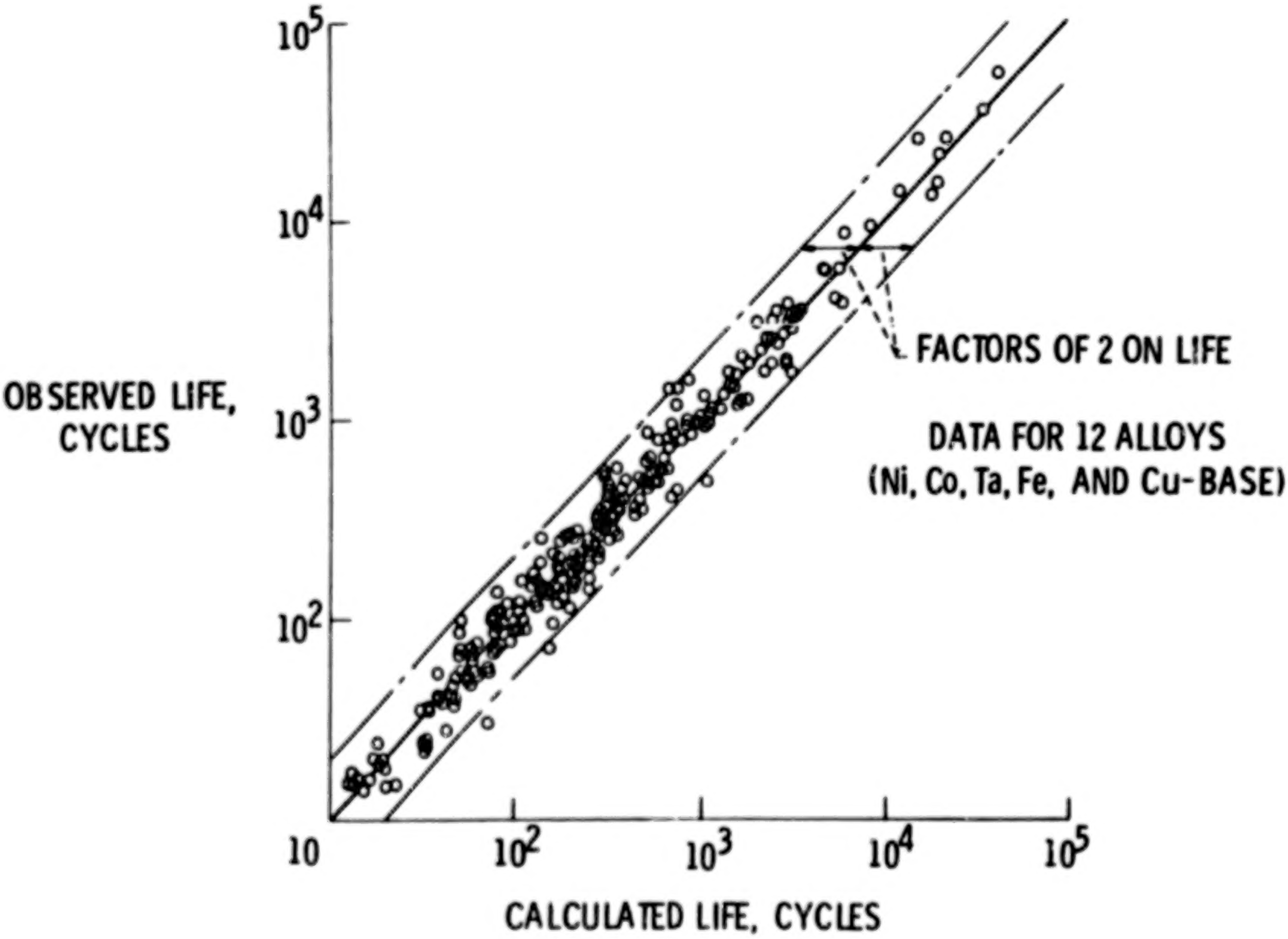

Figure 15

BOUNDS ON LIFE

In addition to correlating high-temperature, low-cycle fatigue data, the ability of the method to predict cyclic lives has also been addressed. The major advantage of the method is its ability to place upper and lower bounds on cyclic lifetime. For most materials, the PP cycle is the least damaging and gives the greatest lifetime whereas the CP cycle is the most damaging and is associated with the lowest life possible due to creep-fatigue.

The method of SRP can also predict the transition in cyclic lives between the upper bound and a lower bound as the cyclic testing frequency, for example, is reduced. A schematic is shown in figure 16 for the transition between PP and CC.

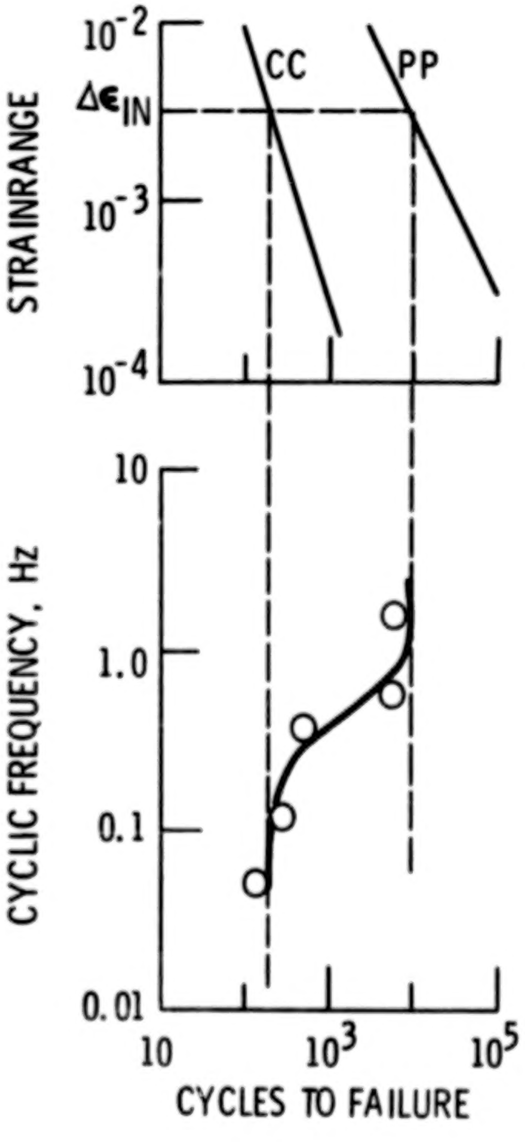

Figure 16

ESTIMATIONS FOR STRAINRANGE PARTITIONING LIFE RELATIONS

We realized that the SRP life relations may not be available for a particular material that a designer might be interested in using. We thus provided a procedure (ref. 7) for estimating the four SRP life relations from a knowledge only of materials tensile ductility D_p and creep ductility D_c. The constants in these equations were arrived at by correlating these measured ductilities with the SRP data for a large number of materials. There are two equations for the CP life relation. The first is to be used when the creep cracking is transcrystalline and the second is for when the cracking is intercrystalline. The life relations estimated by these equations, shown in figure 17, are in agreement with measured life relations to within a factor of approximately three in cyclic lifetime. The greater the ductility, the greater the resistance to failure by cyclic inelastic deformation. These equations also help to predict whether the SRP life relations are sensitive to test temperature. For example, if the ductility of an alloy does not change appreciably with temperature, it would be predicted that the SRP life relations would be insensitive to test temperature. This would be a distinct advantage in the analysis of thermal fatigue cycling with temperatures varying throughout the cycle. Two such materials that we have studied exhibit this desirable behavior. Results of our analyses of these materials are shown in the next figure.

$$\Delta\varepsilon_{PP} = 0.50\, D_P (N_{PP})^{-0.60}$$

$$\Delta\varepsilon_{PC} = 0.25\, D_P (N_{PC})^{-0.60}$$

$$\Delta\varepsilon_{CC} = 0.25 (D_C)^{0.60} (N_{CC})^{-0.60}$$

$$\Delta\varepsilon_{CP} = 0.20 (D_C)^{0.60} (N_{CP})^{-0.60} \quad \text{(TRANSCRYSTALLINE)}$$

$$\text{OR} \quad \Delta\varepsilon_{CP} = 0.10 (D_C)^{0.60} (N_{CP})^{-0.60} \quad \text{(INTERCRYSTALLINE)}$$

Figure 17

TEMPERATURE INSENSITIVITY OF SRP LIFE RELATIONS

The SRP life relations for two steels were measured at a single baseline test temperature appropriate to each (ref. 8), as indicated by the open circles in figure 18. Additional SRP-type test cycles, as indicated by the closed circles, were conducted at higher and lower test temperatures and their lives were predicted based upon the baseline SRP life relations. Since the ductilities for these materials did not vary appreciably over the temperature range studied, the SRP life relation also did not vary appreciably, and the predictions were therefore quite accurate, being within about a factor of two in cyclic lifetime.

It should be pointed out that although the life relations may not be functions of temperature, the stress-strain relationships and the creep rate versus stress relationships are still highly sensitive to temperature.

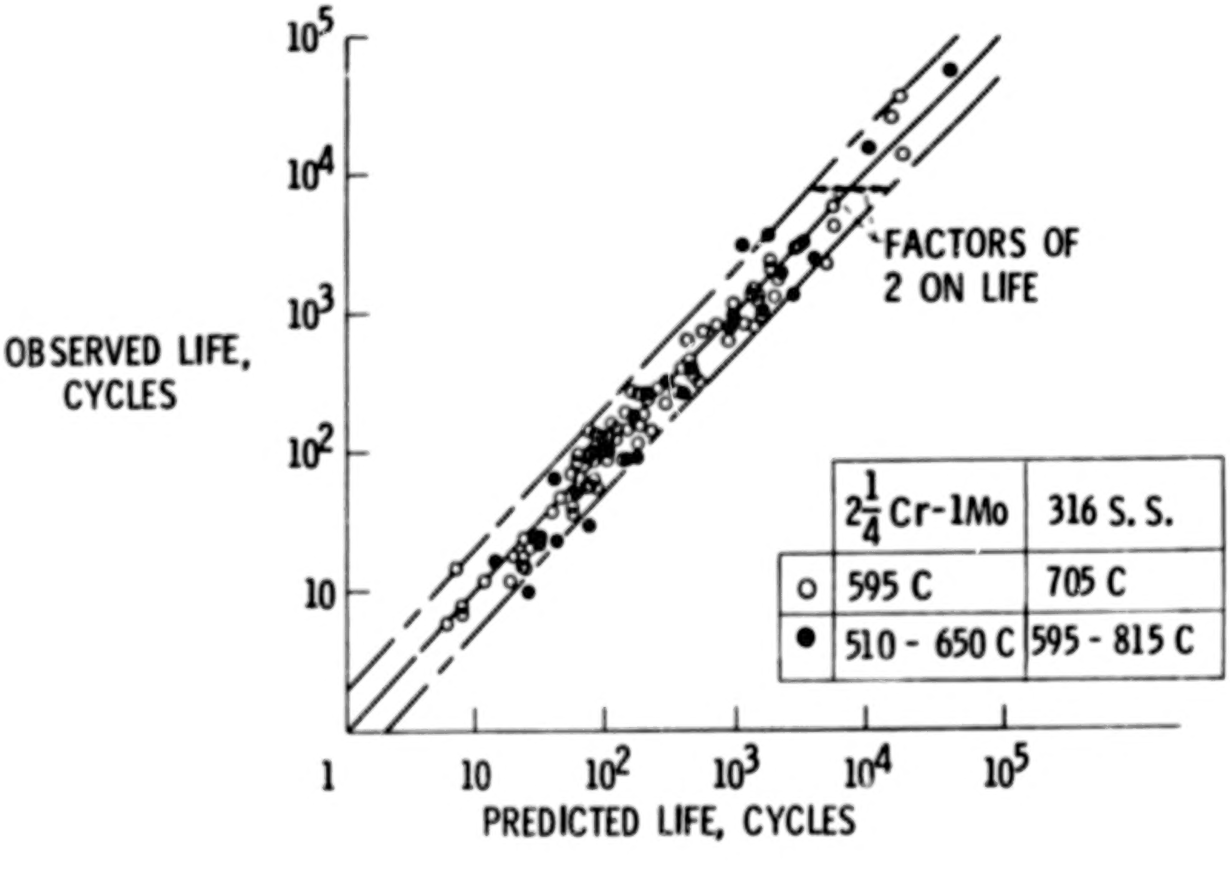

Figure 18

MULTIAXIAL EFFECTS

Multiaxial states of stress are known to affect the inelastic straining behavior of materials as well as their fatigue behavior. We have developed a two-step procedure to account for these multiaxial stress effects when using the Strainrange Partitioning Method.

We begin by determining the four SRP life relations from uniaxial tests. Referring to figure 19, the first step in dealing with a multiaxial stress state is to determine the Equivalent Inelastic Strainrange using the von Mises yield criteria. This takes care of the multiaxiality on the inelastic straining behavior. This is also called the flow or shear behavior. The second step is to determine the degree of hydrostatic stress present. If the hydrostatic stress is tensile, the life relations are decreased, but if the hydrostatic stress is compressive, the life relations are increased. Equations for making the required calculations are included in refs. 9 and 10. We have found the two-step approach to be more accurate than forcing a single multiaxial criterion to correlate uniaxial and multiaxial states of stress in fatigue.

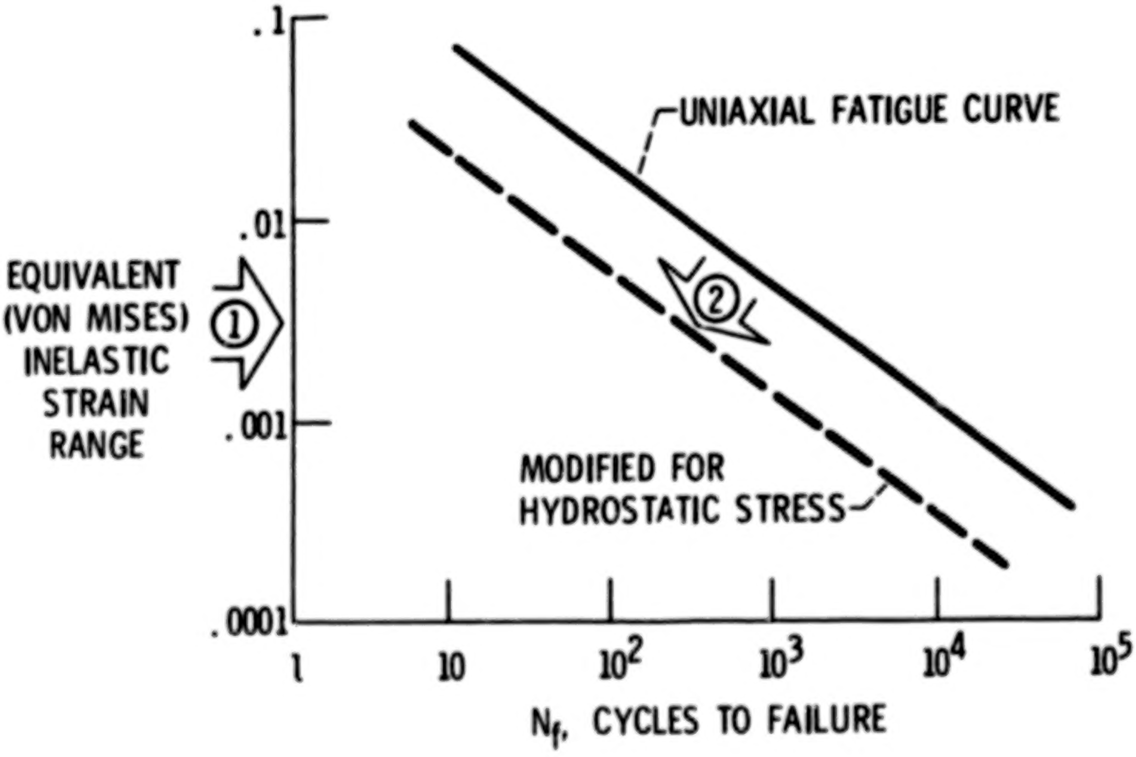

Figure 19

MEAN STRESS EFFECTS

Mean stresses may occur during low-cycle fatigue and thermal fatigue. Their damaging or beneficial influence must be determined in order to accurately predict cyclic lifetime. The effect of mean stresses on high-cycle fatigue life is well understood and established procedures exist for calculating their influence on life. These effects can be very large. However, in the low-cycle fatigue region, their effects are not as great, and at large enough strain ranges and low enough cyclic lives, the effect decreases to zero. This trend is shown in the figure. Here, in the high-cycle region, where the stress-strain response is linearly elastic, mean stresses have their full effect. Typically, compressive mean stresses improve life and tensile mean stresses decrease life. As shown schematically in figure 20, the mean stress effect decreases toward zero at the lower number of cycles to failure. We have developed a relatively simple procedure (ref. 11) for accounting for the effects of mean stress in the low- and intermediate-cycle fatigue region. This procedure is based upon the Morrow Equation for the Goodman diagram which was derived for high-cycle fatigue behavior.

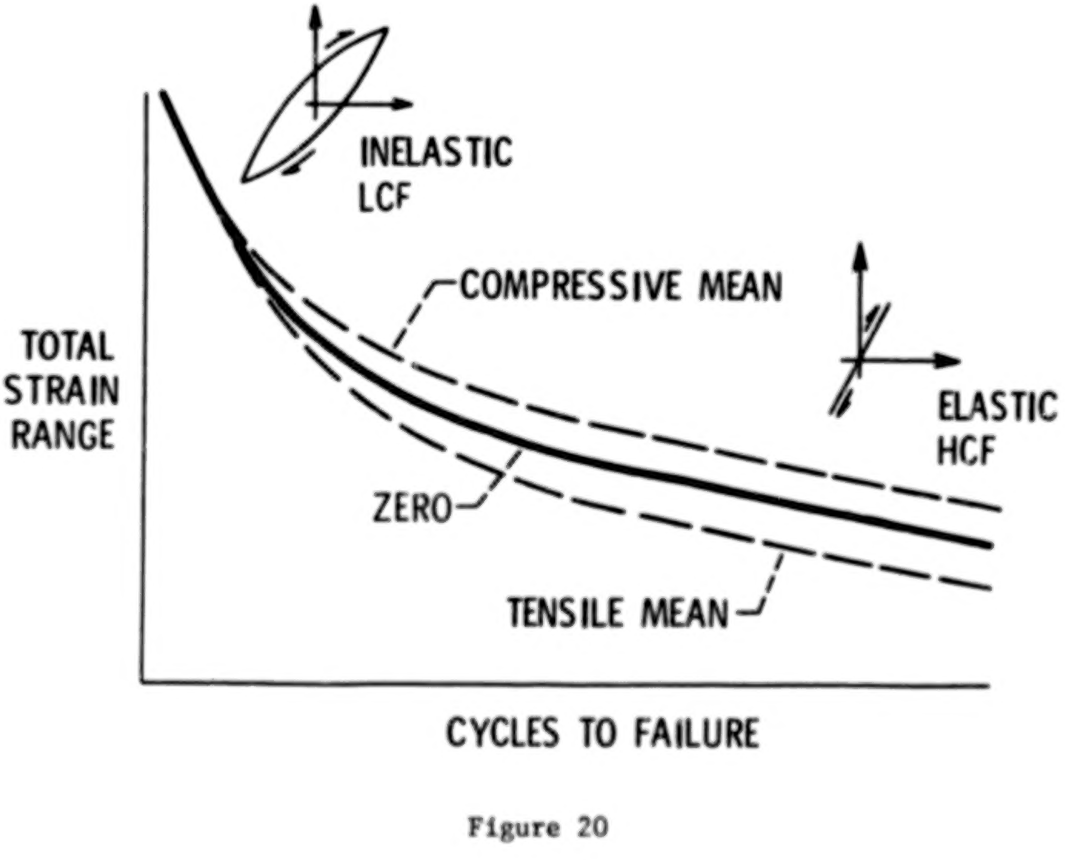

Figure 20

EFFECTIVE IMPLEMENTATION OF STRAINRANGE PARTITIONING

Up to this point in the presentation, I have discussed many of the details of the life prediction methods that have been developed at the NASA Lewis Research Center. I have concentrated mainly on the Method of Strainrange Partitioning. We do realize that to implement the method places a burden upon the materials engineer who must provide the necessary material characterization properties, and a similar burden is placed upon the structural analyst who must do a more thorough job of calculating the localized inelastic strains that occur in a high-temperature component part. For example, the materials engineer must determine the four SRP life relations for the material, and if these are functions of temperature, must determine them at enough isothermal temperatures to permit interpolation and extrapolation as needed. He must also provide the structural analyst with the cyclic constitutive equations that characterize the cyclic stress-strain-creep-time-temperature relations of the material. The structural analyst must then anticipate the thermal and mechanical loading on a component part, to identify the most critical locations where failures may originate, and then calculate the local stresses and strains. The inelastic strains must then be partitioned into their creep and plastic portions in order to predict a cyclic lifetime using Strainrange Partitioning.

If these advanced capabilities are available, then the Method of Strainrange Partitioning has many attributes that represent a vast improvement over previously proposed methods of life prediction.

ATTRIBUTES OF STRAINRANGE PARTITIONING

The method of Strainrange Partitioning is general enough to permit a thorough characterization of the creep-fatigue behavior of materials. As indicated in figure 21, the method is generic and applicable to any creep-fatigue cycle, including thermal mechanical cycling. It can provide upper and lower bounds on cyclic lifetime with a minimum of analysis, and it can readily account for the effects of such factors as: Frequency, Hold Time, Waveshape, Temperature, State of Stress, Mean Stress, and Strain Ratchetting.

Research is in progress for improving the applicability of the method to the solution of practical engineering design problems.

For example, some current research is focused on casting the method in terms of the total strainrange rather than just the inelastic strainrange.

Although considerable work has been done toward the development of the method, further research and development are needed to make the method a practical tool for routine analysis and life prediction of turbine engine hot section components.

In addition to SRP, there are a number of life prediction approaches under development by other research organizations. These include variations of the Time and Cycle Fraction Method, and other approaches that consider cyclic frequency or cyclic inelastic straining rate as the primary variables governing time-dependent damage accumulation. Since few of these address the problems of nonrepetitive cycles (i.e., cumulative fatigue cycling), we have recently researched procedures to deal with this phenomenon.

- CHARACTERIZES CREEP-FATIGUE BEHAVIOR OF ALLOYS
- PROVIDES BOUNDS OF CYCLIC LIFE
- PREDICTS EFFECTS OF:
    - FREQUENCY
    - HOLD TIME
    - WAVESHAPE
    - TEMPERATURE
    - STATE OF STRESS
    - RATCHETTING
- APPLICABLE TO ANY COMPLEX THERMAL-MECHANICAL STRAIN CYCLE

Figure 21

DOUBLE LINEAR DAMAGE RULE FOR FATIGUE

Simple procedures have been developed and verified (ref. 12) for treating the difficult problem of nonlinear cumulative fatigue crack initiation damage under complex loading histories. The Double Linear Damage Rule (DLDR) is a concept arrived at through viewing the fatigue process as two sequential phases: the first, Phase I, associated with microscopic changes in the surface layer of material being fatigued, and the second, Phase II, with the propagation of microcracks to the point that is classified as fatigue crack initiation on the macroscopic engineering level.

The application of the newly proposed rule involves two steps, each similar to the conventional application of the classical Miner Linear Damage Rule. When the sum of the cycle ratios based on Phase I lives reaches unity, Phase I is presumed complete, and further loadings are summed as cycle ratios based on Phase II lives. Once Phase II cycle ratios sum to unity, failure by macrocrack initiation is presumed to occur. No other physical properties or material constants than those normally required in a conventional Miner Linear Damage Rule analysis are required for application of the DLDR. Examples of the application of the approach are shown in figure 22.

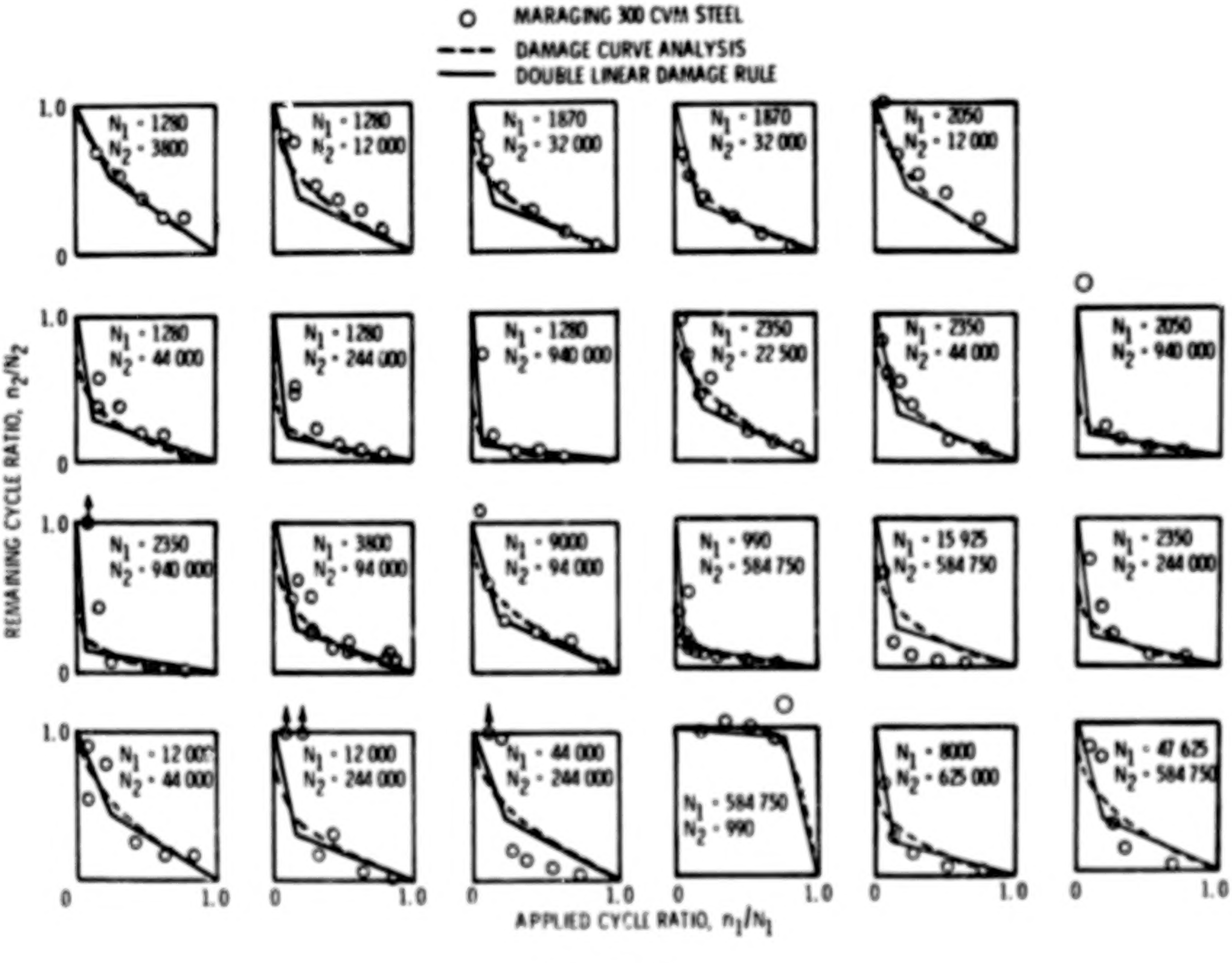

Figure 22

TURBINE COMPONENT LIFE PREDICTION

We have an intensive program aimed at generating the controlled experimental data needed for the development and verification of these life prediction methods. As shown in figure 23, we are using a variety of specimens ranging in complexity from the simple laboratory specimen to actual gas turbine engine components.

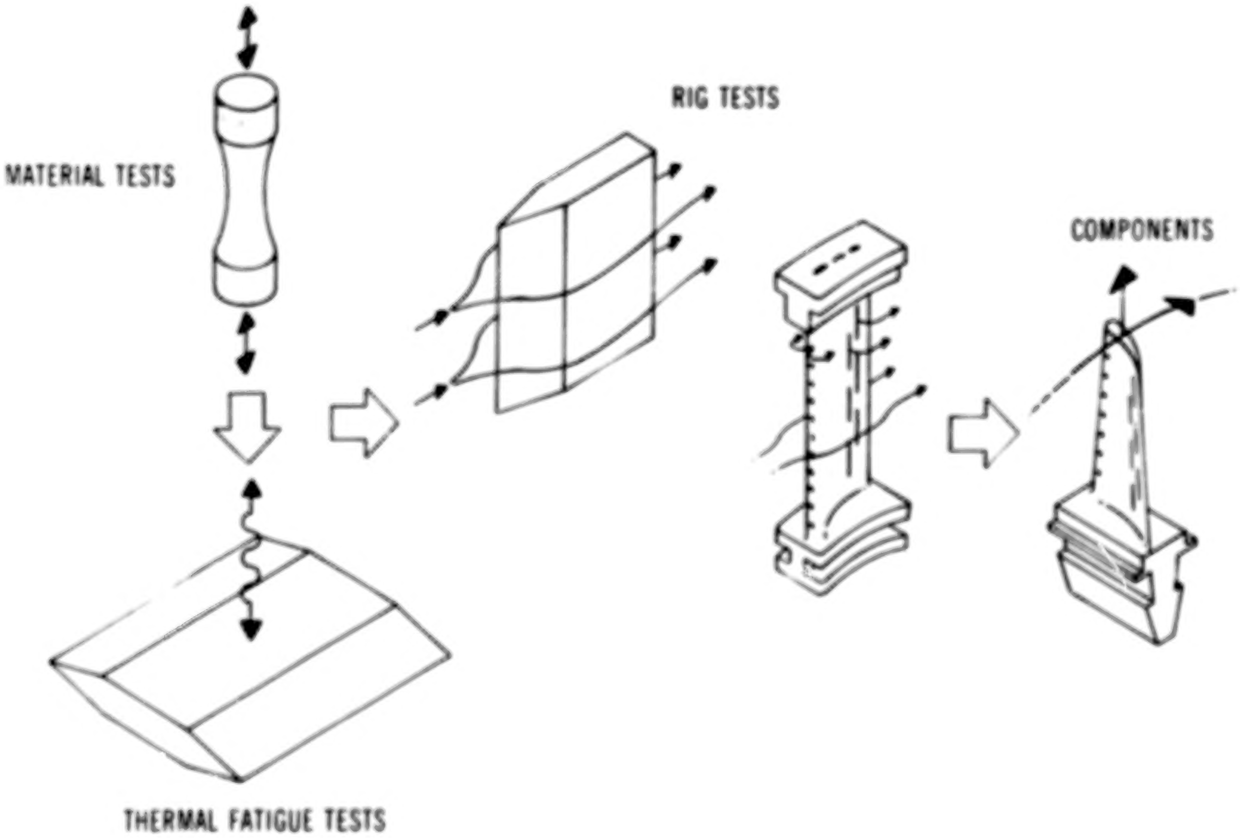
MATERIAL TESTS
RIG TESTS
COMPONENTS
THERMAL FATIGUE TESTS

Figure 23

REFERENCES

1. Manson, S. S.: Behavior of Materials Under Conditions of Thermal Stress. NACA TN-2933, 1953.

2. Manson, S. S.: Fatigue: A Complex Subject - Some Simple Approximations. Exp. Mech., Vol. 5, No. 7, 1965, pp. 193-226.

3. Manson, S. S. and Halford, G. R.: A Method of Estimating High-Temperature Low-Cycle Fatigue Behavior of Materials. Proc. of Int. Conf. on Thermal & High-Strain Fatigue. Metals & Metallurgy Trust, London, 1967, pp. 154-170.

4. Taira, S.: Lifetime of Structures Subjected to Varying Load and Temperature. Creep in Structures, N. J. Hoff, ed.; Academic Press, New York, 1962, pp. 96-124.

5. Manson, S. S.; Halford, G. R.; and Spera, D. A.: The Role of Creep in High-Temperature Low-Cycle Fatigue. Advances in Creep Design, A. I. Smith & A. M. Nicolson, eds., Halsted Press, 1971, pp. 229-249.

6. Manson, S. S.; Halford, G. R.; and Hirschberg, M. H.: Creep-Fatigue Analysis by Strain-Range Partitioning. Symposium on Design for Elevated Temperature Environment, ASME, 1971, pp. 12-28. (NASA TM X-67838, 1971)

7. Halford, G. R.; Saltsman, J. F.; and Hirschberg, M. H.: Ductility Normalized-Strainrange Partitioning Life Relations for Creep-Fatigue Life Prediction. Proceedings of Conf. on Environmental Degradation of Engineering Materials. Virginia Tech Printing Dept., V.P.I. & State Univ., Blacksburg, VA, 1977, pp. 599-612.

8. Halford, G. R.; Hirschberg, M. H.; and Manson, S. S.: Temperature Effects on the Strainrange Partitioning Approach for Creep-Fatigue Analysis. STP 520, ASTM, 1973, pp. 658-669. (NASA TM X-68023, 1972)

9. Manson, S. S. and Halford, G. R.: Multiaxial Rules for Treatment of Creep-Fatigue Problems by Strainrange Partitioning. 1976 ASME-MPC Symposium on Creep-Fatigue Interaction, MPC-3, ASME, 1976, pp. 299-322. (NASA TM X-73488, 1976)

10. Manson, S. S. and Halford, G. R.: Discussion. Multiaxial Low-Cycle Fatigue of Type 304 Stainless Steel. Blass, J. J. and Zamrik, S. Y., 1976 ASME-MPC Symposium on Creep-Fatigue Interaction, MPC-3 ASME, 1976, pp. 129-159.

11. Halford, G. R. and Nachtigall, A. J.: The Strainrange Partitioning Behavior of an Advanced Gas Turbine Disk Alloy, AF2-1DA. J. Aircraft, Vol. 17, No. 8, 1980, pp. 598-604. (NASA TM-79179, 1979)

12. Manson, S. S. and Halford, G. R.: Practical Implementation of the Double-Linear Damage Rule & Damage Curve Approach for Treating Cumulative Fatigue Damage. Int. J. Fracture, Vol. 17, No. 2, 1981, pp. 169-192. Also, Vol. 17, No. 4, 1981, pp. R35-R42.

BLANK PAGE

FIBROUS CERAMIC INSULATION

Howard E. Goldstein
NASA Ames Research Center
Moffett Field, California

INTRODUCTION

In the late 60's and early 70's it became apparent that reusable heat shields would be required to provide thermal protection for the Space Shuttle Orbiter System. Ames Research Center therefore embarked on a program to develop an in house competence in the technology of reusable ceramic fibrous insulation. Ames had for many years been one of the leading centers in the country for aeroconvective testing of heat shield materials using our extensive arc plasma test facility (Ref. 1). In order to contribute to the development of this new class of materials, which was expected to be used on the Space Shuttle, we felt that it was important to understand the materials properties and fabrication process. As our in-house capabilities improved we expanded our goals to include the development of higher temperature, more durable, stronger, rigid and flexible ceramic heat shield materials. The program led to significant new materials developments by the mid-1970's. Among those were improved coatings (Ref. 2), stronger, higher temperature tile materials (Ref. 3) and numerous contributions toward the supporting technology for aeroconvective and mechanical testing of the materials (Ref. 4).

The thrust of the program today is to develop improved reusable ceramic heat shield materials to enhance the Shuttle and enable development of new vehicles such as Advanced Space Transportation Vehicles, Aerobraking Orbital Transfer Vehicles and Advanced Military Spacecraft.

This paper will describe some of the materials that have been developed and their manufacturing processes, properties and applications.

THERMAL PROTECTION MATERIALS DEVELOPMENT PROCESS

The development cycle of new materials from concept to system application is normally so lengthy that, from the start of a program like the Space Shuttle (1972) to its manufacturing phase (1978-1983), the possibility of incorporating new materials concepts is very remote.

The approach at Ames for the development of new materials for space transportation is depicted on this chart. The group is small, interdisciplinary and has all the necessary facilities within the organization to both develop and test new thermal protection materials. New materials are developed and screened internally. Only the reasonably mature innovations are presented to higher management for approval of procurement action for competitive commercial small-scale manufacturing. This essentially closed-loop system allows rapid transition from concept to finished prototype, shortening the development time for new materials considerably.

An example of how rapidly this can be accomplished is development of Fibrous Refractory Composite Insulation (Refs. 5 & 6). It was conceived in July 1977; patent disclosure was in April 1978; and a competitive procurement was awarded in January 1979 to pilot plant it. In January 1981 acceptable preproduction material was delivered by LMSC and in January 1982 first flight hardware delivery for installation on the third Space Shuttle was accomplished.

This extremely short time span from concept through flight hardware delivery is unusual in the field of material development and is attributed to a significant degree to the organization and management approach utilized in this program. Transfer of this technology to industry in a timely manner has been accomplished through an effective working relationship with the contractors that has evolved over a number of years.

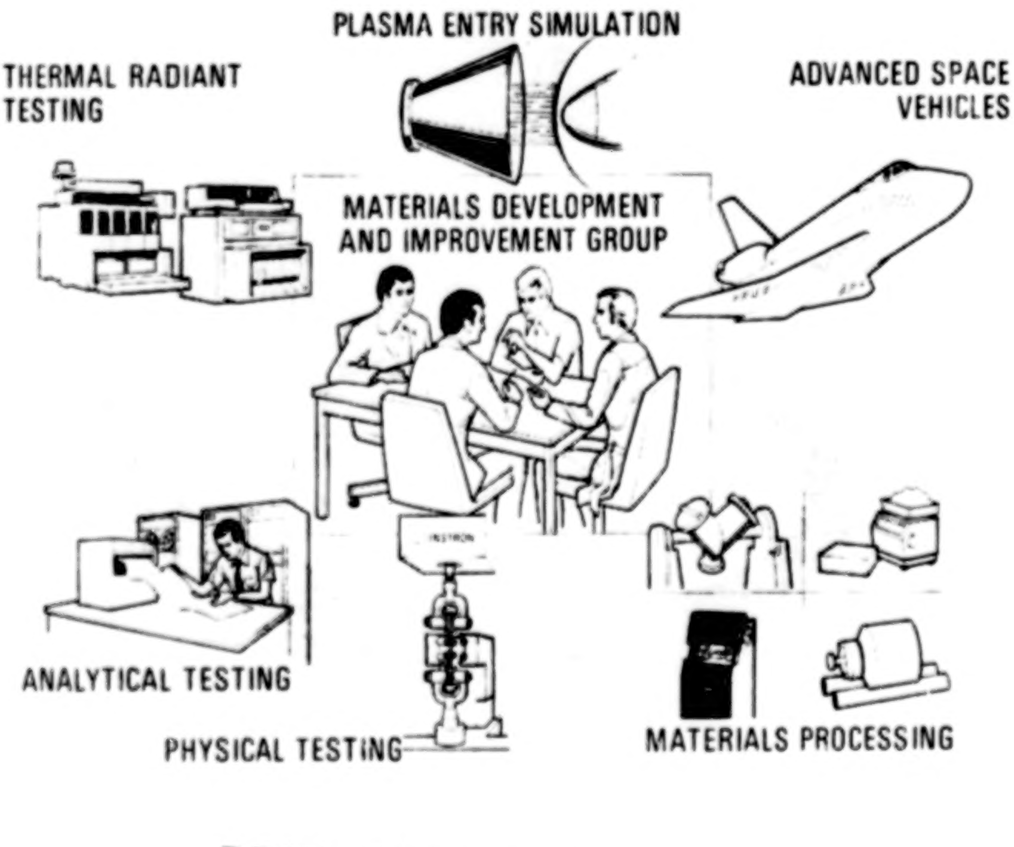

FRCI-20-12 REUSABLE SURFACE INSULATION

This figure shows typical coated and uncoated Reusable Surface Insulation (RSI) tile. RSI is a generic name which describes any coated fibrous insulation materials used on the external surface of the Space Shuttle Orbiter. Among these materials are the rigid ceramics such as FRCI, a fiber-fiber rigid composite insulation; LI-900 and LI-2200 all silica rigid ceramic insulations; and flexible materials such as Fibrous Reusable Surface Insulation (FRSI), a Nomex felt blanket, and Advanced Flexible Reusable Surface Insulation (AFRSI), a glassy ceramic quilted material that will be described subsequently.

The material shown in this figure is a High Temperature Reusable Surface Insulation (HRSI) with the Reaction Cured Glass coating (Ref. 2). The specific tile material shown is FRCI-20-12 which was developed in the late 1970's by Ames (Refs. 5 & 6). LMSC, who developed the first all silica RSI (Ref. 7), manufactures all the rigid RSI materials for the Space Shuttle program. These rigid RSI materials are all fibrous bonded ceramics. They all are low density (0.12 to 0.35 gm/cm^3), extremely thermal-shock resistant, have high-temperature capability in excess of 1260°C and have very low thermal conductivities.

SPACE SHUTTLE RSI TILE SYSTEM

The tile system used on the Space Shuttle has been designed to meet many operational constraints. This cutaway drawing illustrates the various components of the system. Tiles are made of either pure silica fibers (LI-900 and LI-2200) or a composite of silica and aluminoborosilicate (FRCI) fiber. A Reaction Cured Glass coating (0.04 cm thickness) provides a handleable, high-emittance thermal control coatings. If undamaged, it is waterproof. Tiles are bonded with a silicone rubber to a Nomex felt strain isolation pad which in turn is bonded to the aluminum substrate. This strain isolation system prevents excessive thermal or mechanical stresses from being transferred from the rigid aluminum structure into the relatively fragile tiles. The silicone rubber adhesive and Nomex felt were chosen because they have maximum temperature capabilities in excess of 290°C and will not embrittle at temperatures as low as -56°C.

During development of the Space Shuttle Orbiter it became clear that a tougher system that would be less subject to debonding, more resistant to impact damage and have higher temperature capability than the original silica tiles was desirable. As a result of these perceived needs the LI-2200 (Ref. 3) was developed in the mid-seventies and the FRCI family of materials during the 1977-79 time period (Ref. 5 & 6). These materials have been implemented to correct design problems and to generally upgrade the system during development of the Shuttle Orbiter. The higher temperature stronger LI-2200 along with the adoption of a surface densification process for both LI-900 and LI-2200 helped correct a debonding problem discovered in late 1978 (Ref. 8). FRCI-20-12 will provide a weight savings over the earlier LI-2200 for certain areas of the Shuttle on the third and fourth orbiters.

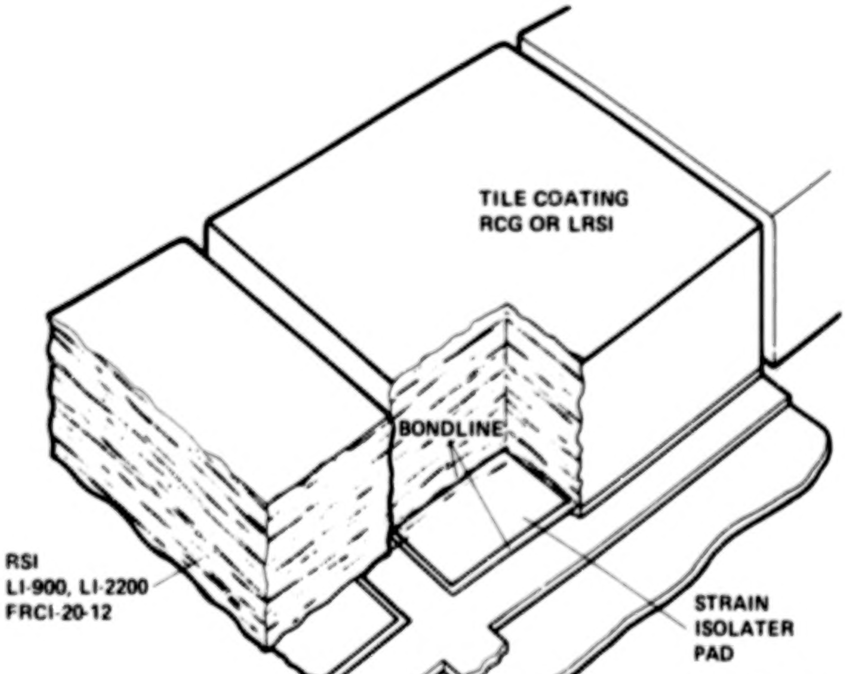

FRCI MANUFACTURING PROCESS

This figure illustrates the manufacturing process for FRCI. Silica fibers and aluminoborosilicate fibers are cleaned, mixed in deionized water to obtain a slurry, cast, dried, sintered and machined using numerically controlled machine tools to exact sizes. The tiles are then coated, dried and glazed with the appropriate ceramic coating, producing a fiber-fiber composite having controlled anisotropic properties. Strength and thermal conductivity in the plane perpendicular to the pressing direction are much higher than through the thickness, for instance.

Raw materials and processing parameters must be carefully controlled to obtain a reproducible product. The sintering temperature is typically controlled within ±10°C in order to be able to meet required density tolerances of ±10%. FRCI-20-12 is stable towards devitrification of the silica fibers at surface use temperatures above 1260°C as a result of both the careful control of the raw materials chemistry and the fiber to fiber ratios used.

As noted earlier, LMSC is now manufacturing FRCI-20-12 for the Space Shuttle Orbiters after Columbia. Pilot plant contracts have been let to make small quantities of FRCI-40-20 a newer, higher temperature, stronger version of the material.

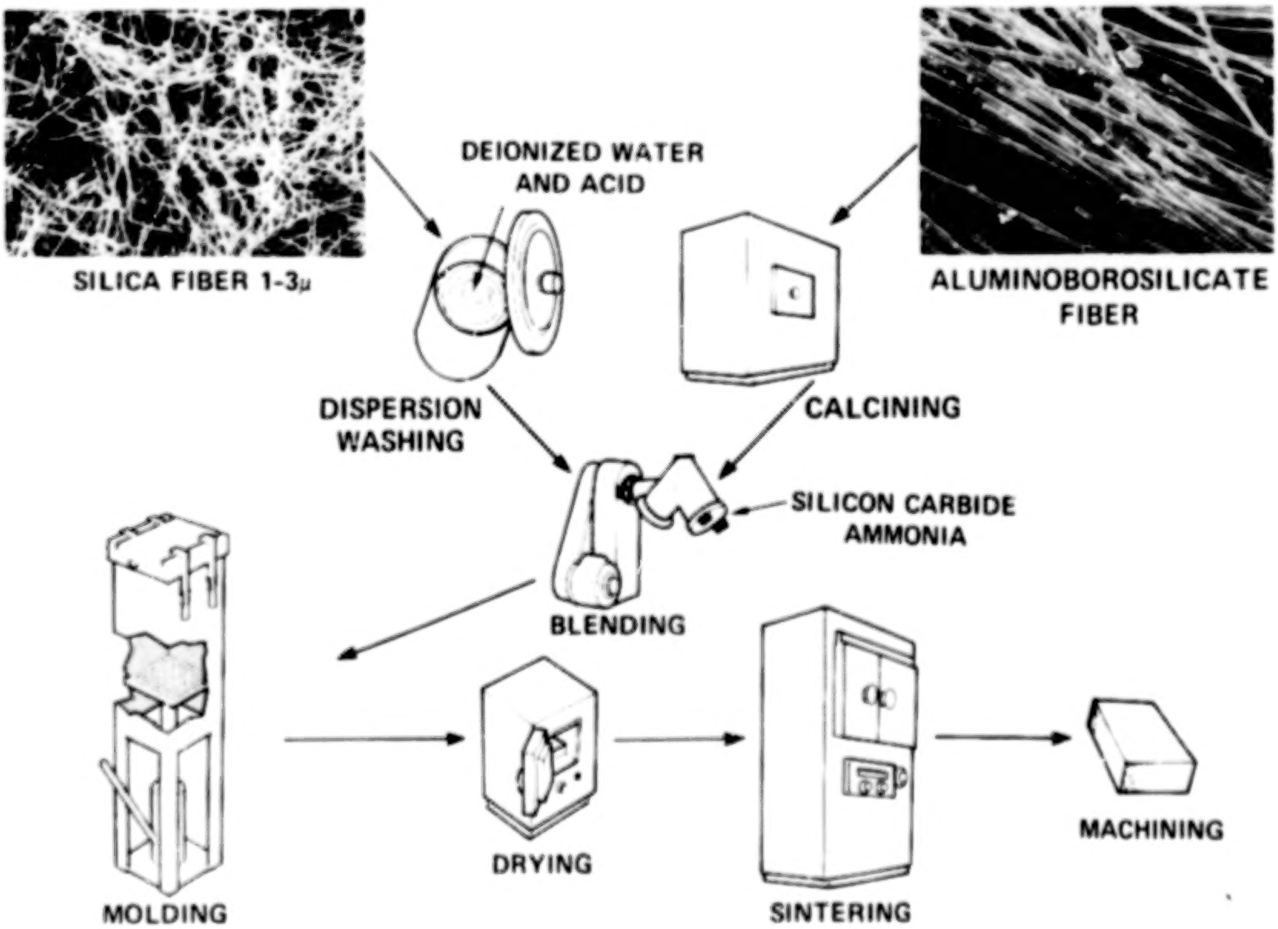
SILICA FIBER 1-3μ
DEIONIZED WATER AND ACID
ALUMINOBOROSILICATE FIBER
DISPERSION WASHING
CALCINING
SILICON CARBIDE AMMONIA
BLENDING
MOLDING
DRYING
SINTERING
MACHINING

MICROSTRUCTURAL COMPARISON OF SILICA

(LI-2200) AND COMPOSITE (FRCI-20-20) RSI

This figure compares the microstructure of FRCI to LI-2200. One can see that much better fiber bonding occurs in the FRCI as a result of the fluxing of the silica by boron oxide vaporized from the aluminoborosilicate fiber during sintering. This improved bonding causes FRCI to have much higher strength than LI-2200. Small diameter fibers contribute to the material having a relatively high strain to failure (>0.5%). These two properties plus the low thermal expansion coefficient of FRCI result in it having extraordinarily good resistance to thermal shock. Typically, dropping a piece of FRCI at 1260°C into liquid nitrogen will cause no damage.

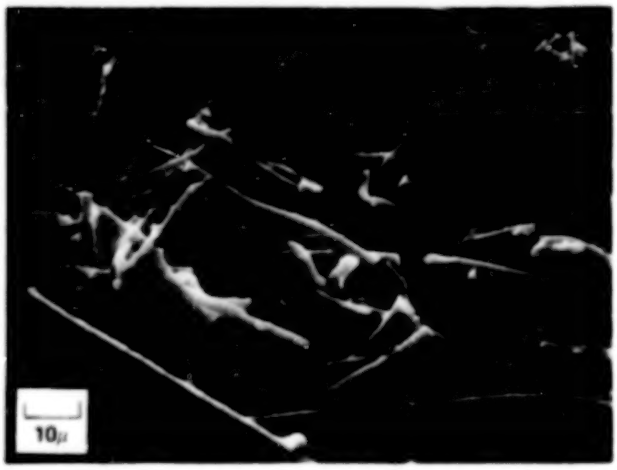

LI-2200 ρ = **0.352 g/cm^3 (22 lbm/ft^3)**

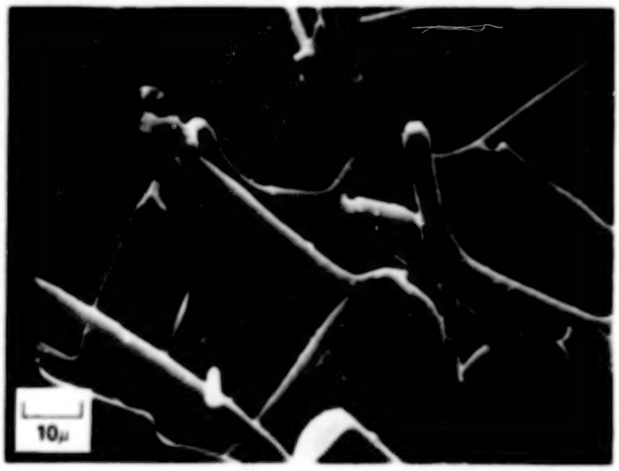

FRCI 20-20 ρ = **0.320 g/cm^3 (20 lbm/ft^3)**

COMPARISON OF TENSILE STRENGTH OF FRCI AND ALL SILICA MATERIALS

Average and minimum strength of FRCI-20-12 with LI-2200 and LI-900 in both in plane (strong) and through the thickness (weak) directions are shown. The important values for design are the minimums. FRCI-12 has a minimum 50% higher than LI-2200 and four times that of LI-900 even though its density is only 55% of LI-2200. These data demonstrate the important effect of improved bonding on strength.

Based on our experience with FRCI, which was the first fiber composite rigid insulation, studies are now being pursued to develop other such composites. These composites will have equivalent or improved strength and resistance to thermal shock with higher temperature capability. Materials with a continuous service capability of 1500 to 1650°C may be possible.

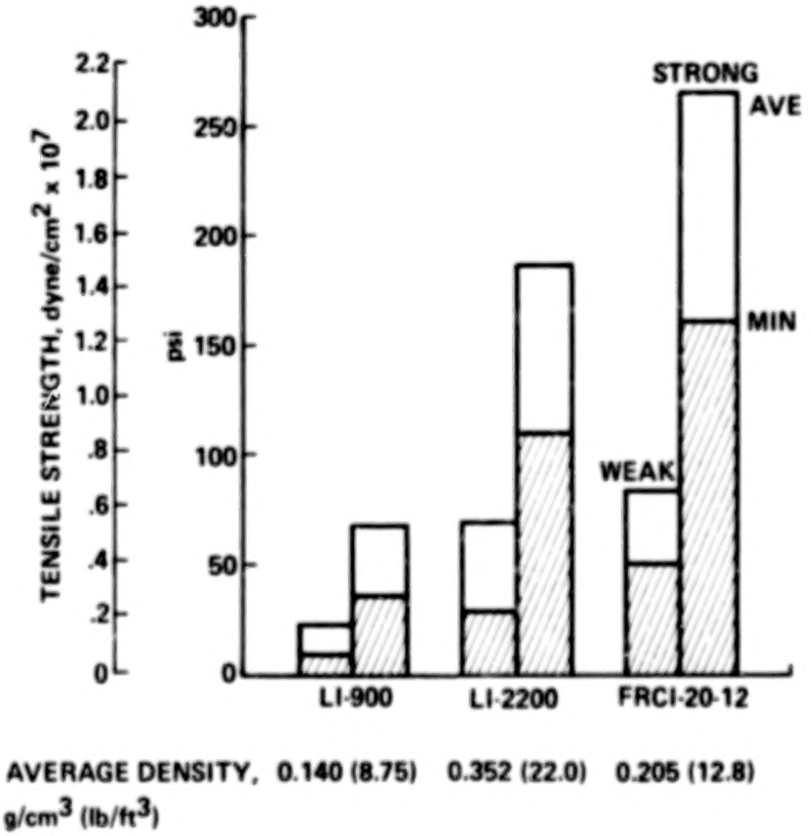

THERMAL CONDUCTIVITY OF FRCI COMPARED TO LI-900

The high temperature conductivity of both all silica RSI and FRCI is controlled by the average fiber diameter of the material. As this figure shows FRCI-20-12 has about a 10% higher thermal conductivity than LI-900. The difference exists because the aluminoborosilicate fibers are about 11 microns compared to 2-3 microns for silica. For practical purposes this difference in thermal conductivity is negligible since the uncertainty in the measurements is equivalent to the difference. Note also that the conductivity is both pressure and temperature dependent. At low pressure and high temperatures these materials have lower conductivities than any commercially available insulation with comparable temperature capability and density. No rigid commercial material has equivalent thermal shock resistance.

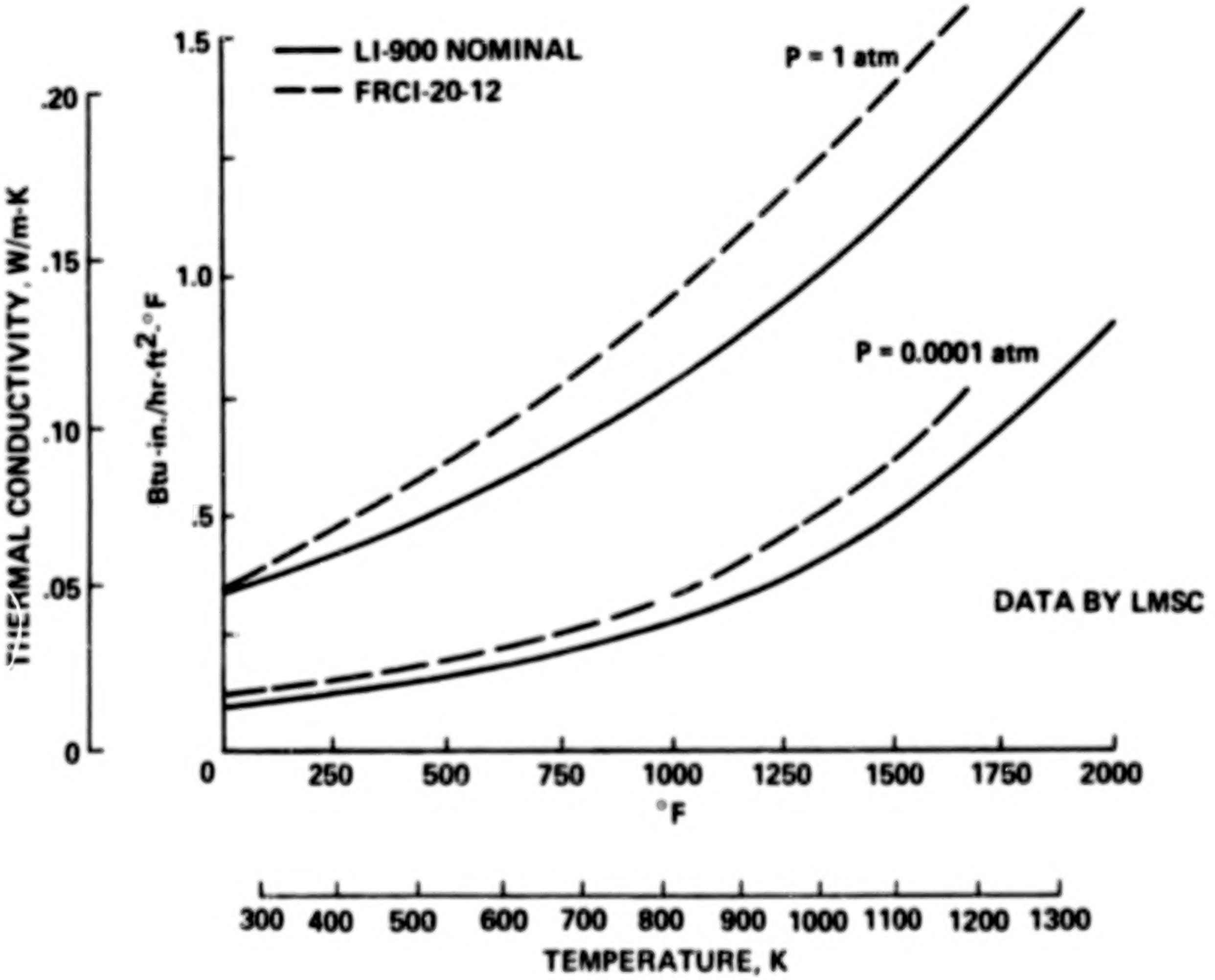

ADVANCED FLEXIBLE REUSABLE SURFACE INSULATION (AFRSI)

AFRSI is a quilt like material made of two layers of glass cloth with a layer of fibrous silica felt between them. The quilt, which varies in thickness from one to five centimeters, is sewn together with silica glass thread. It has a temperature capability in excess of 650°C. Similar materials have been used for many years to insulate jet engines.

AFRSI was conceived in 1975 as a result of test failures with the commercially available flexible ceramic insulations in simulated Space Shuttle launch environments. Shuttle launch acoustics, rain and aeroconvective heating were so severe that no commercial material could totally meet the requirements. Since the AFRSI concept is similar to commercial materials it could be manufactured using existing equipment and technology. Between 1975 and 1979 a series of arc plasma and wind tunnel tests and laboratory studies were performed to evaluate and modify the materials. Successive improvements were made by the manufacturer, Johns-Manville, at Ames direction.

In 1979 AFRSI was adopted for the Shuttle. About two square meters were installed on the Columbia between flights 1 and 2. The Orbiter maneuvering systems (OMS) pods on the second Orbiter Challenger are insulated with it and nearly all white tiles (approximately $185m^2$) will be replaced with it on Orbiters Discovery and Atlantis.

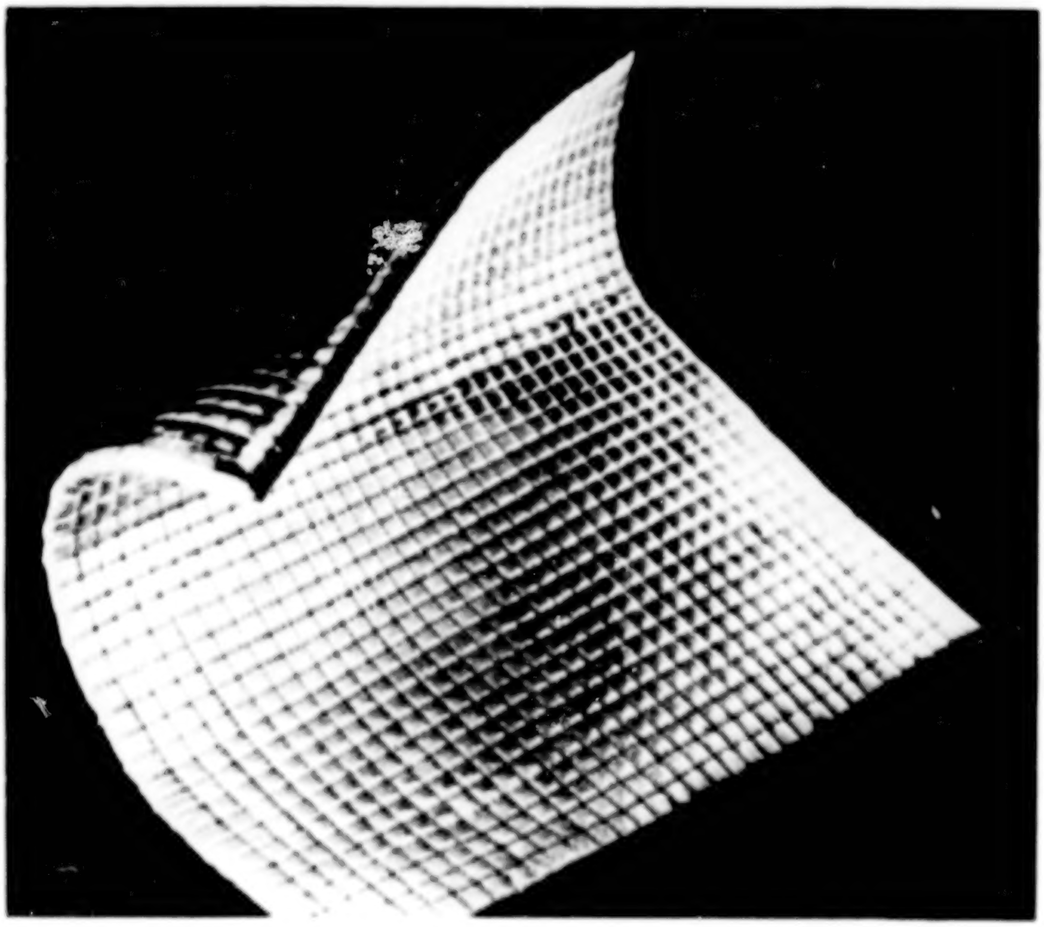

AFRSI CONSTRUCTION

The ARFSI external cover is 570 or 593 silica cloth. A fiberglass cover is used on the internal surface which is then bonded to the Shuttle skin with silicone resin. It is filled with silica fiber felt, having an effective density under 0.16 gm/cm^3. The composite is sewn together with Q-24 silica thread and treated with a silicone water repellent so that it will remain waterproof after long term exposure to surface temperatures above 600°C.

Transonic flow tests showed that heavy thread and relatively stiff cloth were required for AFRSI to survive the launch aeroacoustic environment. The failure mechanism for earlier versions was breaking of the sewing thread which allowed flutter of the outer cloth until the whole cover tore away. The failure mechanism with the current components is slow abrasion of the outer cloth which is easily seen before there is any risk of a catastrophic failure.

Temperature capability of AFRSI depends on the choice of cloth and thread, and the overall sequence of environments to which it is exposed. The original goal was to survive in excess of 650°C for 100 atmospheric entries after exposure to weathering on the launch pad and the orbital environment. Sequenced environmental testing has shown that current AFRSI has a maximum multiple use temperature of 750°C. Single use temperature is in excess of 1000°C.

AFRSI does not transmit stresses because of its construction and is totally resistant to thermal shock. Design of a load carrying structure using this material is much easier then with rigid RSI because strain compatibility with the substrate is not a concern.

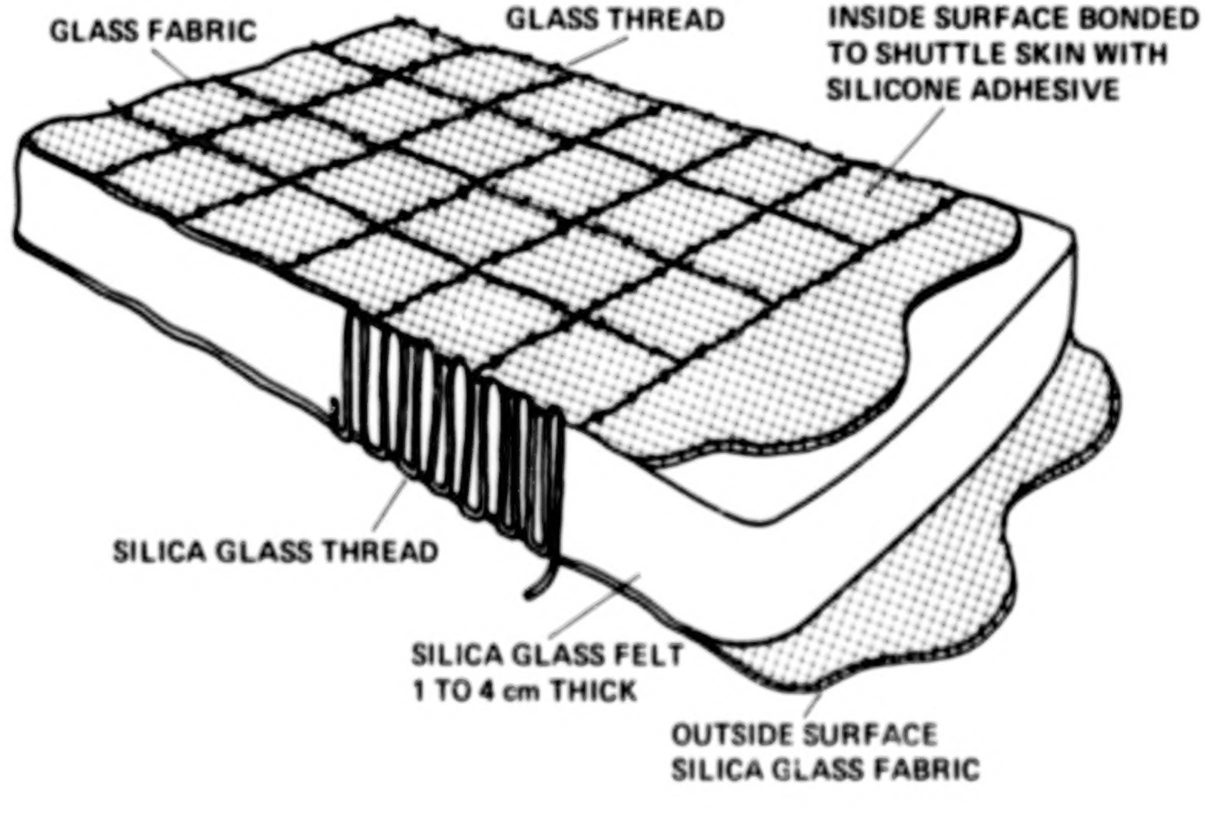
GLASS FABRIC
GLASS THREAD
INSIDE SURFACE BONDED TO SHUTTLE SKIN WITH SILICONE ADHESIVE
SILICA GLASS THREAD
SILICA GLASS FELT 1 TO 4 cm THICK
OUTSIDE SURFACE SILICA GLASS FABRIC

THERMAL CONDUCTIVITY OF AFRSI

The thermal conductivity of AFRSI is essentially equivalent to that of rigid RSI because the same silica fiber is used in both. Conductivity at low pressures and high temperatures is exceptionally low. AFRSI optical properties can be easily tailored by coating, impregnating or changing the surface cloth to an appropriately opacified glass, without degrading temperature capability. This ability to tailor the properties should contribute to the potential for commercial applications.

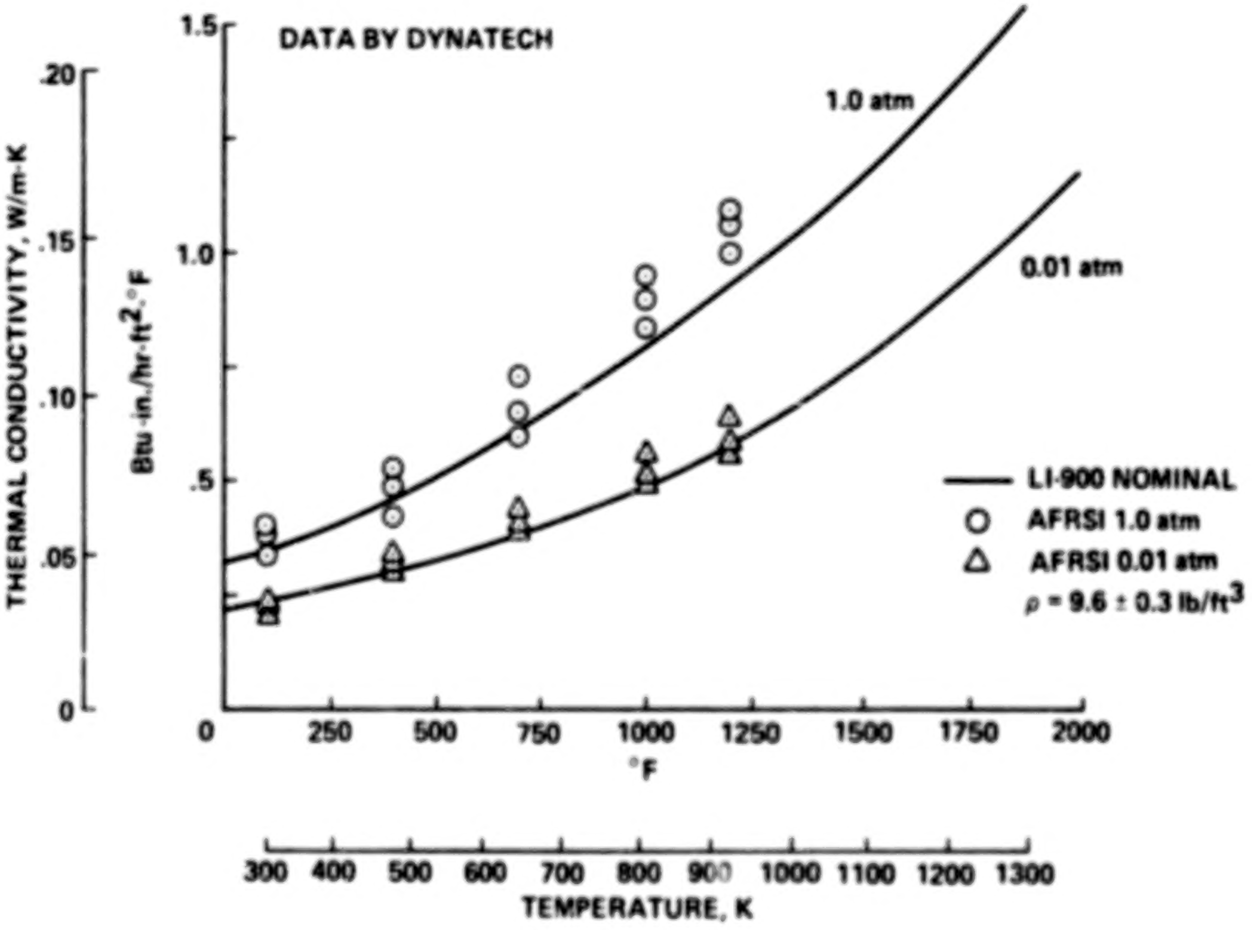

CONCLUSION

New high technology fibrous ceramic insulators have been developed. These materials have unique properties in terms of thermal conductivity, resistance to thermal shock, temperature capability and controlled density. It is probable during the next few years that less expensive versions of these materials will become available in the marketplace, as applications develop to utilize their unique characteristics.

At Ames we are committed to advancing this technology by developing higher temperature, higher strength rigid fibrous ceramic insulation materials for use on advanced Space Transportation Systems. The goal for second generation flexible heat shield materials will be to have higher temperature capability and more resistance to the aeroacoustic environment experienced in transonic, supersonic and hypersonic flight regimes. It may be feasible to design these materials so that the drag and lift characteristics can be optimized in the flight regime of interest. The current materials are the benchmark on which we will base our future research. For the use of space to become truly economical future thermal protection systems must become less exotic, cheaper, and tougher. In the next decade we hope to provide materials to accomplish these goals.

REFERENCES

1. Larson, H. K., Centolanzi, F. J., Vojvodich, N. S., Goldstein, H. E., Covington, M. A., and Matting, F. W. Environmental Testing for Evaluation of Space Shuttle Thermal Protection Materials and Systems. NASA TMX-2273, Vol. II, Paper 10. Presented at NASA Space Shuttle Technology Conference, March 1971.

2. Goldstein, H. E., Leiser, D. B., Katvala, V. Reaction Cured Borosilicate Glass Coating for Low Density Fibrous Silica Insulation. Presented June 7, 1977 at the Boron in Glass Ceramics Conference, Alfred University, Alfred, New York. Published in Borate Glass Structure, Properties, Applications, Plenum Publishing Company, 1978.

3. Goldstein, H. E., Leiser, D. B., Smith, M., and Stewart, D. A. Opacified Silica Reusable Surface Insulation (RSI) for Thermal Protection of the Space Shuttle Orbiter. Presented August 25, 1977 at the Fifteenth International Thermal Conductivity Conference, Ottawa, Canada. Published in Thermal Conductivity 15, Plenum Publishing Company, 1978.

4. Larson, H. K., Goldstein, H. E.. Space Shuttle Orbiter Thermal Protection Materials Development and Testing. Presented March 3, 1978 at the 4th Aerospace Testing Conference of the Institute of Environmental Sciences, Los Angeles, Calif.

5. Leiser, D. B., Smith, M., Goldstein, H. E. Developments in Fibrous Refractory Composite Insulation. Ceramic Engineering and Science Proceedings. Volume I, No. 7-8 (B) July-August, 1980.

6. Leiser, D. B., Smith, M., and Goldstein, H. E. Fibrous, Refractory Composite Insulation. NASA Case No. ARC 11169-1, April, 1978. Patent No. 4,148,962, April 10, 1979.

7. Beaseley, R. M., Izu, Y. D., et al. Fabrication and Improvement of LMSC's All-Silica RSI. Presented at NASA Symposium on Reusable Surface Insulation for Space Shuttle, NASA TMX-2719, Vol. I, Nov. 1972.

8. Korb, L. J., Morant, C. A., Calland, R. M., and Thatcher, C. S. The Shuttle Orbiter Thermal Protection System, Ceramic Bulletin, pp. 1188 to 1193, Vol. 60, No. 11, 1981.

RESEARCH ON ULTRA-HIGH-TEMPERATURE MATERIALS - MONOLITHIC CERAMICS, CERAMIC MATRIX COMPOSITES, AND CARBON/CARBON COMPOSITES

T. J. Miller and H. H. Grimes
NASA Lewis Research Center
Cleveland, Ohio

TRENDS IN HIGH-TEMPERATURE MATERIALS

Efficiency in heat engines is directly related to the maximum allowable operating temperatures of the materials used in the hot section of the engine. The impetus to increase engine efficiency and performance has led to continuing improvements in material use temperatures. Figure 1 shows the increase in material use temperatures over the past three decades for superalloys used for turbine blades. Today's high-temperature superalloys can be used at temperatures up to approximately 2000° F without cooling. With cooling and the application of thermal barrier coatings, the superalloy operating temperatures can be increased somewhat. However, to permit significant increases in operating temperatures, new classes of materials will be required.

The Lewis Research Center (Lewis) is conducting research on three classes of materials that show potential for significant increases in operating temperatures. Another common advantage of these materials is that they contain readily available raw materials. These materials, monolithic ceramics, ceramic matrix composites, and carbon/carbon composites, are defined as follows:

Monolithic ceramic: a brittle, high-strength, refractory material composed of metallic and nonmetallic atoms. The materials being studied at Lewis are silicon carbide and silicon nitride.

Ceramic matrix composite: a ceramic matrix reinforced with high-strength ceramic filaments. The composites being studied at Lewis are silicon-carbide-reinforced silicon nitride, graphite, and silicon-carbide-reinforced oxide glasses.

Carbon/carbon composite: a carbon matrix reinforced with a carbon or graphite filament. The reinforcements can be either single-filament yarns or a woven cloth.

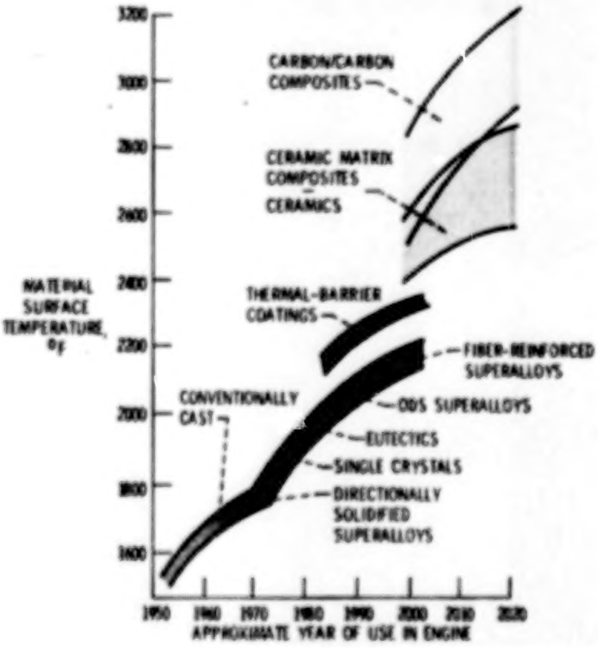

Figure 1

OVERVIEW OF ULTRA-HIGH-TEMPERATURE MATERIALS

The three classes of materials discussed in this paper offer the common advantages of the potential for significant increase in operating temperatures and the use of readily available materials. They also have other potential benefits and liabilities, which are summarized in figure 2.

Of the three materials dicussed in this paper, the most work has been done on monolithic ceramics. Research on monolithic ceramics has been conducted for many years and several development programs have fabricated parts for engine testing made of these materials (refs. 1 to 3). The most recent efforts to develop ceramic components for heat engines are the Department of Energy-sponsored Ceramic Applications in Turbine Engines (CATE) and Advanced Gas Turbine (AGT) projects, which are managed by Lewis (refs. 4 to 12). The work to date on monolithic ceramics has shown that these materials have good high-temperature strength and good oxidation resistance, but they are brittle and currently have low reliability. Improving the reliability is the major challenge for monolithic ceramic materials. The range of maximum operating temperatures for monolithic ceramics is 2400° F to 3000° F.

Ceramic matrix composite materials show the potential for improved toughness while maintaining good high-temperature strength and oxidation resistance. The major challenge with ceramic matrix composites is the fabrication of a dense body with uniformly distributed fibers that results in the desired material properties. Despite considerable interest in these materials, they are still in very early stages of research. The maximum operating temperature for ceramic matrix composites is projected to be approximately 3000° F (ref. 13).

Carbon/carbon composite materials offer the potential for good strength and toughness at very high temperatures (up to 4500° F) (ref. 14). These materials also have a very low density, less than 25 percent of the density of superalloys and 50 percent of the density of monolithic ceramics and ceramic matrix composites. The major challenges associated with these materials are reduction of the long and costly processing times currently required and development of improved ways of oxidation prevention.

MATERIAL TYPE	MAJOR POTENTIAL BENEFITS	MAJOR LIABILITIES	MAXIMUM OPERATING TEMPERATURE
MONOLITHIC CERAMICS	GOOD HIGH TEMPERATURE STRENGTH • OXIDATION RESISTANCE	BRITTLENESS • LOW RELIABILITY	2400°F TO 3000°F
CERAMIC MATRIX COMPOSITES	GOOD HIGH TEMPERATURE STRENGTH • TOUGHNESS • OXIDATION RESISTANCE	FABRICATION	3000°F
CARBON/CARBON COMPOSITES	GOOD STRENGTH AT VERY HIGH TEMPERATURE • TOUGHNESS • LOW DENSITY	OXIDATION • FABRICATION	4500°F

Figure 2

STATUS OF MONOLITHIC CERAMIC MATERIALS

Research on monolithic ceramic materials has been under way for many years (ref. 1). During this time, these materials have demonstrated many desirable characteristics (refs. 2 and 3); some of these are listed in figure 3. The major drawback of monolithic ceramic materials is low reliability. Two curves are shown in figure 3 which compare the reliability of today's monolithic ceramic materials and metals. In each case, the curves represent a typical strength distribution for these materials. For the metal, shown as a dashed line, a narrow range of strengths is indicated. Correspondingly, the strength of each component of the metal varies slightly from the average strength of the sample. One measure of this deviation in strength is the Weibull modulus(m). A high Weibull modulus corresponds to a material with a small strength deviation from the average. A Weibull modulus typical for a metal is approximately 40.

The distribution of strengths for current monolithic ceramics is represented in figure 3 as a solid line. The strength of each component of this material varies widely from the average strength of the sample. The Weibull modulus for current ceramic materials is approximately 10, which corresponds to a low material reliability. The low reliability results from a combination of the inherent brittleness of the material and the inclusion of very small flaws (20 to 50μm) in the material that can initiate failure. These flaws are introduced into the material as inclusions, voids, or surface defects during the processing of the material. The improvement of reliability is the focus of the Lewis research effort for monolithic ceramic materials.

CERAMIC MATERIALS HAVE DEMONSTRATED:

- ***GOOD HIGH TEMPERATURE STRENGTH***
- ***GOOD OXIDATION RESISTANCE***
- ***GOOD EROSION RESISTANCE***
- ***NET SHAPE FABRICATION CAPABILITY***

BUT

- ***LOW RELIABILITY***

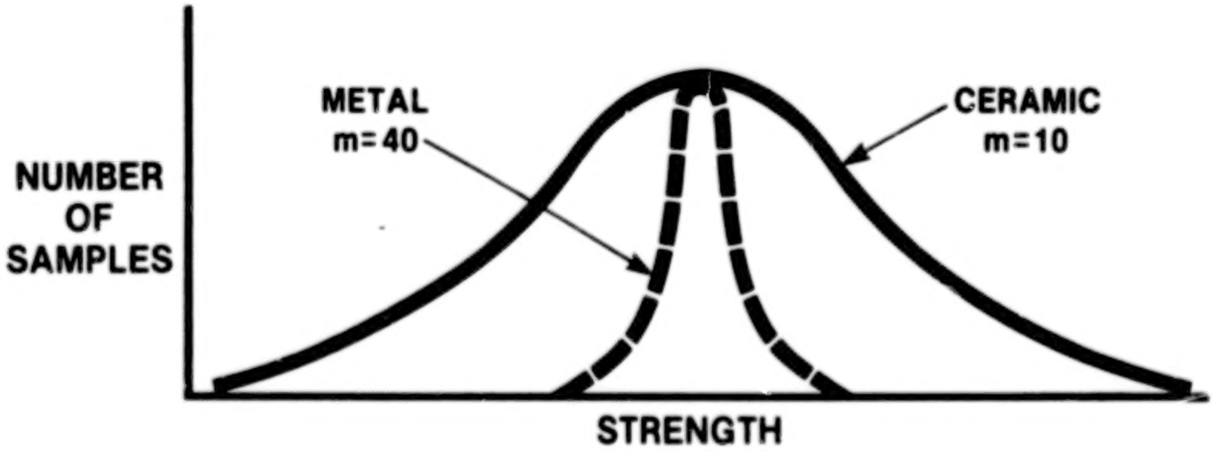

Figure 3

MONOLITHIC CERAMIC MATERIAL PROCESSING

A simplified diagram for the processing of monolithic ceramic materials is shown in figure 4. These materials require an ultra-fine (submicrometer size particle) starting powder. This powder is currently obtained by grinding or milling coarser commercial powders (e.g., silicon carbide or silicon nitride) until the required particle size is achieved. Sintering additives are required in the processing of these materials to achieve a fully dense final part. These additives must be thoroughly blended with the starting powders. Typical sintering aids for silicon nitride are refractory oxides (i.e., yttria); aids for silicon carbide are boron and carbon.

To make a part or shape of this material, several processes can be applied to form a green (unsintered) body. Some of the processes currently being used to make parts of ceramic materials are isopressing, injection-molding, and slip-casting. Parts can also be made by hot-pressing, but they usually require considerable grinding to achieve final shape; this process can be very expensive.

The next step in processing is densification of the green body to a fully dense part. Two of the processes that are used for densification are sintering and hot isostatic pressing (HIPing). Sintering is the application of high temperature to densify the part. Hot isostatic pressing is the application of both high temperature and very high pressure to densify the part. During this densification process a linear shrinkage in the part of approximately 17 percent (typical for sintered material) can result. The result of these process steps is a fully dense monolithic ceramic body.

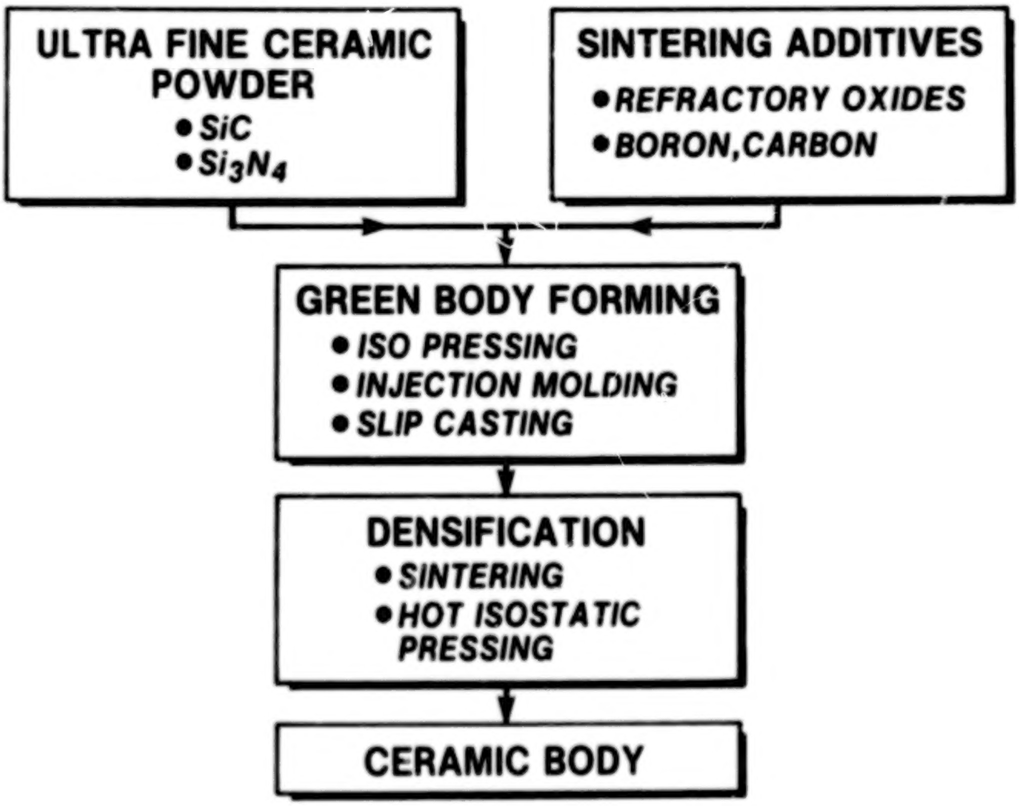
ULTRA FINE CERAMIC POWDER
• SiC
• Si3N4
SINTERING ADDITIVES
• REFRACTORY OXIDES
• BORON, CARBON
GREEN BODY FORMING
• ISO PRESSING
• INJECTION MOLDING
• SLIP CASTING
DENSIFICATION
• SINTERING
• HOT ISOSTATIC PRESSING
CERAMIC BODY

Figure 4

LEWIS MONOLITHIC CERAMIC RESEARCH PROGRAM

The objective of the Lewis Monolithic Ceramics Research Program is to develop technology for ceramic materials with improved reliability by understanding the interrelationships between starting powder, densification process, microstructure, and properties. This program is shown schematically in figure 5. The materials included in the program are sintered silicon carbide (SSC), sintered silicon nitride (SSN), and sintered-reaction-bonded silicon nitride (SRBSN). The major emphasis in the program is densification; however, the program also includes powder processing, nondestructive evaluation, and material evaluations.

Starting powders and sintering aids are obtained from commercial sources and are ground and blended together to achieve an ultra-fine powder with uniformly distributed sintering aids. Test bars are prepared and processed through one of the two densification processes selected for study - hot isostatic pressing (HIPing) and high N_2 pressure sintering. Each of these densification processes will be further described later in this paper. Nondestructive evaluation of the test bars is performed at selected steps in the processing to identify the source of flaws introduced into the bars. Selected material evaluations (strength, microstructure evaluation, distribution of strength, and fractographic analysis) are then conducted to determine the effect of changes in processing parameters on the fully dense ceramic test bars.

This program is iterative and provides feedback at each processing step to identify the most significant parameters that affect the reliability of monolithic ceramic materials.

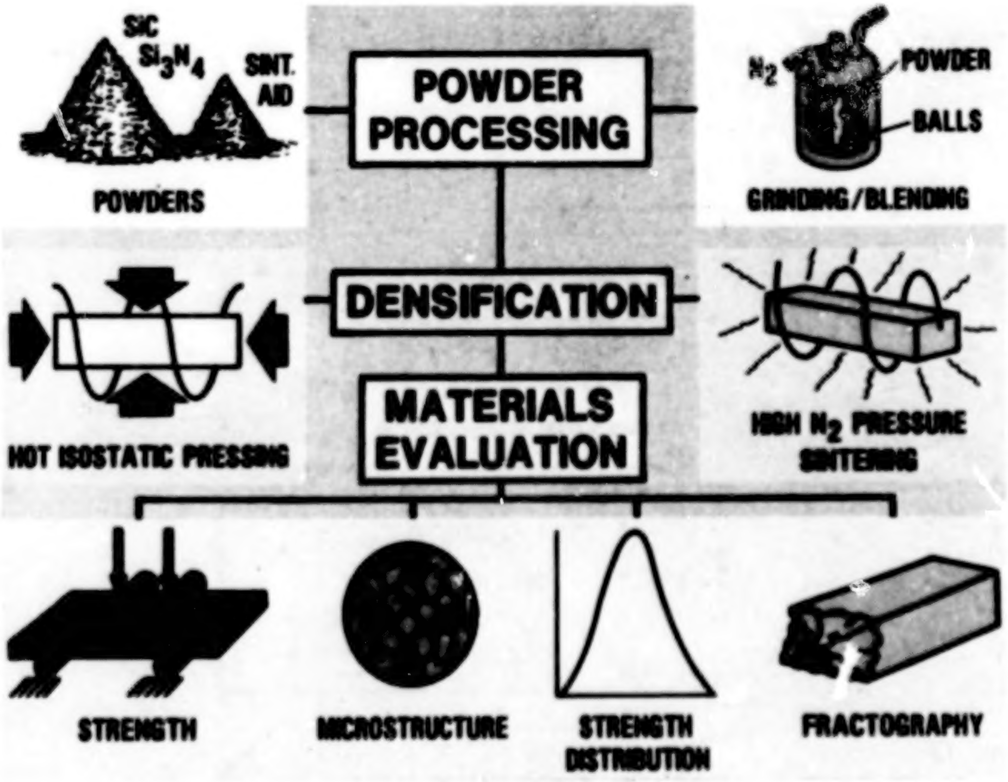
SiC
Si_3N_4
SINT. AID
POWDERS
POWDER PROCESSING
N_2
POWDER
BALLS
GRINDING/BLENDING
DENSIFICATION
HOT ISOSTATIC PRESSING
MATERIALS EVALUATION
HIGH N_2 PRESSURE SINTERING
STRENGTH
MICROSTRUCTURE
STRENGTH DISTRIBUTION
FRACTOGRAPHY

Figure 5

LEWIS MONOLITHIC CERAMIC RESEARCH APPROACHES TO DENSIFICATION

As discussed earlier, densification is the major emphasis of the Lewis Monolithic Ceramics Research Program. The two approaches to densification in the program are HIPing and high N_2 pressure sintering. Lewis has facilities, shown in figure 6, for conducting both of these densification processes.

HIPing is a process that uniformly applies very high temperatures and pressure to the part being processed. The Lewis HIP unit has been designed to operate at the very high temperatures necessary for ceramic materials. The unit is capable of a maximum operating temperature of 3990° F and a maximum operating pressure of 20 000 psi using argon gas as the pressure medium. HIPing studies are being conducted on SSC and SRBSN. The results of the early HIPing studies conducted to date at Lewis are presented in reference 15.

High N_2 pressure sintering is a process that uniformly applies nitrogen pressure and very high temperatures to the part being processed. The Lewis high N_2 pressure sintering unit is capable of up to 1000 psi nitrogen pressure and 3720° F temperature. This process is particularly effective for silicon nitride materials because it permits higher sintering temperatures and lower levels of sintering aids to be used.

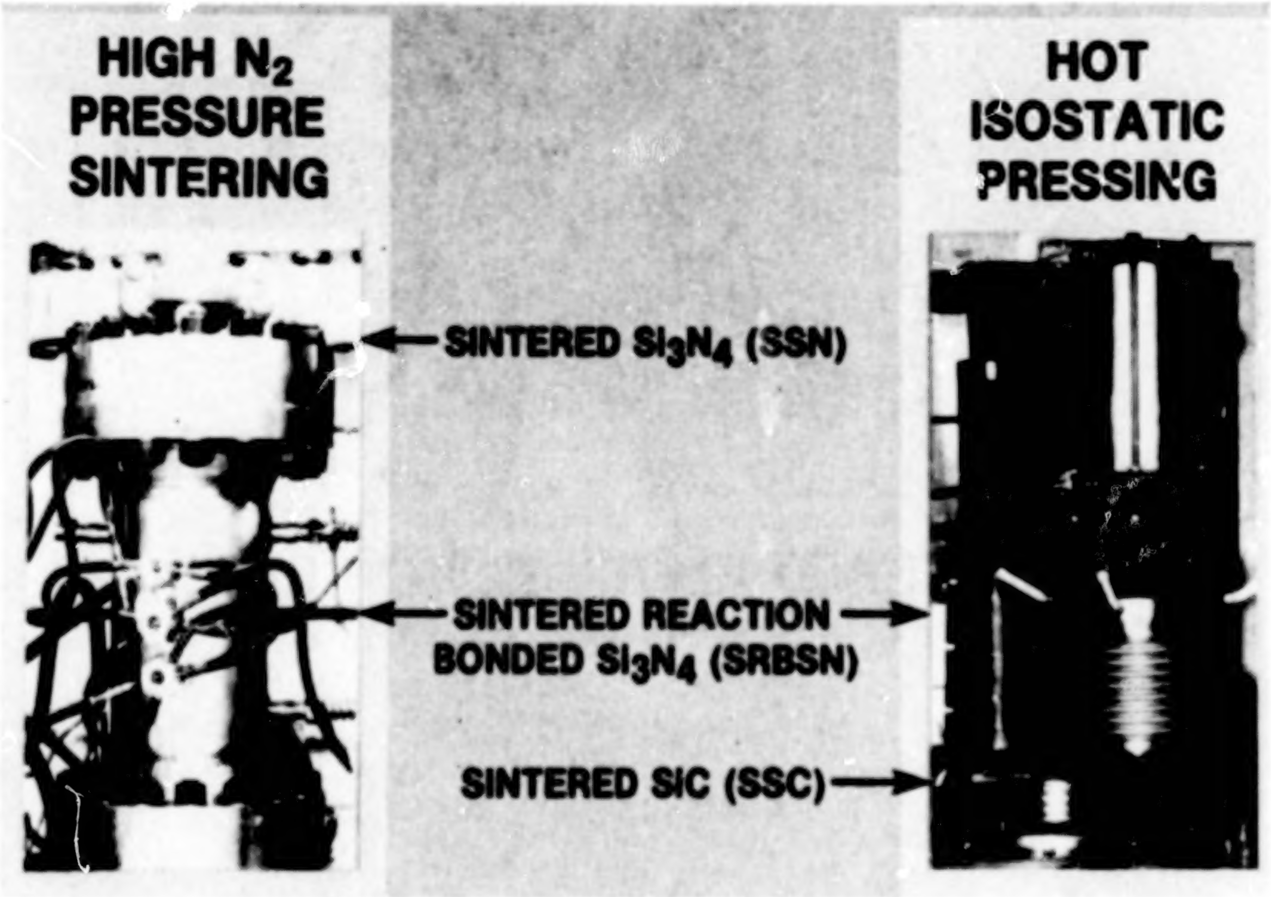
HIGH N2 PRESSURE SINTERING
HOT ISOSTATIC PRESSING
SINTERED Si3N4 (SSN)
SINTERED REACTION BONDED Si3N4 (SRBSN)
SINTERED SiC (SSC)

Figure 6

MONOLITHIC CERAMIC RADIAL TURBINE ROTOR

Monolithic ceramic gas turbine components are currently being developed in the CATE and AGT projects (refs. 4 to 12). As an example of current fabrication technology, figure 7 shows a ceramic radial turbine rotor that was made for this project by the Carborundum Company. This rotor is designed for a 100 hp automotive gas turbine engine. This 6-inch-diameter rotor is made of sintered silicon carbide by injection-molding and meets the final dimensional specifications (blade shape, blade thickness, tolerances, etc.) in the as-sintered state. Ceramic turbine rotors are also being developed for the AGT project by AiResearch Casting Company, Ford Motor Company, and GTE Laboratories.

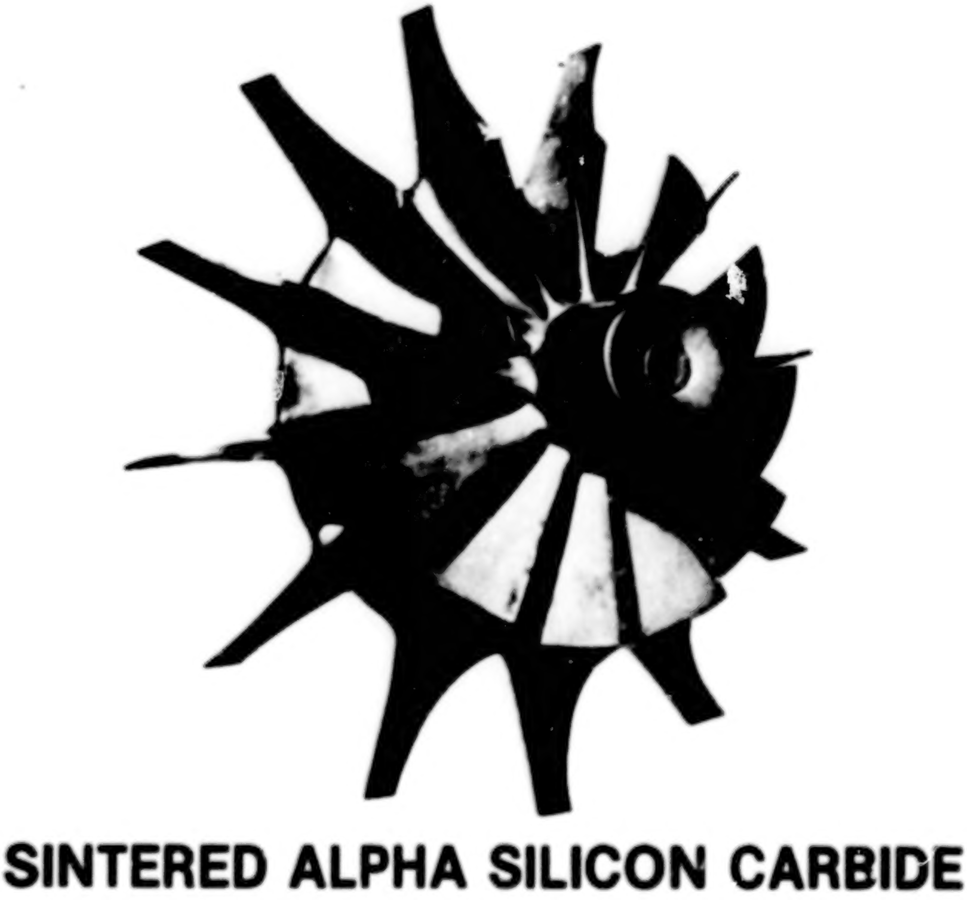

Figure 7

STATUS OF CERAMIC MATRIX COMPOSITES

Although monolithic ceramics offer potential for use in oxidative environments at high temperature, their brittleness may limit their use in certain structural applications. A promising approach to improving the toughness of brittle materials is reinforcement with fine filaments or fibers. The fibers contribute both to increased strain-to-failure of the material and to limited growth of fatal cracks. The success of this approach has recently been demonstrated by glass ceramic matrix composites produced by the United Technologies Research Center (ref. 13). These composites, which are comprised of lithium aluminum silicate (LAS) glass ceramic reinforced with silicon carbide fibers, show a nearly 10-fold improvement in fracture toughness over the unreinforced ceramic (fig. 8). The units of fracture toughness are ksi x $\sqrt{\text{in.}}$ in this figure. This improvement extends to temperatures over 2000° F, above which temperature the composite's utility is limited by the softening of the LAS glass ceramic.

Attempts to reinforce higher temperature ceramics have not been so successful (ref. 16), primarily due to fiber strength degradation related to:

1. fiber/matrix interactions at the higher fabrication temperatures;

2. recrystallization of the reinforcing fibers at these temperatures;

3. fiber fracture due to processing-induced abrasion and stresses.

CERAMIC MATRIX COMPOSITES OFFER—

- ***HIGH TEMPERATURE CAPABILITY***
- ***OXIDATION RESISTANCE***
- ***IMPROVED TOUGHNESS***

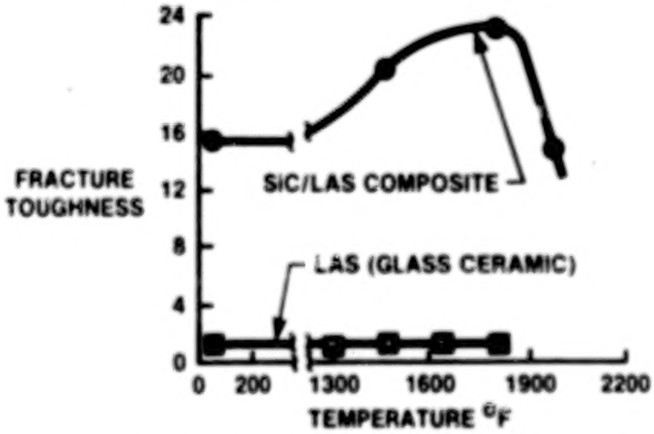

BUT, HIGHER TEMPERATURE CERAMIC MATRIX COMPOSITES DEGRADE DURING FABRICATION DUE TO—

- ***FIBER/MATRIX INTERACTIONS***
- ***FIBER RECRYSTALLIZATION***
- ***MECHANICAL TRAUMA***

Figure 8

STATUS OF CARBON/CARBON COMPOSITES

Carbon/carbon composites have shown good strength and toughness over an even wider temperature range (ref. 14). This material, however, which has a composition similar to a piece of coal, must be protected in oxidizing environments (fig. 9). Generally, this protection is achieved through the use of ceramic coatings. But, in applications where catastrophic oxidation of a component due to a failed coating would be intolerable, the oxidation rate may be retarded by the incorporation of oxidation-inhibiting materials into the matrix. Another major problem with carbon/carbon composites is the long repetitive processing required to prepare dense materials. These process times can exceed 800 hours and contribute significantly to the cost.

For both carbon/carbon and ceramic matrix composites, designs for optimum strength and toughness have not been possible because the fracture mechanisms and effects of composite parameters are poorly understood. The Lewis research program to study these composites addresses this problem, as well as the problems of fabrication, oxidation, and thermal stability.

CARBON/CARBON COMPOSITES OFFER—

- ***GOOD STRENGTH AT VERY HIGH TEMPERATURES***
- ***TOUGHNESS***
- ***LOW DENSITY***

BUT, PRESENT PROBLEMS WITH CARBON/CARBON INCLUDE—

- ***OXIDATION***
  - NEEDS COATINGS
  - INTRINSIC OXIDATION RESISTANCE
- ***FABRICATION***
  - LONG/REPETITIVE PROCESSING TO ACHIEVE DENSITY

Figure 9

HIGH TEMPERATURE NONMETALLIC COMPOSITE FABRICATION

A better understanding of the Lewis program may be gained by reviewing the fabrication processes of the two composite materials (fig. 10). Reinforcing filaments of silicon carbide, alumina, and carbon are all currently being prepared commercially from polymer precursors using conventional fiber-spinning plus a pyrolysis step. These small-diameter, high-strength filaments are flexible and can be spun and woven into yarn, cloth, or other preform shapes. Matrix materials in powder or gel forms, or precursor materials which can be converted to the final matrix material, can be introduced into the preforms at relatively low temperatures. The matrix is then densified either by sintering, hot-pressing, or chemical conversion of a precursor to a higher temperature material. However, because carbon melts at such a high temperature, the only practical method of preparation of a carbon matrix is by pyrolysis of a precursor. If extensive shrinkage occurs during the pyrolysis process, the infiltration/densification cycle will have to be repeated to obtain a dense composite body. This repetition, of course, contributes significantly to the processing time required.

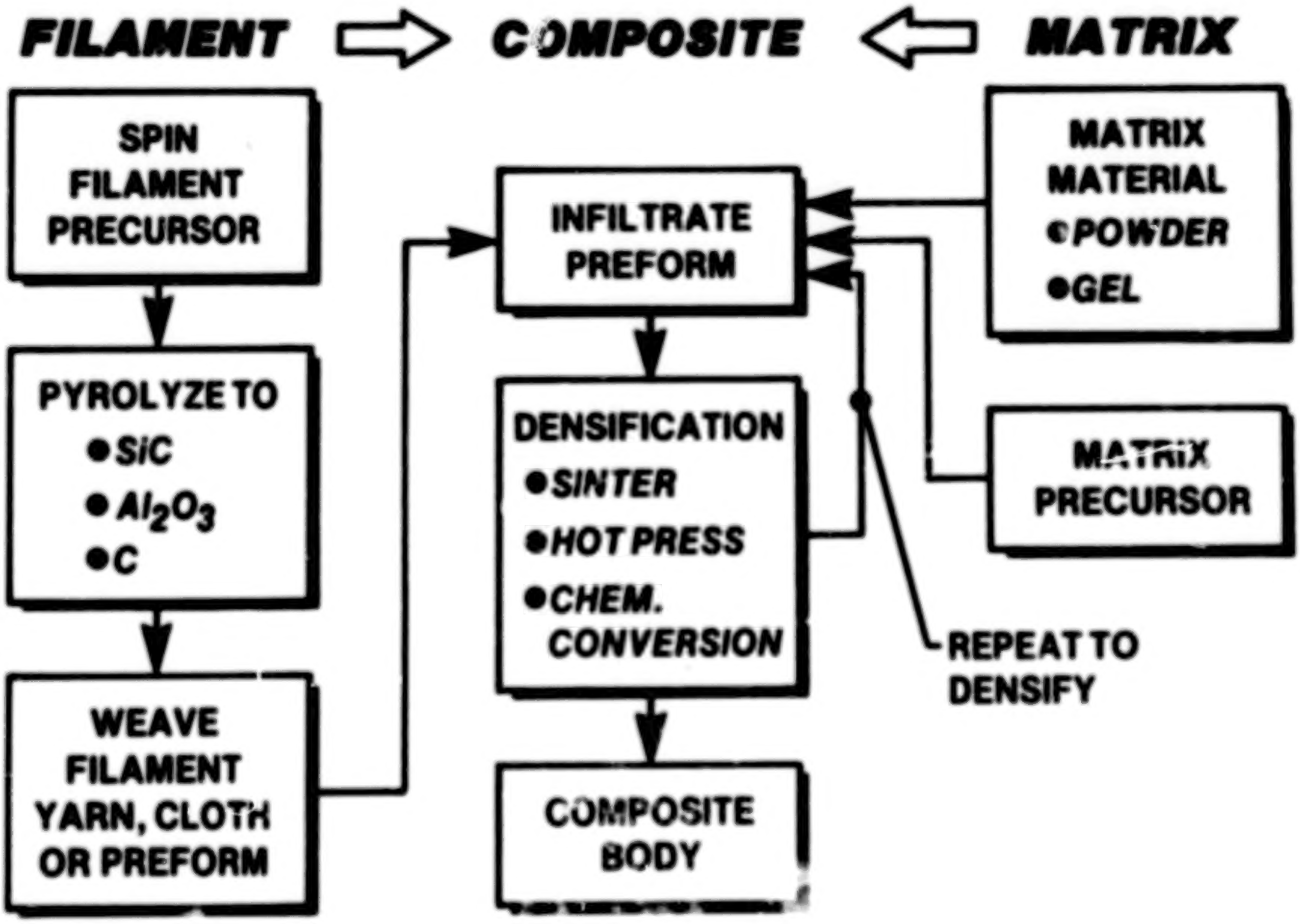
FILAMENT
COMPOSITE
MATRIX
SPIN FILAMENT PRECURSOR
PYROLYZE TO
●SiC
●Al₂O₃
●C
WEAVE FILAMENT YARN, CLOTH OR PREFORM
INFILTRATE PREFORM
DENSIFICATION
●SINTER
●HOT PRESS
●CHEM. CONVERSION
COMPOSITE BODY
MATRIX MATERIAL
●POWDER
●GEL
MATRIX PRECURSOR
REPEAT TO DENSIFY

Figure 10

LEWIS CARBON/CARBON AND CERAMIC MATRIX COMPOSITES RESEARCH PROGRAM

The Lewis carbon/carbon research program (fig. 11) seeks to reduce processing time and cost through development of more processible matrix precursors with improved char yields. The approach here is to find ways to prepare condensed carbon ring structures through more extensive in-situ crosslinking at lower temperatures. In addition, we will attempt to make these composites more oxidatively stable by incorporating oxidation inhibitors into the matrix through the use of modified polymer precursors. These inhibitors do not replace the need for coatings on the carbon/carbon structure, but rather they inhibit rapid oxidation if the coating should fail. Another research group in the Materials Division at Lewis is studying the coatings problem.

In our ceramic matrix composites program, we again address the processibility problem. The goal here is to fabricate silicon carbide filament-reinforced silicon nitride matrix composites via lower temperature methods. One approach is to produce silicon nitride by in-situ pyrolysis of polymer $(Si-N)_n$ compounds which have been deposited in a filament preform. Pyrolysis should occur at temperatures well below those at which degradation occurs between filament and matrix. This approach should also eliminate the traumatic effects of pressing. However, as with carbon/carbon composites, this processing may require repeated infiltration and densification to achieve a dense matrix. A second approach involving somewhat higher processing temperatures (but still below those required for hot pressing or sintering ceramics) involves the reaction of a porous silicon powder matrix with nitrogen to form silicon nitride. This reaction has been studied by ceramists at Lewis since it is also used to prepare monolithic reaction-bonded silicon nitride (refs. 17 and 18).

Another major element of the program is the study of the fracture behavior of brittle filament/brittle matrix composites. Few guidelines exist to help in the design of a carbon/carbon matrix composite for optimum strength and toughness. Our approach here is a systematic study of the fracture behavior of both classes of composites to determine the effects of the materials' properties, component size and geometry, and composite design. With this knowledge, we will develop analytical models which will permit optimization of composite strength and toughness. Computer models designed originally to provide similar understanding of metal matrix composites (ref. 19) are presently being modified to aid in this task.

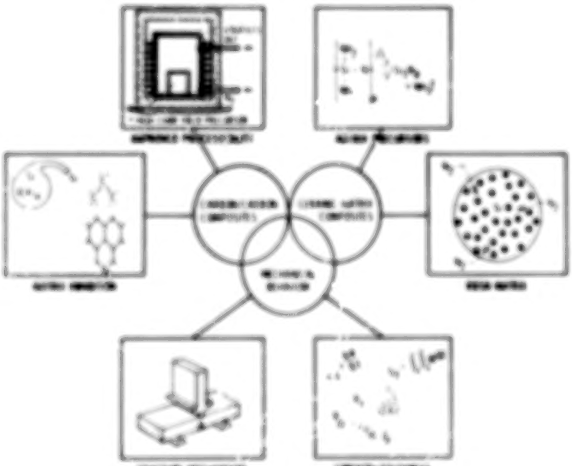

Figure 11

CARBON/CARBON COMPOSITES

An example of the state of the art in carbon/carbon composite applications is shown in figure 12. This figure shows a prototype carbon/carbon component made by General Electric Co. (private communication). The component is a one-piece bladed turbine rotor which, in service, would have to be coated to prevent oxidation. At the lower left is a representative coated carbon/carbon microstructure showing the reinforcing filaments aligned in several directions. At the top of this figure, the silicon carbide oxidation coating can be seen.

Other gas turbine engine applications for which carbon/carbon composites are being studied include exhaust nozzle flaps and seals, augmenters, combustors, and acoustic panels.

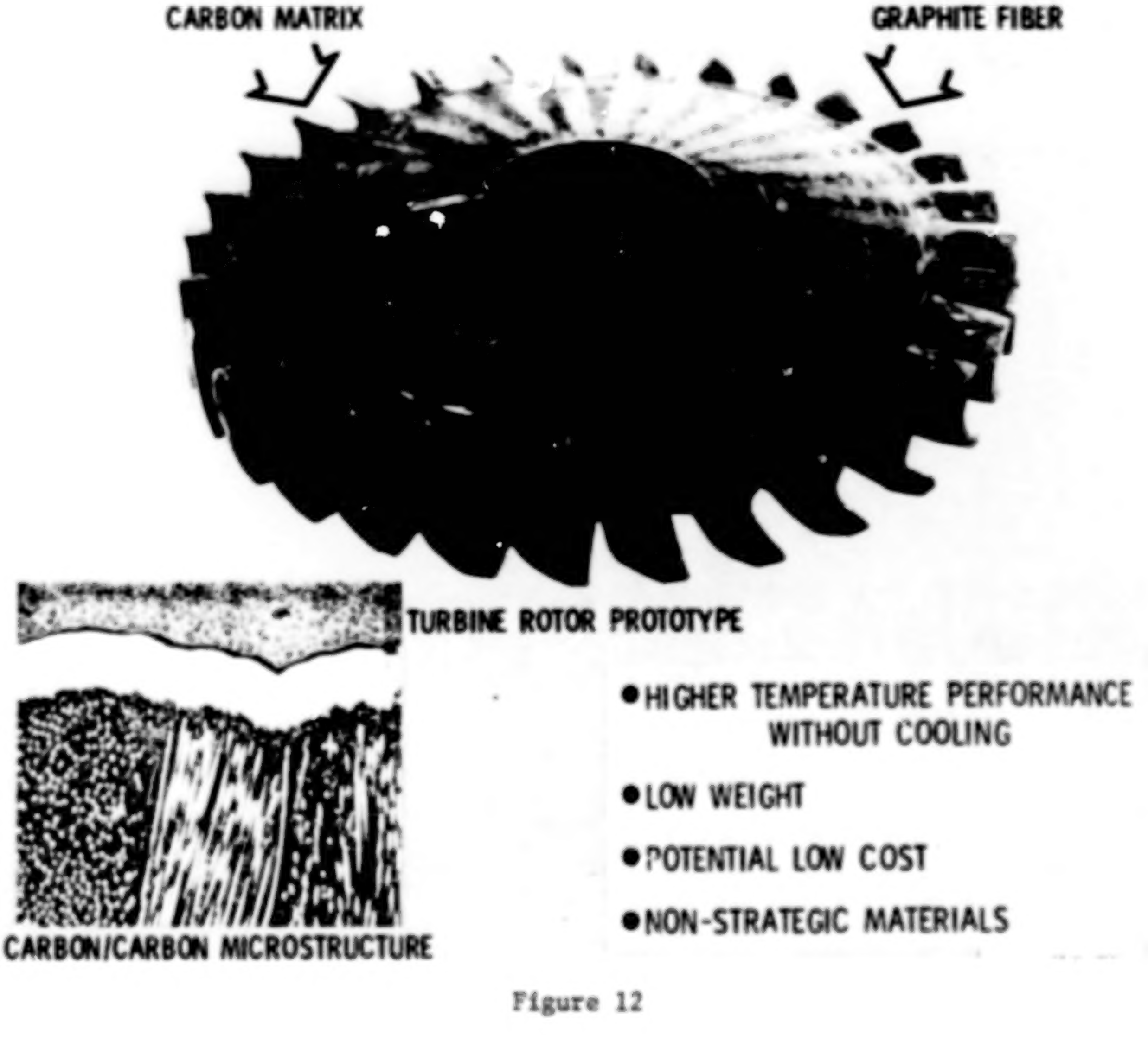

- HIGHER TEMPERATURE PERFORMANCE WITHOUT COOLING
- LOW WEIGHT
- POTENTIAL LOW COST
- NON-STRATEGIC MATERIALS

Figure 12

CERAMIC MATRIX COMPOSITES

The ceramic matrix composite technology is less developed than the carbon/carbon technology. The most mature ceramic matrix composite is probably the silicon carbide filament-reinforced glass ceramic (LAS) composite of United Technologies (ref. 13). This material is currently being considered for several applications in both the aerospace and automotive industries. The coupon shown in figure 13 is being studied for use in a divergent seal in the exhaust section of a gas turbine engine. This reinforced glass ceramic shows a factor of 2 to 5 times improvement in strength, and a factor of 4 to 10 times improvement in toughness over unreinforced glass ceramic. The improved toughness may be due, in part, to the fiber pullout seen in the fracture surface at the lower left.

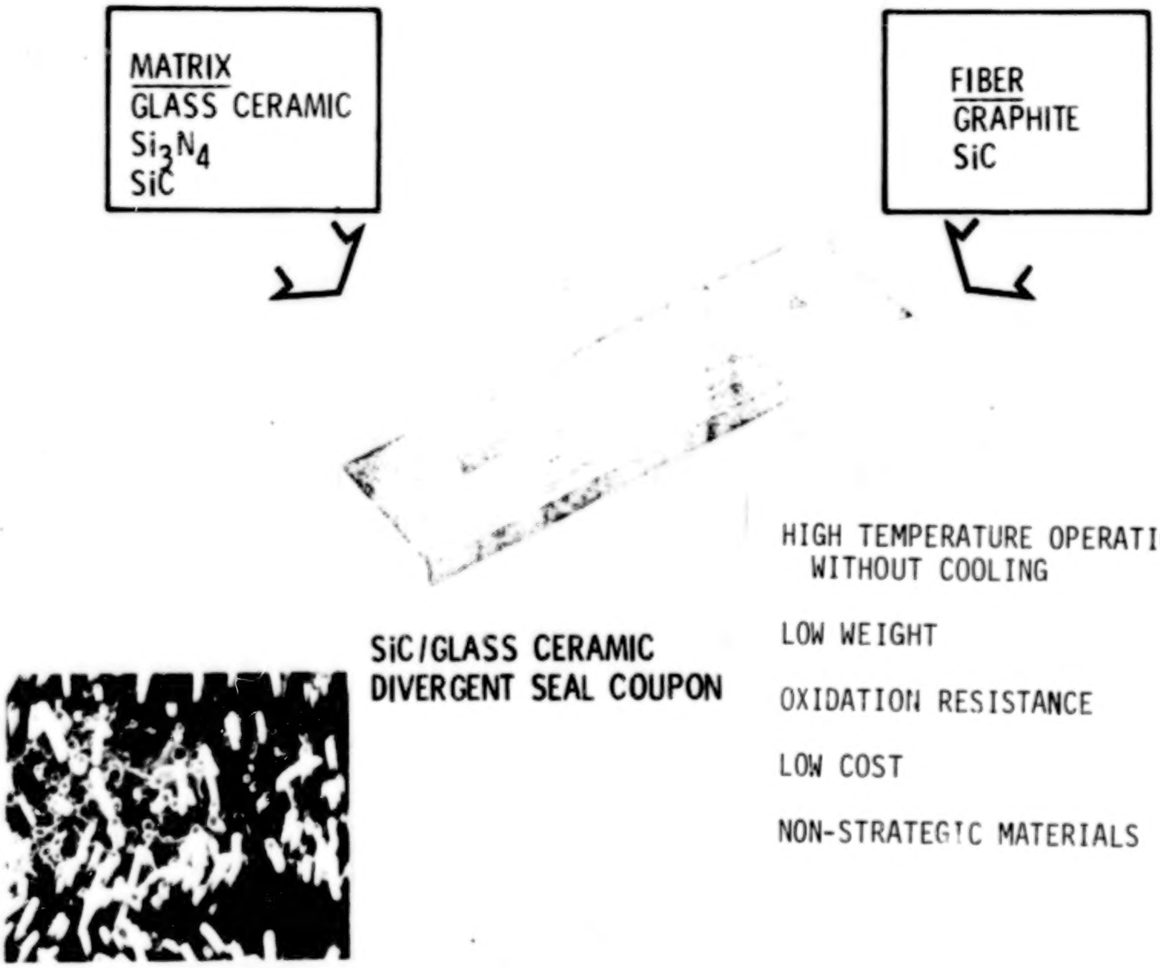

MATRIX
GLASS CERAMIC
Si_3N_4
SiC

FIBER
GRAPHITE
SiC

SiC/GLASS CERAMIC DIVERGENT SEAL COUPON

FRACTURE SURFACE

HIGH TEMPERATURE OPERATION WITHOUT COOLING

LOW WEIGHT

OXIDATION RESISTANCE

LOW COST

NON-STRATEGIC MATERIALS

Figure 13

CONCLUDING REMARKS

Monolithic silicon carbide and silicon nitride, silicon-carbide-reinforced silicon nitride composites, and coated carbon/carbon composites offer potential as very-high-temperature structural materials for a variety of aerospace and terrestrial applications. The Lewis research program focuses on the key challenges that must be met to realize the potential benefits of these materials. Application of these materials will improve the efficiency and performance of heat engines, while reducing the requirements for strategic materials in superalloys.

REFERENCES

1. Rice, R. W.: An Assessment of the Use of Ceramics in Heat Engines. NRL Memorandum Report 4499, 1981.

2. Katz, R. N.: Ceramics for Vehicular Engines: State of the Art. AMMRC MS 80-2, 1980.

3. McLean, A. F.: Ceramic Technology for Automotive Turbines. Ceramics Bulletin, vol. 61, no. 8, 1982, pp. 861, 865, 871.

4. Hudson, S. M.; et al.: Ceramic Applications in Turbine Engines. Progress Report for Period 1, July 1979 to 31 December 1979. (Detroit Diesel Allison; NASA Contract DEN3-17). NASA CR-159865, 1980.

5. Byrd, J. A.; et al.: Ceramic Applications in Turbine Engines. Progress Report for Period 1, January 1980 to 30 June 1980. (Detroit Diesel Allison; NASA Contract DEN3-17). NASA CR-165197, 1980.

6. Rackley, R.; et al.: Advanced Gas Turbine (AGT) Powertrain System Development for Automotive Applications. Progress Report Number 1 (October 1979 - June 1980). (AiResearch Manufacturing Company of Arizona; NASA Contract DEN3-167). NASA CR-165175, 1980.

7. Helms, H. H.; et al.: Advanced Gas Turbine (AGT) Powertrain System Development for Automotive Applications. First Semiannual Report (October 1, 1979 - June 30, 1980). (Detroit Diesel Allison; NASA Contract DEN3-168). NASA CR-165178, 1981.

8. Helms, H. H.; et al.: Advanced Gas Turbine (AGT) Powertrain System Development. Second Semiannual Report (July 1, 1980 - December 31, 1980). (Detroit Diesel Allison; NASA Contract DEN3-168). NASA CR-165504, 1981.

9. Rackley, R.; et al.: Advanced Gas Turbine (AGT) Powertrain System Development for Automotive Applications. Second Semiannual Progress Report (July 1980 - December 1980). (Garrett Turbine Engine Company; NASA Contract DEN3-167). NASA CR-165329, 1981.

10. Byrd, J. A.; et al.: Ceramic Applications in Turbine Engines. Progress Report for Period 1, July 1980 to 31 December 1980. (Detroit Diesel Allison; NASA Contract DEN3-17). NASA CR-165494, 1981.

11. Helms, H. H.; et al.: Advanced Gas Turbine (AGT) Power Train System Development. Third Semiannual Report (January 1, 1981 - June 30, 1981). (Detroit Diesel Allison; NASA Contract DEN3-168). NASA CR-165504, 1981.

12. Helms, H. H.; et al.: Advanced Gas Turbine (AGT) Power Train System Development. Fourth Semiannual Report (July 1, 1981 - December 31, 1981). (Detroit Diesel Allison; NASA Contract DEN3-168). NASA CR-167875, 1982.

13. High Temperature Metal and Ceramic Matrix Composites for Oxidizing Atmosphere Applications. National Materials Advisory Board Report, NMAB-376, 1981.

14. Delmonte, J.: Technology of Carbon and Graphite Fiber Composites. Van Nostrand Reinhold Company, New York, 1981.

15. Watson, G. K.; and Moore, T. J.: Hot Isostatic Pressing of Structural Ceramics at NASA. To be published in the Nineteenth Summary Report of Automotive Technology Contractor's Coordination Meeting, October 1982.

16. Fairbanks, J. W.; and Rice, R. W.: Proceedings of the 1977 DARPA/NAVSEA Ceramic Gas Turbine Demonstration Engine Program Review. Battelle Metals and Ceramics Information Center, MCIC-78-36, 1977.

17. Herbell, T. P.; and Glasgow, T. K.: Developing Improved Reaction Sintered Silicon Nitride. 15th Summary Report of DOE Highway Vehicle Systems Contractors, CONF-781050, 1979.

18. Herbell, T. P.; Glasgow, T. K.; and Shaw, N. J.: Reaction Bon[illegible] Nitride Prepared from Wet Attrition - Milled Silicon. Ceramic [illegible] and Science Proceedings, vol. 1, no. 7-8(B); 1980. (Also published as [illegible] TM-81428.)

19. Adams, D. F.; and Murphy, D. P.: Analysis of Crash Propagation as an Energy Absorption Mechanism in Metal Matrix Composites. Tech. Rep. UWME-DR-101-102-1, Univ. of Wyoming, Dept. of Mech. Eng., 1981.

BLANK PAGE

292

RECENT ADVANCES IN CARBON-CARBON MATERIALS SYSTEMS

Donald R. Rummler
NASA Langley Research Center
Hampton, Virginia

INTRODUCTION

The development and/or improvement of materials systems for application to aerospace vehicles is a continuing research activity within NASA. The evolution of aerospace materials (figure 1) has been coupled with the development of faster vehicles and more efficient engines since the beginning of flight. In many cases the development of new or improved materials enabled the vehicle or engine advances. This continuing evolution has always pointed toward stronger, stiffer, lighter, and higher use temperature materials.

One of the most recent materials systems to evolve for aerospace application is reinforced carbon-carbon (RCC). This class of materials will have application to thermal protection systems, hot structures, and engines that may operate at temperatures in excess of 4000°F.

This paper will briefly discuss carbon-carbon materials and new oxidation-resistant coating developments for carbon-carbon and will highlight potential areas of application. A short bibliography of selected references is included that describe carbon-carbon materials and related technology in detail.

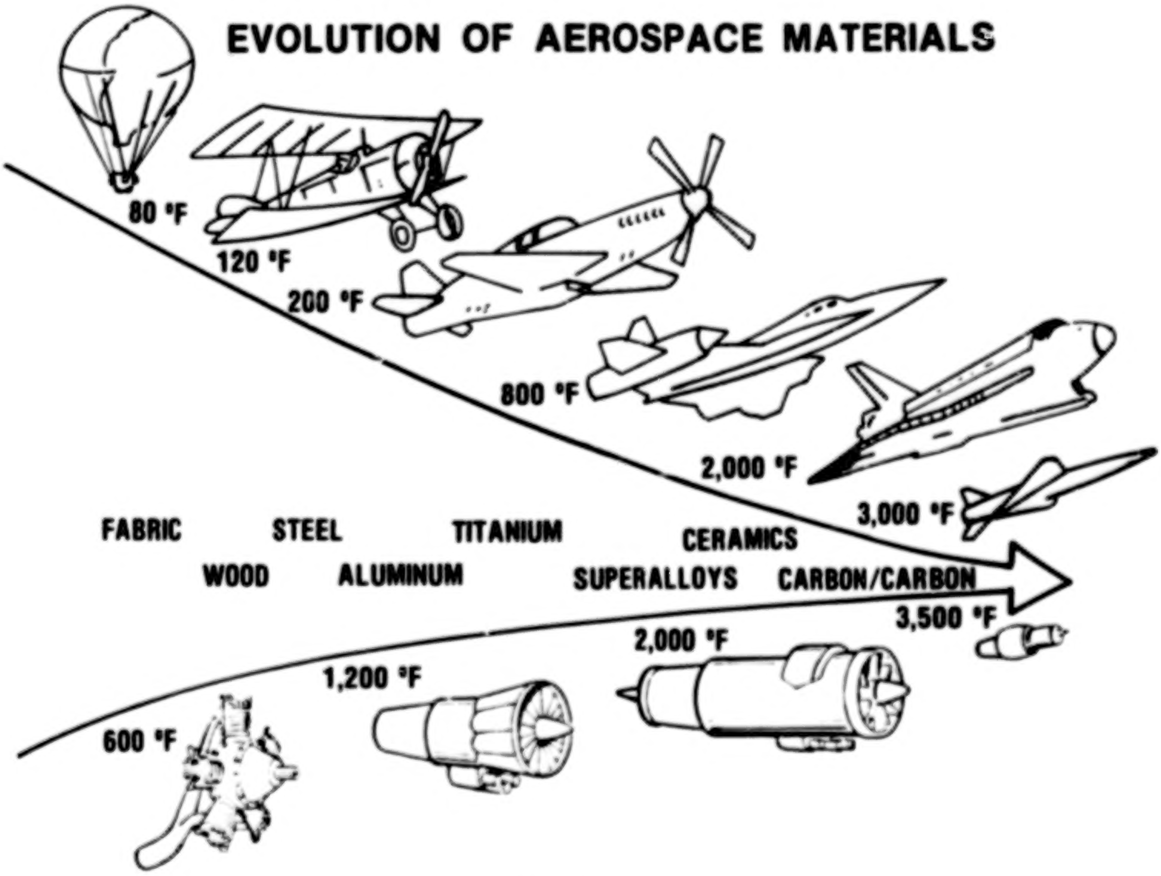
EVOLUTION OF AEROSPACE MATERIALS

Figure 1

SHUTTLE THERMAL PROTECTION SYSTEM

The materials systems used for the Shuttle Orbiter thermal protection system (TPS) are shown in figure 2. Most of the Orbiter surface is covered with silica-based ceramic tiles. However, a small percentage of the surface (the nose cap and leading edges) is exposed to temperatures up to 3000°F. This environment is beyond the capabilities of the silica tiles. Candidate materials for these areas included oxide ceramics, coated refractory metals, bulk graphite, and carbon-carbon. The material selected was reinforced carbon-carbon (RCC), one member of the growing family of carbon-carbon materials. For this application, the RCC is coated with silicon carbide and then impregnated with silica to provide oxidation protection to the carbon-carbon substrate.

The selection of RCC was based upon the following requirements: (1) maintenance of reproducible strength levels to 3000°F, (2) sufficient stiffness to resist flight loads and large thermal gradients, (3) low coefficient of thermal expansion to minimize induced thermal stresses, (4) oxidation resistance sufficient to limit strength reduction, (5) tolerance to impact damage, and (6) manufacturing processes within the state of the art.

It is this rare combination of properties that makes the emergence of carbon-carbon materials such a rich area for materials research and development. When they are fully developed carbon-carbon materials may represent the same kind of breakthrough in high-temperature materials as was provided by the development of nickel- and cobalt-based superalloys.

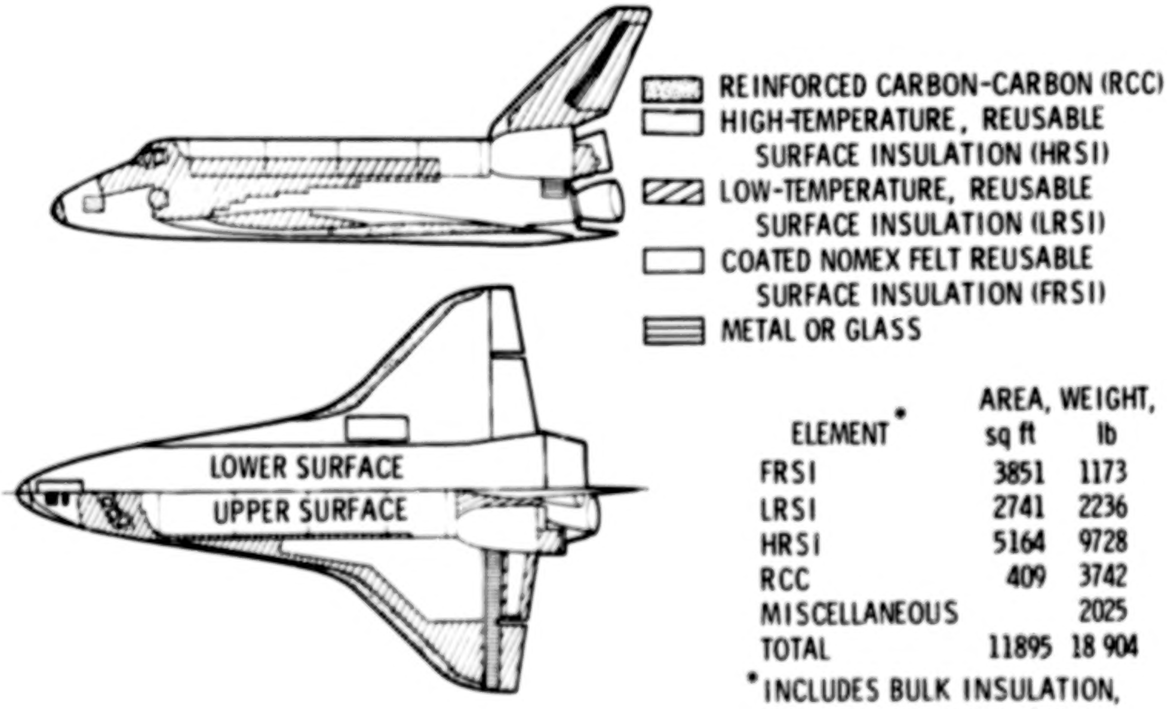

▨ REINFORCED CARBON-CARBON (RCC)
☐ HIGH-TEMPERATURE, REUSABLE SURFACE INSULATION (HRSI)
▨ LOW-TEMPERATURE, REUSABLE SURFACE INSULATION (LRSI)
☐ COATED NOMEX FELT REUSABLE SURFACE INSULATION (FRSI)
▤ METAL OR GLASS
LOWER SURFACE
UPPER SURFACE

ELEMENT*	AREA, sq ft	WEIGHT, lb
FRSI	3851	1173
LRSI	2741	2236
HRSI	5164	9728
RCC	409	3742
MISCELLANEOUS		2025
TOTAL	11895	18 904

*INCLUDES BULK INSULATION, THERMAL BARRIERS, AND CLOSEOUTS

Figure 2

CARBON-CARBON ATTRIBUTES

Carbon-carbon materials are a generic class of composites much like the graphite/epoxy family of polymer matrix composites (figure 3). They can be made in a wide variety of forms, from one-dimensional to n-dimensional, using unidirectional tows, tapes, or woven cloth. Because of this multiformity their mechanical properties can be readily tailored. Currently our primary research interest is in two-dimensional (2-D) carbon-carbon materials that use woven carbon cloth as a precursor. The properties and applications discussed in this paper will concentrate on 2-D carbon-carbon materials.

Carbon materials have high strength and stiffness potential as well as high thermal and chemical stability in inert environments. They must, however, be protected with coatings and/or surface sealants when used in an oxidizing environment.

Carbon-carbon materials have high thermal conductivity and low thermal expansion. These two properties combine to make carbon-carbon materials very resistant to thermal shock. Low density (about 70 percent of that of aluminum alloys) is an additional desirable property of this class of materials.

- MULTIFORMITY

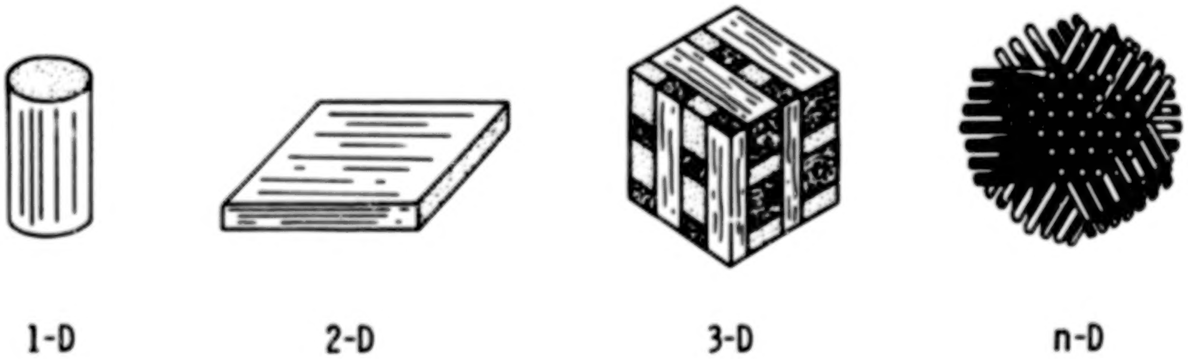

- HIGH STRENGTH POTENTIAL
  $\sigma_{ULT} > 40\,000$ psi $E > 10^7$ psi
- HIGH THERMAL AND CHEMICAL STABILITY
  $T_{MP} > 7400\ ^\circ F$ $K \sim 60$ BTU - in/hr - ft^2 - $^\circ F$ $\alpha \sim 2 \times 10^{-6}\ ^\circ F^{-1}$
- LOW DENSITY
  $\rho < 0.07$ lbm/in^3

Figure 3

STRENGTH EFFICIENCY OF VARIOUS MATERIALS

The effect of temperature on the ratio of tensile strength to density for several classes of high-temperature materials is shown in figure 4. The major advantage of carbon-carbon materials for high-temperature applications is that they do not lose strength as the use temperature is increased. This is in contrast to other structural materials such as superalloys and ceramics.

This figure shows three levels of carbon-carbon strength efficiency. The first, labeled Shuttle material, is the strength level of the RCC material used in the Shuttle thermal protection system. Even though this material is made with low-strength carbon fibers, its strength efficiency is superior to both superalloys and ceramics at temperatures above 1800°F. Recent research has led to the development of an advanced carbon-carbon (ACC) that is twice as strong as the RCC. This material is currently being evaluated by a number of laboratories. The ACC material is made up using woven carbon cloth. If unidirectional carbon fiber tapes are interplied with woven cloth to create a hybrid ACC, its strength in at least one direction can be increased to 50,000 psi or more. Research on hybrid ACC is just beginning.

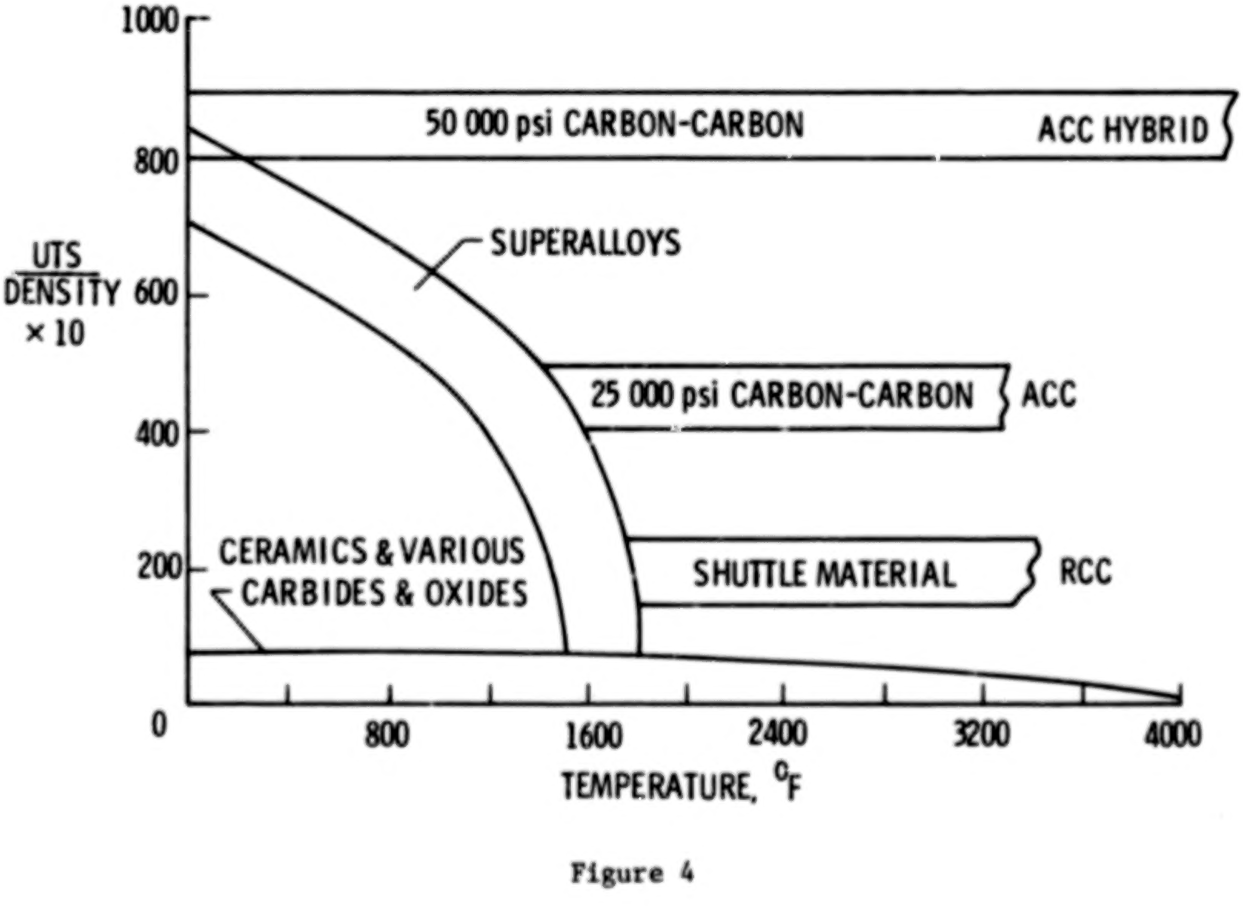

Figure 4

BEST DOCUMENT AVAILABLE

TYPICAL MANUFACTURING CYCLE OF 2-D Carbon-Carbon

A summary of the fabrication steps involved in the manufacture of a 2-D carbon-carbon part is shown in figure 5. First the woven graphite fabric, which is preimpregnated with phenolic resin, is laid up as a phenolic-graphite laminate in a mold and is autoclave cured. Once cured, the part is pyrolyzed to form a carbon matrix surrounding the graphite fibers. The part is then densified by multiple furfural alcohol reimpregnations and pyrolyzations. The resulting carbon-carbon part is ready for use in inert environments. The process is very time consuming. For instance, a single pyrolysis step may take more than 70 hours in a low-temperature inert-atmosphere furnace. Research is currently under way to reduce the processing time and consequent cost of carbon-carbon parts.

For application in oxidizing environments, such as on the Shuttle, the carbon-carbon parts must be coated and sealed to protect them. For the Shuttle application the outer surfaces of the parts are converted to silicon carbide in a high-temperature diffusion coating process. Because of differences in thermal expansion between the silicon carbide and the carbon-carbon part, the coating develops microcracks when the part is cooled from the coating temperature. For the Shuttle these cracks are impregnated with tetraethyl orthosilicate (TEOS). The TEOS process leaves silica (SiO_2) in all of the microcracks, greatly enhancing the oxidation protection of the carbon-carbon substrate. Recent research has been concentrating on the application of surface sealants to further improve oxidation resistance. These improvements will be discussed later in this paper.

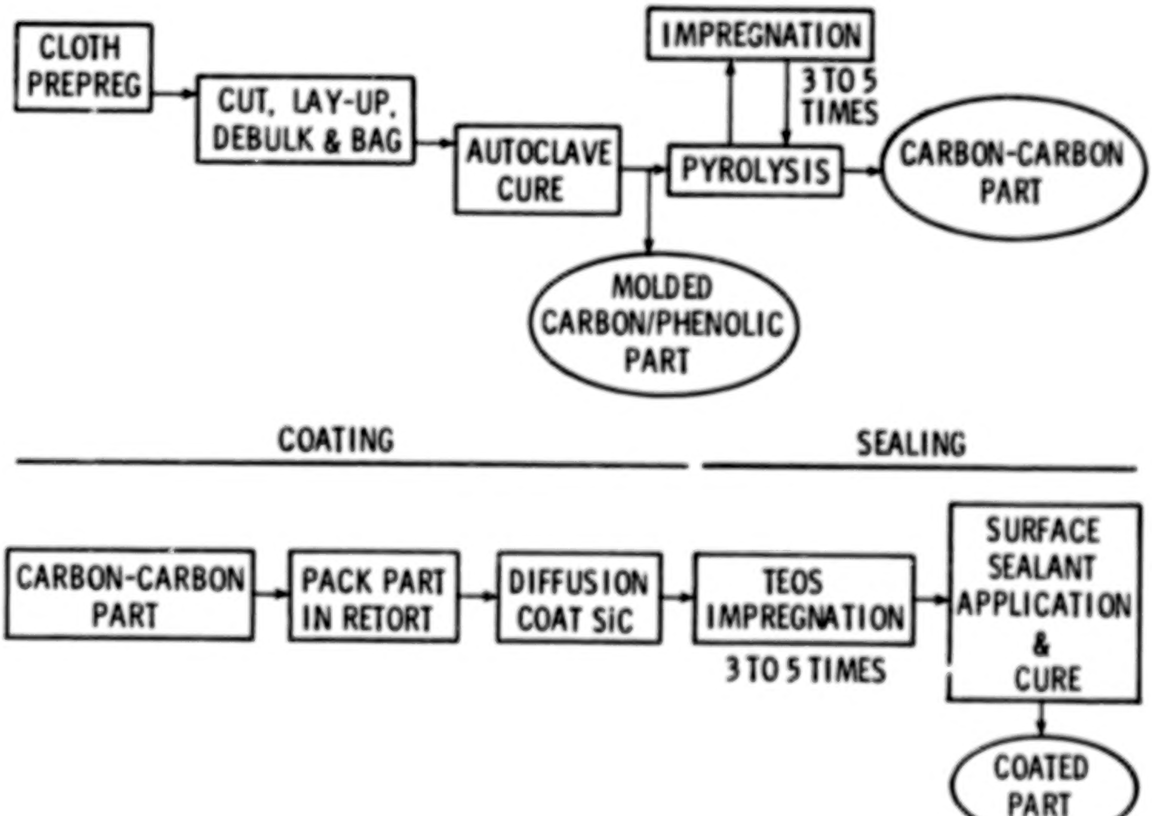
CLOTH PREPREG
CUT, LAY-UP, DEBULK & BAG
AUTOCLAVE CURE
IMPREGNATION
3 TO 5 TIMES
PYROLYSIS
CARBON-CARBON PART
MOLDED CARBON/PHENOLIC PART
COATING
SEALING
CARBON-CARBON PART
PACK PART IN RETORT
DIFFUSION COAT SiC
TEOS IMPREGNATION
3 TO 5 TIMES
SURFACE SEALANT APPLICATION & CURE
COATED PART

Figure 5

MICROSTRUCTURE OF TEOS-SEALED RCC

Details of the TEOS-impregnated coated RCC microstructure are presented in figure 6. The top photomicrograph shows the woven and layered nature of the carbon-carbon as well as the integral silicon carbide coating. The enlargement of the silicon carbide coating shows traces of the outer layer of the carbon-carbon, was converted to silicon carbide during the coating process. A microcrack is also visible in the coating. The cracks are due to the differences in thermal expansion between the coating and the carbon-carbon matrix.

The close-up of the carbon-carbon microstructure shows the individual graphite fibers imbedded in the carbon matrix. Minor porosity in the matrix is also evident. A pore-free microstructure may not be desirable since pores probably act as crack stoppers and improve impact resistance.

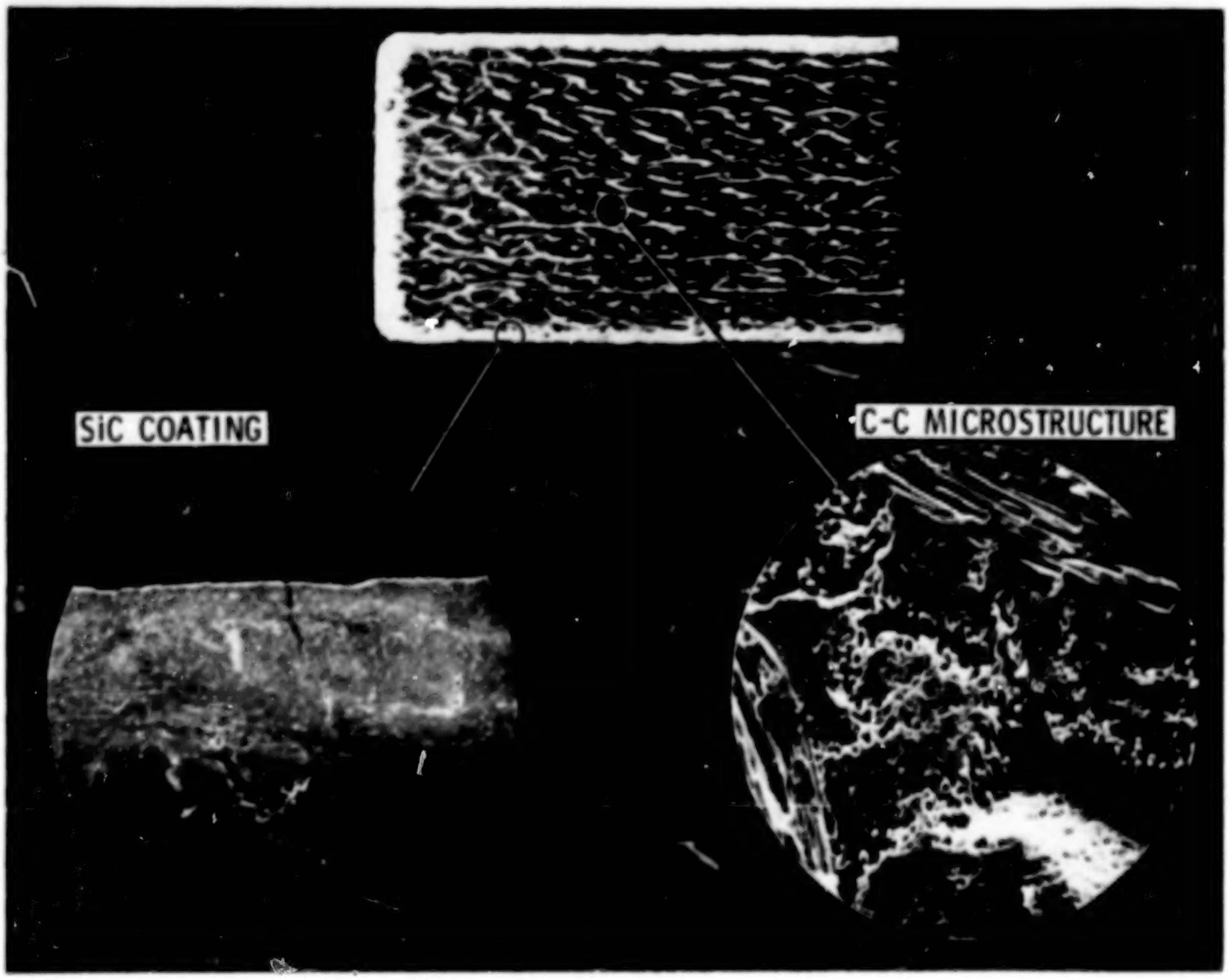

Figure 6

TYPICAL 2-D CARBON-CARBON STRESS-STRAIN BEHAVIOR

Typical stress-strain behavior for a 2-D carbon-carbon material is shown in figure 7. The material in this case is the advanced carbon-carbon (ACC) with 20 plies of woven graphite fabric. The warp of all plies is in the same direction. The stress-strain behavior is linear up to a stress level of about 16 ksi. Above 16 ksi the material is nonlinear and the differences in behavior in tension and compression and in the warp and fill directions become evident.

The behavior of the material depends on both the type and direction of loading. This was not unexpected since most composites show a similar sensitivity to the type and direction of loading. What is somewhat surprising is that the material is not completely brittle; it exhibits some nonlinearity prior to failure. A typical ceramic would not be expected to exhibit this nonlinear behavior and would fail in a completely brittle manner.

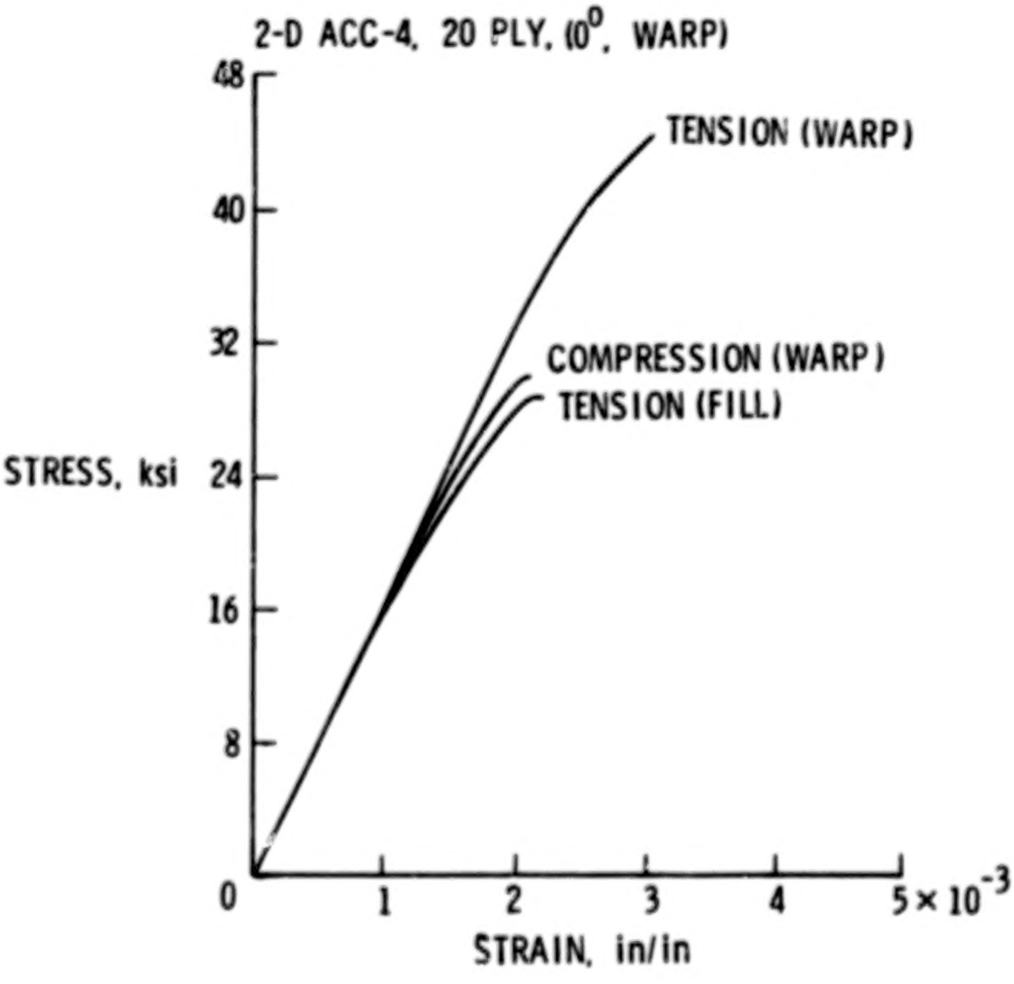

Figure 7

COMPARISON OF 2-D CARBON-CARBON PROPERTIES

The wide range of mechanical properties currently available in carbon-carbon is illustrated in figure 8. These data are from room-temperature tests. However, since strength properties do not degrade with increasing temperature these data are also typical of data generated at temperatures up to 4000°F. The fiber, the weave, the lay-up, and the number of densification steps can be changed to tailor the mechanical properties. Tensile strength can be higher or lower than compressive strength. Elastic modulus can be the same in tension and compression or it can be different. So far we have not been very successful with our attempts to improve in-plane shear or out-of-plane tensile properties.

We will continue our research efforts to characterize, understand, and improve the properties of carbon-carbon materials. Emphasis is being placed on improving in-plane shear and out-of-plane tensile strength so that the full potential of these materials can be realized.

MATERIAL	RCC	ACC-3	ACC-4
FIBER	WCA (RAYON)	T300 (PAN)	T300 (PAN)
WEAVE	SQUARE	8-HARNESS	8-HARNESS
ORIENTATION	X-PLY	QUASI-ISTROPIC	0^{0}(WARP)
IN-PLANE			
TENSILE STRENGTH, ksi	7.5	16	44
TENSILE MODULUS, msi	2	11	16
COMPRESSIVE STRENGTH, ksi	24	16	28
COMPRESSIVE MODULUS, msi	4.4	11	16
SHEAR STRENGTH, ksi	1.8	1.0	2.0
OUT-OF-PLANE			
TENSILE STRENGTH, ksi	0.8	0.4	0.5

Figure 8

IMPROVED OXIDATION-RESISTANT COATINGS - 1000°F THERMAL CYCLES

Early work on the Shuttle program established a correlation between mass loss, temperature, air pressure, and time in order to be able to predict RCC mass loss during the complex reentry heating cycle. This was necessary to evaluate end-of-life strength of parts exposed to different thermal environments. This correlation is used to compare the expected performance of Shuttle baseline RCC with ACC-3, which has been coated, impregnated with TEOS, and sealed with a low-temperature glass former. The improvement in oxidation resistance as a result of our recent research on coating sealants is shown in figure 9. Here the 1000°F maximum temperature during the thermal cycle simulates the temperature that might be encountered in a leading-edge attachment area. At a mass loss of 0.05 lb/ft^2 the improvement in mission life is a factor of 3 for ACC compared to Shuttle baseline RCC.

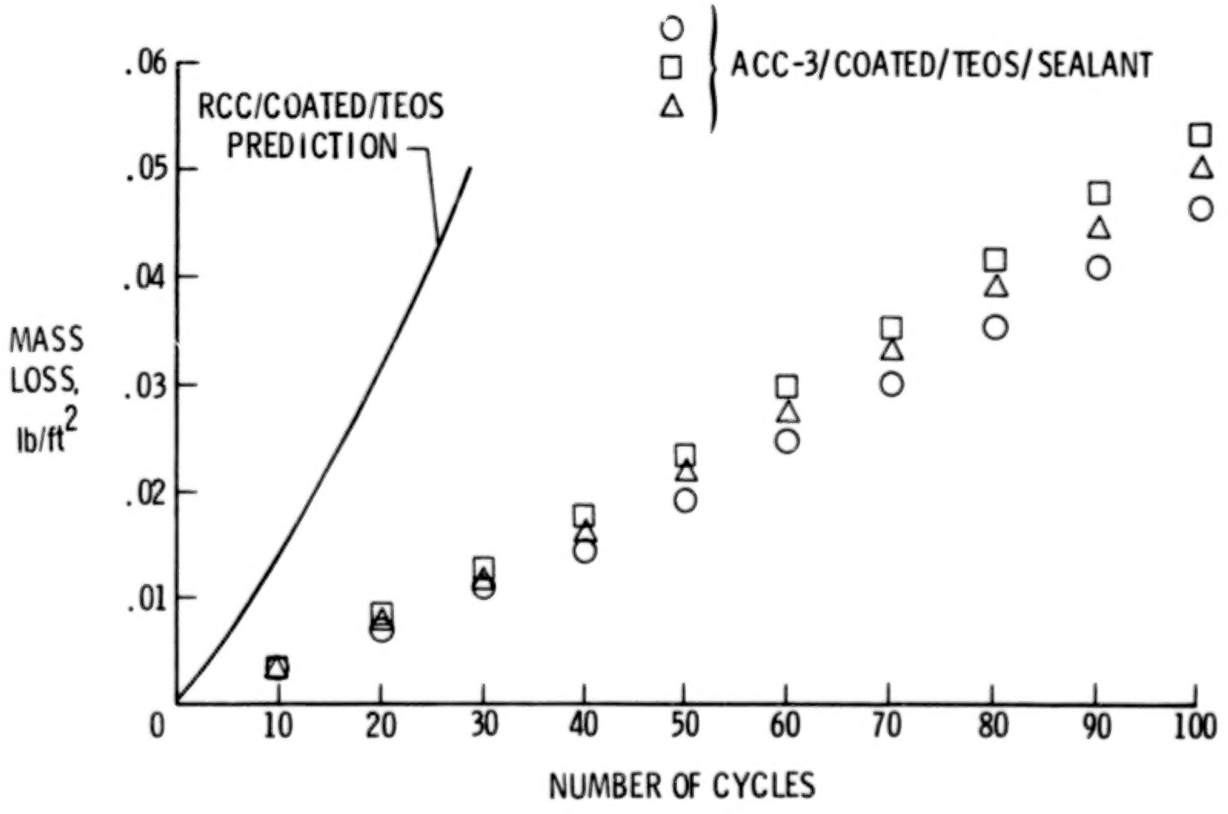

Figure 9

IMPROVED OXIDATION-RESISTANT COATING - 2450°F THERMAL CYCLES

As in the previous figure, the mass loss characteristics of coated and sealed ACC are compared to predicted RCC baseline behavior. The data in figure 10 are for a maximum-temperature thermal cycle of 2450°F. This cycle simulates the type of thermal history that would be expected on the outer surface of the Shuttle leading edge. Although the predicted mass loss for the RCC is only 0.02 lb/ft^2 after 100 simulated missions, the oxidation resistance of the coated and sealed ACC is twice as good as the baseline RCC.

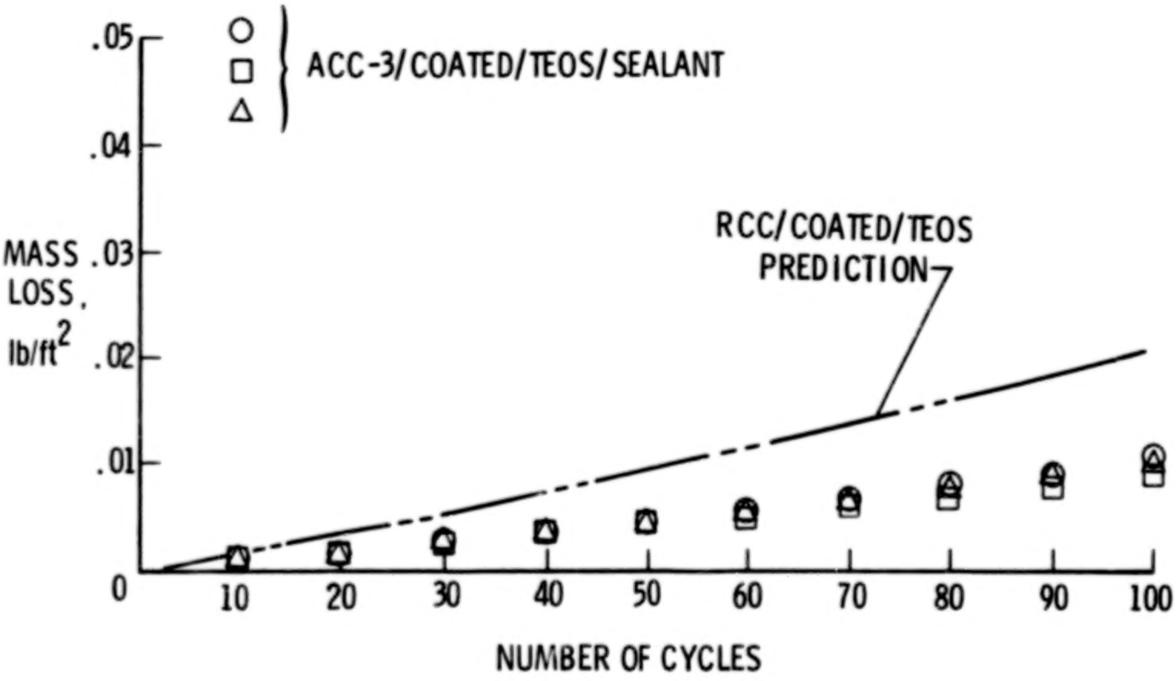

Figure 10

BEST DOCUMENT AVAILABLE

EFFECT OF COATING/SEALANT ON MASS LOSS

Because oxidation of the silicon carbide baseline coating will form a protective layer of glass when RCC parts are exposed to temperatures above 1600°F, we have concentrated our most recent sealant experiments below the protective oxide formation temperature. Figure 11 shows a comparison of mass loss following a 10-hour exposure to atmospheric-pressure air at 1000°F for three carbon-carbon materials systems. The RCC/SiC/TEOS represents the Shuttle baseline system. The ACC/SiC/TEOS/MAP is one of our coated and sealed advanced carbon-carbon materials. As we have seen before, the addition of a low-temperature glass former significantly reduces mass loss. Recently, we have further improved oxidation resistance by modifying the baseline silicon carbide coating (DSIC). This doped and sealed coating has 25 times the oxidation resistance of the Shuttle baseline RCC material.

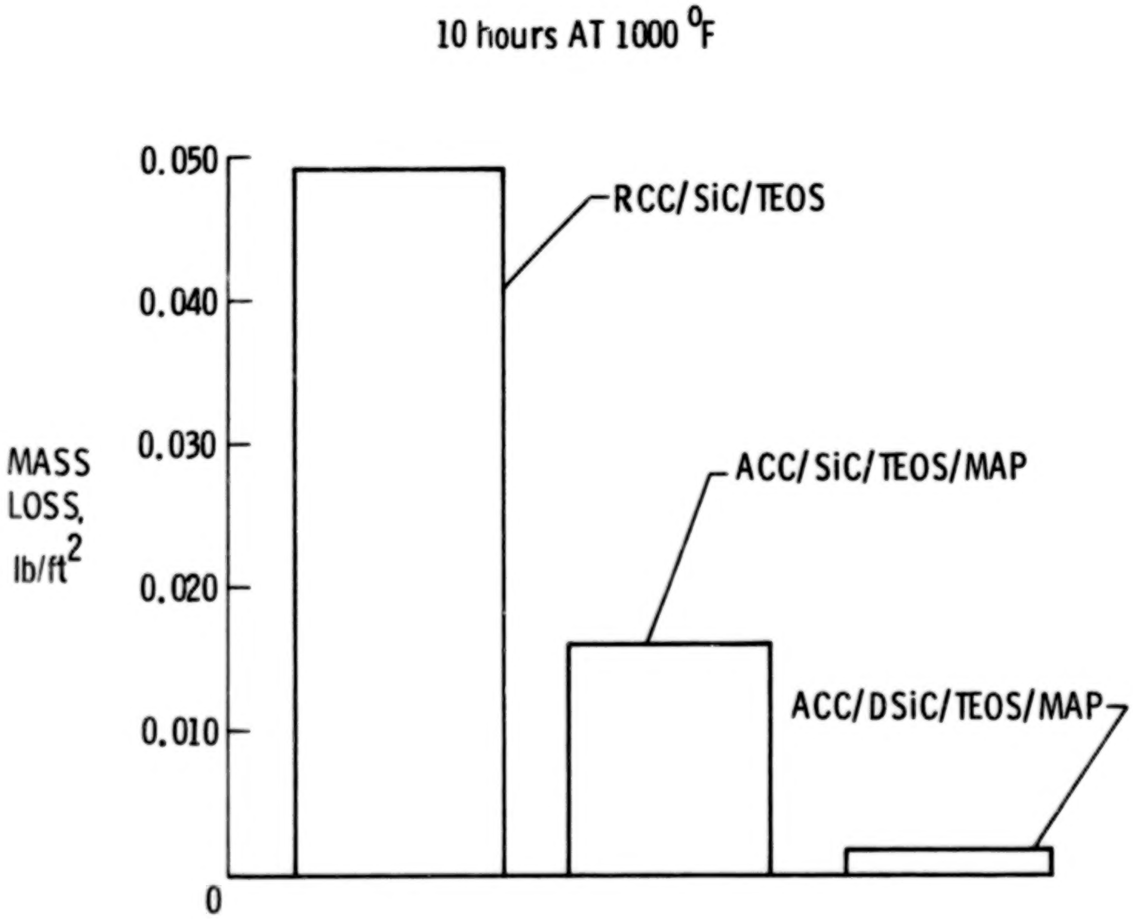

Figure 11

CARBON-CARBON COMPOSITES

A brief summary of the present state of carbon-carbon technology is presented in figure 12. Carbon-carbon composites offer a unique combination of properties. In nonoxidizing environments they retain room-temperature mechanical properties up to temperatures in excess of 4000°F. For application in oxidizing environments, current coatings limit maximum use temperatures to about 2900°F. Their high thermal conductivity and low thermal expansion make carbon-carbon composites excellent candidates for applications involving thermal shock.

Because of the variety of fibers, weaving patterns, and lay-up procedures that can be used for carbon-carbon composites, their mechanical properties can be tailored over a wide range to fit the application.

A strong research activity in carbon-carbon materials is building in this country. Major emphasis is being placed on understanding materials behavior. These research activities should lead to improved matrix properties (particularly in-plane shear and out-of-plane tensile strengths), improved oxidation-resistant coatings with higher use temperatures, longer lifetimes, and less costly fabrication methods.

The first generation of this new class of structural materials is available today. The rest of this paper will briefly discuss some of the aerospace applications for carbon-carbon that are currently being explored.

- UNIQUE COMBINATION OF PROPERTIES
- PROPERTIES CAN BE TAILORED
- STRONG RESEARCH BASE TO IMPROVE PERFORMANCE
- FIRST GENERATION AVAILABLE TODAY

Figure 12

MULTIPOST PANEL CONCEPT

The development of advanced carbon-carbon (ACC) was instigated by the desire to make available to the Shuttle program a thermal protection system that would be more durable and impact resistant than the current reusable surface insulation (RSI). As the mechanical properties of the ACC and the oxidation resistance of the new coating systems improved, it became apparent that an ACC-based TPS might be feasible. We have recently completed an assessment of alternate thermal protection systems for the Space Shuttle Orbiter. This study demonstrated that ACC-based TPS is both feasible and weight competitive with the current RSI-based TPS. ACC is a particularly attractive candidate for TPS locations that experience surface temperatures above 1800°F.

One of the ACC-based TPS concepts to emerge from this study is shown in figure 13. The multipost panel concept utilizes a series of 36-inch-by-36-inch ACC cover plates (outer surface) to bridge airloads to the aluminum substructure and to reradiate reentry thermal energy just as do the current RSI tiles. Since the RSI tiles are, on the average, 6 inches by 6 inches on the surface, these ACC panels would each replace 36 Orbiter tiles. The outer panel is suppported by multiple posts that separate the cover plate from the substructure. The posts are configured to minimize induced thermal stresses as the ACC panel thermally expands. Fibrous insulation packages are used between the outer panel and the aluminum to insulate the substructure from the entry thermal energy that is not rejected by reradiation.

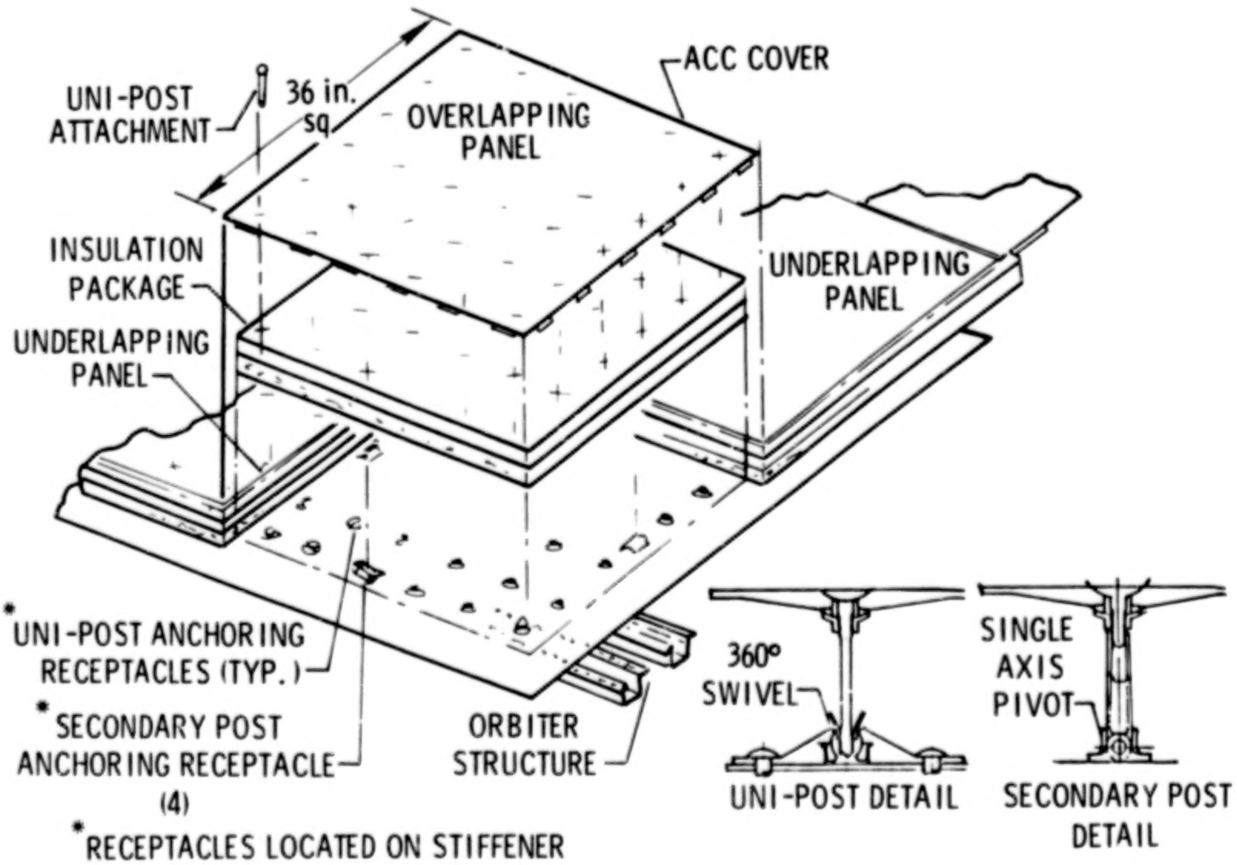
UNI-POST
ATTACHMENT
36 in. sq
OVERLAPPING PANEL
ACC COVER
INSULATION PACKAGE
UNDERLAPPING PANEL
UNDERLAPPING PANEL
*UNI-POST ANCHORING RECEPTACLES (TYP.)
*SECONDARY POST ANCHORING RECEPTACLE (4)
*RECEPTACLES LOCATED ON STIFFENER
ORBITER STRUCTURE
360° SWIVEL
UNI-POST DETAIL
SINGLE AXIS PIVOT
SECONDARY POST DETAIL

Figure 13

CARBON-CARBON HOT STRUCTURE FOR SPACE SHUTTLE

The current use of RCC for the nose cap and leading edges of the Shuttle can be considered a hot-structure application of carbon-carbon. These parts must transmit thermomechanical loads to the aluminum substructure. They are also similar to the previously discussed panel TPS in that insulation packages must be used behind them to protect the substructure from overheating.

Recently we have begun to look at "true" hot-structure applications of ACC. Such an application is shown in figure 14. Potential Orbiter carbon-carbon hot structures are the rudders, speed brakes, ailerons, and the body flap. For these applications carbon-carbon would perform the dual role of primary structure and thermal protection system. Since the primary structure can operate at high temperature, no insulation would be required. If ACC hot structure can be developed for these retrofittable control surfaces, a potential weight saving of 2500 pounds exists for conventional two-skin construction. If an open-face aileron (only a single aerodynamic skin) can be developed, the potential weight saving is 5000 pounds per vehicle.

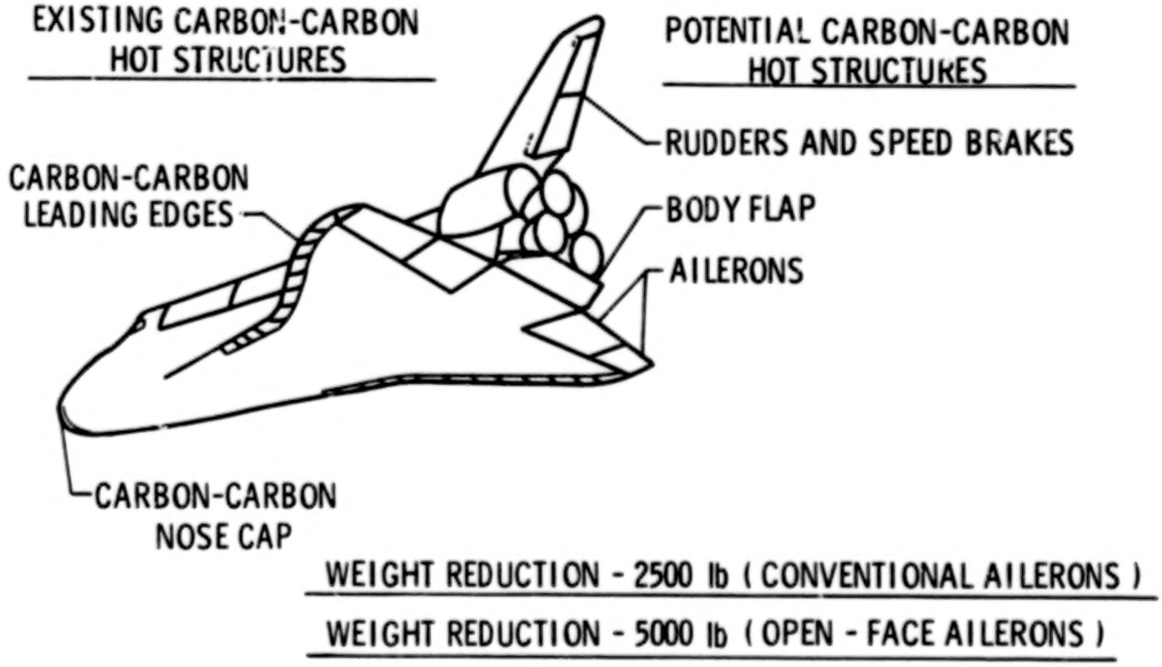
EXISTING CARBON-CARBON HOT STRUCTURES
POTENTIAL CARBON-CARBON HOT STRUCTURES
RUDDERS AND SPEED BRAKES
CARBON-CARBON LEADING EDGES
BODY FLAP
AILERONS
CARBON-CARBON NOSE CAP
WEIGHT REDUCTION - 2500 lb (CONVENTIONAL AILERONS)
WEIGHT REDUCTION - 5000 lb (OPEN - FACE AILERONS)

Figure 14

ACC OPEN-FACE HOT-STRUCTURE SHUTTLE CONTROL SURFACES

A concept for an ACC open-face hot-structure Shuttle control surface is presented in figure 15. In this case we show the body flap. The ACC torque tube would use the existing aft body cove. The single aerodynamic surface would be stiffened with ACC ribs. The feasibility of eliminating the top aerodynamic surface will be investigated in wind tunnel tests.

Our preliminary structural studies of this concept indicate that mechanical fastners would be required to operate at high temperatures. This poses potential structural design problems because of the large difference in thermal expansion between carbon-carbon and any metallic fastener. To minimize these potential problems we are currently developing a fastener concept called DAZE (differential &, zero strain).

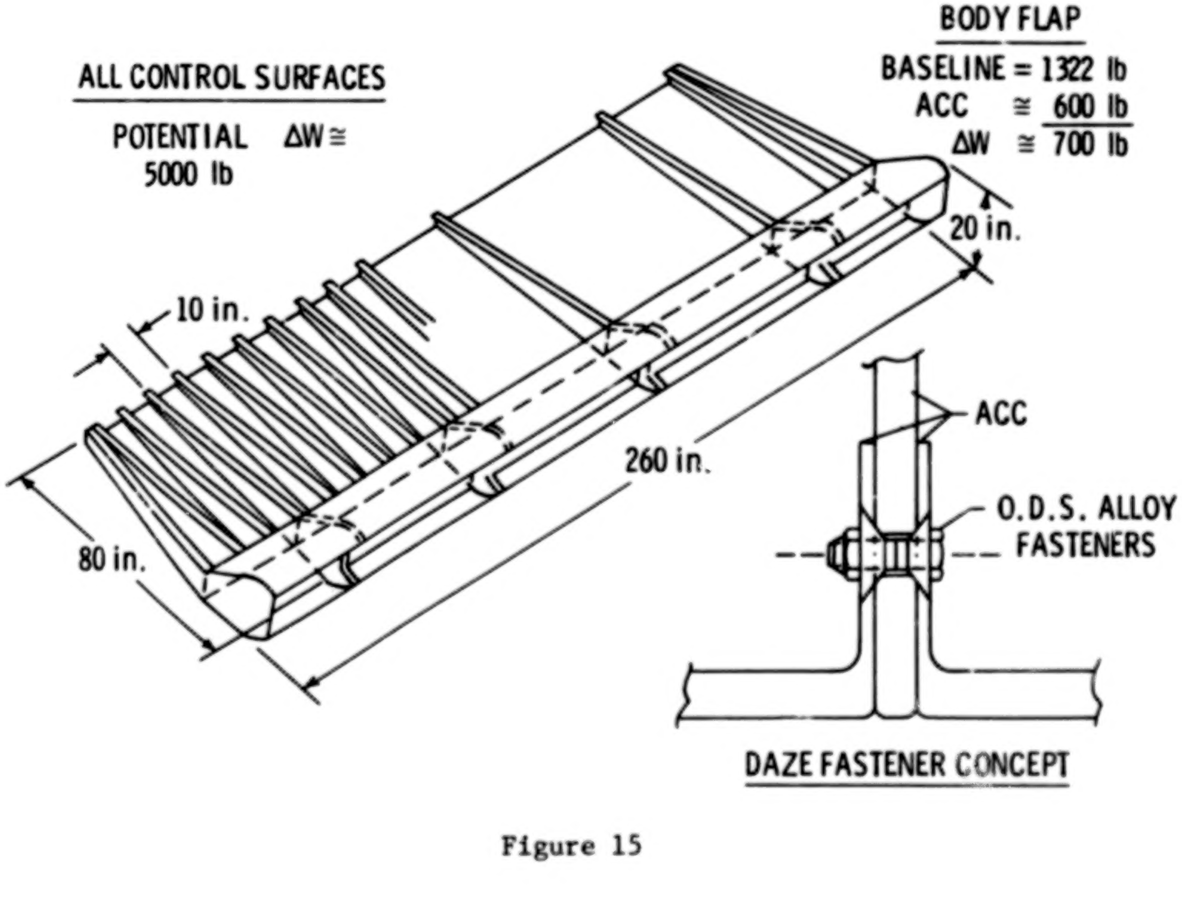
ALL CONTROL SURFACES
POTENTIAL ΔW ≅ 5000 lb
BODY FLAP
BASELINE = 1322 lb
ACC ≅ 600 lb
ΔW ≅ 700 lb
20 in.
10 in.
260 in.
80 in.
ACC
O.D.S. ALLOY FASTENERS
DAZE FASTENER CONCEPT

Figure 15

FASTENER CONCEPT FOR LARGE CARBON-CARBON HOT STRUCTURES

The thermal expansion mismatch between high-temperature metallic fasteners and carbon-carbon causes many potential structural design problems. The DAZE fastener concept is illustrated in figure 16. This concept utilizes a conventional metallic bolt surrounded by two intersecting cones. The joint is tightened at room temperature sufficiently to prevent relative motion between the carbon-carbon parts under the expected design loads. During service at high temperature the joint does not loosen up because the cones expand and slide along the conical surfaces of the carbon-carbon parts. This expansion of the cones prevents the bolt from losing tension. Sufficient radial clearance between the bolt and the carbon-carbon parts is established during assembly to avoid introduction of tensile loads into the carbon-carbon when the joint is hot. The feasibility of this concept has been demonstrated by thermally cycling two pieces of graphite that had been joined using two DAZE fasteners. After four cycles to 1600°F the joints were still snug with no apparent damage to the graphite parts. A snug-fitting conventional fastener failed the graphite in tension during a single thermal cycle. The tensile loads were introduced by the radial expansion of the metallic bolt.

We are continuing to evaluate the DAZE concept both in house and on contract. This concept may represent a breakthrough in high-temperature mechanical fastening.

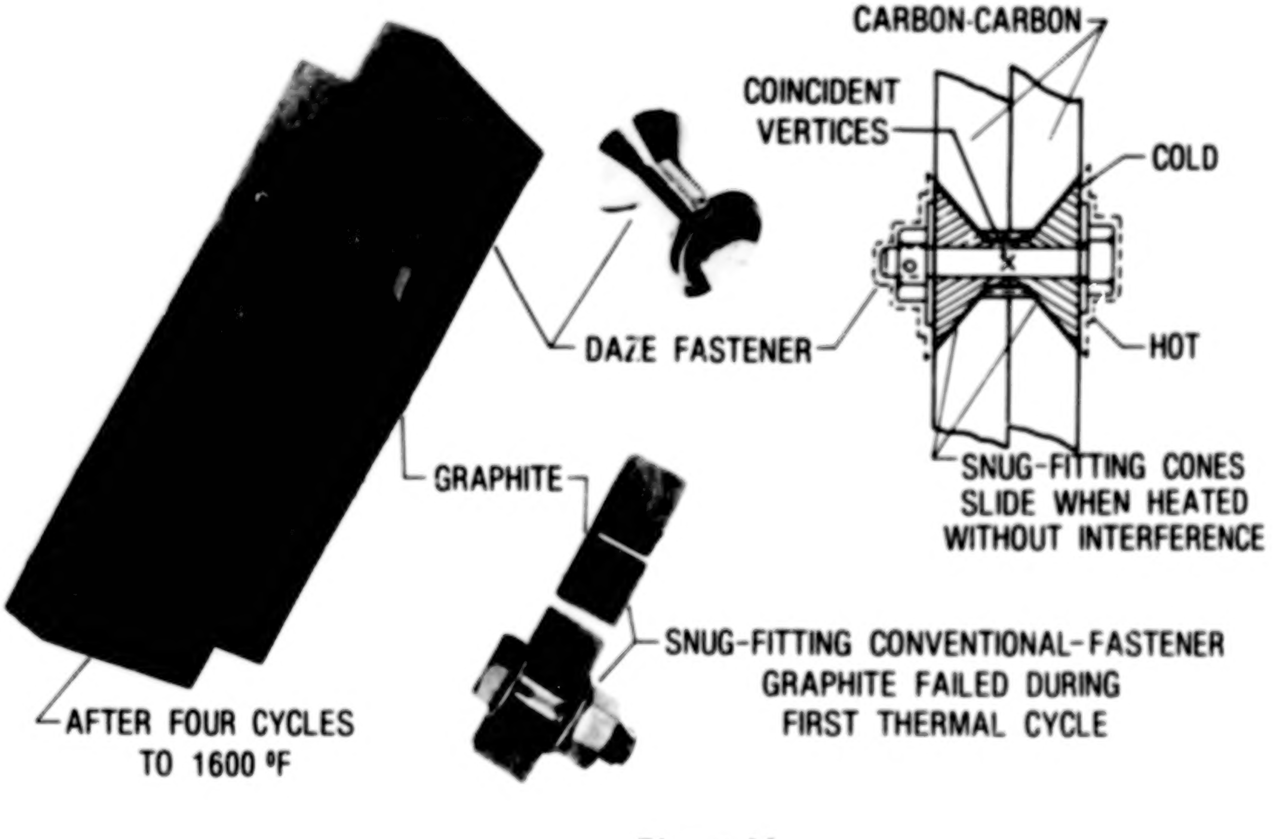
CARBON-CARBON
COINCIDENT VERTICES
COLD
DAZE FASTENER
HOT
GRAPHITE
SNUG-FITTING CONES SLIDE WHEN HEATED WITHOUT INTERFERENCE
SNUG-FITTING CONVENTIONAL-FASTENER GRAPHITE FAILED DURING FIRST THERMAL CYCLE
AFTER FOUR CYCLES TO 1600 °F

Figure 16

ACC TRUSS CORE PANEL

Initial studies for some carbon-carbon applications indicate that a monolithic carbon-carbon structure, such as the one proposed for the Orbiter body flap, will not be weight/cost competitive with current structures. It will be necessary to use internally reinforced or lightweight carbon-carbon constructions such as rib-stiffened sheet or truss core panels.

An initial effort to fabricate a truss core advanced carbon-carbon part is illustrated in figure 17. In this figure the panel has been cut in half to reveal the truss core. This part uses thin-gage face sheets and core. In addition, the fabrication procedures yielded a part with built-in panel closeouts. The integral panel closeout makes feasible the possibility of coating only the outside surfaces of the part for use in oxidizing environments. Research will continue in the development of lightweight carbon-carbon configurations.

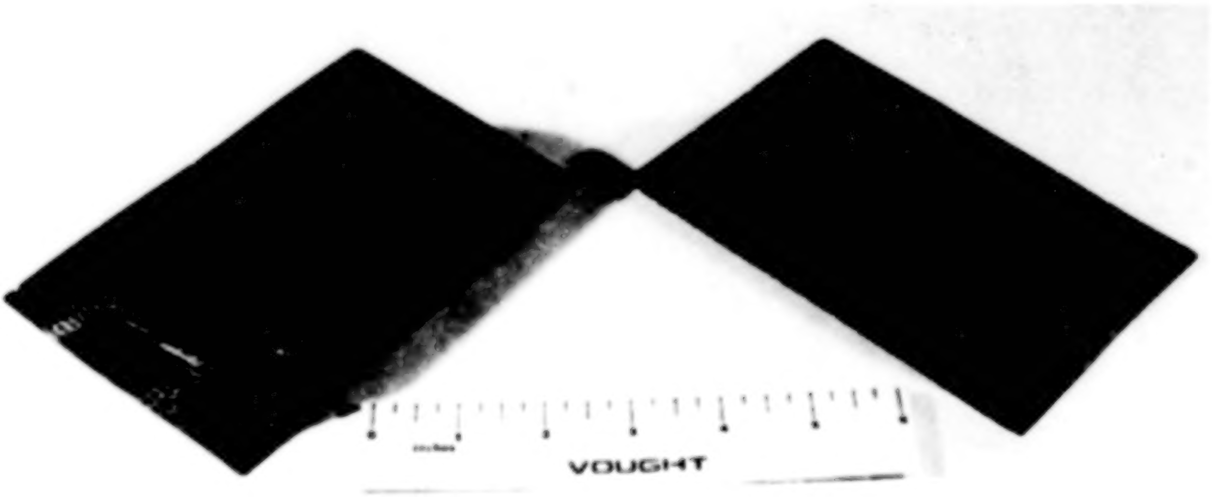

Figure 17

SUMMARY

A summary of the recent advances and expected future improvements in advanced carbon-carbon materials systems is presented in figure 18. The ACC family of carbon-carbon materials represents a significant improvement in strength and stiffness over the baseline RCC material. In the future, hybrid ACC constructions offer the possibility of additional improvements in strength and stiffness. Methods will have to be found to increase in-plane shear and out-of-plane tensile strengths so that the full potential of the ACC matrix materials can be realized.

The concurrent ACC and coating research activities have led to significant improvements in the oxidation resistance of coatings for ACC. Matrix strength retention after exposure to the expected use environment will continue to be an important criterion for coating improvements. Continued research on doped silicon carbide coatings and advanced coating sealants is expected to yield additional improvements in matrix oxidation protection and increase maximum use temperatures.

In the area of ACC applications, our initial efforts show that ACC is both a feasible and attractive candidate material class for both TPS and hot-structure applications. We will continue to pursue these application areas both analytically and experimentally. Particular emphasis will be placed on continued development of the DAZE fastener concept for mechanical joints.

- MATRIX
  - IMPROVED STRENGTH AND STIFFNESS
  - HYBRID CONSTRUCTIONS
  - SHEAR PROPERTIES
- COATINGS
  - IMPROVED OXIDATION RESISTANCE
  - STRENGTH RETENTION
  - DOPED SiC
  - IMPROVED SEALANTS
- APPLICATIONS
  - TPS
  - HOT STRUCTURE

Figure 18

BIBLIOGRAPHY

1. Marshall, Sittig, Ed.: Carbon and Graphite Fibers - Manufacture and Applications. Noyes Data Corporation, Park Ridge, NJ 07656.

2. Hays, D.: An Assessment of Alternate Thermal Protection Systems for the Space Shuttle Orbiter. NASA CR-3548, Apr. 1982.

3. Becker, P. R.: Leading-Edge Structural Material System of the Space Shuttle. Bulletin of American Ceramic Society, pp. 1210-1214, vol. 60, no. 11, 1981.

4. While, D. M.: Development of Advanced Carbon-Carbon (ACC) Composites, vols. I, II and III, NASA CR-165842-(1,2, and 3), July 1982.

5. Fitzer, E. and Huttner, W.: Structure and Strength of Carbon/Carbon Composites. J. Phys. D: Appl. Phys., vol. 14, pp. 342-371, 1981.

6. Adams, D. F.: Longitudinal Tensile Behavior of Unidirectional Carbon-Carbon Composites. J. Composite Materials, vol. 8, pp. 320-332, Oct. 1974.

7. Davis, H. O.: Material and Process Effects on Carbon/Carbon Shear Strength. AIAA Paper No. 75-1253, 1975.

8. Bilow, N., et al: Arylacetylenes as High Char Forming Matrix Resins. SAMPE Journal, pp. 19-23, May/June 1982.

9. Stroud, C. W.; and Rummler, D. R.: Mass Loss of TEOS-Coated RCC Subjected to the Environment at the Shuttle Wing Leading Edge. NASA TM-83203, Sept. 1981.

10. Medford, J.E.: Multi-Cycle Plasma Arc Evaluation of Oxidation Inhibited Carbon-Carbon Material for Shuttle Leading Edges. ASME Paper Number 72-ENAV-26, August 1972.

11. McKinis, F. K.: Shuttle LESS Subsurface Attack Investigation. LTV Aerospace Corporation Report No. 221Rp00241, Vought Corporation, December 1974.

12. Medford, J.E.: Prediction of Oxidation Performance of Reinforced Carbon-Carbon Material for Space Shuttle Leading Edges. AIAA Paper 75-730, 1975.

13. Dicus, Dennis L.; Hopko, Russell, N.; and Brown, Ronald D.: Ablative Performace of Uncoated Silicone Modified and Shuttle Baseline Reinforced Carbon Composites. NASA TN D-8358, Dec. 1976.

14. Curry, Donald M.; Johansen, K. J.; and Stephens, Emily W.: Reinforced Carbon-Carbon Oxidation Behavior in Convective and Radiative Environments. NASA TP-1248, Aug. 1978.

15. Stroud, C. W.; and Rummler, Donald R.: Mass Loss of a TEOS Coated Reinforced Carbon-Carbon Composite Subjected to a Simulated Shuttle Entry Environment. NASA TM-81799, 1980.

TURBINE ENGINE MATERIALS DURABILITY RESEARCH

S. R. Levine and C. A. Stearns
NASA Lewis Research Center
Cleveland, Ohio

INTRODUCTION

Turbine engine hot-section materials are subjected to aggressive chemical and thermomechanical environments. High-temperature environmental attack of dollar-intensive turbine components reduces turbine efficiency and can limit life. The bottom line, of course, is that high-temperature environmental attack costs you money. The objective of materials durability research at Lewis is to understand the mechanisms of alloy and coating attack and the effects of interaction with the environment on mechanical behavior. This base of understanding provides the foundation for developing life prediction methods and identifying strategies for controlling attack.

The major thrusts of our research can be grouped into the categories of environmental attack and control strategies or surface protection. Under environmental attack, which encompasses environmental effects on mechanical properties, we are concerned with oxidation attack, hot corrosion attack and life prediction. In the surface protection area, our major thrusts have been metallic coatings and ceramic thermal barrier coatings, and to these we have recently added a new area of research - coatings for carbon-carbon composites. Rather than skimming over all of these areas, this paper will cover only two areas - oxidation research and thermal barrier coating research. This will exemplify our philosophy while providing some depth of coverage for each topic. Recent reviews of the other areas of research are available (1-3).

SCHEMATIC VIEWS OF SURFACES OF OXIDIZED METALS

Three oxidation cases, as illustrated in figure 1, are of concern when dealing with the oxidation of nickel-base and cobalt-base superalloys and the coatings one might use to protect these materials at high temperature. Protection is derived from the ability to form an adherent, slowly growing oxide scale. The parabolic oxidation case is primarily of academic interest since it is rarely observed in cyclic oxidation. The systems that display this behavior generally form oxides that grow too rapidly to be useful as high-temperature protective scales, such as nickel oxide. Chromium oxide is another commonly encountered high-temperature oxide scale. This oxide is desirable under static conditions since it is generally tenacious and grows more slowly than nickel oxide. However, Cr_2O_3 undergoes oxidative vaporization in a high-temperature, high-velocity environment and this limits its utility. The final case, that of spalling, is exemplified by aluminum oxide and spinels. These oxides grow relatively slowly, do not vaporize, and only exhibit partial spallation. Thus, they have proven to be the most desirable protective scales for superalloys and their coatings.

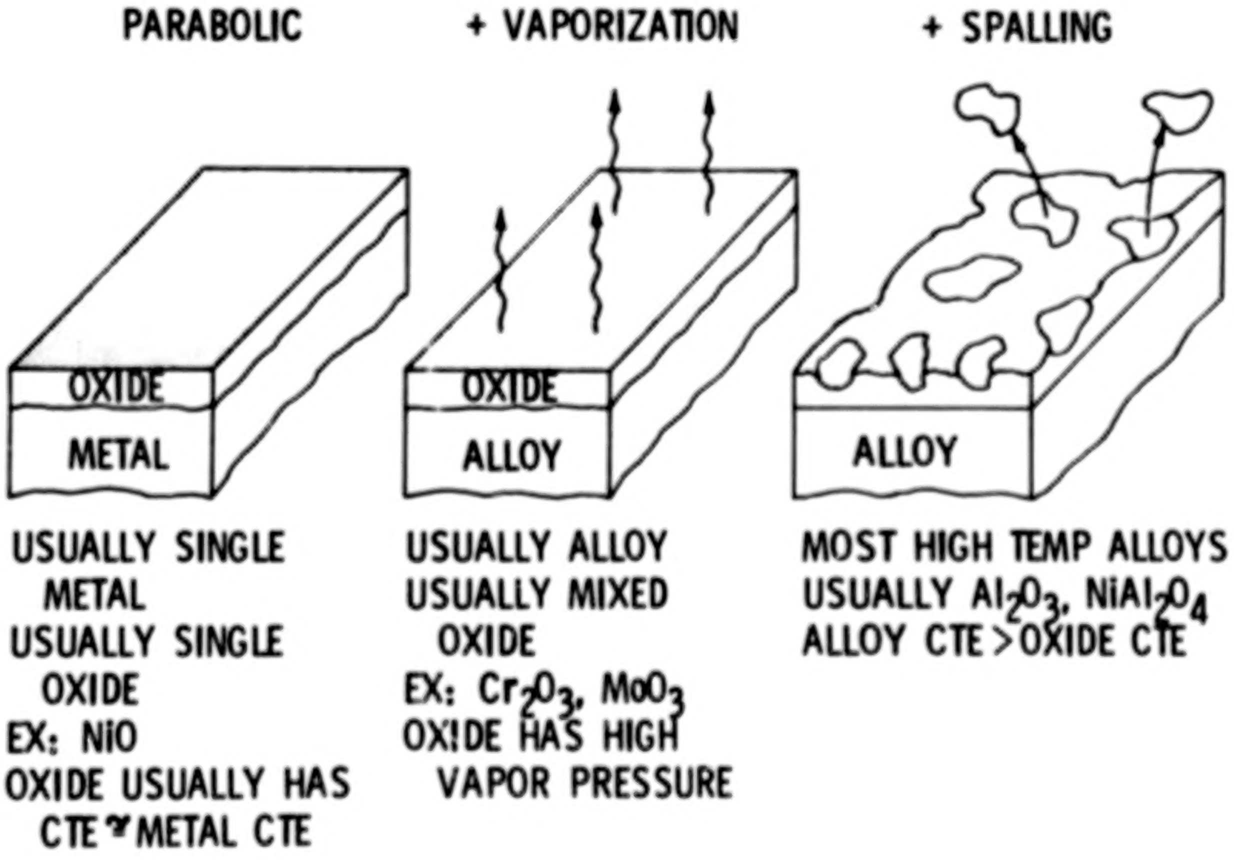
PARABOLIC
+ VAPORIZATION
+ SPALLING
OXIDE
METAL
OXIDE
ALLOY
ALLOY
USUALLY SINGLE METAL
USUALLY SINGLE OXIDE
EX: NiO
OXIDE USUALLY HAS CTE ≈ METAL CTE
USUALLY ALLOY
USUALLY MIXED OXIDE
EX: Cr_2O_3, MoO_3
OXIDE HAS HIGH VAPOR PRESSURE
MOST HIGH TEMP ALLOYS
USUALLY Al_2O_3, $NiAl_2O_4$
ALLOY CTE > OXIDE CTE

Figure 1

TYPES OF OXIDATION BEHAVIOR

Qualitative examples of the cyclic oxidation curves one might see with the three cases just discussed are illustrated in figure 2. The parabolic case, e.g. NiO, can be characterized by the parabolic rate constant, k_p. For an oxide which grows parabolically, but has a relatively high vapor pressure, such as Cr_2O_3, the linear vaporization constant, k_v, must be used in addition to k_p. For a system where the oxide grows parabolically, vaporizes at temperature, and partially spalls after each thermal cycle, the oxidation curve becomes quite complicated. However, the dashed curve gives an adequate representation and this involves a second linear constant, k_s, to account for spalling.

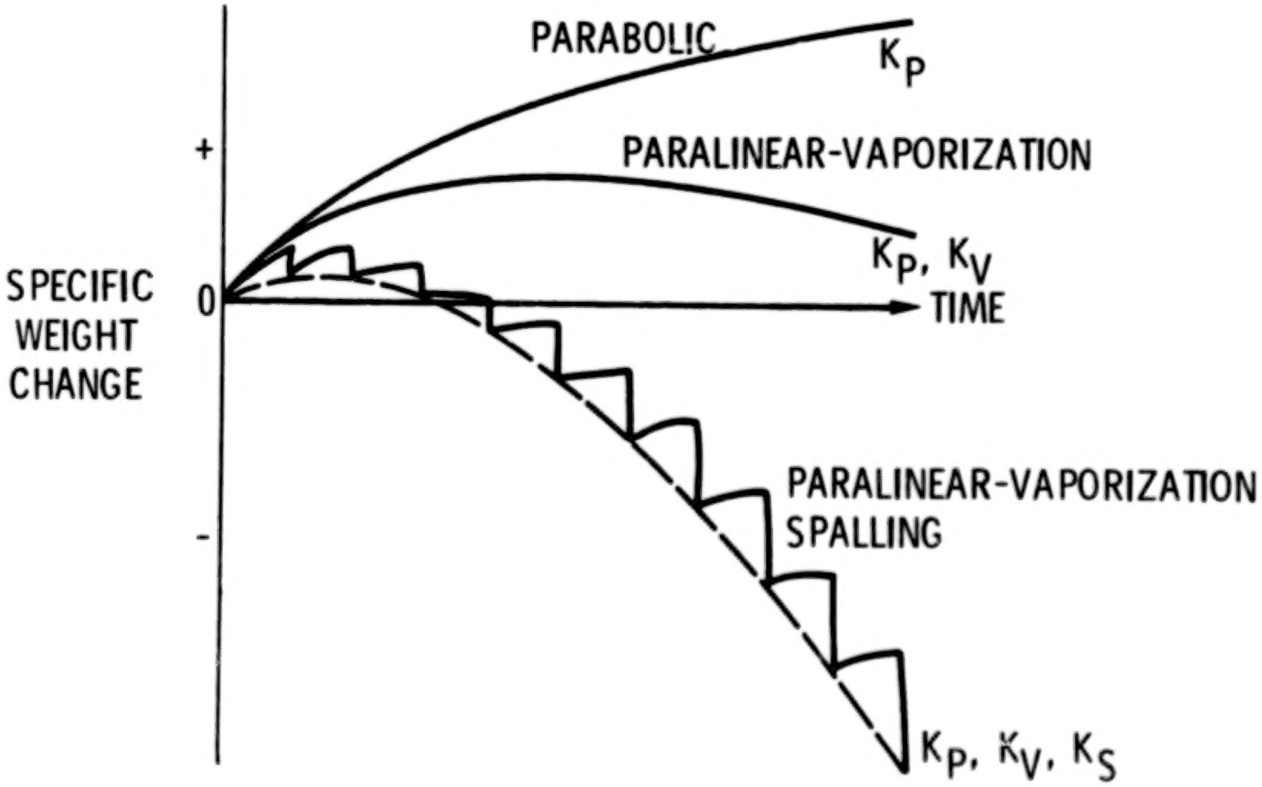

Figure 2

FUNDAMENTALS OF PROTECTIVE Al_2O_3 GROWTH

Because of the technological importance of aluminum oxide as a high-temperature protective scale, extensive studies of its growth behavior and morphology have been carried out (4). As a result it has been postulated, based on morphological evidence from the oxide scale-metal interface, that alumina grows most rapidly via grain boundary diffusion. This model has been verified by measurements of k_p as a function of grain size. The fact that large grain scales grow more slowly holds forth the promise for improving the protective capability of alumina scales through microstructural control (J. L. Smialek, unpublished research). (See fig. 3.)

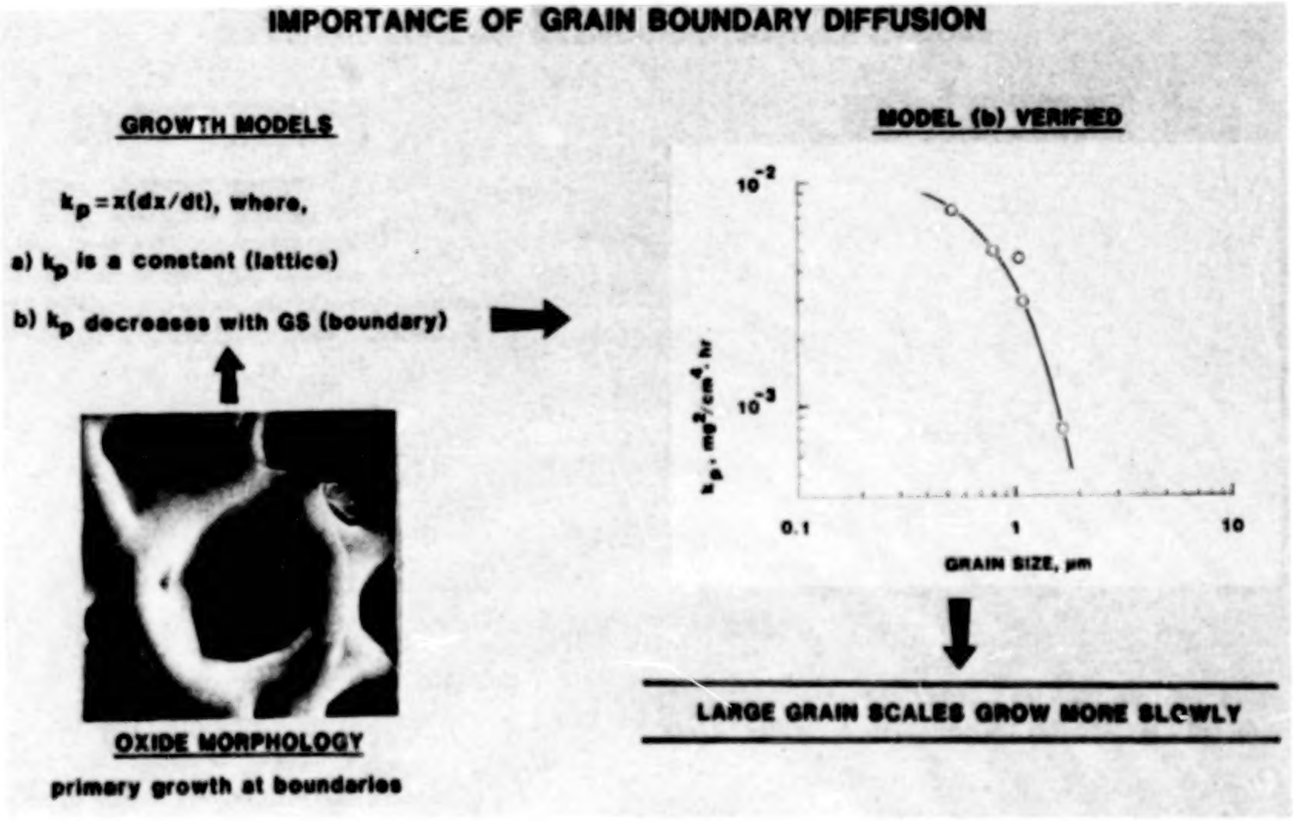

IMPORTANCE OF GRAIN BOUNDARY DIFFUSION

GROWTH MODELS

$k_p = x(dx/dt)$, where,

a) k_p is a constant (lattice)

b) k_p decreases with GS (boundary)

OXIDE MORPHOLOGY

primary growth at boundaries

MODEL (b) VERIFIED

LARGE GRAIN SCALES GROW MORE SLOWLY

Figure 3

SEM MICROGRAPHS OF SPALLED Al_2O_3 SCALES

The rate of aluminum depletion controls the capability of an alloy or coating to be protected as a consequence of forming an aluminum oxide scale. In the case of an alloy of "infinite" thickness, aluminum oxide spallation is the depletion mechanism while the kinetics of subscale diffusion determines the capability for Al_2O_3 scale formation. Therefore, both spallation and subscale diffusion must be modeled to predict alloy environmental life. The scanning electron microscope micrographs of figure 4 illustrate two types of spalling behavior. The Ni-40Al alloy exemplifies spalling to exposed metal over a fraction of the surface area. The Ni-Cr-Al-Zr alloy displays spalling within the oxide scale over a fraction of the surface area.

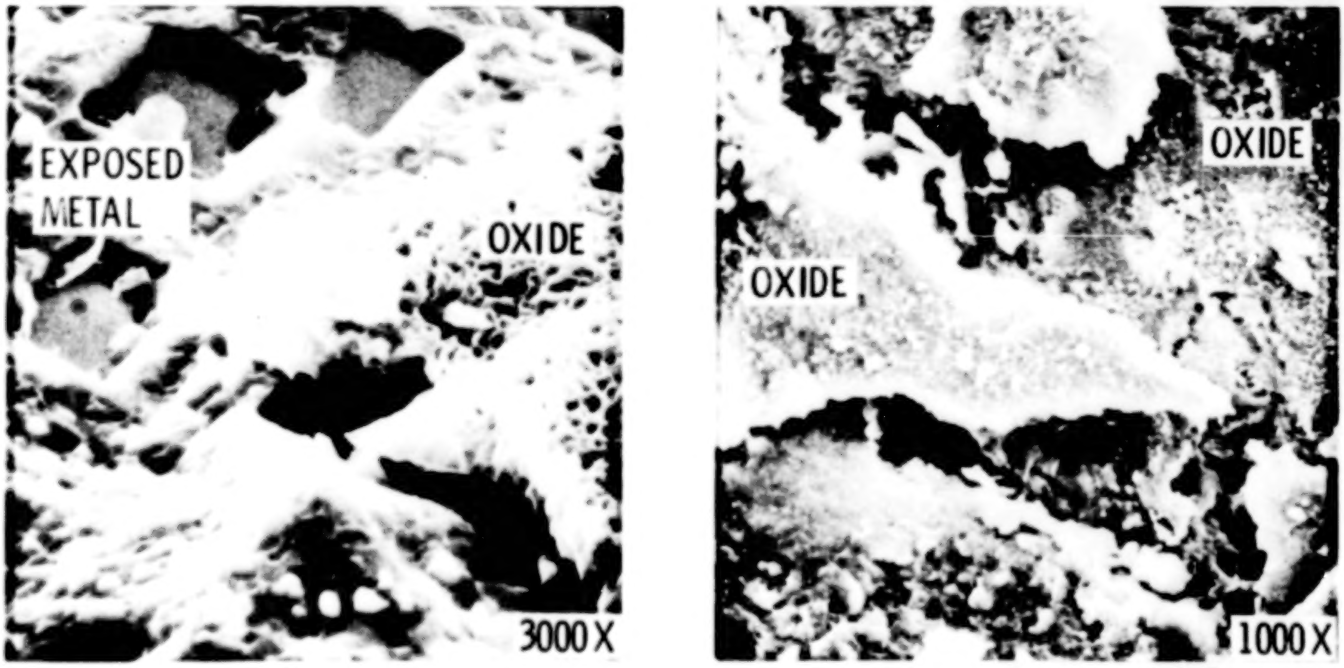

Ni-40 Al, 1200° C, 217 CYCLES

Ni-15Cr-24Al-0.3Zr, 1100° C, 500 CYCLES

Figure 4

CYCLIC OXIDATION VISUALIZATION

A cyclic oxidation model has been developed to predict aluminum depletion via spallation (C. E. Lowell, et al: Cyclic Oxidation of Superalloys. Proceedings of the International Conference on High-Temperature Corrosion, in press). In its simplest form, this model requires input data from isothermal oxidation tests only. The parameters required are the parabolic growth constant and a spalling fraction, Q. To model the actual behavior of the oxide surface, Q can be a constant spall fraction or can vary with oxide scale thickness. Also, Q can be set up to cover the case of spalling to bare metal or spalling within the oxide scale. For this detailed modeling, appreciable morphological data is also required. These various cases have been run using a computer model. Figure 5 illustrates three frames from a motion picture for a 400 segment model wherein the oxide spalls back 80 percent and with the spall fraction a function of scale thickness. At the end of the first heating cycle a uniform oxide scale has formed. Upon cooling, some oxide has spalled. After 100 cycles the surface structure becomes quite complex.

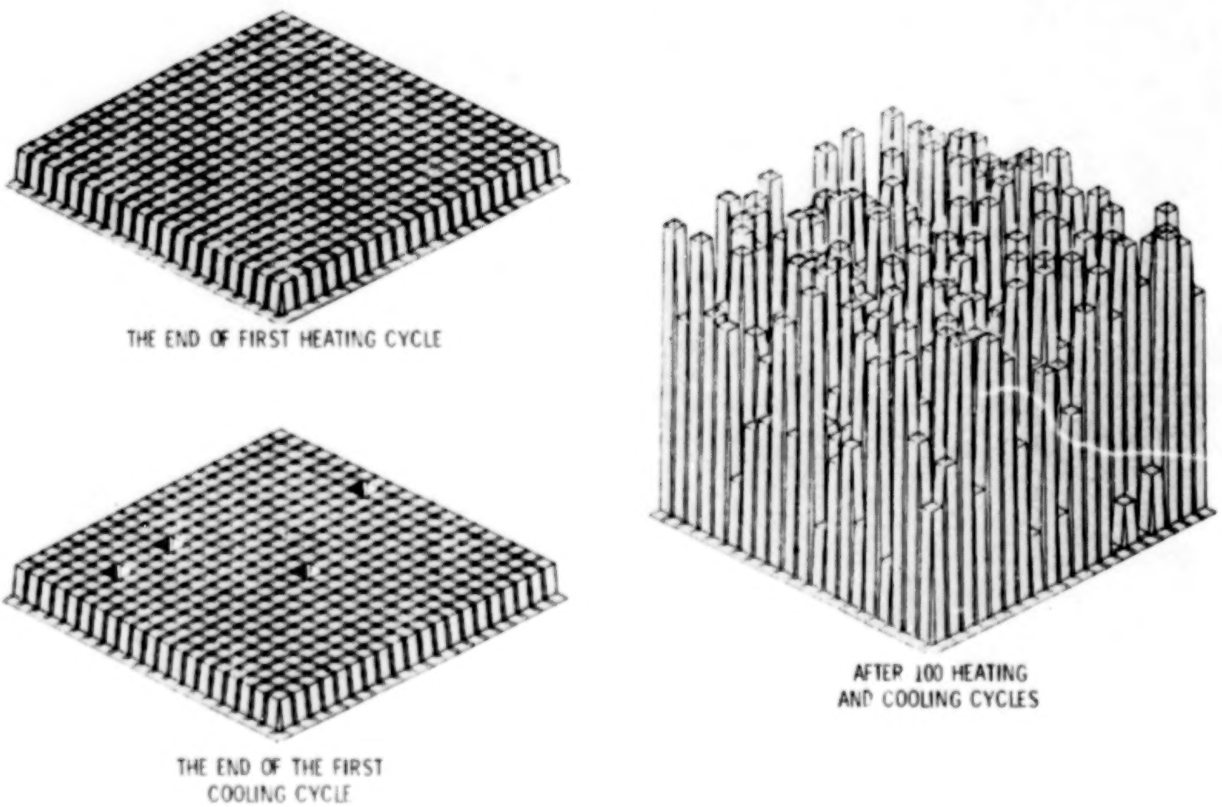

$K_p = 0.02$, $Q_0 = 0.02$, $NS = 400$

THE END OF FIRST HEATING CYCLE

THE END OF THE FIRST
COOLING CYCLE

AFTER 100 HEATING
AND COOLING CYCLES

Figure 5

CYCLIC OXIDATION PREDICTIONS FOR TWO SPALL MODELS

Figure 6 illustrates the results of the Monte Carlo calculations for two spall models - bimodal as illustrated in figure 5 and uniform constant fraction of the scale. The parameters used in these calculations fit the oxidation behavior of the oxide dispersion strengthened alloy TD-NiCrAl at 1200° C. The outcome of the calculations does not show a significant difference between the models. This turns out to be true in all cases. This greatly simplifies the calculations and permits the use of simple isothermal test results to model cyclic oxidation. The model can readily account for cycle frequency. The output of the computation gives retained oxide, metal consumption and specific weight change as a function of time or cycles.

MONTE CARLO, $K_p = 0.02$, $Q_0 = 0.02$

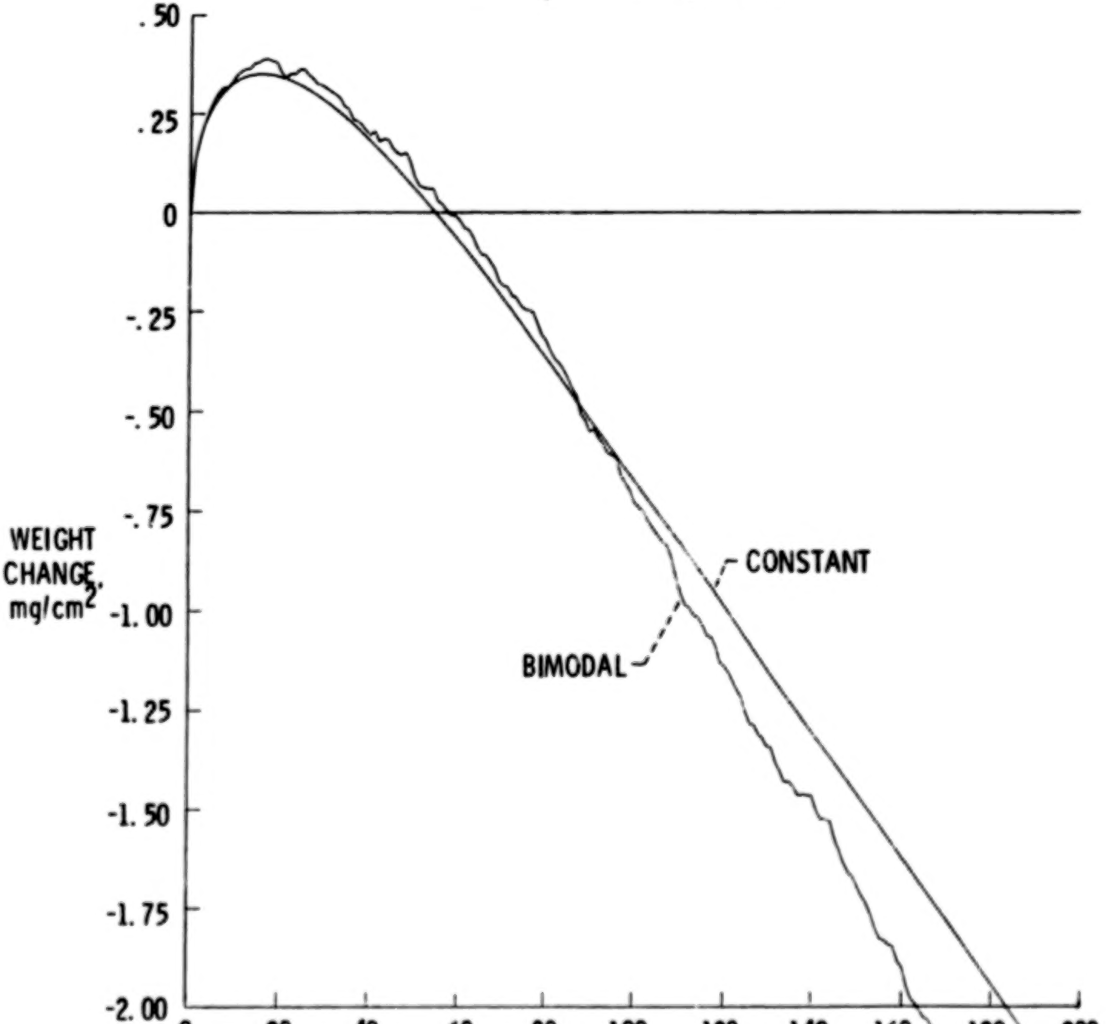

Figure 6

PREDICTIONS FROM ISOTHERMAL DATA AGREE WITH CYCLIC DATA

In figure 7, the results of a cyclic furnace oxidation experiment at 1200° C for an alumina forming NiCrAlZr alloy are compared with predictions from the cyclic oxidation model. The parameters for the model were determined from a short time isothermal test. Agreement is quite good out to 2500 1-hour cycles. At this point, a change in slope for the cyclic oxidation data is evident due to a change in the oxidation mechanism. At this point, the subscale can no longer provide aluminum at a sufficient rate and less protective oxides are formed.

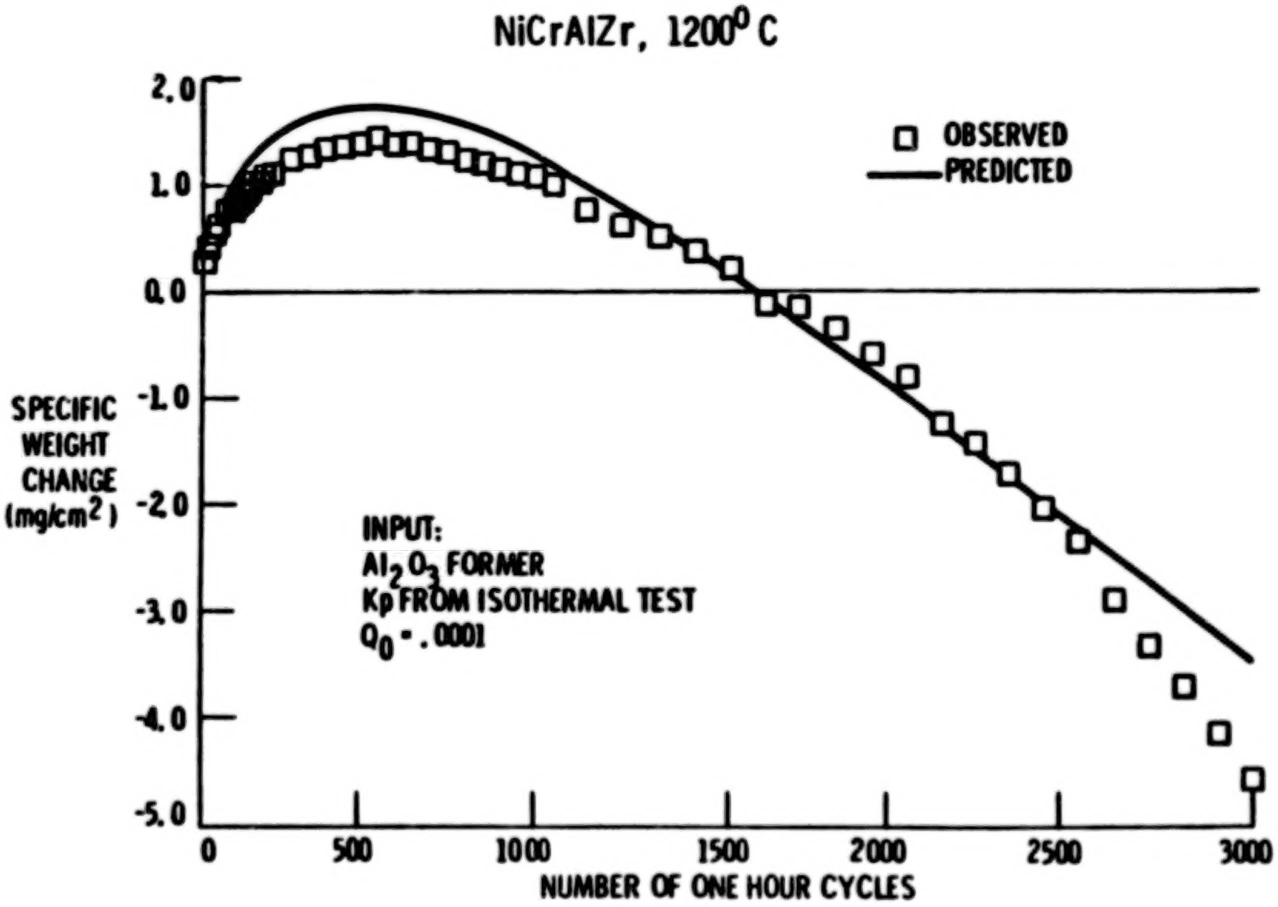

Figure 7

SUBSCALE DIFFUSION LIMITS OXIDATION LIFE

The key to predicting oxidation life then becomes integrating the cyclic oxidation model which accounts for aluminum depletion via oxide spallation with a subscale diffusion model which predicts the rate at which aluminum can diffuse to the surface. As illustrated in figure 8, at some critical concentration at the subscale surface, aluminum can no longer be supplied at a rate sufficient to meet the spalling demand and less protective oxides are formed. The subscale diffusion model has been developed (5) and it is being joined to the cyclic oxidation model.

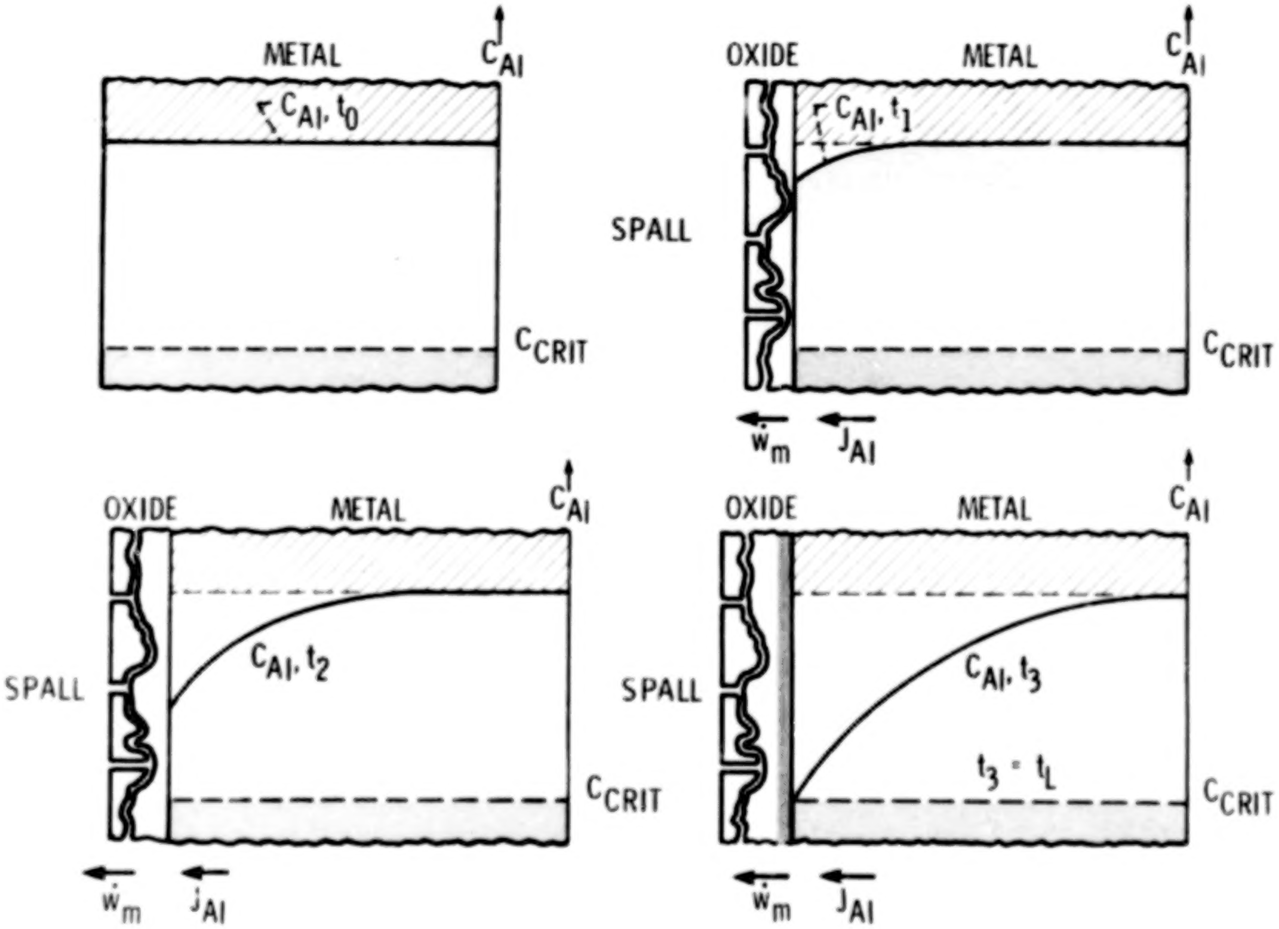
METAL
C_{Al}
C_{Al}, t_0
C_{CRIT}
OXIDE
METAL
C_{Al}
C_{Al}, t_1
SPALL
C_{CRIT}
$\dot{w}_m$
J_{Al}
OXIDE
METAL
C_{Al}
C_{Al}, t_2
SPALL
C_{CRIT}
$\dot{w}_m$
J_{Al}
OXIDE
METAL
C_{Al}
C_{Al}, t_3
SPALL
$t_3 = t_L$
C_{CRIT}
$\dot{w}_m$
J_{Al}

Figure 8

ENVIRONMENTAL AND SUBSTRATE REACTIONS DEGRADE COATINGS

In the case of finite metallic protective coatings, be they diffusionally formed aluminides or MCrAlY (M=Ni or Co) overlays, two distinct aluminum depletion mechanisms need to be dealt with - oxidation and interdiffusion. Figure 9 illustrates the nature and extent of these processes for a NiCrAlY overlay coating. Here the aluminum-rich NiAl phase in NiCrAlY has been over-etched so that it stands out. From these photomicrographs, it is evident that the diffusion reaction between the coating and substrate is of great importance. This has been documented for both aluminide (6) and overlay coatings (7). Also, some progress has been made toward controlling the kinetics of the reaction (7) and an effort to develop a diffusion model for coating life prediction is under way.

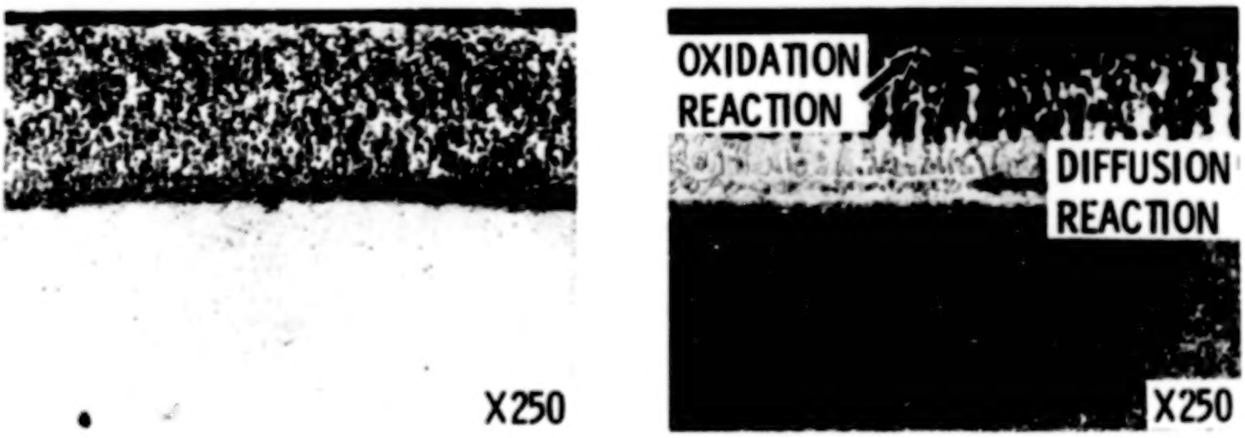

AS-DEPOSITED NiCrAlY COATING

AFTER 200 hr AT 2000° F

Figure 9

SCHEMATIC OF THERMAL BARRIER COATING CONCEPT

Figure 10 introduces a new subject - thermal barrier coatings. Conventional airfoils in the early turbine stages of advanced aircraft gas turbines are cooled with air bled from the compressor. Such cooling and protection from the environment by a metallic coating are required to permit useful component lives while attaining the thermodynamic efficiency benefits of high cycle temperatures. The addition of a thin oxide ceramic layer to such an airfoil adds a significant thermal resistance - hence coatings of this class are called thermal barrier coatings (TBC). Such coatings are most commonly zirconia-based ceramics applied by plasma spraying. A typical microstructure is shown in figure 10. The function of the metallic coating has now been expanded to that of a bond coat. The addition of a ten mil ceramic layer can easily result in a 100° C reduction in metal temperature. This capability offers the options of improved component durability through metal temperature reduction or improved cycle efficiency through reduced cooling air use and/or higher cycle temperature (8).

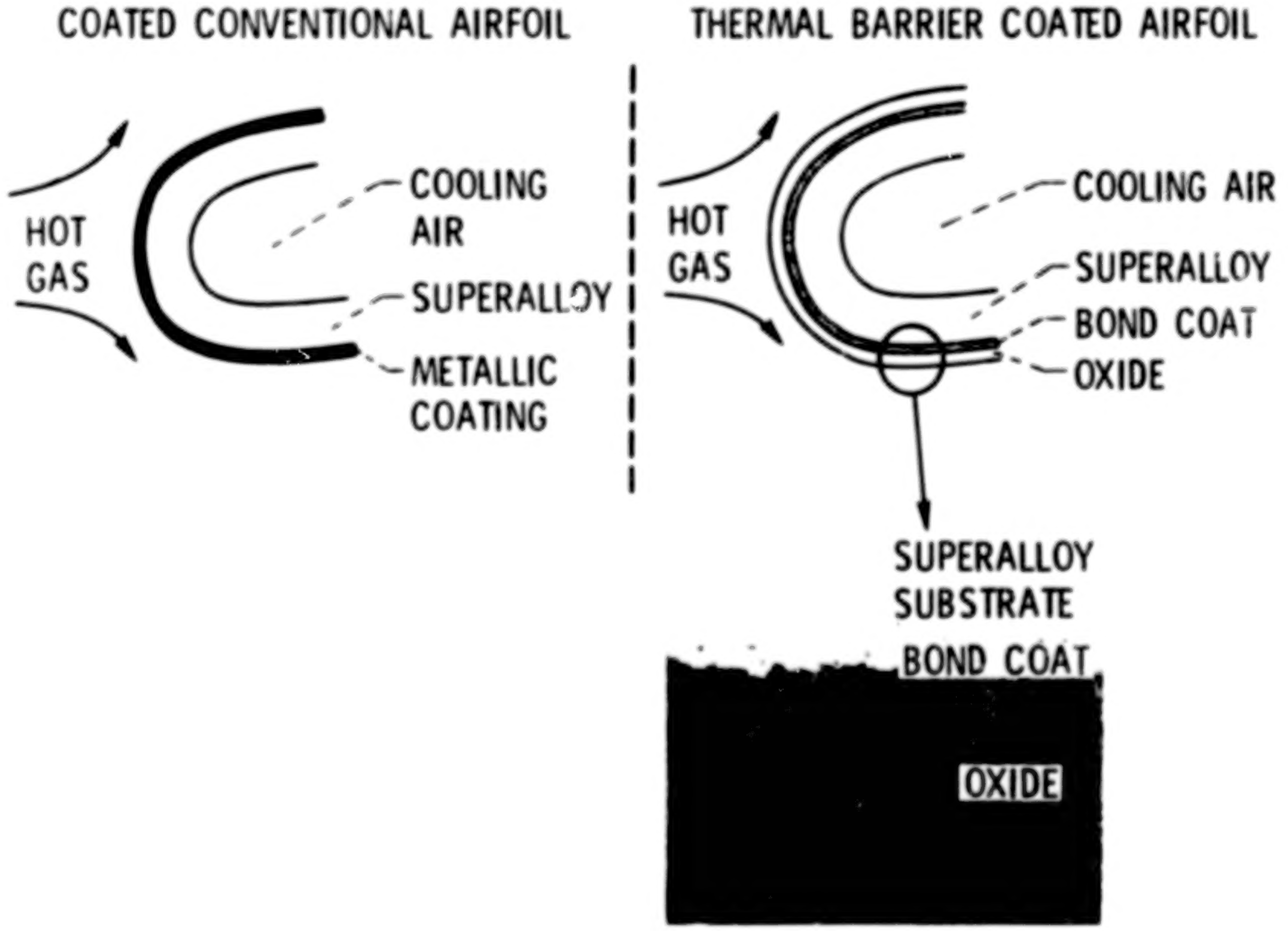
COATED CONVENTIONAL AIRFOIL
HOT GAS
COOLING AIR
SUPERALLOY
METALLIC COATING
THERMAL BARRIER COATED AIRFOIL
HOT GAS
COOLING AIR
SUPERALLOY
BOND COAT
OXIDE
SUPERALLOY SUBSTRATE
BOND COAT
OXIDE

Figure 10

APPLICATIONS OF THERMAL BARRIER COATINGS

Figure 11 illustrates some current and projected future applications of TBC in aircraft gas turbines. Such coatings were introduced to JT8D combuster liners in the late 60's to extend life. They are now being introduced in an advanced JT9D as first stage vane platform coatings in conjunction with a revised cooling system wherein impingement/convection cooling is being used in place of film cooling (9). This results in reduced manufacturing cost, reduced cooling air use yielding higher SFC, and improved durability. Both of these applications involve non-critical static parts. In the late 80's, TBC may begin to be used on turbine airfoils. In initial applications, it is expected that the coatings will be used only to extend life. Our ultimate objective is to provide the research and technology base to permit their ultimate use on the leading edges of advanced aircraft gas turbine first stage blades for performance improvement.

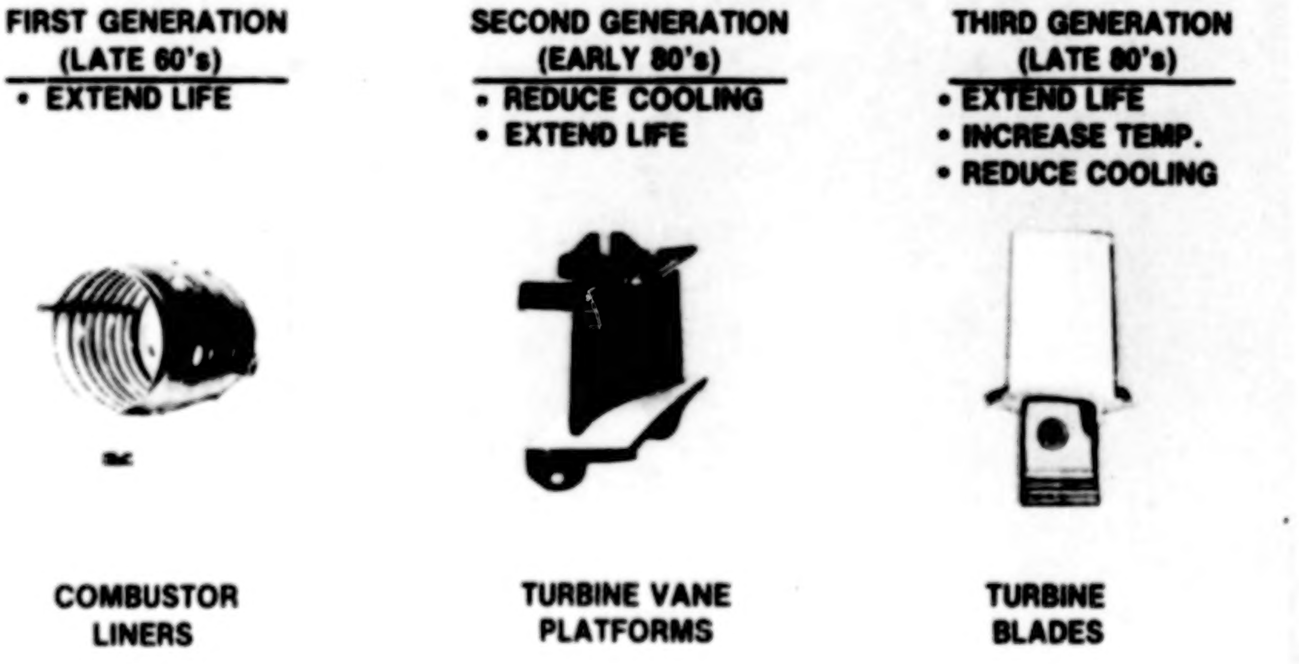
FIRST GENERATION
(LATE 60's)
• EXTEND LIFE
SECOND GENERATION
(EARLY 80's)
• REDUCE COOLING
• EXTEND LIFE
THIRD GENERATION
(LATE 80's)
• EXTEND LIFE
• INCREASE TEMP.
• REDUCE COOLING
COMBUSTOR
LINERS
TURBINE VANE
PLATFORMS
TURBINE
BLADES

Figure 11

TYPICAL JT9D - 7E ENGINE TEST RESULTS OF TBC COATED BLADES

The current impetus for TBC research was derived from the successful test of two layer coatings on air-cooled first-stage blades in a J-75 research engine. The coatings tested survived 500 cycles between full power and flameout (10). A typical first-stage blade from a more recent and more severe test in a JT9D, figure 12, indicated that the ZrO_2 . 12 weight percent Y_2O_3/NiCrAlY coating is not yet ready as an add-on coating for first-stage blades. The coating was intact on the blade platform, suction surface, and most of the pressure surface. Analysis indicated that failures occurred in regions of combined high temperature and compressive stress (11).

NO-COST CONTRACT WITH P & W; 264 hr - 1424 CYCLES

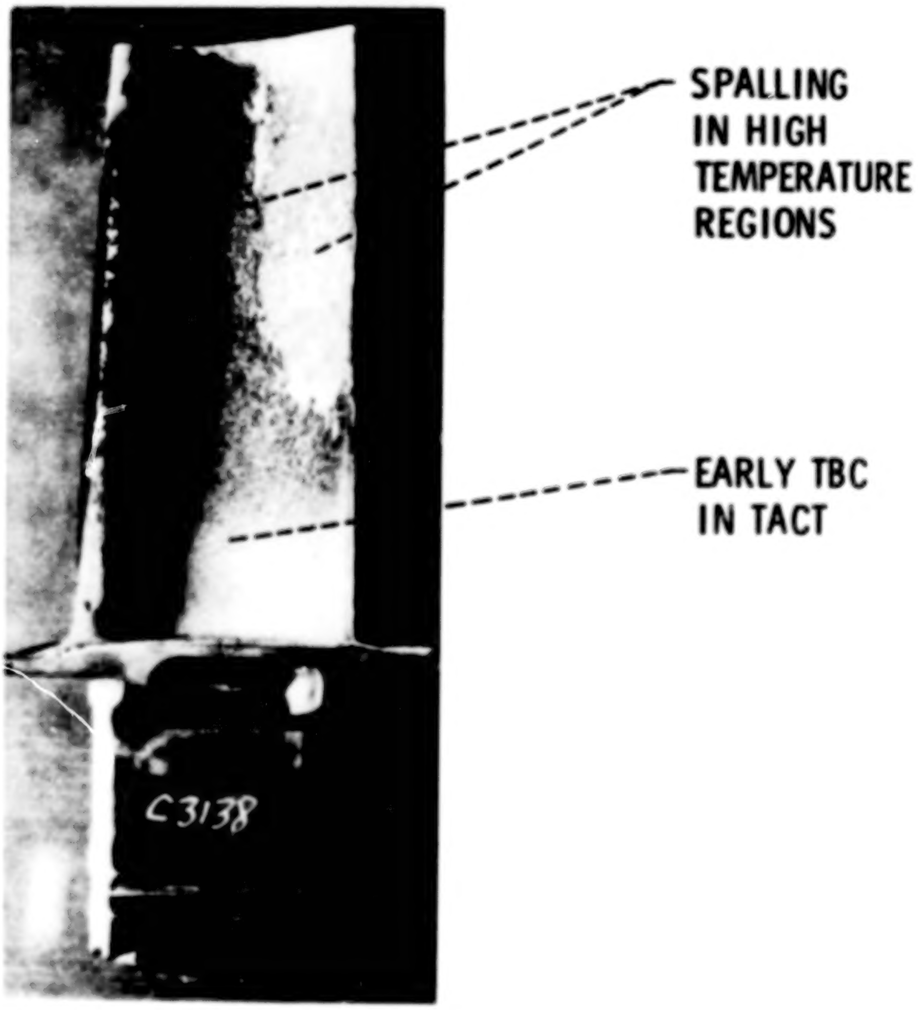

Figure 12

THERMAL BARRIER COATING PERFORMANCE

Based on the results of the JT9D test, it was clear that significant advances in TBC performance and in understanding of TBC behavior were required. The major thrusts of our effort are outlined in figure 13. In the areas of coating composition and structure, significant improvements in coating performance have been made and some of these will be discussed. The understanding of coating behavior in response to thermal stress and environmental degradation will provide the basis for correct design of coated components and will thus enable effective use of thermal barrier coatings.

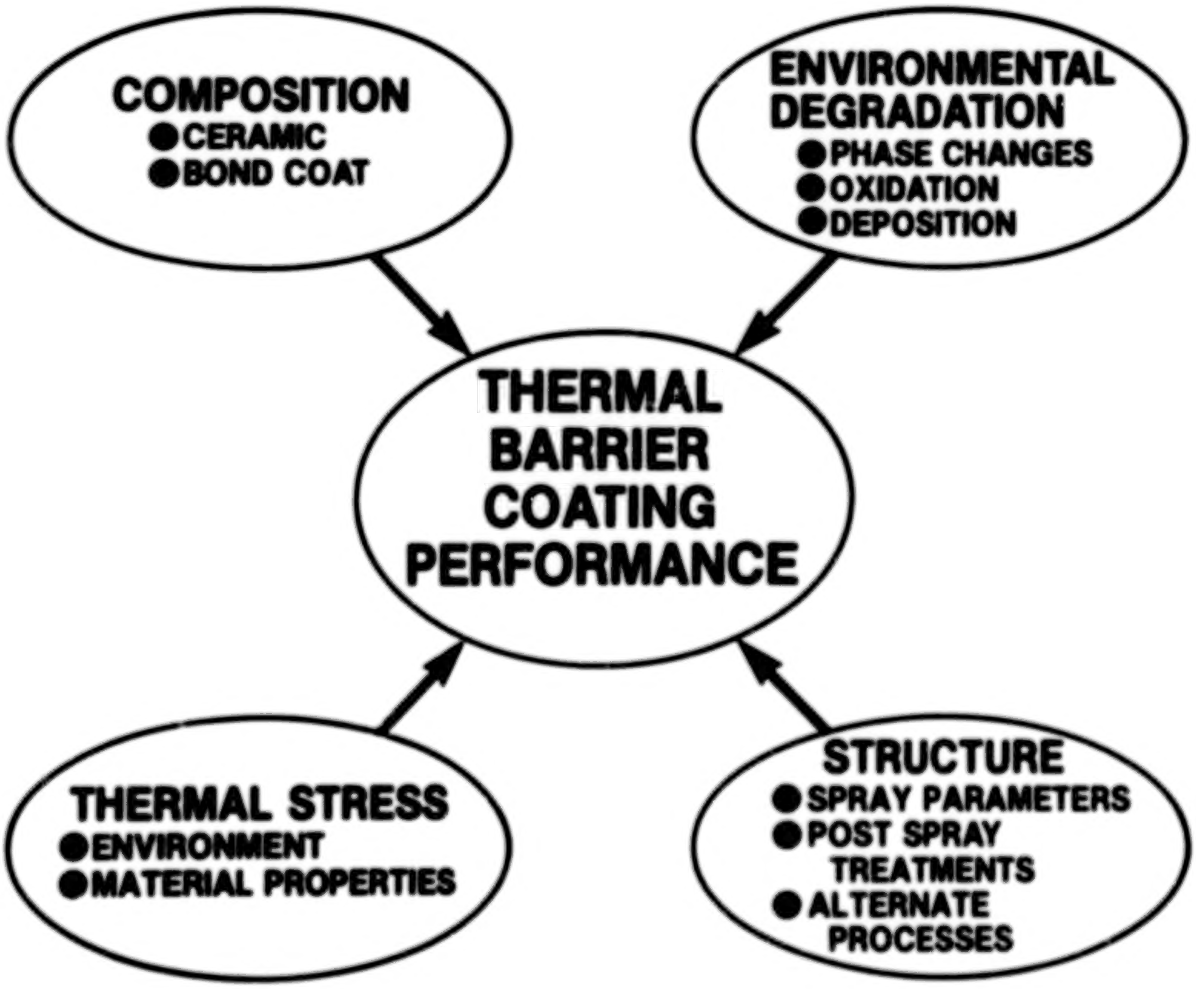
COMPOSITION
●CERAMIC
●BOND COAT
ENVIRONMENTAL DEGRADATION
●PHASE CHANGES
●OXIDATION
●DEPOSITION
THERMAL BARRIER COATING PERFORMANCE
THERMAL STRESS
●ENVIRONMENT
●MATERIAL PROPERTIES
STRUCTURE
●SPRAY PARAMETERS
●POST SPRAY TREATMENTS
●ALTERNATE PROCESSES

Figure 13

RESPONSE OF CERAMIC COATING TO STRESS OPPOSITE TO THAT OF BULK CERAMICS

One of the most important elements of understanding in both the processing of TBC and their use is the realization that conventional wisdom with regard to stresses in the ceramic does not apply. As illustrated in figure 14, TBC readily withstand tensile stresses which in this case have been induced by bending a coated metal strip around a mandrel. The coating is retained in tensile loaded areas of the convex surface. However, the ceramic has spalled from the concave surface where it was loaded in compression. The location of the failures are within the ceramic close to the bond coat-ceramic interface. This location is the weak link in ceramic coatings (12). The sensivity of ceramic coatings to compressive stress implies that processing should be carried out to minimize compressive residual stress (9). Also, components should be designed to minimize compressive stress generation during transients. However further investigation is required to find a solution to the longer term problem of stress relaxation at temperature and the implications on cooldown for a low coefficient of thermal expansion (CTE) TBC on a superalloy with higher CTE.

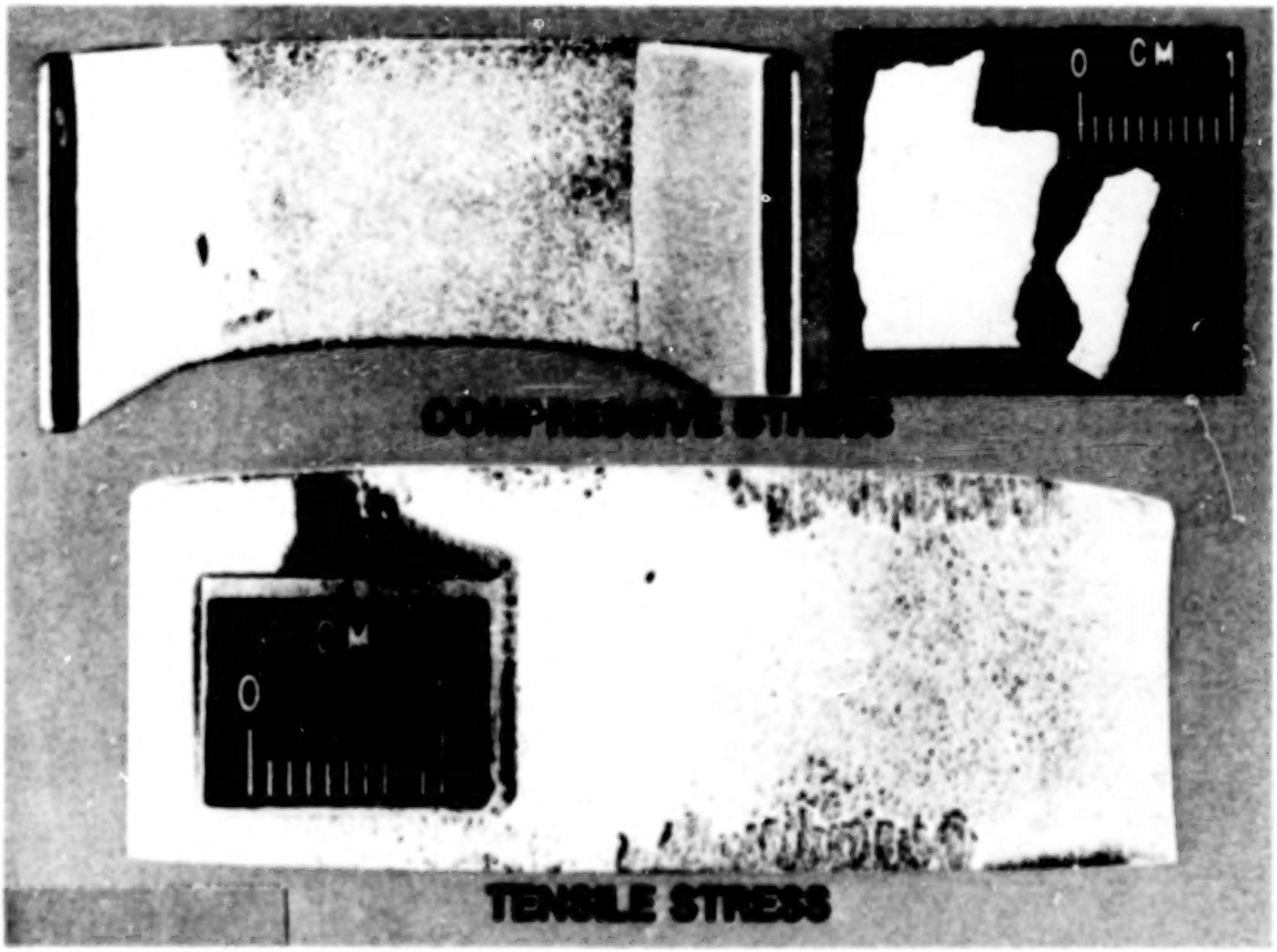

Figure 14

COATING COMPOSITION HAS IMPACT ON COATING LIFE

Early TBC research was oriented toward identifying zirconia based ceramics that were fully cubic phase stabilized rather than compositions that would undergo transformations between the cubic, tetragonal and monoclinic phases. The transformation from cubic or tetragonal to monoclinic was regarded as particularly undesirable because of its disruptive volume expansion. The early NASA ZrO_2 - 12 weight per cent Y_2O_3 coating fell into the category of a fully cubic phase stabilized zirconia (13). An investigation of the effect of yttria stabilizer level on ZrO_2 - Y_2O_3 TBC life revealed that the most durable coatings were obtained with partially stabilized zirconias (about 6 weight per cent yttria) applied to low yttrium NiCrAlY bond coats (14). The 4 weight per cent yttria stabilized zirconia (YSZ) composition was undesirable due to excessive monoclinic phase formation. In hot corrosion-inducing environments, 8 weight per cent YSZ has proven to be more durable than 6 weight per cent YSZ (15). Therefore, the 6 to 8 weight per cent range has been the focus of recent research. (See fig. 15.)

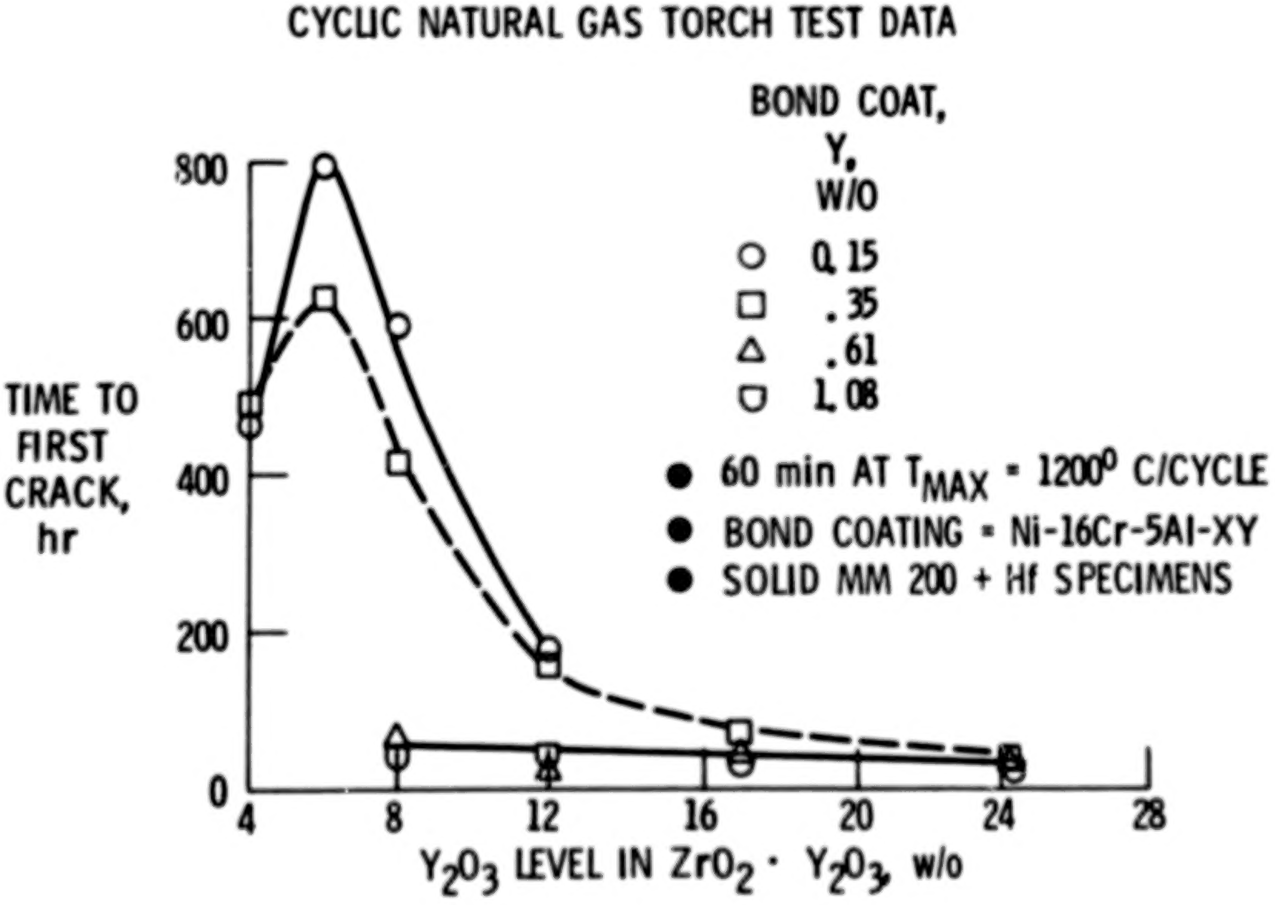

Figure 15

TBC FAILURE MECHANISMS

Thermal barrier coatings can fail due to thermal stress or due to thermally activated processes such as creep of the ceramic or bond coat, oxide sintering, or bond coat oxidation. These latter processes may degrade the coating to the point where thermal stress is the mechanism responsible for ceramic spallation. Separating these two major categories of failure mechanisms has proven to be a difficult process. However, by varying the length of the thermal cycle, it is possible to project two life curves for the pure failure mechanisms as shown at the upper left of figure 16. Early results in Mach 0.3 burner rig tests for a TBC with an oxidation prone Ni-16Cr-6Al-0.3Y bond coat seemed to indicate that thermal stress was responsible for coating failure (16). With more oxidation resistant bond coats, a mixed failure mode was identified (17), but the controlling mode could not be pinned down. By going to cycles of short duration (30 seconds) so that thermal stress was the only permissible failure mechanism, it was shown that thermal stress alone can not induce failure in the Mach 0.3 burner rig test (fig. 16). In the short cycle test, the coating survived 10,000 cycles without failure. However, a few cycles of longer duration, or pre-exposure of the coating in air for about 20 hours at 1250° C resulted in sufficient thermal degradation to cause coating failure (18). In cyclic thermal exposures at higher rates of heat input, as might be found in an engine, the role of thermal stress vs thermally activated processes remains to be determined. Based on the JT9D test and subsequent analysis, it is postulated that thermal stress may become dominant as the heat flux increases. A high pressure burner rig, soon to be constructed at Lewis, will be used to determine TBC failure mechanisms at advanced engine conditions.

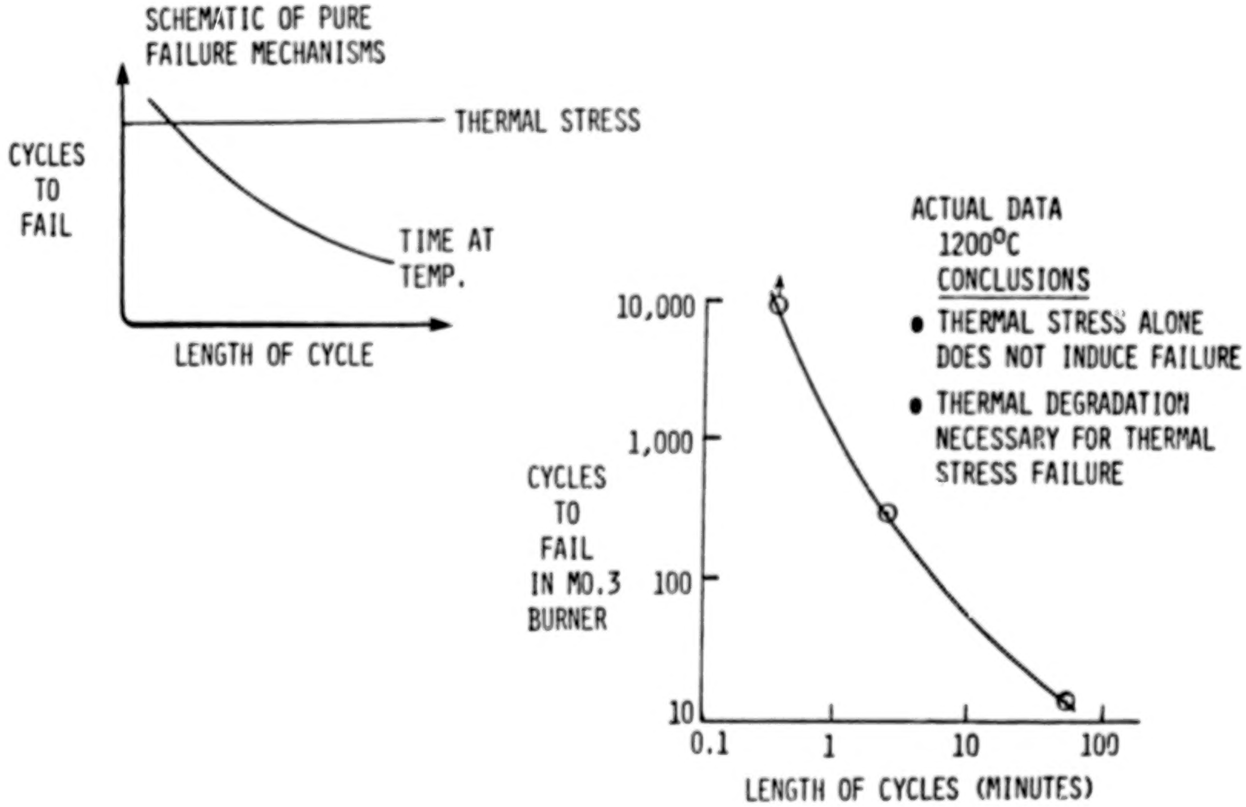

Figure 16

LIFE EXTENSION FOR THERMAL BARRIER COATINGS (TBC)

As pointed out earlier, the bond coat plays a dual role in a TBC. It provides oxidation and hot corrosion protection for the superalloy substrate while providing a good mechanical bond between the substrate and ceramic coating. The oxidation of the bond coat has been identified as a key potential failure mechanism for TBC (17,18). Significant improvements to the durability of TBC have been made through the use of more oxidation resistant bond coat compositions combined with improved plasma spray processing (17,19,20) as illustrated in figure 17(17). The improved compositions have high Cr and Al contents to provide a greater reservoir of protective oxide scale formers. Processing improvements include higher power levels and additions of hydrogen to the arc gas. Further improvements through low pressure plasma spray processing (21) can be anticipated.

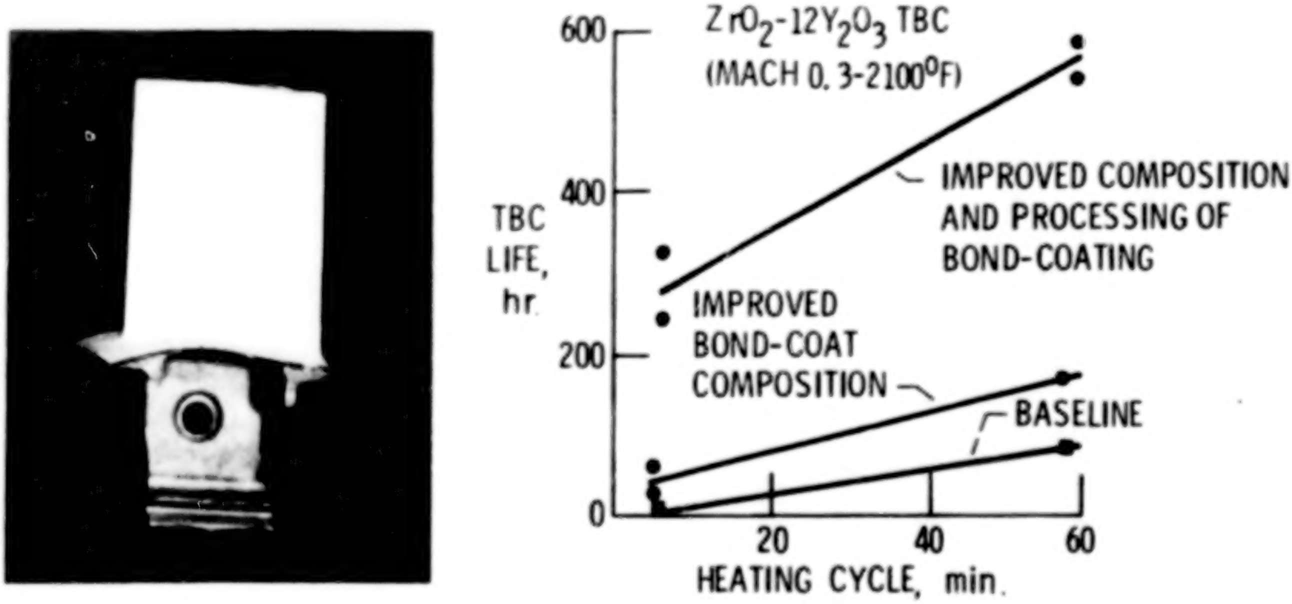

MATERIAL/PROCESS IMPROVEMENTS PRODUCE
- **10X LIFE IMPROVEMENT**

OR
- **100°C TEMPERATURE INCREASE**

OVER CURRENT THERMAL BARRIER COATINGS

Figure 17

THERMAL BARRIER COATING (TBC) TECHNOLOGY TRANSFER

Development of advanced technology, such as TBC, by NASA does little good unless it can be effectively transferred to industry. Lewis has entered into a number of cooperative agreements (contractual or informal) with various industrial concerns to transfer TBC to the user by providing hands-on experience. The results of some of these ventures are reported in the literature (22,23). Figures 18 and 12 illustrate some of the ventures in which we have participated, and the results and benefits obtained.

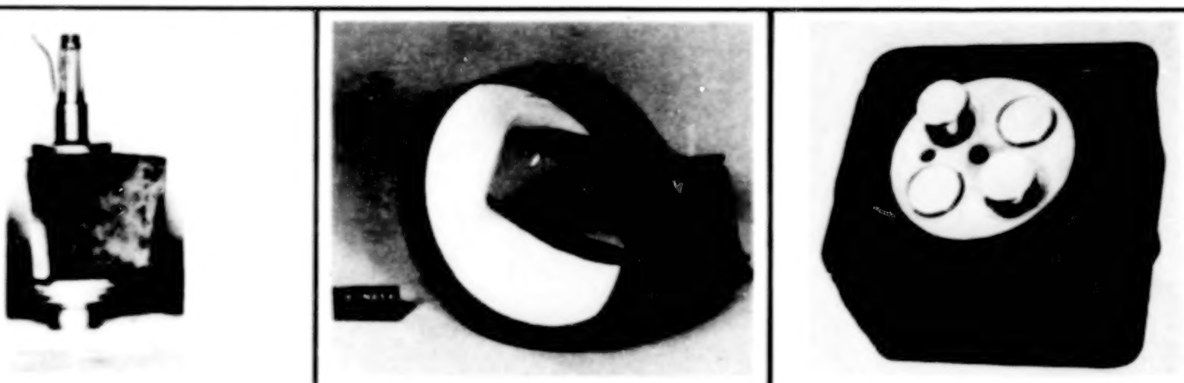

ADVANCED GAS TURBINE VANES

- APPLICATION OF TBC TO DDA/ATEGG VANES PREVENTED CRACKING AND MELTING

GAS TURBINE COMBUSTOR TRANSITION SECTIONS

- NASA TBC ADHERED PREVENTING WARPING OF TRANSITION SECTIONS

DIESEL ENGINE HEAD AND VALVES

- TBC ADHERED AND PROVIDED SOME OF THE REQUIRED INSULATION

Figure 18

REFERENCES

1. Grisaffe, S. J.; Lowell, C. E.; and Stearns, C. A.: High Temperature Environmental Effects on Metals. Risk and Failure Analysis for Improved Performance and Reliability, J. J. Burke and V. Weiss, eds., Plenin Publishing Corp., 1980, pp. 225-242.

2. Stearns, C. A.; Kohl, F. J.; and Rosner, D. E.: Combustion System Processes Leading to Corrosive Deposits. NASA TM-81752, 1981.

3. Merutka, J. P.: Progress in Protective Coatings for Aircraft Gas Turbines - A Review of NASA Sponsored Research. NASA TM-82740, 1981.

4. Smialek, J. L.: Microstructure of Al_2O_3 Scales Formed on NiCrAl Alloys. NASA TM-81676, 1981.

5. Nesbitt, J. A.: Solute Transport During the Cyclic Oxidation of Ni-Cr-Al Alloys. NASA CR-165544, 1982.

6. Smialek, J. L.; and Lowell, C. E.: Effects of Diffusion on Aluminum Depletion and Degradation of NiAl Coatings. J. Electrochem. Soc., Vol. 121, 1974, pp. 800-805.

7. Gedwill, M. A.; Glasgow, T. K.; and Levine, S. R.: A New Diffusion-Inhibited Oxidation-Resistant Coating for Superalloys. NASA TM-82687, 1981.

8. Levine, S. R.; Miller, R. A.; and Hodge, P. E.: Thermal Barrier Coatings for Heat Engine Components. SAMPE Quarterly, Vol. 12, 1980, pp. 20-26.

9. Sheffler, K. D.; and Graziani, R. A.: JT9D Thermal Barrier Coated Vanes. NASA CR-167964, 1982.

10. Liebert, C. H.; Jacobs, R. E.; Stecura, S.; and Morse, R.: Durability of Zirconia Thermal-Barrier Ceramic Coatings on Air-Cooled Turrbine Blades in Cyclic Jet Engine Operation. NASA TM X-3410, 1976.

11. Sevcik, W. R.; and Stoner, B. L.: An Analytical Study of Thermal Barrier Coated First Stage Blades in a JT9D Engine. NASA CR-135360, 1978.

12. Levine, S. R.: Adhesive/Cohesive Strength of a ZrO_2-12 w/o Y_2O_3/NiCrAlY Thermal Barrier Coating. NASA TM-73792, 1977.

13. Stecura, S.: Two-Layer Thermal Barrier Coating for High Temperature Components. Ceramic Bulletin, Vol. 56, 1977, pp. 1081-1089.

14. Stecura, S.: Effects of Compositional Changes on the Performance of a Thermal Barrier Coating System. NASA TM-78976, 1978.

15. Hodge, P. E.; Miller, R. A.; and Gedwill, M. A.: Evaluation of Hot Corrosion Behavior of Thermal Barrier Coatings. NASA TM-81520, 1980.

16. McDonald, G.; and Hendricks, R. C.: Effect of Thermal Cycling on ZrO_2-Y_2O_3 Thermal Barrier Coatings. NASA TM-81480, 1980.

17. Gedwill, M. A.: Burner Rig Evaluation of Thermal Barrier Coating Systems for Nickel-Base Alloys. NASA TM-81683, 1981.

18. Miller, R. A.; and Lowell, C. E.: Failure Mechanisms of Thermal Barrier Coatings Exposed to Elevated Temperatures. Thin Solid Films, Vol. 95, 1982, pp. 265-273.

19. Stecura, S.: Effects of Yttrium, Chromium, and Aluminum Concentrations in Bond Coatings on the Performance of Zirconia Yttria Thermal Barriers. NASA TM-79206, 1979.

20. Stecura, S.: Effects of Plasma Spray Parameters on Two-Layer Thermal Barrier Coating System Life. NASA TM-81724, 1981.

21. Pennisi, F. J.; and Gupta, D. K.: Tailored Plasma Sprayed MCrAlY Coatings for Aircraft Gas Turbine Applications. NASA CR-165234, 1981.

22. Liebert, C. H.; and Stepka, F. S.: Industry Tests of NASA Ceramic Thermal Barrier Coatings - for Gas Turbine Engine Applications. NASA TP-1425, 1979.

23. Liebert, C. H.; and Levine, S. R.: Further Industrial Tests of Ceramic Thermal-Barrier Coatings. NASA TP-2057, 1982.

DURABILITY OF AIRCRAFT COMPOSITE MATERIALS

H. Benson Dexter
NASA Langley Research Center
Hampton, Virginia

INTRODUCTION

Since the early 1970's, the NASA Langley Research Center has had programs under way to develop a data base and establish confidence in the long-term durability of advanced composite materials for aircraft structures. A series of flight service programs are obtaining worldwide service experience with secondary and primary composite components installed on commercial and military transport aircraft and helicopters. Included are spoilers, rudders, elevators, ailerons, fairings and wing boxes on transport aircraft and doors, fairings, tail rotors, vertical fins, and horizontal stabilizers on helicopters. Materials included in the evaluation are boron/epoxy, Kevlar/epoxy, graphite/epoxy and boron/aluminum. Inspection, maintenance, and repair results for the components in service are reported. The effects of long-term exposure to laboratory, flight, and outdoor environmental conditions are reported for various composite materials. Included are effects of moisture absorption, ultraviolet radiation, and aircraft fuels and fluids. Figure 1 summarizes some points of the aircraft composite materials program.

DURABILITY OF AIRCRAFT COMPOSITE MATERIALS

- FLIGHT SERVICE OF COMPOSITE COMPONENTS
  - TRANSPORT AIRCRAFT
  - HELICOPTERS
- ENVIRONMENTAL EFFECTS ON COMPOSITES
  - WORLDWIDE GROUND-BASED OUTDOOR EXPOSURE
  - FLIGHT EXPOSURE OF MATERIAL COUPONS
  - CONTROLLED LABORATORY EXPOSURE

Figure 1

FLIGHT SERVICE COMPOSITE COMPONENTS ON TRANSPORT AIRCRAFT

Confidence in the long-term durability of advanced composites is being developed through flight service of numerous composite components on transport aircraft. Emphasis has been on commercial aircraft because of their high utilization rates, exposure to worldwide environmental conditions, and systematic maintenance procedures. The composite components currently being evaluated on transport aircraft are shown in figure 2. Eighteen Kevlar/epoxy fairings have been in service on Lockheed L-1011 aircraft since 1973. In April 1982 eight graphite/epoxy ailerons developed under the NASA ACEE program were installed on four L-1011 aircraft for service evaluation. One hundred and eight graphite/epoxy spoilers have been in service on six different commercial airlines in worldwide service since 1973. Thirteen graphite/epoxy DC-10 upper aft rudders are in service on five commercial airlines and three boron/aluminum aft pylon skins have been in service on DC-10 aircraft since 1975. Ten graphite/epoxy elevators have been in service on B-727 aircraft since 1980. In addition to the commercial aircraft components shown in figure 2, two boron/epoxy reinforced aluminum center-wing boxes have been in service on U.S. Air Force C-130 transport aircraft since 1974.

L-1011 FAIRING AND AILERON

B-737 SPOILER

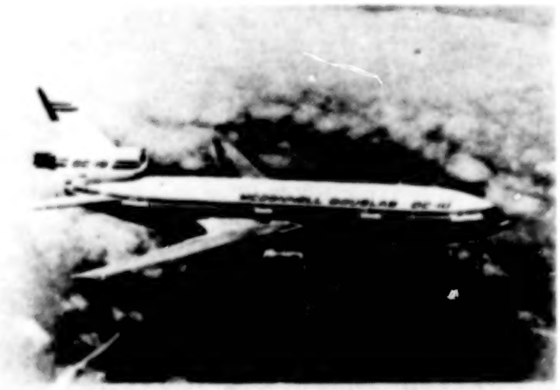
DC-10 RUDDER AND AFT PYLON

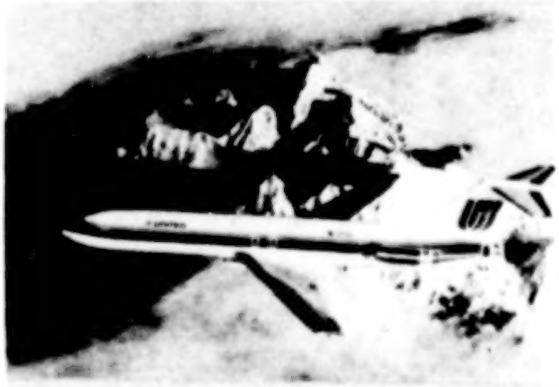
B-727 ELEVATOR

Figure 2

ACEE COMPOSITE SECONDARY STRUCTURES

The three major U.S. commercial transport manufacturers have been under NASA contract to design, fabricate, and test the major secondary composite components shown in figure 3. The components were developed as part of the NASA Aircraft Energy Efficiency (ACEE) Program. Each of the components has been certified by the FAA and flight service evaluation is under way. The three components utilize different design concepts. The graphite/epoxy rudders are multi-rib stiffened, the elevators are constructed with graphite/epoxy skins and Nomex honeycomb sandwich, and the aileron design features a syntactic-core sandwich with graphite/epoxy facesheets. An overall mass saving of 25 percent was achieved for the three components when compared to the production aluminum designs.

BOEING 727 COMPOSITE ELEVATOR

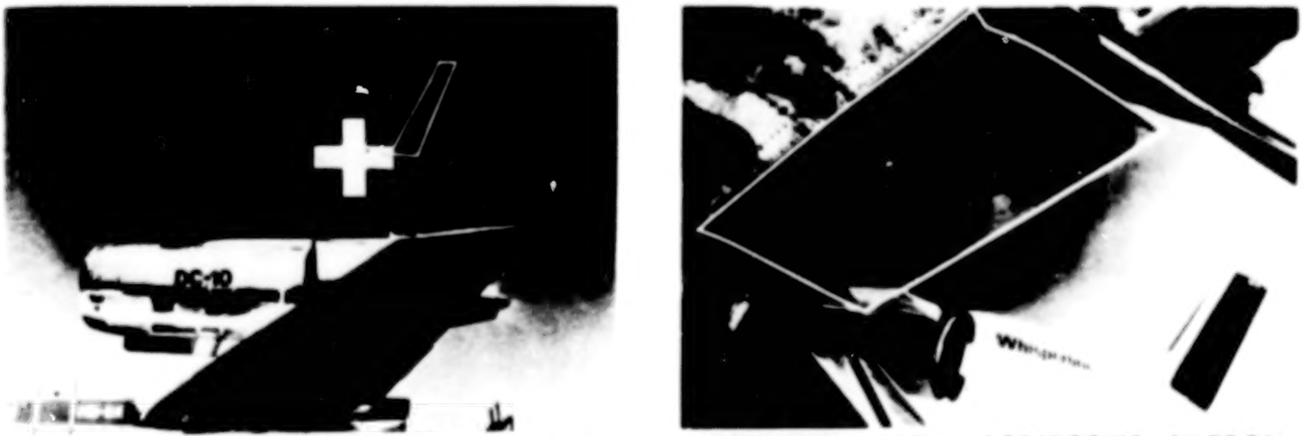

DOUGLAS DC-10 COMPOSITE RUDDER

LOCKHEED L-1011 COMPOSITE AILERON

Figure 3

FLIGHT SERVICE COMPOSITE COMPONENTS ON HELICOPTERS

Composite components are being evaluated in service on commercial and military helicopters, as shown in figure 4. Forty shipsets of Kevlar/epoxy doors and fairings and graphite/epoxy vertical fins are being installed on Bell 206L commercial helicopters for 5 to 10 years of service evaluation. The helicopters are operating in diverse environments in Alaska, Canada, and the U.S. Gulf Coast. Selected components will be removed from service for residual strength testing. Ten tail rotors and four horizontal stabilizers will be removed from S-76 production helicopters to determine the effects of realistic operational service environments on composite primary helicopter components. Static and fatigue tests will be conducted on the components removed from service and the results will be compared with baseline certification test results. In addition, several hundred composite coupons exposed to the outdoor environment will be tested for comparison with the component test results. A Kevlar/epoxy cargo ramp skin is being evaluated on a U.S. Marine Corps CH-53D helicopter. The laminated fabric skin may encounter severe handling such as rough runway abrasion and impact. Maintenance characteristics of the Kevlar skin will be compared with those of production aluminum skin.

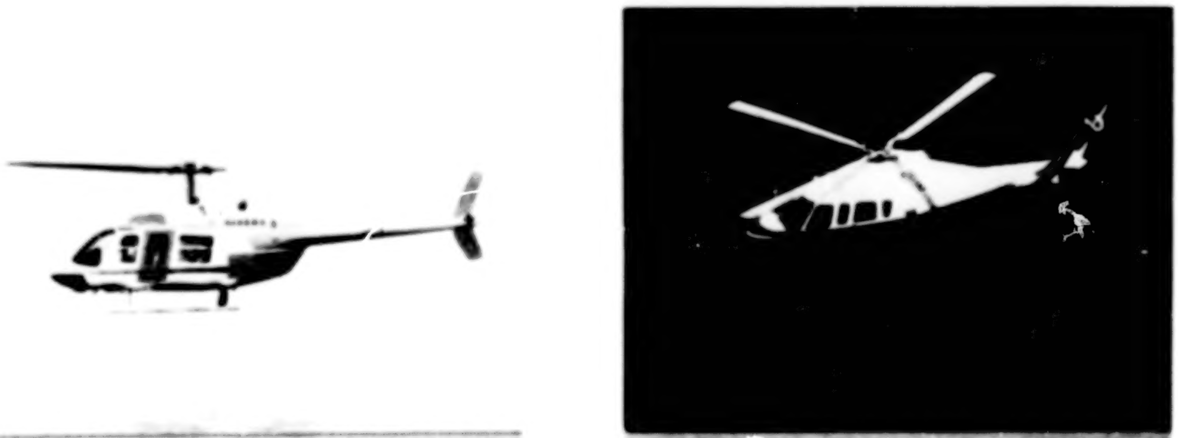

206L DOORS, FAIRING AND VERTICAL FIN

S-76 TAIL ROTOR AND HORIZONTAL STABILIZER

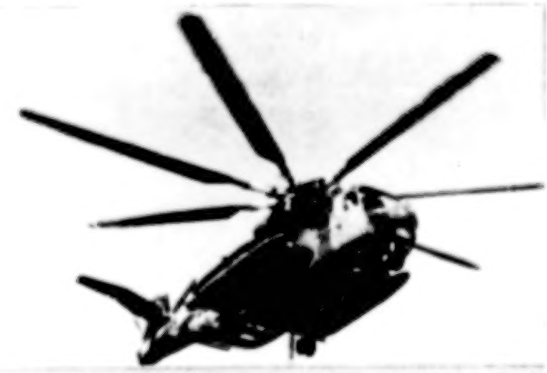

CH-53 CARGO RAMP SKIN

Figure 4

BELL 206L HELICOPTER COMPOSITE COMPONENTS

The four composite components that are being evaluated on the Bell 206L are shown in figure 5. Four different structural design concepts are used in the composite components. The forward fairing is a sandwich structure with a single ply of Kevlar/epoxy fabric co-cured on a polyvinylchloride foam core. The vertical fin is constructed with graphite/epoxy facesheets bonded to a Fibertruss honeycomb core. The litter door is constructed with Kevlar/epoxy fabric and has local reinforcement at load introduction points (hinges and latch assembly). The litter door is a hollow section with inner and outer skins and unidirectional Kevlar/epoxy tape is used in the post area and in the hat-section stiffeners. The baggage door is constructed with Kevlar/epoxy fabric facesheets and Nomex honeycomb core. Additional reinforcements are added in the area of the latch and along the edges.

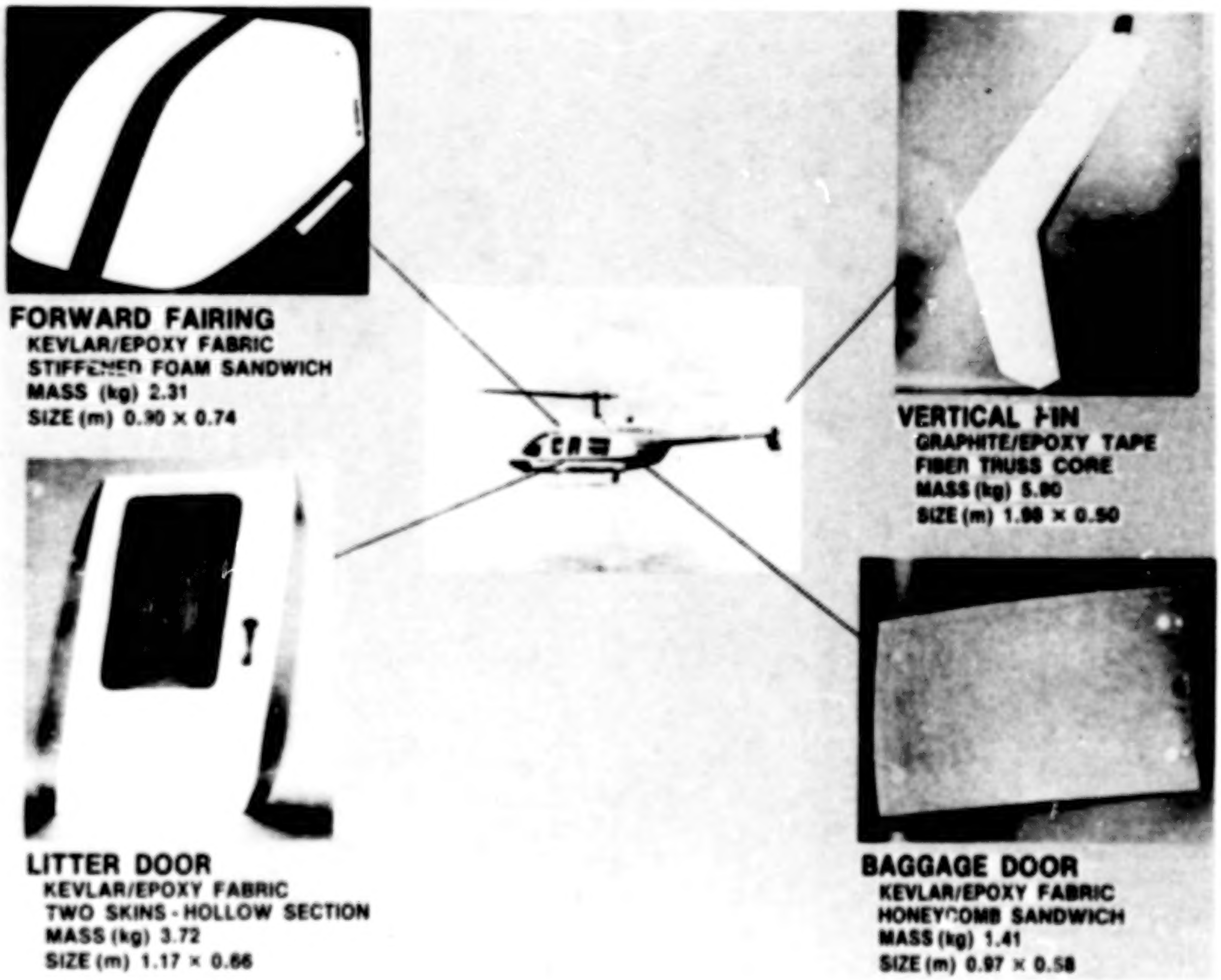
FORWARD FAIRING
KEVLAR/EPOXY FABRIC
STIFFENED FOAM SANDWICH
MASS (kg) 2.31
SIZE (m) 0.90 × 0.74
VERTICAL FIN
GRAPHITE/EPOXY TAPE
FIBER TRUSS CORE
MASS (kg) 5.90
SIZE (m) 1.98 × 0.50
LITTER DOOR
KEVLAR/EPOXY FABRIC
TWO SKINS - HOLLOW SECTION
MASS (kg) 3.72
SIZE (m) 1.17 × 0.86
BAGGAGE DOOR
KEVLAR/EPOXY FABRIC
HONEYCOMB SANDWICH
MASS (kg) 1.41
SIZE (m) 0.97 × 0.58

Figure 5

SIKORSKY S-76 HELICOPTER COMPOSITE COMPONENTS

The two composite components that are being evaluated on the Sikorsky S-76 are shown in figure 6. The composite components are baseline designs for the S-76 and are currently in commercial production. The tail rotor has a laminated graphite/epoxy spar with a glass/epoxy skin. The horizontal stabilizer has a Kevlar/epoxy torque tube with graphite/epoxy spar caps, full-depth Nomex honeycomb sandwich core, and Kevlar/epoxy skins. Components have been removed from helicopters and tested after 2 years of service. In addition, small coupons exposed to the outdoor environment were tested and results were compared to baseline values. No significant reduction in either component or coupon strengths was noted. Measured moisture levels were similar to results obtained from other environmental effects programs sponsored by NASA Langley.

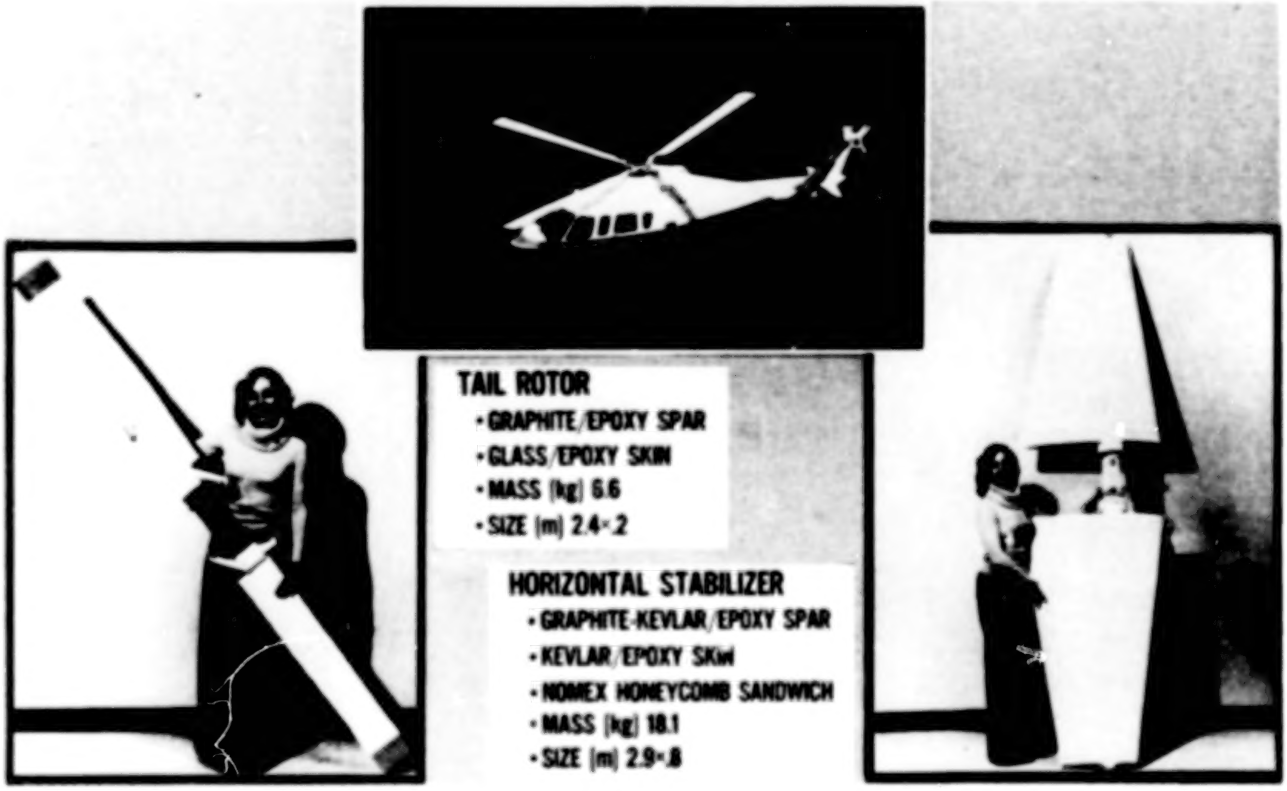
TAIL ROTOR
•GRAPHITE/EPOXY SPAR
•GLASS/EPOXY SKIN
•MASS (kg) 6.6
•SIZE (m) 2.4×.2
HORIZONTAL STABILIZER
•GRAPHITE-KEVLAR/EPOXY SPAR
•KEVLAR/EPOXY SKIN
•NOMEX HONEYCOMB SANDWICH
•MASS (kg) 18.1
•SIZE (m) 2.9×.8

Figure 6

NASA COMPOSITE STRUCTURES FLIGHT SERVICE SUMMARY

A total of 300 composite components have been in service with numerous operators, including foreign and domestic airlines, the U.S. Army, the U.S. Marines, and the U.S. Air Force. The NASA Flight Service Program was initiated in 1973 for the components indicated in figure 7. Over 2.5 million component flight hours have been accumulated with the high-time aircraft having more than 24,000 hours. Some of the graphite/epoxy DC-10 upper aft rudders have been accumulating flight service time at a rate of over 300 hours per month during the past 6 years. The 108 graphite/epoxy spoilers installed on B-737 aircraft have accumulated the highest total component flight hours, over 1.7 million, during 9 years of service. Over 66,000 total component flight hours have been accumulated on the 206L and S-76 composite helicopter components.

AIRCRAFT COMPONENT	TOTAL COMPONENTS	START OF FLIGHT SERVICE	CUMULATIVE FLIGHT HOURS	
			HIGH TIME AIRCRAFT	TOTAL COMPONENT
L-1011 FAIRING PANELS	18	JANUARY 1973	23 130	409 590
737 SPOILER	108	JULY 1973	24 290	1 712 470
C-130 CENTER WING BOX	2	OCTOBER 1974	6 080	12 100
DC-10 AFT PYLON SKIN	3	AUGUST 1975	19 240	55 810
DC-10 UPPER AFT RUDDER	13*	APRIL 1976	22 420	186 970
727 ELEVATOR	10	MARCH 1980	7 180	65 630
L-1011 AILERON	8	MARCH 1982	1 180	7 210
S-76 TAIL ROTORS AND HORIZONTAL STABILIZERS	14	FEBRUARY 1979	3 670	32 070
206L FAIRING, DOORS, AND VERTICAL FIN	124**	MARCH 1981	900	34 000
GRAND TOTAL	300			2 515 850

JUNE 1982

* 7 MORE RUDDERS TO BE INSTALLED

** 36 MORE COMPONENTS TO BE INSTALLED

Figure 7

RESIDUAL STRENGTH OF GRAPHITE/EPOXY SPOILERS

The large number of spoilers with graphite/epoxy skins allows planned retrievals from flight service without seriously impairing the total exposure. Six spoilers, which include two of each of three material systems used in fabricating the spoilers, are selected at random for removal from service annually. The six spoilers are shipped to Boeing for ultrasonic inspection. Three of the spoilers are returned to service after inspection and three are tested to failure to compare residual strengths with the strength of 16 new spoilers that were tested early in the program. Tests have been completed on all three graphite/epoxy systems after 6 years of service and the seventh-year test has been completed on a spoiler constructed with T300/5209. Results of tests conducted to date are shown in figure 8.

The strengths for the individual spoilers generally fall within the same scatter band as was defined by strengths of the new spoilers. The results indicate essentially no degradation in strength after the 7-year period of service for the materials indicated. In addition, stiffness measurements for the graphite/epoxy spoilers indicate essentially no reduction in stiffness as a result of 7 years of service exposure.

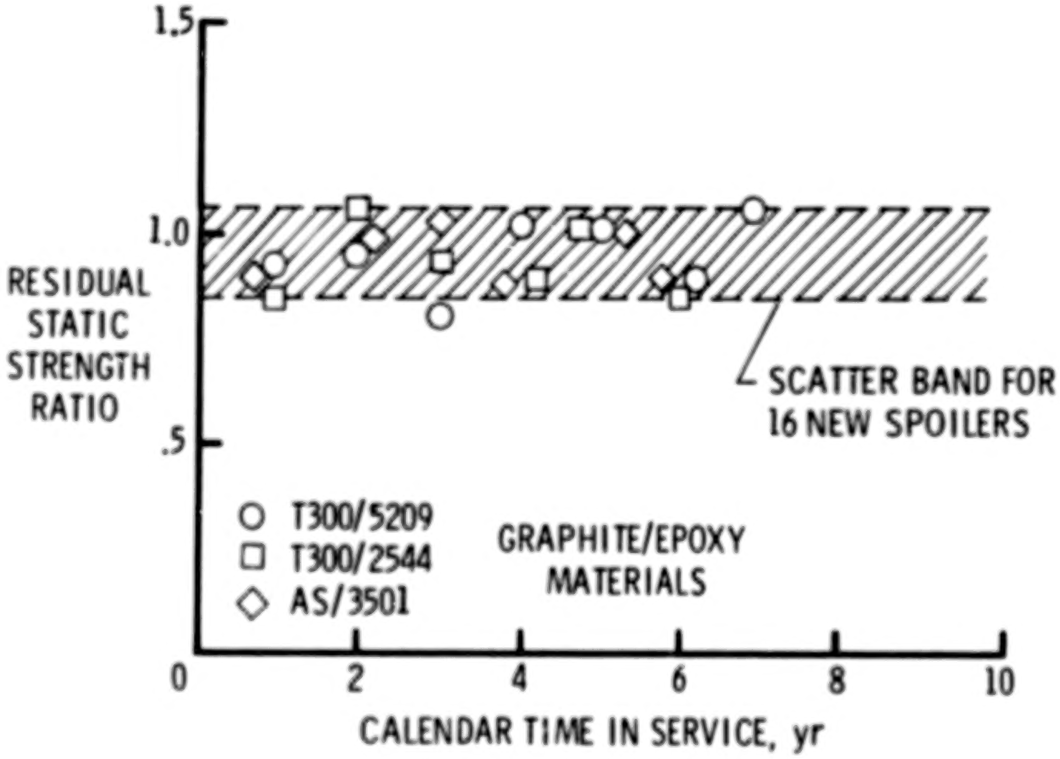

Figure 8

NASA COMPOSITE COMPONENT INSPECTION AND MAINTENANCE RESULTS

The composite components in the NASA Flight Service Evaluation Program are being inspected at periodic intervals to check for damage, defects, or repairs that may occur during normal aircraft operation. The composite components are being inspected by the aircraft operators and manufacturers, and in some cases both visual and ultrasonic inspection methods are being used, as indicated in figure 9.

The Kevlar/epoxy fairings on the L-1011 aircraft have incurred minor impact damage from equipment and foreign objects. Fiber fraying and fastener hole elongations have been noted on all the fairings but no repair has been required. The B-737 graphite/epoxy spoilers have encountered several types of minor damage or defects. Included are spar and doubler corrosion, cuts and dents, and delaminations. Some repairs are being prepared by the airlines but most repairs have been done at Boeing. One of the boron/aluminum aft pylon skins on the DC-10 aircraft was removed from service because of surface corrosion. This corrosion is believed to have been caused by improper surface preparation during panel fabrication.

Minor rib-to-skin disbonds have been detected on two DC-10 rudders. Also, three rudders have encountered minor lightning strikes and one rudder was damaged during ground handling. Minor lightning strikes have also been discovered on two graphite/epoxy elevators. One elevator has been damaged by ground handling. Overall, excellent performance has been achieved with the NASA flight service composite components.

COMPONENT	INSPECTION INTERVAL, months	INSPECTION METHODS	STATUS
L-1011 FAIRING PANELS	12	VISUAL	MINOR IMPACT DAMAGE, FIBER FRAYING AND HOLE ELONGATIONS
737 SPOILER	12	VISUAL ULTRASONIC	INFREQUENT MINOR DAMAGE REPAIRED AT BOEING
DC-10 AFT PYLON SKIN	12	VISUAL	ONE SKIN PANEL REMOVED DUE TO CORROSION
DC-10 UPPER AFT RUDDER	3, 12	VISUAL ULTRASONIC	MINOR RIB-TO-SKIN DISBOND ON TWO RUDDERS; MINOR LIGHTNING STRIKE ON THREE RUDDERS; GROUND HANDLING DAMAGE ON ONE RUDDER
727 ELEVATOR	13	VISUAL	MINOR LIGHTNING STRIKE ON TWO ELEVATORS; GROUND HANDLING DAMAGE ON ONE ELEVATOR

Figure 9

B-737 SPOILER IN-SERVICE DAMAGE AND REPAIR

During the first nine years of flight service there have been 67 instances in which graphite/epoxy spoilers have received damage in service sufficient to require repairs. Typical damage includes graphite/epoxy skin blisters, trailing-edge delamination, miscellaneous cuts and dents, and corrosion of the aluminum spar and doublers, as shown in figure 10. Over one-half of the damage incidents were caused by a design problem wherein actuator rod-end interference caused upper surface skin blisters. The actuator rods have been modified to prevent future damage. Nineteen repairs have been required as a result of corrosion damage to the aluminum spar and aluminum doublers. The corrosion initiates at a spar splice and is probably caused by moisture intrusion through a crack in the sealant material coupled with manufacturing defects in the aluminum surface preparation and corrosion protection schemes. Bondline fatigue in the spar splice area probably contributes to crack initiation and subsequent corrosion. There have been no incidents of galvanic corrosion between the graphite/epoxy skins and the aluminum honeycomb substructure. There have been ten incidents of cuts and dents caused by airline use and four trailing-edge delaminations that were apparently caused by normal aircraft maintenance and moisture intrusion.

Overall, excellent in-service performance has been achieved with the graphite/epoxy spoilers. Several of the airline maintenance executives have expressed the opinion that significantly fewer problems have been experienced with the graphite/epoxy spoilers compared to production aluminum spoilers.

PROBLEM	NUMBER OF INCIDENTS	PERCENT OF TOTAL	CAUSE
BLISTER ABOVE CENTER HINGE FITTING	34	51	DESIGN
SPAR AND DOUBLER CORROSION	19	28	DESIGN/MFG.
MISCELLANEOUS CUTS AND DENTS	10	15	AIRLINE USE
TRAILING-EDGE DELAMINATION	4	6	ENVIRONMENT

Figure 10

DC-10 COMPOSITE RUDDER LIGHTNING DAMAGE

Three of the graphite/epoxy upper aft rudders flying on DC-10 aircraft have sustained minor lightning strikes. The rudder that encountered the most severe strike is shown in figure 11. The damage was localized in an area measuring approximately 1.3 cm by 4.0 cm near the trailing edge of the structural box. The paint layer and four of the outer layers of the graphite/epoxy were removed by the lightning strike. Dry graphite fibers around the edge of the damaged region suggested that the epoxy resin had been vaporized by intense heat generated by the lightning strike. Repair of the rudder was performed in accordance with repair procedures established at the time the graphite/epoxy rudders were certified by the FAA. The repair consisted of a fiberglass cloth patch and a room temperature curing epoxy adhesive. The other two rudders were repaired in a similar manner using either fiberglass or graphite cloth. All three repairs were performed by airlines maintenance personnel and the aircraft resumed scheduled airline service.

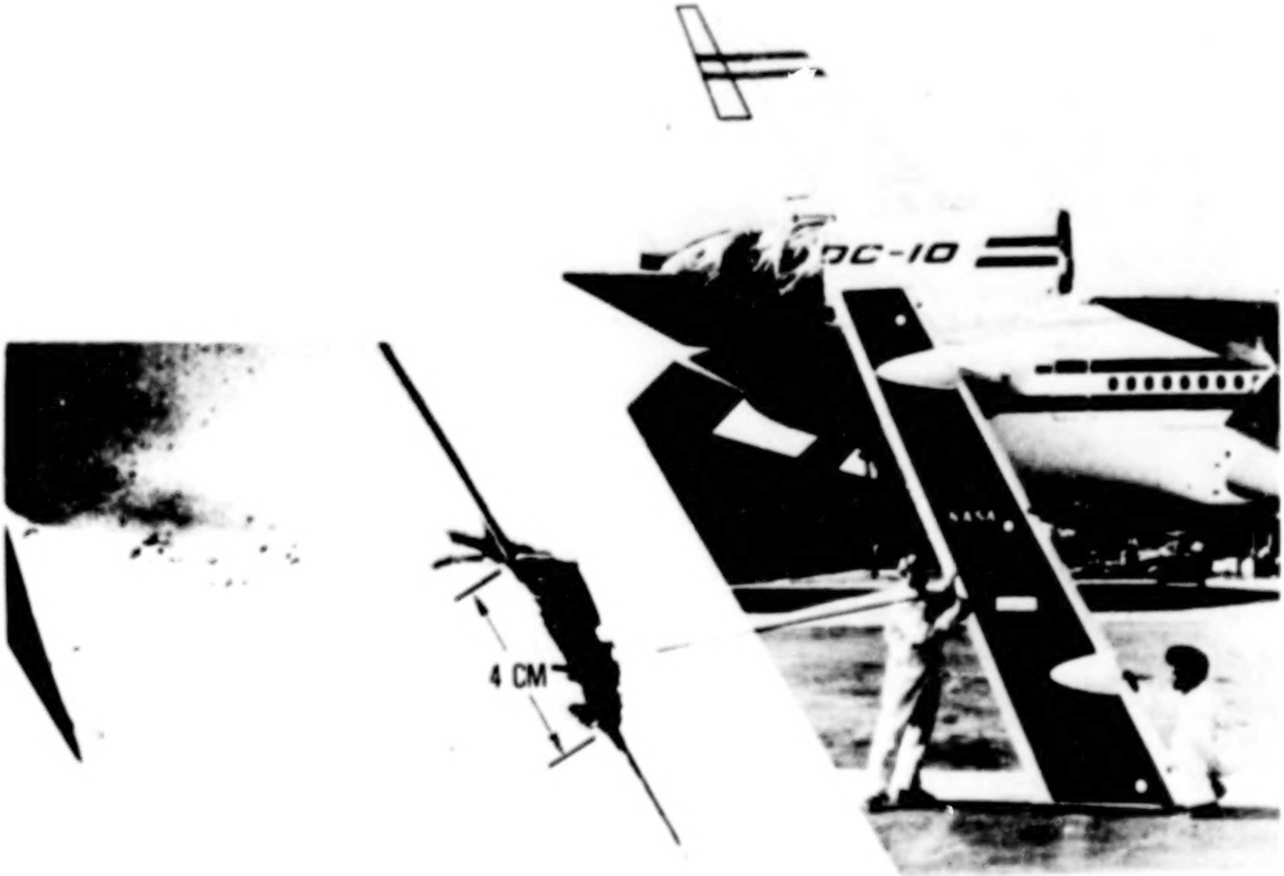

Figure 11

ENVIRONMENTAL EFFECTS ON LONG-TERM DURABILITY OF COMPOSITE MATERIALS FOR COMMERCIAL AIRCRAFT

Concurrent with the flight evaluation of structural composite components, NASA initiated programs to determine the outdoor ground, flight, and controlled laboratory environmental effects on composite materials, as shown in figure 12. Included are effects of moisture absorption, ultraviolet radiation, aircraft fuels and fluids, and sustained tensile stress. Specimens configured for various mechanical property tests are exposed to real-time environmental conditions on aircraft in scheduled airline service and at various ground stations around the world. Composite specimens are also exposed to controlled laboratory environments including temperature, relative humidity, and simulated ultraviolet radiation. The tests, involving more than 17,000 composite specimens, are scheduled to run for up to 10 years. The results of these tests will be correlated to provide a broad data base for environmental effects on composite materials.

- GROUND EXPOSURE – 10 YEARS AT AIRPORTS
- FLIGHT EXPOSURE – 10 YEARS ON AIRPLANES
- LABORATORY EXPOSURE – CONTROLLED CONDITIONS
- CORRELATE AND ANALYZE RESULTS

Figure 12

WORLD-WIDE ENVIRONMENTAL EXPOSURE OF COMPOSITE MATERIALS

Composite test specimens are being exposed to outdoor environmental conditions at the ground station locations shown in figure 13. Specimens are mounted on racks and positioned on building rooftops where they are exposed to ambient environmental conditions. Test specimens are configured for interlaminar shear, flexure, compression, and tension tests. Stressed and unstressed tension specimens are being exposed to assess the effects of sustained tensile load. Some specimens are unpainted to evaluate the effects of weathering on unprotected resin matrix materials, while other specimens are painted to evaluate protection afforded by standard aircraft paint. The materials being evaluated include several different graphite/epoxy and Kevlar/epoxy systems. Specimens are removed from the racks at intervals of 1, 2, 3, 5, 7, and 10 years to evaluate mass and mechanical property changes.

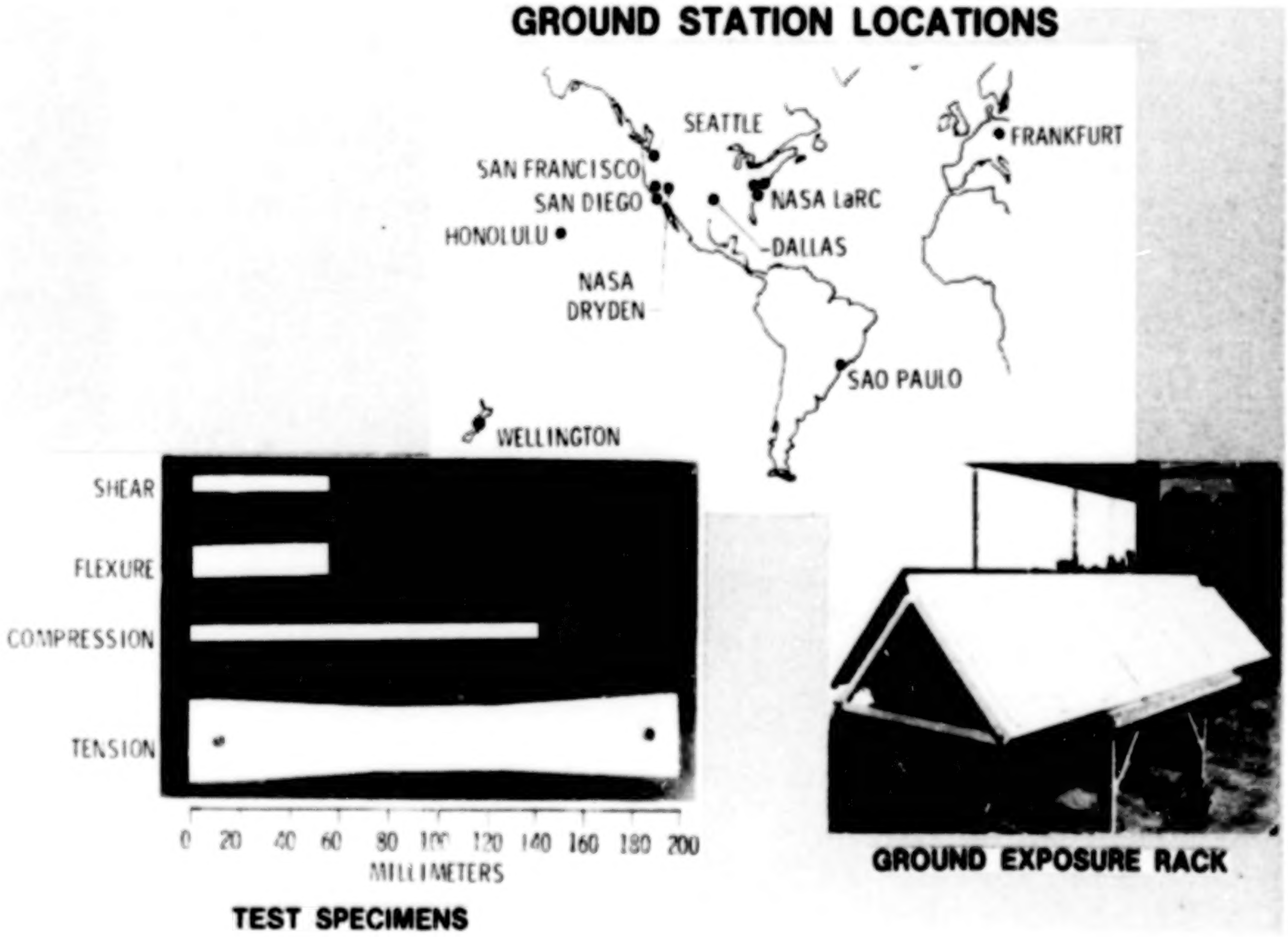
GROUND STATION LOCATIONS
SEATTLE
FRANKFURT
SAN FRANCISCO
SAN DIEGO
NASA LaRC
HONOLULU
DALLAS
NASA DRYDEN
SAO PAULO
WELLINGTON
SHEAR
FLEXURE
COMPRESSION
TENSION
0 20 40 60 80 100 120 140 160 180 200
MILLIMETERS
TEST SPECIMENS
GROUND EXPOSURE RACK

Figure 13

MOISTURE ABSORPTION DURING GROUND EXPOSURE

The moisture contents of four graphite/epoxy and two Kevlar/epoxy material systems after 5 years of exposure at six exposure sites are shown in figure 14. The data shown were obtained from flexure specimens that were exposed on outdoor racks located at Hampton, Virginia; San Diego, California; Sao Paulo, Brazil; Wellington, New Zealand; Honolulu, Hawaii; and Frankfurt, Germany. Each point plotted represents an average value for eighteen specimens, three at each of the six locations. The graphite/epoxy materials have stabilized after 5 years but the Kevlar/epoxy materials are apparently still gaining a slight amount of moisture. The Kevlar/epoxy materials and T300/2544 have moisture levels of about 2 percent. AS/3501 graphite/epoxy has a moisture content of about 1 percent, while both T300/5209 and T300/5208 graphite/epoxy have moisture contents of about 0.5 percent. The low value in the 5 year scatter band, in all cases, represents specimens exposed in Frankfurt, Germany; the high value for all material systems except T300/5209 represents specimens exposed in Sao Paulo, Brazil. Additional moisture absorption data will be obtained after 7 and 10 years of outdoor exposure.

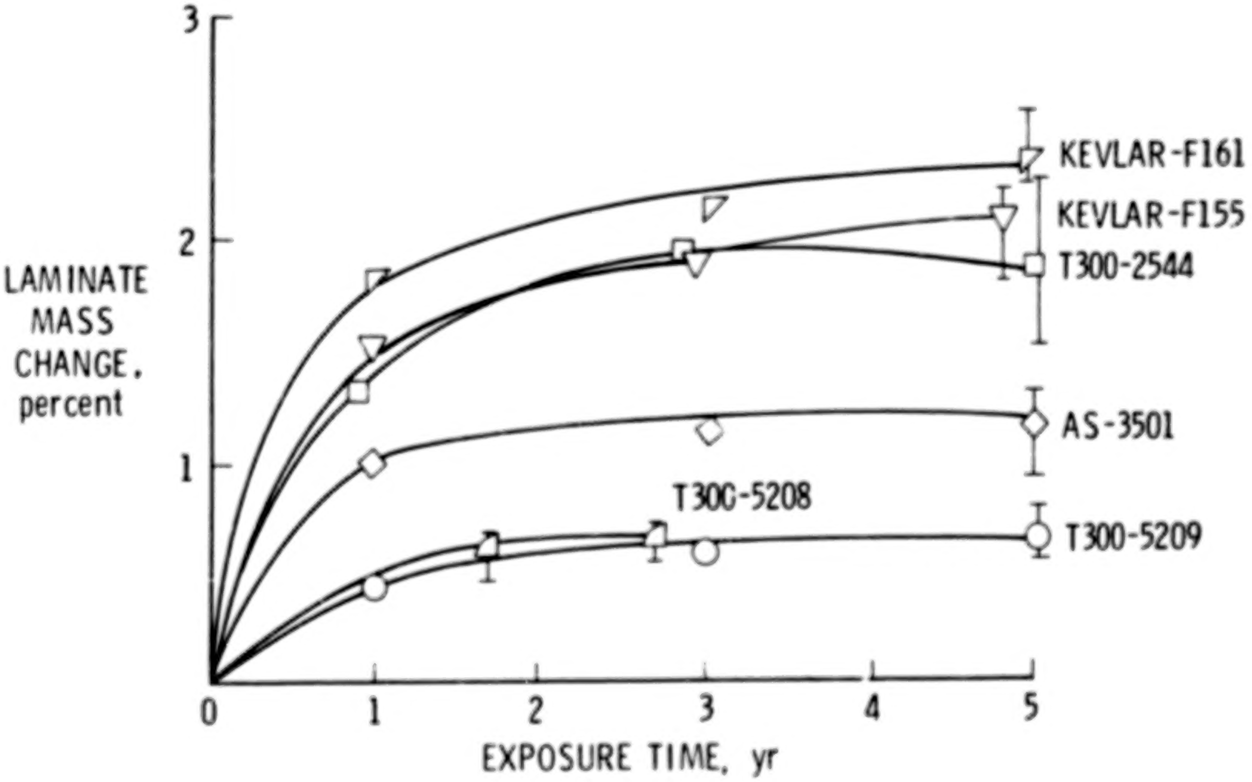

Figure 14

RESIDUAL STRENGTH OF COMPOSITE MATERIALS AFTER WORLDWIDE OUTDOOR EXPOSURE

Data obtained to date on specimens from four graphite/epoxy and two Kevlar/epoxy systems are shown in figure 15. The data points represent a comparison of the average strength values at six exposure sites with the average baseline strength value for that material system. The shaded area represents a plus-or-minus 10 percent scatter in the baseline strength values. Results of flexure tests indicate little or no degradation in strength over the 7-year exposure period. Compression strengths indicate a slight downward trend, but are still close to the baseline values after 7 years. Short beam shear strength is apparently influenced more by outdoor environmental exposure. The shear strengths for the T300/2544 graphite/epoxy and Kevlar/F-155 systems have dropped below the scatter band of the baseline test results. All the results presented in figure 15 are for unpainted specimens and several of the materials show evidence of surface deterioration due to solar radiation exposure. It is expected that the flexure strength will start to degrade as more matrix resin is leached away and more surface fibers become free. The data obtained to date confirm that the short beam shear strength tests are more sensitive to variations in matrix properties than the flexure or compression tests. One additional set of test specimens remains to be tested after 10 years of outdoor exposure.

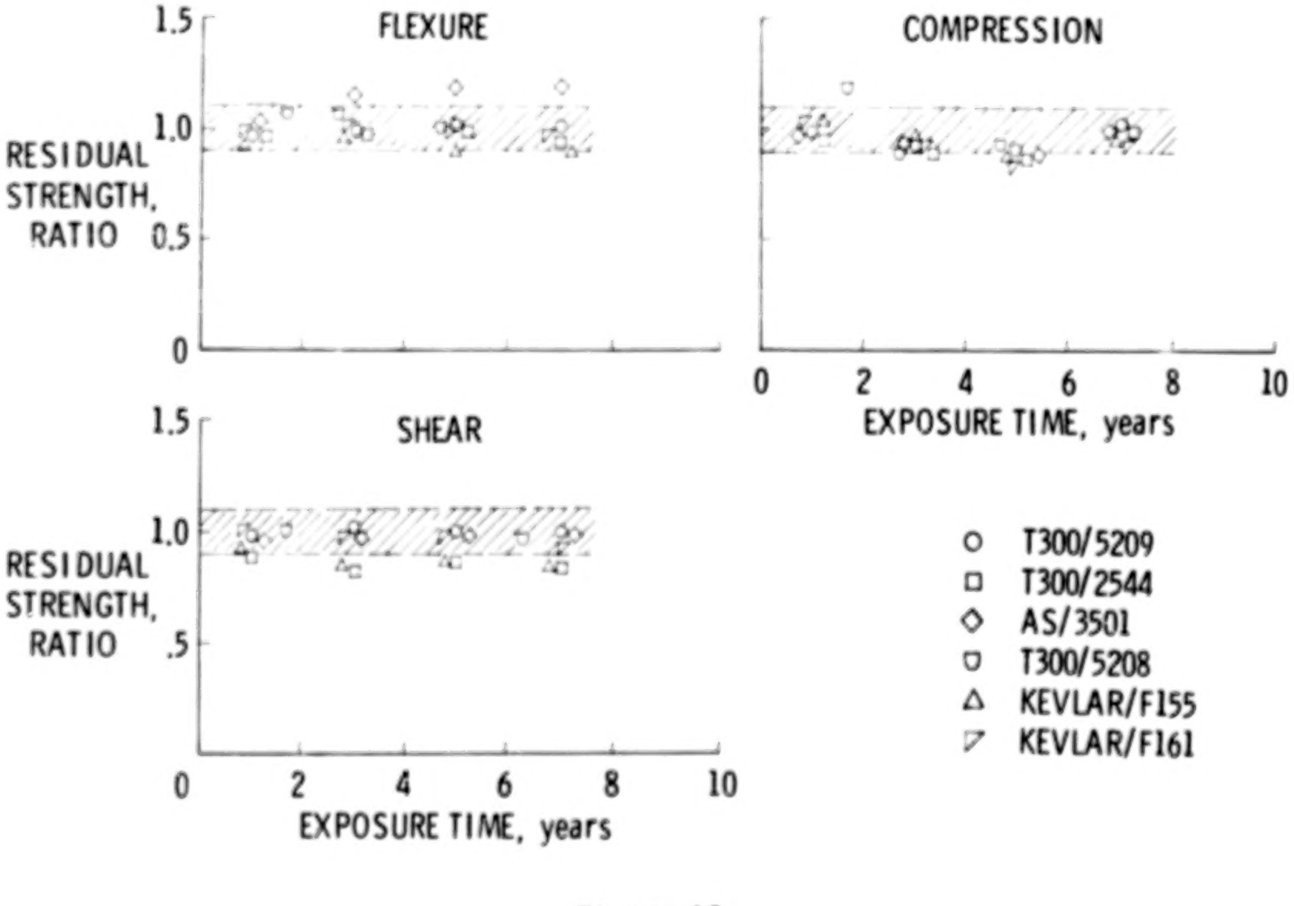

Figure 15

RESIDUAL TENSILE STRENGTH AFTER SUSTAINED STRESS OUTDOOR EXPOSURES

Effects of sustained stress during outdoor environmental exposure are evaluated by exposing tension specimens to 40 percent of ultimate baseline strength. Residual tensile strengths of T300/5208 quasi-isotropic laminated specimens after 7 years of outdoor exposure at the Langley Research Center and San Francisco are shown in figure 16. The residual tensile strength is within the scatter band for the strength of unexposed specimens. Results indicate that the T300/5208 quasi-isotropic tensile specimens were unaffected by either outdoor environment or sustained tensile stress at the two exposure sites indicated. Additional data will be obtained after 10 years of outdoor exposure.

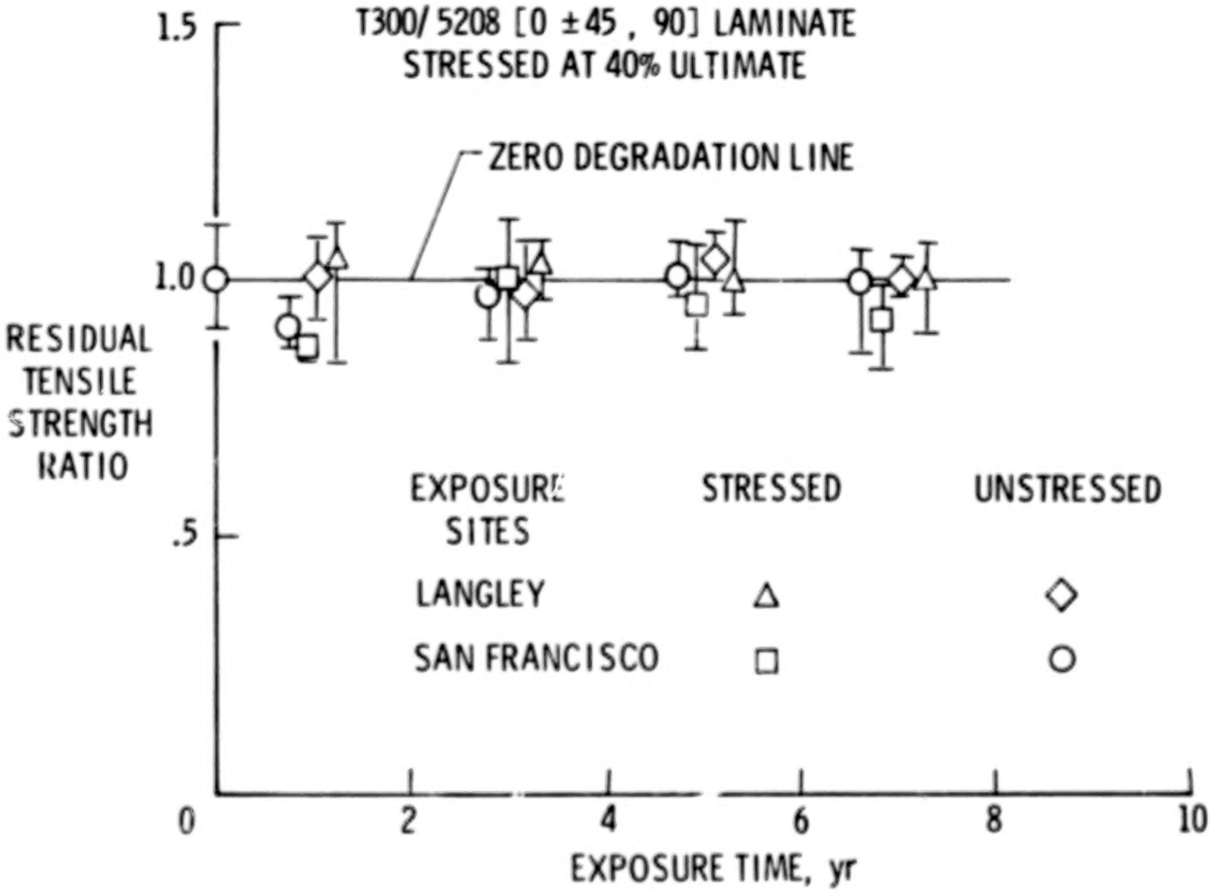

Figure 16

EFFECT OF AIRCRAFT FLUIDS ON COMPOSITE MATERIALS AFTER 5 YEARS OF EXPOSURE

Although aircraft composite structures are exposed almost continuously to various levels of moisture in the atmosphere, they are frequently exposed to various other fluids used in aircraft such as fuel and hydraulic fluid. The effects of various combinations of these fluids on composite materials have been evaluated after 5 years of exposure. Specimens were exposed to six different environmental conditions as follows: ambient air, water, JP-4 fuel, Skydrol, fuel/water mixture, and fuel/air cycling. The water, JP-4 fuel, and Skydrol were replaced monthly to maintain fresh exposure conditions. Specimens exposed in the fuel/water mixture were positioned with the fuel/water interface at the center of the test specimens. The fuel/air cycling environment consisted of 24 hours of fuel immersion followed by 24 hours of exposure to air. Residual tensile strengths of T300/5208 graphite/epoxy, T330/5209 graphite/epoxy, and Kevlar 49/5209 specimens after exposure to the six environments are shown in figure 17. The residual tensile strength of T300/5208 was not degraded by any of the six environments indicated in figure 17. The most degrading environment on the T300/5209 and Kevlar 49/5209 materials was the fuel/water combination. The T300/5209 specimens lost about 11 percent in tensile strength, whereas the Kevlar 49/5209 specimens lost about 25 percent in tensile strength. The ambient air results are consistent with other data obtained from the NASA Langley sponsored ground and flight environmental studies. The tests reported in figure 17 were more severe than actual aircraft flight exposures and the results should represent an upper bound on material property degradation.

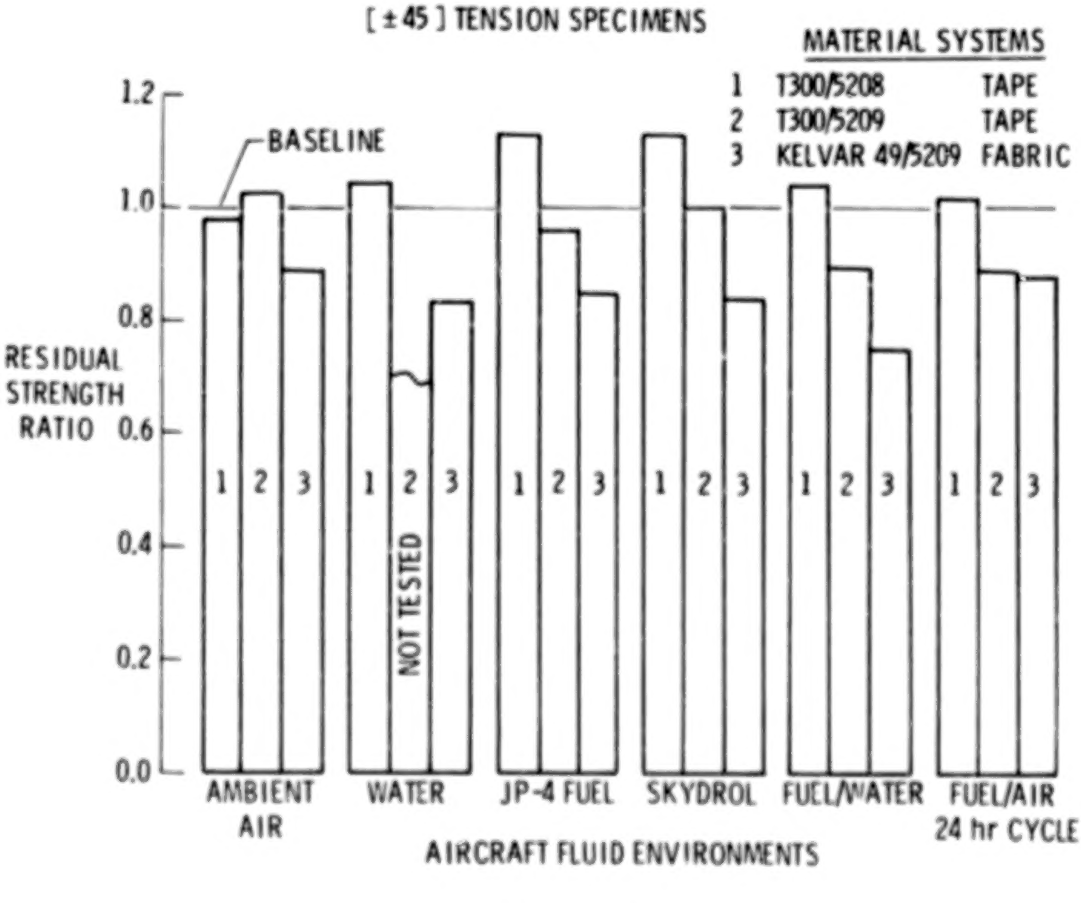

Figure 17

SURFACE DEGRADATION OF AS/3501 GRAPHITE/EPOXY

Scanning electron micrographs were taken of AS/3501 graphite/epoxy flexure specimens with no outdoor exposure and after 5 years of outdoor exposure. The micrograph shown on the left of figure 18 indicates that all the surface fibers are coated with resin for the specimen with no outdoor exposure. The micrograph shown on the right of figure 18 indicates that the surface fibers are no longer coated with resin after 5 years of outdoor exposure. The 5 years of weathering has removed the outer layer of resin and bare graphite fibers are visible.

As with controlled laboratory weatherometer results, these micrographs substantiate the need to keep graphite/epoxy composite aircraft structures painted to prevent ultraviolet radiation damage to composite matrix materials.

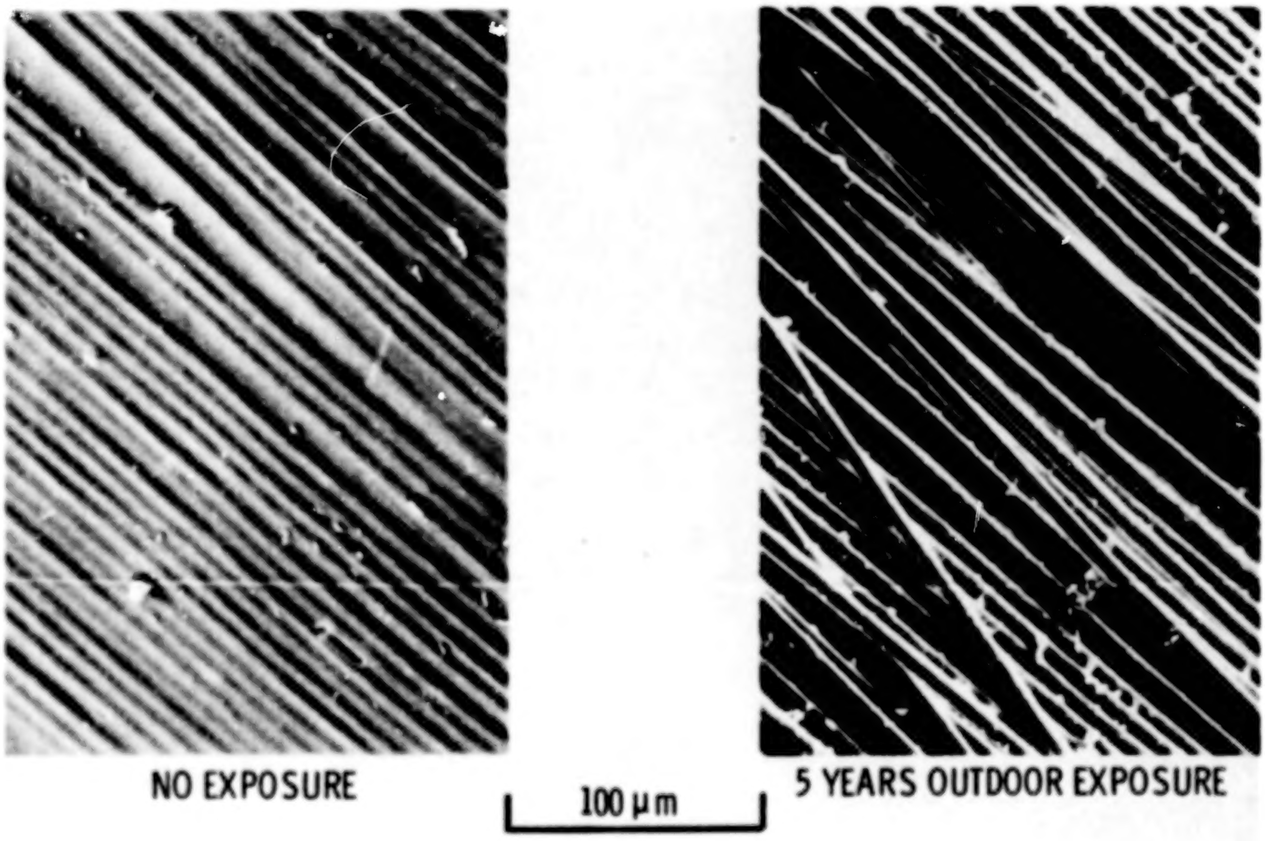

Figure 18

CONCLUDING REMARKS

The NASA Langley Research Center has sponsored design, development, and flight service evaluation of 300 composite aircraft components. Excellent in-service performance and maintenance experience have been achieved during 9 years and over 2.5 million hours of flight service. No significant degradation has been observed in residual strength of composite components or environmental exposure specimens after 7 years of service or exposure. Results obtained to date indicate that composite surfaces must be painted with standard aircraft polyurethane paint to protect the matrix from ultraviolet degradation. Test results also indicate that Kevlar/epoxy composites absorb more moisture than most widely used graphite/epoxy composites and a larger reduction in residual strength results for the Kevlar composite systems. Additional details on the programs discussed herein can be found in references 1 through 8.

Confidence developed through NASA-sponsored service evaluation, environmental testing, and advanced composite component development programs has led commercial transport and helicopter manufacturers to make production commitments to selected composite components (fig. 19).

- EXCELLENT IN-SERVICE PERFORMANCE AND MAINTENANCE EXPERIENCE HAVE BEEN ACHIEVED WITH OVER 300 COMPOSITE COMPONENTS DURING 9 YEARS AND OVER 2.5 MILLION HOURS OF FLIGHT SERVICE

- NO SIGNIFICANT DEGRADATION HAS BEEN OBSERVED IN RESIDUAL STRENGTH OF COMPOSITE COMPONENTS OR ENVIRONMENTAL EXPOSURE SPECIMENS AFTER 7 YEARS OF SERVICE OR EXPOSURE

- CONFIDENCE DEVELOPED THROUGH NASA SERVICE EVALUATION, ENVIRONMENTAL TESTING, AND ADVANCED COMPOSITE COMPONENT DEVELOPMENT PROGRAMS HAS LED COMMERCIAL TRANSPORT AND HELICOPTER MANUFACTURERS TO MAKE PRODUCTION COMMITMENTS TO SELECTED COMPOSITE COMPONENTS

Figure 19

REFERENCES

1. Lehman, G. M.: Flight-Service Program for Advanced Composite Rudders on Transport Aircraft. First Annual Summary Report, McDonnell Douglas Corporation, NASA CR-145385, July 1977.

2. Dexter, H. Benson: Composite Components on Commercial Aircraft. NASA TM-80231, March 1980.

3. Dexter, H. Benson and Chapman. Andrew J.: NASA Service Experience with Composite Components. Presented at the 12th National SAMPE Technical Conference, Seattle, WA, October 7-9, 1980.

4. Dexter, H. Benson: Durability of Commercial Aircraft and Helicopter Composite Structures. Proceedings of the Critical Review: Techniques for the Characterization of Composite Materials, AMMRC MS 82-3, May 1982.

5. Kizer, J. A.: Program for Establishing Long-Time Flight Service Performance of Composite Materials in the Center Wing Structure of C-130 Aircraft-Phase V-Flight Service and Inspection, NASA CR-165770, October 1981.

6. Stone, R. H.: Flight Service Evaluation of Kevlar-49/Epoxy Composite Panels in Wide-Bodied Commercial Transport Aircraft-Eighth Annual Flight Service Report, NASA CR-165841, March 1982.

7. Tanimoto, E. Y.: Effects of Long-Term Exposure to Fuels and Fluids on Behavior of Advanced Composite Materials, NASA CR-165763, August 1981.

8. Coggeshall, Randy L.: 737 Graphite Composite Flight Spoiler Flight Service Evaluation, Seventh Annual Report, NASA CR-165826, March 1982.

BLANK PAGE

DURABILITY OF SPACECRAFT MATERIALS

Darrel R. Tenney
NASA Langley Research Center
Hampton, Virginia

INTRODUCTION

Composite materials will be used for future space missions such as communication antennae, solar reflectors, satellite power systems, and a space operations center because of their unique combination of high specific stiffness and low coefficient of thermal expansion. (See fig. 1.) For long-life space missions (10-20 years), the durability of these materials in the hostile space environment has been identified as a key materials technology need.

This paper reviews NASA Langley's research efforts on the space durability of materials, including radiation effects on polymer matrix composites and films, dimensional stability of polymer matrix composites and tension-stabilized cables, and thermal control coatings. Research to date has concentrated on establishing a fundamental understanding of space environmental effects on current graphite-reinforced composites and polymer systems, and development of analytical models to explain observed changes in mechanical, physical, and optical properties. As a result of these research efforts, new experimental facilities have been developed to simulate the space environment and measure the observed property changes. Chemical and microstructural analyses have also been performed to establish damage mechanisms and the limits for accelerated testing. The implications of these results on material selection and system performance are discussed and additional research needs and opportunities in the area of tougher resin/matrix and metal/matrix composites are identified.

FOCAL MISSIONS FOR ADVANCED TECHNOLOGY DEVELOPMENTS

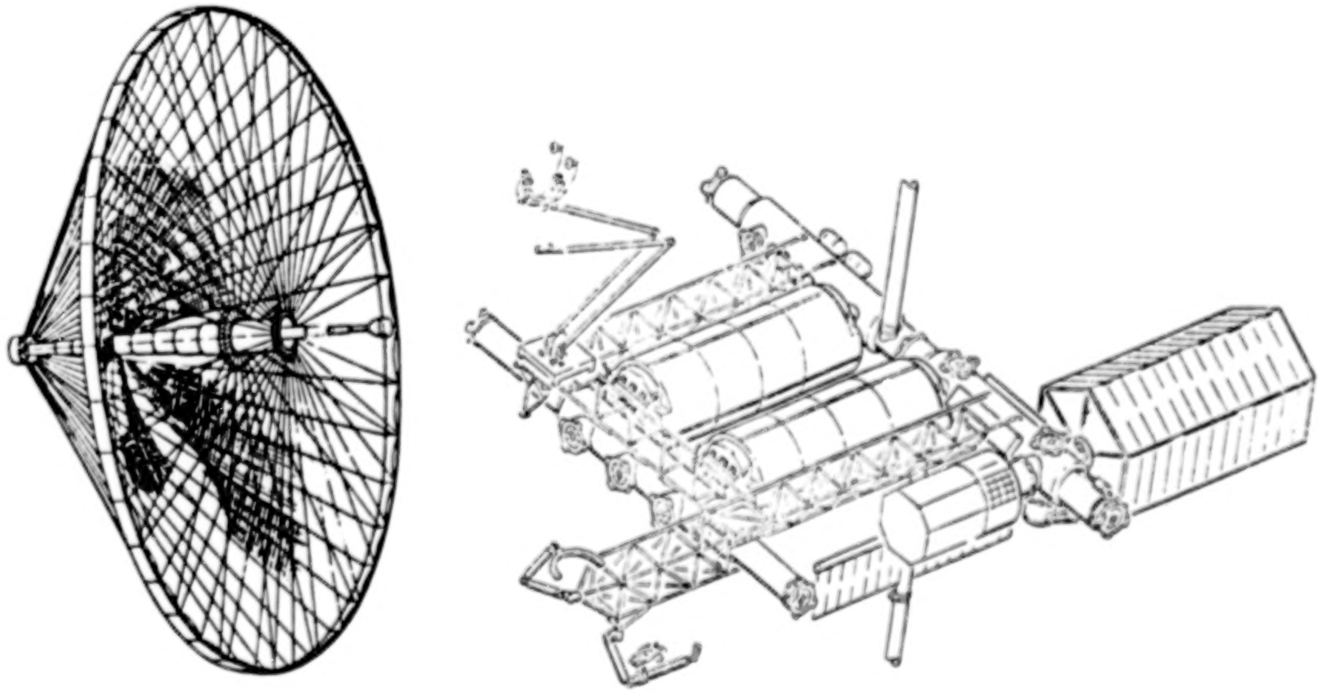

Figure 1

HIGH-STIFFNESS LOW-THERMAL-EXPANSION SPACE MATERIALS

Structural requirements generally focus on light weight, high stiffness, and dimensional stability. Conventional aerospace materials such as aluminum and titanium do not provide these characteristics, whereas advanced graphite reinforced composites do. The coefficient of thermal expansion (CTE) values and specific stiffnesses of graphite composites and selected other low-expansion materials are compared in figure 2. Quartz and ULE (titanium silicate glass) fall within the preferred range of CTE values but do not provide the needed stiffness. A range of values is shown for both the graphite/resin and graphite/metal composites, indicating the flexibility that these composites offer for tailoring properties by varying the fiber type and ply orientation. Graphite/resin and graphite/metal composites both provide the needed CTE values and can be selected for a particular application depending on the stiffness requirements. Graphite/glass has a very low CTE and high stiffness but its low thermal conductivity may make it undesirable in applications where large thermal gradients could cause warping of the structure.

Metal matrix composites (graphite/aluminum and graphite/magnesium) research for space structures is being conducted in several Department of Defense programs. Resin matrix composites (graphite/epoxy, graphite/polyimide, and graphite/advanced resins) research is the primary focus of the NASA program. Each of the composite materials has potential advantages for large space structures. Continued research on both classes of composite materials is warranted to assure their technology readiness and to provide the designer with material options for optimum structural design.

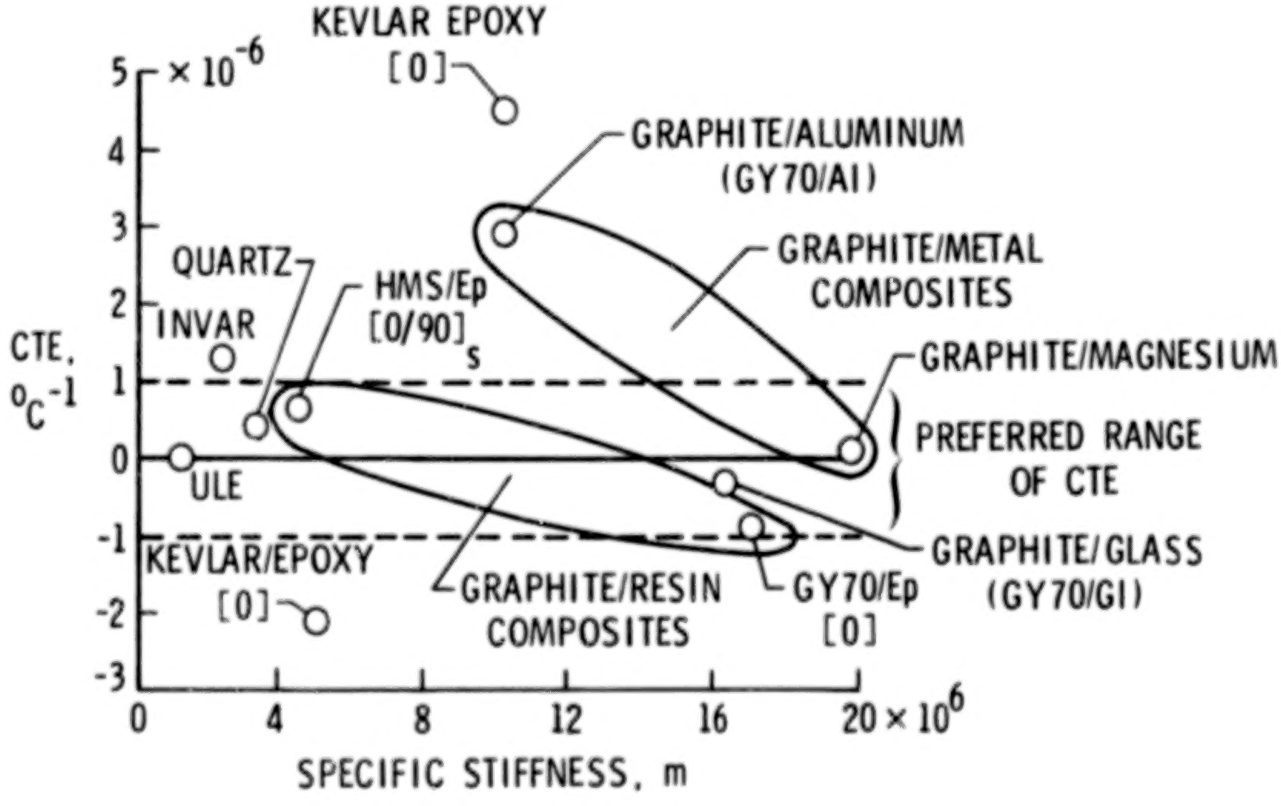

Figure 2

DURABLE SPACE MATERIALS

Space-durable materials are a necessary requirement to achieving long-life space structures. (See fig. 3.) As previously noted, materials of construction will include advanced metal and polymer matrix composites, coatings for thermal control, polymer films, and adhesives. In low Earth orbit (LEO), materials will be subjected to repeated thermal cycles from approximately +200°F to -200°F, to UV radiation, and to ultra-high vacuum. Micrometeoroids and space debris are also considered as hazards in LEO. For higher orbits, such as goesynchronous Earth orbit (GEO), the materials will also be subjected to large doses of high-energy electrons and protons. The primary concerns for resin matrix composites are radiation-induced changes in mechanical and physical properties and dimensional stability, as well as microcracking due to residual stresses produced during thermal cycling. Similarly, the residual strains produced by the thermal expansion mismatch between the fibers and the matrix in metal matrix composites are likely to affect the dimensional stability of these materials.

Long-life coatings are required to keep the spacecraft system within design temperature limits. Degradation of the optical properties of these coatings by UV and particulate radiation and by contamination appears to be a significant problem that must be solved to achieve long-life systems (10 to 20 years).

The ability to predict the long-term performance of all classes of materials in space must be a central part of any durability program and may require flight experiments for verification of ground exposure data and analytical predictions.

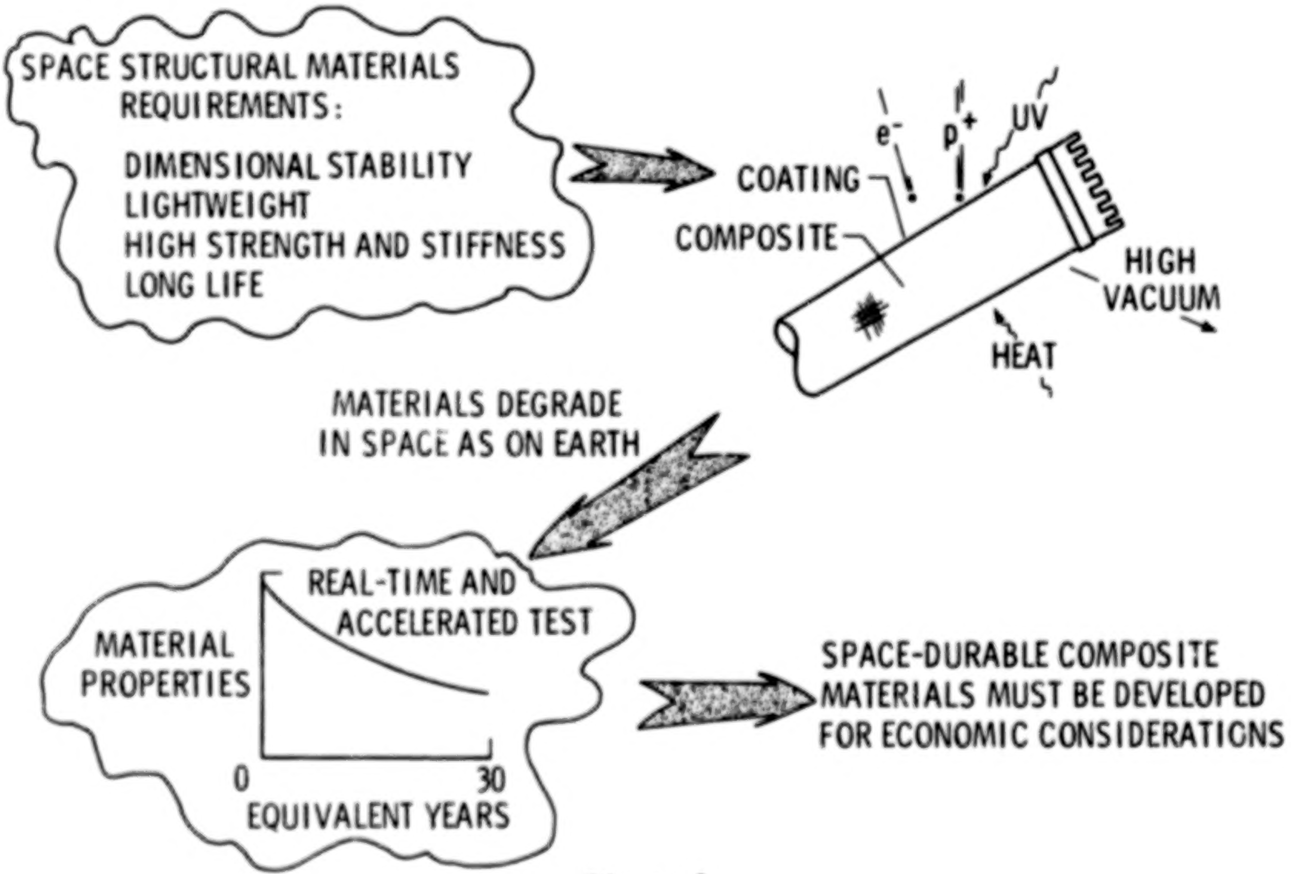
SPACE STRUCTURAL MATERIALS REQUIREMENTS:
DIMENSIONAL STABILITY
LIGHTWEIGHT
HIGH STRENGTH AND STIFFNESS
LONG LIFE
e⁻
p⁺
UV
COATING
COMPOSITE
HIGH VACUUM
HEAT
MATERIALS DEGRADE IN SPACE AS ON EARTH
MATERIAL PROPERTIES
REAL-TIME AND ACCELERATED TEST
0
30
EQUIVALENT YEARS
SPACE-DURABLE COMPOSITE MATERIALS MUST BE DEVELOPED FOR ECONOMIC CONSIDERATIONS

Figure 3

SPACE MATERIALS DURABILITY LABORATORY

Figure 4 shows a schematic of the Space Materials Durability Laboratory at NASA Langley. The laboratory is dedicated to the evaluation of the effects of space radiation on composite materials. This laboratory has a 2.5-MeV proton accelerator, a 1-MeV electron accelerator, and a solar simulator, all focused on a 12-inch-diameter target in a clean ultra-high-vacuum chamber. The accelerators were selected to cover the most prevalent energy range found in space for generation of bulk damage to composite materials.

Two smaller single-parameter exposure chambers are also being developed for in situ chemical characterization studies. In these chambers, polymer films are subjected to low-energy (100 KeV) electrons. Chemical and physical properties such as weight loss, outgassing and condensible products, infrared (IR) absorption, and dynamic moduli are followed during the irradiation. Mechanical properties of the films are obtained after irradiation. These characterizations serve as a sensitive measure of the radiation interaction and provide data for development of mechanistic models of the interaction process.

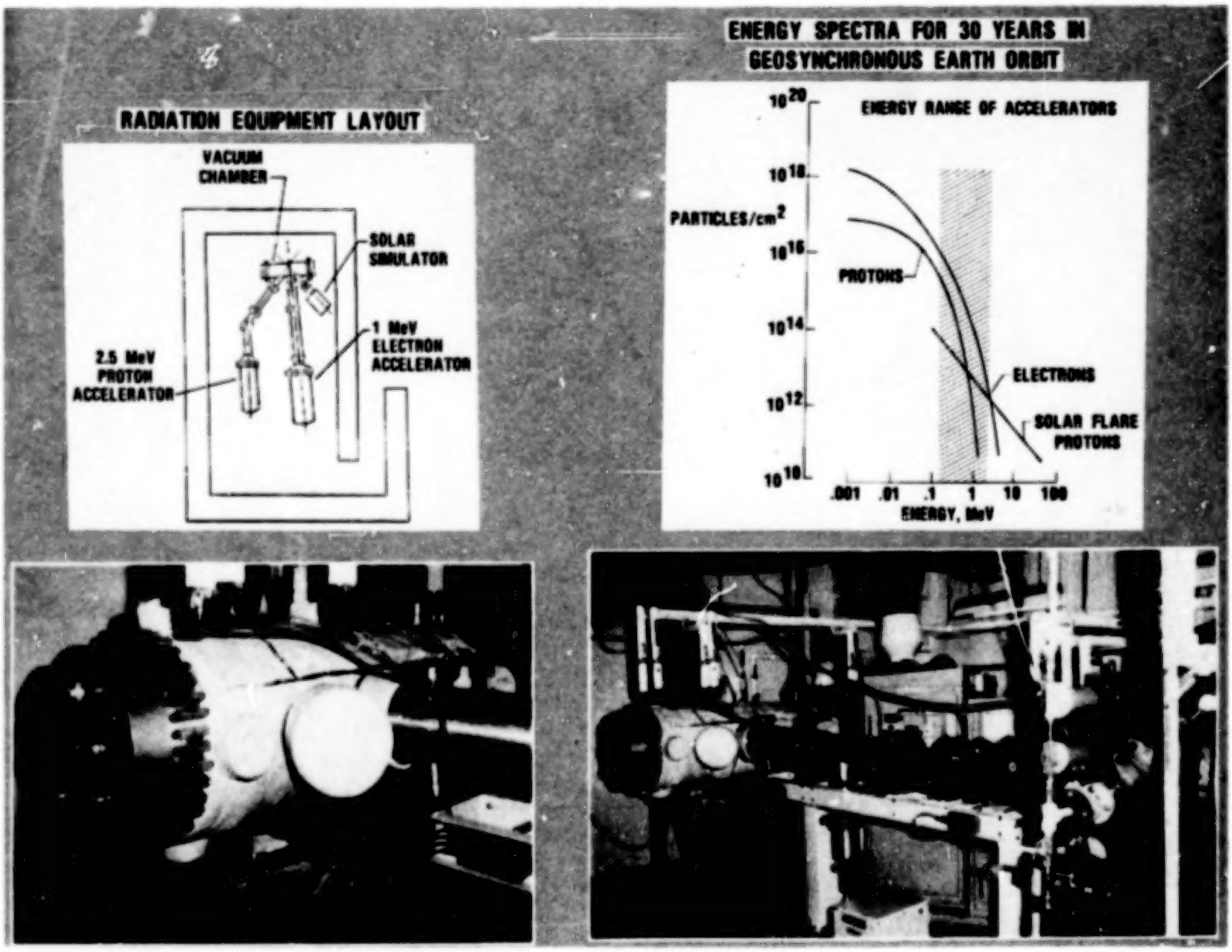
4
RADIATION EQUIPMENT LAYOUT
VACUUM CHAMBER
SOLAR SIMULATOR
1 MeV ELECTRON ACCELERATOR
2.5 MeV PROTON ACCELERATOR
ENERGY SPECTRA FOR 30 YEARS IN GEOSYNCHRONOUS EARTH ORBIT
ENERGY RANGE OF ACCELERATORS
PARTICLES/cm^2
10^{20}
10^{18}
10^{16}
10^{14}
10^{12}
10^{10}
PROTONS
ELECTRONS
SOLAR FLARE PROTONS
.001 .01 .1 1 10 100
ENERGY, MeV

Figure 4

TEMPERATURE OF POLYSULFONE FILM AND COMPOSITES DURING ELECTRON RADIATION

Because real-time exposures to evaluate space materials are not practical, a test acceleration methodology must be established that can be used to accurately predict long-term performance from short-time data. Test variables such as temperature, particle energy, dose rate, and type of energy must be evaluated to develop this methodology. Figure 5 shows the effect of dose rate (test acceleration rate) on sample temperature for both polysulfone films and a graphite/polysulfone composite (4-ply, unidirectional). Because of the low thermal conductivity of polymers and difficulties in maintaining good contact with the specimen cooling plate, the temperature of the composite specimen was found to increase substantially with dose rate. For polysulfone films, contact with the cooled base plate was easier to achieve and the maximum temperature at 10^8 rads/hr was about 50°C. This is significantly below its glass transition temperature (190°C) and no major effect due to temperature is anticipated. High specimen temperatures, particularly those near the glass transition temperature, may change the radiation interaction mechanism and therefore produce material changes not representative of changes expected in actual service. For composites, long and thus expensive tests are required.

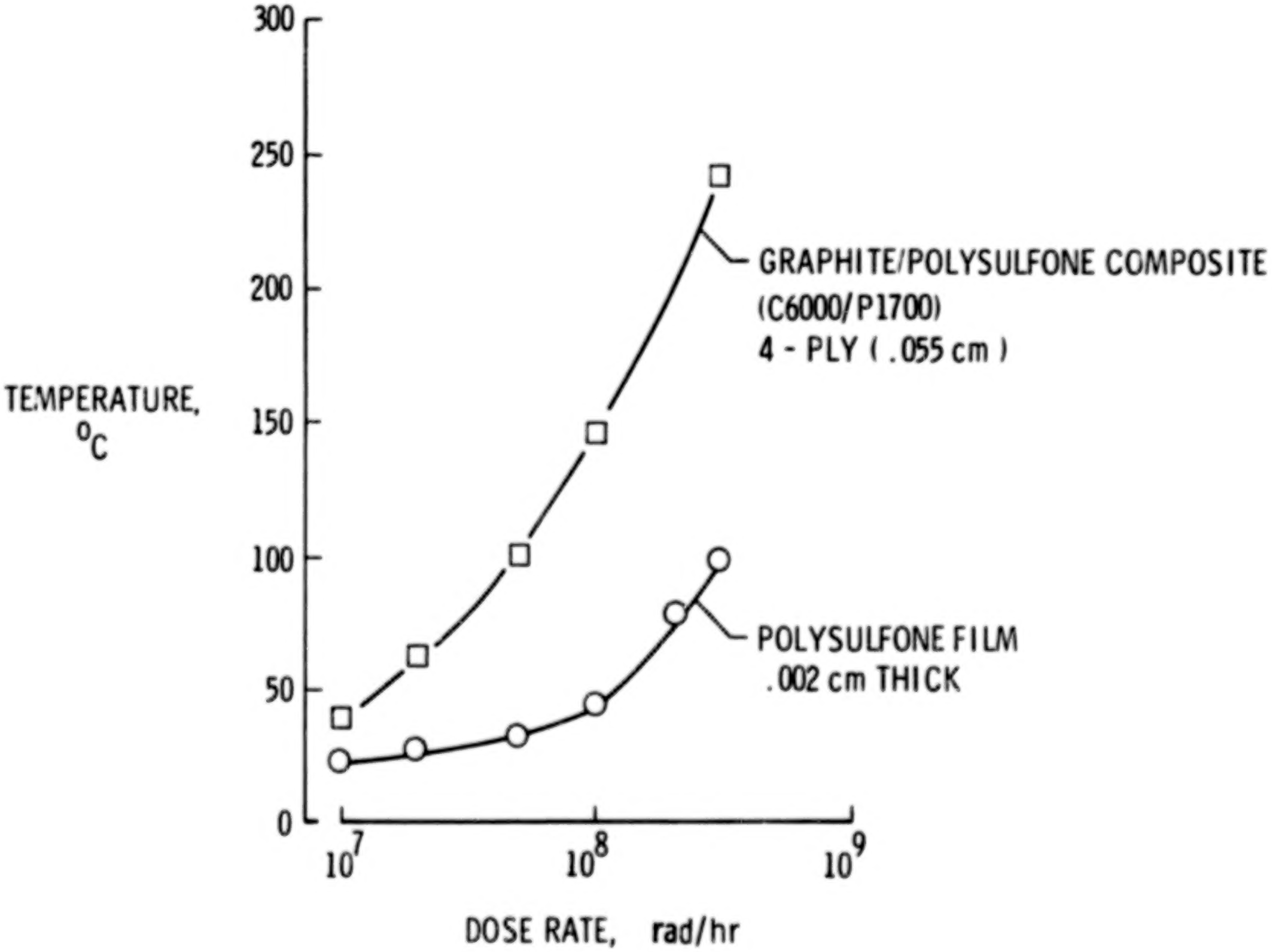

Figure 5

RADIATION EFFECTS ON FLEXURAL PROPERTIES OF A GRAPHITE/EPOXY COMPOSITE

The effect of radiation on composite mechanical properties has not been fully explored. However, limited data have shown that radiation does not significantly affect mechanical properties. An example of the limited data available is shown in figure 6. The flexural strength of small (1.2 x 2.5 cm) unidirectional specimens of T300/5208 graphite/epoxy composite after exposure to electron radiation is plotted as a function of absorbed dose in rads. These miniature specimens were used because of the small diameter of the electron beam. Exposures in vacuum for doses up to and including 8 x 10^9 rads are shown. The fiber direction was in the direction of specimen length (longitudinal), so the flexural properties were fiber dominated. The flexural strength appears to increase slightly with dose - approximately 4 percent at 8 x 10^9 rads. However, the size of the confidence band is large and could mask small changes in flexural properties. This scatter is typical of composite specimens and is a major problem in conducting environmental effects studies on composites.

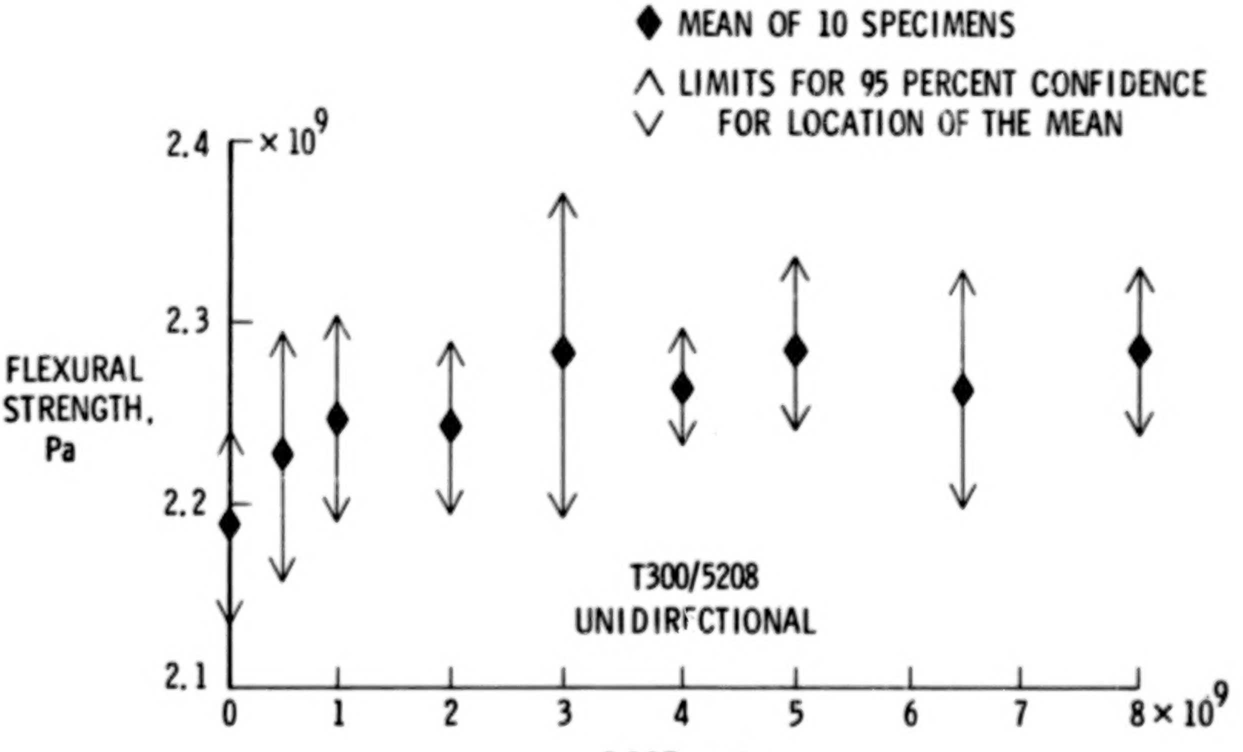

Figure 6

EFFECT OF ELECTRON RADIATION ON THE MODULUS OF POLYSULFONES

Thermoplastics with improved properties are being actively considered for structural applications. One class that has received considerable attention for space and aircraft application is polysulfones. To assess long-term durability of these materials in space, a series of four materials, each with a different chemical structure, was exposed to either an electron or a proton environment using several different dose rates and particle energy sufficient to give a unifom dose through the polymer film. The absorbed dose was varied between 10^8 and 10^{10} rads. Film samples of all materials were used because chemical characterization of films is much easier than for composites and provides a more sensitive measure of radiation damage.

The effect of total electron dose on the observed modulus of the four polysulfone films is shown in figure 7. Modulus values were obtained using an automated Rheovibron Dynamic Viscoelastometer with all data obtained at a frequency of 3.5 Hz. When determining modulus, the film sample was inserted, removed, and reinserted several times to eliminate sample mounting effects. All reported values are the average of at least three measurements.

For all materials, modulus increased as dose increased and the threshold value for a major change in modulus appears to be near 10^9 rad. The percent increase ranges from about 24 percent for P-1700 to 58 percent for Radel 5000. This increase with dose suggests that crosslinking is occurring in all materials, particularly above 10^9 rad.

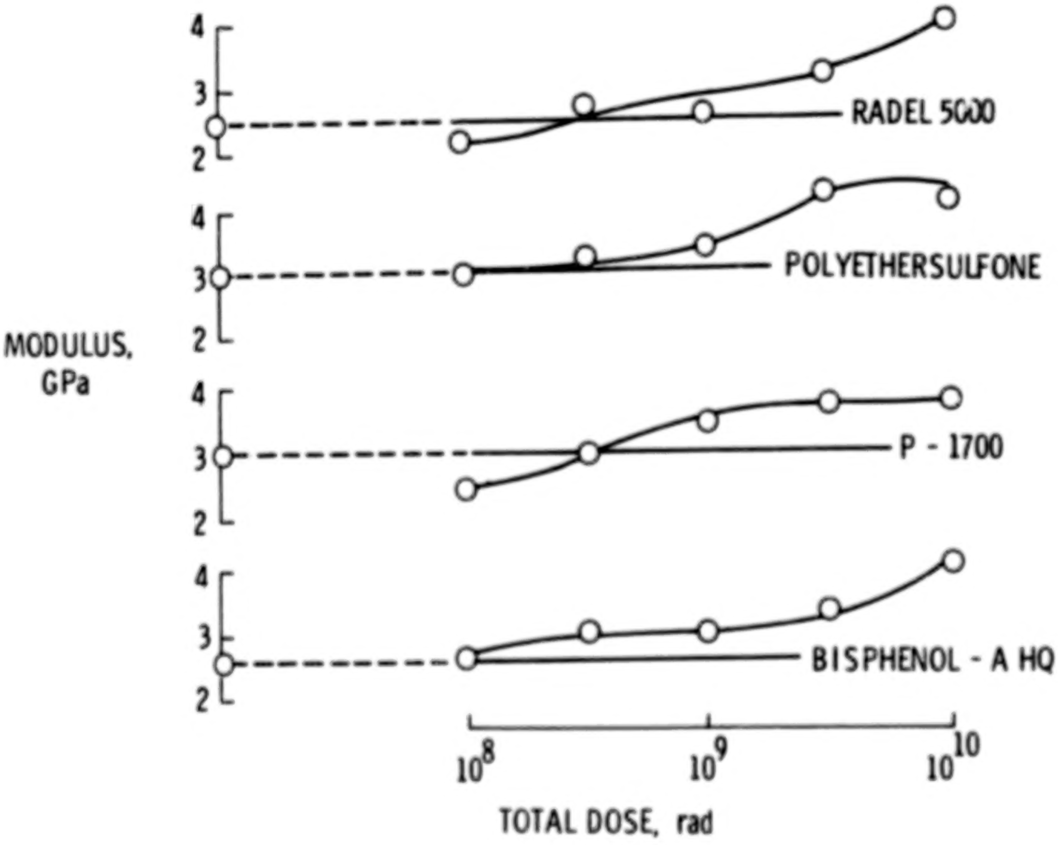

Figure 7

INFRARED SPECTRA OF ELECTRON-IRRADIATED P-1700

Two infrared spectra, each made from a film of P-1700 are shown in figure 8. This polysulfone is representative of the four materials studied. The lower curve represents the portion from 1600 to 600 cm^{-1} frequency of the IR spectrum of nonirradiated polyethersulfone. The upper curve represents that same portion of the spectrum of polyethersulfone irradiated with electrons to 10^{10} rads. The SO_2 absorption band occurs at approximately 1400 cm^{-1}, which can clearly be seen as an absorption peak (an inverted peak) on the nonirradiated curve. However, after irradiation this peak is greatly diminished. Near 1300 and 1150 cm^{-1} are the asymmetric and symmetric ϕ-SO_2-ϕ absorption bands, respectively. These bands are present in the lower curve, but they have almost disappeared in the upper curve of the irradiated material. At approximately 1070 cm^{-1}, the C-O-C absorption band that appears on the spectrum for the nonirradiated specimen is absent in the spectrum for the irradiated polyethersulfone. The spectra shown here are the two extremes of the data actually obtained. The spectra of those specimens irradiated at lower doses resemble the spectrum of the nonirradiated material, and as the dose was increased, the spectra approached that of the curve at 10^{10} rads. All four polysulfones exhibited this same basic trend, with the SO_2, ϕ-SO_2-ϕ, and C-O-C bands being the most significantly affected by the radiation. The proton data, not shown here, also followed this trend, but the magnitude of change is less.

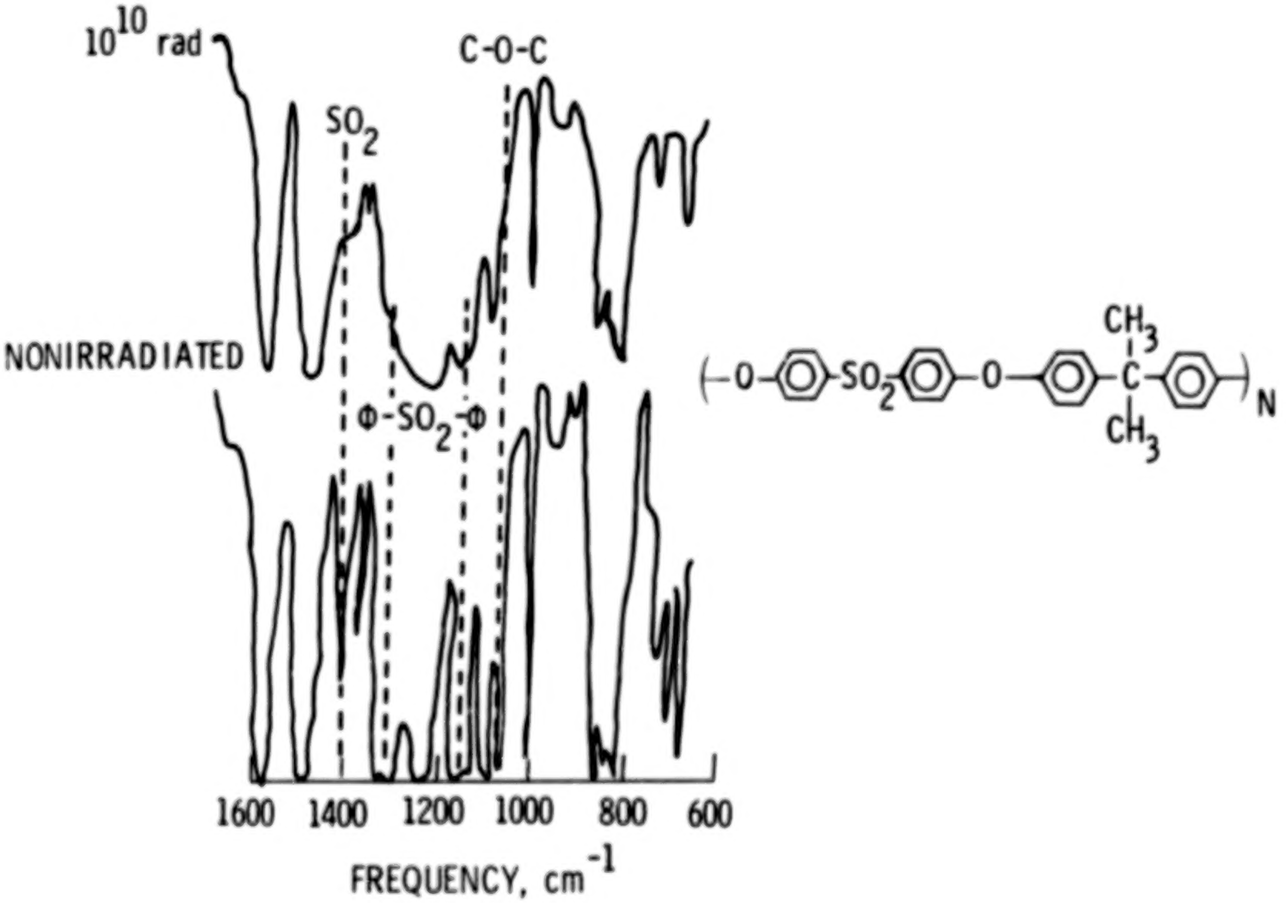

Figure 8

NORMALIZED ELEMENTAL COMPOSITION OF IRRADIATED P-1700

Following irradiation of each polysulfone film, a chemical analysis was performed to determine changes in elemental composition. Figure 9 shows this elemental composition data for one material (P-1700), normalized relative to the chemical analysis of the starting material, as a function of total dose. Similar chemical analysis data were obtained on all polysulfones studied and showed trends as presented in this figure. The analysis showed considerable loss of oxygen and moderate losses of sulfur and hydrogen. The threshold for a major decrease in oxygen occurs near 2 x 10^8 rads. About 24 percent of the initial oxygen content is lost for P-1700 at 10^{10} rads and that loss could establish sites for crosslinks. This apparent loss is supported by the diminished absorption bands associated with oxygen in the IR data. The breaking of an oxygen bond by irradiation and subsequent combination of oxygen atoms to form oxygen molecules, which could then be lost to the surroundings, would explain the decrease in oxygen content and the diminished absorption bands. The loss of oxygen atoms from -SO_2- linkages creates sites for crosslinking to adjacent chains and thus could explain the observed increase in modulus at high radiation doses.

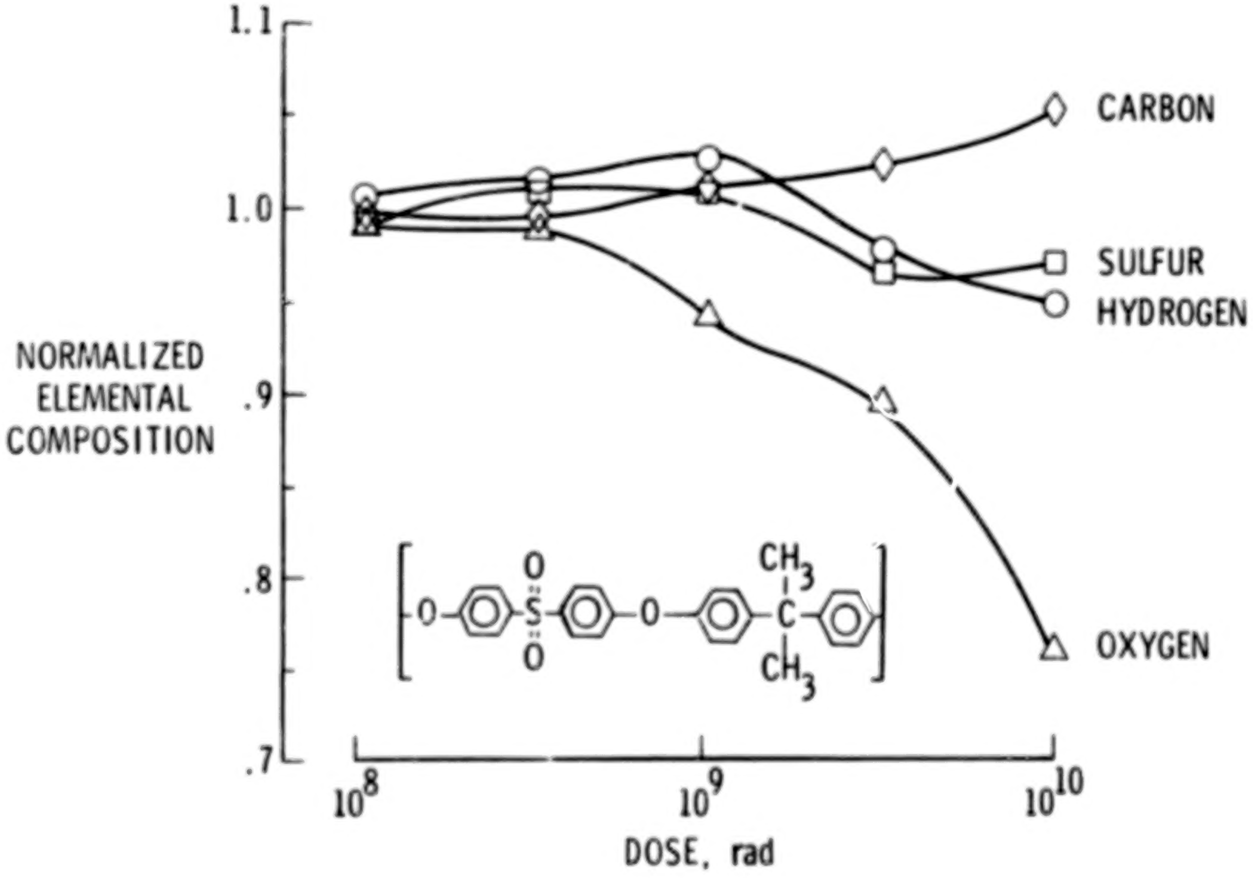

Figure 9

DIMENSIONAL STABILITY OF SPACE STRUCTURES

The performance characteristics of many large space structures are dependent upon their dimensional stability. One example of this is a space communications system, as shown in figure 10, in which small dimensional changes may cause a defocusing of the antenna and a corresponding loss in efficiency. The materials to be used in these structures include graphite cables, organic matrix composites, and metal/matrix composites. The primary factors controlling the dimensional stability of these materials include both thermal and mechanical load cycling, moisture desorption, radiation exposure, and microcracking. These factors may cause permanent changes in the thermoelastic properties, as well as permanent residual strains in the composite materials.

NASA Langley has undertaken a program to determine the dimensional stability of composite materials. This includes studying the effects of thermal cycling, radiation, and processing variability on these composites, both experimentally and analytically. Research to date has focused on the development of precise laser-based measurement systems for measuring small dimensional changes in composites and the effect of microcracking on the dimensional stability. The current effort on commercially available graphite/epoxy composites will be expanded in the future to include advanced composite systems, including hybrids, tougher resin/matrix composites, and advanced metal/matrix composites. The dimensional stability aspects of candidate tension-stabilized cable materials is also being investigated.

FACTORS CONTROLLING DIMENSIONAL STABILITY

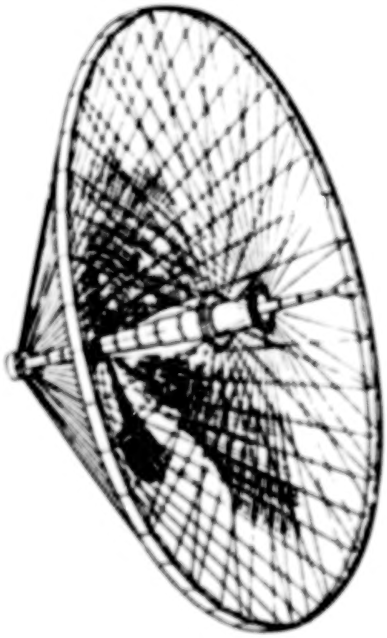

HOOP/COLUMN ANTENNA

- CABLES
  - THERMAL CYCLING
  - MECHANICAL LOADING
- ORGANIC MATRIX COMPOSITES
  - MOISTURE DESORPTION
  - THERMAL CYCLING
  - MECHANICAL LOADING
  - MICROYIELDING (CAUSED BY MATRIX MICROCRACKING)
  - RADIATION
- METAL MATRIX COMPOSITES
  - THERMAL CYCLING
  - MECHANICAL LOADING

Figure 10

TECHNIQUES FOR MEASURING SMALL THERMAL STRAINS

The composite laminates used in structures in which dimensional stability is critical will have CTE's approaching zero. Two laser interferometer systems capable of detecting strains on the order of 1×10^{-6} have been developed - a moire interferometer and a Priest interferometer. The moire interferometry technique is similar to conventional methods of moire strain analysis except that a fringe multiplication phenomenon is employed. This allows the use of a relatively coarse grating on the specimen and a much finer grating for the reference. By observing selected diffraction orders, the resolution is dependent upon the frequency of the reference grating and not that of the coarse specimen grating (0.025-inch-thick silicone or epoxy replicated onto the surface). The specimen and reference grating are illuminated with a collimated beam from a 5-mW He-Ne laser and are mounted in an environmental chamber capable of cycling between 422 K (300°F) and 116 K (-250°F). Measurements are made by counting interference fringes between gage marks cast in the specimen grating.

A Priest interferometer measures the displacement of an unknown specimen relative to two parallel rods of a known low-expansion reference material. A schematic of the Priest interferometer developed in this study is shown in figure 11. The interferometer is enclosed in a chamber in which the temperature of circulating air is controlled by a resistance heater and liquid nitrogen. A He-Ne laser illuminates the interferometer through a window in the top of the chamber. The fringe pattern is recorded by a camera. A similar setup is being used in a thermal vacuum chamber to make measurements of specimens being cycled in vacuum.

SCHEMATIC DIAGRAM OF PRIEST INTERFEROMETER

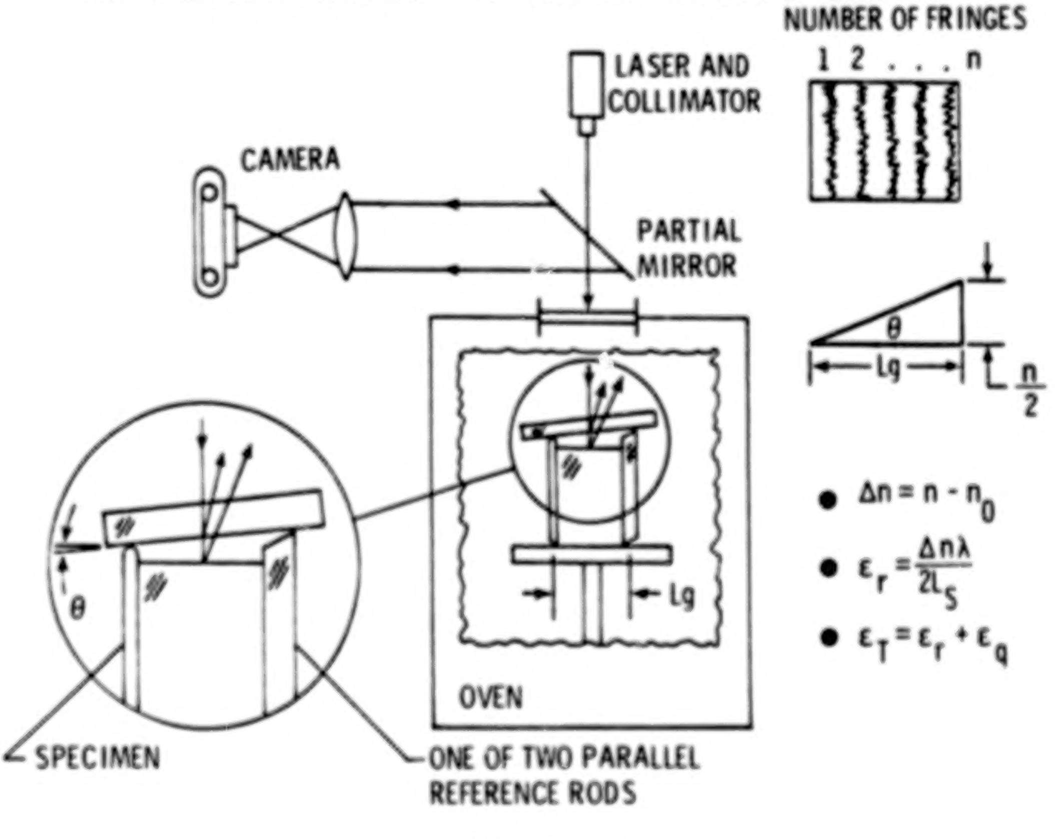
NUMBER OF FRINGES
1 2 . . . n
LASER AND COLLIMATOR
CAMERA
PARTIAL MIRROR
θ
Lg
n/2
θ
Lg
OVEN
SPECIMEN
ONE OF TWO PARALLEL REFERENCE RODS
• $\Delta n = n - n_0$
• $\varepsilon_r = \frac{\Delta n \lambda}{2L_S}$
• $\varepsilon_T = \varepsilon_r + \varepsilon_q$

Figure 11

THERMAL EXPANSION OF UNIDIRECTIONAL AND ISOTROPIC T300/5208 Gr/Ep LAMINATES

Typical thermal expansion data collected for unidirectional and quasi-isotropic T300/5208 graphite/epoxy over a temperature range from -150°C to 100°C are shown in figure 12. These data show the large range of CTE values that can be obtained in composites depending on the laminate configuration. As can be seen, unidirectional T300/5208 provides a very small CTE, -0.13×10^{-6} to 0.17×10^{-6} per °C, over the entire temperature range. The expansion behavior of these laminates is expected to bound the behavior of the laminates chosen for space structures. These data for different graphite fibers and resins are essential for verification of analyses used for tailoring laminates to achieve required stiffness and low CTE.

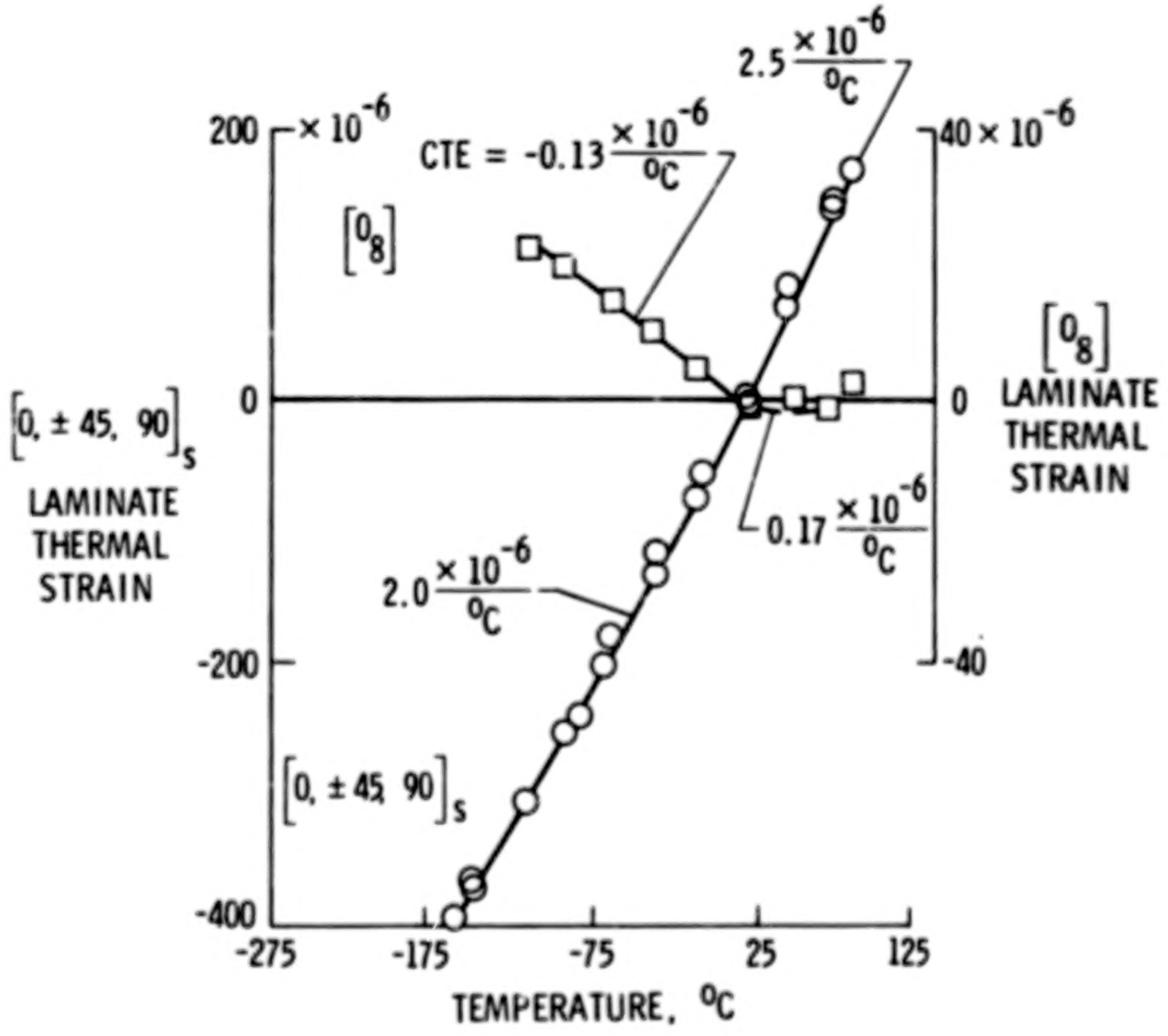

Figure 12

MICROCRACKING IN COMPOSITES

Microcracks are small cracks in the matrix of organic composites that extend parallel to the fiber direction. They occur when the internal stresses exceed the transverse strength of an individual lamina. The two primary causes of microcracking are mechanical and thermal loads.

A limited amount of research has been conducted concerning the causes and effects of microcracking in composites. Repeated thermal cycling has been shown to cause microcracking in graphite/epoxy laminates, which causes the CTE to approach that of the unidirectional material. A typical example of this thermal microcracking is shown in figure 13. Research has also shown that residual strains due to microcracking of up to 20 $\mu\varepsilon$ may develop in graphite/epoxy during the first cooling cycle to -143°C. What was lacking in past research was a quantitative relationship between the amount of microcracking and changes in CTE. This was the main focus of the current research.

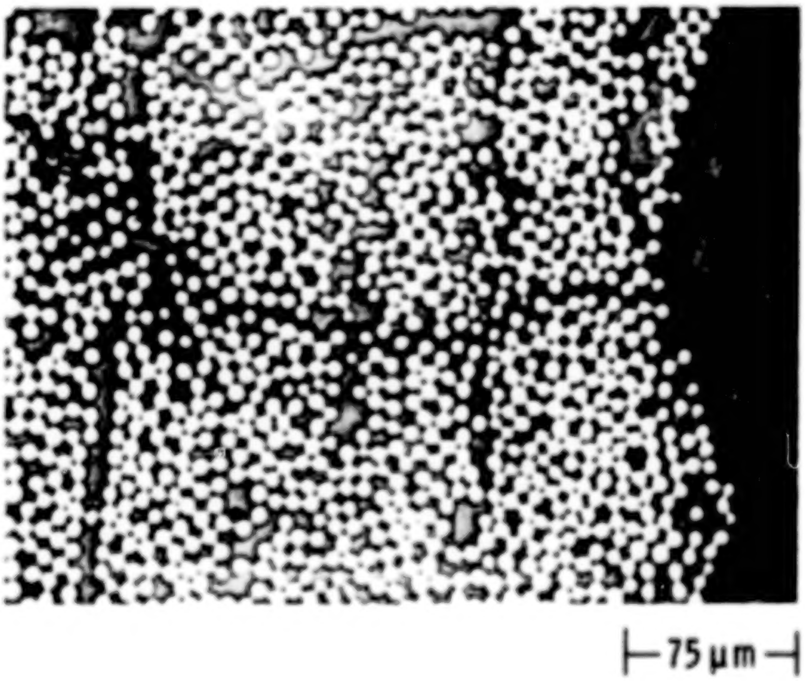

Figure 13

MODELING THE EFFECT OF MICROCRACKING ON CTE OF COMPOSITES

The effect of microcracks on the CTE was modeled with a finite-element analysis. A generalized plane strain formulation was used with four noded linear general quadrilateral isoparametric elements capable of handling orthotropic material properties.

Numerical results were generated for the $[0_m/90_n]_s$ (m, n = 1, 2, 3) class of laminates using typical material properties for T300/5208. Results are presented in the form of CTE as a function of linear crack density in the 90° plies, which was varied from zero to three cracks per mm. The value of three cracks per mm was found to be an upper limit on the crack density formed in these materials during the experimental phase of this research.

The results for this family of laminates are shown in figure 14. As would be expected, the laminate configuration with the largest percentage of 90° plies experienced the largest reduction in CTE. The CTE at three cracks per mm for the three laminates, $[0/90_3]_s$, $[0_2/90_2]_s$, and $[0_3/90]_s$, was reduced by approximately 80, 65, and 40 percent, respectively. For all of these laminates the CTE was reduced in a direction towards the value of the CTE for the unidirectional material, -0.1×10^{-6} per °C, and approached a stabilized value after approximately two cracks per mm.

EFFECT OF MICROCRACKS ON THE CTE OF $[0_m/90_n]_s$ LAMINATES

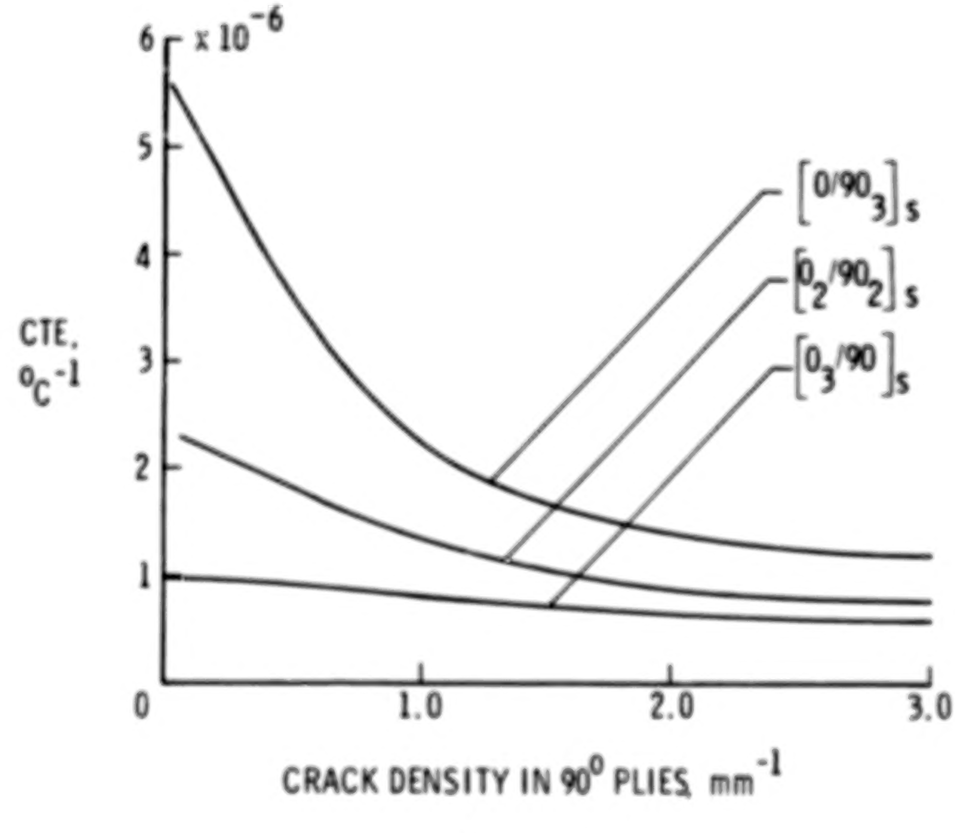

Figure 14

BEST DOCUMENT AVAILABLE

THERMAL CYCLING EFFECTS ON THE CTE OF GRAPHITE/MAGNESIUM COMPOSITES

Graphite-reinforced metal/matrix composites are an emerging new class of composites that have good potential for space applications. These materials can be fabricated with high-modulus (100 msi) pitch fibers to give a very low coefficient of thermal expansion (CTE). In addition, metal/matrix composites have a higher thermal conductivity than polymer/matrix composites and are therefore more resistant to thermal distortions resulting from through-thickness temperature gradients. Also, these composites are very stable in the space environment, are not affected by space radiation, and are very low outgassing materials. However, the thermal cycling response of these materials is one area of concern. Typical data collected on a three-ply graphite/magnesium composite manufactured with 45 volume percent pitch fibers are shown in figure 15. Upon cycling from room temperature to 60°C the CTE was observed to be approximately 0.95 x 10^{-6} °C^{-1}. However, when the material was cycled to low temperature, the CTE was observed to change during the first several thermal cycles, as indicated. After approximately six cycles from room temperature to -80°C, the low-temperature CTE approached that observed at higher temperatures. This type of transient behavior is related to the state of residual stress in the composites due to the difference in expansion between the graphite fibers and the magnesium matrix. Considerable effort is being expended to characterize and quantify the thermal cycling response of these materials. To achieve a uniform CTE over a large temperature range, cyclic preconditioning of subelements made with graphite/magnesium may be required for precision space structures.

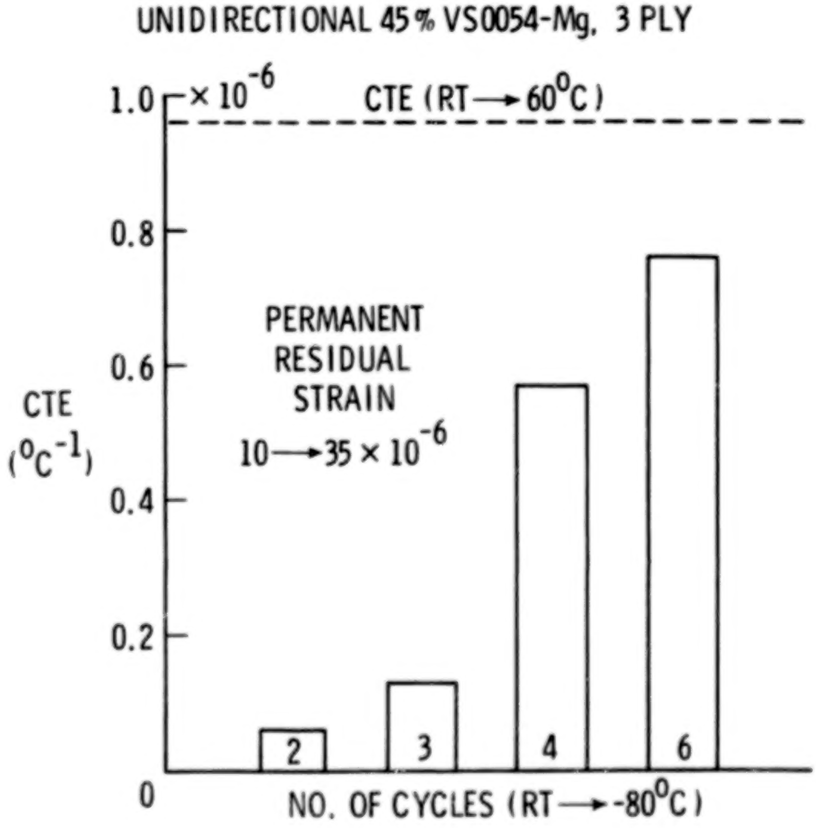

Figure 15

IMPROVED TENSION-STABILIZED CABLE MATERIALS

Lightweight deployable cables are currently being used in certain antenna designs to shape the mesh reflector surfaces. Current cables are made of quartz fibers because quartz has a low thermal expansion, is inherently stable in the space environment, and can be made in small-diameter fibers. A typical cable, approximately 450 με in diameter, is composed of approximately 2000 individual quartz fibers, 9 με in diameter, held together by a Teflon cross wrap. One of the problems with this type of construction is the difficulty in aligning the fibers and keeping them aligned during handling and storage of the cables. This results in a small (60×10^{-6}) but significant residual strain in the cable when subjected to repeated load or thermal cycles. Also, considerable variability is observed in this residual strain, making it difficult to accurately bias this out during fabrication when the precise length of each cable is determined.

The results of a recent program conducted to develop an improved cable are summarized in figure 16. Two major improvements were made that significantly advanced space cable technology. Unidirectional composites were made by impregnating the bare fibers with Teflon while holding the fibers straight under tension to achieve a better alignment of fibers and minimize the amount of twist in the fiber along the cable. This resulted in a substantial increase in the relative stiffness of the cable and reduction in residual strain after repeated thermal/mechanical cycling. Further improvements were achieved by using graphite fibers in place of the quartz fibers.

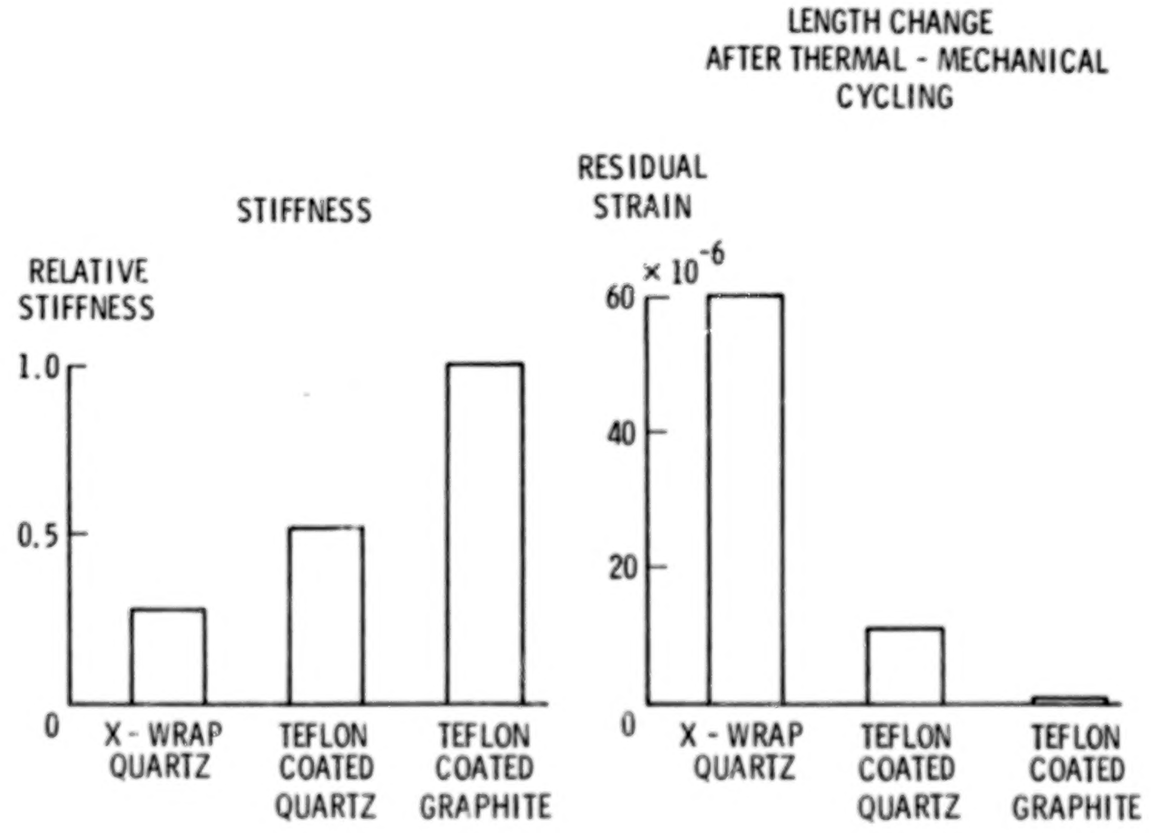

Figure 16

THERMAL CONTROL COATING REQUIREMENTS FOR SPACE STRUCTURES

The basic requirement for thermal control coatings is to keep spacecraft components within allowable temperature limits. Thermal designers have two major problems. The first occurs when the temperature limit is dictated only by the solar heat input (for example, large-area structures) and the second occurs when both solar and internal heat are thermal inputs (for example, a manned habitat). In each case a coating with a different ratio of solar absorptance to thermal emittance is required. In figure 17 the coating requirements for a composite structure in GEO are compared to the requirements for a manned habitat in LEO. The major differences are: (1) low-emittance coatings are required for the composite structure to reduce the extent of cooldown during a solar occult, (2) coating to be used in GEO must be able to withstand high-energy electrons and protons in addition to UV, and (3) a higher electrical conductivity is required in GEO to eliminate spacecraft charging. Contamination would be a major source of coating performance degradation for the manned habitat because of contaminants from the Shuttle. However, repair or refurbishment of coatings can be considered for this application but not for GEO.

	COMPOSITE STRUCTURE GEO	MANNED HABITAT LEO
OPTICAL PROPERTIES	α/ε - SELECTABLE WITH $\varepsilon \leq 0.3$	α/ε - SELECTABLE WITH $\varepsilon \geq 0.8$
TEMPERATURE	-100^0 TO $+80^0$C	-100^0 TO $+40^0$C
ENVIRONMENT	UV, e^-, p^+, VAC, ΔT	UV, VAC, ΔT
ELECT. CONDUCTIVITY	$\leq 10^{-8}$ (ohm^{-1}-cm^{-1})	10^{-8} - 10^{-17} (ohm^{-1} - cm^{-1})
LIFETIME	10 TO 20 YEARS	10 YEARS

Figure 17

LIMITATIONS OF CURRENT THERMAL CONTROL COATINGS

Figure 18 summarizes some of the existing and previously used radiator thermal control coating materials and identifies the major problem with each of these materials. The table also points out that no low-emittance paint-type coatings are available for use on large space structural components. Because of the weight penalty associated with use of this type of coating on small, thin-gage tubular structural elements, organic-matrix white-paint coatings would not likely be considered. New coating concepts that are easily adapted to any structural configuration and have good long-term durability in the radiation (ionized particle and UV) environment must be developed.

RADIATOR COATINGS (LOW ABSORPTANCE, HIGH EMITTANCE)

COATING	PERFORMANCE
S-13 GLO (ZnO/RTV-602)	RTV 602 DISCONTINUED, NEW SILICONE BINDER FOR QUALIFICATION
ZOT (Zn_2TiO_4/SILICATE)	ABSORBS MOISTURE, HARD TO CLEAN
Z-93 (ZnO/SILICATE)	ABSORBS MOISTURE, EASILY CONTAMINATED
Al OR Ag/TEFLON	LARGE AREA APPLICATION DIFFICULT

STRUCTURAL COATINGS (LOW ABSORPTANCE, LOW EMITTANCE)

NO QUALIFIED PAINT-TYPE COATINGS AVAILABLE

Figure 18

DEVELOPMENT OF NEW THERMAL-CONTROL COATINGS

To achieve long-lived (10-15 years) space structures, space-durable coatings are required. Current thermal-control coatings are generally considered to degrade significantly after 5 to 7 years in orbit. NASA has undertaken a program to develop long-life, UV-resistant thermal-control coatings for space systems with tailored optical and electrical properties (fig. 19). In addition, these coatings must be capable of being applied over a large area of coverage. Both metallic- and oxide-vapor-deposited coatings will be evaluated for laminated polymer/matrix composites. The solar absorptance to emittance ratio will be tailored for operation over a -50°C to +100°C temperature range. These coatings will be exposed to electrons, protons, and UV radiation under space flight conditions to evaluate their long-term space durability. Contamination effects will also be evaluated to develop coatings with minimum sensitivity to contamination. A necessary requirement for these coatings is that they be low outgassing and thermally stable.

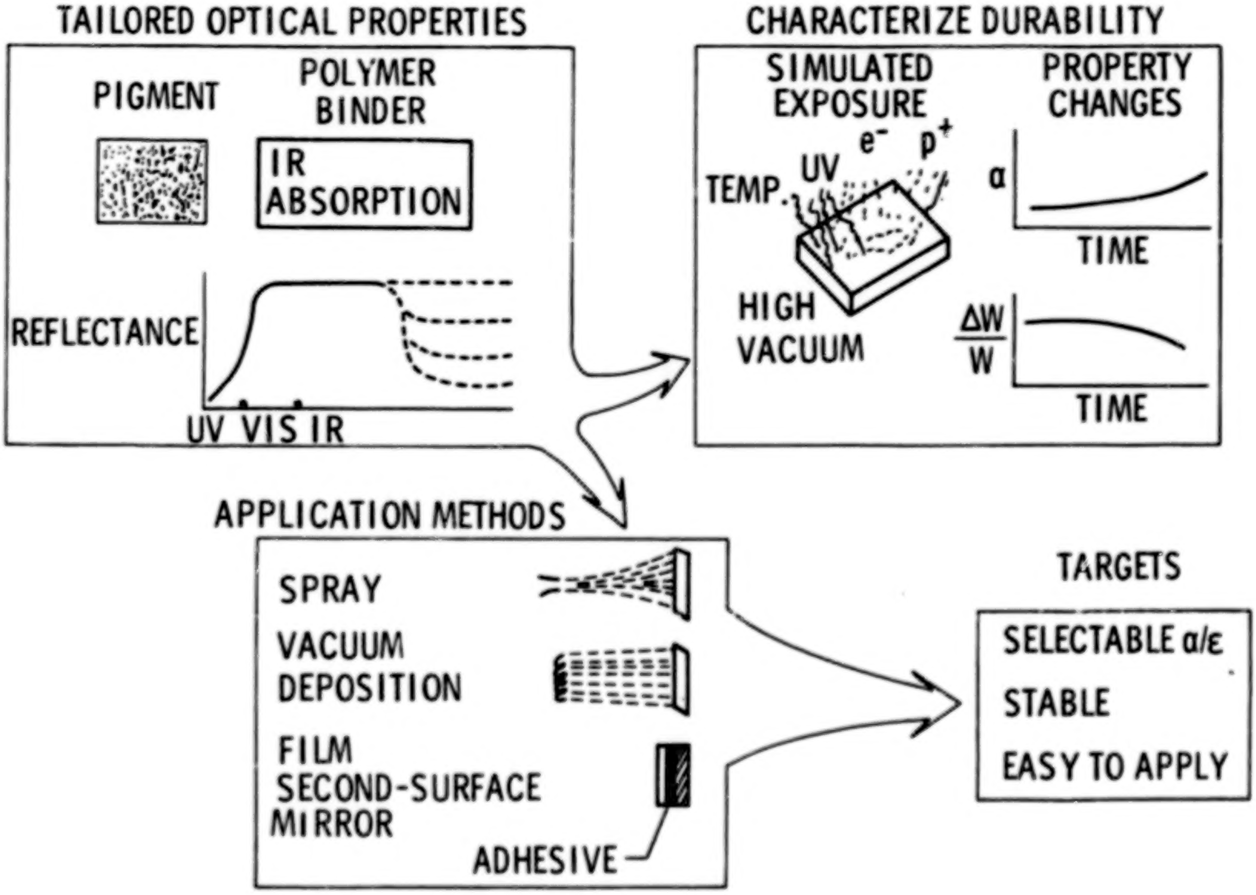
TAILORED OPTICAL PROPERTIES
PIGMENT
POLYMER BINDER
IR ABSORPTION
REFLECTANCE
UV VIS IR
CHARACTERIZE DURABILITY
SIMULATED EXPOSURE
PROPERTY CHANGES
TEMP.
UV
e^-
p^+
HIGH VACUUM
α
TIME
ΔW/W
TIME
APPLICATION METHODS
SPRAY
VACUUM DEPOSITION
FILM SECOND-SURFACE MIRROR
ADHESIVE
TARGETS
SELECTABLE α/ε
STABLE
EASY TO APPLY

Figure 19

LDEF FLIGHT EXPERIMENT

In addition to development of new coating concepts, Langley has also maintained a continuing role in both ground testing and development of flight tests of coatings. A Langley coatings experiment will be flown on the Long Duration Exposure Flight (LDEF) spacecraft. The objectives of LDEF are to determine the effects of both the Shuttle-induced environment and the space radiation environment on selected sets of spacecraft thermal-control coatings. The experimental approach is to passively expose samples of thermal-control coatings to Shuttle-induced and space radiation environments, return the samples for postflight evaluation and compare with preflight measurements to determine the effects of environmental exposure. Two additional sets of samples will remain in the laboratory and will be analyzed for comparison with the flight data. Optical measurements of the samples will include total normal emittance and spectral reflectance. The experiment will use a 15.2-cm-deep tray and an Experiment Exposure Control Canister (EECC) to provide protection for some of the samples against the launch and reentry environment. The EECC will be programmed to open about 2 weeks after LDEF deployment and close prior to LDEF Shuttle retrieval (fig. 20).

Some samples will not be housed in the EECC and will be exposed to the Shuttle-induced environment during launch and reentry. Comparison of data from these samples with that of samples the EECC will yield information about possible contamination-induced degradation effects.

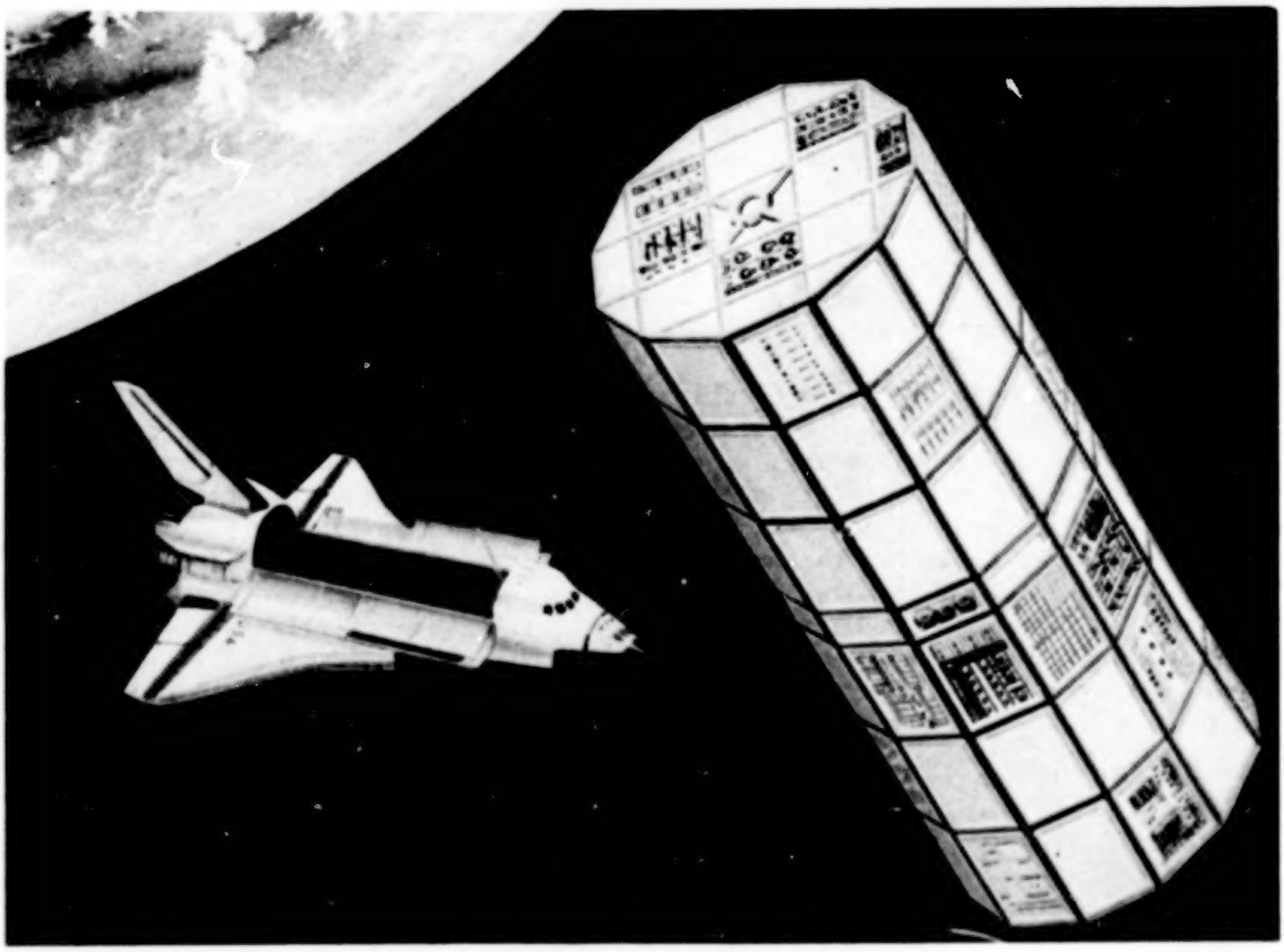

Figure 20

CONCLUDING REMARKS

Polymer/matrix composite materials will be used for future space structures because of their excellent properties. Test results suggest that currently available composites will not undergo significant mechanical property changes for 20 to 30 years of service in space. No significant degradation has been observed in residual strength of composites upon laboratory exposure to electron radiation doses to 5 x 10^9 rads (equivalent to 30 years exposure in GEO). However, results to date are preliminary and were obtained using high dose rates (30 to 60 hours of test to simulate 30 years of exposure). Longer term low-dose-rate tests that are more representative of the conditions expected in space need to be conducted to determine if dose rate effects are significant. These tests are under way.

Extensive chemical characterization of polymer films exposed to radiation doses expected in space have shown that radiation does produce significant chemical changes. Degradation mechanisms have been established for a polysulfone and similar studies are ongoing on a number of other polymers. The point at which mechanical property changes appear has yet to be established. Radiation degradation models currently under development are expected to aid in understanding how radiation damage occurs in polymers and how chemical and mechanical properties are changed.

Thermal expansion measurements of composites are difficult because of the orthotropic nature of composites and because of their low coefficient of thermal expansion. To make precision strain measurements of composites, two laser interferometer techniques were developed. The effect of mechanically induced microcracks on the CTE was determined experimentally and an analysis was formulated to predict the observed changes. Results showed that microcracks reduce the CTE towards the value for the unidirectional material, and the reduction is a function of both the crack density and laminate configuration. Research in the area of improved cable materials has resulted in the development of a Teflon-impregnated graphite cable with a higher stiffness, lower CTE, and greatly reduced residual strain compared to the conventional quartz cable.

An assessment of current coatings indicates that they will not meet the thermal-control requirements for large space structures. Existing white paint coatings are heavy and undergo significant degradation in optical properties in 5 years of space exposure. Langley is working on new advanced coatings concepts including unique particulate and UV-radiation-stable polymer films that may be suitable for thermal-control coatings and blankets. The development of a clear polyimide offers good potential for developing improved coatings. The planned coating experiment on LDEF will provide useful data for evaluating Shuttle contamination of coatings and for verification of ground-based simulation tests.

BIBLIOGRAPHY

1. Large Space Systems Technology - 1980, Vols. I and II, NASA CP-2168.

2. Large Space Systems Technology - 1981, Vols. I and II, NASA CP-2215, 1981.

3. Bush, H. G.; and Heard, J. L.: Recent Advances in Structural Technology for Large Deployable and Erectable Spacecraft. NASA TM-81905, Oct. 1980.

4. Wright, R. L. (Editor): The Microwave Radiometer Spacecraft - A Design Study. NASA RP-1079, Dec. 1981.

5. Russell, R. A.; Campbell, T. G.; and Freeland, R. E.: A Technology Development Program for Large Space Antennas. NASA TM-81902, 1980.

6. Moritz, J.: Measurement of Radiation Belt Protons in the Energy Range 0.25 to 1.65 MeV on Board the Satellite "AZUR." J. Geophy., 37, 1971.

7. Vette, J. I.; Locero, A. B.; and Wright, J. A.: Models of the Trapped Radiation Environment, V. II: Inner and Outer Zone Electrons. NASA SP-3024, 1967.

8. Teague, M. J.; Chan, K. W.; and Vette, J. I.: AE6: A Model Environment of Trapped Electrons for Solar Maximum. NASA TM X-72597, 1976.

9. Kircher, J. F.; and Bowman, R. E.: Effects of Radiation on Materials and Components. Reinhold Publ. Co., New York, 1964.

10. Fornes, R. E.; Memory, J. D.; and Naranong, N.: "Effect of 1.33 MeV γ Radiation and 0.5 MeV Electrons on the Mechanical Properties of Graphite Fiber Reinforced Composites," J. Applied Polym Sci. 26: 2061-2067 (1981).

11. Santos, B.; and Sykes, G. F.; Radiation Effects on Polysulfone Films. Presented at 13th National SAMPE Tech. Conf. (Mt. Pocono, PA), Oct. 1981.

12. Marayama, T.: Dynamic Mechanical Analysis of Polymeric Material. Materials Science Monographs 1, Elsevier Scientific Publishing Co., NY, 1968.

13. Bowles, D. E.; Post, D.; Herakovich, C. T.; and Tenney, D. R.: Moire Interferometry for Thermal Expansion of Composites. Experimental Mechanics, Vol. 21, No. 12, Dec. 1981.

14. Short, J. S.: Thermal Expansion of Graphite/Epoxy Composite Laminates Bewtween 116 and 366 K. M. S. Thesis, Virginia Polytechnic Insitute and State University, Blacksburg, VA, July 1982.

15. Camahort, J. L.; Rennhack, E. H.; and Coons, W. C.: Effects of Thermal Cycling Environment on Graphite/Epoxy Composites. ASTM STP 602, 1976.

16. Eselun, S. A.; Neubert, H. D.; and Wolff, E. G.: Microcracking Effects on Dimensional Stability. Presented at 24th National SAMPE Conf. (San Francisco, CA), May 8-10, 1979.

17. Bowles, D. E.: The Effect of Microcracking on the Thermal Expansion of Gr/Ep. Large Space Systems Technology - 1981, NASA CP-2215, Nov. 1981.

18. Tompkins, S. S.; and Williams, S. L.: Effects of Thermal Cycling on Residual Mechanical Properties of C6000/PMR-15 Graphite Polyimide. Presented at AIAA 23rd SDM Conference (New Orleans, LA), May 1982.

19. Harris, F. W.; and Seymour, R. B.: Structure-Solubility Relationships in Polymers, Acadmic Press, NY, 1977.

20. St. Clair, A. K. and Taylor, L. T.: Incorporation of Metal Related Materials into Electrically Neutral Polymers. J. Macromol. Sci-Chem. A16(11), 1981.

MATERIALS PROCESSING IN SPACE

W. A. Oran
NASA Headquarters
Washington, DC

ABSTRACT

A brief overview of the current Materials Processing in Space Program will be given, including a tentative schedule of flight experiments. Some recent results of processing materials (e.g., polymers and eutectic materials) in a microgravity environment will be given, along with a discussion on additional proposed flight experiments. Ground-based results and the rationale for flight experimentation will be presented for other materials processes, including crystal growth.

Overall objectives and major areas of research of the Materials Processing in Space Program are shown in figure 1.

MATERIALS PROCESSING IN SPACE (MPS)

GOAL

PROVIDE RESEARCH BASE AND ESTABLISH STS FACILITY USAGE

O TO ACHIEVE IMPROVED PROCESSING METHODS AND MATERIALS OF TECHNOLOGICAL INTEREST

O TO ASSIST EARLY COMMERCIALIZATION OF SPACE PROCESSING

CURRENT AREAS OF ACTIVITY

O CRYSTAL GROWTH

O SOLIDIFICATION

O FLUID AND CHEMICAL PROCESSES

O CONTAINERLESS PROCESSING

O BIOLOGICAL MATERIALS SEPARATION

Figure 1

Specific areas of research supported by the Materials Processing in Space Program are shown in figure 2.

MPS APPLIED RESEARCH AND DATA ANALYSIS

AREA	THRUST
1. CONTAINERLESS TECHNOLOGY	DEVELOPMENT OF UNIQUE STATE-OF-ART PROCESSING TECHNOLOGY, ACOUSTIC, ELECTROSTATIC, ELECTROMAGNETIC, JET. WE ARE LEADERS IN THIS FIELD.
2. CONTAINERLESS SCIENCE	HIGH-PURITY GLASS NEW OXIDE GLASSES HIGH-TEMPERATURE PROCESSING HIGH-TEMPERATURE THERMOPHYS. MEAS. CORROSIVE REACTIONS BASIC NUCLEATION STUDIES FUSION TARGET TECHNOLOGY
3. CRYSTAL GROWTH	GROWTH FROM VAPOR GROWTH FROM SOLUTION GROWTH FROM MELT
4. SOLIDIFICATION PROCESS	UNDERSTANDING CASTING REDUCING CONVECTIVE EFFECTS IMMISCIBLE MATERIALS COOPERATIVE GROWTH
5. SPACE MATERIALS SYSTEM	DEVELOPMENT OF REQUIREMENTS AND TECHNIQUES FOR EXTRA-TERRESTRIAL MATERIALS PROCESSING
6. BIOLOGICAL PROCESSING	SEPARATION TECHNIQUES SEPARATION OF VIABLE CELLS SEPARATION OF PROTEIN
7. FLUID BEHAVIOR	FLUID DYNAMICS OF SPACE PROCESSING CRITICAL POINT PHENOMENA
8. PROGRAM SUPPORT	SCIENCE AND DISCIPLINE WORKING GROUPS, OUTSIDE PEER REVIEW SUPPORT
9. COMMERCIAL MPS	IDENTIFY COMPANIES AND ARRANGEMENTS FOR COMMERCIALIZATION
10. COMBUSTION	INFLUENCE OF CONVECTION ON COMBUSTION
11. CLOUD PHYSICS	INFLUENCE OF CONVECTION ON CLOUD FORMATION

Figure 2

A chronology of past and proposed flight experiments for the United States Materials Processing in Space Program is shown in figure 3.

FLIGHT EXPERIMENTS

1974 - 1975

- OVER 50 MATERIALS PROCESSING EXPERIMENTS PERFORMED ON SKYLAB AND APOLLO SOYUZ TEST PROGRAM

1982

- 4 RESEARCH EXPERIMENTS
- 1 PRECOMMERCIAL EXPERIMENT

POLYMERIC REACTION STUDIES
ELECTROPHORETIC SEPARATION

1983

- 4 RESEARCH EXPERIMENTS
- 3 PRECOMMERCIAL EXPERIMENTS

POLYMERIC REACTION STUDIES
ELECTROPHORETIC SEPARATION
VAPOR CRYSTAL GROWTH
IMMISCIBLE ALLOY FORMATION
CONTAINERLESS PROCESSING

1984

- 15 RESEARCH EXPERIMENTS
- 3 PRECOMMERCIAL EXPERIMENTS

ELECTROPHORETIC SEPARATION
CONTAINERLESS PROCESSING
UNDERCOOLING/RECALESCENCE STUDIES
VAPOR CRYSTAL GROWTH
IMMISCIBLE ALLOY FORMATION
BLOOD RHEOLOGY
OXIDE GLASS FORMATION
MARANGONI BUBBLE FLOW
SOLUTION CRYSTAL GROWTH

Figure 3

Some applications of results obtained in microgravity investigation to ground-based processing technology are shown in figure 4.

Magnetic field breeds Skylab-like semiconductors

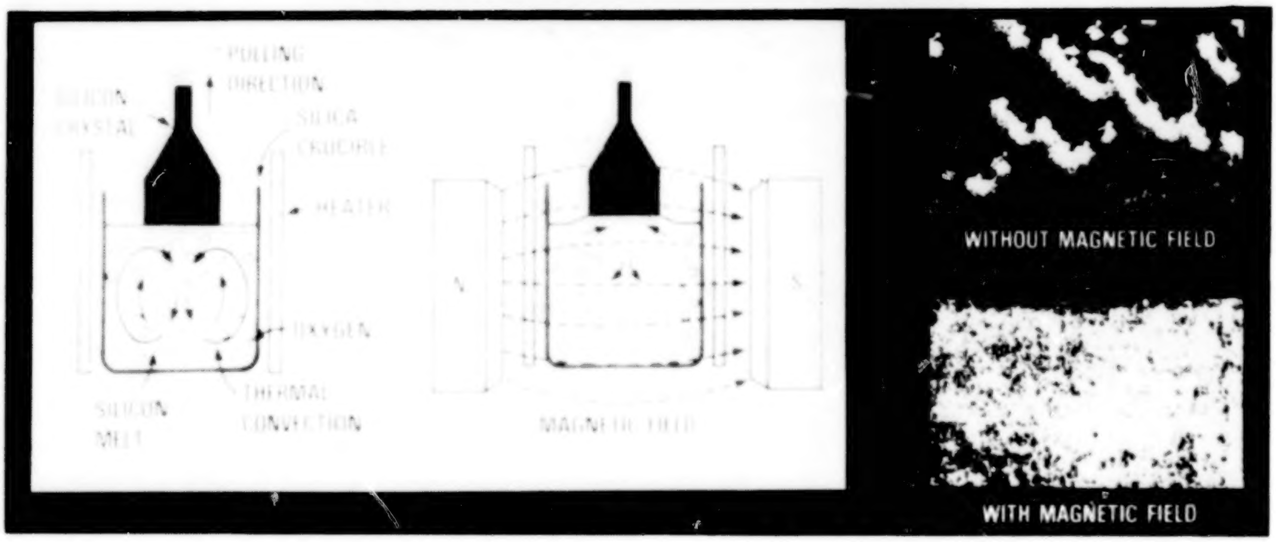
PULLING DIRECTION
SILICON CRYSTAL
SILICA CRUCIBLE
HEATER
OXYGEN
SILICON MELT
THERMAL CONVECTION
N
S
MAGNETIC FIELD
WITHOUT MAGNETIC FIELD
WITH MAGNETIC FIELD

Figure 4

Figure 5 shows a comparison of crystals of HgCdTe grown by vapor transport on Earth. The lower photographs show the results of growing in a vertical thermally stabilizing configuration, while the upper photographs show the results of growing in a horizontal configuration.

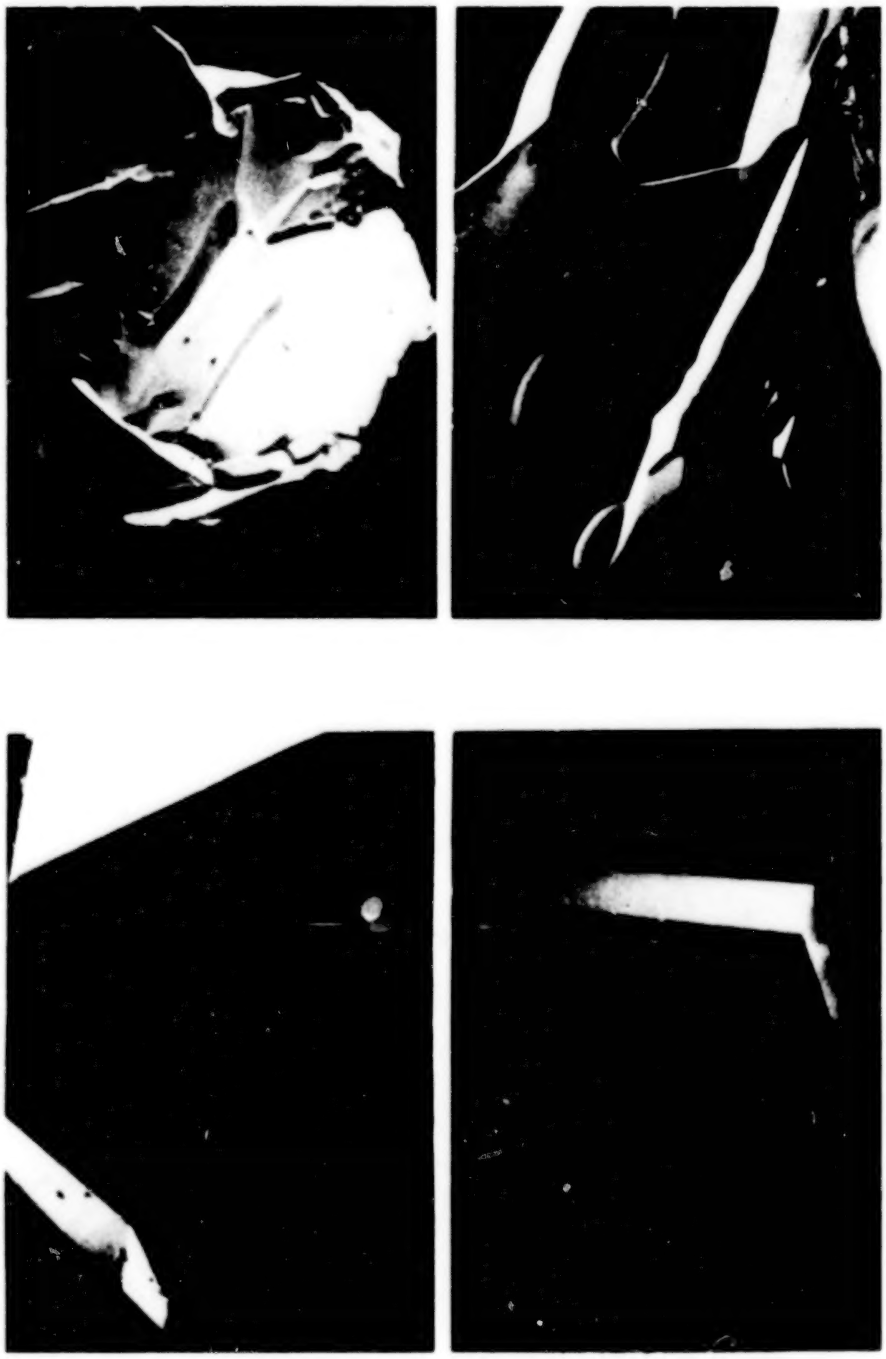

Figure 5

Micrographs of Bi/MnBi eutectic grown under similar conditions are shown in figure 6. The Bi/MnBi was grown in sealed quartz cartridges in a Bridgman-Stockbarger furnace.

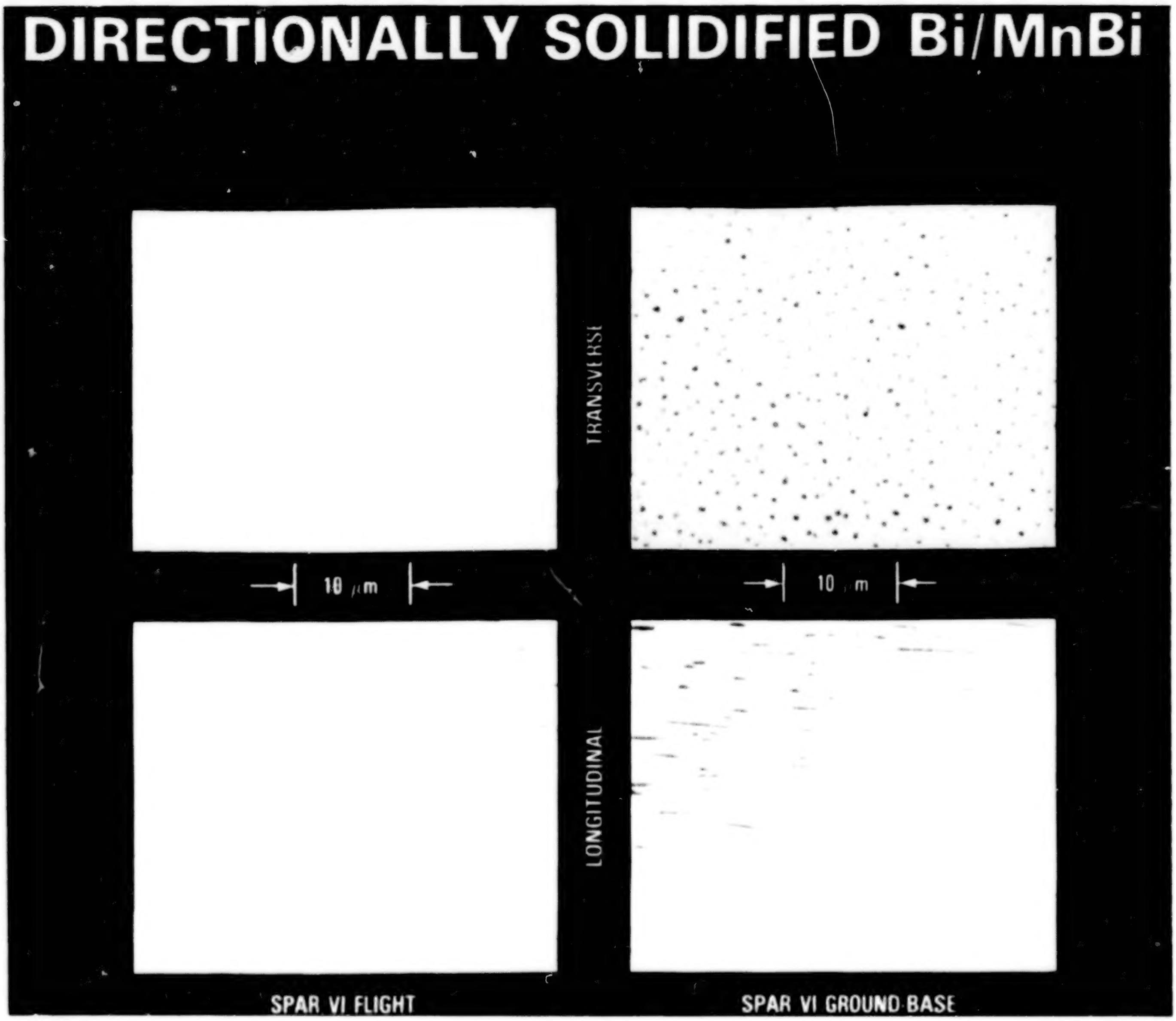
DIRECTIONALLY SOLIDIFIED Bi/MnBi
TRANSVERSE
10 μm
10 μm
LONGITUDINAL
SPAR VI FLIGHT
SPAR VI GROUND BASE

Figure 6

Figure 7 shows a chronology of microgravity separation studies.

PAST

- 1972-73 ELECTROPHORESIS TECHNOLOGY STUDIES - APOLLO
- 1975 STATIC COLUMN ELECTROPHORESIS STUDIES - ASTP

PRESENT

- 1982 PRECOMMERCIAL CONTINUOUS FLOW ELECTROPHORESIS

RECENT RESULTS FROM STS-4

- SEPARATION VOLUME EXCELLENT
- SAMPLE QUANTITY EXTREMELY GOOD
- MOBILITY, SEPARATION UNIMPAIRED

Figure 7

Commercial MPS participants, present and proposed, are shown in figure 8.

COMMERCIAL MPS PARTICIPANTS: PRESENT AND PROPOSED

- JOINT ENDEAVOR AGREEMENT

  INDUSTRY BUILDS HARDWARE WHICH FLIES AS NASA MPS PAYLOAD - NO EXCHANGE OF FUNDS BY NASA - INDUSTRY DERIVES A PRE-COMMERCIAL PRODUCT IN LOW-G ENVIRONMENT OF SPACE

  - MCDONNELL DOUGLAS (SIGNED JANUAR[illegible]0) USES CONTINUOUS FLOW ELECTROPHORESIS APPARATUS TO DEVELOP COMMERCIALLY USEFUL PHARMACEUTICAL MATERIALS
  - GTI CORPORATION - (SIGNED JANUARY 20, 1982) WILL MAKE VARIOUS ALLOYS FOR SALE TO UNIVERSITY AND INDUSTRIAL RESEARCHERS
  - MICROGRAVITY RESEARCH ASSOCIATES, INC. (PROPOSED) WILL GROW GALLIUM ARSENIDE CRYSTALS FOR ELECTRONIC AND COMPUTER APPLICATIONS

- TECHNICAL EXCHANGE AGREEMENT

  PROVIDES FOR SHORT-DURATION LOW-G TIME ON DROP TUBES/ DROP TOWER AND KC-135 - NO EXCHANGE OF FUNDS

  - DEERE AND COMPANY (SIGNED JUNE 29, 1981) EXPLORE PROPERTIES BASIC TO CASTING PROCESS
  - DUPONT (SIGNED JANUARY 27, 1982) EXPLORE CATALYTIC PROPERTIES OF ALLOYS
  - INCO RESEARCH AND DEVELOPMENT CENTER, INC. (SIGNED JANUARY 28, 1982) EXPLORE ELECTROPLATING PROCESS AT LOW-G
  - HONEYWELL ELECTROOPTICAL SYSTEMS STUDY OF MERCURY CADMIUM TELLURIDE

Figure 8

TRIBOLOGY

Donald H. Buckley
NASA Lewis Research Center
Cleveland, Ohio

INTRODUCTION

Tribology is the study of the adhesion, friction, wear, and lubricated behavior of materials in solid-state contact. The function of tribological research is to bring about a reduction in the adhesion, friction, and wear of mechanical components to prevent their failure and provide long, reliable component life through the judicious selection of materials, operating parameters, and lubricants.

Mechanical systems such as bearings, gears, and seals are examples of components involving tribology. Wherever, however, two or more solid surfaces are in contact with relative motion between the surfaces, tribology is involved. Such mundane activities as a man's morning shave involve both friction and corrosive wear, and considerable tribological research has gone into increasing blade life and reducing friction and shaving discomfort. More complex tribological systems are gyro bearings and instrumentation gears requiring attention to many elements.

The objective of the present paper is to review the adhesion, friction, and wear properties of materials and some of the factors influencing these properties. The forms of lubrication and types of lubricants will also be discussed.

ADHESION AND FRICTION

In a conventional atmospheric environment, the oxygen present in the air interacts with freshly generated metal and alloy surfaces to produce surface films; namely, oxides. These oxides play a very strong role in the adhesion, friction, and wear behavior of metals and alloys. In the absence of these oxides, very strong adhesion, high friction coefficients, and ultimately cold welding of materials from one surface to another are observed. If, for example, two normal metal surfaces are placed inside a vacuum environment with a system capable of achieving pressures to 10^{-10} torr, and the surfaces are very carefully cleaned with argon ion bombardment and then brought into touch contact, adhesion of one surface to the other will immediately occur. Attempts at tangential motion will cause a growth in the area adhered at the interface, that is, in the real contact area with an ultimate complete seizure of the surfaces one to another. With this occurrence, the surfaces are generally severely disrupted (refs. 1 and 2).

When adhered surfaces are separated, the adhesion at the interface between the two dissimilar solid surfaces is sufficiently strong to prevent fracture at the interface, but fracture does generally occur in the cohesively weaker of the two materials in contact (ref. 3). An example of such behavior is shown in the photomicrograph of figure 1. This figure represents the results of an experiment conducted in a vacuum chamber where two solid surfaces were brought into contact; the surfaces had been cleaned in vacuum. Adhesion occurred at the interface, and when separation of the solid surface was attempted, fracture occurred in one of the two materials, leaving material transferred to the opposite surface.

The actual area of real contact at the interface can be seen in figure 1 by a careful examination of the interface region. There appear to be voids in the interface region where complete and intimate solid-state contact across the interface did not occur. However, a great portion of the interfacial area does reflect solid-to-solid contact in adhesive bonding. This adhesive bond was generated as a result of attempting to slide one surface over the other. This resulted in growth in the adhered junctions at the interface, leaving only a small area wherein no intimate contact of the two solid surfaces occurred. On separation, the adhesive bond at the interface remained intact and fracture occurred in one of the solids, as indicated in figure 1 by the rough piece which remained on the solid surface.

This type of adhesion and transfer behavior is observed for all clean metal surfaces and alloys in solid-state contact. That is, when the environmentally contributed surface films, namely the oxides, are removed, such adhesion is observed with strong bonding and friction coefficients measured in excess of 100 under such circumstances. The surfaces of solids such as metals and alloys are so sensitive to the contact region microenvironment that the admission of very small adsorbate concentrations from the environment to the solid surface can markedly reduce adhesion and friction. For example, fractions of a monolayer on the solid surface will produce a marked reduction in the adhesion and corresponding static friction coefficients for metal in contact (ref. 4).

In addition to metals and alloys, nonmetallic materials are also markedly influenced by the presence of the environment in their adhesion, friction, and wear behavior. The presence of adsorbates on ceramic materials such as aluminum oxide has a pronounced influence on the friction coefficients measured for aluminum oxide (ref. 5).

Polymeric materials are also affected by the presence of environmental constituents on their surfaces. For example, nylon serves as a good solid self-lubricating material in certain mechanical applications. Nylon, however, depends upon the presence of adsorbed moisture for its effective lubrication; that is, for its low friction and wear properties. In the absence of moisture, nylon will not lubricate effectively and it becomes a poor tribological material (ref. 5). Carbon materials are heavily used in mechanical devices such as dynamic seals and are extremely sensitive to environment and environmental constituents.

The flying of aircraft at high altitudes results in excessive wear in carbon generator brush materials; this was established during the second World War. Careful analysis of the aircraft surfaces revealed that the excessive wear of carbon materials, carbon bodies at high altitudes, was due to a reduction in the ambient pressure, and more particularly with the reduction of moisture in the environment. Carefully controlled experiments in the laboratory subsequently demonstrated that carbon lubricates effectively in the presence of moisture, exhibiting low friction, low wear, and little tendency to adhere. In the absence of moisture, however, carbon exhibits extremely heavy wear and becomes a very poor friction and wear material. In fact, by simply reducing the ambient pressure from 760 torr of air to an ambient pressure of approximately 1 torr, a 1,000-fold change in wear properties occurs. Thus, moisture is a lubricant and is needed on these surfaces and at the interface between two carbon bodies in relative contact and in motion, or between the carbon body and some other material in solid-state contact (ref. 5).

If one considers the environment not only as an ordinary air containing principally oxygen and nitrogen with some water vapor, but also considers vapors of hydrocarbons as constituents of the environment, then the particular hydrocarbon molecular structure that may be present in the environment can have a very pronounced influence upon the adhesion, friction, and wear behavior of materials in contact. For example, careful cleaning of iron surfaces in a vacuum environment will result in the generation of extremely energetic surfaces that will adhere one to another when brought into contact with cold welding occurring readily. If, however, a small amount of hydrocarbon gas is admitted to the vacuum chamber and allowed to absorb on the clean iron surface, a structure will develop which will provide that surface with a protective film.

Further, clean iron surfaces will chemisorb nearly all hydrocarbons (ref. 6). The hydrocarbon film will reduce adhesion, friction, and wear because the surface energy has been reduced by the hydrocarbon molecules on the surface. The energy on the clean iron surface available for bonding across the interface to another solid surface has been taken up in the interaction of the clean iron surface with the lubricating molecules absorbing on it. The particular molecular structure, however, of the adsorbing hydrocarbon will also affect the tribological behavior. That is, a slight modification in the molecule will produce sensitivities in adhesion, friction, and wear. These slight differences indicate extreme sensitivity in the tribological behavior of materials to environment and environmental constituents. This effect can be demonstrated by the adsorption of a simple hydrocarbon such as ethylene oxide onto an iron surface and exposure of that same surface to a different simple hydrocarbon with a slightly modified molecular structure, something such as ethylene chloride (or as it is commonly called, vinyl chloride).

If clean iron single crystal surfaces of the same orientation are exposed to equivalent concentrations of these two simple hydrocarbons, namely ethylene oxide and vinyl chloride, entirely different surface structures result. The differences can be seen in the LEED (Low Energy Electron Diffraction) patterns presented in figure 2.

LEED is a device which permits examination of the structural arrangement of atoms in the outermost atomic layer of the solid surface. Thus, in figure 2, we see the molecular arrangement in the diffraction pattern for the adsorbed ethylene oxide and vinyl chloride on the iron surface in the two patterns. Equivalent concentrations of each specie were provided. Thus, everything is constant except the particular molecular structure. The ethylene oxide exhibits the basic ethylene structure with oxygen present in the molecule. Vinyl chloride exhibits essentially the same structure as the ethylene, but chlorine is substituted for oxygen. This subtle difference in the structures, however, causes marked differences in surface coverage (see LEED patterns, fig. 2).

With the ethylene oxide, the six diffraction spots in a hexagonal array indicate that the ethylene oxide molecule completely masked or covered the iron surface. No diffraction spots are seen for the iron in the diffraction pattern of figure 2. A close packing of the molecules of ethylene oxide on the iron surface provides a very effective and continuous surface film.

In contrast to ethylene oxide, however, the vinyl chloride structure is much more open with less-than-complete surface coverage and bonding of vinyl chloride to the surface. The four bright diffraction spots with vinyl chloride adsorption, seen in a rectangular array in figure 2, are associated with the iron. Thus, vinyl chloride does not provide complete coverage, and nascent iron is still exposed at the surface.

As one might anticipate, differences in adhesion and friction behavior are observed with these two films present. With the ethylene oxide, the adhesive forces are appreciably reduced between two clean iron surfaces in contact. Further, the friction forces are less for the ethylene oxide on the iron surface than are observed with the vinyl chloride present. Thus, slight differences in the molecular structure of hydrocarbons present in the microenvironment of solid surfaces in contact can influence the tribological behavior of those surfaces.

WEAR

Various recognized mechanisms cause surfaces to wear. The more common types are adhesion, abrasion, corrosion, erosion, cavitation, fretting, and fatigue. Some of these mechanisms will be briefly discussed.

Adhesive Wear

Adhesion has already been discussed with reference to figure 1. The transfer resulting from the interfacial adhesion is adhesive wear. Material has been lost from one surface and transferred to another. Adhesive wear can occur for a wide variety of materials brought into contact. Abrasive wear, however, is limited to those situations where a very hard material contacts a softer material, or where hard particles are sandwiched between two softer surfaces (e.g., particles of sand in a bearing). Abrasion occurs when a softer surface is cut or micromachined by a harder surface or particle.

Abrasive Wear

One might intuitively anticipate that the resistance of a material to abrasive wear is strongly a function of the hardness of the surface being abraded. The harder the surface, the greater should be the resistance to abrasion; this has been experimentally demonstrated (ref. 7).

In figure 3 resistance to wear is plotted as a function of hardness for the surface of various metals. The data of figure 3 indicate a direct relation between the hardness of the metal being abraded and its abrasive wear resistance.

The abrasion of solid surfaces involves wear to the abrasive as well as wear to the surface being abraded. For example, with such relatively hard abrasive materials as single crystal aluminum oxide (sapphire) and titanium dioxide (rutile), the resistance to wear is very much a function of their orientation. With certain atomic planes contacting steel, wear resistance of the abrasive substance is greater than for other orientations. This resistance is demonstrated in the data of figure 4 for titanium dioxide.

A marked variation in the wear rate of titanium dioxide (fig. 4) occurs with changes in orientation. Between the minimum and maximum it varies by a factor of seven times. Thus, abrasion can result in wear to the abrasive as well as to the surface being abraded; the latter can be minimized by giving consideration to the physical and mechanical properties of the abrasive material.

Corrosive Wear

The surfaces of solids play an extremely important role in corrosive wear. In corrosive wear, material is lost from a solid as a direct result of chemical interactions of the solid surface with the environment. The active environmental constituent can be the lubricant, an additive, or a component of the surrounding atmosphere. The relative motion between solid surfaces in contact aggravates surface attrition by continuously exposing fresh surface for reaction.

Materials which are very effective lubricants under certain conditions can become extremely reactive under another set of conditions. The lubrication of alloys with halogen-containing lubricants is a good example.

In figure 5 for a cobalt alloy lubricated by a chlorinated fluorocarbon, wear at temperatures to 300° C is extremely low. The values in figure 5 are 100 times less than those obtained for the unlubricated surfaces. Above 300° C, however, the rate of wear begins to increase markedly. This increase is due to excessive chemical reactivity of the chlorine of the chlorinated fluorocarbon with the cobalt surface.

Examination of the cobalt alloy surface after sliding revealed copious quantities of cobalt chloride. This particular compound is an extremely good solid-film lubricant and accounts for the low wear to 300° C. Above that temperature cobalt chloride continues to form, but in such large quantities that the cobalt alloys are consumed as a result of excessive surface reactivity. Thus, effective lubrication, with solid films of the type described here, is a matter of controlled corrosion. A reaction product should form to reduce friction and wear, as in figure 5, but that quantity should be limited.

The data of figure 5 also indicate that no correlation between friction and wear can be drawn from information about one or the other. Corrosive wear is an excellent example of this concept. Wear may increase due to the excessive reactivity, but friction may decrease because of the low shear strength of the reaction product formed.

Corrosive wear can be brought about by increasing temperature, as indicated in figure 5. Similar effects can be produced by both increased loading and increased rubbing speeds.

A wide variety of material properties affects wear behavior. As already indicated with reference to figure 4, the crystallographic orientation of materials affects wear. This property holds true not only for the wear of nonmetals, but for metals as well (ref. 8).

Crystal structure is another property of materials which influences wear. Transformation in a metal from one crystal structure to another can result in notable changes in wear. This effect is indicated for tin in figure 6. The wear track width is plotted as a function of temperature, and is relatively constant until the temperature for the transformation of tin from a diamond structure (gray tin) to that of the tetragonal (white tin) is approached. At that point wear begins to increase. The tetragonal tin structure has greater ductility than the diamond form.

A further manifestation of the effect of crystal structure is observed when layer lamellar solids are in rubbing contact with metals. With these solids shear readily occurs along basal planes, and transfer to the metal surface is readily observed; this can be seen in table I. In the table pyrolytic boron nitride transfers to all metals except gold and silver; poor adhesion accounts for this failure.

In practical engineering applications, metals are not used in their elemental form, but rather as alloys. The alloying elements can have varying effects on wear. For example, in figure 7, adding 10-atomic-percent aluminum to copper does not affect its rate of wear. The addition of 10-atomic-percent of alloying element such as silicon, tin, or indium to copper does, however, appreciably reduce wear (fig. 7).

The wear behavior differences for copper alloyed with various elements are maintained even with variations in the concentration of the lubricant additive, as is indicated in figure 8 for the alloys copper-10-atomic-percent aluminum and copper-10-atomic-percent indium. At all concentrations of stearic acid, wear is greater with aluminum alloyed with copper than it is for indium alloyed with copper.

LUBRICATION

Liquids

The purpose of lubrication is to separate surfaces in relative motion by a material which has a low resistance to shear so that the surfaces do not sustain major damage. This low-resistance material can be any of a variety of different species (e.g., adsorbed gases, chemical reactions films, liquids, solid lubricants), some of which have already been discussed.

Depending on the type of intervening film and its thickness, a number of lubrication regimes can be identified. A classical way of depicting some of these regimes is by use of the well-known Stribeck curve (fig. 9). Stribeck (ref. 9) performed comprehensive experiments on journal bearings around 1900. He measured the coefficient of friction as a function of load, speed, and temperature. He had difficulty, however, condensing this data into usable form. Some years later, Hersey (ref. 10) performed similar experiments and devised a plotting format based on a dimensionless parameter. The Stribeck curve, or more appropriately, the Stribeck-Hersey curve, takes the form of the coefficient of friction as a function of the viscosity of the liquid (Z), velocity (N), and load (P) parameter, ZN/P.

At high values of ZN/P which occur at high speeds, low loads, and at high viscosities, the surfaces are completely separated by a thick (>0.25 μm

($>10^{-5}$ in.)) lubricant film. This area is that of hydrodynamic lubrication where friction is determined by the rheology of the lubricant. For nonconformal concentrated contacts where loads are high enough to cause elastic deformation of the surfaces and pressure-viscosity effects on the lubricant, another fluid film regime, elastohydrodynamic lubrication (EHL), can be identified. In this regime film thickness (h) may range from 0.025 to 2.5 μm (10^{-6} to 10^{-4} in.).

As film thickness becomes progressively thinner, surface interactions start taking place. This regime of increasing friction, which combines asperity interactions and fluid film effects, is referred to as the mixed-lubrication regime.

Finally, at low values of the ZN/P parameter, one enters the realm of boundary lubrication. This regime is characterized by the following:

1. This regime is highly complex, involving metallurgy, surface topography, physical and chemical adsorption, corrosion, catalysis, and reaction kinetics.
2. The most important aspect of this regime is the formation of protective surface films to minimize wear and surface damage.
3. The formation of these films is governed by the chemistry of the film-forming agent, as well as the surface of the solid and other environmental factors.
4. The effectiveness of these films in minimizing wear is determined by their physical properties, which include shear strength, thickness, surface adhesion, film cohesion, melting point or decomposition temperature, and solubility.

Besides the Stribeck-Hersey curve (fig. 9) already described, an idealized plot of wear rate as a function of relative load can also delineate the various lubrication regimes and some wear transitions (fig. 10, ref. 11).

Region OA of figure 10 encompasses the regimes of hydrodynamic and EHL, the latter as point A is approached. Since no surface interactions occur in this region except for startup or shutdown, little or no wear occurs. (This excludes rolling-element fatigue, which can occur without surface interactions.) Region AX is the mixed-lubrication regime where surface interactions begin to occur at A and become more prevalent as point X is approached. Wear is low because fluid film effects still exist.

Next there is region XY in figure 11, which is the region of boundary lubrication. The degree of metal-to-metal contact and the wear rate increase as the load increases. Wear is mild and tends to be corrosive to the left of B and adhesive to the right of B. The location of B is quite variable and depends on the corrosivity of the lubricant formulation. For a noncorrosive lubricant, adhesive wear can occur at X. On the other hand, a corrosive additive can extend the boundary regime to Z^1 before boundary film failure occurs. Region YZ is the regime of severe wear where severe adhesion and scoring occur. Machinery cannot operate successfully in this region, and, therefore, the location of this transition point is quite important. At point Z total surface failure occurs, followed by seizure.

In the boundary lubrication regime many properties of the liquid lubricant become important. These include shear strength, film thickness, melting point, and chemical reactivity with the surface. Operating variables which will affect lubricant film performance include load, speed, temperature, and atmosphere, as already discussed. Additives present in the lubricant to serve specific functions will also affect behavior. These additives include anti-wear, anti-foam, antioxidants, viscosity improvers, and others. A good review of boundary lubrication can be found in reference 12.

Solids

At temperatures below which liquid lubricants become solid, and above which they either thermally or oxidatively decompose, solids are used. The solids include inorganic compounds, polymers, and low-shear-strength metals. A review of the subject can be found in reference 13.

Of solid lubricants, those most widely used and studied are the layer-lattice inorganic compounds. These materials have a hexagonally layered crystal structure. Their shear properties are anisotropic with preferred planes for easy shear parallel to the basal planes of the crystallites. In some of the compounds such as molybdenum disulfide (MoS_2), a low shear strength is intrinsic to the pure material, while in others, notably graphite, the presence of absorbed gases or intercalated "impurities" between the basal planes appears to be necessary to develop desirable friction characteristics. The most common representatives of this class of lubricants are graphite and the dichalcogenides, notably MoS_2 and WS_2.

The maximum useful temperatures for solid lubricants depend strongly upon the composition of the ambient atmosphere, the required life at temperature, factors such as oxygen availability at the lubricated surface (is the coating openly exposed to the atmosphere, or shielded within conforming bearing surfaces?), air flow rates, lubricant particle size, and the influence of adjuvants and binders.

Dichalcogenides

The maximim temperature for lubrication with MoS_2 in an air atmosphere is limited by oxidation to about 400° C under favorable conditions. Some oxidation kinetics data for loosely compacted MoS_2 powders of 1μ average particle size are given in figure 11(a) from reference 13. At a modest airflow rate over the compact, 50 percent of the MoS_2 was oxidized to molybdic oxide (MoO_3) in 1 hour at 400° C. At a six-times-higher airflow rate, the temperature for an oxidation half-life of 1 hour was reduced to 300° C. Figure 1(b) compares the oxidation kinetics of MoS_2 and WS_2 at the lower airflow rate. The curves for MoS_2 and WS_2 intersect, with MoS_2 oxidizing more rapidly above about 340° C.

Friction experiments were conducted with a pin-on-disk apparatus using a hemispherically tipped pin in sliding contact with the flat surface of a rotating disk. A comparison of the oxidation data of figure 11 and the friction data of figure 12(b) (ref. 13) shows that the loss of lubricating ability of MoS_2 and WS_2 in air coincides with the temperatures at which rapid conversion to the oxides occurs.

Figure 12(a) also shows that both compounds lubricate to much higher temperatures in a nonreactive argon atmosphere. In an inert gas or vacuum, the maximum useful temperature is a function of the thermal dissociation rates, rather than the oxidation rates of the lubricants. Thermal dissociation rates and the friction coefficients of molybdenum and tungsten disulfides, diselenides, and ditellurides in vacuum have been systematically studied (ref. 14). The major results, summarized in table II, indicate that the disulfides are the most stable, the diselenides are intermediate, and the ditellurides are the least stable. However, thin, burnished films of the diselenides with their higher densities evaporate more slowly than the disulfides. Apparently, for the very thin, burnished films, the evaporation rates were the controlling factor in determining the maximum temperature for effective lubrication. The limiting temperatures for a significant wear life of these coatings ranged from 600° to 700° C.

Vacuum-deposited coatings are increasingly being used in tribological applications; these fall into two main composition categories: soft-lubricating coatings, and very hard, wear-resistant coatings. The methods of application are also in two principal categories: sputtering and ion-plating. These techniques have been rapidly adopted by industry especially for aerospace applications. A very large variety of these vacuum-deposited coatings is becoming available for lubrication application.

The most common vacuum-deposited tribological coatings are the sputtered dichalogenides, especially MoS_2 and ion-plated soft metals such as gold. These coatings are often very thin, on the order of 2000 to 5000 Å in thickness. Compounds such as MoS_2 are usually applied by sputtering, because with proper procedures, pure, essentially stoichiometric, compounds can be deposited. In contrast, ion-plating tends to dissociate chemical compounds. However, ion-plating is an appropriate technique for the deposition of elemental metals because (1) dissociation is obviously not a problem; (2) high ion-impact energies can be used to enhance adhesion; (3) excellent throwing power is achieved when coating parts with complex shapes; and (4) rapid deposition rates can be achieved.

Sputtered hard coats are used primarily for wear control. The oxidation temperatures and hardness of some important carbides and nitrides are presented in table III. Coatings of all of the compounds listed are hard enough to be expected to have good wear resistance, assuming adequate bond to the substrate can be achieved. However, a considerable variation in oxidation resistance exists. Chromium carbide, boron carbide, silicon nitride, and silicon carbide are oxidatively stable to at least 1000° C, while tungsten and titanium carbides oxidize during long-duration exposure in air at temperatures above about 540° C. Tungsten carbide tends to oxidize more rapidly than titanium carbide because its oxides are volatile at high temperature, and their sublimation tends to accelerate the oxidation.

Titanium nitride is another promising hard-coat material, but it too will convert to the oxide above 550° C. However, some TiC- and TiN-sputtered coatings have shown surprisingly good resistance to oxide conversion at higher temperatures than those listed in table III. Oxidation occurs, but the rate is very low, probably because of high coating density and the passivating nature of the initially formed oxide films, which protect the coating against catastrophic oxidation.

CONCLUDING REMARKS

The adhesion, friction, and wear behavior of materials in solid-state contact are strongly dependent upon material properties and environmental factors. Adsorbed surface films and oxides on metals markedly influence tribological behavior.

Relatively subtle differences in the molecular structure of hydrocarbons can profoundly influence adhesion and friction. With liquid lubrication, distinct regimes of lubrication are identified. Both the physical properties of the lubricant and operating variables affect lubricant performance.

With solids as high-temperature lubricants, both thermal and oxidative stability are important, as well as the lubricating properties of the solids over a broad temperature range. Techniques such as ion-plating and sputtering are being increasingly used for the application of solid film lubricants.

REFERENCES

1. Buckley, D. H.; and Johnson, R. L.: Friction and Wear of Hexagonal Metals and Alloys as Related to Crystal Structure and Lattice Parameters in Vacuum. ASLE Trans., vol. 9, no. 2, 1966, pp. 121-135.
2. Tabor, O.: Junction Growth in Metallic Friction: The Role of Combined Stresses and Surface Contamination. Proc. Roy. Soc. (London), A, vol. 251, 1959.
3. Buckley, D. H.: Definition and Effect of Chemical Properties of Surfaces in Friction, Wear and Lubrication. NASA TM-73806, 1978.

4. Wheeler, D. R.: Effect of Adsorbed Chlorine and Oxygen on the Shear Strength of Iron and Copper Junctions. J. Appl. Phys., vol. 47, no. 3, Mar. 1976, pp. 1123-1130.
5. Buckley, D. H.: Friction, Wear and Lubricating in Vacuum. NASA SP-277, 1971.
6. Buckley, D. H.: Adsorption of Ethylene Oxide and Vinyl Chloride on an Iron (011) Surface and Effect of these films on Adhesion. NASA TN D-5999, 1970.
7. Khruschov, M. M.: Resistance of Metals to Wear by Abrasion, as Related to Hardness. Proceedings of the Conference on Lubrication and Wear. Institution of Mechanical Engineers, London, 1957, pp. 655-659.
8. Buckley, D. H.; and Johnson, R. L.: Friction and Wear of Hexagonal Metals and Alloys as Related to Crystal Structure and Lattice Parameters in Vacuum. ASLE Trans., vol. 9, 1966, pp. 121-135.
9. Stribeck, R.: Characteristics of Plain and Roller Bearings. Z.V.D.I., vol. 46 (1902).
10. Hersey, M. D.: The Laws of Lubrication of Horizontal Journal Bearings. J. Wash. Acad. Sci., vol. 4, 1914, pp. 542-52.
11. Beerbower, A.: Boundary Lubrication. Scientific and Technical Applications Forecasts, Department of the Army, DAHC-19-69-C-0033, 1972.
12. Jones, W. R., Jr.: Boundary Lubrication Revisited. NASA TM-82858, 1982.
13. Sliney, H. E.: Solid Lubricant Materials for High Temperature - A Review. Dry Bearings, Tribology International Journal, 1982.
14. Brainard, W. A.: The Thermal Stability and Friction of the Disulfides and Ditellurides of Molybdenum and Tungsten in Vacuum. (10^{-9} to 10^{-6} torr). NASA TN D-5141, 1969.

TABLE I. - TRANSFER OF MATERIAL FOR VARIOUS METALS IN SLIDING CONTACT WITH PYROLYTIC BORON NITRIDE

Metal	Metal to boron nitride	Boron nitride to metal
Aluminum	No	---
Titanium	No	Yes
Iron	No	Yes
Platinum	No	Yes
Copper	No	Yes
Gold	No	No
Silver	No	No
Tantalum	--	Yes
Niobium	--	Yes
Zirconium	--	Yes
Vanadium	--	Yes
Rhodium	--	Yes

TABLE II. - RESULTS OF THERMAL STABILITY AND FRICTIONAL EXPERIMENTS IN VACUUM OF 10^{-9} to 10^{-6} TORR

Compound	Probable onset of thermal dissociation as detected by TGA °C	Dissociation products first detected by mass spectrometry, °C	Maximum temperature at which burnished films provided effective lubrication, °C
MoS_2	930	1090	650
WS_2	870	1040	730
$MoSe_2$	760	980	760
WSe_2	700	930	760
$MoTe_2$	700	700	540
WTe_2	700	700	(a)

[a] Friction coefficient greater than 0.2 at all temperatures.

TABLE III. - BULK PROPERTIES OF SOME HARD-COAT MATERIALS[a]

Material	Microhardness, kg/mm^2	Oxidation temperature[b], °C
B_4C	4200	1090
TiC	3200	540
SiC	2900	1650
Cr_3C4	2650	1370
WC	2050	540
Si_3N4	2000	1400
TiN	1950	540
Cr_203	[c]1800	----

[a] Data from: Engineering Properties of Ceramic Materials, Battelle Memorial Institute, Published by American Ceramic Society, Columbus, Ohio, 1966.

[b] Temperature for appreciable detrimental oxidation passivating oxide films form at lower temperatures.

[c] Estimated conversion from published Moh hardness of 9.

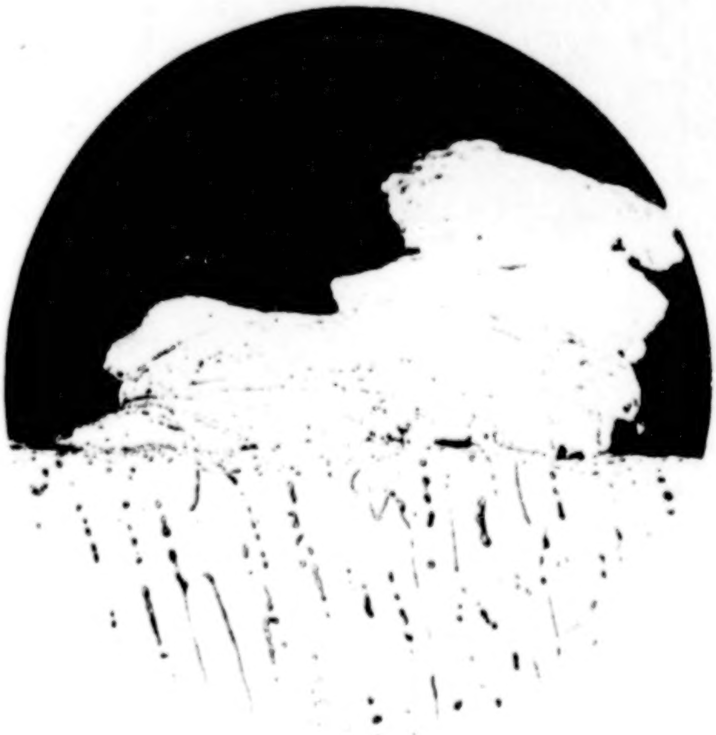

Figure 1.- Severe surface welding resulting from unlubricated sliding (2% Al-Ni alloy from 10^{-9} mm Hg vacuum experiment).

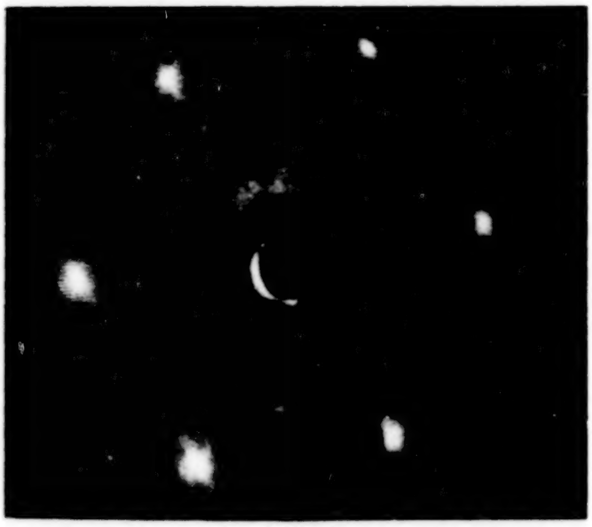

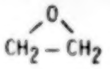

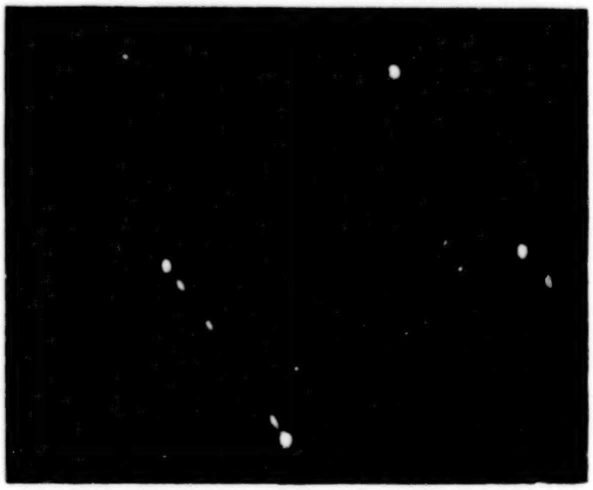

$CH_2=CHCl$

Figure 2.- LEED patterns obtained with two polymer forming hydrocarbons on iron (001) surface (100 L exp.).

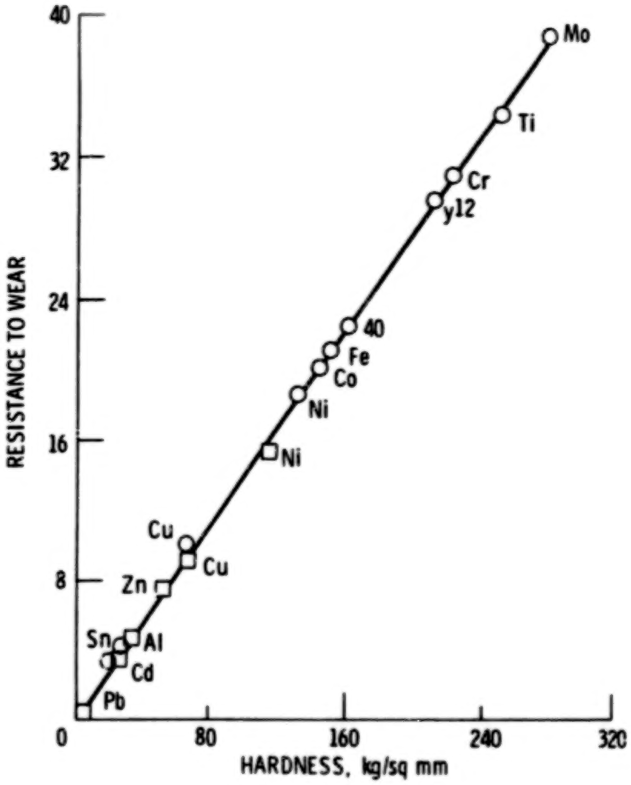

Figure 3.- Resistance to wear as a function of hardness. (See ref. 7.)

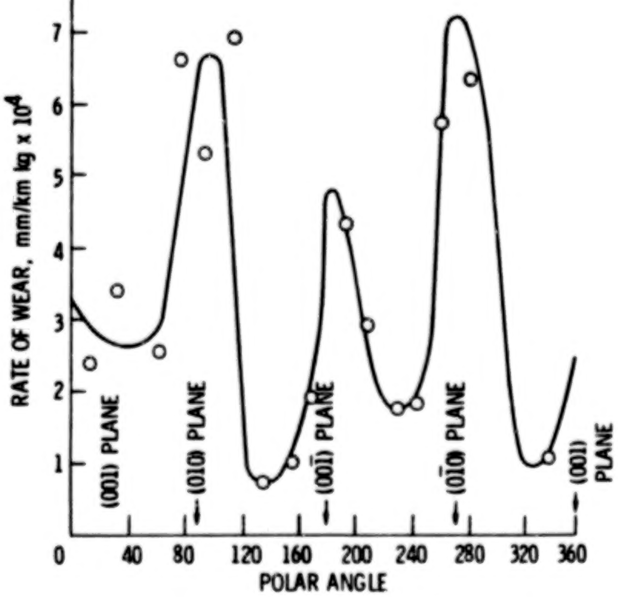

Figure 4.- Rate of wear of a rutile single-crystal sphere on a great circle in the plane of the a- and c-axes. C-axis is normal to plane of sliding at 0° and 180°. Slide direction is in plane of great circle.

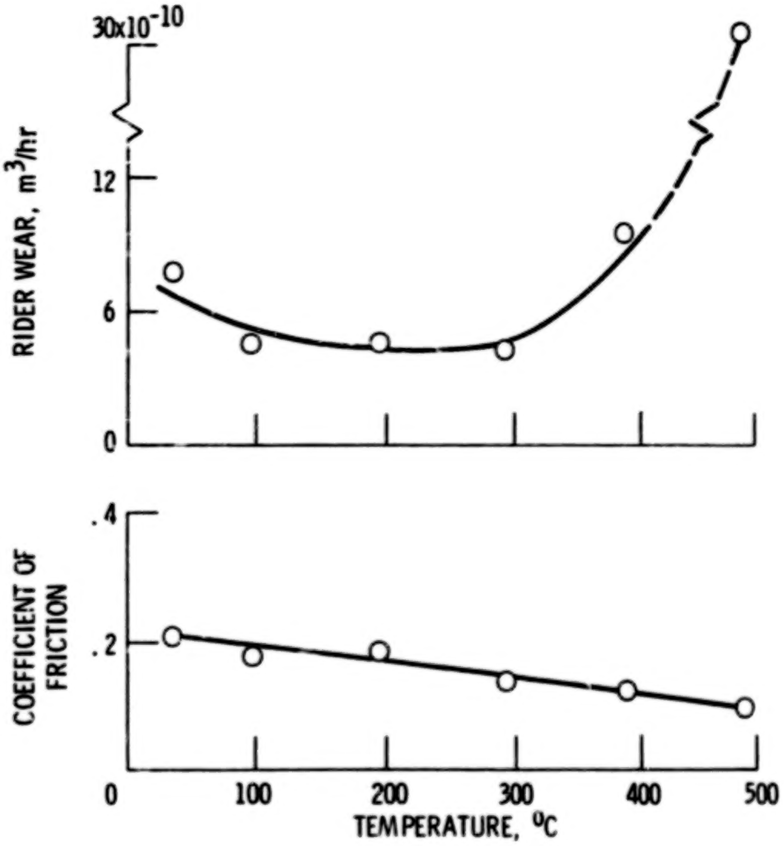

Figure 5.- Friction and wear of cobalt alloy sliding on itself at various temperatures and lubricated with a chlorinated fluorocarbon.

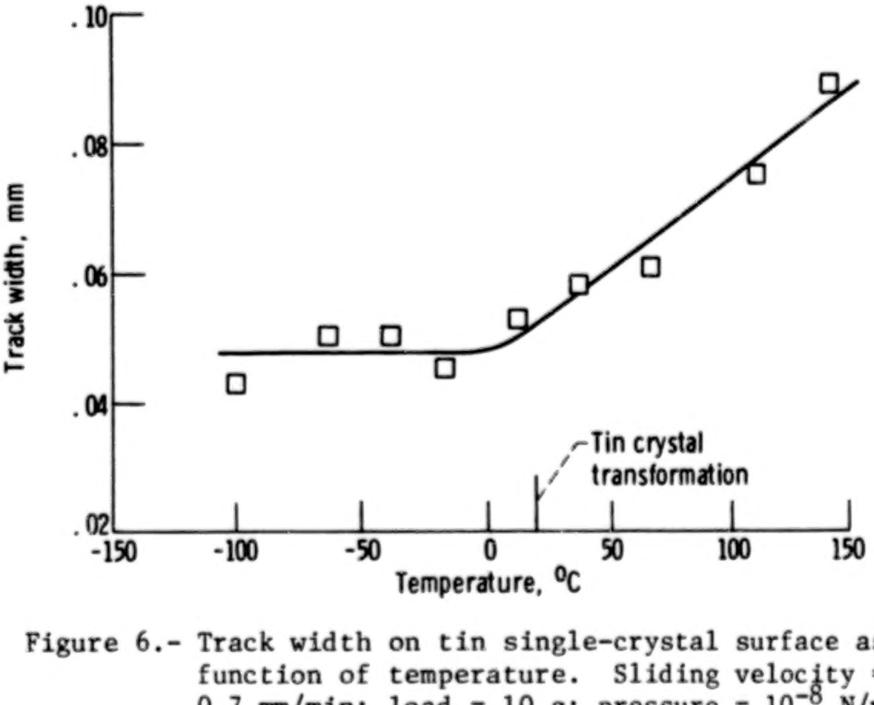

Figure 6.- Track width on tin single-crystal surface as function of temperature. Sliding velocity = 0.7 mm/min; load = 10 g; pressure = 10^{-8} N/m^2 (10^{-8} N/m^2); rider = iron (110); single pass.

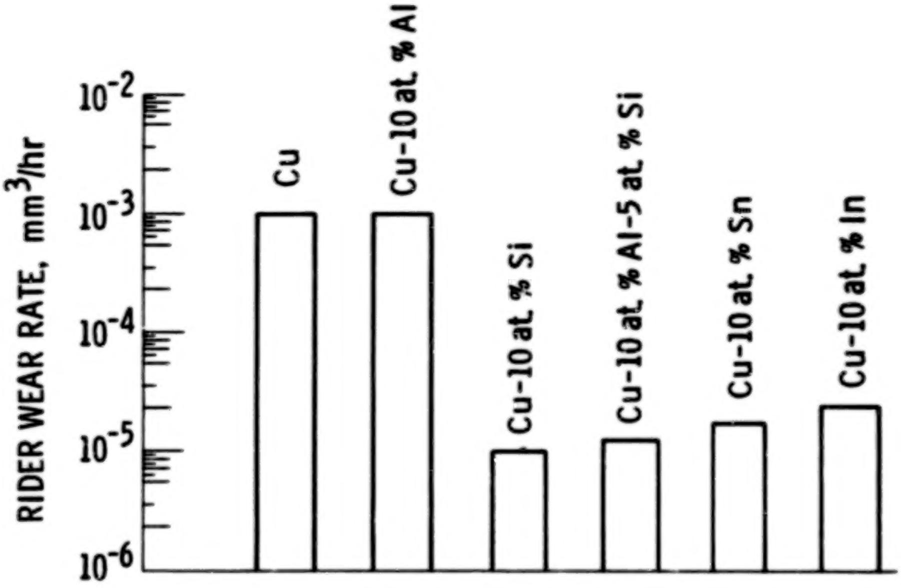

Figure 7.- Rider wear for various copper alloys sliding on themselves in hexadecane containing 0.1 volume percent stearic acid. Load = 250 g; sliding velocity = 300 cm/min; temperature = 25°C.

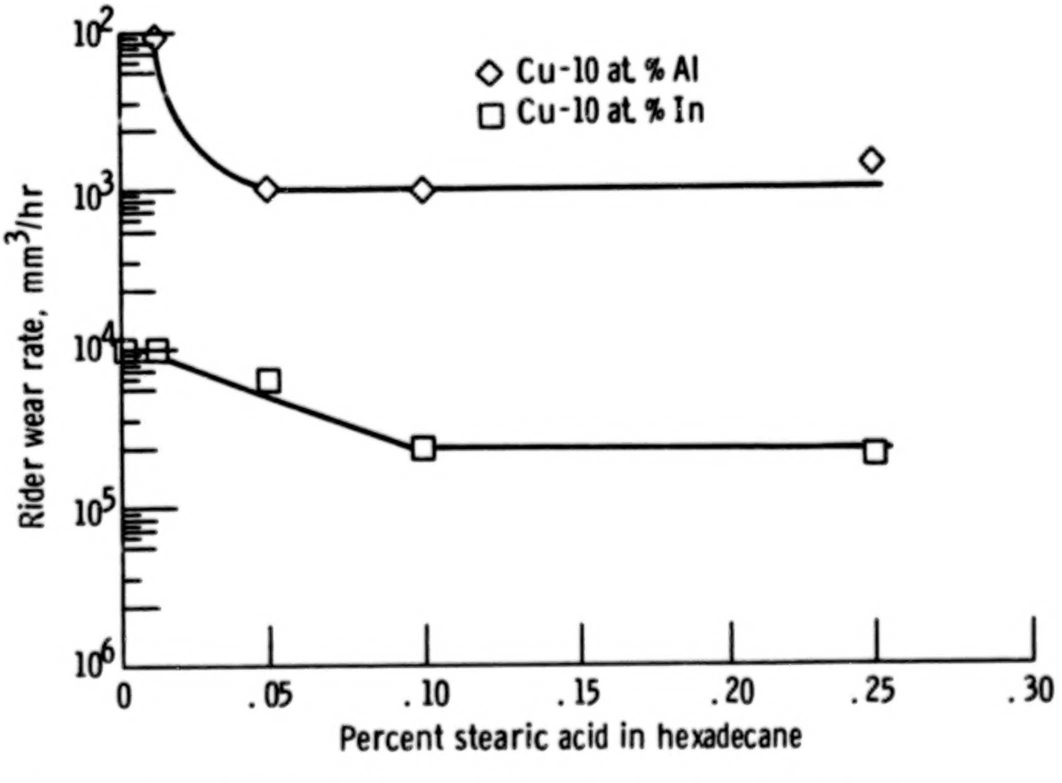

Figure 8.- Rider wear rate for two copper alloys sliding on themselves with various concentrations of stearic acid in hexadecane as lubricant. Load = 500 g, sliding velocity = 300 cm/min; temperature = 25°C.

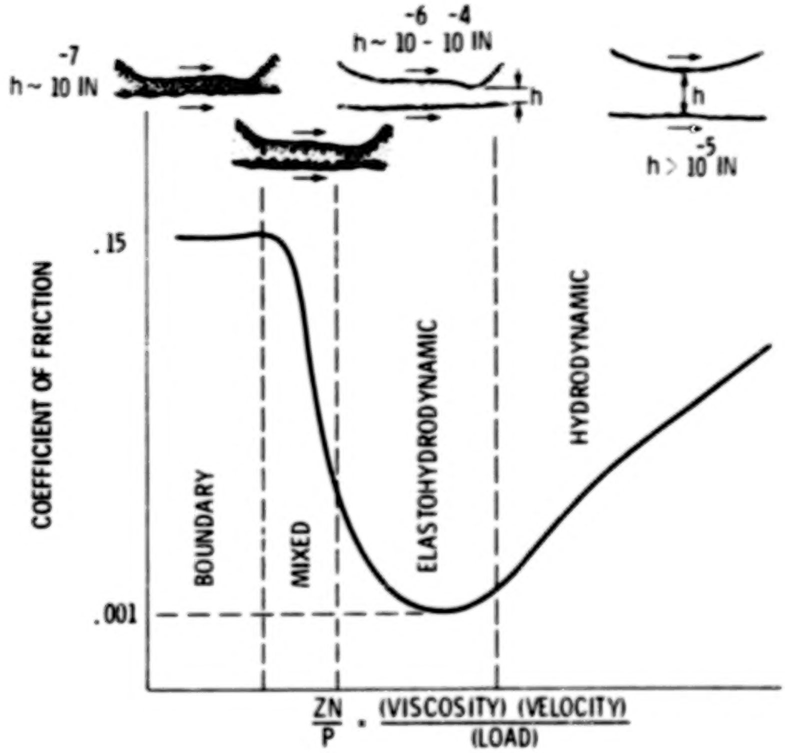

Figure 9.- Coefficient of friction as a function of speed-velocity-load parameter (Stribeck-Hersey curve). (See ref. 9.)

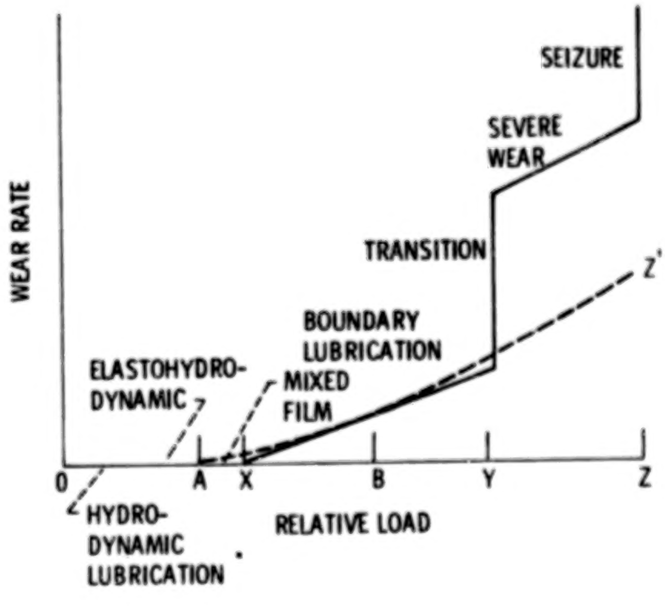

Figure 10.- Wear rate as a function of relative load depicting the various regimes of lubrication (ref. 11).

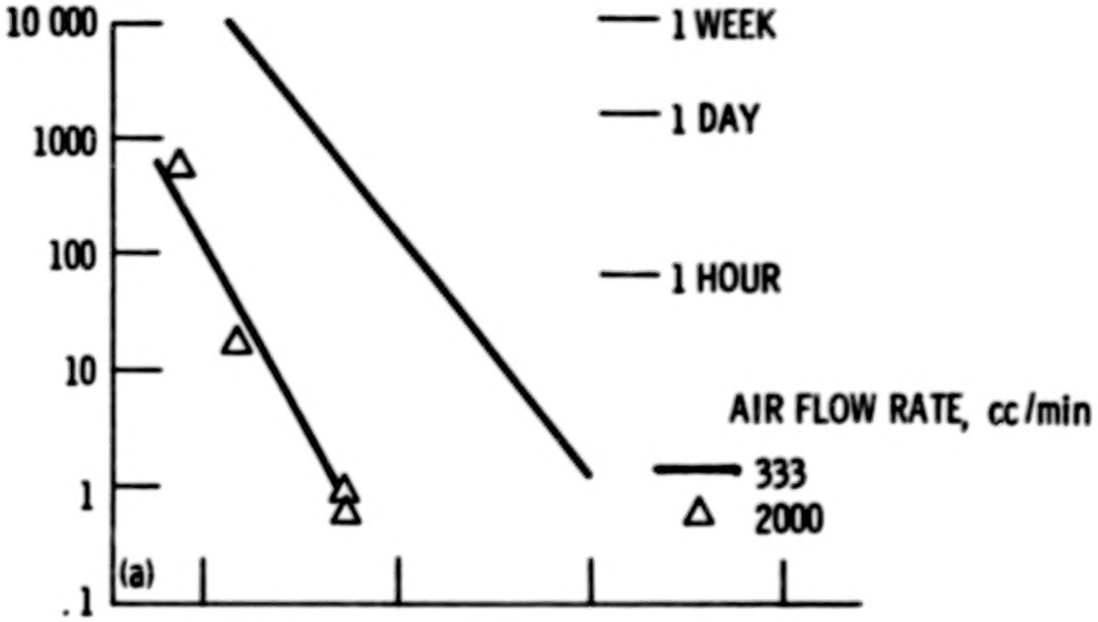

(a) Oxidation characteristics of MoS_2 at two air flow rates.

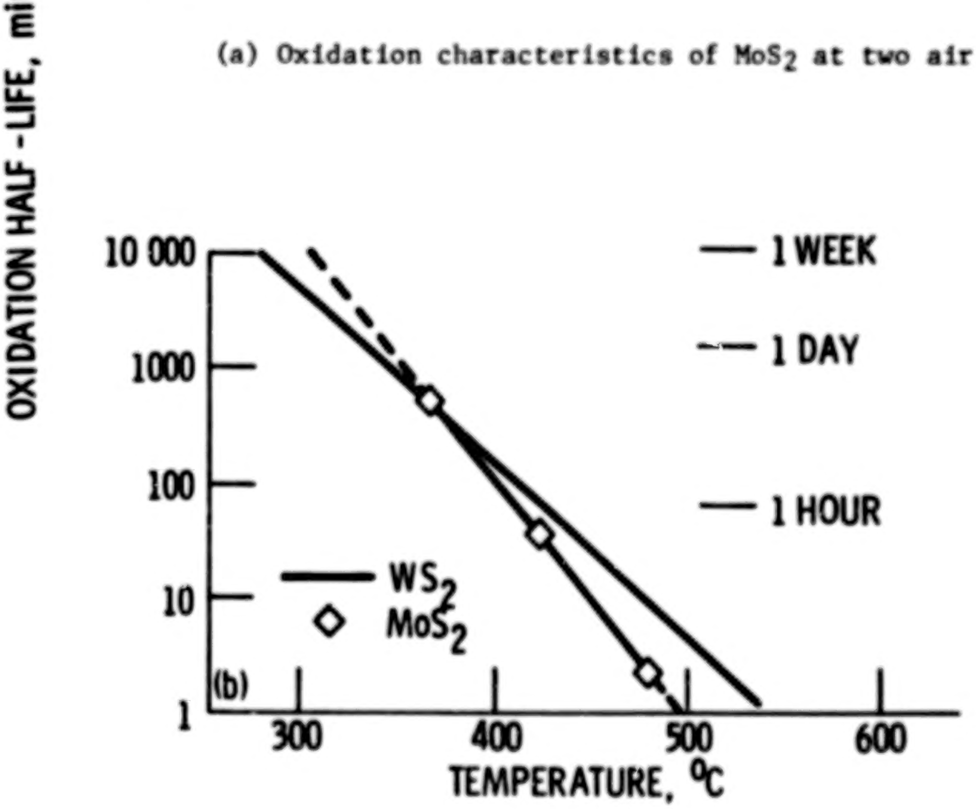

(b) Comparative oxidation of WS_2 and MoS_2 air flow rate, 1/3 L/min.

Figure 11.- Oxidation kinetics of MoS_2 and WS_2. Average particle size = 1 μm; compact density = 50%.

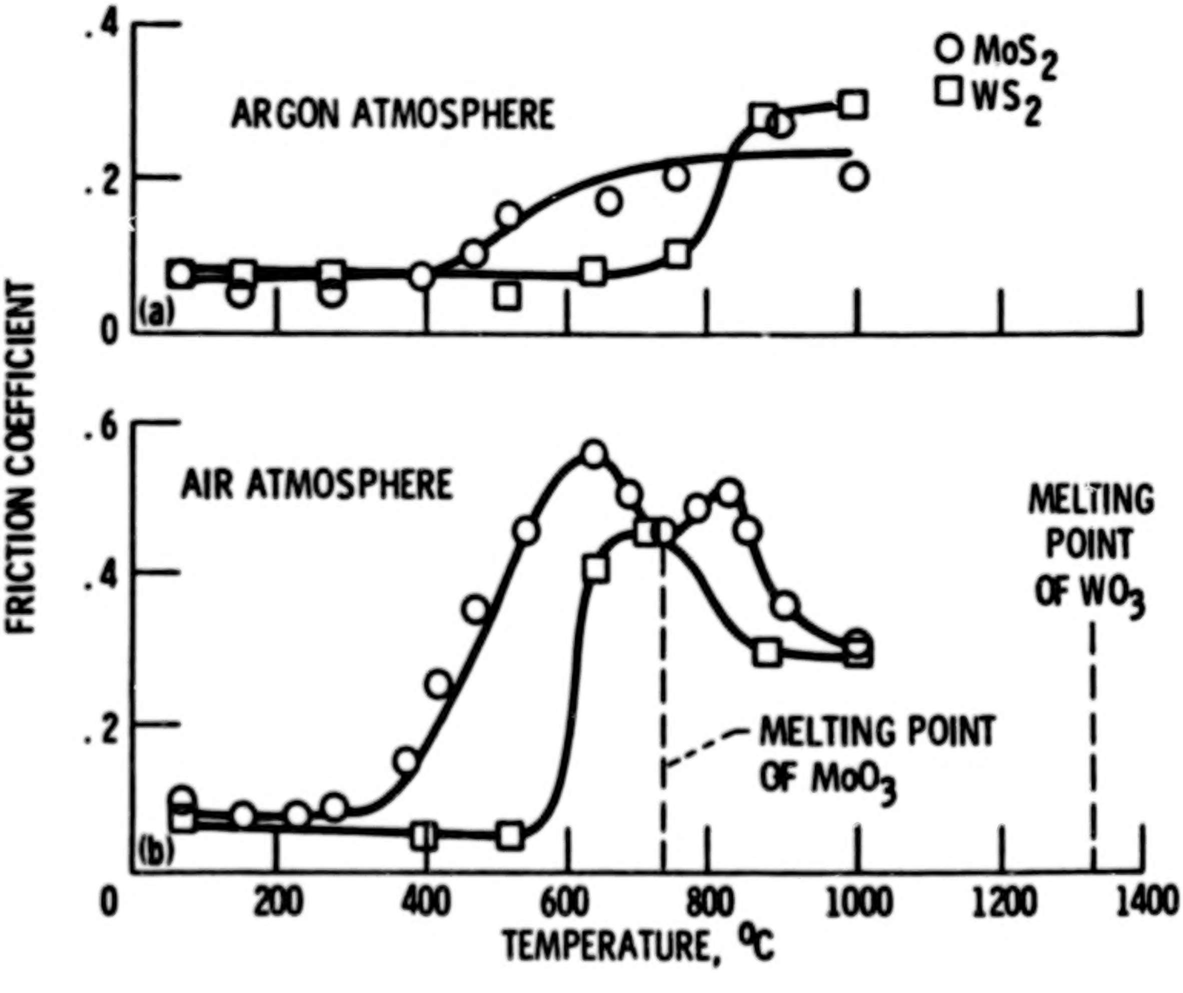

Figure 12.- Friction characteristics of MoS_2 and WS_2 in argon and in air.

BEST DOCUMENT AVAILABLE

BLANK PAGE

FUNDAMENTALS OF ULTRASONIC NDE FOR MICROSTRUCTURE/MATERIAL PROPERTY INTERRELATIONS

A. Vary
NASA Lewis Research Center
Cleveland, Ohio

INTRODUCTION - PRELIMINARY CONSIDERATIONS

In its most general context, nondestructive evaluation (NDE) is a branch of materials science that is concerned with all aspects of the uniformity, quality, and serviceability of materials and structures. Therefore, NDE should not be defined solely by the current emphasis on the detection of overt flaws. On the broadest scale, NDE addresses the integrated effect of defects and the material environment in which the defects reside. This calls for NDE technology that can characterize inherent material properties as well as individual defects. In this case the emphasis is on the evaluation of microstructural and morphological factors that govern mechanical strength/toughness, dynamic performance, and residual life (ref. 1).

There are many NDE techniques that can to varying degrees characterize material properties (ref. 2). Herein, the focus is on ultrasonic techniques because of their wide potential for materials characterization. All the material properties and conditions listed in figure 1, for example, are amenable to ultrasonic evaluation (ref. 3). In this paper some fundamental aspects of ultrasonic NDE for material properties and microstructure assessment are given. Ultrasonic wave interaction concepts, some recent findings, and practical ramifications are illustrated. The concepts are discussed in nonmathematical, narrative form. Additional information can be found in the references cited herein.

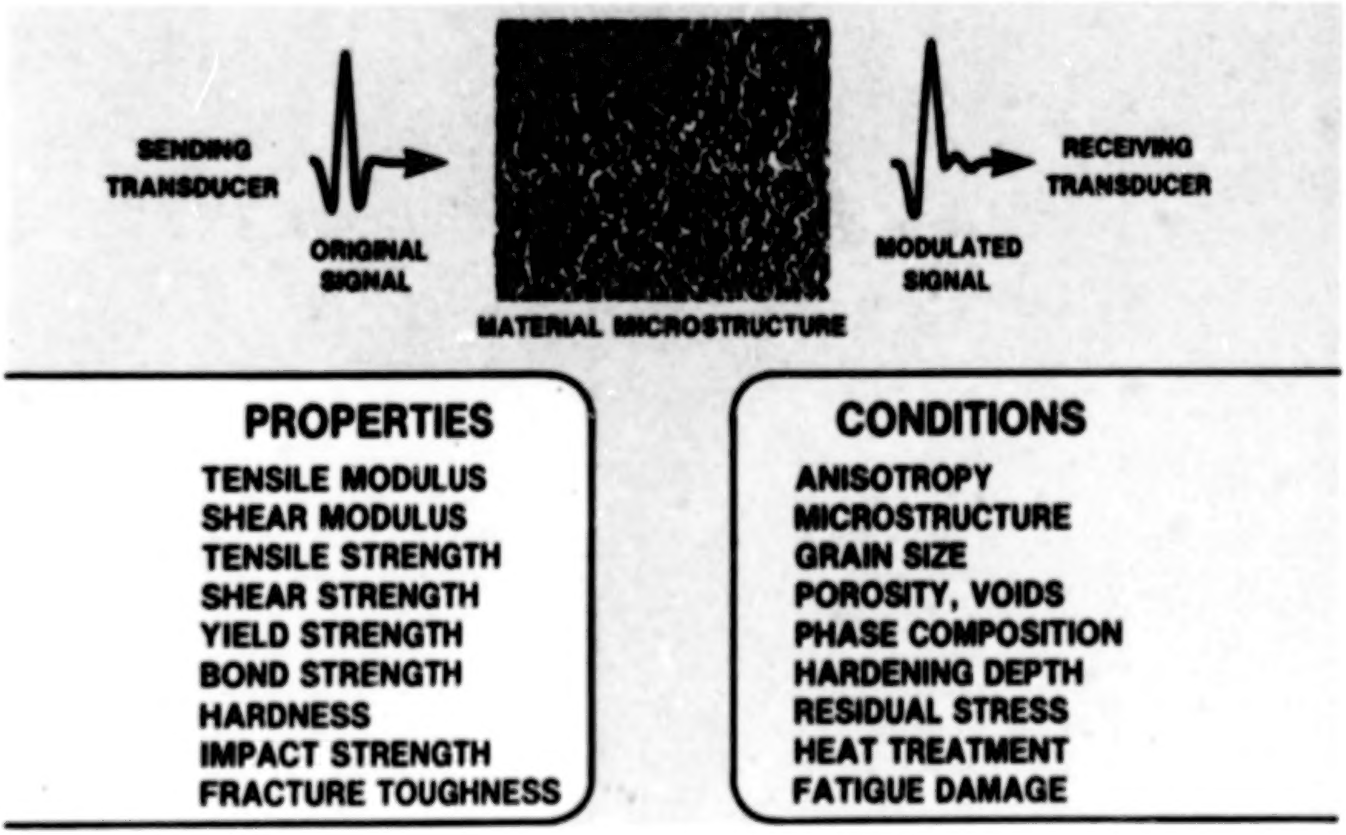
SENDING TRANSDUCER
ORIGINAL SIGNAL
MATERIAL MICROSTRUCTURE
MODULATED SIGNAL
RECEIVING TRANSDUCER
PROPERTIES
TENSILE MODULUS
SHEAR MODULUS
TENSILE STRENGTH
SHEAR STRENGTH
YIELD STRENGTH
BOND STRENGTH
HARDNESS
IMPACT STRENGTH
FRACTURE TOUGHNESS
CONDITIONS
ANISOTROPY
MICROSTRUCTURE
GRAIN SIZE
POROSITY, VOIDS
PHASE COMPOSITION
HARDENING DEPTH
RESIDUAL STRESS
HEAT TREATMENT
FATIGUE DAMAGE

Figure 1

ULTRASONIC INTERACTIONS WITH MICROSTRUCTURE

The basis for ultrasonic materials characterization lies in the analysis of wave interactions with microstructure. Material microstructure and grain morphology affect ultrasonic wave velocity and attenuation. These same factors also affect material properties and dynamic performance. For example, velocity measurements correlate with elastic moduli and residual stresses. Attenuation measurements correlate with mechanical properties such as strength, hardness, and toughness. Both velocity and attenuation measurements correlate with microstructural factors that influence or govern material properties and performance. A basis for these correlations is suggested in figure 2. Spontaneous stress waves that arise during dislocation movements, deformation, cracking, and fracture failure are ultrasonic in nature. It is reasonable, therefore, to expect that by introducing benign ultrasonic probe waves one can interrogate the microstructure and infer its effect on the stress waves that interact with it during deformation, failure, etc. An approach to ultrasonic materials characterization consists of treating the microstructure as having a mathematically definable modulation transfer function that governs stress wave propagation. The analysis then proceeds by comparing output versus input signals as indicated in figure 1. An especially useful method involves frequency domain signal deconvolution procedures to determine the ultrasonic attenuation characteristics of a sample of material (ref. 4).

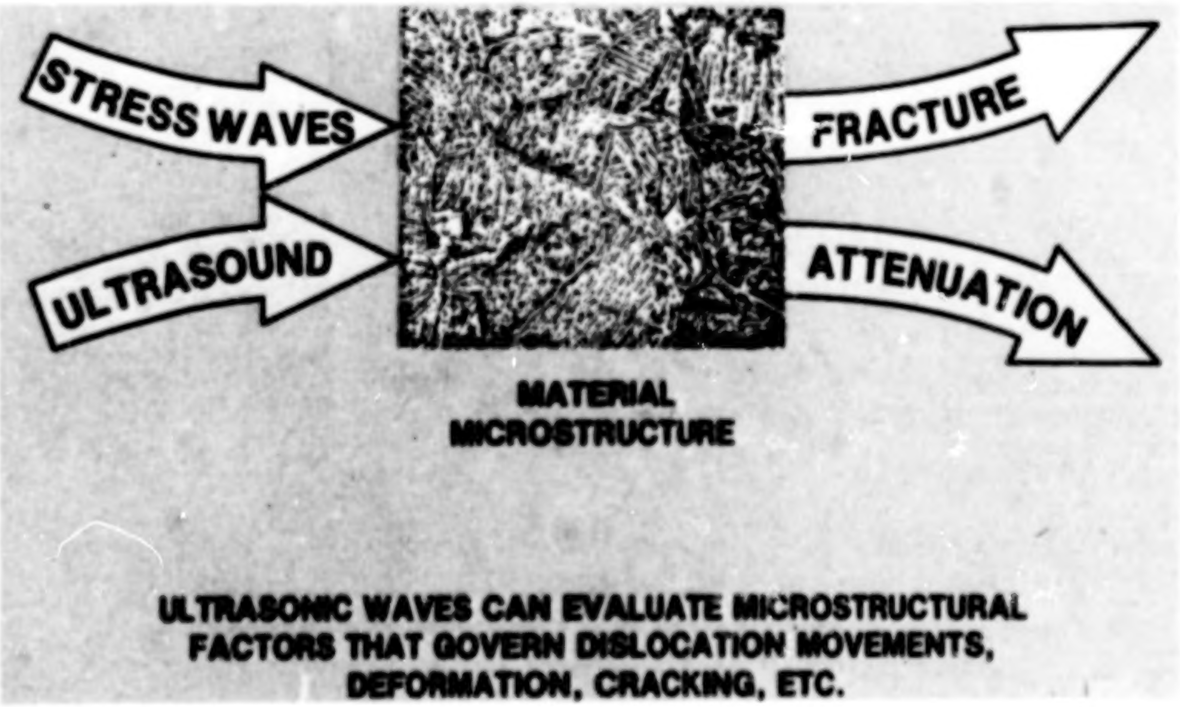

ULTRASONIC WAVES CAN EVALUATE MICROSTRUCTURAL FACTORS THAT GOVERN DISLOCATION MOVEMENTS, DEFORMATION, CRACKING, ETC.

Figure 2

ULTRASONIC VERIFICATION OF MATERIAL PROPERTIES

Tensile strength, yield strength, and fracture toughness are examples of extrinsic material properties that depend on microstructure and grain morphology in polycrystalline aggregates that constitute typical structural materials. Herein, we will concentrate on illustrative examples of ultrasonic measurement of fracture toughness in metals. Increased toughness in structural materials means increased resistance to catastrophic fracture failure due to sudden crack growth. Tougher materials tolerate larger naturally occurring or fatigue-induced cracks. One goal of NDE is to detect and characterize cracks that are greater than a critical size and likely to cause catastrophic fracture failure. The criterion for what constitutes a critical crack size presupposes that a material's fracture toughness is known. The usual way to determine fracture toughness is to conduct destructive tests on samples of material. Representative toughness indexes, such as the plane strain fracture toughness or drop weight tear test values, are used to calculate critical crack size (ref. 5). But this does not satisfy the need for verification of the actual toughness of the material in which the cracks reside. This need can only be met by NDE techniques that characterize material properties. As indicated in figure 3, ultrasonic attenuation measurements can be used to verify fracture toughness once calibration curves are established for a given material.

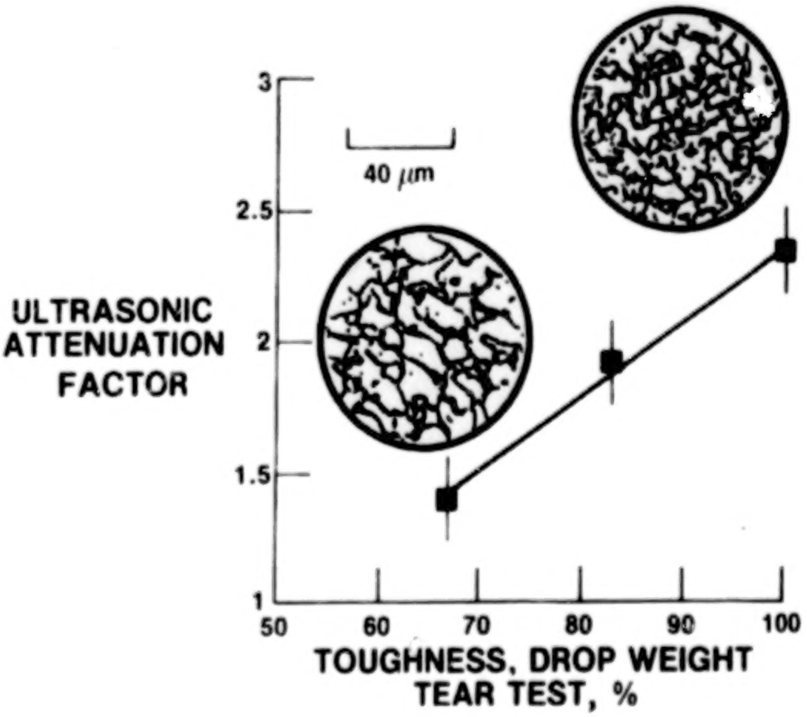

A CORRELATION BETWEEN AN ULTRASONIC FACTOR AND TOUGHNESS IS SHOWN.

EACH DATA POINT REPRESENTS A DIFFERENT HEAT OF STEEL.

THE BARS INDICATE THE SCATTER ASSOCIATED WITH THE ULTRASONIC MEASUREMENT.

PHOTOMICROGRAPHS SHOW THAT GRAIN SIZE DECREASES WITH INCREASED TOUGHNESS AND ATTENUATION.

Figure 3

ANALYTICAL BASIS FOR ULTRASONIC PREDICTION OF TOUGHNESS

Although significant empirical correlations of ultrasonic attenuation and velocity with material mechanical properties exist, the theoretical bases for predicting extrinsic properties such as toughness are only now being investigated. A recent development initiated at the NASA Lewis Research Center invokes a stress wave interaction (SWI) model and the interrelation of ultrasonic attenuation and microstructure. The SWI model postulates that spontaneous stress waves generated during crack nucleation and onset of rapid unstable crack growth strongly interact with specific microstructural features. The SWI model has been successfully used to derive equations that predict experimentally observed correlations (e.g., fig. 4). For polycrystalline aggregates the predicted relation consists of a power function between the "characteristic length" factor and ultrasonic attenuation factor. The characteristic length factor consists of the ratio of plane strain fracture toughness and yield strength. The square of this ratio is proportional to the plastic or "process" zone size at the tip of a crack verging toward instability. Tougher materials exhibit larger process zones and, hence, a greater degree of crack blunting. SWI theory and empirical data (as in fig. 4) agree in identifying the ultrasonic attenuation properties of material microstructure as significant in determining the process zone size and, concomitantly, the material toughness (ref. 6).

CORRELATION OF ULTRASONIC AND FRACTURE TOUGHNESS FACTORS FOR THREE METALS

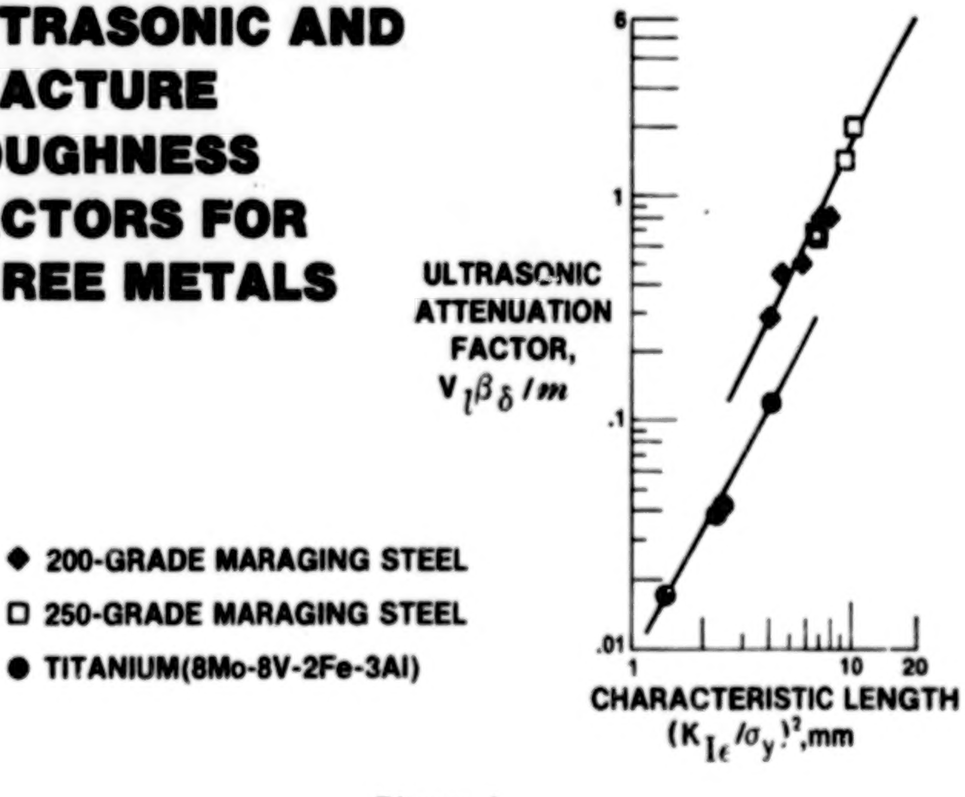

Figure 4

ELEMENTS IN ULTRASONIC PREDICTION OF MATERIAL TOUGHNESS

A holistic approach to predicting toughness, ultimate strength, and similar properties involves three basic elements: a stress wave interaction (SWI) model, a microcrack nucleation mechanics (MNM) model, and a microstructure transfer function (MTF) model (see fig. 5). The SWI model invokes the concept that energy absorption sites are activated by spontaneous stress waves emitted at the onset of catastrophic crack growth. These sites are associated with distributed microstructural features that resonantly absorb stress wave energy. The model assumes that there is a threshold wavelength commensurate with the mean dimension of critically interacting microstructural features, e.g., second phase particles, precipitates, etc. The mode of stress wave interaction with critical microfracture sites is described by an appropriate microcrack nucleation mechanics (MNM) model. The MNM model delineates the specific ultrasonic energy absorption mechanism peculiar to a given material's microstructure, grain morphology, boundary spacing, etc. The SWI and MNM models are supplemented by the microstructure transfer function (MTF) model which is required for characterizing the material microstructure. The MTF model is the basis for nondestructive characterization of ultrasonic propagation properties of the material. Appropriate combinations of the three models can be used to derive analytical expressions that predict correlations between ultrasonic and material property factors, as indicated in figure 5.

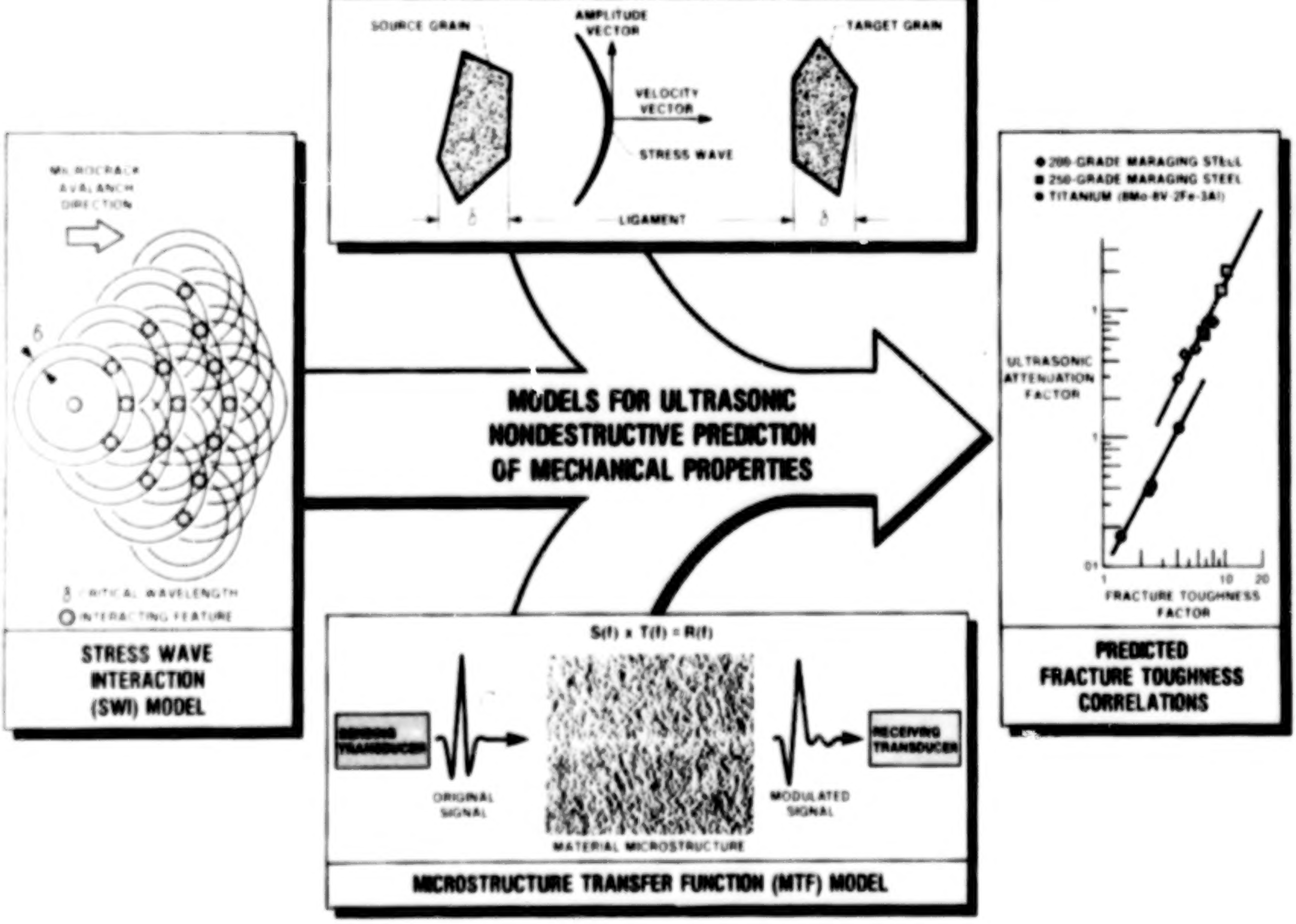
MICROCRACK NUCLEATION MECHANICS (MNM) MODEL
SOURCE GRAIN
AMPLITUDE VECTOR
VELOCITY VECTOR
STRESS WAVE
TARGET GRAIN
δ
LIGAMENT
δ
MICROCRACK AVALANCH DIRECTION
δ
δ CRITICAL WAVELENGTH
INTERACTING FEATURE
STRESS WAVE INTERACTION (SWI) MODEL
MODELS FOR ULTRASONIC NONDESTRUCTIVE PREDICTION OF MECHANICAL PROPERTIES
200-GRADE MARAGING STEEL
250-GRADE MARAGING STEEL
TITANIUM (8Mo-8V-2Fe-3Al)
ULTRASONIC ATTENUATION FACTOR
1
1
01
1
10
20
FRACTURE TOUGHNESS FACTOR
PREDICTED FRACTURE TOUGHNESS CORRELATIONS
S(f) x T(f) = R(f)
ORIGINAL SIGNAL
MATERIAL MICROSTRUCTURE
MODULATED SIGNAL
RECEIVING TRANSDUCER
MICROSTRUCTURE TRANSFER FUNCTION (MTF) MODEL

Figure 5

IDENTIFICATION OF CRITICAL MICROSTRUCTURAL FEATURES

A case study helps illustrate the role of critical microstructural features in governing material properties such as fracture toughness. Moreover, it will be seen that ultrasonic measurements based on stress wave interaction (SWI) and associated models can help identify the critical features. When assessment of microstructure is based solely on photomicrographs, it is not always apparent what feature governs material performance. Judging from figure 3, one might infer that increasing fracture toughness can be associated with decreasing average grain size. This basis for ranking toughness may be correct for low carbon steels and other materials with similar microstructures. However, for materials with a more complex microstructure, such as that shown in figure 6, we do not have a priori criteria for ranking fracture toughness simply by examination of photomicrographs. In this latter case, and in general, the ranking can be accomplished with the aid of ultrasonic measurements and the previously mentioned models.

By using the SWI and associated models, one can derive equations relating ultrasonic and toughness factors. There is a particular equation that is valid only if one of the factors is the critical dimension associated with the microstructural feature that influences or governs fracture toughness. It is found that the best correlation of ultrasonic and toughness data occurs when the equation is evaluated using the correct (i.e., critical microstructural) dimension (see fig. 7).

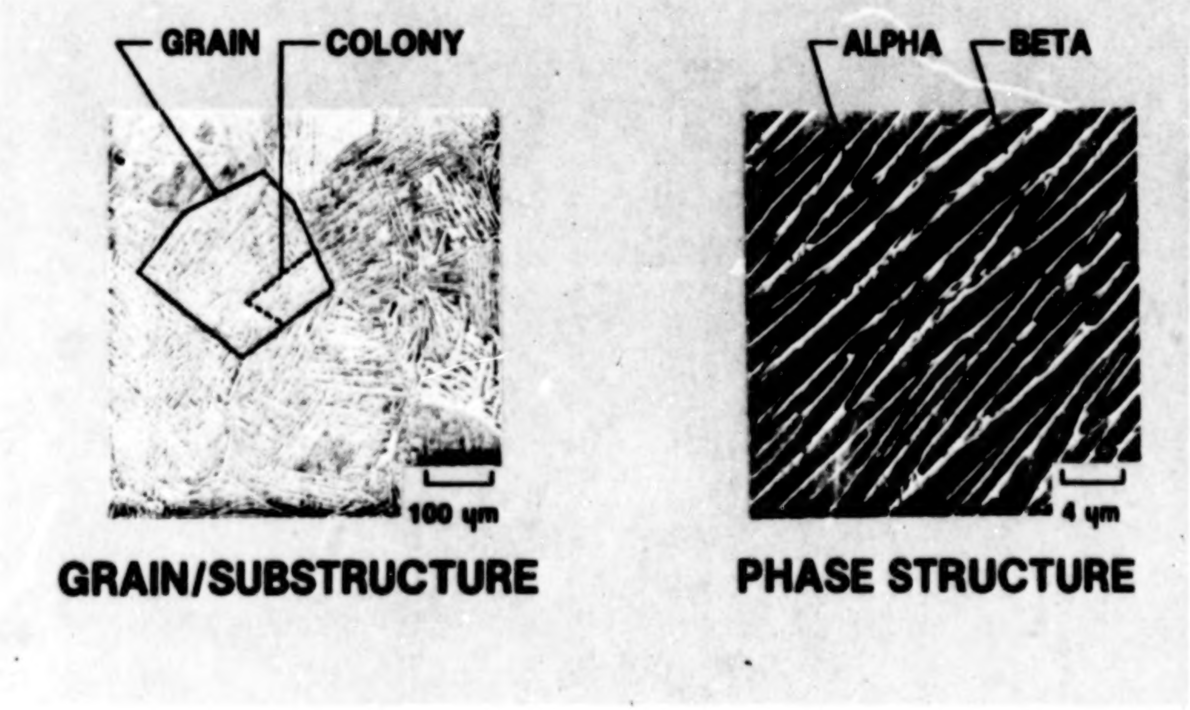

WHICH MICROSTRUCTURAL FACTOR GOVERNS FRACTURE TOUGHNESS?

Figure 6

IDENTIFICATION OF CRITICAL MICROSTRUCTURAL FEATURES (Concluded)

In the case of the titanium alloy depicted in figures 6 and 7, there are three levels of microstructure: grains, colonies, and alternating alpha/beta phases, each with its own characteristic dimension. The question is which of these features exerts the greatest influence on toughness. The question has been answered experimentally and in conformance with the previously discussed analytical models (ref. 7). The results shown in figure 7 indicate that the best empirical correlation and also best agreement with theoretical expectations occur with data based on the beta-phase thickness. The alpha-phase thickness was found to be significant but less critical from the ultrasonic viewpoint. Colony size was weakly influential while the grain size was indeterminate in affecting toughness in the titanium alloy. Further analysis confirmed that the beta phase comprised the critical microstructural feature because of its high dislocation density and high attenuation (i.e., high energy absorption) for ultrasonic waves.

In all the cases studied thus far the experimental results agree with predictions based on the SWI and associated models mentioned previously. These models appear to be at least valid starting points for predicting and explaining correlations between ultrasonic and fracture toughness measurements. However, it should be admitted that we are only at a preliminary stage in establishing fundamental precepts for ultrasonic NDE of extrinsic properties.

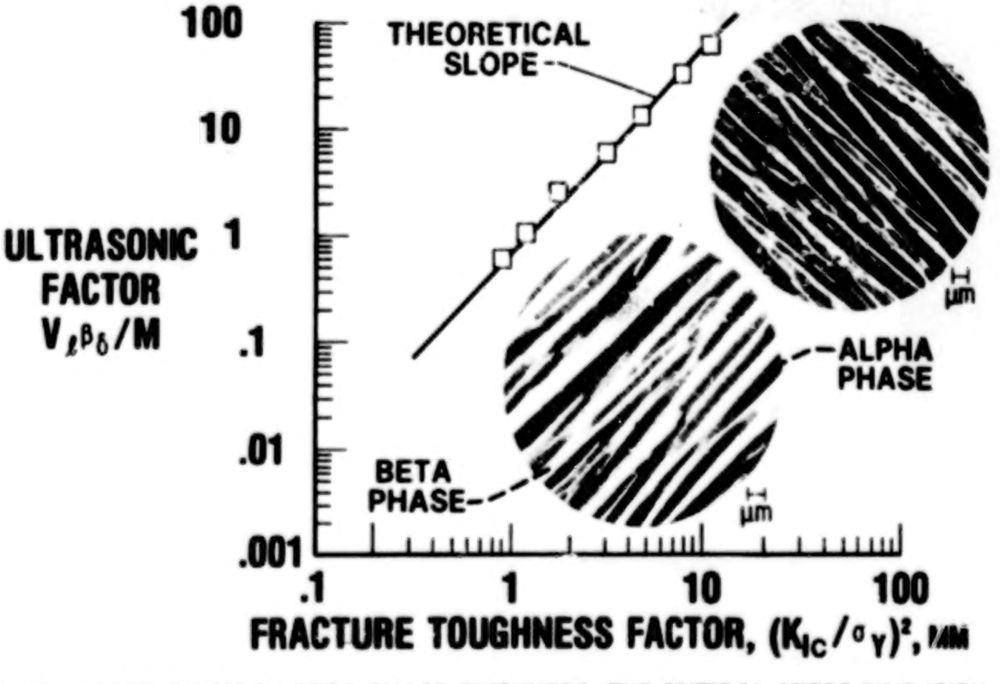

- ★ DATA BASED ON MEAN BETA PHASE THICKNESS, THE CRITICAL MICRO-DIMENSION
- ★ SLOPE OF LINE THROUGH DATA CONFORMS WITH STRESS WAVE INTERACTION MODEL
- ★ MODEL PREDICTS RELATION FOUND BETWEEN ULTRASONIC & TOUGHNESS FACTORS

Figure 7

PRACTICAL IMPLICATIONS - CONCLUSIONS

Among the obvious practical applications of the ultrasonic technology mentioned herein are those of material property assessment and verification. As indicated in figure 8, immediate benefits can be realized by ultrasonic measurement of fracture toughness and related properties. This would satisfy a widely recognized need for rapid, inexpensive alternatives to conventional destructive methods for fracture toughness testing (ref. 5).

The preceding text summarized concepts and experimental findings concerning nondestructive materials characterization. For illustrative purposes, there was some focus on ultrasonic assessment of fracture toughness. There are, however, ramifications that extend beyond toughness or any other extrinsic property. Therefore, the emphasis was on interrelations of ultrasound, microstructure, and extrinsic properties to indicate the potential scope of NDE. It should be apparent that NDE technology can span a rather large area of interest ranging from parts inspection to materials research. From the research viewpoint, the ultrasonic technology cited herein can contribute to better understanding of factors that govern material performance and also contribute guidance to microstructure tailoring to achieve better performance. This is in addition to the more standard role of ultrasonics for defect and materials characterization.

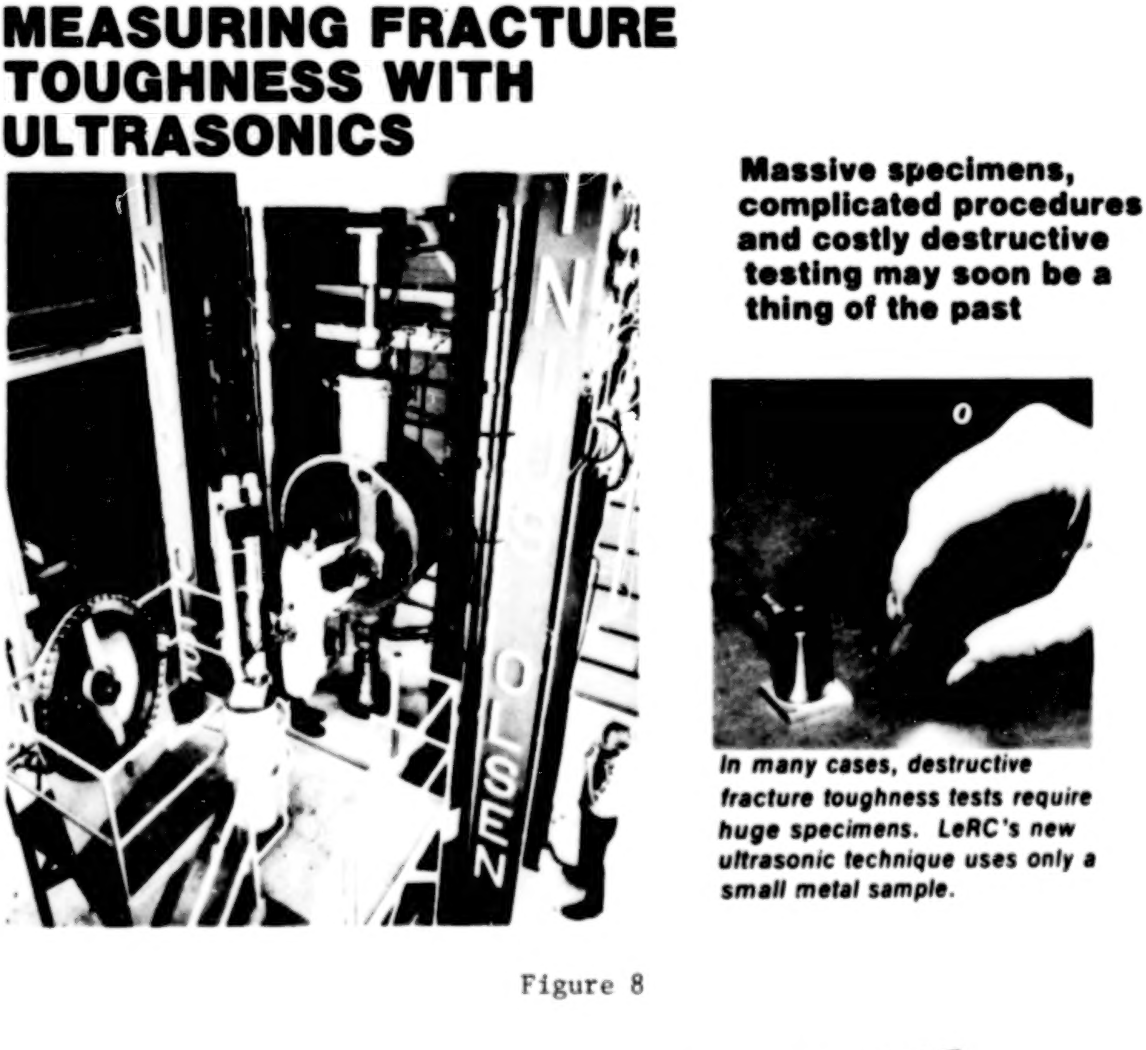

MEASURING FRACTURE TOUGHNESS WITH ULTRASONICS

Massive specimens, complicated procedures and costly destructive testing may soon be a thing of the past

In many cases, destructive fracture toughness tests require huge specimens. LeRC's new ultrasonic technique uses only a small metal sample.

Figure 8

REFERENCES

1. Bever, M. B., ed.: Nondestructive Evaluation. Encyclopedia of Materials Science and Engineering. Pergamon Press, Oxford, 1982.

2. Vary, A.: Nondestructive Evaluation Technique Guide. NASA SP-3079, 1973.

3. Vary, A.: Ultrasonic Measurement of Material Properties. Research Techniques in Nondestructive Testing, R. S. Sharpe, ed., Academic Press, 1980, pp. 159-204.

4. Vary, A.: Concepts and Techniques for Ultrasonic Evaluation of Material Mechanical Properties. Mechanics of Nondestructive Testing, W. W. Stinchcomb, ed., Plenum Press, 1980, pp. 123-141.

5. Rapid Inexpensive Tests for Determining Fracture Toughness. NMAB 328, National Academy of Sciences, 1976.

6. Vary, A.: Correlations Between Ultrasonic and Fracture Toughness Factors in Metallic Materials. Fracture Mechanics, C. W. Smith, ed., ASTM STP 677, 1979, pp. 563-578.

7. Vary, A.; and Hull, D. R.: Interrelation of Material Microstructure, Ultrasonic Factors, and Fracture Toughness of a Two Phase Titanium Alloy, NASA TM-82810, 1982.

ADVANCES IN NONDESTRUCTIVE EVALUATION TECHNOLOGY

Joseph S. Heyman
NASA Langley Research Center
Hampton, Virginia

INTRODUCTION

Quantitative nondestructive evaluation (NDE) is becoming one of the fastest growing fields paralleling the importance of technology in most specializations. Materials are being pushed to their limits of strength, life, and temperature with extreme pressure on economy, requiring quantitative measurement to characterize materials' properties. Development of new sensors, technologies, and applications is at an exciting threshold. However, of most importance, a fundamental understanding of the physical limitations of a given technology is helping to focus research on those topics that have the highest potential of a major breakthrough.

Research at NASA Langley's Materials Characterization Instrumentation Section has followed the philosophy of improving the science base of NDE and advancing the state of the art of quantitative interpretability of physical measurements of materials. (See fig. 1.) Most of the effort has been applied to advanced ultrasonics. New methods are evolving that separate materials' parameters, in contrast with some conventional methodologies in which several different properties simultaneously affect the choosen measurement. Thus separated, "images" of materials similar to X-ray photos may be studied independently. One such image may be material elastic properties, another may represent material stress, while a third may localize material attenuation. These additional quantitative results can have considerable impact on the correct interpretation of NDE data for a critical part.

In this paper we shall examine details of several R&D programs choosen to highlight our last several years. A brief look at acoustic nonlinear theory will introduce the basis upon which some exciting instrumentation has been developed. Applications of these technologies will be presented in the area of stress measurement, characterization of metal heat treatment, and evaluation of material internal structure. A second focus of the program is on quantitative transducers/measurements that have resulted in better data in irregular inhomogeneous materials such as composites. Examples are presented of new capabilities resulting from these advances that include fatigue and impact damage evaluation.

The future of the research program is most exciting with new imaging and measurement theories being combined with new physical understanding of materials. At present, our future programs thrust will focus on linear and nonlinear acoustics, thermal mapping for flaws, new sensors, and, of most importance, a science base upon which all these concepts must be built. To build without improving the science base is to risk a stale technology.

NONDESTRUCTIVE RESEARCH AT NASA LANGLEY

- IMPROVE SCIENCE BASE OF NDE
- DEVELOP MATERIAL MEASUREMENTS WHICH DEPEND ON ISOLATED MATERIAL PROPERTIES
- IMPROVE INTERPRETABILITY OF NDE IMAGES
- ADVANCE THEORY/APPLICATIONS OF NONLINEAR ACOUSTICS
- IMPROVE MEASUREMENTS OF MATERIAL STRESS
- IMPROVE TECHNOLOGIES FOR STRUCTURAL NDE

Figure 1

THEORY OF NONLINEAR ACOUSTICS

Figure 2 presents in a simplified fashion a stress-strain curve of two materials. The upper curve shows a "linear" material response and the Hookeian equation that describes the material behavior. In reality, higher order elastic properties are already "operating" on the material behavior, even in the straight-line figure. The lower curve shows gross nonlinearity that requires many terms in the non-Hookeian equation to correctly describe its behavior. For both of these cases nonlinear acoustics has played an important role in measuring material properties.

Our nonlinear acoustics research program is developing the correct physical models that describe how important material properties can be measured. For example, current research on stress in materials has resulted in a model of material elasticity that includes for the first time the important contributions of residual stress. Other theoretical efforts have identified thermodynamic properties of materials that may result in a measurement technique capable of determining internal material stress/strain. A long-term goal of the program is to develop elements of an equation of state for solids to understand how to quantitatively measure important material properties.

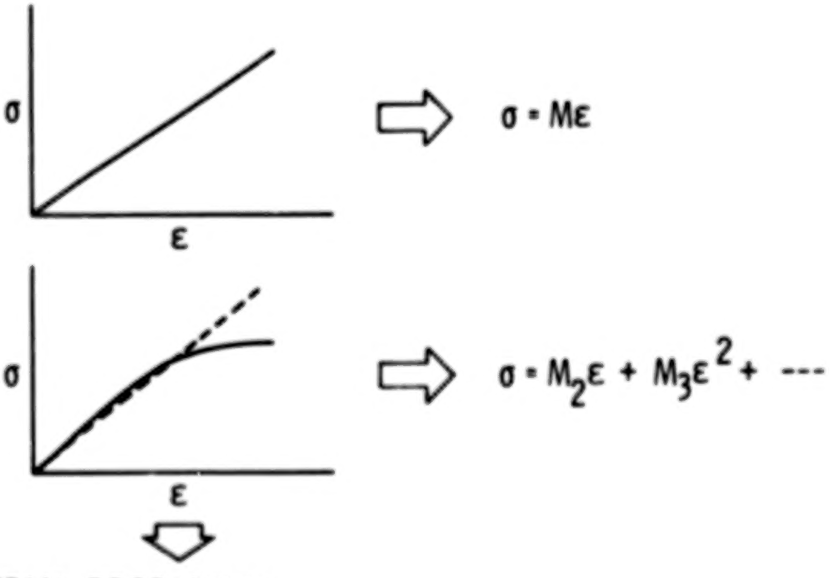

NONLINEAR MATERIAL PROPERTIES

- ENGINEERING MODULUS DEPENDS ON STRAIN AND STRAIN RATE
- MATERIAL THERMODYNAMIC PROPERTIES (e.g. COEFFICIENT OF THERMAL EXPANSION, THERMAL CONDUCTIVITY)
- IMPACT STRENGTH - SHOCK WAVE EFFECTS
- OPTICAL REFRACTIVE INDEX VARIATIONS WITH RESPECT TO σ, TEMPERATURE

Figure 2

APPLIED LOAD CHANGES ACOUSTIC SPECTRA

Figure 3 shows the experimental acoustic spectra of a simple threaded fastener for four levels of applied load. The spectra predicted from acoustic theory represent the resonances of the tested bolt in the range of the 200th harmonic. With increasing stress load, each harmonic shifts down in frequency as shown in the figure. The linear shift with respect to stress is predicted from acoustic nonlinear theory and can be used to determine preload in critical fasteners. These tests have led to the development of precision measurement instruments which are capable of determining stress in critical fasteners.

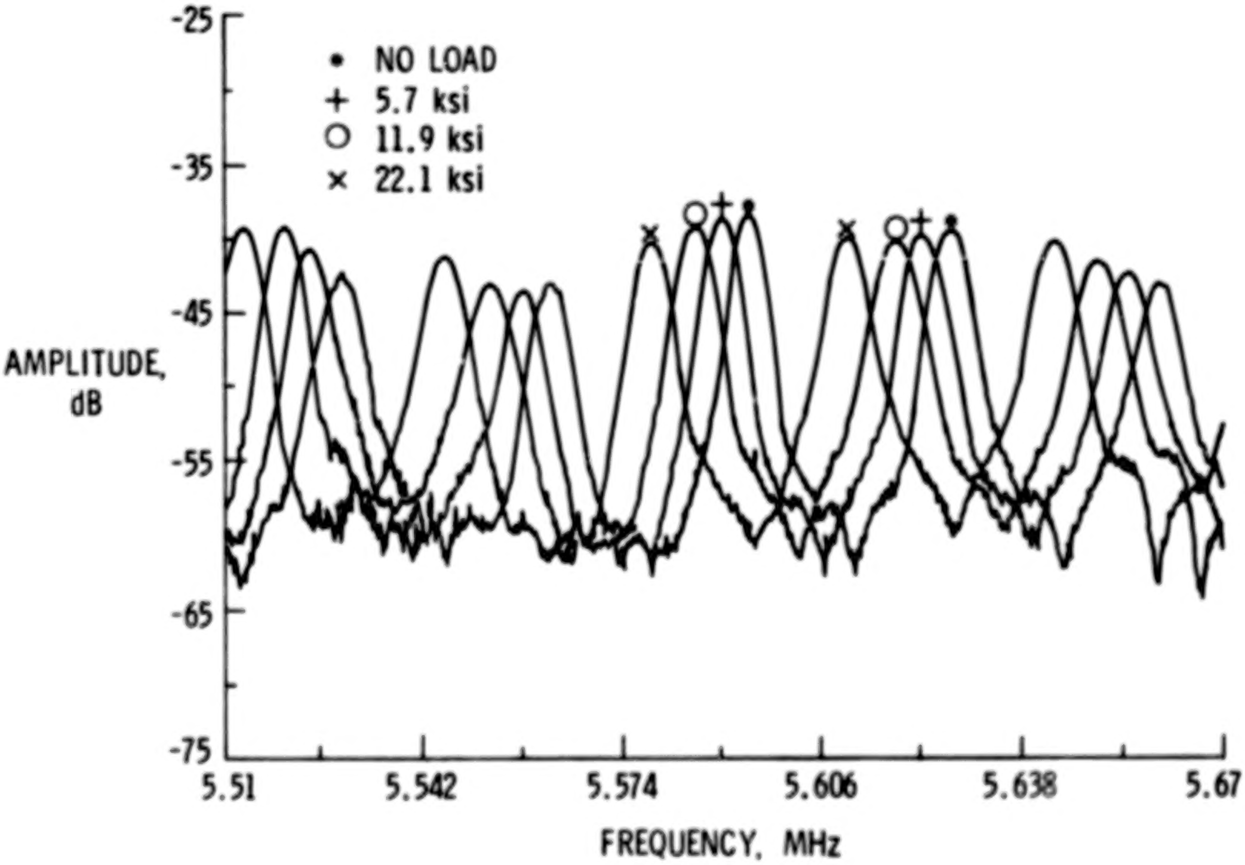

Figure 3

NEW ULTRASONIC STRAIN MEASUREMENT TECHNIQUE

When a solid is placed under tension, it not only elongates, it also undergoes a change in sound speed as predicted by nonlinear theory. The change in acoustic properties is similar to the combined effects of elongating a pipe organ tube (strain) and replacing the tube's air with a gas of lower sound speed. The resulting tone will decrease. As shown in figure 4, a stress of 54 ksi applied to an aluminum rod produced a normalized frequency decrease of $\Delta v/v = 16 \times 10^{-3}$. Strain for that same load was 6×10^{-3} and normalized acoustic velocity decrease was $\Delta v/v = 16 \times 10^{-3}$.

This data shows that the state of the art for ultrasonic technology/analysis has reached that of strain gages. An additional important feature is that the ultrasonic system measures strain directly in the member being strained, not in an externally applied gage to which the strain must be coupled. This improvement in measurement technology goes far beyond strain sensing. It represents a new tool for materials testing allowing higher order elastic properties to be easily determined.

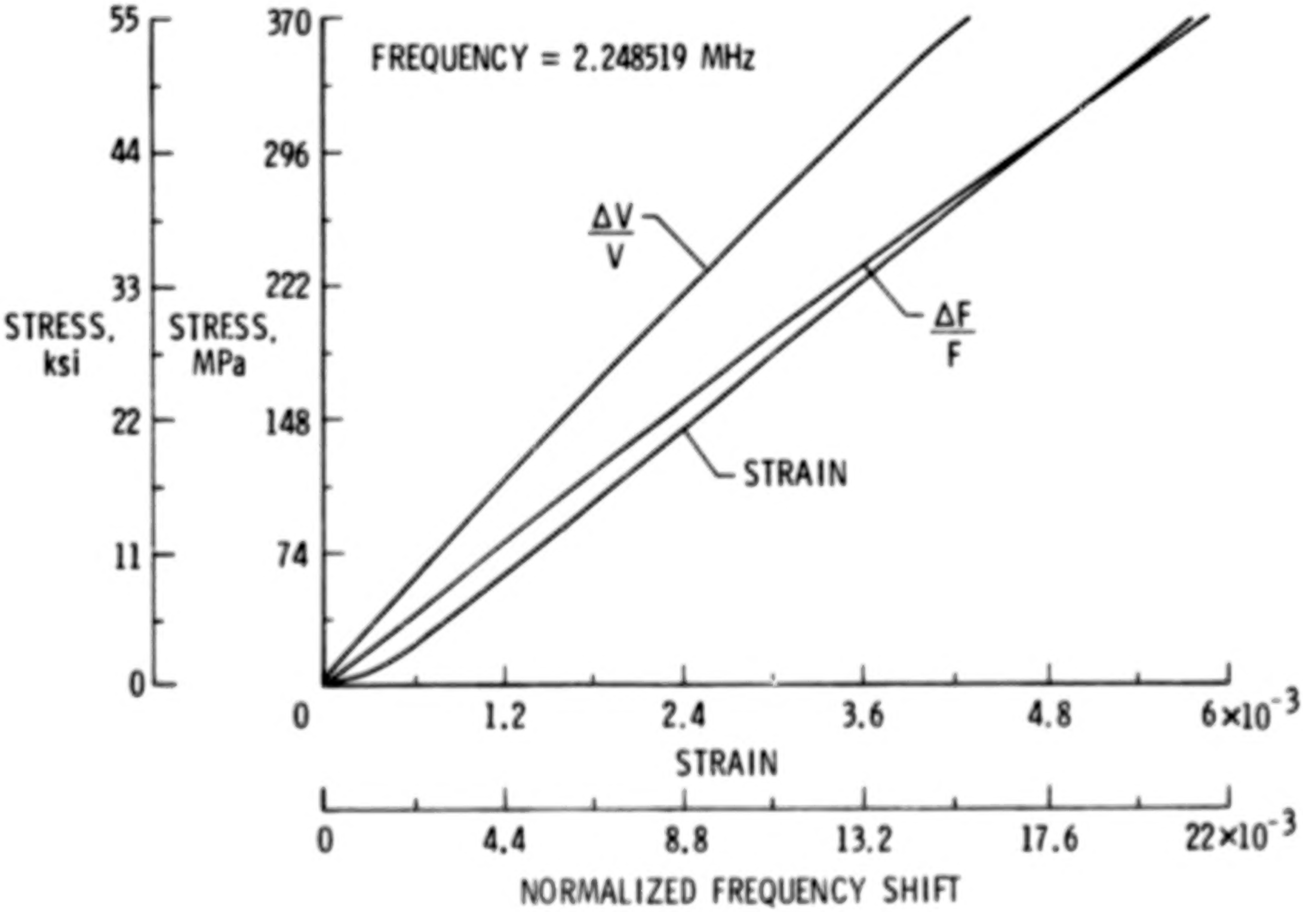

Figure 4

ULTRASONIC CHARACTERIZATION OF ALUMINUM HEAT TREATMENT

The data in figure 5 was obtained from the same threaded rod (not a standard tensile geometry) of the previous figure after it was annealed to simulate thermal loss of strength. Instead of failure occurring at a load of 54 ksi, the aluminum plastically flowed at 28 ksi and failed at 39 ksi. Measurements of sound velocity at zero load (related to the second-order modulus) showed little variation between quenched and annealed material and thus are not useful for identifying "soft" aluminum.

The nonlinear acoustic properties, however, measured from the "linear range" of this figure have been able to clearly identify the "soft" aluminum. The most sensitive of these parameters is the normalized shear wave change in frequency per unit stress. A 30-percent change occurred from annealed to quenched in that parameter for these tested samples. In similar tests we have applied advanced nonlinar acoustic measurements to stressed materials to examine new methods of determining residual stress.

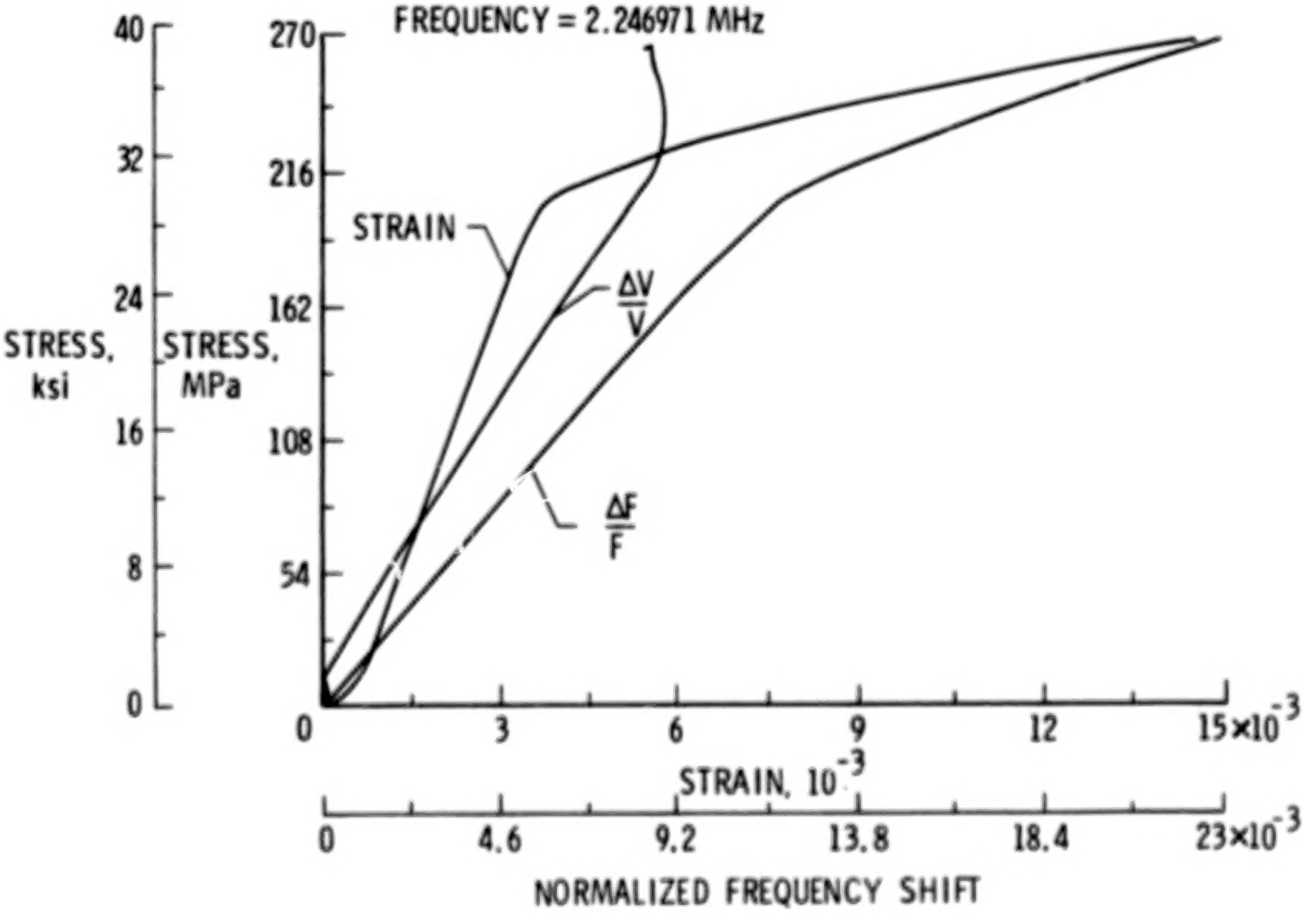

Figure 5

ULTRASONIC C-SCAN TECHNOLOGY

Ultrasonic C-scans represent an outstanding method of investigating internal properties of materials nondestructively. In effect, the resulting data appears as an ultrasonic "X-ray" - that is, an image of the tested part projected on a two-dimensional plane. In general, a transducer source emits ultrasonic waves that are usually focused by a lens and propagate through a material to a receiving transducer. Usually, a liquid couplant or bath used to increase the coupling efficiency requires a water tank or "squirters" for the test. The transducers (used singly in reflection or in pairs) are moved in a scanning configuration, building up an acoustic image of the material (fig. 6). We have developed extensive technological improvements in analysis and instrumentation for C-scan measurements. Examples include tone burst spectroscopy for quantitative measurements, spectral line fitting for data analysis, and integrated backscattering for improved imaging.

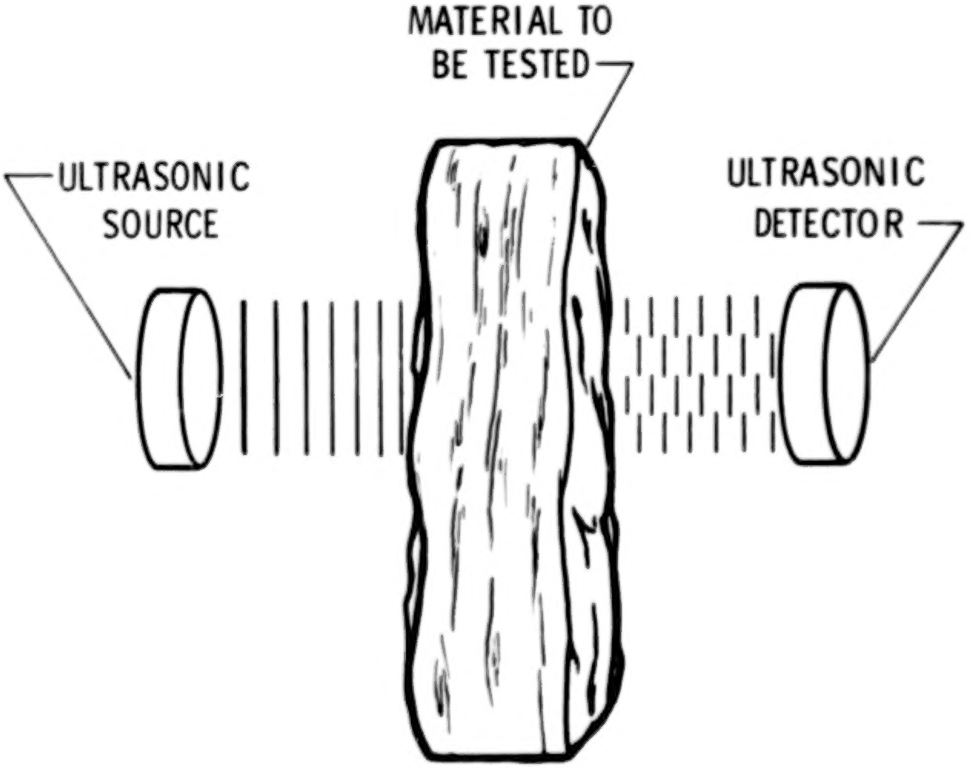

Figure 6

NEW TRANSDUCER TECHNOLOGY FOR NDE

One of the most severe limitations of the current quality of NDE images is the transducer itself. Conventional transducers are phase sensitive and as such are affected by the shape of the acoustic phase front incident on them. For accurate measurement of acoustic attenuation in materials, a phase-insensitive device is necessary. We have developed the first practical acoustic power detector that is insensitive to wave front phase distortion.

Figure 7 shows two ultrasonic C-scan images of the letters "NASA" machined in a metal plate. The upper image, obtained with conventional phase-sensitive transducers (PZT), is highly distorted by phase artifacts, especially at letter interfaces. The lower figure, obtained with our phase-insensitive acousto-electric transducer (AET), shows clear letters, representing a more quantitative measurement technique.

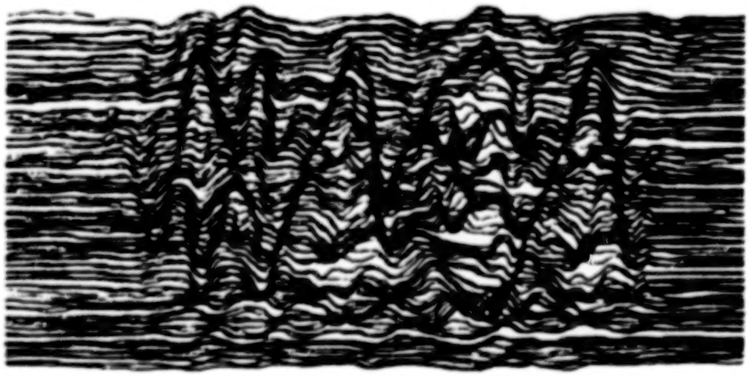

PZT

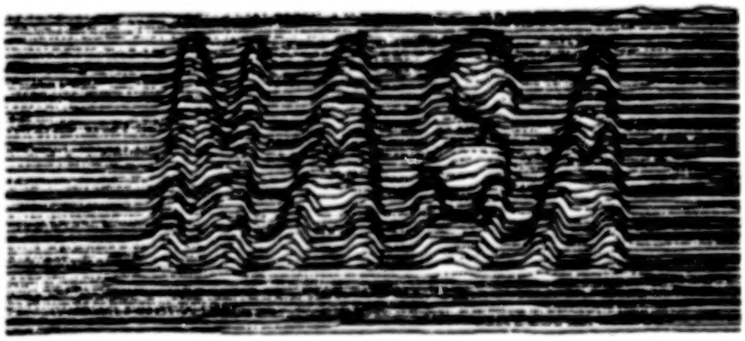

AET

Figure 7

APPLICATION OF THE AET FOR QUANTITATIVE NDE

The phase-insensitive AET discussed in the previous figure represents a significant improvement in the state of the art for absorption measurements. An example of the improved accuracy of ultrasonic absorption measurements is shown in figure 8. A threaded fastener is shown loaded asymmetrically by an angled washer. A conventional PZT transducer mounted on the right side of the bolt was used to generate and measure an ultrasonic wave. The phase-insensitive AET mounted on the left of the bolt also measured the ultrasonic wave.

The four oscilloscope photos show the effect of increasing load on the bolt. Note that the PZT signal decreases, nulls, and then increases with load while the AET signal remains constant. There is no actual loss of acoustic amplitude for this case, only a "wrong" signal from the PZT caused by phase cancellation. Artifacts such as this may lead to incorrect analyses of critical parts and costly unnecessary repairs.

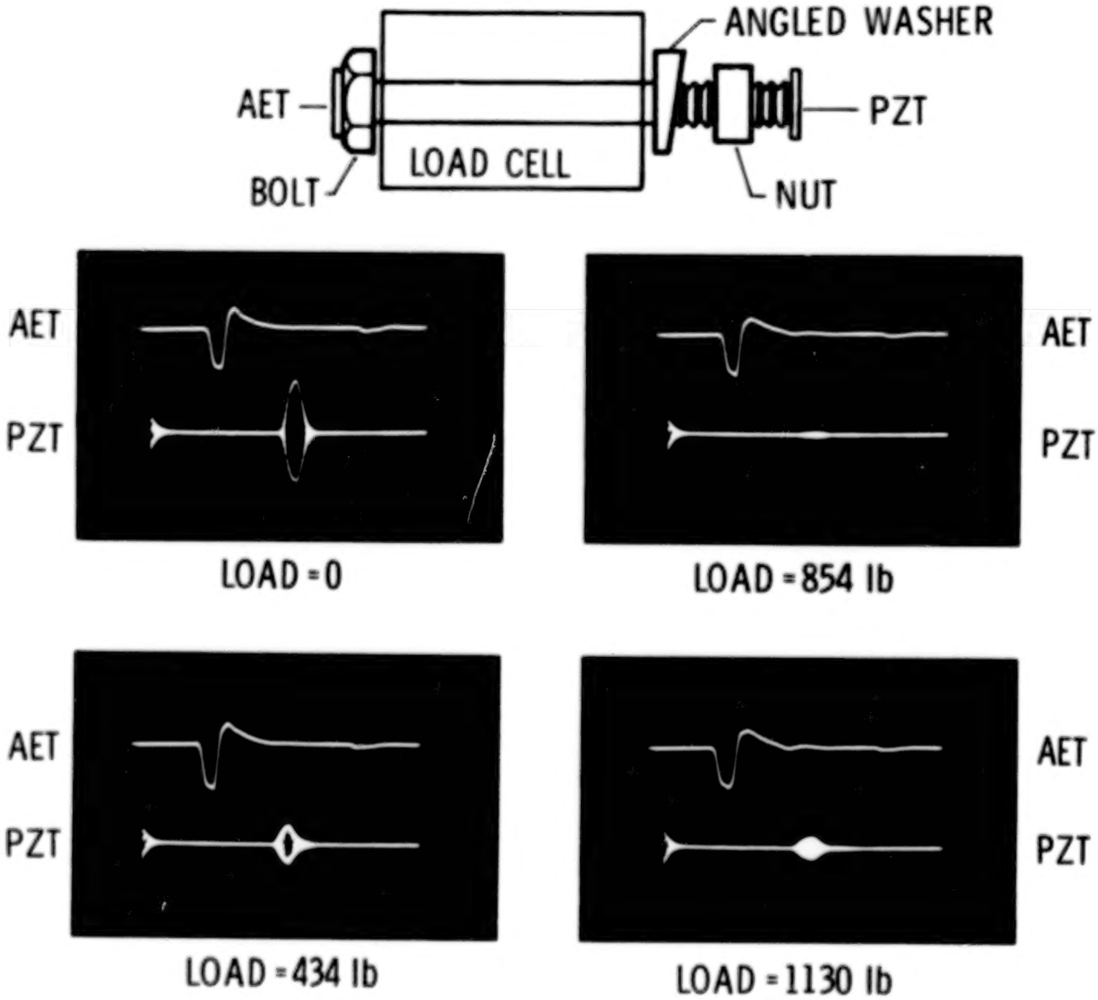

LOAD = 0

LOAD = 854 lb

LOAD = 434 lb

LOAD = 1130 lb

Figure 8

TONE BURST ACOUSTIC SPECTROSCOPY (TBS)

The block diagram (fig. 9) below shows a new acoustic spectroscopy system that eliminates gating influences on spectra. Conventional acoustic spectroscopy utilizes short pulses or step-like signals. The Fourier transform of such signals depends on the detailed pulse rise, pulse width, and pulse fall, which influence the spectra measured for pulse propagation through samples. Also, since all the energy is generated in a short period of time (typically nanoseconds), the pulse is quite large in amplitude, leading to nonlinearities in the transducer.

In contrast, the TBS technique uses wide signal gates (several microseconds), which require lower amplitude signals but over longer times. By tracking the frequency emitted by the gates with a spectrum analyzer, a pure acoustic spectra is obtained without gating artifacts.

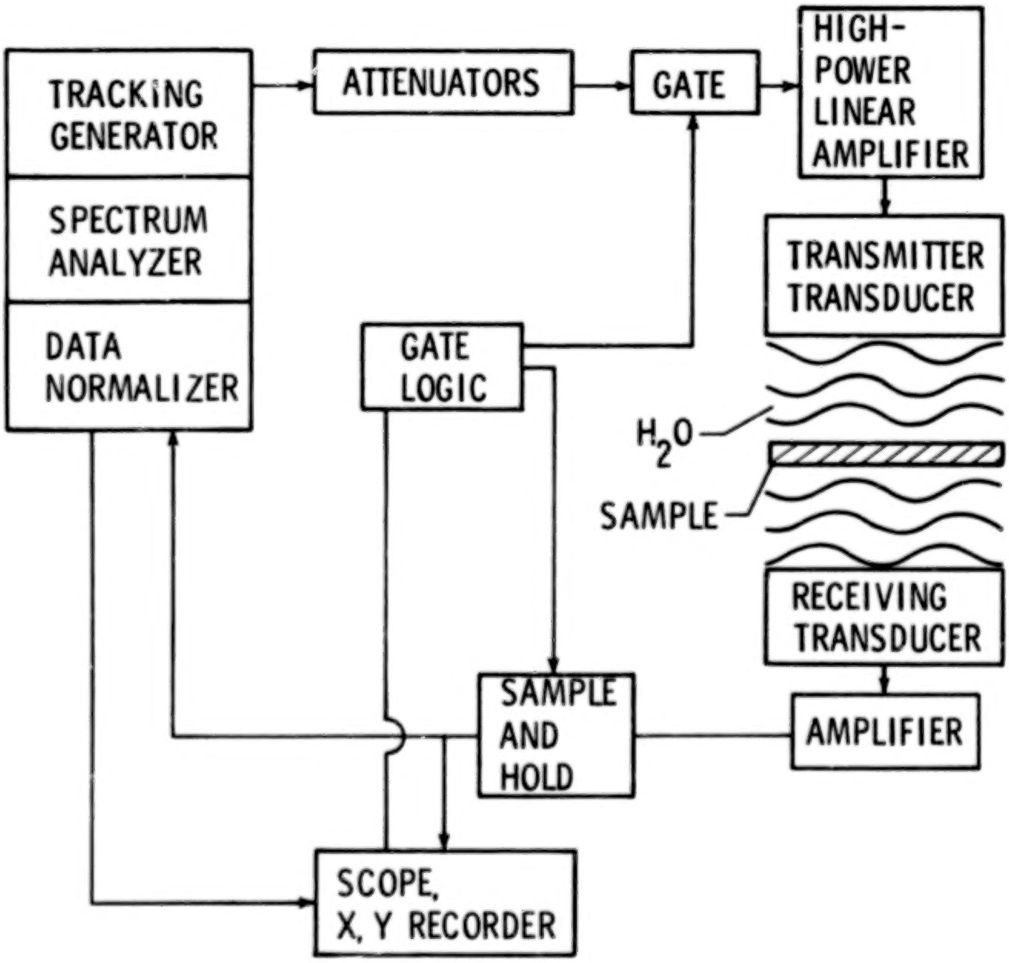
TRACKING GENERATOR
SPECTRUM ANALYZER
DATA NORMALIZER
ATTENUATORS
GATE
HIGH-POWER LINEAR AMPLIFIER
TRANSMITTER TRANSDUCER
GATE LOGIC
H_2O
SAMPLE
RECEIVING TRANSDUCER
SAMPLE AND HOLD
AMPLIFIER
SCOPE, X, Y RECORDER

Figure 9

AET POWER SPECTRA OF COMPOSITES

The data in figure 10 was obtained by combining the TBS system of the previous figure with the AET power transducer to achieve a first for irregular inhomogeneous material - clear spectral characterization for NDE analysis. The acoustic spectra represent longitudinal standing harmonic modes of the sample, which was a laminated graphite/epoxy composite.

The composite sample was clamped in a test machine and fatigued until cracks developed on the sample sides. The cracks were measured with a replicating technique and the fatigued samples were ultrasonically examined. The fatigue-induced damage increased the acoustic absorption, decreasing the amplitude of the resonance spectra, as shown in the figure. Such research may result in a measurement technology capable of assessing the degree of fatigue damage in composites.

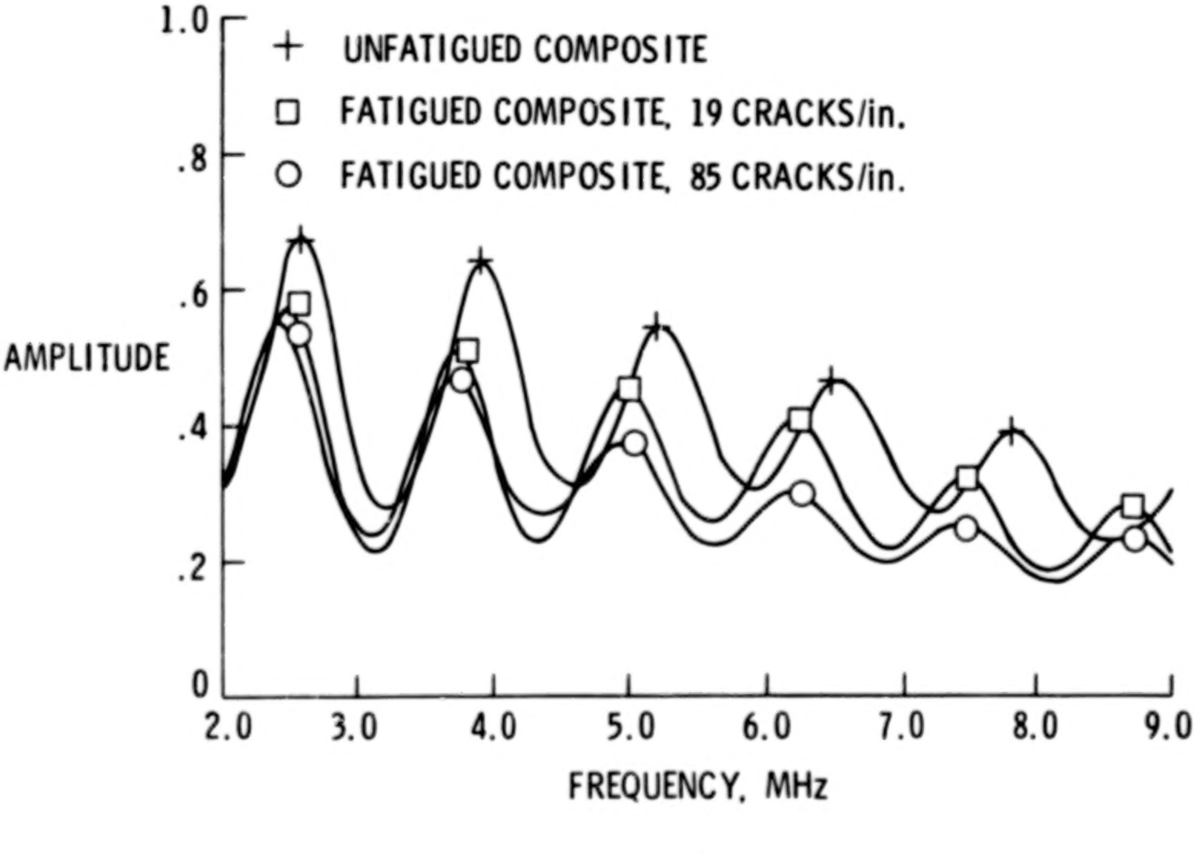

Figure 10

TRANSDUCER MEASURES 10^{-8} INCHES

A new broadband electrostatic transducer measures displacement of less than 10^{-8} inches in water. The high-resolution capability of this newly patented device is a result of a novel fabrication technique insuring exacting parallelism of elements and internal pressurization to maintain precision internal spacing. The transducer is simply a capacitor with one stationary plate and one "plate" composed of an 11-mm-thick metal film (fig. 11). This device has been used to examine absolute ultrasonic wave amplitudes with frequencies up to 30 MHz. It has been quite successful as a standard to which other transducers may be compared.

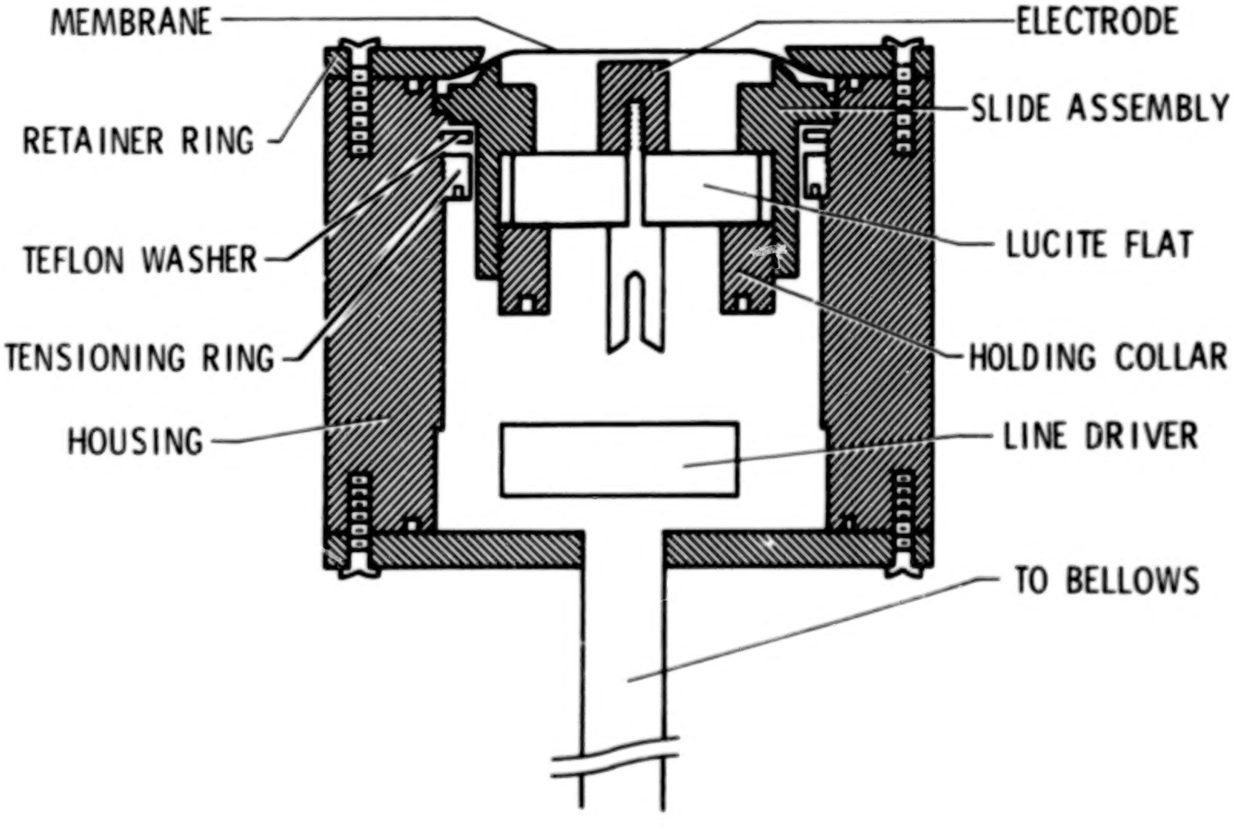
MEMBRANE
ELECTRODE
RETAINER RING
SLIDE ASSEMBLY
TEFLON WASHER
LUCITE FLAT
TENSIONING RING
HOLDING COLLAR
HOUSING
LINE DRIVER
TO BELLOWS

Figure 11

QUANTITATIVE NDE IMAGING

This advanced C-scan (fig. 12) brings together many subelements of our NDE research program. The details shown are of impact damage to a graphite/epoxy composite based on tone burst spectroscopy combined with a power transducer (AET). The image on the right shows surface damage only at the site of impact since the physics of the imaging represents impedance reflections. Using the same C-scan data we obtained an image based on the slope of the attenuation versus frequency curve, which is independent of impedance. Thus, a totally different image was generated from the same data, representing different material physics. The slope data shows damage off center from the impact on a 45° ply. This internal damage, not seen with conventional methods, represents attenuation mechanisms such as scattering from cracks.

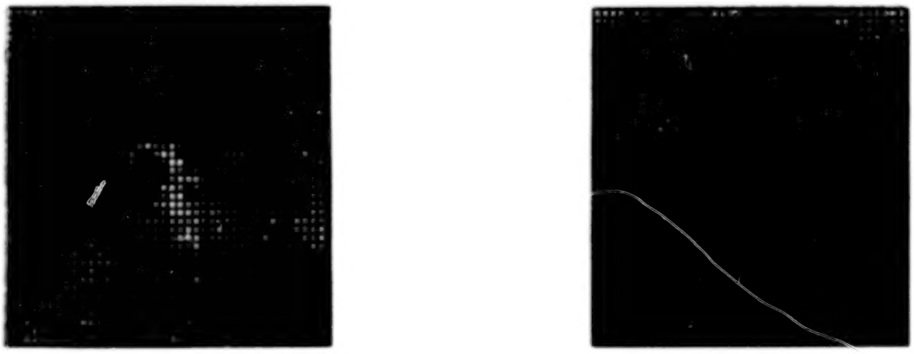

SLOPE, dB/MHz-cm

INTERCEPT, dB

ACOUSTOELECTRIC RECEIVER

4 TO 8 MHz

Figure 12

IN SITU FIBER SENSOR FOR COMPOSITE STRAIN AND ACOUSTIC EMISSION

Figure 13 shows a block diagram of an optical fiber interferometer developed to improve the reliability of composites through monitoring. The technique involves optically coupling reference fibers to fibers embedded in the composite matrix. The result is a set of optical fringes which, when spatially filtered, results in an optical signal proportional to strain. Results of an acoustic emission event (left) and cantilever beam strain (right) are shown.

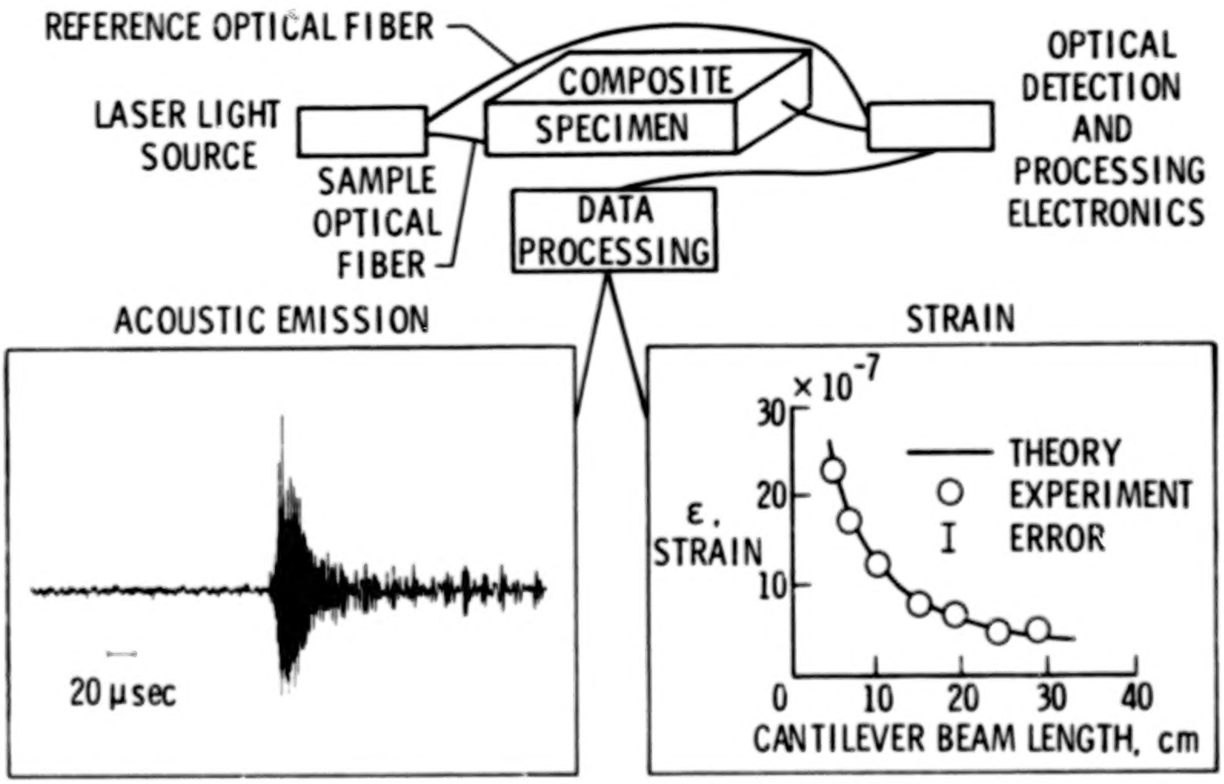
REFERENCE OPTICAL FIBER
LASER LIGHT SOURCE
COMPOSITE SPECIMEN
OPTICAL DETECTION AND PROCESSING ELECTRONICS
SAMPLE OPTICAL FIBER
DATA PROCESSING
ACOUSTIC EMISSION
20 μsec
STRAIN
× 10⁻⁷
30
20
10
ε, STRAIN
THEORY
EXPERIMENT
ERROR
0
10
20
30
40
CANTILEVER BEAM LENGTH, cm

Figure 13

ULTRASONIC TECHNOLOGY UTILIZATION-MINING

Two applications of our in-house research on ultrasonic propagation in stressed solids have helped improve mining technology. The first is a mine roof bolt tension monitor that measures bolt tension ultrasonically. The second (fig. 14) is an in situ rock strain sensor. The figure on the left shows an artist's impression of how the system would function in a mine shaft. The figure on the right shows a compressive test on Longmont sandstone, comparing the sensitivity of strain gage data ($\Delta a/a$) with that of ultrasonic data ($\Delta F/F$). The relative change in natural velocity in the $\Delta F/F$ curve shows that the ultrasonic sensor is 100 times more sensitive to the applied load than the conventional strain gage, and, more importantly, it measures strain directly in the rock itself.

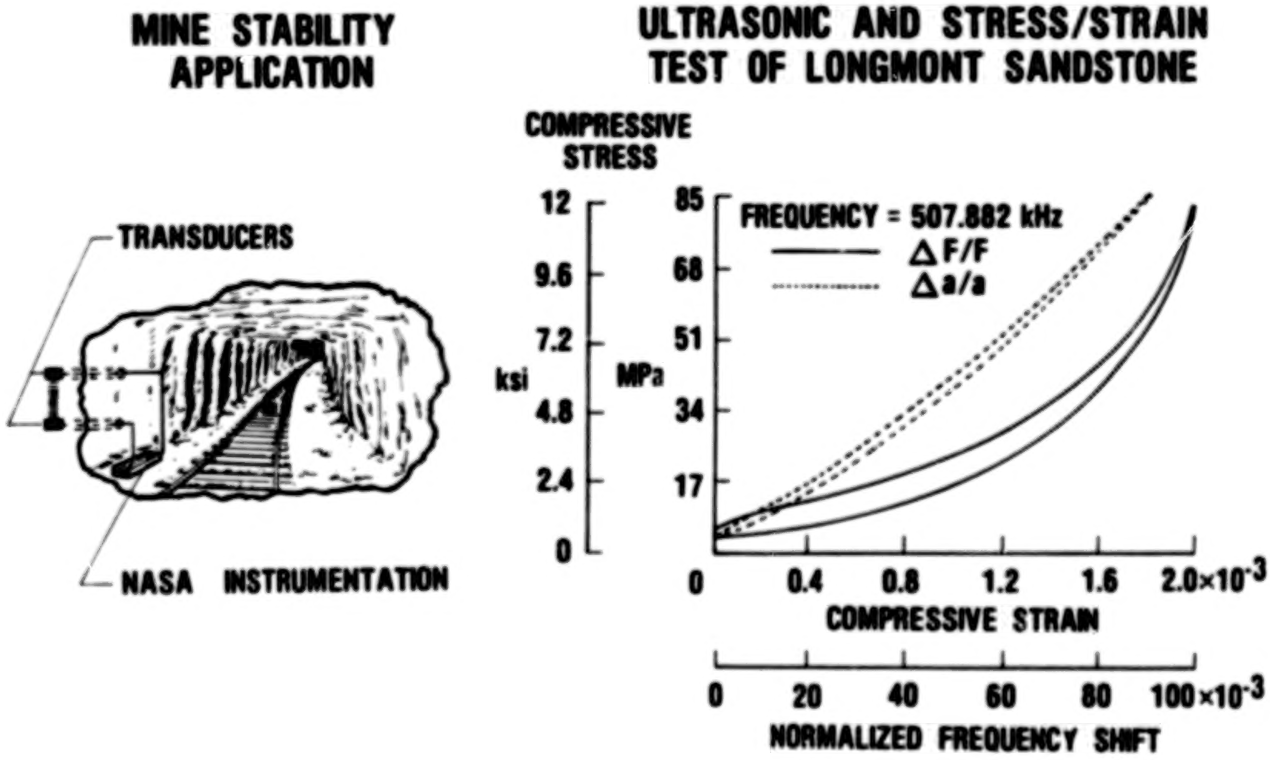

MINE STABILITY APPLICATION

ULTRASONIC AND STRESS/STRAIN TEST OF LONGMONT SANDSTONE

Figure 14

ULTRASONIC TECHNOLOGY UTILIZATION - SKIN BURNS

A technique developed in part by one of our researchers is being optimized to detect the level of burn damage to human skin. The treatment of skin burn would improve significantly if the burn physician could distinguish third-degree burns (killed tissue) from second-degree burns (viable tissue). In this technique a short high-frequency wave is launched into the tissue in question. The depth of burn, which is related to the degree of burn, is measured from the ultrasonic signal. As shown in figure 15, the technique detects the outer layer of skin (epidermis), the burn interface (depth of burn), and the fat interface (total depth of skin tissue). With this technique optimized for skin burn analysis, the prognosis for burn patients may improve significantly.

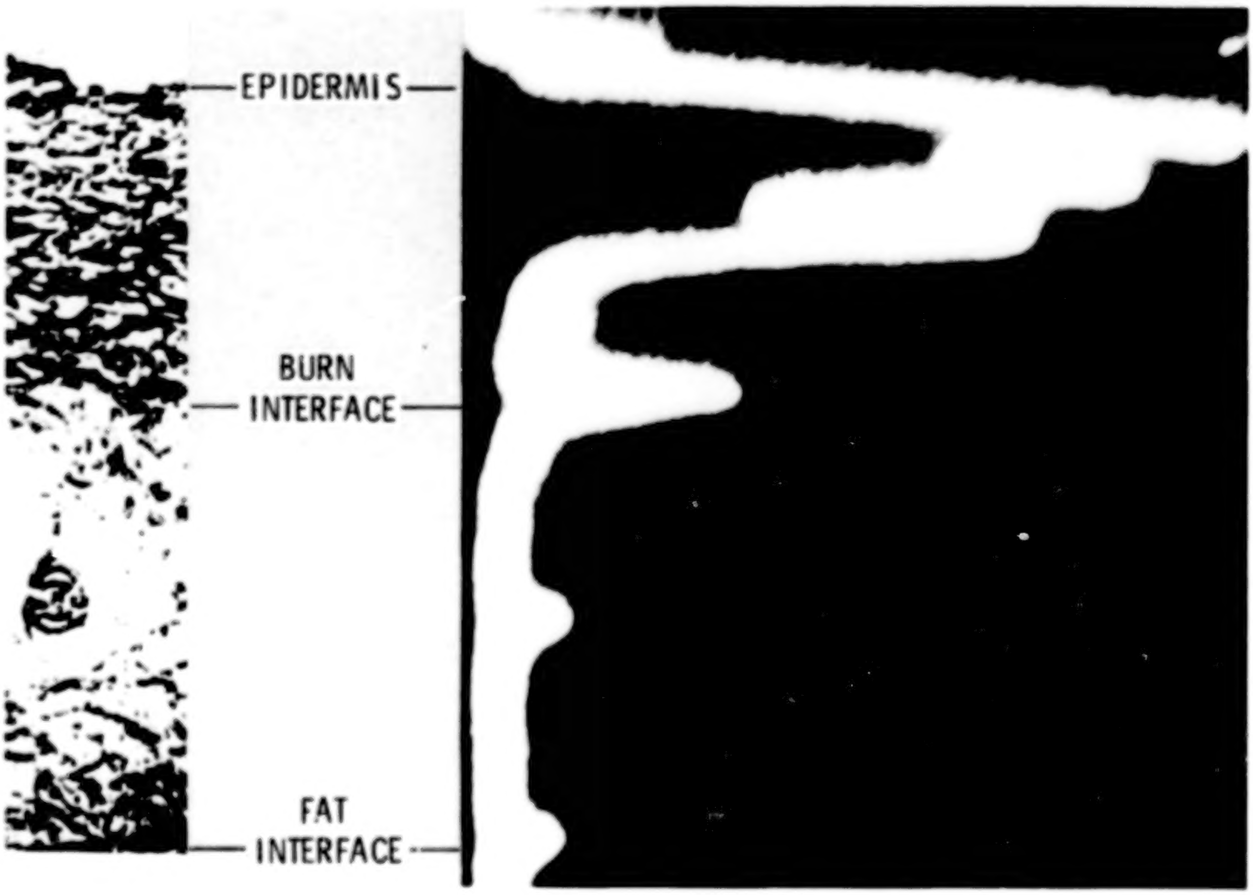

Figure 15

CONCLUSION

This paper has examined nondestructive research at NASA Langley Research Center. In order to fully meet the challenge of the future we must address problems of nondestructive measurements in materials (fig. 16).

- WE MUST IMPROVE NDE SCIENCE BASE
- IMPROVE NDE TECHNOLOGY
- DESIGN FOR INSPECTION
- DEVELOP QUANTITATIVE MATERIALS CHARACTERIZATION INSTRUMENTATION

Figure 16

BIBLIOGRAPHY

1. Cantrell, John H., Jr.: Anharmonic Properties of Solids from Measurements of the Stress Acoustic Constant, ASTM Journal of Testing and Evaluation, September 1982.

2. Cantrell, John H., Jr.: Generalized Gruneisen Tensor from Solid Nonlinearity Parameters, Physics Review, 21, pp. 4191-4195, 1980.

3. Heyman, Joseph S.: A CW Ultrasonic Bolt Strain Monitor, Experimental Mechanics, 17, pp. 183-187, 1977.

4. Heyman, Joseph S.: CW Ultrasonic Bolt Tensioning Monitor, United States Patent #4,062,227, 1977.

5. Heyman, Joseph S.: Pseudo Continuous Wave Instrument, United States Patent #4,117,731, 1978.

6. Blume, R. J.: Review of Scientific Instruments, 34, p. 1400, 1963.

7. Heyman, Joseph S.: Pulsed Phase Locked Loop Strain Monitor, NASA Patent Disclosure LAR 12772-1, 1980.

8. Heyman, Joseph S., and Chern, Engmin J.: Characterization of Heat Treatment of Aluminum Based on Ultrasonic Determination of the Second and Third Order Elastic Constants, Proceedings of IEEE Ultrasonics Symposium, October 1981.

9. Joseph S. Heyman, and Chern, Engmin J.: Ultrasonic Measurements of Axial Stress, ASTM Journal of Testing and Evaluation, September 1982.

10. Breazeale, M. A.; Cantrell, John H., Jr.; and Heyman, Joseph S.: Ultrasonic Wave Velocity and Attenuation Measurements, Methods of Experimental Physics, Edmonds, P. D., Ed., Academic Press, New York, 1981.

11. Heyman, Joseph S., and Cantrell, John H., Jr.: Effects of Material Inhomogeneities on Ultrasonic Measurements: The Problem and a Solution, Nondestructive Evaluation and Flaw Criticality for Composite Materials, ASTM STP 696, R. B. Pipes, Ed., pp. 45-56, 1979.

12. Heyman, Joseph S.: Phase Insensitive Acoustoelectric Transducer, Journal of Acoustical Society of America, 64, pp. 243-249, 1978.

13. Cantrell, John H., Jr., and Heyman, Joseph S.: Ultrasonic Spectrum Analysis Using Frequency-Tracked Gated RF Pulses, Journal of the Acoustical Society of America, 67, pp. 1623-1628, May 1980.

14. Claus, R. O., and Cantrell, John H., Jr.: Detection of Ultrasonic Waves in Solids by an Optical Fiber Interferometer, Proceedings of 1980 IEEE Ultrasonics Symposium, Boston, MA, November 1980.

15. Claus, R. O., and Cantrell, John H., Jr.: DC Calibration of the Strain Sensitivity of a Single Mode Optical Fiber Interferometer, Proceedings of 1981 IEEE Ultrasonics Symposium, Chicago, IL, October 1981.

16. Claus, R. O., and Cantrell, John H., Jr.: Optical Probing of Pulsed Acoustic Surface Waves Using Wideband Differential Interferometry, accepted for publication in Acoustics Letters.

17. Cantrell, John H.: Ultrasonic Determination of Thermodynamic Threshold Parameters for Irreversible Cutaneous Burns, Journal of Acoustical Society of America, August 1982.

1. Report No.
NASA CP-2251

2. Government Accession No.

3. Recipient's Catalog No.

4. Title and Subtitle
ADVANCED MATERIALS TECHNOLOGY

5. Report Date
November 1982

6. Performing Organization Code
505-33-33-01

7. Author(s)
Charles P. Blankenship and Louis A. Teichman, compilers

8. Performing Organization Report No.
L-15537

9. Performing Organization Name and Address
NASA Langley Research Center
Hampton, VA 23665

10. Work Unit No.

11. Contract or Grant No.

12. Sponsoring Agency Name and Address
National Aeronautics and Space Administration
Washington, DC 20546
and
American Institute of Aeronautics and Astronautics
New York, New York 10104

13. Type of Report and Period Covered
Conference Publication

14. Sponsoring Agency Code

15. Supplementary Notes

16. Abstract

This publication is a compilation of papers presented at the NASA/AIAA Advanced Materials Technology Seminar held at NASA Langley Research Center on November 16-17, 1982. Collectively, these papers depict the broad scope of NASA's Materials Technology Program. Each paper provides a brief overview of a technical area in which NASA has a significant research focus. The technical areas include composites, polymer science, metallic materials (aluminum, titanium, and superalloys), materials processing technology, materials durability in the aerospace environment, ceramics, fatigue and fracture mechanics, tribology, and nondestructive evaluation (NDE). The technical program covers research being conducted at four NASA centers: Ames Research Center, Moffett Field, California; Langley Research Center, Hampton, Virginia; Lewis Research Center, Cleveland, Ohio; and Marshall Space Flight Center, Huntsville, Alabama.

17. Key Words (Suggested by Author(s))
Composites
Metals
Ceramics
Polymer chemistry
Nondestructive evaluation (NDE)

18. Distribution Statement
Unclassified - Unlimited

Subject Category 23

19. Security Classif. (of this report)
Unclassified

20. Security Classif. (of this page)
Unclassified

21. No. of Pages
446

22. Price
A19

For sale by the National Technical Information Service, Springfield, Virginia 22161

NASA-Langley, 1982

441